Université de Lille

Doctoral School: Science of Matter, Radiation and Environment

Discipline: Theoretical, Physical and Analytical Chemistry

Dissertation

Unravelling the chlorine chemistry using simulations from the molecular scale to the global scale

by

Zainab SROUR

Thesis submitted in partial fulfilment of the requirements for the degree of Doctor of Philosophy of the University of Lille

Defended on **September 26th, 2023**

Defence Committee

Jury president	Pr. Celine TOUBIN	University of Lille
Reviewer	Pr. René FOURNET	University of Lorraine
Reviewer	Dr. Didier HAUGLUSTAINE	Institut Pierre - Simon Laplace - IPSL
Examiner	Dr. Loic BOSLAND	Institut de Radioprotection et de Sûreté Nucléaire - IRSN
Thesis Director	Dr. Florent LOUIS	University of Lille
Thesis co-director	Dr. Valérie FEVRE-NOLLET	University of Lille
Thesis co-director	Dr. Virginie MARECAL	CNRM Météo-France

Ecole Doctorale : Science de la Matière, du Rayonnement et de l'Environnement

Filière : Chimie Théorique, Physique, et analytique

Thèse de Doctorat

Etudes par Simulations Numériques de la Chimie Atmosphérique du Chlore

présentée par

Zainab SROUR

pour obtenir le Grade de Docteur de l'Université de Lille

Soutenance le **26 septembre 2023**

Composition du Jury

Présidente du jury	Pr. Celine TOUBIN	Université de Lille
Rapporteur	Pr. René FOURNET	Université de Lorraine
Rapporteur	Dr. Didier HAUGLUSTAINE	Institut Pierre - Simon Laplace - IPSL
Examinateur	Dr. Loic BOSLAND	Institut de Radioprotection et de Sûreté Nucléaire - IRSN
Directeur de thèse	Dr. Florent LOUIS	Université de Lille
Co-directrice de thèse	Dr. Valérie FEVRE-NOLLET	Université de Lille
Co-directrice de thèse	Dr. Virginie MARECAL	CNRM Météo-France

Abstract

The discovery of the ozone hole over the Antarctic in the 1970s established the significance of gas-phase halogenated species in the atmosphere. These species play a crucial role in tropospheric and stratospheric chemistry, influencing ozone budget, atmospheric concentrations of key species (such as OH, NO_x, and volatile organic compounds), and halogen interactions. Numerous studies have explored halogen chemistry using global models, however, most of the focus has been on bromine and iodine due to their higher reactivity compared to chlorine. This preference arises from the greater chemical stability of HCl compared to other halogen acids (HX, where X = Br, I).

This thesis aims to unravel the chlorine chemistry in the troposphere starting from the molecular up to the global scales. This is done through the employment of different numerical tools: (i) quantum chemistry tools to predict the reactivity and thermokinetic parameters of the reaction between OH radicals and CH_2ClOOH, which are challenging to obtain experimentally, (ii) the kinetic model "ASTEC" to determine the reactivity of gaseous chlorinated compounds on a short time scale; and (iii) the chemistry transport model "MOCAGE" to evaluate the impact of chlorine on the global atmospheric budget.

The results show that the reaction between CH_2ClOOH and OH radicals is of atmospheric interest with an overall rate constant 6.55×10^{-11} cm^3 molecule^{-1} s^{-1} at 298 K computed at the M06-2X/6-311++G(3df,3p) level of theory. The kinetic modelling showed that the daytime reactivity of chlorinated compounds is more important than the night-time reactivity governed by photolysis and reactivity with OH radicals. Moreover, the global modelling by MOCAGE showed that the chlorine atmospheric budget is not only affected by chemical transformation, but also, it is altered by the physical processes including transport and deposition.

Key words:

Résumé

La découverte du trou d'ozone au-dessus de l'Antarctique dans les années 1970 a mis en évidence l'importance des espèces halogénées en phase gazeuse dans l'atmosphère. Ces espèces jouent un rôle crucial dans la chimie troposphérique et stratosphérique, en influençant le bilan d'ozone, les concentrations atmosphériques d'espèces clés (telles que OH, NO_x et les composés organiques volatils) et les interactions avec les halogènes. De nombreuses études ont exploré la chimie des halogènes à l'aide de modèles globaux, mais l'accent a surtout été mis sur le brome et l'iode en raison de leur plus grande réactivité par rapport au chlore. Cette préférence s'explique par la plus grande stabilité chimique du HCl par rapport aux autres acides halogénés (HX, où X = Br, I).

Cette thèse vise à élucider la chimie du chlore dans la troposphère, de l'échelle moléculaire à l'échelle globale. Pour ce faire, différents outils numériques sont utilisés : (i) des outils de chimie quantique pour prédire la réactivité et les paramètres thermocinétiques de la réaction entre le radical OH et CH_2ClOOH, qui sont difficiles à obtenir expérimentalement, (ii) le modèle cinétique "ASTEC" pour déterminer la réactivité des composés chlorés gazeux sur une courte échelle de temps ; et (iii) le modèle de transport chimique "MOCAGE" pour évaluer l'impact du chlore sur le bilan atmosphérique global.

Les résultats montrent que la réaction entre CH_2ClOOH et le radical OH présente un intérêt atmosphérique avec une constante de vitesse globale de $6{,}55 \times 10^{-11}$ cm^3 molécule^{-1} s^{-1} à 298 K calculée au niveau M06-2X/6-311++G(3df,3p) de la théorie. La modélisation cinétique a montré que la réactivité diurne des composés chlorés est plus importante que la réactivité nocturne régie par la photolyse et la réactivité avec les radicaux OH. En outre, la modélisation globale par MOCAGE a montré que le bilan atmosphérique du chlore n'est pas seulement affecté par la transformation chimique, mais qu'il est également modifié par les processus physiques, y compris le transport et le dépôt.

Mots clés :

Chimie atmosphérique, simulations numériques, Chlore, Chimie quantique, Modèle chimie-transport

Acknowledgments

The completion of this thesis is a significant milestone in my academic journey, representing years of research, dedication, and motivation. However, no scholarly endeavour is accomplished in isolation. Throughout this journey, countless individuals provided me invaluable support, guidance, and inspiration that lead to the success of the thesis.

It all started in April, 2019 when I received a scholarship for my second year of Master studies, which allowed me to enrol in the International Master's degree program in "Atmospheric Environment" at the University of Lille. In that year, I had the opportunity to perform my MSc research internship in PC2A laboratory. The internship, being my first contact with research activities, allowed me to continue my studies with a PhD thesis, which is a collaboration between **PC2A laboratory** and **CNRM Météo-France**. This work would not have been possible without the funding I received from the **University of Lille** and **LabEx CaPPA**.

First and foremost, I would like to express my deepest gratitude and appreciation to my thesis supervisor, **Dr. Florent LOUIS** for his invaluable advice, continuous support, and patience during this thesis. His knowledge and experience have raised the quality of this work and given me the motivation to always go on. Thanks to **Dr. Valérie FEVRE-NOLLET**, who was my co-supervisor. Her supervision and support throughout this journey were invaluable. Her smile and positivity were always inspiring and pushing me forward. Special thanks go **Dr. Virginie MARECAL**. I really appreciate all the valuable time we spent together, as she was teaching me the methodology of the new model, how to carefully analyse, and present the results in a clear manner. I am extremely lucky to be working with my supervisors who were not only knowledgeable scientists, but humble leaders, motivational speakers, and great friends. They all wanted to have the best version of "Zainab" who is confident and free to express and share all her ideas and thoughts.

I would like to express my sincere gratitude to all PC2A laboratory member, starting with the director **Benjamin HANOUNE**, all technical and administrative staff, namely **Pascal DEMAUX** and **Louisguillaume LEBIKINGOLOT** who are always helping during emergency cases of computer troubles. Thanks to all the team member in PC2A specifically **Pr. Abderrahman EL BAKALI**, **Dr. Marc RIBAUCOUR**, **Dr. Patrick LEBÈGUE,** and of course **Sonia TAAMALLI**. Sonia, thank you so much, for always being by my side since my day-one at PC2A laboratory. I don't want even to think how would it be without you. Your continuous support and our invaluable discussions were indispensable throughout the journey.

I would also like to thank all the members at CNRM Méteo-France, for the excellent work environment they provided and their kind help and support that made the time I spent at their laboratory wonderful and fruitful. Special thanks to **Sophie PELLETIER**, **Jonathan GUTH**, **Jonathan AMERIC**, **Joaquim ARTETA**, and **Martin CUSSAC**. Thank you for teaching me how to use the model, helping me when I get horrible errors, and giving me the codes, you were developing.

Table of Contents

Table of Figures

Table of Tables

Table of Appendices

General introduction

The hypothesis that chlorine atoms can catalytically deplete stratospheric ozone was put forth more than two decades ago, and it has been the main source of inspiration for much of what we know about atmospheric chlorine-containing gases. The discovery of chlorofluorocarbons (CFCs) as one of the main carriers of chlorine into the stratosphere brought attention to emissions from consumer goods and industrial processes as drivers of global pollution. The reduction of stratospheric ozone caused by rising CFC concentrations may result in increased levels of biologically damaging ultraviolet light at the earth's surface. Aside from CFCs, there are other natural and anthropogenic chlorine-containing gases that can also add chlorine to the atmosphere.

Chlorine-containing gases can be classified according to their estimated reactivity into three groups: gases with atmospheric lifetimes of a few hours or days are reactive gases, gases with lifetimes less than 6 months are chlorinated very-short lived species, and gases with longer lifetimes like chlorofluorocarbons are chlorinated long-lived species. The reactivity of the "reactive gases" is considered to be more important at a short time scale (few days or hours), that they mostly affect the chemistry of the troposphere, and are not transported into the stratosphere. This is not true when talking about the chlorinated very-short lived species whose lifetimes allow their maintenance in the troposphere to be later injected into the stratosphere. Moreover, CFCs are known to be inert in the troposphere. In *Chapter I*, chlorine chemistry in both troposphere and stratosphere is further developed.

In the context of this thesis, the chemistry of atmospheric chlorine is investigated by various numerical tools including: quantum chemistry tools, 0D model, and global model.

From the **quantum chemistry** aspect, the presence of a chlorine atom on a carbon site lowers the energy of the C-H bond by about 17 kJ mol^{-1}, making the species more reactive and the hydrogen abstraction easier with lower activation energy. This leads to faster formation of the corresponding radicals. In this work, the reactivity between OH radicals, the most important oxidant in the troposphere, and chloromethyl hydroperoxide (CH$_2$ClOOH) is investigated. The importance of this reaction lies in the fact that CH$_2$ClOOH is a significant intermediate in the low-temperature combustion processes and in the atmospheric photochemical oxidation of chlorinated hydrocarbons. By quantum chemistry tools, the thermokinetic properties of this reaction are determined. Details about the quantum chemistry tools applied, computational methods, and the results are presented in *Chapter II*.

Thermokinetic properties obtained by quantum chemistry tools are essential in atmospheric models, as they are used as input parameters. Atmospheric models simulate the main atmospheric processes including solar radiation, meteorology, emissions, transport, chemical processing, and removal processes of gases and aerosols (Jacobson, 2005). They aim to better understand the air composition and its physical and chemical properties. In this work, two types of models are operated.

General introduction

Firstly, a kinetic zero-dimensional box model, named **ASTEC**, is employed. ASTEC, **A**ccident **S**ource **T**erm **E**valuation **C**ode, developed by both French Nuclear Safety Institute (IRSN), allows to figure out the speciation and reactivity of the so-called "reactive chlorine-containing gases" in the troposphere at a global scale. This is done through the implementation of 388 reactions of organic and inorganic chlorinated species into the model and running it at a very short time scale. Therefore, species with lifetimes shorter than the simulation period are reacting and making up the chlorine cycle by this model. ASTEC model is described, with the methodology followed and results achieved are given in ***Chapter III***.

After that, **MOCAGE**, **M**odel **O**f atmospheric **C**hemistry **A**t lar**GE** scale, is utilized. It is a three-dimensional chemistry-transport model developed by the National Centre of Meteorological Research (CNRM). MOCAGE models the chemical composition of the troposphere and stratosphere from global to regional scales. This type of models is usually run for long periods allowing the simulation of longer-lived species than those simulated by ASTEC. Chemistry-transport models can also take benefit of the simplified mechanisms built by 0D models. They are capable of simulating the behaviour of chlorinated short-lived species, and even long-lived ones. MOCAGE components are all described in ***Chapter IV*** with all processes and results.

Therefore, the complementarity between the three different aspects applied in this thesis can be summarized by ***Figure Intro-1***.
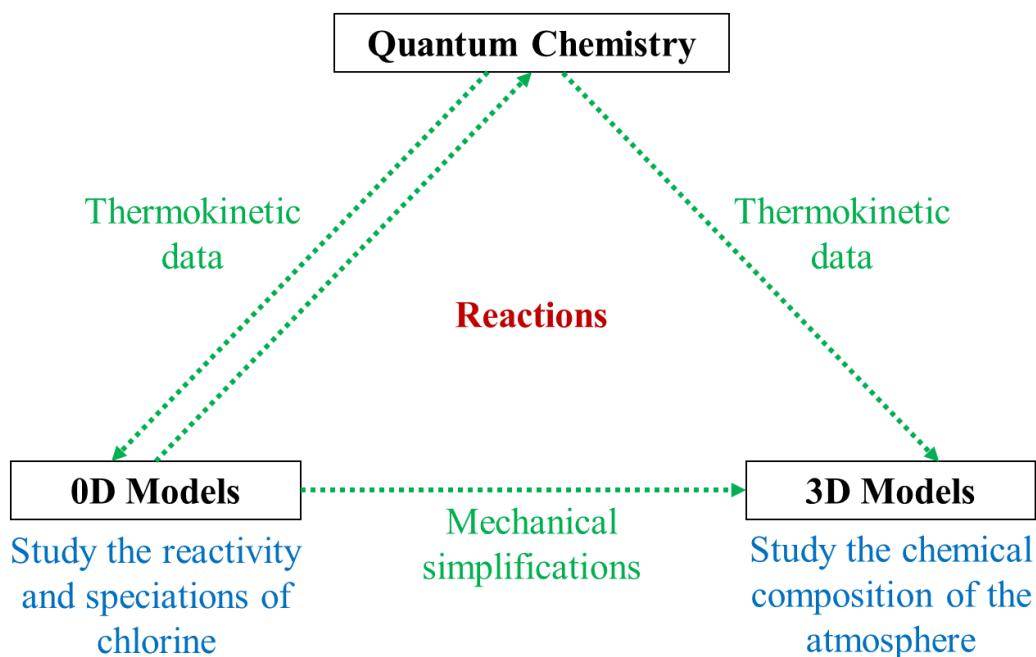
Figure Intro-1: *Diagram illustrating the complementarity between the three approaches used.*

General introduction

The studies performed during this PhD thesis were carried out as a collaboration between research groups from two laboratories:

- **PC2A:** Physico-Chimie des Processus de Combustion et de l'Atmosphère, Villeneuve d'Ascq, UMR 8522, Université de Lille & CNRS;
- **CNRM**: Centre National de Recherches Météorologiques , Toulouse, France, UMR 3589 Météo-France & CNRS.

The work is done under the supervision of Dr. Florent LOUIS (PC2A, ULille), Dr. Valérie FEVRE-NOLLET (PC2A, ULille), and Dr. Virginie MARECAL (CNRM, CNRS). This thesis is funded by the **University of Lille** (50%) and **LabEx CaPPA**, **Lab**oratoire d'**Ex**cellence - **C**hemical **a**nd **P**hysical **P**roperties of the **A**tmosphere, (50%).

This thesis is a part of group 3 at PC2A laboratory that is dedicated to the molecular simulations of the environmental processes. This team treats five different themes including:

- Theme 1: Iodine chemistry from the plant to the atmosphere,
- Theme 2: Thermodynamics of chemical interactions at high temperature of ATF (Accident Tolerant Fuel) type nuclear fuels,
- Theme 3: Study of the atmospheric reactivity of halogenated compounds, mercury and pesticides,
- Theme 4: Physicochemical modelling of pollutant adsorption,
- Theme 5: Theoretical study of the reaction mechanisms of PAHs (Polycyclic Aromatic Hydrocarbons).

The objectives of this thesis lie in the treatment of theme 3, where we attempt to model the chemistry of chlorine in the atmosphere.

Chapter I.   Atmospheric chlorine chemistry

I.1. Generalities

I.1.1.   The atmosphere

Gaze upwards, and you'll behold the wonders influenced by Earth's atmosphere. The clouds adorning the sky, the gentle wind swaying trees and flags, and even the warm touch of sunlight on your face are all outcomes of this remarkable phenomenon.

Extending from the planet's surface to a distance of up to 10,000 kilometres (km), Earth's atmosphere gradually merges into the vastness of space. Although there isn't a unanimous agreement among scientists regarding the precise upper boundary of the atmosphere, they concur that the majority of it resides in proximity to Earth's surface, within a range of approximately 8 to 15 km.

Despite oxygen being vital for most life on Earth, it constitutes only a fraction of our atmosphere. The composition of Earth's atmosphere predominantly consists of nitrogen, accounting for about 78%, followed by oxygen at 21%. Argon makes up 0.9%, while the remaining 0.1% comprises various other gases, including trace amounts of carbon dioxide, methane, and neon.

The atmosphere can be categorized into five distinct layers based on temperature (*Figure I-1*). The **troposphere**, closest to the surface, extends from around 7 to 15 km above the Earth. It exhibits its greatest thickness at the equator and thins out considerably towards the North and South Poles. This layer houses the majority of the atmosphere's mass, approximately 75% to 80%. It is also where most of the water vapor, dust, and ash particles reside, explaining the prevalence of clouds in this level. Temperatures in the troposphere decrease as altitude increases.

Above the troposphere lies the **stratosphere**, stretching from the tropopause (the upper boundary of the troposphere) to an altitude of approximately 50 km. Unlike the troposphere, temperatures in the stratosphere rise with increasing altitude. This layer harbours a notable concentration of ozone (O_3), a molecule composed of three oxygen atoms, forming the ozone layer. The ozone layer absorbs a portion of the incoming solar radiation, shielding life on Earth from potentially harmful ultraviolet (UV) light and contributing to the temperature elevation observed at higher altitudes.

The stratopause marks the upper limit of the stratosphere. Beyond it, the **mesosphere** prevails, spanning up to about 85 km above the Earth's surface. Temperatures in the mesosphere decline as altitude increases. In fact, the coldest temperatures in the entire atmosphere are found near the top of the mesosphere, plummeting to approximately -90°C. While the atmosphere is relatively thin here, it still possesses enough density for meteors to disintegrate upon entry, resulting in the phenomenon known as "shooting stars". The upper boundary of the mesosphere is referred to as the mesopause.

Chapter I. Atmospheric chlorine chemistry
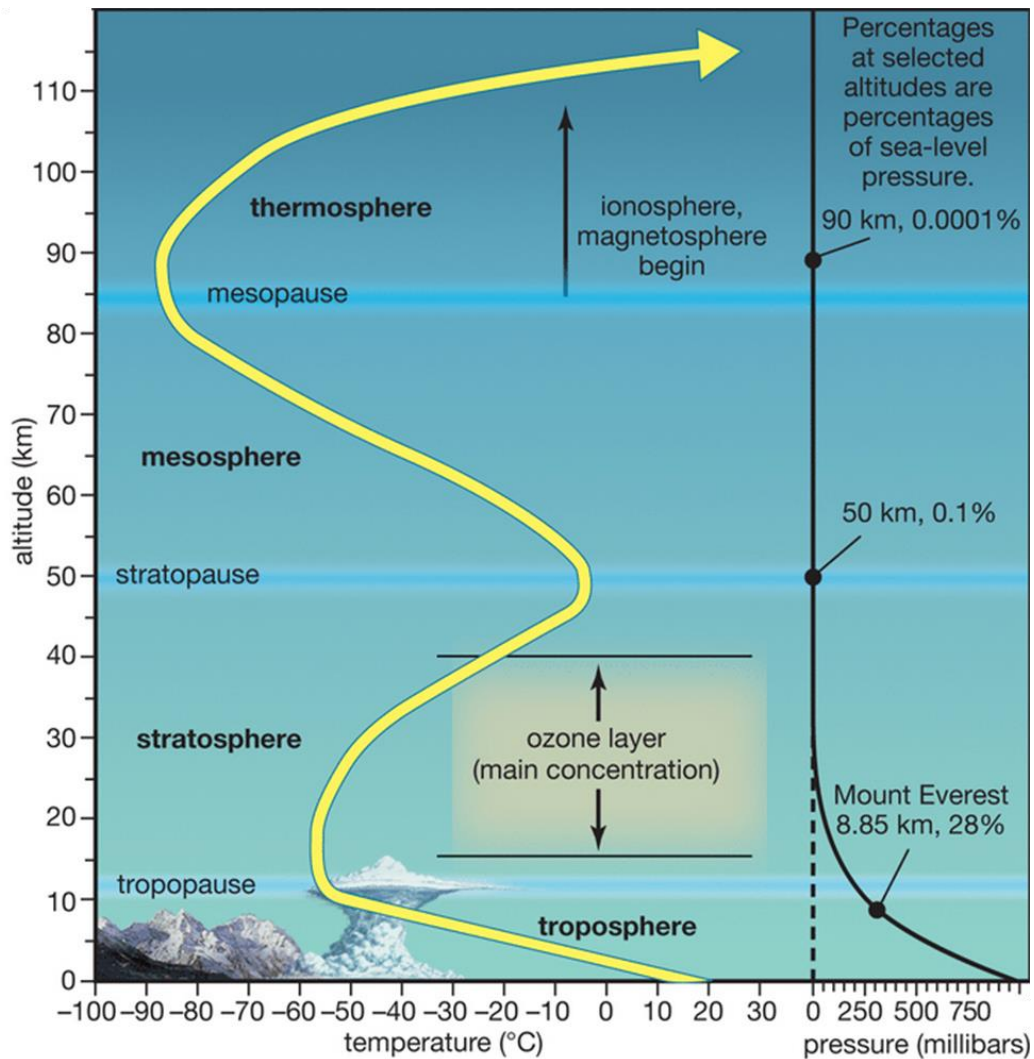
Figure I-1: *The physical vertical structure of the atmosphere as a function of altitude. (Fahad, 2021).*

Above the mesopause lies the **thermosphere**, extending to around 400 km. Despite limited knowledge about this region, it is understood that temperatures rise with increasing altitude. The upper reaches of the thermosphere experience intense heating from solar radiation, with temperatures soaring as high as 2000°C.

Finally, the outermost layer blending into what is traditionally considered outer space is the **exosphere**. At this height, the gravitational pull of Earth is so weak that gas molecules can escape into the expanse of space.

It is worth mentioning that the upper part of the mesosphere, together with the thermosphere and exosphere form the **ionosphere**. The regions of this layer are not considered separate, such as the more familiar troposphere and stratosphere. Instead, it is formed out of the ionized regions embedded with the mentioned atmospheric layers.

Chapter I. Atmospheric chlorine chemistry

I.1.2. Chlorine element

Chlorine, symbolized by Cl and atomic number 17, is the second-lightest member of the halogen group. It occupies a position on the periodic table between fluorine and bromine, displaying properties that lie between these two elements. Chlorine is the 19th most abundant element in the Earth's crust and the second most common element found in the ocean, making it the 23rd most prevalent element in nature.

There is a total of nine isotopes of chlorine, ranging from mass numbers 32 to 40. However, only three isotopes occur naturally. The stable isotopes ^{35}Cl and ^{37}Cl make up 75.77% and 24.23% of naturally occurring chlorine, respectively (IUPAC, 1991). Another isotope, ^{36}Cl, is radioactive and has a half-life of 3.0×10^5 years. The primary source of ^{36}Cl is its production in the atmosphere induced by cosmic radiation. The ratio of ^{36}Cl to stable chlorine ^{35}Cl in the environment is approximately 10^{-17} (Argento *et al.*, 2010).

Chlorine finds applications in various domains, most notably in water disinfection for sewage and industrial waste treatment, contributing significantly to sanitation procedures. It is also used as a bleaching agent in paper and cloth production and is a key ingredient in cleaning products such as household bleach. Additionally, chlorine is utilized in the manufacturing of chlorides, chlorinated solvents, pesticides, polymers, synthetic rubbers, and refrigerants.

Exposure to chlorine, primarily through inhalation, can have detrimental effects on human health. Symptoms typically appear shortly after exposure and may include airway irritation, wheezing, sore throat, coughing, as well as eye and skin irritation. The severity of these health effects depends on factors such as the route, dosage, and duration of chlorine exposure. High levels of chlorine inhalation can lead to pulmonary oedema, a condition characterized by fluid accumulation in the lungs, with the onset potentially delayed by several hours. Contact with compressed liquid chlorine can cause frostbite on the skin and eyes.

In the broader context, atmospheric chlorine holds significance in several areas. It plays a role in determining the acidity of precipitation, particularly in remote regions. It is considered an important intermediate in oxidation reactions within the marine troposphere and contributes to the atmospheric corrosion of metals and alloys. Furthermore, reactive chlorine serves as a source of stratospheric chlorine, which contributes to the destruction of O_3. Lastly, it is believed to be a factor in the uptake and damage of foliage (Graedel and Keene, 1995).

I.2. Tropospheric chlorine chemistry

Different forms of chlorine, both organic and inorganic, are released into the atmosphere. Understanding the chemistry of chlorine in the troposphere is crucial as it significantly impacts atmospheric composition and air quality.

Over time, the total amount of chlorine in the troposphere has been steadily decreasing since its highest levels recorded in 1993-1994 (*Figure I-2*) (Laube and Tegtmeier, 2022). The peak of annual average total chlorine from controlled and uncontrolled substances was approximately 3660 parts per trillion (ppt) in 1994. The rate of decline slowed down from 39 ppt per year between 1995 and 1996 to 3.6 ppt per year between 2012 and 2016. However, it

has recently accelerated again to an average of 15.1 ± 3.6 ppt per year between 2016 and 2020. This recent acceleration is primarily attributed to changes in substances not regulated by the Montreal Protocol, specifically CH_3Cl and Very Short-Lived Substances (VSLSs).
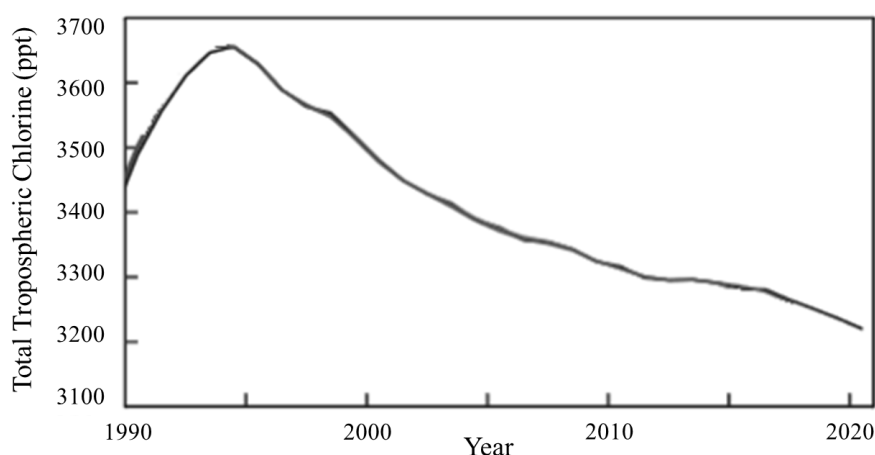
Figure I-2: *Near-surface total tropospheric chlorine from the combined global ground-based measurement networks (Laube and Tegtmeier, 2022).*

Previous studies on halogen chemistry in the troposphere mainly focused on bromine and iodine due to their higher reactivity (Wang, X. *et al.*, 2019). Atomic chlorine has a significant impact on air quality, and understanding the behaviour of chlorinated species in the troposphere is particularly important for climate considerations, as it reacts highly with volatile organic compounds (VOCs), especially the greenhouse gas CH_4 (Saiz-Lopez and von Glasow, 2012). Additionally, atomic chlorine reacts with various components of the troposphere, leading to the formation of diverse organic and inorganic chlorinated species. These species further degrade to form additional compounds such as molecular chlorine (Cl_2) and chlorine nitrite ($ClNO_2$) (Haskins *et al.*, 2019; Schmidt *et al.*, 2016; Sherwen *et al.*, 2016; Simpson *et al.*, 2015).

The significance of tropospheric chlorine lies in its oxidative capacity. For example, the oxidation rates of VOCs by atomic chlorine are 1 to 2 orders of magnitude higher than their reaction with hydroxyl (OH) radicals (Yi *et al.*, 2021). Moreover, atomic chlorine influences the production rates of peroxyalkyl (RO_2) compounds, thereby affecting the formation of O_3 in the troposphere (Li *et al.*, 2020). Furthermore, chlorinated species alter the distribution of odd hydrogen ($HO_x = HO_2 + OH$) and nitrogen oxides ($NO_x = NO_2 + NO$) (Badia *et al.*, 2019).

In summary, understanding tropospheric chlorine chemistry involves identifying the sources of chlorine compounds and highlighting their role in initiating reactions with VOCs, NO_x, and O_3.

Chapter I. Atmospheric chlorine chemistry

I.2.1. Sources of chlorine

The ocean serves as the primary natural source of atmospheric chlorine emissions, but studies have shown that human activities also contribute significantly to the release of chlorine (Tham *et al.*, 2016; Thornton *et al.*, 2010; Wang *et al.*, 2016). In 1990, the Global Emissions Inventory Activity (GEIA) developed the Reactive Chlorine Emission Inventory (RCEI), which estimated that the anthropogenic inorganic chloride emissions reached 12,900 gigagrams (Gg) (1 Gg = 10^9 g) (Keene *et al.*, 1999). These emissions were categorized as 49% from biomass burning (BB), 36% from coal combustion, and 16% from waste incineration. However, it's important to note that this inventory is based on data from 1990 and has not been updated since.

According to The Scientific Assessment of Ozone Depletion, the average annual chlorine mixing ratio in the troposphere was 3287 ppt in 2016, encompassing both organic and inorganic chlorinated species (Engel and Rigby, 2018). In this section, our goal is to compile and categorize all the sources of chlorinated organic and inorganic species.

Zhang *et al.* (2022) conducted a study on global emissions of HCl and of pCl, which is Cl from continental sources. ***Figure I-3*** presents the historical trends of HCl, pCl, and tCl (total Cl) emissions. The upper panels of the figure illustrate these trends for various source sectors, while the lower panels focus on different regions. It is important to note that the emissions from open biomass burning (BB) are not represented in the lower panel of the figure.

In the following, some of the main sources of chlorine in the atmosphere are elaborated and categorized into three classes: marine, terrestrial, and anthropogenic sources.
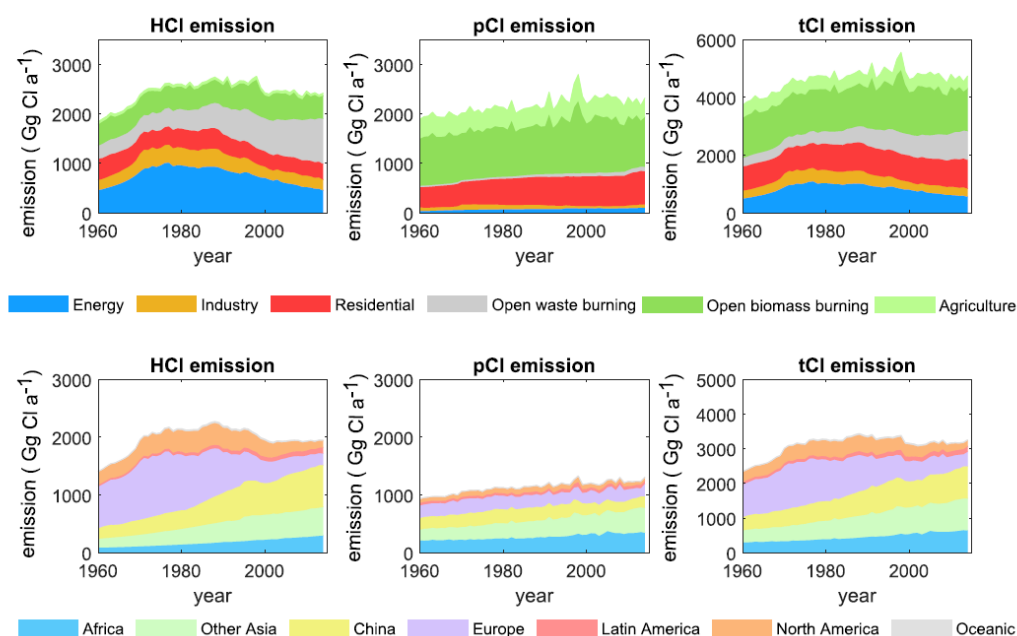
Figure I-3: *Trends of the evolution of annual HCl, pCl and total Cl (tCl) emissions by sectors (upper panel) and regions (lower panel) over years. The emission from open biomass burning are not included in the lower panel (Zhang et al., 2022).*

Chapter I. Atmospheric chlorine chemistry

I.2.1.1.   Marine sources

The generation of Sea-Salt Aerosol (SSA) by turbulence at the air-sea interface is the major source of atmospheric chlorine, which is emitted in the form of chloride ions (Cl^-) (Graedel and Keene, 1995). These ions are directly released into the troposphere through sea spray, influenced by factors such as wind speed and sea surface temperature. However, a large portion of this chloride is rapidly removed through deposition. Only a small fraction of these ions is transformed into the gas phase as hydrochloric acid (HCl), nitryl chloride ($ClNO_2$), and other species.

HCl formation can occur when SSA Cl^- is displaced by strong acids like H_2SO_4 and HNO_3, as described by the following reactions (Wang, X. *et al.*, 2019):

$$Cl^- + HNO_3 \rightleftharpoons HCl + NO_3^- \qquad\qquad\qquad\qquad\qquad \textit{\textbf{R1}}$$
$$Cl^- + H_2SO_4 \rightleftharpoons HCl + HSO_4^- \qquad\qquad\qquad\qquad\qquad \textit{\textbf{R2}}$$

The mixing ratios of HCl in marine surface air tend to be high in polluted coastal areas, where significant sources of HNO_3 and H_2SO_4 from anthropogenic NO_x and SO_2 emissions drive the displacement of acid from SSA (Wang, X. *et al*., 2019).

In coastal regions with high levels of pollution from NO_x, Cl^- ions react with gaseous dinitrogen pentoxide (N_2O_5) through a heterogeneous uptake process. This night-time reaction leads to the formation of $ClNO_2$ as described by the reaction (***R3***). Sherwen *et al*. (2016) and Wang X. *et al*. (2019) used the GEOS-Chem model to calculate that this process accounted for the emission of 650 Gg (Cl) yr^{-1} in 2005 and 1810 Gg (Cl) yr^{-1} in 2016, respectively.

$$N_2O_5 \text{ (g)} + Cl^- \text{ (aq)} \rightarrow ClNO_2 \text{ (g)} + NO_3^- \text{ (aq)} \qquad\qquad\qquad \textit{\textbf{R3}}$$
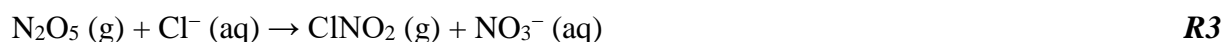
Moreover, ocean is considered as a primary of source of certain organic chlorinated species. For instance, 360 Gg of $CHCl_3$ are estimated to be released by the ocean per year (McCulloch, 2003). In addition, the sea-to-air fluxes of C_2HCl_3 and C_2Cl_4 are estimated to be 280.3 and 221.7 nmol m^{-2} day^{-1}, respectively.

I.2.1.2.   Terrestrial sources

Terrestrial sources can also contribute to the presence of chlorinated species in the environment. Some examples of terrestrial sources of chlorinated species include:
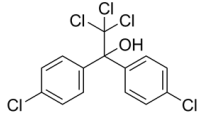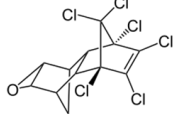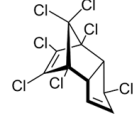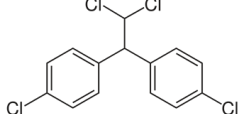
- Agricultural processes:

In their study, Redeker *et al.* (2003) demonstrated that certain chlorofluorocarbons (CFCs) and halons can be emitted from rice paddies. Specifically, they identified the release of CFC-11 (CCl_3F), CFC-12 (CCl_2F_2), CFC-113 ($C_2Cl_3F_3$), CFC114 ($C_2Cl_2F_4$), Halon-1211 ($CBrClF_2$), and Halon-2402 ($C_2Br_2F_4$) from these agricultural areas. Additionally, chlorocarbons such as CH_3Cl, CH_2Cl_2, $CHCl_3$, CCl_4, C_2Cl_4, C_2H_5Cl, CH_3CCl_3 were found to be emitted alongside CFCs and halons. Among these emissions, CH_3Cl was identified as the most significant, with median emissions of 1.2 µg m^{-2} h^{-1}.

Chapter I. Atmospheric chlorine chemistry

Furthermore, organic chlorinated compounds are widely utilized as pesticides (Jayaraj *et al.*, 2016). These compounds release chlorine-containing substances, such as HOCl and HCl, into the atmosphere. They can also generate reactive organic chlorinated radicals, which can further degrade in the environment. This degradation process has the potential to give rise to toxic substances that pose risks to both human health and the environment. ***Table I-1*** provides a range of these species, indicating their varying persistence in the environment, ranging from a few days to up to ten years.

Table I-1: *Some organochlorine pesticides, their lifetimes, their chemical formula and structure (Jayaraj et al., 2016).*

Species	Dicofol	Dieldrin	Heptachlor	Dichloro diphenyl dichloroethane (DDE)
Lifetime	60 days	9 months	2 years	10 years
Formula and Structure	$C_{14}H_9Cl_5O$	$C_{12}H_8Cl_6O$	$C_{10}H_5Cl_7$	$C_{14}H_{10}Cl_4$

- Volcanic activity:

Volcanic emissions play a significant role in introducing halogens into the atmosphere. When volcanoes erupt, one of the primary halogens released is chlorine, predominantly in the form of HCl. A notable example is the eruption of Mount Samalas in 1257, where Vidal *et al.* (2016) estimated an emission of a total of 227 Tg of HCl.

During volcanic eruptions, HCl can be directly injected into the stratosphere. Upon entering this layer of the atmosphere, rapid chemical reactions occur, transforming the initially emitted HCl into highly reactive chlorinated species such as chlorine monoxide (ClO) and chlorine dioxide (OClO). This conversion is a result of various reactions involving sunlight and other atmospheric constituents. These reactive compounds have significant implications for atmospheric chemistry and the overall composition of the stratosphere. They play a crucial role in stratospheric ozone depletion.

It is worth mentioning that the source of volcanic emissions is not only the volcanic eruptions in the troposphere and the stratosphere that are sporadic, but most importantly, the continuous passive degassing from the volcanoes (von Glasow *et al*., 2009). In addition, the chemical composition of volcanic emissions can vary according to the type of magma from one volcano to another and according to volcanic activity. For instance, ***Table I-2*** shows the chemical composition of the gaseous emissions of volcanoes based on Gerlach (2004) and Textor *et al.* (2004). HCl is the main halogenated species released by volcanoes (0.84%).

Chapter I. Atmospheric chlorine chemistry

Table I-2: The distribution (in %) of the chemical species emitted by volcanoes according to Gerlach (2004) and Textor et al. (2004).

					Trace gases		Halogens		
Chemical species	H_2O	CO_2	SO_2	H_2S	H_2	CO	HCl	HF	HBr
Percentage (%)	50-90	1-40	1-25	1-10	0.5	0.03	0.84	0.061	0.0025

- Biomass burning:

BB serves as a significant source of various trace constituents in the atmosphere, making it an important factor in atmospheric chemistry. When biomass is burned, emissions of several compounds occur, including CH_3Cl, CH_2Cl_2, $CHCl_3$, and CH_3CCl_3, as identified by Lobert *et al.* (1999).

Among these compounds, CH_3Cl stands out as the most substantial natural contributor to organic chlorine in the atmosphere. To better understand the levels of CH_3Cl in different locations and time periods, ***Table I-3*** provides the mixing ratios for this compound.

In addition to organic chlorine, inorganic chlorine compounds such as hydrogen chloride (HCl) and particulate chloride (pCl) have been recognized as the dominant forms of chlorine emitted from BB. However, the distribution and behaviour of HCl and pCl in the air are influenced by several factors, including temperature, aerosol surface area, and liquid water content, as elucidated by Lobert *et al.* (1999).

Recent estimates by Yang *et al.* (2022) suggest that BB emissions of HCl and pCl amount to approximately 30 Gg and 120 Gg (Cl) yr^{-1}, respectively. These figures underscore the significant contribution of BB to the release of chlorine-containing compounds into the atmosphere.

I.2.1.3. Anthropogenic sources

Organic chlorinated species primarily originate from human activities, known as anthropogenic sources. Anthropogenic activities, including industrial processes, emissions from chlorine-containing solvents, and the use of chlorinated disinfectants, also release significant amounts of chlorine compounds into the troposphere. Dichloromethane (CH_2Cl_2) is an example of such a compound, and it is released into the environment through the use of foam plastic products, metal cleaning processes, and as a solvent (Simmonds *et al.*, 2006). According to the findings of Bednarz *et al.* (2022), an estimated emission flux of 1 Tg yr^{-1} of CH_2Cl_2 occurred in 2017, based on atmospheric observations and inversion analysis.

Trichloromethane ($CHCl_3$), commonly known as chloroform, is primarily used in industrial applications as a feedstock for the production of HCFC-22, which itself has various uses both as an emissive and non-emissive compound (Bednarz *et al.*, 2022). In 2015, it was estimated that the emission flux of $CHCl_3$ reached 324 Gg yr^{-1}, with China identified as the dominant source location.

Another organic chlorinated compound is C_2Cl_4, which is produced through dry cleaning applications. Claxton *et al.* (2020) reported emission fluxes ranging between 83 and 103 Gg yr^{-1} for C_2Cl_4 in 2016.

Furthermore, trichloroethene (C_2HCl_3) is predominantly used as a degreasing solvent (Simmonds *et al.*, 2006). From 1988 to 1996, its emissions remained relatively constant at approximately 240 Gg yr^{-1}.

It's worth noting that these organic chlorinated species, originating from anthropogenic sources, require careful monitoring and management due to their potential environmental and health impacts. Understanding their emission sources and fluxes is essential for developing effective strategies to minimize their release and mitigate their effects on ecosystems and human well-being.

I.2.2.   Measurements of the concentrations of chlorinated species

Methyl chloride (CH_3Cl) is the most abundant halogenated hydrocarbon in the atmosphere (Yokouchi *et al.*, 2000). It has received much attention as being a natural source of atomic Cl in the stratosphere. Oceanic emissions are thought to be the main source of CH_3Cl, and BB is the second largest source. Different campaigns were made to measure the concentrations of CH_3Cl in the free troposphere at different locations (***Table I-3***).

Moreover, quantification of chlorinated inorganic species in the atmosphere is the interest of different studies. Some of these studies and their results are depicted in ***Table I-4***.

In ***Table I-4***, all measurements of HCl are compiled by Crisp *et al*. (2014). For $ClNO_2$, values are compiled by Wang, X. *et al*. (2019). Cl_2 measurements are taken from Hall *et al.* (2020). In addition, for some chlorinated organic species, measurements are collected in ***Table I-5***.

Table I-3: *Measurements of the mixing ratios of CH$_3$Cl in the atmosphere.*

Location	GPS coordinates	Measurement dates	Concentration (ppt)			Reference
			Min	Max	Average	
Polar NH	-	1981 - 1996	-	-	580	(Khalil and Rasmussen, 1981)
Middle NH	-	1981 - 1996	-	-	597	(Khalil and Rasmussen, 1981)
Tropical NH	-	1981 - 1996	-	-	615	(Khalil and Rasmussen, 1981)
Polar SH	-	1981 - 1996	-	-	620	(Khalil and Rasmussen, 1981)
Middle SH	-	1981 - 1996	-	-	598	(Khalil and Rasmussen, 1981)
Tropical SH	-	1981 - 1996	-	-	573	(Khalil and Rasmussen, 1981)
Indian Ocean	9° 59' S - 69° 59' E	Feb - Mar 1999	-	-	542	(Scheeren *et al.*, 2002)
Arabian Sea	12° 26' N - 63° 0' E	Feb - Mar 1999	-	-	666	(Scheeren *et al.*, 2002)
Bay of Bengal	15° 39' N - 87° 38' E	Feb - Mar 1999	-	-	757	(Scheeren *et al.*, 2002)
Mace Head, Ireland	53° 19' N - 9° 54' E	Feb 1998	-	-	576	(Simmonds *et al.*, 2004)
Mace Head, Ireland	53° 19' N - 9° 54' E	Jun 2001	-	-	522	(Simmonds *et al.*, 2004)
Cape Grim, Tasmania	40° 38' S - 144° 43' E	Feb 1998	-	-	529	(Simmonds *et al.*, 2004)
Cape Grim, Tasmania	40° 38' S - 144° 43' E	Jun 2001	-	-	551	(Simmonds *et al.*, 2004)
Mt. Cimone	45° 58' N - 11° 3' E	Jun - Aug 2017	-	-	557	(Cristofanelli *et al.*, 2020)

Chapter I. Atmospheric chlorine chemistry

Table I-4: Measurements of the mixing ratios of inorganic chlorinated species (HCl, ClO, OClO, atomic Cl, ClNO$_2$, HOCl, and Cl$_2$) in the atmosphere.

Location	GPS coordinates	Measurement dates	Concentration (ppt) Min	Max	Average	References
HCl						
Manhattan, NY	40° 47' N - 73° 57' W	Jul - Aug 1976	1000	9000	4000	(Rahn *et al.*, 1979)
Reims, France	49° 15' N - 4° 1' E	Dec 1978 - Jun 1979	1	100	-	(Marché *et al.*, 1980)
Columbus, Ohio	39° 57' N - 83° 0' W	Sep 1980 - Oct 1980	30	1000	350	(Spicer, 1986)
Bermuda	32° 18' N - 64° 45' W	Jul - Sep 1988	200	400	-	(Keene *et al.*, 1990)
U.S. East Coast	1° 18' N - 103° 55' E	Jul - Sep 1988	500	1200	-	(Keene *et al.*, 1990)
Sweden	59° 40' N - 14° 31' E	Jan 1990	200	1000	-	(Lindgren, 1992)
Sweden	59° 40' N - 14° 31' E	Jul 1990	100	600	-	(Lindgren, 1992)
Sweden	59° 40' N - 14° 31' E	Sep 1990	20	300	-	(Lindgren, 1992)
Virginia Key, Florida, USA	25° 44' N - 80° 8' W	Jan 1992	-	268	-	(Pszenny *et al.*, 1993)
Tudor Hill, Bermuda	32° 15' N - 64° 52' W	Apr - May 1996	100	900	-	(Keene and Savoie, 1998)
Nara, Japan	34° 17' N - 135° 52' E	Jun 1994 - May 1995	800	1500	1100	(Matsumoto and Okita, 1998)
Dumont d' Urville, Antarctica	55° 26' S - 68° 59' W	Dec 2000 - Dec 2001	30	300	-	(Jourdain and Legrand, 2002)
Manhattan, NY	40° 47' N - 73° 57' W	Jul 1999 - Jun 2000	10	2000	300	(Bari *et al.*, 2003)
Bronx, NY	40° 50' N - 73° 52' W	Jul 1999 - Jun 2000	10	1800	300	(Bari *et al.*, 2003)
Sao Vicente Island, Cape Verde	16° 0' S - 24° 0' W	May - Jun 2007	50	600	-	(Lawler *et al.*, 2009)
Cape Verde	16° 0' N - 24° 0' W	June 2009	1	35	-	(Lawler *et al.*, 2011)
Erie, CO	40° 0' N - 105° 6' W	Feb - Mar 2011	23	1250	-	(Young *et al.*, 2013)
Sacramento Delta, CA	38° 29' N - 121° 33' W	May - Jun 2010	0	1900	270	(Crisp *et al.*, 2014)
Central California Coast	32° 42' N - 117° 9' W	May - Jun 2010	0	2800	440	(Crisp *et al.*, 2014)
Southern California Coast	32° 34' N - 117° 3' W	May - Jun 2010	0	16000	2200	(Crisp *et al.*, 2014)
ClO						
Great Salt Lake, UT	41° 10' N - 112° 36' W	Oct 2000	4	15	-	(Stutz *et al.*, 2002)
OClO						
Arctic (Amundsen Gulf)	70° 30' N - 122° 30' W	Spring 2008	-	24	-	(Pöhler *et al.*, 2010)
Atomic Cl						
Alert, Northwest Territories	82° 30' N - 62° 17' E	Apr 2 - Apr 15, 1992	-	0.003	-	(Jobson *et al.*, 1994)
Alert, Nunavut, Canada	82° 29' N - 62° 21' W	Apr 14 - May 10, 1998	-	0.003	-	(Boudries and Bottenheim, 2000)

Table I-4: *Continued.*

Location	GPS coordinates	Measurement dates	Concentration (ppt)			References
			Min	Max	Average	
ClNO$_2$						
Houston, TX, USA	29° 45' N - 95° 22' W	Aug - Sep 2008	-	-	1200	(Osthoff *et al.*, 2008)
Boulder, CO, USA	40° 0' N - 105° 16' W	Feb 2009	-	-	450	(Thornton *et al.*, 2010)
Calgary, AB, Canada	51° 2' N - 114° 3' W	Spring 2010	5	250	-	(Mielke *et al.*, 2011)
Calgary, Alberta, Canada	51° 2' N - 114° 3' W	Apr 2010	-	-	250	(Mielke *et al.*, 2011)
Los Angeles, CA, USA (marine)	33° 42' N - 118° 17' W	May - Jun 2010	-	-	2100	(Riedel *et al.*, 2012)
Kleiner Feldberg, Germany	50° 13' N - 8° 26' W	Summer 2011	3	800	-	(Phillips *et al.*, 2012)
Boulder, CO, USA	40° 0' N - 105° 16' W	Feb - Mar 2011	-	-	1300	(Riedel *et al.*, 2014)
Pasadena, CA, USA (in land)	34° 8' N - 118° 8' W	May - Jun 2010	-	-	3600	(Mielke *et al.*, 2013)
Calgary, AB, Canada	51° 2' N - 114° 3' W	Spring 2011	5	338	-	(Mielke *et al.*, 2016)
Hong Kong, China	22° 16' N - 114° 9' E	Nov - Dec 2013	-	-	4700	(Wang *et al.*, 2016)
Olympic Park, South Korea	37° 31' N - 127° 7' E	May - Jun 2016	-	-	780	(Jeong *et al.*, 2019)
University of Manchester, UK	53° 28' N - 2° 13' W	Oct 30 - Nov 11, 2014	-	506	58	(Priestley *et al.*, 2018)
HOCl						
Cape Verde	16° 0' N - 24° 0' W	June 2009	5	173	-	(Lawler *et al.*, 2011)
University of Manchester, UK	53° 28' N - 2° 13' W	Oct 30 - Nov 11, 2014	-	9	2	(Priestley *et al.*, 2018)
Cl$_2$						
Eastern Long Island, NY	40° 45' N - 73° 55' W	Jun 1996	15	150	-	(Spicer, 1986)
Irvine, CA	33° 41' N - 117° 49' W	Fall 2005	3	20	-	(Finley and Saltzman, 2006)
La Jolla, CA	32° 48' N - 117° 16' W	Jan 2006	1	26	-	(Finley and Saltzman, 2008)
Cape Verde	16° 0' N - 24° 0' W	Jun 2009	1	35	-	(Lawler *et al.*, 2011)
Barrow, AK	71° 32' N - 156° 28' W	Spring 2009	1	400	-	(Liao *et al.*, 2014)
Northern America	-	-	20	250	-	(Faxon *et al.*, 2015)
Arctic MBL in Barrow, Alaska	-	-	-	400	-	(Faxon *et al.*, 2015)
University of Manchester, UK	53° 28' N - 2° 13' W	Oct 30 - Nov 11, 2014 (day)	0	17	2	(Priestley *et al.*, 2018)
University of Manchester, UK	53° 28' N - 2° 13' W	Oct 30 - Nov 11, 2014 (night)	0	5	0	(Priestley *et al.*, 2018)

Chapter I. Atmospheric chlorine chemistry

Table I-5: *Measurements of the mixing ratios of organic chlorinated species (CH_2Cl_2, $CHCl_3$, CH_3CCl_3, and C_2Cl_4) in the atmosphere.*

Location	GPS coordinates	Measurement dates	Concentration (ppt)		Reference
			LOD	Average	
CH_2Cl_2					
Indian Ocean	9° 59' S – 69° 59' E	Feb – Mar 1999	-	8	(Scheeren *et al.*, 2002)
Arabian Sea	12° 26' N – 63° 0' E	Feb – Mar 1999	-	22	(Scheeren *et al.*, 2002)
Bay of Bengal	15° 39' N – 87° 38' E	Feb – Mar 1999	-	26	(Scheeren *et al.*, 2002)
Cape Grim, Tansamia	40° 38' S – 144° 43' E	1998-2000	-	9	(Cox *et al.*, 2003)
Alert, Canada	82° 29' N – 62° 21' W	1989 – 1996	-	47	(Gautrois *et al.*, 2003)
Mace Head, Ireland	53° 17' N – 9° 54' W	1998-2004	-	301	(Simmonds *et al.*, 2006)
Cape Grim, Tansamia	40° 38' S – 144° 43' E	1998-2004	-	9	(Simmonds *et al.*, 2006)
Canada and Greenland	-	2008	-	36	(Simpson *et al.*, 2011)
Europe	-	1998 – 2002	-	25	(Leedham Elvidge *et al.*, 2015)
Africa	-	2000	-	22	(Leedham Elvidge *et al.*, 2015)
India	-	1998 – 2000	-	22	(Leedham Elvidge *et al.*, 2015)
North and Central Atlantic	-	2009 – 2011	-	32	(Leedham Elvidge *et al.*, 2015)
$CHCl_3$					
Pacific Ocean	15° 30' N – 148° 11' E	15 Feb 1990	0.35	15	(Atlas *et al.*, 1993)
Pacific Ocean	10° 25' S – 165° 35' E	10 Mar 1990	0.35	6	(Atlas *et al.*, 1993)
Indian Ocean	9° 59' S – 69° 59' E	Feb – Mar 1999	-	3	(Scheeren *et al.*, 2002)
Arabian Sea	12° 26' N – 63° 0' E	Feb – Mar 1999	-	7	(Scheeren *et al.*, 2002)
Bay of Bengal	15° 39' N – 87° 38' E	Feb – Mar 1999	-	8	(Scheeren *et al.*, 2002)
CH_3CCl_3					
Indian Ocean	9° 59' S – 69° 59' E	Feb – Mar 1999	-	66	(Scheeren *et al.*, 2002)
Arabian Sea	12° 26' N – 63° 0' E	Feb – Mar 1999	-	67	(Scheeren *et al.*, 2002)
Bay of Bengal	15° 39' N – 87° 38' E	Feb – Mar 1999	-	65	(Scheeren *et al.*, 2002)
CH_3CCl_3					
Bay of Bengal	15° 39' N – 87° 38' E	Feb – Mar 1999	-	3	(Scheeren *et al.*, 2002)
Mexico City	22° 30' N – 100° 0' W	Spring 2006	-	4	(Barletta *et al.*, 2009)
Mace Head	53° 17' N – 9° 54' W	1998-2004	-	5	(Simmonds *et al.*, 2006)
Cape Grim, Tansamia	40° 38' S – 144° 43' E	1998-2004	-	81	(Simmonds *et al.*, 2006)

Chapter I. Atmospheric chlorine chemistry

I.2.3. Reactivity of HCl

HCl, among the inorganic chlorinated compounds emitted into the atmosphere, plays a crucial role as the main reservoir of chlorine in the troposphere. Therefore, understanding the reactivity of HCl in the troposphere is of great importance. HCl in the gas phase is directly released into the atmosphere through various processes, including the combustion of chloride-containing fuels (such as waste incineration, BB, and coal combustion), volcanic emissions, water treatment, and manufacturing processes (Keene *et al.*, 1999; Khalil *et al.*, 1999; McCulloch *et al.*, 1999), in addition to the acid displacement by SSA as mentioned in *section I.2.1.1*, which is the main source of atmospheric HCl.

Once HCl is released into the atmosphere, it can react with OH radicals to form atomic Cl through the reaction (***R4***).

$$HCl + OH \rightarrow Cl + H_2O \qquad\qquad\qquad\qquad\qquad\qquad\qquad \textbf{\textit{R4}}$$

The atmospheric lifetime of HCl resulting from this reaction is approximately 35.6 hours when the tropospheric OH concentration is 1×10^7 radicals cm^{-3}. Consequently, HCl serves as a significant source of daytime recycling of atomic chlorine (Fan *et al.*, 2021). According to Wang, X. *et al.* (2019), this pathway leads to an annual production of 9720 Gg of atomic chlorine.

I.2.4. Tropospheric fate of inorganic chlorinated species

According to Sherwen *et al.* (2016), approximately 70% of inorganic chlorine released into the troposphere is deposited over the oceans. This deposition is more significant in regions with high precipitation such as the Intertropical Convergence Zone, Maritime continents, and the Indian Ocean, while it is less significant in polar regions where precipitation and emissions are lower. The deposited inorganic chlorine exists in the form of HCl, HOCl, and ClONO$_2$, where 94, 5.1, and 1.1% of the total tropospheric release of these species are being deposited, respectively.

For these species, the Henry's law constants are given in *Table I-6*. Henry's law constants are given by the following expression:

$$H^{cp} = \frac{H^{cc}}{RT}$$

$$\Leftrightarrow \ln H^{cp} = \ln H^{cc} + \ln\left(1/R\right) + \ln\left(1/T\right)$$

$$\Rightarrow \frac{d\ln H^{cp}}{d(1/T)} = \frac{d\ln H^{cc}}{d(1/T)} + \frac{d\ln(1/T)}{d(1/T)} = \frac{d\ln H^{cc}}{d(1/T)} + 1 \qquad\qquad \textbf{\textit{Eq. I-1}}$$

In the above equation (***Eq. I-1***), H^{cp} (mol L^{-1} atm^{-1}) represents the solubility defined via concentration, which depends on the concentration of a species in the aqueous phase and the partial pressure of that species in the gas phase under equilibrium conditions. H^{cc} is the dimensionless ratio between the aqueous-phase concentration of a species and its gas-phase concentration. R and T are the ideal gas constant and temperature, respectively (Sander, 2015).

Chapter I. Atmospheric chlorine chemistry

Table I-6: *Henry's law constants H^{cp} and H^{cc} of HCl, HOCl, and ClONO2.*

Species	Henry's law constant (H^{cp}) at 298 K (mol L^{-1} atm^{-1})	d(ln H^{cc})/ d(1/T) (K)	Reference
HCl	7.1×10^{15}	5.9×10^3	(Sander, 2015)
HOCl	6.5×10^3	5.9×10^3	(Sander, 2015)
ClONO2	∞	-	(Sander, 2015)

In ***Table I-6***, the effective Henry's law is given for HCl which considers the rapid dissociation of HCl in water. It depends on the pH of the medium, where it is assumed 4.5 for a typical cloud droplet (Sherwen *et al*., 2016). Moreover, when Henry's law constant for ClONO2 is considered equal to infinity, it means that this species is very soluble in the droplet.

On the other hand, the photolysis of inorganic chlorinated species plays a significant role in their loss and the production of atomic chlorine. After sunrise, species such as Cl_2, $ClNO_2$, HOCl, and ClONO2 undergo rapid photolysis, and their lifetimes can be found in ***Table I-9***. Atomic chlorine then reacts with tropospheric O_3 through a highly reactive reaction (***R5***) to form chlorine monoxide (ClO), which leads to the destruction of O_3 in the troposphere and stratosphere.

$$Cl + O_3 \rightarrow ClO + O_2 \qquad\qquad\qquad \textbf{\textit{R5}}$$

Burkholder *et al*. (2020) proposed a rate constant of 1.2×10^{-11} cm^3 molecule^{-1} s^{-1} for reaction ***R5***. ClO can subsequently react with the hydroperoxyl radical HO_2 (***R6***) to form the stable intermediate hypochlorous acid (HOCl), which can be directly photolyzed (***R7***) to regenerate atomic chlorine and initiate the cycle starting with reaction ***R5***. The formation and loss of ClO (***R5*** and ***R6***) and HOCl (***R6*** and ***R7***) can be summarized by reaction ***R8***, which represents the overall reaction involving the destruction of tropospheric O_3 through its reaction with HO_2 (Sherwen *et al*., 2016).

$$ClO + HO_2 \rightarrow HOCl + O_2 \qquad\qquad\qquad \textbf{\textit{R6}}$$
$$HOCl + h\nu \rightarrow Cl + OH \qquad\qquad\qquad \textbf{\textit{R7}}$$
$$\textbf{Net:}\ O_3 + HO_2 \rightarrow OH + 2O_2 \qquad\qquad\qquad \textbf{\textit{R8}}$$

Additionally, HOCl and ClONO2 can react with acidic Cl-containing aerosol particles to form Cl_2, which can partition into the gas phase. These reactions, denoted as ***R9*** and ***R10***, respectively, can occur during both day and night, ensuring the formation of Cl_2 during the night that is subsequently photolyzed during the day (Riedel *et al*., 2012).

$$HOCl + Cl\ (aq) + H^+\ (aq) \rightarrow Cl_2 + H_2O \qquad\qquad\qquad \textbf{\textit{R9}}$$
$$ClONO_2 + Cl\ (aq) + H^+\ (aq) \rightarrow Cl_2 + HNO_3 \qquad\qquad\qquad \textbf{\textit{R10}}$$

Furthermore, $ClNO_2$ undergoes a similar reaction on acidic Cl-containing particles (like SSA), resulting in the formation of Cl_2 and nitrous acid (HONO) (Roberts *et al*., 2008).

$$ClNO_2 + Cl\ (aq) + H^+\ (aq) \rightarrow Cl_2 + HONO \qquad\qquad\qquad \textbf{\textit{R11}}$$
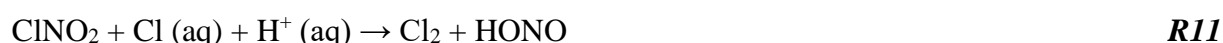
Chapter I. Atmospheric chlorine chemistry

I.2.5.   Reactivity of chlorinated very-short lived species

Halogenated Very-Short Lived Substances (VSLS) are a group of gases that exhibit tropospheric lifetimes of approximately 6 months or less when present near the Earth's surface (Engel and Rigby, 2018). These relatively short lifetimes make them comparable to, or even shorter than, the timescales associated with tropospheric transport. As a result, the distribution of these substances in the troposphere is characterized by significant spatial variations.

Among the primary chlorine-containing VSLS released into the atmosphere are methylene chloride (CH_2Cl_2), chloroform ($CHCl_3$), 1,2-dichloroethane (CH_2ClCH_2Cl), trichloroethylene (C_2HCl_3), and tetrachloroethylene (C_2Cl_4). ***Table I-7*** provides information on the annual mean lifetimes of some of these chlorine-containing VSLS, specifically their susceptibility to oxidation by OH radicals in both the Boundary Layer (BL) and Upper Troposphere (UT).

Table I-7: *Annual mean local lifetime of Cl-VSLS (days) with respect to OH oxidation in the Boundary Layer and the Upper Troposphere (Hossaini et al., 2019).*

Species	BL	UT
CH_2Cl_2	102	245
$CHCl_3$	102	252
C_2Cl_4	61	158
CH_2ClCH_2Cl	43	127

The emission of VSLS into the atmosphere can occur through natural sources, such as oceanic emissions, as well as through human activities, including industrial processes. Detailed information about the sources of VSLS can be found in ***section I.2.1***, where various natural and anthropogenic emission pathways are discussed.

Once released into the troposphere, VSLS undergo a range of processes that contribute to their transformation and redistribution. These processes include oxidation by OH radicals, photolysis, washout (removal by precipitation), and convection. Through these mechanisms, the original Source Gases (SG) can undergo chemical reactions and physical transformations, leading to the formation of different Product Gases (PG). Notably, when SG and PG enter the stratosphere, they release their halogen content, which can then participate in the cycle of O_3 destruction. This phenomenon has been studied extensively, and the involvement of VSLS in O_3 depletion has been well-documented (Engel and Rigby, 2018). A summary of these processes is depicted in ***Figure I-4***.

Chapter I. Atmospheric chlorine chemistry
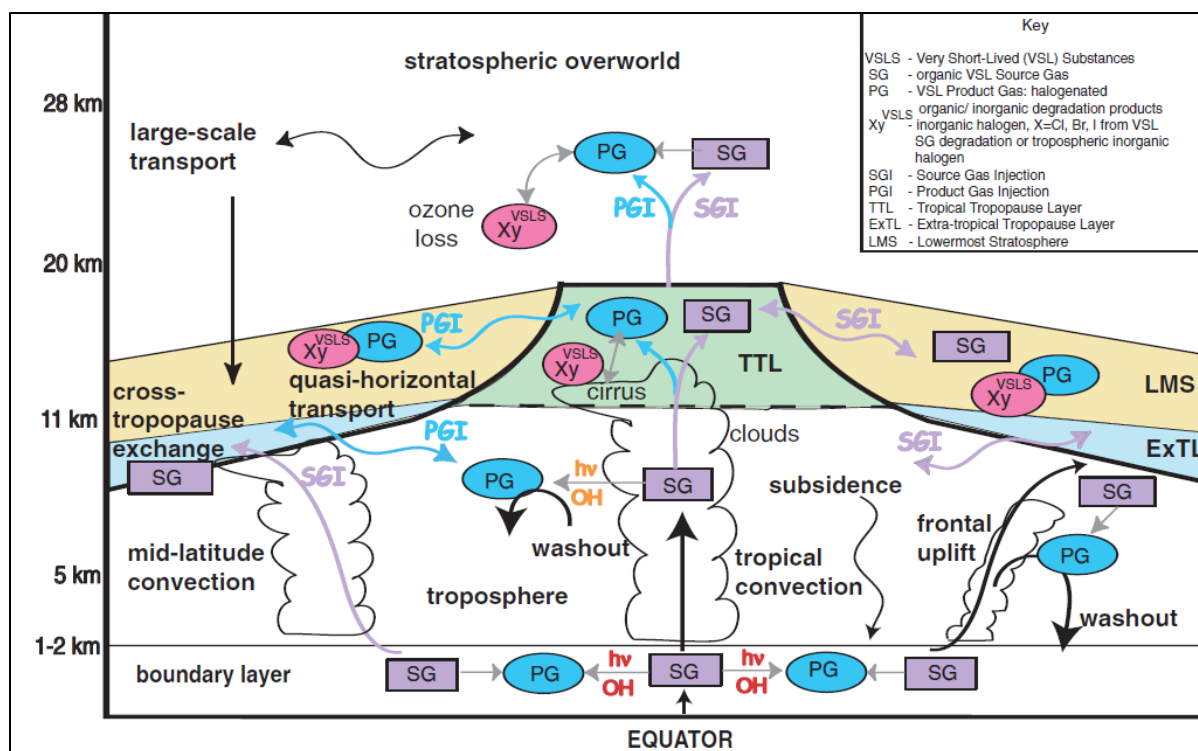
Figure I-4: *Scheme showing the principal pathways transporting SGs and PGs between troposphere and stratosphere at different latitudes (Engel and Rigby, 2018).*

I.2.6.   Reactivity of chlorine with VOCs

The role of chlorine (Cl) atoms in tropospheric oxidation has been the subject of extensive research, as evidenced by numerous studies (Badia *et al.*, 2019; Fan and Li, 2022; Faxon *et al.*, 2013; Finley and Saltzman, 2006; Hoffmann *et al.*, 2019; Hossaini *et al.*, 2016; Le Breton *et al.*, 2018; Li *et al.*, 2016; Liu *et al.*, 2017; Peng *et al.*, 2022; Saiz-Lopez and von Glasow, 2012; Sander *et al.*, 2011; Sherwen *et al.*, 2016; Sommariva and von Glasow, 2012; X. Wang *et al.*, 2019). These investigations have revealed the involvement of chlorinated inorganic compounds, such as $ClNO_2$, Cl_2, HOCl, and $ClONO_2$, in releasing chlorine atoms primarily through a process called photolysis, as well as through other minor pathways. As a result, the highly reactive chlorine atoms readily react with VOCs present in the atmosphere.

One of the key reactions between Cl and VOCs is hydrogen abstraction, where the chlorine atom removes a hydrogen atom from the VOC molecule (referred to as RH). This leads to the formation of an alkyl radical and hydrogen chloride (HCl), as represented by the reaction (***R12***). The resulting alkyl radical (R) can further react with molecular oxygen (O_2) to form peroxyalkyl radicals (RO_2) through the reaction (***R13***). These peroxyalkyl radicals can then participate in a complex series of reactions, ultimately leading to the production of various oxygenated organic compounds and potentially contributing to the formation of secondary organic aerosols (SOAs).

Chapter I. Atmospheric chlorine chemistry

In addition to its involvement in VOC oxidation, atomic Cl facilitates the conversion of nitric oxide (NO) to nitrogen dioxide (NO$_2$) through the reaction (**R14**). This process contributes to the production of O$_3$ in polluted regions where NO$_x$ levels are high. However, Cl can react directly with O$_3$, forming chlorine monoxide (ClO) and oxygen (O$_2$) in the reaction (**R17**). These reactions demonstrate the interconnected nature of chlorine chemistry with the formation and degradation of O$_3$ (Xia *et al.*, 2021).

Cl + RH → R + HCl	**R12**
R + O$_2$ + M → RO$_2$ + M	**R13**
RO$_2$ + NO → RO + NO$_2$	**R14**
NO$_2$ + hν (λ < 424 nm) → O (^{3}P) + NO	**R15**
O (^{3}P) + O$_2$ + M → O$_3$ + M	**R16**
Cl + O$_3$ → ClO + O$_2$	**R17**

Furthermore, Cl radicals can also undergo addition reactions with VOCs, resulting in the addition of a chlorine atom to the VOC molecule and the formation of chlorinated products. The formation of chlorinated VOCs is particularly relevant in the presence of chlorine-containing species like chlorine oxides (Cl$_2$ and ClNO$_2$) or hypochlorous acid (HOCl).

The rate constants (k$_{Cl}$) obtained from **Table I-8**, which provides the rate constants for the reactions of VOCs with atomic Cl and OH radicals (k$_{OH}$) at 298 K, are the ones used for kinetic modelling of chlorine chemistry (**Chapter III**). The rate constants for the reactions with OH radicals are recommended by the JPL Evaluation (Burkholder *et al.*, 2020). Analysis of **Table I-8** reveals that chlorine exhibits higher reactivity towards most VOCs compared to OH radicals. The reaction rates of chlorine radicals with many alkanes, such as methane, ethane, and propane, as well as alcohols like methanol, are typically one to two orders of magnitude greater than the corresponding reactions with OH radicals. The difference in reactivity is slightly smaller for alkenes and alkynes, with acetylene exhibiting a k$_{Cl}$/k$_{OH}$ ratio of 1.58. This higher reactivity of chlorine radicals can have significant implications for the atmospheric lifetimes and fate of VOCs, as well as influence the formation of O$_3$ and secondary pollutants.

In conclusion, the oxidation of VOCs by chlorine radicals contributes to the complex chemistry occurring in the atmosphere. It has important implications for air quality, the formation of secondary pollutants, and the overall oxidative capacity of the troposphere. Understanding the role of chlorine in VOC oxidation is crucial for accurately representing atmospheric chemistry in models and assessing its impacts on the environment.

Table I-8: *Comparison of rate constants (cm^3 molecule^{-1} s^{-1}) for OH (k_{OH}) and Cl (k_{Cl}) for reactions with common VOCs at 298 K.*

VOC	k_{Cl}	k_{OH}	k_{Cl}/k_{OH}
Methane CH$_4$	1.11×10^{-13} (a)	6.30×10^{-15} (g)	1.76×10^1
Ethane C$_2$H$_6$	5.43×10^{-11} (b)	2.50×10^{-13} (h)	2.17×10^2
Propane C$_3$H$_8$	1.40×10^{-10} (c)	1.12×10^{-12} (i)	1.25×10^2
Propene C$_2$H$_4$	2.93×10^{-10} (d)	7.90×10^{-12} (j)	3.71×10^1
Acetylene C$_2$H$_2$	2.13×10^{-10} (e)	1.35×10^{-10} (k)	1.58×10^0
Methanol CH$_3$OH	7.13×10^{-11} (f)	9.10×10^{-13} (l)	7.84×10^1

(a) (Bryukov *et al.*, 2002)　　　　　　　　　　(e) (Kaiser, 1992)

(b) (Bryukov *et al.*, 2003)　　　　　　　　　　(f) (Jodkowski *et al.*, 1998)

(c) (Atkinson et al., 2001)　　　　　　　　　　(g) (Bonard *et al.*, 2002)

(d) (Knyazev *et al.*, 1999)

(h) The recommended value (Burkholder *et al.*, 2020) for k_{OH} (298 K) is an average of the results reported at room temperature (Abbatt *et al.*, 1990; Baulch *et al.*, 1985; Bourmada *et al.*, 1987; Cavalli *et al.*, 1998; Clarke *et al.*, 1998; Crowley *et al.*, 1996; DóBé *et al.*, 1992; Donahue *et al.*, 1998; Finlayson-Pitts *et al.*, 1993; Heathfield *et al.*, 1998; Howard and Evenson, 1976; Lee and Tang, 1982; Leu, 1979; Li *et al.*, 2000; Overend *et al.*, 1975; Schiffman *et al.*, 1991; Schmidt *et al.*, 1985; Smith, C. A. *et al.*, 1984; Stachnik *et al.*, 1986; Talukdar *et al.*, 1994; Tully *et al.*, 1983, 1986; Wallington *et al.*, 1987; Zabarnick *et al.*, 1988).

(i) The recommended value (Burkholder *et al.*, 2020) for k_{OH} (298 K) is the average of the results reported at room temperature (Bryukov *et al.*, 2004; Clarke *et al.*, 1998; DeMore and Bayes, 1999; Donahue *et al.*, 1998; Droege and Tully, 1986; Kozlov *et al.*, 2003; Mellouki *et al.*, 1994; Morin *et al.*, 2015; Talukdar *et al.*, 1994)

(j) (Cleary *et al.*, 2006)

(k) (Smith, G. P. *et al.*, 1984)

(l) The recommended value (Burkholder *et al.*, 2020) for k_{OH} (298 K) is the average of direct studies by (Overend and Paraskevopoulos, 1978), (Ravishankara and Davis, 1978), (Hägele *et al.*, 1983), (Meier *et al.*, 1984), (McCaulley *et al.*, 1985), (Wallington and Kurylo, 1987), (Hess and Tully, 1989), (Jiménez *et al.*, 2003) and (Dillon *et al.*, 2005)

Chapter I. Atmospheric chlorine chemistry

I.2.7. Lifetimes of chlorinated species in the troposphere

Species in the atmosphere are primarily eliminated through their interaction with OH radicals and UV photolysis, mainly occurring in the gas phase. Consequently, the local lifetimes of these species can be expressed as follows:

$$(\tau_{local})^{-1} = (\tau_{OH})^{-1} + (\tau_J)^{-1} \qquad \textit{Eq. I-2}$$

where (τ_{OH}) and (τ_J) represent the lifetimes resulting from the reaction with OH radicals and UV photolysis, respectively (Engel and Rigby, 2018).

Table I-9 presents the measured lifetimes of various organic and inorganic chlorinated species in the troposphere under different conditions.

Table I-9: *Lifetimes of some inorganic chlorinated species measured at different conditions in the troposphere.*

Species	Lifetime	Reference	Specific conditions
Cl_2	Few min	(Wang, X. *et al.*, 2019)	Due to photolysis
	7 min	(Peng *et al.*, 2022)	Due to photolysis
	35.6 h	(Fan *et al.*, 2021)	Due to reaction with OH ([OH] = 1×10^7 radicals cm^{-3})
	20 days	(Kim *et al.*, 2008)	Due to photolysis and reaction with OH ([OH] = 1×10^6 radicals cm^{-3})
HCl	1 - 2 days	(Sanhueza and Garaboto, 2002)	Due to reactivity in free troposphere
	15 days	(Crisp *et al.*, 2014)	Due to reactivity in polluted marine boundary layer
HOCl	Few min	(Wang, X. et al., 2019)	Due to photolysis
$ClNO_2$	> 30 h	(Eger *et al.*, 2019)	Due to reactivity in the nocturnal marine boundary layer
	1 - 2 h	(Xia *et al.*, 2021)	Photochemical lifetime at 10:00 am in northern China
$ClONO_2$	10 h	(Lou *et al.*, 2022)	

I.3. Stratospheric chlorine chemistry

In 1985, an important scientific discovery was made by Joe Farman, Brian Gardiner, and Jonathan Shanklin. They reported significant and unexpected reductions in stratospheric O_3 levels over the Antarctic stations of Halley and Faraday (Farman *et al.*, 1985). Their data revealed a decline in O_3 levels during the austral spring months, starting in the late 1970s, after about 20 years of relatively stable values (***Figure I-5***). By 1984, the thickness of the stratospheric O_3 layer over Halley in October had decreased to about two-thirds of its earlier levels, leading to the identification of the phenomenon known as the Antarctic ozone hole. Farman *et al.* (1985) boldly proposed a link between this O_3 depletion and the use of CFCs, which are commonly found in aerosol cans and cooling devices like refrigerators. This ground-breaking finding had a profound impact on the fields of atmospheric science and chemical kinetics and resulted in global changes in environmental policies.
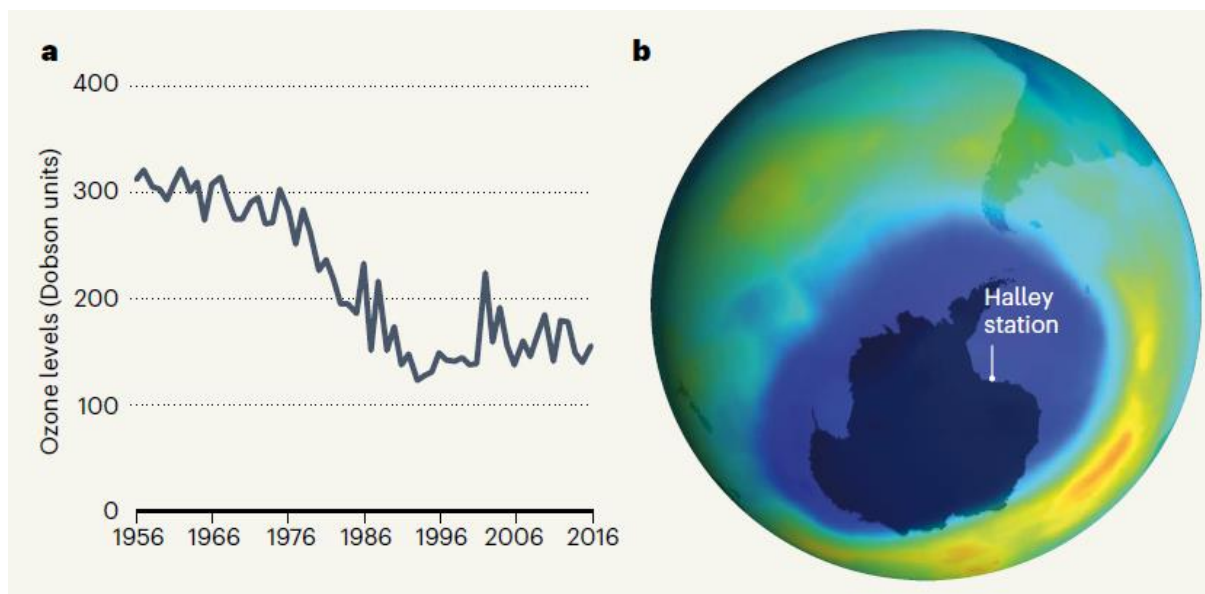
Figure I-5: *(a) The evolution of the ozone total column over the Halley time series. (b) The satellite ozone map for 10 September 2000, when ozone depletion was close to its maximum: blue indicate slow ozone levels; red, high levels. The position of the Halley station is indicated.*

For over 50 years, the stability of the stratospheric O_3 layer had been a matter of great interest for scientists, the public, and policymakers due to its crucial role in protecting life on Earth's surface from harmful UV radiation. The potential depletion of global O_3 by nitrogen oxide pollutants prompted extensive research on the influence of aviation on the ozone layer (Crutzen, 1970). A study by Molina and Rowland (1974) suggested that chlorine monoxide (ClO) produced from CFCs could have a similar O_3-depleting effect.

Although the expected depletion was initially considered relatively small and distant in the future, it posed serious threats such as increased incidence of skin cancers and ecological damage. Consequently, international policymakers concluded that a cautious strategy for O_3 protection was necessary. In March 1985, the United Nations Vienna Convention for the Protection of the Ozone Layer was signed, calling for further O_3 research but lacking legally binding goals for CFC reductions.

A few months later, Farman *et al.*'s (1985) report on the one-third loss of the springtime ozone layer over Antarctica was published. The paper's strengths lay in the authors' meticulous analysis of the seasonal patterns of change and the utilization of two different instruments to detect these changes. The authors suggested that Antarctica's extremely cold temperatures during winter and spring made the region uniquely susceptible to the growth of inorganic chlorine derived from CFCs in the atmosphere, although their proposed chemical mechanism was later found to be incorrect. This single paper had a transformative effect, abruptly reshaping the careers of hundreds of scientists and dozens of diplomats worldwide.

Chapter I. Atmospheric chlorine chemistry

In 1986, the first measurements of chlorine monoxide (ClO) (de Zafra et $al.$, 1987) and another O_3-depleting compound derived from CFCs, chlorine dioxide (OClO) (Solomon et $al.$, 1987), were obtained at the US station in McMurdo. These compounds were approximately 100 times more abundant there than in other locations. The definitive evidence linking CFCs to O_3 depletion came from aircraft measurements taken in 1987. Anderson et $al.$ (1989) revealed a significant increase in ClO levels (comparable to those in McMurdo) and a simultaneous decrease in O_3 concentrations as the aircraft flew south from Chile into the Antarctic.

These independently obtained datasets provided compelling evidence that the Antarctic region was indeed uniquely sensitive to chlorine compounds (Solomon, 1990), confirming Farman et $al.$'s (1985) initial suggestion. Unusual changes in the atmospheric abundances of related chemicals were also observed. Furthermore, satellite monitoring confirmed that the depletion extended over a vast region, typically spanning up to about 20 million square km.

The response of policymakers to Farman and colleagues' paper was initially reserved. They were cautious about disrupting the delicate diplomatic progress made under the Vienna Convention until the scientific findings were firmly established. However, they argued that the convention encompassed precautionary principles. Consequently, even as research planes were flying from Chile, policymakers signed the 1987 Montreal Protocol on Substances that Deplete the Ozone Layer. This agreement aimed to halt the production and consumption of O_3-depleting substances at their current rates, with future meetings scheduled to consider further production reductions. Subsequently, in 1995, the Nobel Prize in Chemistry was awarded to Paul Crutzen, Mario Molina, and Sherwood Rowland for their ground-breaking work in atmospheric chemistry, particularly their discoveries regarding the formation and decomposition of O_3 ("Nobel Prize in Chemistry," 1995), recognizing the role of CFCs in stratospheric O_3 depletion.

I.3.1. Impact of chlorine on ozone destruction

Chlorine is released into the stratosphere through various "chlorine SGs", including CH_3Cl, CFCs, and hydrochlorofluorocarbons (HCFCs) (von Clarmann, 2013). These SGs, such as CH_3Cl, CF_2Cl_2 (CFC-12), CCl_3F (CFC-11), CHF_2Cl (HCFC-22), CH_3CCl_3 (methyl chloroform), CCl_4 (CFC-10), and $CF_2ClCFCl_2$ (CFC-113), play a significant role in the release of chlorine in the stratosphere. While CH_3Cl is predominantly of natural origin (Khalil et $al.$, 1999), CFCs are mainly of anthropogenic origin and are commonly used as refrigerants and propellants. These gases have low reactivity in the troposphere and lower stratosphere, enabling them to resist breakdown and rainout in the lower atmosphere, eventually reaching the stratosphere. The partitioning of the primary sources of atomic Cl entering the stratosphere in the early 1990s, including CFCs, HCFCs, as well as CH_3Cl and HCl is depicted in ***Figure I-6***.

Once in the stratosphere, chlorine source gases face destruction primarily through UV photolysis, leading to the release of atomic chlorine (Cl) (Rowland, 1990). This process occurs in the mid-stratosphere, where the energy from UV radiation breaks the chlorine SG apart, liberating reactive chlorine atoms. These chlorine atoms play a crucial role in stratospheric chemistry, particularly in the depletion of O_3 molecules.
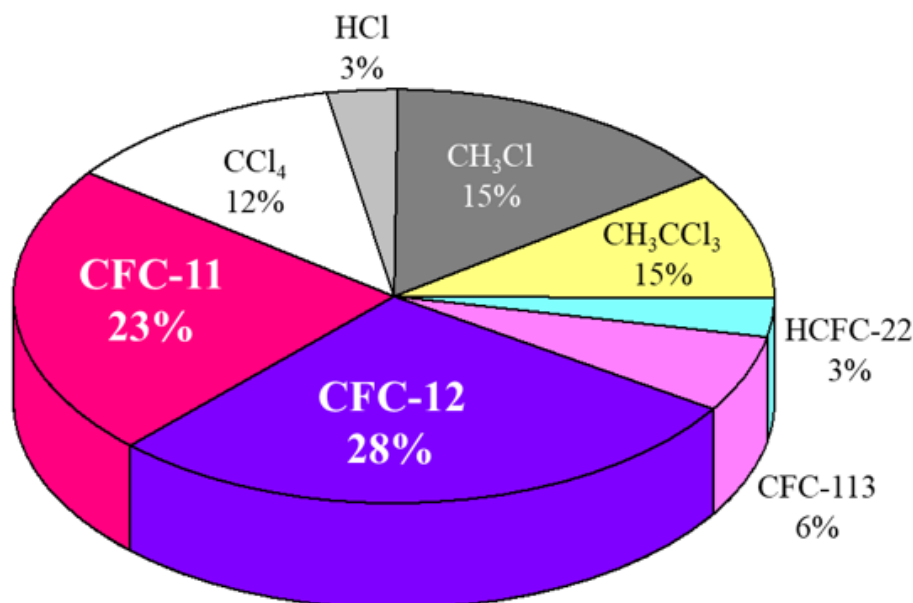
Figure I-6: *Primary sources of chlorine entering the stratosphere in the early 1990s (NOAA Chemical Sciences, 1994).*

The depletion of O_3 in Cycle 1 (illustrated in ***Figure I-7***) involves two distinct chemical reactions. The cycle can commence with either ClO or Cl. When initiating with ClO, the initial reaction is the combination of ClO and O to produce Cl and O_2. Subsequently, Cl reacts with O_3, regenerating ClO and consuming O_3 in the process while generating another O_2. The overall reaction can be summarized as atomic oxygen (O) reacting with O_3 to yield two oxygen molecules (O_2). The cycle then restarts with another interaction between ClO and O. Chlorine functions as a catalyst for O_3 depletion since Cl and ClO are regenerated with each completion of the reaction cycle, making them available for further O_3 destruction. Atomic oxygen is generated when solar ultraviolet (UV) radiation interacts with O_3 and O_2 molecules. Cycle 1 holds particular significance in the stratosphere at tropical and middle latitudes, where solar UV radiation is most intense.

Additionally, significant O_3 depletion occurs during late winter and early spring in polar regions when the levels of ClO are high. In such cases, reaction cycles initiated by the interaction of ClO with another ClO (Cycle 2, ***Figure I-8***) or the interaction of ClO with BrO (Cycle 3, ***Figure I-8***) effectively deplete O_3. The net reaction, in both cases, involves the transformation of two O_3 molecules into three oxygen (O_2) molecules. The reaction between ClO and BrO provides two pathways for the formation of Cl and Br gases, which contribute to O_3 loss. The O_3 depletion caused by Cycles 2 and 3 (***Figure I-8***) is catalytic, similar to the illustration shown in ***Figure I-7*** for Cycle 1, because chlorine and bromine gases react and regenerate during each completion of the reaction cycle. Sunlight is necessary to complete each cycle and maintain elevated levels of ClO. During polar nights and other dark periods, O_3 cannot be depleted by these reactions.

Chapter I. Atmospheric chlorine chemistry
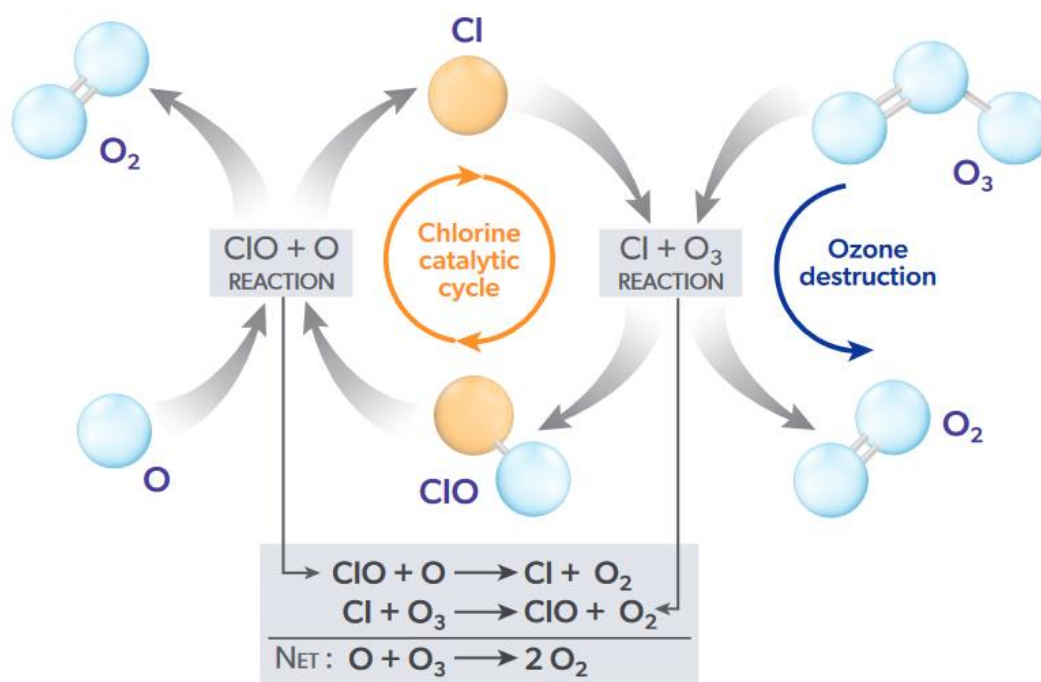
Figure I-7: *Ozone destruction Cycle 1.*

CYCLE 2:

$$ClO + ClO \rightarrow (ClO)_2$$
$$(ClO)_2 + h\nu \rightarrow ClOO + Cl$$
$$ClOO \rightarrow Cl + O_2$$
$$2(Cl + O_3 \rightarrow ClO + O_2)$$

NET: $\quad 2O_3 \rightarrow 3O_2$

CYCLE 3:

$$ClO + BrO \rightarrow Cl + Br + O_2$$
$$OR \begin{pmatrix} ClO + BrO \rightarrow BrCl + O_2 \\ BrCl + h\nu \rightarrow Cl + Br \end{pmatrix}$$
$$Cl + O_3 \rightarrow ClO + O_2$$
$$Br + O_3 \rightarrow BrO + O_2$$

NET: $\quad 2O_3 \rightarrow 3O_2$
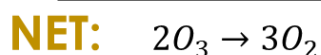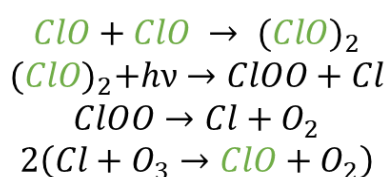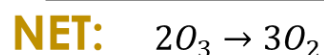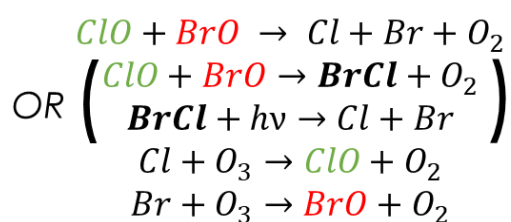
Figure I-8: *Polar ozone destruction Cycles 2 and 3.*

Furthermore, ClO can react with NO_2 (**R18**) to form $ClONO_2$ through a gaseous reaction. $ClONO_2$ can be hydrolysed by water droplets in Polar Stratospheric Clouds (PSC) through a heterogeneous reaction in the lower stratosphere (**R19**). This process converts the stable chlorine reservoir species ($ClONO_2$) into active chlorine, which can catalytically destroy O_3 (Solomon, 1990).

$ClO + NO_2 + M \rightarrow ClONO_2 + M$ $\hspace{6cm}$ **R18**
$ClONO_2 + H_2O \rightarrow HOCl + HNO_3$ $\hspace{5.5cm}$ **R19**
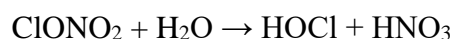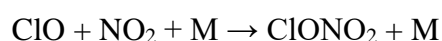
Chapter I. Atmospheric chlorine chemistry

I.4. Chlorine modelling studies

In this work, the modelling of chlorinated species has been done at different scales: the molecular, the kinetic, and the global. In the following, a brief overview of each modelling aspect and its application in understanding the chemistry of chlorinated species in the troposphere.

I.4.1. Chlorine from the quantum chemistry aspect

Accurate assessment of the environmental impact of chlorinated hydrocarbons released into the air requires a detailed understanding of their atmospheric chemistry. Chlorinated hydrocarbons are present in the troposphere at levels somewhat lower than those of major hydrocarbon pollutants. The presence of a Cl atom on a carbon site usually reduces the C-H bond energy by about 17.0 kJ mol^{-1} (Chen and Tschuikow-Roux, 1992; Niedzielski *et al.*, 1984; Sun and Bozzelli, 2001), leading to lower activation energies for abstraction of the hydrogen on the α-carbon ***Figure I-9***. This may lead to a faster formation of chlorinated alkyl radicals and subsequently chlorinated alkyl hydroperoxides (Cohen and Benson, 1987). These species will subsequently react with NO or another organic peroxy radical to form the corresponding chlorinated alkoxy radicals.
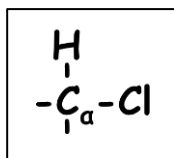
Figure I-9: *A chemical representation of the hydrogen on the α-carbon.*

Quantum chemistry is a branch of physical chemistry that focuses on the application of quantum mechanics to chemical systems. It is a very powerful tool that describes the fundamental behaviour of matter at the molecular scale. It focuses on how the atomic orbitals combine to form individual chemical bonds to give a molecule. It aims to study the thermochemical properties of species and the kinetic parameters of a chemical reaction.

Thermochemical properties obtained by quantum chemistry tools are important for the analysis of the impacts of the corresponding species on the environment. Kinetic data are used as input in atmospheric Chemistry-Transport Models (CTMs).

Basics of quantum chemistry and their applications are detailed later on in ***Chapter II***, in which we study the reactivity between OH radical and chloromethyl hydroperoxide (CH$_2$ClOOH). CH$_2$ClOOH is an important intermediate in low-temperature combustion processes and in the atmospheric photochemical oxidation of chlorinated hydrocarbons (Sun *et al.*, 2000). The lack of experimental studies of the thermodynamic properties of chlorinated alkyl hydroperoxides urged us to compute its missing properties on different levels of theory by quantum chemistry tools, and to determine the reactivity of this species with OH, the most important oxidant in the troposphere.

Chapter I. Atmospheric chlorine chemistry

I.4.2. Chlorine in atmospheric models

Tropospheric chlorine chemistry encompasses the investigation of reactions involving chlorine-containing species within the troposphere. Previous studies (Badia *et al.*, 2019; Eastham *et al.*, 2014; Fan and Li, 2022; Hoffmann *et al.*, 2019; Hossaini *et al.*, 2016; Li *et al.*, 2016; Ordóñez *et al.*, 2012; Peng *et al.*, 2021; Sander *et al.*, 2011; Sander and Crutzen, 1996; Sherwen *et al.*, 2016; Singh and Kasting, 1988; Sommariva and von Glasow, 2012; Soni *et al.*, 2023) have explored this area, which are all listed in ***Table I-10***. For each of the mentioned studies, the total number of reactions of chlorinated species is listed which are further classified in detail based on the nature of the species (organic or inorganic), and the type of the reaction (thermal or photolysis).

Table I-10: *Previous studies involving atmospheric models of gas-phase chlorine chemistry, with their total number of reactions of chlorinated species whether organic or inorganic species, thermal or photolysis reactions.*

Reference	Total number of reactions	Thermal		Photolysis		Model
		organic	inorganic	organic	inorganic	
(Singh and Kasting, 1988)	60	23	25	5	7	1D
(Sander and Crutzen, 1996)	17	5	7	0	5	0D (MOCCA)
(Sander *et al.*, 2011)	44	13	20	3	8	3D (CAABA/MECCA-3.0)
(Sommariva and von Glasow, 2012)	67	18	43	0	6	1D (MISTRA)
(Ordóñez *et al.*, 2012)	42	5	27	3	7	3D (CAM-Chem)
(Eastham *et al.*, 2014)	45	6	29	3	7	3D (GEOS-Chem)
(Sherwen *et al.*, 2016)	55	18	26	2	9	3D (GEOS-Chem)
(Hossaini *et al.*, 2016)	95	67	16	5	7	3D (TOMCAT)
(Li *et al.*, 2016)	24	14	6	1	3	3D (WRF-Chem)
(Badia *et al.*, 2019)	38	12	20	0	6	3D (WRF-Chem)
(Hoffmann *et al.*, 2019)	602	489	38	66	9	3D (SPACCIM)
(Peng *et al.*, 2021)	281	233	38	0	9	0D
(Fan and Li, 2022)	30	18	6	1	5	3D (CMAQ)
(Soni *et al.*, 2023)	35	21	9	0	5	0D (CAABA/MECCA v4.4.2)

In general, atmospheric models simulate the main atmospheric processes including solar radiation, meteorology, emissions, transport, chemical processing, and removal processes of gases and aerosols (Jacobson, 2005). They aim to better understand the air composition and its physical and chemical properties. Concurrently, models are always improved in order to be used for forecasting and prediction of air quality, tropospheric and stratospheric air composition, and climate from the local to the global scales. In this study, we choose to use two different atmospheric models with different applications and purposes.

Chapter I. Atmospheric chlorine chemistry

1. The first is ASTEC (Accident Source Term Evaluation Code), a kinetic zero-dimensional (0D) box model. It was developed by the French Nuclear Safety Institute (IRSN) (Chatelard *et al*., 2016). This model is used to create a complete gas-phase mechanism for a global representation. It includes all reactions involving organic and inorganic chlorinated species in the troposphere. Using this model allows us to figure out the mechanism of the cycling of the very reactive chlorinated species at a very short time scale. A comprehensive description of the model, the methodology, and the results is given in ***Chapter III***.

2. The second is MOCAGE (Model Of atmospheric Chemistry At larGE scale), a three-dimensional (3D) Chemistry-Transport Model (CTM) developed by the National Centre of Meteorological Research (CNRM). MOCAGE allows to model the chemical composition of the troposphere and the stratosphere from regional to global scales. In our study, we aim to implement reactions of organic and inorganic chlorinated species and determine their effects on a longer time scale adding different factors that could affect the reactivity and fate of these species. In ***Chapter IV***, this CTM is described with its various components. The chlorine mechanism implemented and its effect on gaseous species are also presented.

Chapter II.   Molecular modelling

II.1. Introduction

Hydroperoxides are molecules containing an -OOH group. Alkyl hydroperoxides (ROOH) and hydrogen peroxides (H_2O_2) are indicators of the atmospheric oxidative capacity and play a crucial role in gas phase chemistry. The production of these species is initiated via either photodissociation of a light halogenated hydrocarbon, RX, (***R1***) or the oxidation of a hydrocarbon, RH, by hydroxyl (OH) radical (***R2***) yielding an alkyl radical, R, that can readily pick up an oxygen molecule (***R3***) (Wallington *et al*., 1992).

$RX + h\nu \rightarrow R + X$ (X = halogen atom)	***R1***
$RH + OH \rightarrow R + H_2O$	***R2***
$R + O_2 \rightarrow RO_2$	***R3***

In environments with low concentrations of NO_x, RO_2 are mostly involved in reactions that lead to the production of alkyl hydroperoxides ROOH (***R4***) (Anglada *et al*., 2006).

$RO_2 + HO_2 \rightarrow ROOH + O_2$	***R4***

ROOH are relatively stable adducts in the atmosphere that are removed from the troposphere by precipitation (Tyndall *et al.*, 2001). At the same time, it is crucial to study the mechanism of the oxidation of these species in the chemistry of combustion and in atmospheric chemistry. Hence, the structures and thermodynamics of alkyl hydroperoxides have been investigated by several experimental and theoretical studies.

However, the experimental reports on the study of the structural and thermodynamic properties of ROOH and their reactivity are limited (Wang, Z. *et al*., 2019). This is due to several constraints. The detection, quantification, and comprehensive study of the kinetics of organic hydroperoxides pose significant challenges. This is mainly due to the lack of availability of these reactive species in the commercial market, the complexities involved in their synthesis and purification due to their tendency for spontaneous and exothermic decomposition (Kyasa *et al.*, 2013; Vaghjiani and Ravishankara, 1989), and the limitations of the analytical tools (like gas chromatography).

On the other hand, most of the theoretical work on the ROOH has primarily focused on the simplest members of the series, i.e. methyl hydroperoxides (CH_3OOH). Theoretical investigation of structural and thermodynamic parameters has been performed by Sun *et al*. (2000). Luo *et al*. (2011) investigated the mechanism and kinetics of the OH radical with alkyl hydroperoxides CH_3OOH and CH_3CH_2OOH.

Chapter II. Molecular modelling

In their study, Sun *et al*. (2000) extended their research to chlorinated methyl hydroperoxides (CH_2ClOOH, $CHCl_2OOH$, and CCl_3OOH). Understanding the atmospheric chemistry of chlorinated hydrocarbons released into the air is necessary for accurate environmental impact assessment. The presence of a chlorine atom on a carbon site lowers the C-H bond energy by approximately 16.74 kJ mol^{-1}, leading to lower activation energies for hydrogen abstraction at the α-carbon.

Chlorinated alkyl hydroperoxides are important intermediates in low-temperature combustion processes (Sun and Bozzelli, 2001), and understanding the thermodynamic parameters for chlorinated methyl hydroperoxides is crucial for predicting their reaction pathways and rate constants. Due to their rapid interconversion and instability, there are few experimental studies on the thermodynamic properties of alkyl hydroperoxides, making their investigation complex.

In this chapter, structural and thermodynamic properties of CH_2ClOOH are investigated, by theoretical chemistry tools, at two different levels of theory: M06-2X/6-311+G(2df,2p) and MP2/aug-cc-pVTZ. The mechanism and kinetics of the reaction of OH radical with CH_2ClOOH are determined within the atmospheric temperature range. This reaction, depicted in *Figure II-1*, proceeds through several pathways which are:

- H-abstraction pathways:
  - H4 or H5 abstractions: $OH + CH_2ClOOH \rightarrow CHClOOH + H_2O$,
  - H7 abstraction: $OH + CH_2ClOOH \rightarrow CH_2ClOO + H_2O$,
- Cl-abstraction: $OH + CH_2ClOOH \rightarrow CH_2OOH + HOCl$,
- OH-abstraction: $OH + CH_2ClOOH \rightarrow CH_2ClO + H_2O_2$.
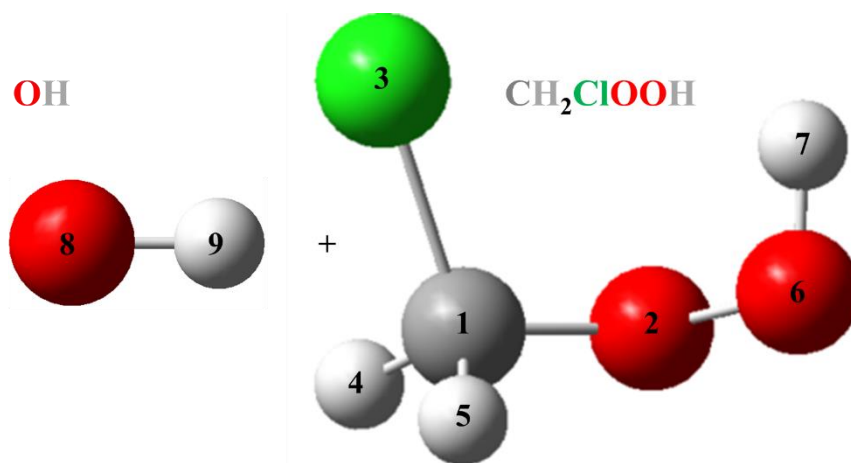
Figure II-1: *Schematic drawing of the reactants with atom labels. Dark grey balls represent carbon atoms, light grey for hydrogen, red for oxygen, and green for chlorine.*

In the following, basics of theoretical chemistry are detailed in ***section II.2***, the computational methods applied are described in ***section II.3***, different thermochemical properties and kinetic parameters are explained in ***section II.4***, and the results are discussed in ***section II.5***.

Chapter II. Molecular modelling

II.2. Theoretical chemistry background

The field of theoretical chemistry arose in the 1930s, utilizing mathematical and physical principles to conduct fundamental studies of chemistry. With the advancement of computational tools in the late 1960s, theoretical chemistry experienced significant growth. The primary aim of this discipline is to investigate the behaviour of electrons within a molecule and to determine key structural parameters such as geometries and vibrational frequencies, as well as the energetics of the chemical species involved in a reaction, including reactants, transition states, products, and molecular complexes.

The Schrödinger equation and Born-Oppenheimer approximation are the basics of this field.

- The Schrödinger equation

The Schrödinger equation, published by Erwin Schrödinger in his 1926 paper titled *"An undulatory theory of the mechanics of atoms and molecules"* (Schrödinger, 1926), is a differential equation, which describes how the wave function representing the state of a particle evolves in time. This time-dependent equation is a cornerstone of quantum physics and governs all phenomena of the microscopic world. The Schrödinger equation is written as:

$$i\hbar\frac{d\Psi}{dt} = \widehat{H}\Psi \qquad\qquad\qquad \textbf{\textit{Eq. II-1}}$$

A purely mathematical function Ψ called a wave function is used to describe a system composed of N particles. The probability of presence of the particles in a volume at a given time is determined by the quantity $|\Psi|^2$. In the Schrödinger equation, $\hbar$ is the reduced Planck constant, t the time and $\widehat{H}$ the Hamiltonian operator. Assuming that $\widehat{H}$ is independent of time, ***Eq. II-1*** can be written as follows:

$$\widehat{H}\Psi = E\Psi \qquad\qquad\qquad \textbf{\textit{Eq. II-2}}$$

where E is the system energy.

The Hamiltonian operator can be written as follows:

$$\widehat{H} = \widehat{T}_n + \widehat{T}_e + \widehat{V}_{ee} + \widehat{V}_{en} + \widehat{V}_{nn} \qquad\qquad \textbf{\textit{Eq. II-3}}$$

In Eq. II-3, $\widehat{T}_n$ the operator associated with the kinetic energy of nuclei, $\widehat{T}_e$ the operator associated with the kinetic energy of electrons, $\widehat{V}_{ee}$ the potential energy associated with electron-electron interactions, $\widehat{V}_{en}$ the potential energy associated with electron-nucleus interactions and $\widehat{V}_{nn}$ the potential energy associated with nucleus-nucleus interactions.

This equation cannot be solved in the majority of cases because it is a second order partial differential equation with a very large number of variables. It is therefore necessary to use approximations to be able to solve it.

Chapter II. Molecular modelling

- Born-Oppenheimer approximation

The Born-Oppenheimer (BO) approximation is the bedrock of quantum mechanical calculations of atomic and molecular systems. It simplifies the calculation of wave functions and energy levels of a molecule. The hypothesis proposed by Born and Oppenheimer states:

"We consider that we can decouple the movement of electrons from that of nuclei, by estimating that their movement is much slower than that of electrons: they are considered fixed in the study of the movement of the electrons of the molecule. Internuclear distances are then treated as parameters."

(Born and Oppenheimer, 1927)

The Hamiltonian operator corresponding to the kinetic energy of the nuclei is therefore neglected.

$$\widehat{T}_n = 0 \qquad\qquad \textbf{\textit{Eq. II-4}}$$

II.2.1. Potential energy surface

The idea of a potential energy surface (PES) for chemical reactions was initially proposed by the French physicist René Marcelin in 1913. Later on, the first calculation of a PES was carried out by Eyring and Polanyi using a combination of experimental data and theoretical methods in 1931.

The PES is a fundamental concept in chemistry that describes the relationship between the energy and geometric structure of a molecule or system. This concept arises from the great mass disparity between nuclei and electrons and may be understood by considering the nucleus immobile with respect to the electrons. Typically represented as a three-dimensional plot, the PES shows the energy as a function of the positions of the atoms or molecules in the system (Kwon *et al.*, 2021). This tool is valuable for predicting the behaviour of molecules in chemical reactions as it can reveal information about potential energy barriers and reaction pathways involved (see ***Figure II-2***).
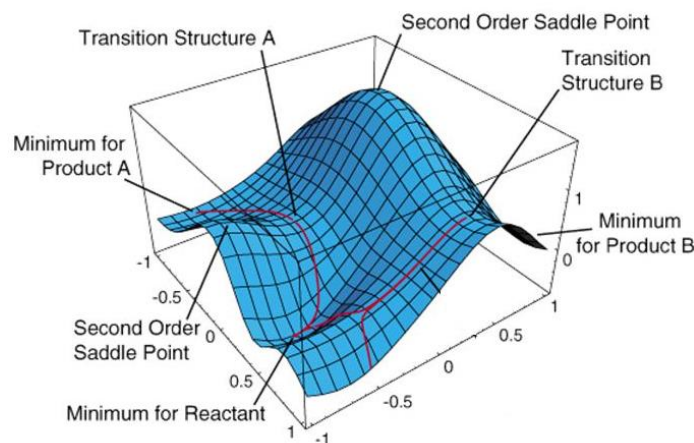
Figure II-2: *Model of the potential energy surface (Schlegel, 2003).*

Chapter II. Molecular modelling

This PES, depicted in ***Figure II-2*** is constructed for only two degrees of freedom of a molecular system. Each point on the surface corresponds to a value of energy linked to two other variables defining the plane above which the surface is drawn. Therefore, each point on the surface represents a different molecular structure.

In quantum mechanics, the Born-Oppenheimer approximation is commonly used to model chemical reactions with the PES. The PES characterizes the molecular structure of a chemical species based on the positions of its atoms' nuclei, with each position corresponding to an energy obtained by solving the Schrödinger equation. The PES is considered to be an effective potential energy function for the relevant degrees of freedom of the nucleus. It is a surface with (3N-6) degrees of freedom for a non-linear chemical species with N atoms, where the six degrees of freedom removed correspond to translations and rotations of the molecular system along the x, y and z axes. For a linear chemical species, the PES has (3N-5) degrees of freedom, where the five degrees of freedom removed correspond to translations of the entire molecular system along the x, y, and z axes and rotations about the x and y axes.

The 3N Cartesian coordinates describe the structure of a molecule, and for a given structure and electronic state, the molecule has a specific energy. The PES describes how the energy of the molecule in a particular state varies according to changes in the structure of the molecule.

II.2.2. Characterization of stationary points

The PES is a not a planar structure (***Figure II-2***), and it shows representative points known as stationary points. These are local and global minima corresponding to optimized molecular structures and a first-order saddle point, namely the transition state.

Each stationary point is characterized by having the first derivative of the potential energy that is zero with respect to all the degrees of freedom of the molecular system. This corresponds to the gradient G defined by the following equation:

$$G_i = \left(\frac{\partial E(x_1, x_2, x_3, \ldots, x_n)}{\partial x_i} \right)_{j \neq i} = 0 \forall i \qquad \textbf{\textit{Eq. II-5}}$$

The direction of curvature (concave or convex) of the PES characterizes the stationary points and therefore the nature of the molecular structures representing these points. The direction of curvature is given by a matrix called Hessian, denoted H. it has the dimension (3N − 6) × (3N − 6) whose elements are the second derivatives of the potential energy.

$$H_{ij} = \left(\frac{\partial^2 E(x_1, x_2, x_3, \ldots, x_n)}{\partial x_i \partial x_j} \right)_{k \neq i,j} \qquad \textbf{\textit{Eq. II-6}}$$

Chapter II. Molecular modelling

After diagonalization of this matrix, the eigenvalues correspond to the force constants k_i of a harmonic oscillator. They quantify the curvature of the PES at this point. The number of imaginary eigenvalues identifies the nature of the stationary point:

- No imaginary eigenvalues: the stationary point is a minimum on the PES and corresponds to a molecular structure at equilibrium. It can be a reactant, a product, or a molecular complex,

- An imaginary eigenvalue: the stationary point, called a first-order saddle point is characterized by a maximum energy for one particular degree of freedom and a minimum for the other degrees of freedom. The surface is convex in the direction of the particular degree of freedom and concave in the directions of the other degrees. It is a point of chemical interest for the reactivity of a system because it is the TS that connects two minima,

- More than one imaginary eigenvalue: the stationary point is an nth-order saddle point characterized by maximum energy for n degrees of freedom. These points have no interest in terms of reactivity.

The construction of the reaction path starts with the identification of the first-order saddle point, the TS. The connection between the TS and the minima (the reactants and products) is determined using the Intrinsic Reaction Coordinate (IRC) that will be described in *section II.3.5*.

II.2.3. Vibrational frequencies and zero-point energies

The harmonic oscillator model describes vibrational frequencies. To define molecular vibrations, 3N coordinates are needed to specify the positions of N atoms in a molecule, as previously stated in *section II.2.1*. Three of these coordinates are used to locate the molecule's centre of mass, or to describe its translational motion as a whole. The remaining (3N-3) coordinates, or degrees of freedom, describe the molecule's internal motion. A non-linear molecule has three independent rotations, one for each of the three axes in a coordinate system fixed at its centre of mass. In contrast, a linear molecule only has two distinct rotations, one for each of the two axes perpendicular to its molecular (z) axis. The number of independent rotations can also be thought of as the number of angles required to describe the molecule's orientation relative to the coordinate system at its centre of mass. All remaining degrees of freedom account for molecular vibrations. Therefore, a non-linear molecule has (3N-6) distinct vibrations, whereas a linear molecule has (3N-5). Each vibration can be modelled as a harmonic oscillator with different parameters.

Each vibrational frequency or wave number can be calculated using the following formula:

$$\bar{\nu} = \frac{1}{2\pi c} \times \sqrt{\frac{k}{\mu}} \qquad\qquad \textit{Eq. II-7}$$

with c the velocity of light in vacuum (c = 3×10^8 m s^{-1}), μ the reduced mass of the compound in kg and k the force constant in kg s^{-2}. Force constants give an indication of the relative

stiffness of bonds. For a molecule, the force constants are obtained by diagonalization of the mass-weighted Hessian matrix. Most of the work in calculating vibrational frequencies is spent in constructing the Hessian. From a mathematical point of view, a Hessian matrix is used to determine points of local maxima or minima.

From the value of the vibrational frequencies, the zero-point energy (ZPE) is calculated from the following equation:

$$ZPE = 1/2 \sum_i^N hc\bar{v}_l \qquad \textbf{\textit{Eq. II-8}}$$

where h is Planck's constant (h = 6.626×10^{-34} J s^{-1}). The ZPE is defined as the vibrational energy that the molecules retain even at absolute zero of temperature. It is the lowest quantized energy level of a quantum mechanical system or, in other words, the energy that remains in the when all other energy forms are removed. In conventional quantum physics, the origin of zero-point energy is the Heisenberg uncertainty principle, which states that, for a moving particle such as an electron, the more precisely one measures the position, the less exact the best possible measurement of its momentum (mass times velocity), and vice versa.

II.3. Computational methods

II.3.1. Levels of theory

All stationary point structures found on the PES are fully optimized using two different methods. These methods and the corresponding levels of theory applied are described below:

II.3.1.1. Second-order Møller-Plesset perturbation theory (MP2)

Møller and Plesset (1934) stated that:

"A perturbation theory is developed for treating a system of n electrons in which the Hartree-Fock solution appears as the zero-order approximation. It is shown by this development that the first order correction for the energy and the charge density of the system is zero. The expression for the second-order correction for the energy greatly simplifies because of the special property of the zero-order solution. It is pointed out that the development of the higher approximation involves only calculations based on a definite one-body problem."

The **MP2** perturbation theory (Møller and Plesset, 1934) is used together with the aug-cc-pVTZ basis set for the light atoms H, C, and O. The "cc-p" means consistently correlated with polarization functions, V means that this base is designed to handle only valence and not core electrons. TZ stands for triple-ζ (Dunning, 1989) nature of the valence base. For Cl atoms, tight d polarization functions (Dunning *et al.*, 2001) have been added to the basis sets (aug-cc-pV(T+d)Z). The prefix "aug" is added to indicate that it is an augmented version of this base by the addition of diffuse functions (Kendall *et al.*, 1992). The wave numbers and zero-point energies computed at the MP2/aug-cc-pVTZ level of theory are adjusted using the scaling factor of 0.953 (Johnson III *et al.*, 2022).

Chapter II. Molecular modelling

The MOLCAS 8.6 program (Aquilante *et al.*, 2020) is used to perform single-point energy calculations at all the stationary points of the reaction profile, employing the coupled cluster theory with single, double, and noniterative triple substitutions (CCSD(T)) in the basis of canonical orbitals. This parallel version of the CC-code, based on the restricted open-shell Hartree-Fock reference (ROHF), was employed for its computational efficiency. To correct for spin contamination introduced by the CCSD procedure, a spin-adaptation scheme was used on the dominant DDVV portion of T_2 excitation amplitudes, while leaving T_1 excitation amplitudes non-adapted (Neogrády *et al.*, 1994; Neogrády and Urban, 1995). The calculation of the triples contribution to the CCSD energy used diagonal Fock matrix elements as denominators. The second-order spin-free Douglas−Kroll−Hess Hamiltonian (Douglas and Kroll, 1974; Hess, 1986) was applied to calculate the scalar relativistic effects within the CCSD(T) method. This resulted in the use of a one-component spin-adapted approach, DK-CCSD(T), which was implemented in MOLCAS 8.6.

Two types of relativistic contraction of the ANO-RCC primitive sets for H(8s4p3d1f), C/O(14s9p4d3f2g), and Cl(17s12p5d4f2g) were adopted. The first one corresponds to the valence quadruple-ζ contraction for H, C, O, and Cl atoms: H[4s3p2d1f], C/O[5s4p3d2f1g], and Cl[6s5p3d2f1g]. For each of these atoms, s, p, d, f, and g are the atomic orbitals that represent the space around a nucleus where there is a high probability to find an electron.

The extensive application of the MP2 level of theory in modelling reactions of atmospheric interest justifies its selection for these studies (Agrawal *et al.*, 2023; Begum and Subramanian, 2014; Ghoshal and Hazra, 2014; Joy and Rajakumar, 2023; Khiri *et al.*, 2018; Louis, 2015, … etc).

II.3.1.2. The Density Functional Theory M06-2X

The Density Functional Theory (DFT) is applied to calculate the electronic structures of atoms, molecules, and solids. It aims to understand, quantitatively, the properties of material from the fundamental laws of quantum mechanics. Through this method, the one-body density is considered as a fundamental variable, rather than using the many-body wave function (Kurth *et al.*, 2005).

Zhao and Truhlar (2008) claimed that M06-2X functional may be classified as hybrid meta-generalized gradient-approximation. It is a high-nonlocality functional with double the amount of nonlocal exchange (2X), and it is parametrized only for non-metals. This functional contains 54% HF electron exchange. Zhao and Truhlar (2008) recommended the use of this level of theory for various applications including thermochemistry, kinetics, and non-covalent interactions. In this work, the basis sets applied to this method are 6-311+G(2df,2p) and 6-311++G(3df,3pd). The terms in these notations stand for:

- **6-311G**: this is a triple split valence basis, where the core orbitals are a contraction of six primitive Gaussian Type Orbitals (GTOs) and the valence split into three functions, represented by three, one, and one GTOs, respectively, i.e. (11s5p) → [4s3p].
- **(+) and (++)**: diffuse functions are normally s- and p-functions and consequently go before the G. They are denoted by (+) or (++), with the first (+) indicating one set of

diffuse s- and p-functions on heavy atoms, and the second (+) indicating that a diffuse s-function is also added to hydrogens. The arguments for adding only diffuse functions on non-hydrogen atoms is the same as that for adding only polarization functions on non-hydrogens. Diffuse functions are described as spherical harmonics times Gaussian functions with small exponents. They are functions with long tails allowing the electrons to be far from the nuclei (Papajak and Truhlar, 2010). They are used for quantitative accuracy.

- Polarization functions are indicated after the G, with a separate designation for heavy atoms and hydrogens. A 6-311++G(2df,2p) is similarly a triple zeta split valence with additional diffuse s and p-functions, and two d- and one f-functions on heavy atoms and diffuse s- and two p-functions on hydrogens. The largest standard Pople style basis set is 6-311++G(3df, 3pd). These types of basis sets have been derived for hydrogen and the first-row elements, and some of the basis sets have also been derived for second and higher row elements. Polarization functions are added to the basis sets to enhance the flexibility of atoms to form chemical bonds in any direction.

The wave numbers and zero-point energies computed at the M06-2X/6-311+G(2df,2p) level of theory are adjusted using the scaling factor of 0.983 (Kanchanakungwankul *et al.*, 2018).

Single-point energy calculations at all the stationary points of the reaction profile were performed at the M06-2X/6-311++G(3df, 3pd) level of theory using the largest Pople style basis set 6-311++G(3df, 3pd). Single-point energy calculations are performed to determine the effect of the basis set on the energetics.

The M06-2X level of theory is recommended by Zhao and Truhlar (2008) for various applications including thermochemistry, kinetics, and non-covalent interactions. Various atmospheric studies have utilized this level of theory before (Dao *et al.*, 2023; Joy and Rajakumar, 2023; Ngo *et al.*, 2023; Rawas *et al.*, 2023)

II.3.2. Stability of the wave function

For each of the stationary points, the stability of the wave function, which is controlled using an algorithm implemented in the Gaussian16 software (Frisch *et al.*, 2016) is being determined. This algorithm applies a constraint on the wave function. If it corresponds to a minimum, it returns to its original state and the wave function is said to be stable.

II.3.3. Spin-Orbit Coupling

The spin-orbit coupling (SOC) of the OH radical arises due to the interaction between the electron spin and its orbital motion around the oxygen atom. This interaction leads to a splitting of the energy levels in the $^2\Pi$ ground state of the OH radical by 139.21 cm^{-1} (Huber and Herzberg, 1979), which can be observed in spectroscopic experiments.

The magnitude of the SOC in the OH radical is relatively weak, as the molecule has a light mass and a small spin-orbit interaction. Nonetheless, the spin-orbit coupling can be detected and measured using advanced experimental techniques such as laser spectroscopy and

magnetic resonance spectroscopy. Based on literature, the value of SOC is -0.836 kJ mol^{-1} according to Hess *et al.* (1982) and Huber and Herzberg (1979) or -0.833 kJ mol^{-1} as given in the NIST-JANAF thermochemical database (Chase, 1998).

It is worth noting that the SOC values for all species, including those containing chlorine, are negligible.

II.3.4. Identification of the Transition State

A transition state is a high-energy state that occurs during a chemical reaction, where the reactants are partially transformed into products. At the TS, the molecules are highly reactive and unstable, and they are characterized by partial bonds and a degree of bond strain. The TS represents the highest point on the reaction energy profile, and the activation energy required to reach the TS is related to the rate of the reaction. The higher the energy barrier, the slower the reaction will be.

The imaginary frequency of a TS, represented by $\nu_i^{\neq}$, is a key characteristic that provides important information about the nature of the TS and the reaction mechanism. refers to a specific vibrational frequency associated with the TS. Unlike real frequencies, which correspond to stable vibrational modes, an imaginary frequency indicates that the TS represents a saddle point on the reaction energy surface. In other words, the imaginary frequency indicates that the TS represents a maximum in some directions and a minimum in others, and that the reaction can proceed in the direction associated with the imaginary frequency.

II.3.5. Intrinsic Reaction Coordin²ate

The starting point for studying a chemical reaction is to determine the location of the reactant, product, and TS geometries on the potential energy surface. Once the TS geometry is obtained, an IRC analysis (Fukui, 1970) may be performed to follow the minimum energy path to reactants and products and verify that this TS does indeed connect the molecular complexes from both reactant and product sides of the reaction of interest, namely MCR and MCP, respectively.

A molecular complex is a temporary species that forms when two or more molecules interact with each other in a reaction. The complex is stabilized by intermolecular forces, such as hydrogen bonding, van der Waals forces, or electrostatic interactions. Molecular complexes can play an important role in chemical reactions.

The IRC path is defined as the steepest descent path in mass-weighted Cartesian coordinates. When the reaction system descends from the TS to the reactant or product on the potential energy surface with infinitesimal velocity, it should follow the IRC path from both forward and reverse directions. The IRC calculations are performed using Gaussian 16 software (Frisch *et al.*, 2016).

In order to simplify, the reaction mechanism can be broken down into the following steps for all pathways:

1. Formation of the MCR: the reactants, OH and CH_2ClOOH here, start to get closer to each other to form the MCR.
2. Formation of the TS: at the TS, the reactants are partially transformed into products. The formation of the TS requires an input of energy, which is related to the activation energy barrier that must be overcome for the reaction to proceed.
3. Formation of the MCP: after passing through the TS, the system may form a molecular complex, which is a temporary species that arises from the interaction of two or more chemical species (molecules or radicals).
4. Formation of the product species: the molecular complex may break down, releasing the final products of the reaction. The products may be further modified or transformed through subsequent chemical reactions in the atmosphere.

II.4. Thermochemical properties and kinetic parameters

II.4.1. Thermochemical parameters

II.4.1.1. Partition functions

For a molecule, the total partition function q_{tot} is expressed according to the following equation:

$$q_{tot} = q_{trans} \times q_{rot} \times q_{vib} \times q_{elec} \qquad \textit{Eq. II-9}$$

where q_{trans}, q_{rot}, q_{vib}, and q_{elec} designate the partition functions of translation, rotation, vibration, and electronic, respectively.

The translational partition function can be written:

$$q_{trans} = (\frac{2\pi M k_B T}{h^2})^{3/2} V \qquad \textit{Eq. II-10}$$

where M is the molar mass, and k_B is the Boltzmann constant. Moreover, T is the temperature, and V is the volume.

The rotational partition function for a non-linear species is written:

$$q_{rot} = \frac{8\pi^2 (2\pi k_B T)^{3/2} (I_x I_y I_z)^{1/2}}{\sigma h^3} \qquad \textit{Eq. II-11}$$

where I_x, I_y, I_z are the moments of inertia of the molecule along the x, y and z axes. The number of symmetry σ is determined by the rotational symmetry of the molecule.

The vibrational partition function is given by the following relation:

$$q_{vib} = \prod_i \frac{1}{1 - exp\left(-\frac{hc\,\overline{v_i}}{k_B T}\right)} \qquad \textbf{\textit{Eq. II-12}}$$

For minima, the vibrational partition function has 3N-6 terms if the molecule is non-linear or 3N-5 if the molecule is linear. For TSs, this same function will have 3N-7 terms (non-linear) and 3N-6 (linear).

The electronic partition function is calculated according to the following formula:

$$q_{elec} = g_{ground\ state} + \sum g_{excited\ state}\, exp(-\Delta\varepsilon_{excited\ state}/k_B T) \qquad \textbf{\textit{Eq. II-13}}$$

with $\Delta\varepsilon_{excited\ state}$ the energy difference between the excited level and the ground state and g the associated energy degeneracy.

The use of statistical thermodynamics makes it possible to calculate the translational, rotational, vibrational, and electronic contributions of the thermodynamic quantities of interest (Irikura, 1998).

a.   Translational contributions

The translational enthalpy contribution at a temperature T is given by the equation:

$$[H(T) - H(0\ K)]_{trans} = \frac{5}{2}RT \qquad \textbf{\textit{Eq. II-14}}$$

with R being the ideal gas constant.

The translational contribution to the standard molar entropy at temperature T (S_{trans}) is defined by the following relation:

$$S_{trans} = R\left[\left(\frac{3}{2}\right)ln\left(\frac{2\pi M}{h^2}\right) + \left(\frac{5}{2}\right)ln(k_B T) - ln(p^{\circ}) + \frac{5}{2}\right] \qquad \textbf{\textit{Eq. II-15}}$$

with p° being the standard pressure.

The translational contribution to the heat capacity at constant pressure at temperature T ($C_{p,trans}$) is given by the equation:

$$C_{p,trans} = \frac{5}{2}R \qquad \textbf{\textit{Eq. II-16}}$$

b.   Rotational contributions

The rotational enthalpy contribution at temperature T for linear and non-linear molecules is given by the following relationships, respectively:

$$[H(T) - H(0\ K)]_{rot} = RT \qquad \textbf{\textit{Eq. II-17}}$$

$$[H(T) - H(0\ K)]_{rot} = \frac{3}{2}RT \qquad \textbf{\textit{Eq. II-18}}$$

The external rotation involves the entire structure of the molecule. This rotational contribution to the absolute standard entropy is calculated using the external symmetry number depending on the symmetry group of the species.

The rotational contribution to the standard molar entropy at temperature T (S_{rot}) is given for a linear and non-linear species by the equations:

$$S_{rot}^{linear} = R\left[ln\left(\frac{8\pi^2 I k_B T}{\sigma h^2}\right) + 1\right] \qquad \textbf{\textit{Eq. II-19}}$$

$$S_{rot}^{non\ linear} = R\left[ln\left(\frac{8\pi^2}{\sigma}\right) + \left(\frac{3}{2}\right)ln\left(\frac{2\pi k_B T}{h^2}\right) + \left(\frac{3}{2}\right)ln(I_A I_B I_C) + \frac{3}{2}\right] \qquad \textbf{\textit{Eq. II-20}}$$

where I_A, I_B, and I_C represent the moments of inertia of the molecule. A, B, and C represent the three directions of space.

The rotational contribution to the heat capacity at constant pressure at temperature T ($C_{p,rot}$) is given for a linear and non-linear species by the equations:

$$C_{p,rot}^{linear} = R \qquad \textbf{\textit{Eq. II-21}}$$

$$C_{p,rot}^{non\ linear} = \frac{3}{2}R \qquad \textbf{\textit{Eq. II-22}}$$

c.   Vibrational contribution

The vibrational enthalpy contribution at temperature T is given by equation:

$$[H(T) - H(0\ K)]_{vib} = RT\sum_i \frac{h v_i}{k_B T}\frac{exp\left(-\frac{h v_i}{k_B T}\right)}{\left(1 - exp\left(-\frac{h v_i}{k_B T}\right)\right)} \qquad \textbf{\textit{Eq. II-23}}$$

where v_i is the vibrational frequency of the normal mode i.

The vibrational contribution to the standard molar entropy at temperature T (S_{vib}) is given by the equation:

$$S_{vib} = -R\sum_i ln\left(1 - exp\left(-\frac{h v_i}{k_B T}\right)\right) + R\sum_i \frac{h v_i}{k_B T}\frac{exp\left(-\frac{h v_i}{k_B T}\right)}{\left(1 - exp\left(-\frac{h v_i}{k_B T}\right)\right)} \qquad \textbf{\textit{Eq. II-24}}$$

The vibrational contribution to the heat capacity at constant pressure at temperature T ($C_{p,vib}$) is given by equation:

$$C_{p,vib} = R\sum_i \left(\frac{h v_i}{k_B T}\right)^2 \frac{exp\left(-\frac{h v_i}{k_B T}\right)}{\left(1 - exp\left(-\frac{h v_i}{k_B T}\right)\right)^2} \qquad \textbf{\textit{Eq. II-25}}$$

d. Electronic contributions

The electronic enthalpy contribution at temperature T is given by equation:

$$[H(T) - H(0\ K)]_{elec} = RT \frac{\Sigma_i\, g_i\left(\frac{\varepsilon_i}{k_B T}\right) exp\left(-\frac{\varepsilon_i}{k_B T}\right)}{\left(\Sigma_i\, g_i exp\left(-\frac{\varepsilon_i}{k_B T}\right)\right)} \qquad \textbf{Eq. II-26}$$

where g_i and ε_i represent the degeneracy and energy of the energy level i corresponding to the excited states. They are denoted g_0 and ε_0 in the case of the ground state.

The electronic contribution to the standard molar entropy at temperature T (S_{elec}) is given by the equation:

$$S_{elec} = R ln\left(\Sigma_i\, g_i exp\left(-\frac{\varepsilon_i}{k_B T}\right)\right) + R \frac{\Sigma_i\, g_i\left(\frac{\varepsilon_i}{k_B T}\right) exp\left(-\frac{\varepsilon_i}{k_B T}\right)}{\left(\Sigma_i\, g_i exp\left(-\frac{\varepsilon_i}{k_B T}\right)\right)} \qquad \textbf{Eq. II-27}$$

The electronic contribution to the heat capacity at constant pressure at temperature T ($C_{p,elec}$) is given by equation:

$$C_{p,elec} = R\left(\frac{\Sigma\, g_i\left(\frac{\varepsilon_i}{k_B T}\right)^2 exp\left(-\frac{\varepsilon_i}{k_B T}\right)}{\left(\Sigma\, g_i exp\left(-\frac{\varepsilon_i}{k_B T}\right)\right)}\right) - R\left(\frac{\Sigma\, g_i\left(\frac{\varepsilon_i}{k_B T}\right) exp\left(-\frac{\varepsilon_i}{k_B T}\right)}{\left(\Sigma\, g_i exp\left(-\frac{\varepsilon_i}{k_B T}\right)\right)}\right)^2 \qquad \textbf{Eq. II-28}$$

II.4.2. Kinetic parameters

II.4.2.1. Transition State Theory TST

In his description of the TST, Eyring (1935) states that:

"Atoms and molecules can collide and combine to form an unstable, high energy complex. When the molecules fall out of this high energy state, they may do so as new and different molecules, or in their original states. The energy required to reach the activated state must be available if the molecules are to change into something new."

The classical transition state theory (TST) is directly based on the minimum energy profile determined by the IRC calculation. In this theory, the TS is placed at the top of this minimum energy path. The velocity constant is calculated using the formulation proposed by Eyring (1935):

$$k_{TST} = \left(\frac{k_B T}{h}\right) \times \frac{Q_{TS}}{\prod Q_{R(s)}} \times e^{-E_0/RT} \qquad \textbf{Eq. II-29}$$

$Q_{R(s)}$ and Q_{TS} refer to the total partition functions of reactants and TS, respectively. E_0 corresponds to the vibrationally adiabatic barrier including all energy corrections (ZPE and SOC corresponding to zero-point energy and spin-orbit coupling respectively). Its formula is given below:

$$E_0 = \Delta E + \Delta E_{ZPE} + \Delta E_{SOC} \qquad \textbf{Eq. II-30}$$

Chapter II. Molecular modelling

II.4.2.2. Kinetic scheme

The rate constant k for the different abstraction pathways involves the MCR, which is a hydrogen-bonded adduct. At first, it was examined using the Singleton and Cvetanovic (1976) recommended scheme for pre-reactive complexes. Our assumption in this context is that the reaction takes place in a two-step mechanism as follows:

$$OH + CH_2ClOOH \overset{k_a}{\rightarrow} MCR \qquad \textbf{\textit{(a)}}$$

$$MCR \overset{k_b}{\rightarrow} OH + CH_2ClOOH \qquad \textbf{\textit{(b)}}$$

and
$$MCR \overset{k_c}{\rightarrow} TS \qquad \textbf{\textit{(c)}}$$
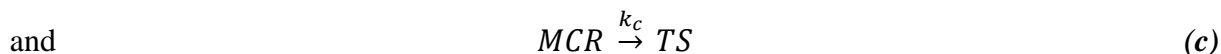
This mechanism involves a rapid pre-equilibrium between the reactants and the pre-reactive complex MCR, followed by an abstraction resulting in the post-reactive complex and the products. When the steady-state conditions are applied to reactions *(a-c)*; the effective reaction rate, r, can be expressed as:

$$r = r_c = k[OH][CH_2ClOOH] \qquad \textbf{\textit{Eq. II-31}}$$

where k is the overall rate constant for each of the studied pathways following the above mechanism, and k can be written as:

$$k = \frac{k_a k_c}{(k_b + k_c)} \qquad \textbf{\textit{Eq. II-32}}$$

Although the energy barrier for k_b is approximately equal to that of k_c, the reverse reaction (*b*) experiences a much greater entropy change compared to the reaction (*c*) leading to the TS. Consequently, k_b is anticipated to be significantly higher than k_c, and k can be expressed in the following manner:

$$k = \frac{k_a k_c}{k_b} = K_{a,b} k_c \qquad \textbf{\textit{Eq. II-33}}$$

In *equation II-33*, $K_{a,b}$ is the equilibrium constant between the isolated reactants and the pre-reactive complex MCR. The basic statistical thermodynamic principles are applied to calculate the equilibrium constant of the first step ($K_{a,b}$), whereas, the classical TST formula is used to calculate k_c:

$$K_{a,b}(T) = \frac{Q_{MCR}(T)}{Q_R(T)} exp\left(\frac{E_R - E_{MCR}}{k_B T}\right) \qquad \textbf{\textit{Eq. II-34}}$$

and
$$k_c(T) = \Gamma(T) \times \frac{k_B T}{h} \times \frac{Q_{TS}(T)}{Q_{MCR}(T)} \times exp\left(-\frac{E_{TS} - E_{MCR}}{k_B T}\right) \qquad \textbf{\textit{Eq. II-35}}$$

where $Q_R(T)$, $Q_{MCR}(T)$, and $Q_{TS}(T)$ are the total partition functions of the reactants, the pre-reactive complex (MCR), and the TS at a temperature T, respectively. E_R, E_{MCR}, and E_{TS} are the total energies at 0 K including the ZPE and SOC corrections, whereas $\Gamma(T)$ refers to the

transmission coefficient used for the tunnelling correction at temperature T; k_B and h are the Boltzmann's and Planck's constants, respectively.

This expression does not account for reaction path degeneracy as the rotational symmetry numbers are already factored into the partition function calculations. To calculate the reaction rate constants using the TST formulation provided by ***Eq. II-32***, it is essential to accurately compute the partition functions of both the pre-reactive complex and the transition state.

II.4.2.3.   Tunnelling effect

In chemical kinetics, tunnelling refers to the phenomenon where reactants are able to pass through a potential energy barrier, even when they do not possess the exact energy to surmount the barrier according to classical mechanics. This is a consequence of the wave-like nature of particles, which allows them to penetrate energy barriers that would be impenetrable according to classical mechanics.

Tunnelling is particularly important for reactions that involve light atoms or small molecules, where the tunnelling probability can be significant. In such cases, the rate of the reaction can be significantly enhanced by tunnelling, which can make the reaction rate comparable to or even faster than that predicted by classical kinetics.

The effect of tunnelling on chemical kinetics can be described mathematically using the TST, which considers the quantum mechanical tunnelling of the reactants through the potential energy barrier. In TST, the rate constant of a reaction is calculated as the product of the collision frequency of the reactants and the probability that they will overcome the potential energy barrier to form the products. The probability of tunnelling through the barrier is represented by the tunnelling correction factor, $\Gamma(T)$, which depends on the shape and height of the barrier, as well as the temperature of the reaction. Moreover, tunnelling can significantly affect the rate and selectivity of chemical reactions.

Within the scope of this investigation, two types of tunnelling correction are being examined: Wigner and Eckart tunnelling. The tunnelling factor, $\Gamma(T)$, typically varies based on the activation barrier of the elemental process in which the atom is being abstracted (or group, in case of OH group abstraction).

The GPOP (Gaussian POst Processor) (Miyoshi, 2022) program was used to extract information from Gaussian output files, to estimate the Eckart tunnelling corrections, and to do the rate constant calculations over the temperature range of interest.

Chapter II. Molecular modelling

a. Wigner tunnelling

Wigner tunnelling assumes that the potential energy barrier is symmetrical and therefore the tunnelling probability can be calculated based on the width of the barrier and the particle's energy (Wigner, 1932). The Wigner tunnelling probability is typically lower than that of Eckart tunnelling, as it relies solely on the particle's energy and the width of the barrier, rather than considering additional factors such as the shape and curvature of the barrier. Wigner tunnelling is given by the following formula

$$\kappa(T) = 1 + \frac{1}{24}\left(\frac{h\nu_i^{\neq}}{k_B T}\right)^2 \qquad\qquad \textit{Eq. II-36}$$

Wigner's approximation works well when $h\nu_i^{\neq} \ll k_B T$.

b. Eckart tunnelling

The Eckart potential function is commonly employed to estimate quantum mechanical tunnelling corrections to theoretically determined rate constants (Eckart, 1930). In this scenario, $\Gamma(T)$ represents the ratio of the quantum mechanical to classical barrier crossing rate, assuming an asymmetrical one-dimensional Eckart function barrier. To achieve this, a 1D function is fitted to approximate the potential and account for the ZPE and SOC corrected barrier, reaction enthalpy at 0 K, and the potential's curvature at the TS. The presence of the complex at the entrance channel implies that there are multiple rotational and vibrational energy levels from where tunnelling may occur. In the complex mechanism, we have assumed that a thermal equilibrium distribution of the rovibrational energy levels is maintained, which corresponds to the high-pressure limiting behaviour. Furthermore, we have assumed that all these levels, ranging from the bottom of the complex's well to the top of the barrier, contribute to tunnelling.

In the reaction OH + CH₂ClOOH, we have carried out a one-dimensional calculation of the tunnelling effect by representing the energy profile of the reaction by an asymmetric Eckart potential. This is defined by the height of the entry barrier V_1 and the exit barrier V_2. The Johnston's (1966) development is used to evaluate Γ^* which is defined by the following expression in the case where $V_2 > V_1$.

$$\Gamma^* = \frac{e^{\left(\frac{V_1}{kT}\right)}}{kT}\int_0^{\infty} \kappa(E)e^{\left(-\frac{E}{kT}\right)}dE \qquad\qquad \textit{Eq. II-38}$$

where κ (E) is the transmission coefficient.

It is clear that at a given temperature, the Γ^* factor depends on 2 topological parameters linked to the reaction path: the entry barrier V_1 and the absolute value of the imaginary frequency at the saddle point.

Chapter II. Molecular modelling

II.5. Results and discussion

Having a comprehension of the degradation process of CH_2ClOOH in the atmosphere is vital for its removal and to evaluate potential risks. Thus, it is highly significant to comprehend the various pathways, intermediate species, and end products involved in the atmospheric oxidation of CH_2ClOOH with OH radicals. Unfortunately, the current knowledge of the degradation of CH_2ClOOH is quite restricted.

II.5.1. Structures of the reactants and products

II.5.1.1. Structures of OH, H₂O, HOCl, and H₂O₂

Here, the optimized structures of the small species involved in the reaction (OH + CH_2ClOOH), which are either reactants (OH) or products (H_2O, HOCl, and H_2O_2) will be presented.

Figure II-3 presents the optimized structures of OH and H_2O. These structures are optimized at the two levels of theory of interest the MP2/aug-cc-pVTZ and M06-2X/6-311+G(2df,2p). The values optimized at the M06-2X level of theory are added on the figure between parentheses. Similarly, **Figure II-4** shows the geometry of HOCl optimized at MP2/aug-cc-pV(T+d)Z and M06-2X/6-311+G(2df,2p). In these two figures, distances are in Angstroms, and bond angles are in degrees.
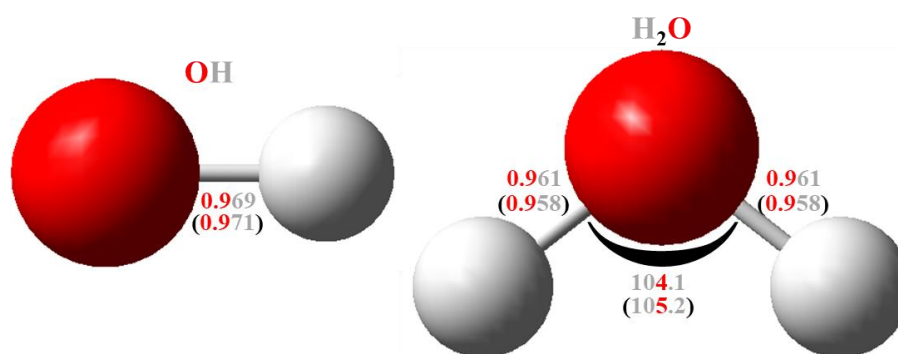
Figure II-3: *Schematic representation of OH and H₂O optimized at the MP2/aug-cc-pVTZ and M06-2X/6-311+G(2df,2p) (values between parentheses). The distances are in Angstroms, and bond angles are in degrees.*
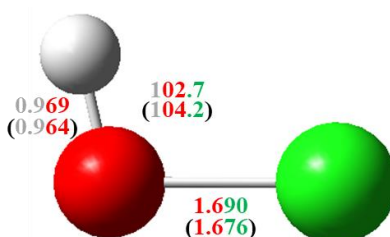
Figure II-4: *Schematic representation of HOCl optimized at the MP2/aug-cc-pV(T+d)Z and M06-2X/6-311+G(2df,2p) (values between parentheses). The distances are in Angstroms, and bond angles are in degrees.*

In the case of H_2O_2, it is necessary to study the variation of the potential energy along the rotation of the dihedral angle HOOH. The potential energy as a function of the dihedral angle is determined by scanning the angles from 0° to 360° at intervals of 10°. The result of the scan is summarized in a graph with maxima and minima. Different minimum and maximum values indicate the presence of different conformers of a species. The differences between the total energy of each conformation and that of the most stable conformer (the one with least energy) gives the barriers for the internal rotation (Sun *et al.*, 2000). The result of the scan of H_2O_2 is given in *Figure II-5*.

At the two levels of theory mentioned, the variation of the potential energy as a function of the dihedral angle HOOH possess the same behaviour with approximately equal barriers. The examination of *Figure II-5* shows the presence of two conformers (1a and 1b) of same potential energy where the value of φ(HOOH) are 113 and 247° (±113°) respectively. Moreover, there are two rotational barriers between the two conformers: a relatively low barrier (4.9 kJ mol⁻¹) and another relatively high one (31.0 kJ mol⁻¹).
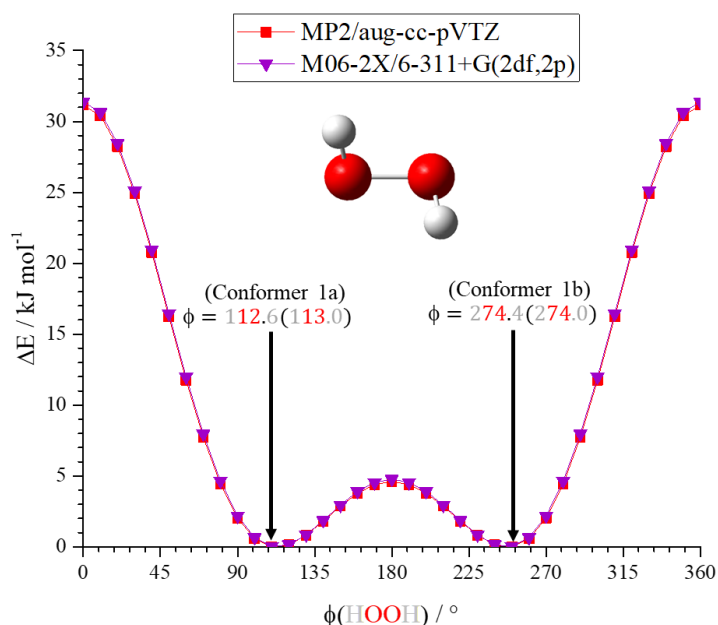
Figure II-5: *Variation of the potential energy of H_2O_2 as a function of the dihedral angle HOOH at MP2/aug-cc-pVTZ and M06-2X/6-311+G(2df,2p) (values between parentheses) levels of theory.*

The structures of the two conformers of H_2O_2 are schematized in ***Figure II-6***.

(Conformer 1a)
$\phi = 112.6(113.0)$

(Conformer 1b)
$\phi = 274.4(274.0)$
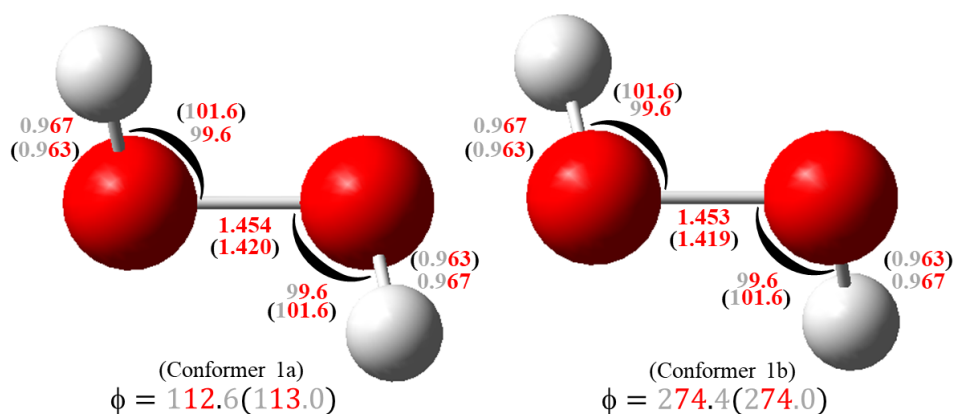
Figure II-6: *Schematic representation of H_2O_2 optimized at MP2/aug-cc-pVTZ and M06-2X/6-311+G(2df,2p) (values between parentheses) levels of theory. The distances are in Angstroms, bond angles and dihedral angles are in degrees.*

The structural parameters of OH, H_2O, HOCl, and H_2O_2 at the two levels of theory are summarized in **Table II-1**. Values taken from literature are also listed, these are the ones recommended by Johnson III *et al.* (2022).

Table II-1: *Geometrical parameters of OH, H_2O, HOCl, and H_2O_2 at the two chosen levels of theory compared to experimental data from literature.*

Species	r (Å)			θ (°)			ϕ (°)	Reference
	O-H	O-O	O-Cl	HOH	HOO	HOCl	HOOH	
OH	0.969							This work, MP2/aug-cc-pVTZ
	0.971							This work, M06-2X/6-311+G(2df,2p)
	0.970							**(Huber and Herzberg, 1979)** **Method: evaluation**
H₂O	0.961			104.1				This work, MP2/aug-cc-pVTZ
	0.958			105.2				This work, M06-2X/6-311+G(2df,2p)
	0.958			**104.5**				**(Hoy and Bunker, 1979)** **Method: evaluation**
HOCl	0.969		1.690			102.7		This work, MP2/aug-cc-pV(T+d)Z
	0.964		1.676			104.2		This work, M06-2X/6-311+G(2df,2p)
	0.973		**1.697**			**102.5**		**(Anderson *et al.*, 1986)** **Method: microwave spectroscopy**
H₂O₂	0.967	1.454			99.6		112.5	This work, MP2/aug-cc-pVTZ
	0.963	1.420			101.6		113.0	This work, M06-2X/6-311+G(2df,2p)
	0.950	**1.475**			**94.8**		**119.8**	**(Redington *et al.*, 1962)** **Method: infrared spectroscopy**

Chapter II. Molecular modelling

After comparing the geometries of the species using the two levels of theory with literature, the following observations were made:

- The bond length values showed very good agreement, with deviations not exceeding 4%.
- For H_2O and HOCl, the values of the bond angles were in very good agreement with deviations not exceeding 2%, while for H_2O_2, an overestimation of 5% and 7% was observed at the MP2 and M06-2X levels, respectively.
- The dihedral angle (HOOH) of H_2O_2 showed good agreement, with an underestimation of 6 and 5% at the MP2 and M06-2X levels, respectively.

When comparing the geometries optimized at the two levels of theory, there is an outstanding agreement among the values of all the parameters, with a maximum deviation of only 2%.

II.5.1.2.   Structure of CH₂ClOOH

Figure II-1 illustrates the conventional representation of CH₂ClOOH, which indicates that the molecule has two rotational axes along the dihedral angles OOCCl and HOOC. ***Figure II-7*** and ***Figure II-8*** display the potential energy curves of these two dihedral angles at two different levels of theory, namely M06-2X/6-311+G(2df,2p) and MP2/aug-cc-pV(T+d)Z, respectively. Based on these curves, it can be inferred that CH₂ClOOH has three distinct conformers, whose geometries are presented in ***Figure II-9***.
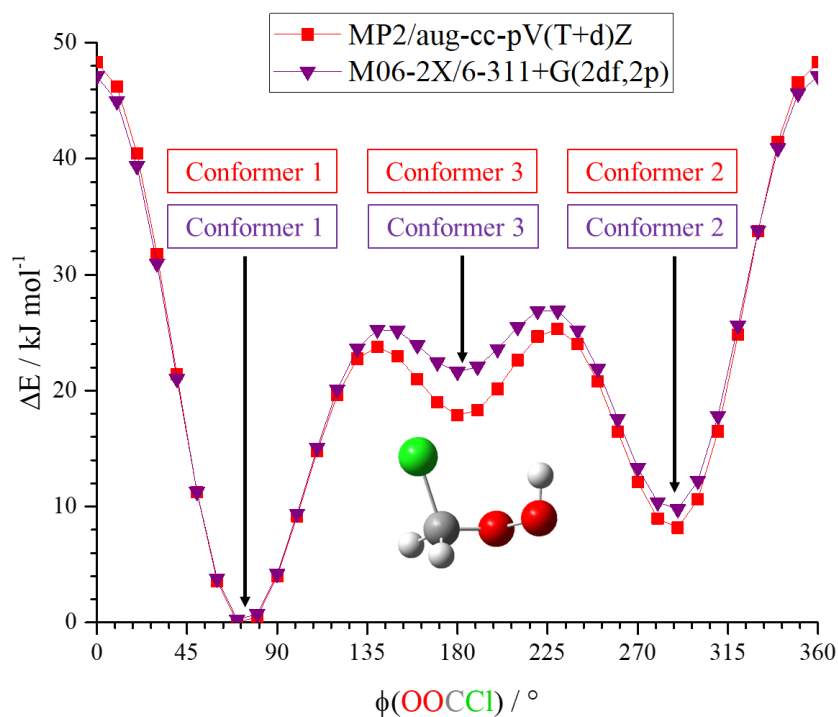
Figure II-7: *Variation of the potential energy of CH₂ClOOH as a function of the dihedral angle OOCCl at MP2/aug-cc-pV(T+d)Z and M06-2X/6-311+G(2df,2p) levels of theory.*
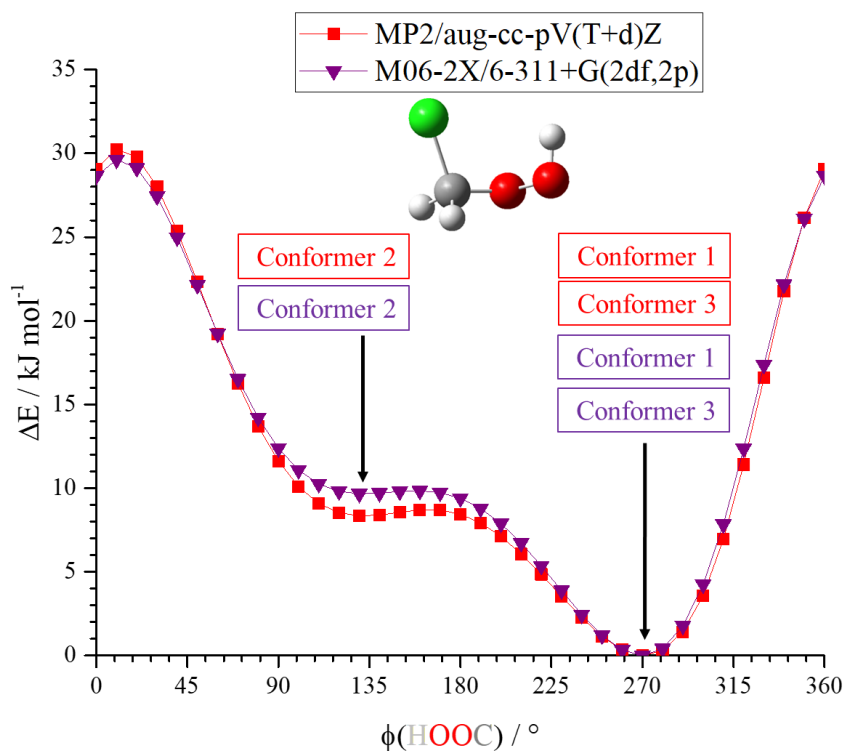
Figure II-8: *Variation of the potential energy of CH₂ClOOH as a function of the dihedral angle HOOC at MP2/aug-cc-pV(T+d)Z and M06-2X/6-311+G(2df,2p) levels of theory.*
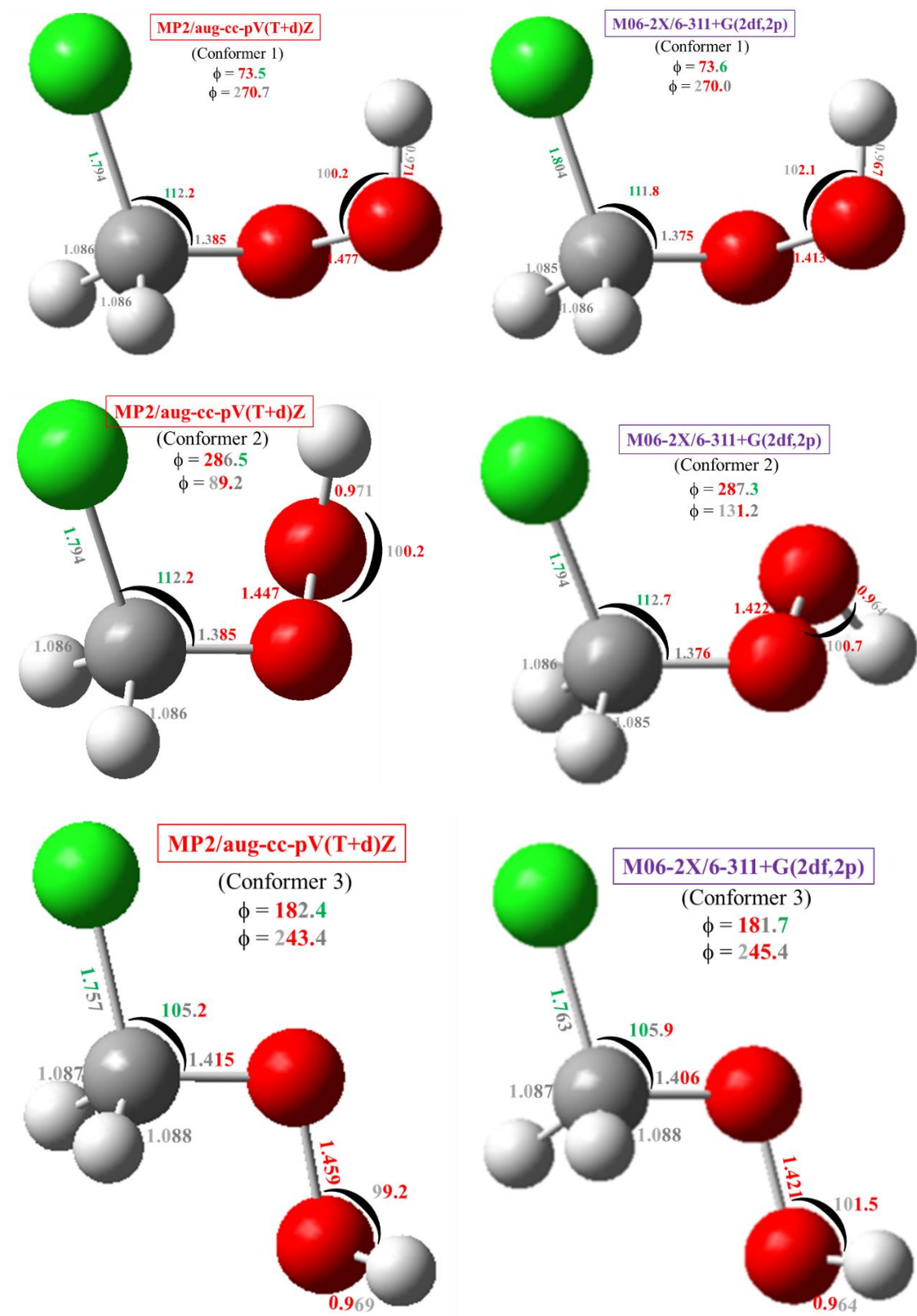
Figure II-9: *Schematic representation of the three conformers of CH$_2$ClOOH optimized at the MP2/aug-cc-pV(T+d)Z and M06-2X/6-311+G(2df,2p). The distances are in Angstroms, bond angles and dihedral angles are in degrees.*

Chapter II. Molecular modelling

Table II-2 lists the geometric parameters of the most stable conformer 1 of CH_2ClOOH, as well as the parameters computed by Wallington *et al.* (1996) and Sun *et al.* (2000). Wallington *et al.* (1996) used the MP2/6-31G(d,p) method to study the reactivity of CH_2ClOOH with Cl radicals, while Sun *et al.* (2000) calculated the structural parameters of this species at the B3LYP/6-31G(d,p) level.

Our computations at the MP2/aug-cc-pV(T+d)Z level show very good agreement with Wallington *et al.*'s (1996) results, with deviations below 1.5% in bond lengths and bond angles. Similarly, the comparison between the results of the DFT levels M06-2X and B3LYP used in our study and Sun *et al.*'s (2000), respectively, show very good agreement with deviations less than 1.5% in all bond lengths and bond angles, except for the r(O6-O2) bond (2.5%) and θ(H7O6O2) angle (5.7%).

Table II-2: *The geometric parameters of CH_2ClOOH as calculated in our study at the two levels of theory and in literature.*

	This work		Sun *et al.* (2000)	Wallington *et al.* (1996)
	MP2/aug-cc-pV(T+d)Z	M06-2X/6-311+G(2df,2p)	B3LYP/6-31G(d,p)	MP2/6-31G(d,p)
r (Å)				
O2-C1	1.385	1.375	1.377	1.390
Cl3-C1	1.794	1.804	1.842	1.792
H4-C1	1.086	1.085	1.090	1.085
H5-C1	1.086	1.086	1.090	1.085
O6-O2	1.477	1.413	1.449	1.461
H7-O6	0.971	0.967	0.974	0.972
θ (°)				
Cl3C1O2	112.2	111.8	112.7	112.7
H4C1O2	105.5	106.3	106.0	104.9
H5C1O2	111.7	111.9	112.5	111.4
O6O2C1	106.7	108.2	107.3	106.2
H7O6O2	100.2	102.1	107.9	99.4
ϕ (°)				
H4C1O2Cl3	116.8	116.9		
H5C1O2Cl3	-119.8	-119.3		
O6O2C1Cl3	73.5	73.6		
H7O6O2C1	-89.3	-90.0		

The conformational analysis of CH_2ClOOH that aims to study the population (N_i) of each of the conformers of this molecule was performed using the Boltzmann's distribution equation that can be written as follows:

$$N_i = \frac{e^{-\frac{\Delta G^{\circ}_T(i)}{RT}}}{\sum_{j=1}^{M} e^{-\frac{\Delta G^{\circ}_T(j)}{RT}}} \qquad\qquad \textbf{\textit{Eq. II-39}}$$

where $\Delta G^{\circ}_T(i)$ is the Gibbs free energy of the conformer (i) at a specific temperature, and M is the number of all conformers present for a specific species of interest.

Chapter II. Molecular modelling

The results of the conformational analysis based on Boltzmann's distribution are summarized in ***Table II-3***.

Table II-3: *The conformational analysis of the different conformers of CH$_2$ClOOH at 298 K computed at DK-CCSD(T)/ANO-RCC-VQZP and M06-2X/6-311++G(3df,3pd).*

	N$_1$	N$_2$	N$_3$
	DK-CCSD(T)/ANO-RCC-VQZP [a]		
250 K	94.9	5.1	0.1
298 K	94.3	5.6	0.1
300 K	94.2	5.7	0.1
	M06-2X/6-311++G(3df,3pd) [b]		
250 K	96.5	3.5	0.0
298 K	96.1	3.9	0.0
300 K	96.9	3.1	0.0

[a] Geometries optimized at MP2/aug-cc-pV(T+d)Z
[b] Geometries optimized at M06-2X/6-311+G(2df,2p)

Table II-3 shows that conformer 1 of CH$_2$ClOOH consistently dominates as the primary conformer, with an abundance exceeding 90.0% at both levels of theory across the three temperatures. In contrast, conformer 2 exists in a significantly lower proportion, ranging between 5.0 to 6.0% at the DK-CCSD(T)/ANO-RCC-VQZP level of theory and between 3.0 to 4.0% at the M06-2X/6-311++G(3df,3pd) level of theory. Conformer 3 of CH$_2$ClOOH is rare and exists in negligible quantities.

II.5.1.3. *Structure of the different radicals: CHClOOH, CH$_2$ClOO, CH$_2$OOH, CH$_2$ClO*

The radical products arising from the reaction pathways between OH and CH$_2$ClOOH are as follows: CHClOOH, resulting from H4 and H5 abstractions; CH$_2$ClOO, resulting from H7 abstraction; CH$_2$OOH, resulting from Cl abstraction; and CH$_2$ClO resulting from OH abstraction. The exploration of the doublet energy surface of all these radical species at the two levels of theory have been performed. Only, the optimized structures of the most stable conformers are shown in ***Figure II-10***.
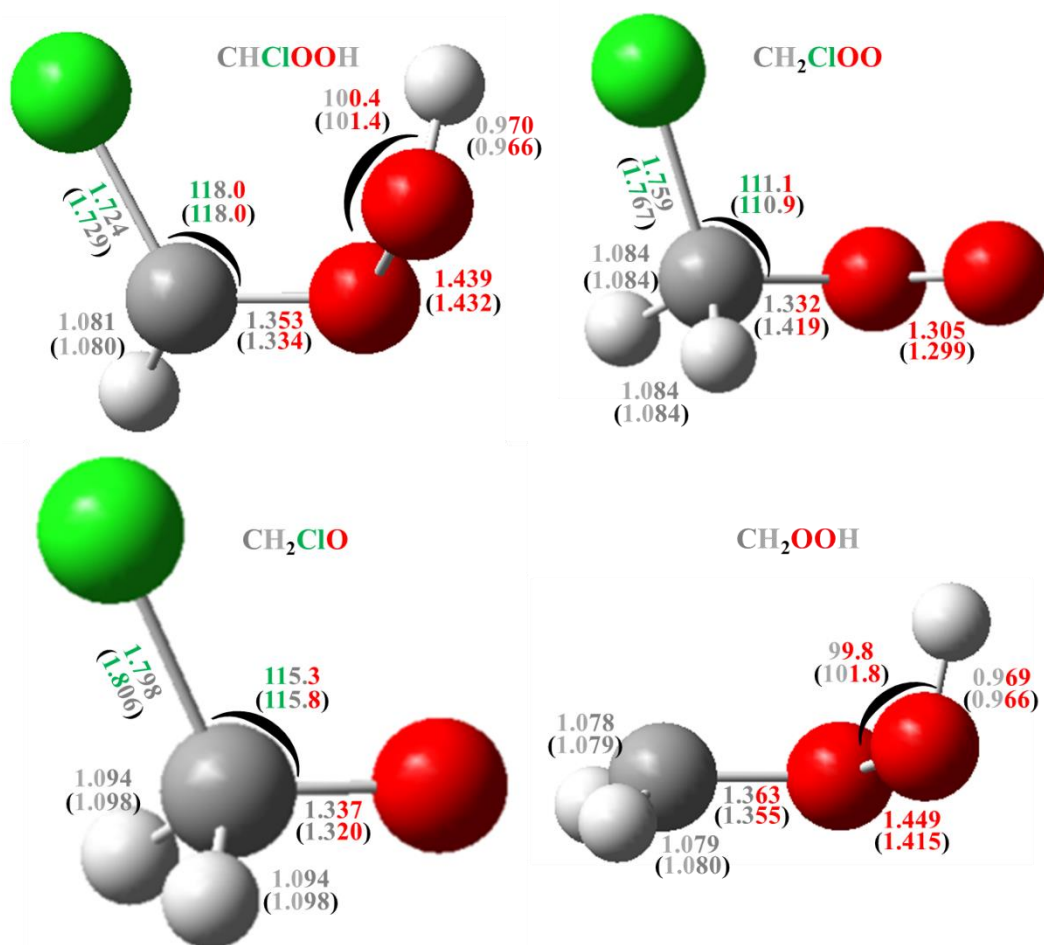
Figure II-10: *Schematic representation of the radical products of the reaction OH + CH₂ClOOH optimized at the MP2 and M06-2X (values between parentheses) levels. The distances are in Angstroms, bond angles and dihedral angles are in degrees.*

II.5.2. Vibrational frequencies, rotational constants, point group, and electronic state of reactants and products

Table II-4 lists the symmetry number, electronic state, and point group of all the reactants and products involved in the reaction OH + CH₂ClOOH. It also shows the values of the vibrational frequencies and zero-point energies of each of the species scaled by a factor of 0.953 (Johnson III *et al.*, 2022) at the MP2/aug-cc-pVTZ and MP2/aug-cc-pV(T+d)Z levels and by a factor of 0.983 (Kanchanakungwankul *et al.*, 2018) at M06-2X/6-311+G(2df,2p). The values of the scaled vibrational frequencies are compared with those available in literature when available.

Our M06-2X calculations exhibit good agreement with our MP2 results when comparing vibrational frequencies for OH, H₂O, and HOCl, with deviations not exceeding 8%. However, for H₂O₂ (conformer 1a), a difference of approximately 14% is observed in the second vibrational mode which represents the stretching of O-O bond. In addition, for CH₂ClOOH (conformer 1), deviations of up to 11% are observed in the second and sixth vibrational modes, showing the bending of the angle H7O6O2 and stretching of O6-O2 bonds, respectively.

Compared to literature (Huber and Herzberg, 1979), M06-2X/6-311+G(2df,2p) demonstrates excellent efficiency in reproducing the vibrational frequencies of OH. For H_2O, an acceptable overestimation of approximately 4.5% is observed in the second and third vibrational modes representing the symmetrical and asymmetrical stretching of O-H bonds, respectively, when compared to Huber and Herzberg (1979) and Shimanouchi (1972). However, M06-2X overestimates the first vibrational mode of HOCl showing the stretching of O-Cl bond by approximately 9%. H_2O_2 (conformer 1a) exhibits a relatively high deviation of up to 17% in the second vibrational mode. CH_2ClOOH (conformer 1) demonstrates very good agreement with Sun *et al.* (2000), with deviations less than 9%. However, when compared to Wallington *et al.* (1996), there is an overestimation in all vibrational modes, reaching about 20% in the second vibrational mode.

MP2 level of theory produces vibrational frequency values that closely match those in literature, with deviations no greater than 8%. This demonstrates that the MP2/aug-cc-pVTZ and MP2/aug-cc-pV(T+d)Z levels of theory are highly effective in computing the vibrational frequencies of the species listed.

Table II-4: *Symmetry number, point group, electronic state, rotational constants, scaled vibrational frequencies, and zero-point energy (ZPE) values for the reactants and products of the reaction OH + CH₂ClOOH computed at different levels of theory and compared with literature.*

Level of theory	Symmetry number	Point group & electronic state	Rotational constants (GHz)	Scaled vibrational frequencies (cm^{-1})	Scaled ZPE (kJ mol^{-1})
OH					
M06-2X/6-311+G(2df,2p)	1	$C_{\infty V}$ - $^2\Pi$	565.46	3726	22.28
MP2/aug-cc-pVTZ	1	$C_{\infty V}$ - $^2\Pi$	567.39	3619	21.64
				3738[a]	
CH₂ClOOH (conformer 1)					
M06-2X/6-311+G(2df,2p)	1	C_1 - ^1A	14.72, 3.63, 3.14	160, 295, 378, 515, 712, 936, 1016, 1131, 1268, 1322, 1420, 1450, 3069, 3149, 3738	122.98
MP2/aug-cc-pV(T+d)Z	1	C_1 - ^1A	14.42, 3.63, 3.13	149, 263, 357, 484, 703, 830, 968, 1045, 1221, 1287, 1320, 1411, 2981, 3065, 3553	117.46
				147[b], 248[b], 337[b], 462[b], 683[b], 782[b], 933[b], 1003[b], 1177[b], 1252[b], 1267[b], 1363[b], 2870[b], 2955[b], 3421[b]	
				148[c], 262[c], 361[c], 487[c], 655[c], 868[c], 983[c], 1082[c], 1250[c], 1315[c], 1372[c], 1437[c], 3046[c], 3130[c], 3651[c]	
CH₂ClOOH (conformer 2)					
M06-2X/6-311+G(2df,2p)	1	C_1 - ^1A	15.48, 3.50, 3.07	142, 149, 366, 507, 722, 927, 1015, 1127, 1272, 1328, 1411, 1447, 3063, 3141, 3786	122.03
MP2/aug-cc-pV(T+d)Z	1	C_1 - ^1A	15.03, 3.52, 3.08	140, 144, 351, 477, 714, 819, 970, 1037, 1224, 1292, 1313, 1409, 2975, 3057, 3594	
CH₂ClOOH (conformer 3)					
M06-2X/6-311+G(2df,2p)	1	C_1 - ^1A	36.46, 2.67, 2.55	103, 268, 281, 417, 826, 995, 1008, 1106, 1210, 1340, 1396, 1497, 3040, 3108, 3777	121.85
MP2/aug-cc-pV(T+d)Z	1	C_1 - ^1A	35.60, 2.67, 2.54	109, 222, 263, 390, 796, 860, 981, 1031, 1163, 1284, 1305, 1462, 2959, 3031, 3590	116.33
CHClOOH					
M06-2X/6-311+G(2df,2p)	1	C_1 - ^2A	15.98, 3.80, 3.20	157, 204, 335, 526, 593, 790, 938, 1137, 1287, 1403, 3180, 3758	85.57
MP2/aug-cc-pV(T+d)Z	1	C_1 - ^2A	15.44, 3.90, 3.23	161, 185, 327, 529, 691, 837, 997, 1246, 1272, 1342, 3085, 3569	85.18
CH₂ClOO					
M06-2X/6-311+G(2df,2p)	1	C_1 - ^2A	17.73, 3.56, 3.20	109, 346, 539, 761, 947, 1020, 1207, 1282, 1337, 1453, 3081, 3163	91.18
MP2/aug-cc-pV(T+d)Z	1	C_1 - ^2A	17.95, 3.52, 3.18	96, ,334, 510, 747, 890, 987, 1139, 1222, 1300, 1417, 2998, 3085	88.09
H₂O					
M06-2X/6-311+G(2df,2p)	2	C_{2V} - $^1A_1$	833.97, 432.48, 284.79	1602, 3823, 3925	55.93
MP2/aug-cc-pVTZ	2	C_{2V} - $^1A_1$	807.77, 436.26, 283.27	1552, 3642, 3762	53.57
				1595[d], 3657[d], 3756[a]	

Table II-4*: Continued.*

Level of theory	Symmetry number	Point group & electronic state	Rotational constants (GHz)	Scaled vibrational frequencies (cm^{-1})	Scaled ZPE (kJ mol^{-1})
				CH$_2$OOH	
M06-2X/6-311+G(2df,2p)	1	C$_1$ - ^{2}A	54.59, 11.52, 9.89	187, 283, 501, 670, 948, 1171, 1213, 1398, 1426, 3108, 3247, 3758	107.12
MP2/aug-cc-pVTZ	1	C$_1$ - ^{2}A	52.26, 11.39, 9.72	183, 280, 467, 685, 852, 1112, 1157, 1307, 1388, 3034, 3179, 3581	103.03
				HOCl	
M06-2X/6-311+G(2df,2p)	1	C$_S$ - ^{1}A'	622.79, 15.42, 15.04	793, 1259, 3792	34.95
MP2/aug-cc-pV(T+d)Z	1	C$_S$ - ^{1}A'	607.83, 15.19, 14.82	731, 1203, 3595	33.07
				724^e, 1276^e, 3794^e	
				CH$_2$ClO	
M06-2X/6-311+G(2df,2p)	1	C$_S$ - ^{2}A''	48.58, 5.82, 5.37	397, 661, 703, 1055, 1109, 1270, 1329, 2935, 2978	74.39
MP2/aug-cc-pV(T+d)Z	1	C$_S$ - ^{2}A''	47.89, 5.84, 5.38	387, 674, 692, 1041, 1054, 1253, 1329, 2897, 2955	73.46
				H$_2$O$_2$ (conformer 1a)	
M06-2X/6-311+G(2df,2p)	2	C$_2$ - ^{1}A	308.41, 27.46, 26.58	374, 1029, 1345, 1545, 3789, 3790	70.47
MP2/aug-cc-pVTZ	2	C$_2$ - ^{1}A	300.50, 26.41, 25.58	367, 883, 1258, 1356, 3608, 3609	66.29
				371^d, 877^d, 1266^d, 1402^d, 3599^d, 3608^d	
				H$_2$O$_2$ (conformer 1b)	
M06-2X/6-311+G(2df,2p)	2	C$_2$ - ^{1}A	308.37, 27.48, 26.59	375, 1031, 1346, 1455, 3789, 3790	70.49
MP2/aug-cc-pVTZ	2	C$_2$ - ^{1}A	300.45, 26.42, 25.60	368, 884, 1258, 1356, 3609, 3609	66.30

[a] Experimental data taken from Huber and Herzberg (1979).

[b] Vibrational frequencies taken from the study of Wallington *et al.* (1996) scaled by a factor of 0.9 at the MP2/6-31G(d,p).

[c] Vibrational frequencies taken from the study of Sun *et al.* (2000) scaled by a factor of 0.9806 (Scott and Radom, 1996) at the B3LYP/6-31G(d,p).

[d] Experimental data taken from Shimanouchi (1972).

[e] Experimental data taken from Jacox (1994).

II.5.3. Standard molar entropies at 298 K for the reactants and products

The standard molar entropies of the reactants and products in the OH and CH_2ClOOH reaction at 298 K are presented in **Table II-5**. The calculations were performed using the M06-2X and MP2 levels of theory and scaled by factors of 0.953 and 0.983, respectively.

Table II-5: *Standard molar entropy at 298 K determined at M06-2X/6-311+G(2df,2p) and MP2/aug-cc-pVTZ levels of theory. Literature values are added when available.*

Species	$S°_{298 K}$ (J mol^{-1} K^{-1}) M06-2X/6-311+G(2df,2p)	$S°_{298 K}$ (J mol^{-1} K^{-1}) MP2/aug-cc-pVTZ	Literature value (J mol^{-1} K^{-1})
OH	183.52	183.49	183.74 (Gurvich *et al.*, 1989) [a]
CH_2ClOOH (conformer 1)	295.05	297.81 [b]	297.21 (Sun *et al.*, 2000) [c]
CH_2ClOOH (conformer 2)	301.49	303.20 [b]	
CH_2ClOOH (conformer 3)	300.34	302.88 [b]	
CHClOOH	304.71	304.46 [b]	
CH_2ClOO	296.92	298.85 [b]	
H_2O	188.65	188.78	188.84 (Cox *et al.*, 1990) [a]
CH_2OOH	273.43	274.64	
HOCl	235.93	236.43 [b]	236.50 (Chase, 1998) [a]
CH_2ClO	270.01	270.29 [b]	
H_2O_2 (conformer 1a)	226.96	227.84	234.52 (Gurvich *et al.*, 1989) [a]
H_2O_2 (conformer 1b)	226.93	227.83	

[a] Value recommended by NIST CCCBDB (Johnson III *et al.*, 2022).
[b] Calculated at MP2/aug-cc-pV(T+d)Z level of theory.
[c] Scaled by a factor of 0.9806 (Scott and Radom, 1996) at the B3LYP/6-31G(d,p).

Our results for OH, CH_2ClOOH, H_2O, and HOCl align well with the literature when computed at both levels of theory. However, there is a discrepancy of approximately 6 J mol^{-1} K^{-1} in the value of H_2O_2 between our calculations and the values recommended by NIST CCCBDB (Johnson III *et al.*, 2022) based on Gurvich *et al.* (1989) work. This difference may be due to the fact that certain vibrational modes need to be treated as internal rotors rather than harmonic oscillators, specifically, the second vibrational mode, which represents the stretching of O-O bond.

II.5.4. Structures of the transition states and molecular complexes

In this section, we will discuss the geometrical parameters of the TSs and molecular complexes for all pathways of the reaction of OH radical with CH_2ClOOH. The parameters for the corresponding products were provided in *section II.5.1.3*.

Please take note that the pathways outlined in the forthcoming sections represent the most energetically favourable transition states associated with each respective pathway. It is important to keep in mind that other transition states may exist, but the focus here is on the most stable ones for the purpose of comprehensive analysis.

II.5.4.1. Study of the H-abstraction pathways

The optimized structures of the molecular complexes and TS of the three H-abstraction pathways at the M06-2X/6-311+G(2df,2p) and MP2/aug-cc-pV(T+d)Z levels of theory are shown in *Figure II-11* and *Figure II-12*, respectively. In these figures, the main geometrical parameters, including the intermolecular distances (shown in dashed lines) and the angle between the three main atoms involved in a given pathways, are mentioned.

The main geometrical changes of the TS were described using the L parameter, which is the ratio between the elongations of the bonds being broken and formed. The value of L parameter is $\delta r(CH)/\delta r(OH)$ for H4 and H5 abstractions, and $\delta r(OH)/\delta r(OH)$ for H7-abstraction, which is relative to its equilibrium value in the reactant/product. The L parameter provides information on whether the TS is reactant-like or product-like (Miller and Smith, 1978); a small value corresponds to the reactant-like structure, while a large value is typical for product-like TSs. *Table II-6* summarizes the geometrical properties, imaginary frequencies, and L parameter for the intermediate species involved in all possible hydrogen abstraction pathways of the reaction OH + CH_2ClOOH.

Regarding the H4 and H5 abstractions, the distance between H and C grows larger as one moves from MCR to MCP, whereas the distance between O and H becomes smaller. Similarly, for the H7 abstraction pathway, the O-H bond of the hydroxyl group in CH_2ClOOH becomes longer from MCR to MCP, while the O-H bond in the resulting H_2O molecule becomes shorter. The imaginary frequency, denoted as $v_i^{\neq}$, is given for each abstraction pathway.

At both levels of theory, the L parameter values are very small ranging between 0.228 and 0.274 at the M06-2X level of theory, and between 0.306 and 0.445 at the MP2 level of theory (*Table II-6*). This indicates that these TSs have a reactant-like character for the three pathways.
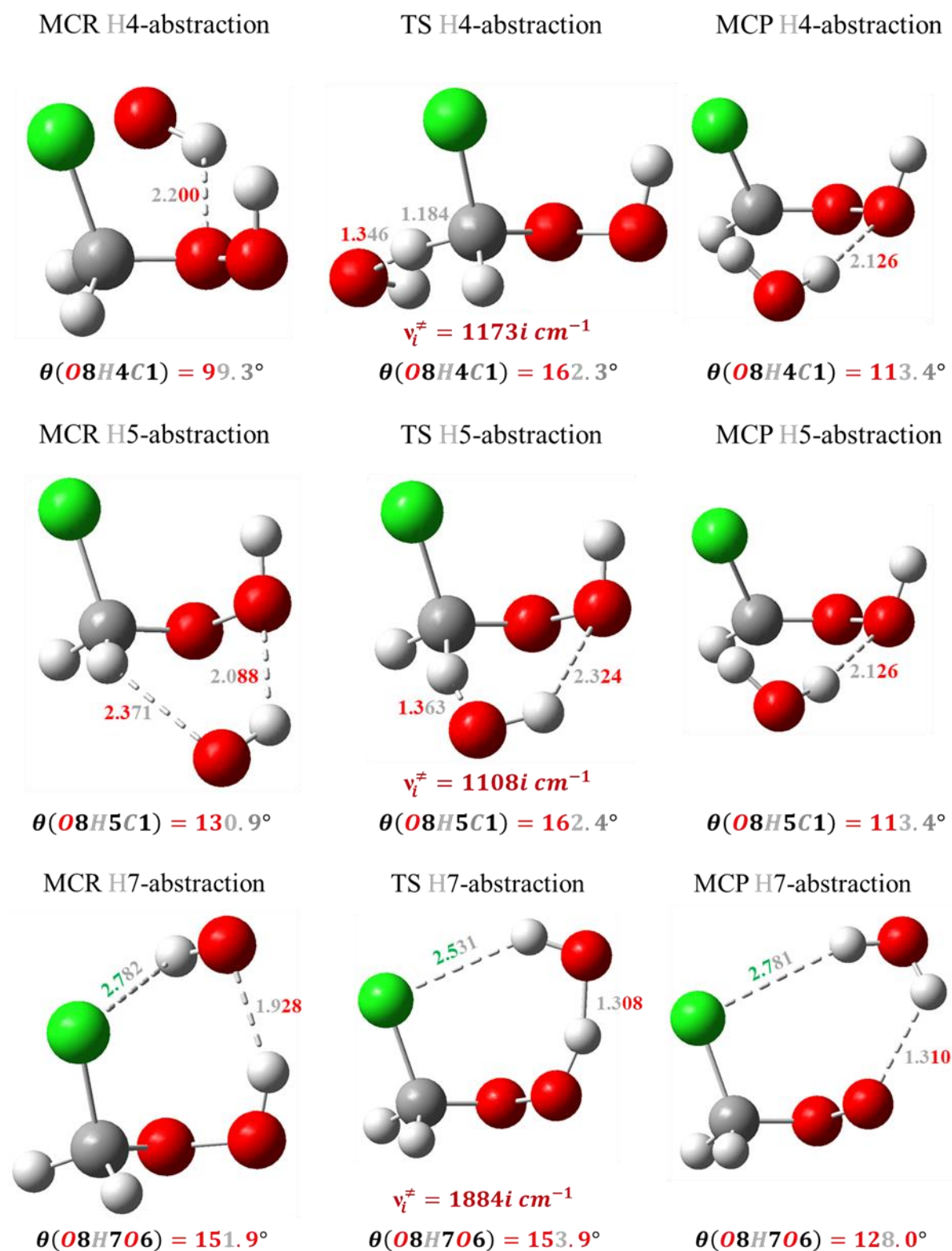
Figure II-11: *Schematic representation of the TS and molecular complexes involved in H-abstraction pathways of the reaction OH + CH$_2$ClOOH optimized at the M06-2X/6-311+G(2df,2p) levels of theory. The main geometrical parameters and intermolecular distances (represented by dashed lines) are only shown. The distances are in Angstroms, and bond angles are in degrees. Imaginary vibrational frequencies of the TSs are added.*
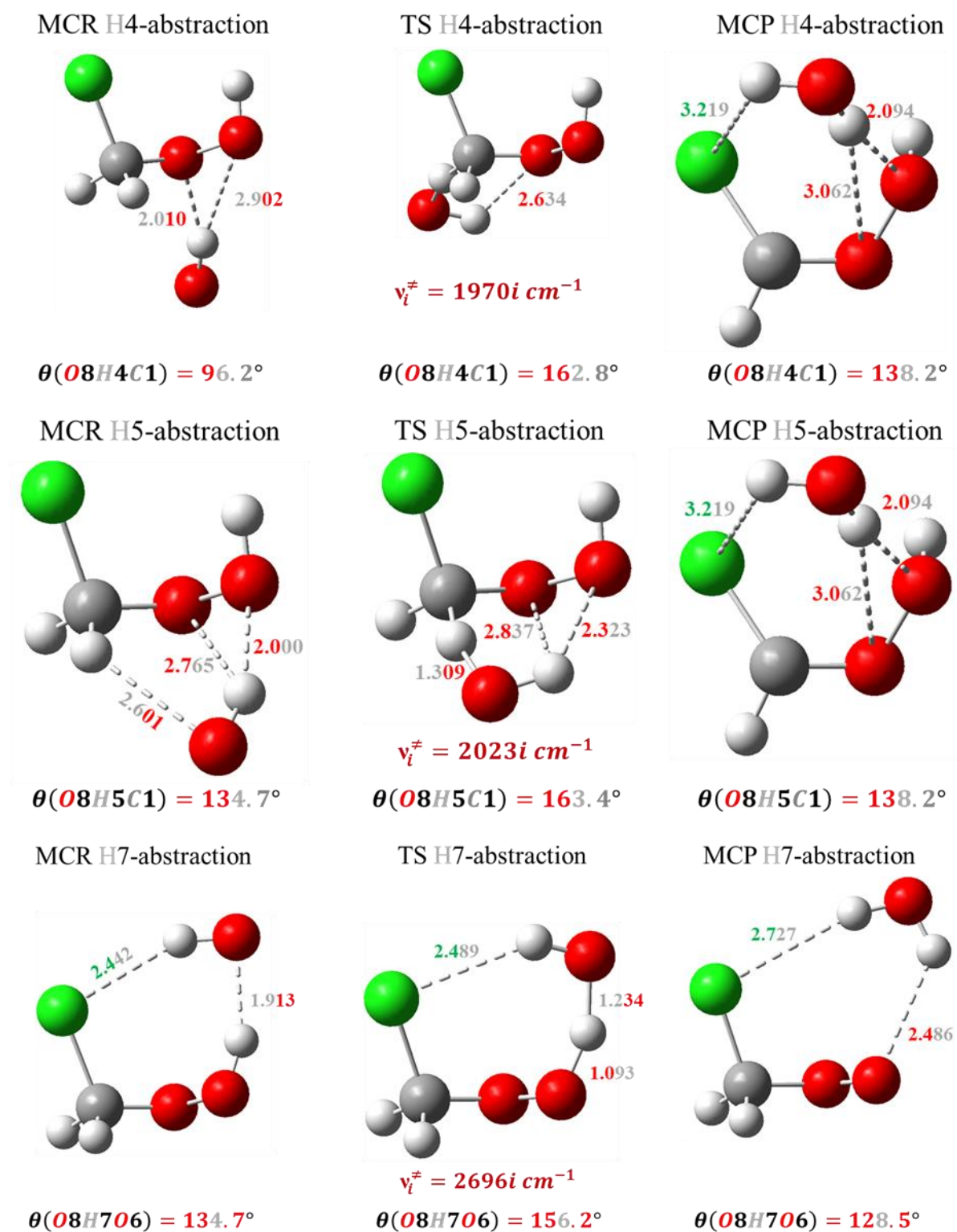
Figure II-12: *Schematic representation of the TS and molecular complexes involved in H-abstraction pathways of the reaction OH + CH₂ClOOH optimized at the MP2/aug-cc-pV(T+d)Z levels of theory. The main geometrical parameters and intermolecular distances (represented by dashed lines) are only shown. The distances are in Angstroms, and bond angles are in degrees. Imaginary vibrational frequencies of the TSs are added.*

Table II-6: *Essential structural parameters for H-abstraction pathways of the reaction OH + CH$_2$ClOOH calculated at the M06-2X/6-311+G(2df,2p) and MP2/aug-cc-pV(T+d)Z levels of theory.*

	r_{H-C} (Å)	r_{O-H} (Å)	θ_{OHC} (°)	$\nu_i^{\neq}$ (cm^{-1})	L
H-abstraction pathways					
H4 - abstraction					
M06-2X/6-311+G(2df,2p)					
MCR-H4	1.085	2.644	99.3		
TS-H4	1.184	1.346	162.3	*1173i*	**0.255**
MCP-H4	2.768	0.961	113.4		
MP2/aug-cc-pV(T+d)Z					
MCR-H4	1.086	3.407	96.2		
TS-H4	1.193	1.303	162.8	*1970i*	**0.315**
MCP-H4	3.012	0.965	138.2		
H5 – abstraction					
M06-2X/6-311+G(2df,2p)					
MCR-H5	1.086	2.371	130.9		
TS-H5	1.178	1.363	162.4	*1108i*	**0.228**
MCP-H5	2.768	0.961	113.4		
MP2/aug-cc-pV(T+d)Z					
MCR-H5	1.086	2.601	134.7		
TS-H5	1.192	1.309	163.4	*2023i*	**0.306**
MCP-H5	3.012	0.965	138.2		
H7 – abstraction					
M06-2X/6-311+G(2df,2p)					
MCR-H7	0.974	1.928	151.9		
TS-H7	1.063	1.308	153.9	*1884i*	**0.274**
MCP-H7	2.310	0.960	128.0		
MP2/aug-cc-pV(T+d)Z					
MCR-H7	0.979	1.913	159.5		
TS-H7	1.093	1.234	156.2	*2696i*	**0.359**
MCP-H7	2.486	0.962	128.5		

For the three hydrogen abstraction pathway, the L parameter is higher when calculated at the MP2/aug-cc-pV(T+d)Z level of theory. In general, computations at the MP2 level often lead to an overestimation of the vibrational adiabatic barrier, resulting in an overestimation of the L-parameter compared to M06-2X level. This discrepancy may be due to the inherent limitations of the MP2 in capturing high-order electron correlation effects, which might be better accounted in the M06-2X level. Moreover, the DFT computations (M06-2X) are usually more consistent and precise. They have computationally lower costs, requiring less time and faster convergence compared to ab-initio calculations (MP2).

II.5.4.2.   Study of the Cl-abstraction pathway

The optimized structures of the molecular complexes and TS of the most favorable pathway of Cl-abstraction at the M06-2X/6-311+G(2df,2p) and MP2/aug-cc-pV(T+d)Z levels of theory are shown in **Figure II-13**.

Within the Cl-abstraction pathway, the bond between C and Cl in CH_2ClOOH lengthens as the reaction progresses from reactants to products, indicating a breakage of the C-Cl bond. Simultaneously, the Cl atom is abstracted by the OH radical, resulting in the formation of a new bond between the oxygen atom (O) of the OH radical and the Cl atom.
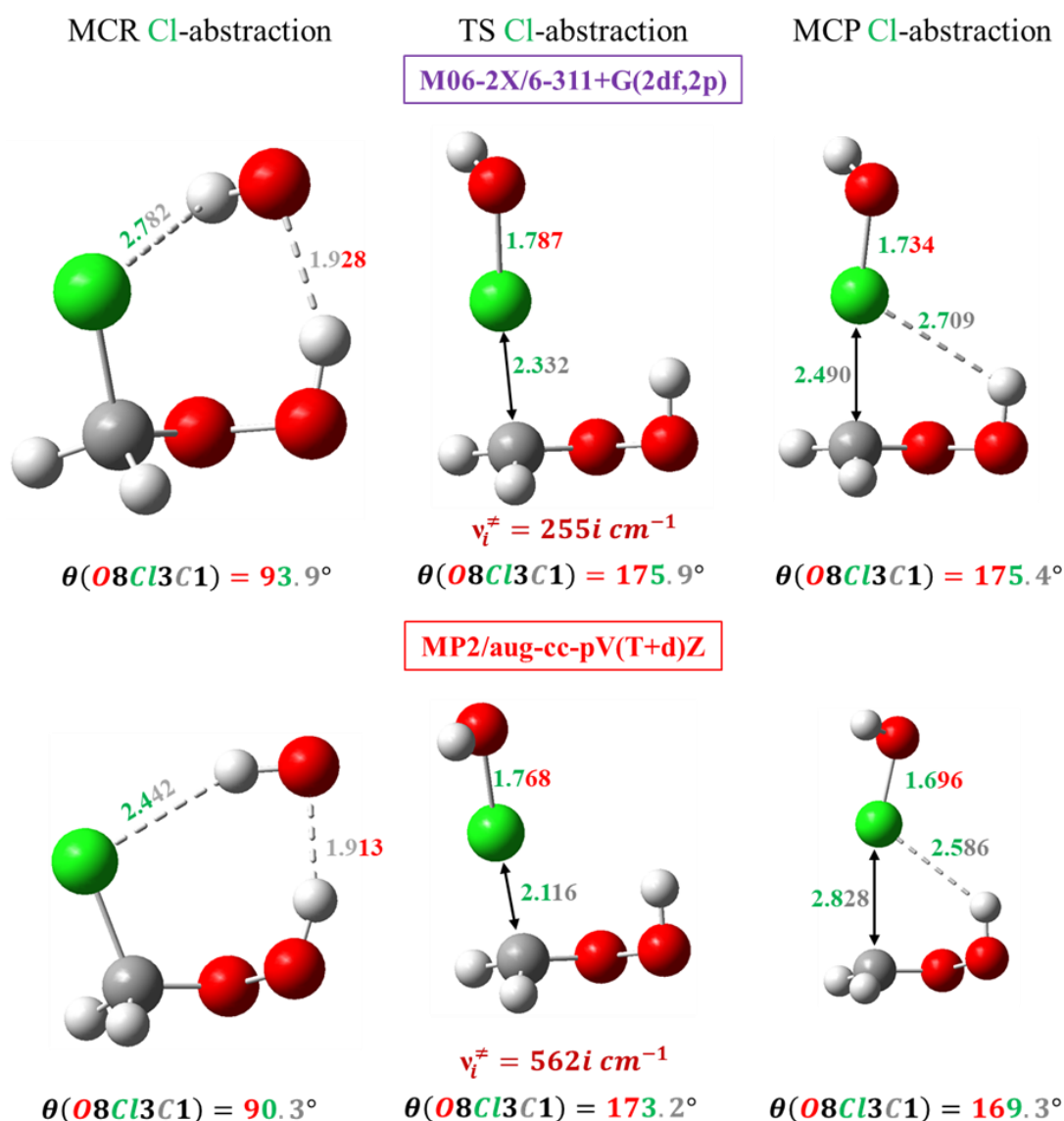
Figure II-13: *Schematic representation of the TS and molecular complexes involved in Cl-abstraction pathway of the reaction OH + CH_2ClOOH optimized at the M06-2X/6-311+G(2df,2p) and MP2/aug-cc-pV(T+d)Z levels of theory. The main geometrical parameters and intermolecular distances (represented by dashed lines) are only shown. The distances are in Angstroms, and bond angles are in degrees. Imaginary vibrational frequencies of the TSs are added.*

Table II-7 summarizes the geometrical properties, imaginary frequencies, and L parameter for the intermediate species involved in Cl-abstraction pathway of the reaction OH + CH_2ClOOH.

Table II-7: *Essential structural parameters for Cl-abstraction pathway of the reaction OH + CH_2ClOOH calculated at the M06-2X/6-311+G(2df,2p) and MP2/aug-cc-pV(T+d)Z levels of theory.*

	r_{Cl-C} (Å)	r_{O-Cl} (Å)	θ_{OClC} (°)	$\nu_i^{\neq}$ (cm^{-1})	L
Cl-abstraction pathway					
M06-2X/6-311+G(2df,2p)					
MCR-Cl	1.815	2.872	93.9		
TS-Cl	2.332	1.787	175.9	*255i*	**4.768**
MCP-Cl	2.490	1.734	175.4		
MP2/aug-cc-pV(T+d)Z					
MCR-Cl	1.812	3.306	90.3		
TS-Cl	2.116	1.768	173.2	*562i*	**4.148**
MCP-Cl	2.828	1.696	169.3		

Furthermore, the TS of the Cl-abstraction pathway has a product-like structure at both levels of theory. This is evident in ***Figure II-13*** where the TS structure shows the detachment of Cl from CH_2ClOOH and the formation of HOCl. Additionally, the value of the L parameter, which is much greater than 1 (4.768 and 4.148 at M06-2X/6-311+G(2df,2p) and MP2/aug-cc-pV(T+d)Z levels, respectively), confirms this result.

II.5.4.3.   Study of the OH-abstraction pathway

Similarly, ***Figure II-14*** illustrates the optimized structures of the molecular complexes and TS for the preferred pathway of Cl-abstraction, as determined by the M06-2X/6-311+G(2df,2p) and MP2/aug-cc-pV(T+d)Z levels of theory.

In this pathway, the OH group of CH_2ClOOH is abstracted by the OH radical. The O-O bond in CH_2ClOOH undergoes stretching, while the distance between the oxygen atoms of the OH radical and the OH group of CH_2ClOOH decreases. Eventually, the reaction ends up in the creation of a H_2O_2 molecule and CH_2ClO radical.

The geometrical properties, imaginary frequencies, and L parameter for the intermediate species involved in OH-abstraction pathway of the OH + CH_2ClOOH reaction at the two levels of theory are summarized in ***Table II-8***.

Furthermore, the small L parameter values calculated at the M06-2X/6-311+G(2df,2p) and MP2/aug-cc-pV(T+d)Z levels of theory, 0.351 and 0.953, respectively, indicate that the TSs possess a reactant-like character.

MCR OH-abstraction   TS OH-abstraction   MCP OH-abstraction

M06-2X/6-311+G(2df,2p)

$\nu_i^{\neq} = 1173i\ cm^{-1}$

$\theta(O8O6O2) = 82.6°$ $\theta(O8O6O2) = 156.2°$ $\theta(O8O6O2) = 124.1°$

MP2/aug-cc-pV(T+d)Z

$\nu_i^{\neq} = 1380i\ cm^{-1}$

$\theta(O8O6O2) = 87.6°$ $\theta(O8O6O2) = 162.5°$ $\theta(O8O6O2) = 100.5°$
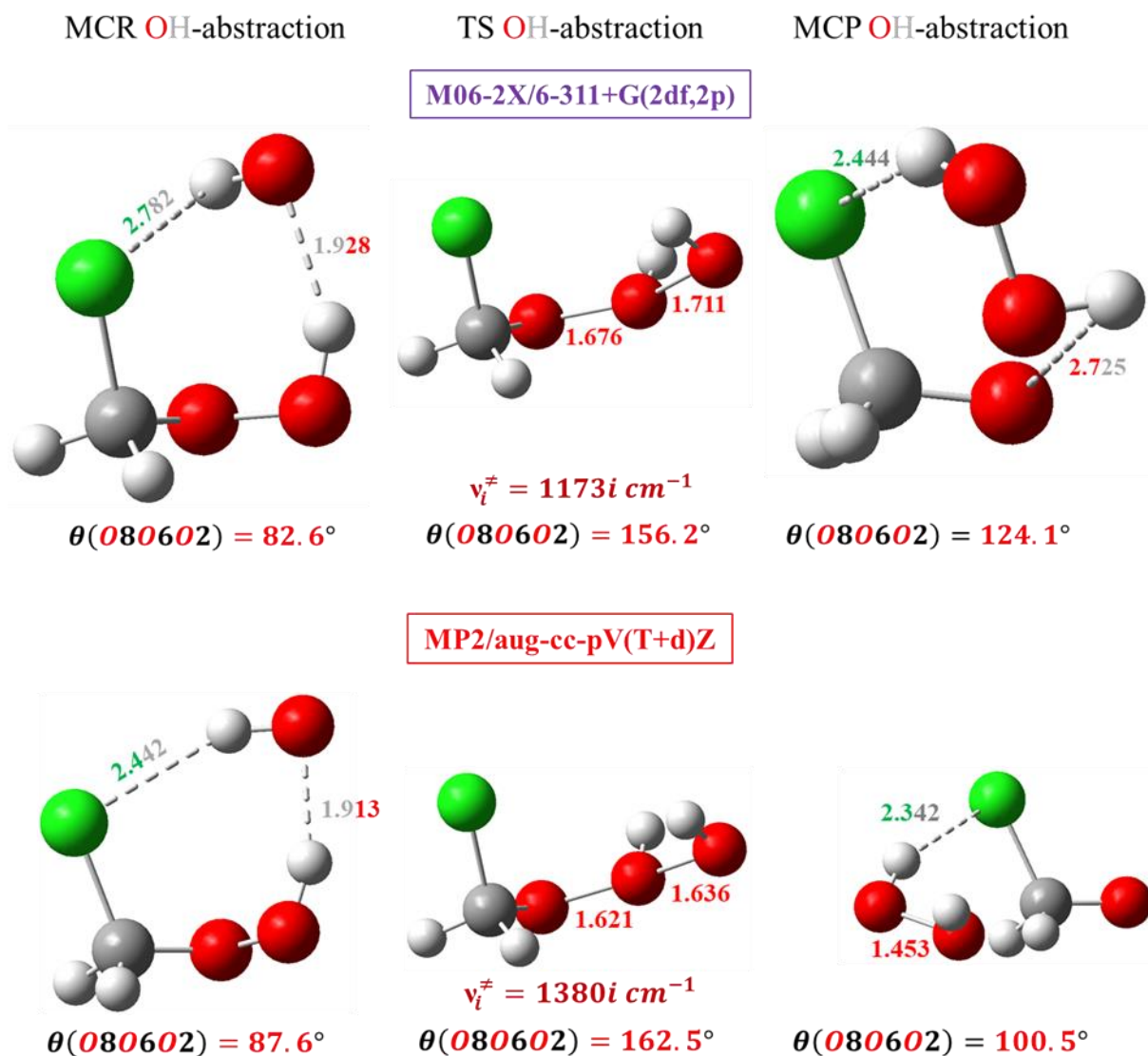
Figure II-14: Schematic representation of the TS and molecular complexes involved in OH-abstraction pathway of the reaction OH + CH₂ClOOH optimized at the M06-2X/6-311+G(2df,2p) and MP2/aug-cc-pV(T+d)Z levels of theory. The main geometrical parameters and intermolecular distances (represented by dashed lines) are only shown. The distances are in Angstroms, and bond angles are in degrees. Imaginary vibrational frequencies of the TSs are added.

Table II-8: *Essential structural parameters for OH-abstraction pathway of the reaction OH + CH$_2$ClOOH calculated at the M06-2X/6-311+G(2df,2p) and MP2/aug-cc-pV(T+d)Z levels of theory.*

	OH-abstraction pathway				
	r$_{O-O}$ (Å)	**r$_{O-O}$ (Å)**	**θ$_{OOO}$ (°)**	**$\nu_i^{\neq}$ (cm^{-1})**	**L**
	M06-2X/6-311+G(2df,2p)				
MCR-OH	1.415	2.824	82.6		
TS-OH	1.711	1.711	156.2	*1155i*	**0.351**
MCP-OH	2.769	1.418	124.1		
	MP2/aug-cc-pV(T+d)Z				
MCR-OH	1.450	2.851	87.6		
TS-OH	1.621	1.636	162.5	*1380i*	**0.953**
MCP-OH	4.186	1.453	100.5		

Similarly, as in the case of hydrogen abstraction (***II.5.4.1***), the L parameter is higher when calculated at the MP2/aug-cc-pV(T+d)Z level of theory. At this level, computations often lead to an overestimation of the vibrational adiabatic barrier, resulting in an overestimation of the L-parameter compared to M06-2X level.

II.5.5. Vibrational frequencies, rotational constants, point group, and electronic state for intermediate species

Table II-9 lists the number of symmetries, electronic states, rotational constants, scaled vibrational frequencies, scaled ZPE, and standard molar entropy for all the intermediate species involved in the reaction pathways discussed in ***section II.5.4***. SOC values are also added to the MCRs and TSs. When the OH group is detached in the TS and MCR structures, the SOC value is equivalent to that of an isolated OH group (-0.836 kJ mol^{-1}). However, the SOC value becomes null when the OH group is attached. All these parameters are computed at the two levels of theory, M06-2X/6-311+G(2df,2p) and MP2/aug-cc-pV(T+d)Z.

Table II-9: *Symmetry number, point group, electronic state, rotational constants; scaled vibrational frequencies, ZPE, spin-orbit coupling (SOC), and standard molar entropy of the intermediate species through the different pathways of the reaction OH + CH$_2$ClOOH calculated at two different levels of theory and compared to literature.*

Species	Symmetry number	Point group & electronic state	Rotational constants (GHz)	Scaled vibrational frequencies (cm^{-1})	Scaled ZPE (kJ mol^{-1})	SOC (kJ mol^{-1})	S°$_{298K}$ (J mol^{-1} K^{-1})
				H4 - abstraction			
				M06-2X/6-311+G(2df,2p)			
MCR (H4-abs)	1	C$_1$ - ^{2}A	3.70, 2.88, 1.90	50, 71, 143, 165, 281, 309, 364, 390, 516, 713, 934, 1018, 1120, 1269, 1321, 1427, 1445, 3075, 3158, 3687, 3719	150.59	-0.836	371.21
TS (H4-abs)	1	C$_1$ - ^{2}A	3.54, 2.86, 1.66	***1173i***, 77, 101, 140, 157, 277, 370, 467, 660, 769, 821, 960, 1014, 1126, 1276, 1291, 1410, 1502, 3097, 3730, 3740	137.49	-0.836	358.69
MCP (H4-abs)	1	C$_1$ - ^{2}A	3.44, 2.78, 1.81	47, 74, 127, 143, 166, 197, 235, 336, 401, 501, 580 ,778, 924, 1128, 1282, 1389, 1614, 3188, 3755, 3800, 3898	142.50		390.95
				MP2/aug-cc-pV(T+d)Z			
MCR (H4-abs)	1	C$_1$ - ^{2}A	6.62, 1.50, 1.27	15, 21, 116, 149, 256, 334, 360, 441, 492, 721, 831, 967, 1028, 1223, 1292, 1323, 1411, 2982, 30, 3535, 3553	144.26	-0.836	395.73
TS (H4-abs)	1	C$_1$ - ^{2}A	3.56, 2.88, 1.67	***1970i***, 82, 100, 139, 157, 262, 348, 445, 598, 763, 800, 932, 1010, 1139, 1222, 1254, 1322, 1439, 3017, 3554, 3590	132.63	0.000	359.88
MCP (H4-abs)	1	C$_1$ - ^{2}A	3.54, 2.52, 1.65	26, 46, 113, 125, 179, 183, 228, 330, 419, 533, 687, 835, 997, 1248, 1275, 1336, 1563, 3089, 3565, 3608, 3733	144.26		400.91
				H5 – abstraction			
				M06-2X/6-311+G(2df,2p)			
MCR (H5-abs)	1	C$_1$ - ^{2}A	5.78, 1.83, 1.64	27, 79, 110, 156, 242, 290, 329, 384, 519, 719, 934, 1008, 1120, 1268, 1319, 1404, 1453, 3066, 3149, 3696, 3724	149.51	-0.836	380.94
TS (H5-abs)	1	C$_1$ - ^{2}A	4.18, 2.72, 2.02	***1108i***, 92, 144, 178, 237, 336, 357, 507, 738, 780, 870, 933, 1011, 1131, 1268, 1292, 1413, 1492, 3116, 3716, 3729	139.62	-0.836	345.90
MCP (H5-abs)	1	C$_1$ - ^{2}A	3.44, 2.78, 1.81	47, 74, 127, 143, 166, 197, 235, 336, 401, 501, 580 ,778, 924, 1128, 1282, 1389, 1614, 3188, 3755, 3800, 3898	146.89		390.95

Table II-9: *Continued.*

Species	Symmetry number	Point group & electronic state	Rotational constants (GHz)	Scaled vibrational frequencies (cm^{-1})	Scaled ZPE (kJ mol^{-1})	SOC (kJ mol^{-1})	S°$_{298K}$ (J mol^{-1} K^{-1})
				H5 – abstraction			
				MP2/aug-cc-pV(T+d)Z			
MCR (H5-abs)	1	C$_1$ - ^{2}A	5.33, 1.77, 1.57	25, 72, 135, 171, 270, 320, 363, 468, 490, 709, 828, 969, 1028, 1223, 1292, 1315, 1419, 2984, 3068, 3531, 3538	144.86	-0.836	378.23
TS (H5-abs)	1	C$_1$ - ^{2}A	4.14, 2.75, 2.03	*2023i*, 101, 128, 167, 234, 324, 338, 478, 679, 746, 819, 886, 982, 1075, 1200, 1245, 1322, 1424, 3027, 3542, 3576	133.32	0.000	348.54
MCP (H5-abs)	1	C$_1$ - ^{2}A	3.54, 2.52, 1.65	26, 46, 113, 125, 179, 183, 228, 330, 419, 533, 687, 835, 997, 1248, 1275, 1336, 1563, 3089, 3565, 3608, 3733	144.26		400.91
				H7 – abstraction			
				M06-2X/6-311+G(2df,2p)			
MCR (H7-abs)	1	C$_1$ - ^{2}A	3.87, 3.28, 1.99	68, 106, 142, 234, 270, 351, 390, 513, 553, 695, 935, 1017, 1138, 1267, 1319, 1450, 1481, 3072, 3153, 3615, 3708	152.39	-0.836	359.01
TS (H7-abs)	1	C$_1$ - ^{2}A	4.66, 2.81, 1.87	*1884i*, 94, 127, 185, 256, 377, 423, 519, 700, 731, 952, 1027, 1134, 1268, 1321, 1390, 1450, 1490, 3077, 3159, 3710	139.89	0.000	343.56
MCP (H7-abs)	1	C$_1$ - ^{2}A	4.00, 2.49, 1.67	24, 49, 105, 108, 142, 201, 253, 347, 539, 756, 945, 1017, 1208, 1279, 1335, 1452, 1612, 3084, 3168, 3806, 3898	151.51		398.09
				MP2/aug-cc-pV(T+d)Z			
MCR (H7-abs)	1	C$_1$ - ^{2}A	3.79, 2.89, 1.81	63, 118, 129, 206, 213, 350, 393, 479, 587, 675, 830, 969, 1064, 1223, 1286, 1392, 1410, 2986, 3071, 3413, 3521	145.82	-0.836	363.95
TS (H7-abs)	1	C$_1$ - ^{2}A	4.74, 2.83, 1.91	*2696i*, 100, 127, 184, 303, 342, 459, 499, 694, 802, 888, 979, 1056, 1229, 1253, 1297, 1410, 2705, 2986, 3072, 3605	143.50	0.000	342.06
MCP (H7-abs)	1	C$_1$ - ^{2}A	3.70, 2.51, 1.61	31, 46, 83, 103, 147, 162, 224, 336, 510, 743, 888, 987, 1145, 1222, 1301, 1417, 1562, 3000, 3089, 3631, 3739	145.74		402.49

Table II-9: *Continued.*

Species	Symmetry number	Point group & electronic state	Rotational constants (GHz)	Scaled vibrational frequencies (cm^{-1})	Scaled ZPE (kJ mol^{-1})	SOC (kJ mol^{-1})	S°$_{298K}$ (J mol^{-1} K^{-1})
				Cl - abstraction pathway			
				M06-2X/6-311+G(2df,2p)			
MCR (Cl-abs)	1	C$_1$ - ^{2}A	3.87, 3.28, 1.99	68, 105, 142, 234, 272, 350, 389, 512, 552, 694, 935, 1017, 1139, 1268, 1318, 1450, 1481, 3072, 3153, 3616, 3709	152.39	-0.836	358.96
TS (Cl-abs)	1	C$_1$ - ^{2}A	9.67, 1.67, 1.49	***255i***, 74, 96, 122, 162, 241, 328, 443, 512, 601, 928, 960, 1122, 1189, 1244, 1433, 1444, 3096, 3234, 3686, 3794	147.79	0.000	362.44
MCP (Cl-abs)	1	C$_1$ - ^{2}A	9.44, 1.63, 1.45	63, 82, 90, 118, 158, 212, 329, 470, 526, 583, 835, 954, 1181, 1184, 1238, 1426, 1439, 3103, 3243, 3697, 3798	147.91		381.90
				MP2/aug-cc-pV(T+d)Z			
MCR (Cl-abs)	1	C$_1$ - ^{2}A	3.79, 2.89, 1.81	63, 118, 129, 206, 215, 350, 392, 479, 587, 675, 830, 969, 1065, 1223, 1286, 1392, 1410, 2986, 3072, 3414, 3512	145.82	-0.836	363.91
TS (Cl-abs)	1	C$_1$ - ^{2}A	9.77, 1.81, 1.60	***562i***, 63, 92, 124, 134, 279, 319, 459, 513, 701, 845, 1034, 1066, 1126, 1184, 1345, 1403, 3004, 3135, 3499, 3620	143.22	0.000	363.49
MCP (Cl-abs)	1	C$_1$ - ^{2}A	8.69, 1.55, 1.38	65, 73, 85, 90, 131, 138, 297, 361, 473, 727, 800, 854, 1115, 1168, 1192, 1335, 1389, 3027, 3173, 3524, 3595	141.23		393.43
				OH – abstraction			
				M06-2X/6-311+G(2df,2p)			
MCR (OH-abs)	1	C$_1$ - ^{2}A	3.87, 3.28, 1.99	68, 106, 142, 235, 271, 350, 390, 513, 553, 695, 935, 1017, 1138, 1268, 1319, 1450, 1481, 3072, 3153, 3616, 3709	152.39	-0.836	358.99
TS (OH-abs)	1	C$_1$ - ^{2}A	5.38, 2.32, 1.72	***1155i***, 44, 64, 175, 232, 327, 422, 472, 500, 687, 952, 1017, 1108, 1200, 1263, 1308, 1433, 3033, 3100, 3743, 3790	148.74	0.000	360.28
MCP (OH-abs)	1	C$_1$ - ^{2}A	4.56, 2.37, 1.65	25, 76, 101, 132, 173, 239, 390, 491, 667 ,717, 1031, 1079, 1119, 1268, 1328, 1376, 1453, 2955, 3013, 3722, 3774	150.28		383.94
				MP2/aug-cc-pV(T+d)Z			
MCR (OH-abs)	1	C$_1$ - ^{2}A	3.79, 2.89, 1.81	63, 118, 129, 206, 214, 350, 392, 479, 586, 675, 830, 969, 1065, 1223, 1286, 1392, 1410, 2986, 3072, 3415, 3512	145.82	-0.836	363.97
TS (OH-abs)	1	C$_1$ - ^{2}A	5.88, 2.21, 1.72	***1380i***, 47, 89, 165, 259, 341, 421, 457, 492, 681, 936, 1039, 1062, 1187, 1275, 1289, 1406, 2954, 3028, 3612, 3631	145.75	0.000	356.64
MCP (OH-abs)	1	C$_1$ - ^{2}A	5.11, 1.81, 1.43	23, 58, 84, 120, 143, 205, 380, 509, 657, 712, 884, 1057, 1069, 1250, 1280, 1331, 1372, 2885, 2956, 3502, 3606	144.07		393.53

II.5.6. Reaction profile and energetics

In this section, all energies are computed at the dual levels of theory: M06-2X/6-311+G(3df,3pd)//M06-2X/6-311+G(2df,2p) and DK-CCSD(T)/ANO-RCC-VQZP//MP2/aug-cc-pV(T+d)Z. For simplicity, they will be referred to by M06-2X/6-311+G(3df,3pd) and DK-CCSD(T)/ANO-RCC-VQZP, respectively.

II.5.6.1. H-abstraction pathways

The energy profile of the H4-abstraction pathway is depicted in **Figure II-15**, and has been analysed at 0 K at two different levels of theory: M06-2X/6-311+G(3df,3pd) and DK-CCSD(T)/ANO-RCC-VQZP. The figure shows the formation of pre-reactive molecular complexes (MCRs) stabilized by 14.6 and 12.0 kJ mol^{-1} with respect to the reactants, respectively. The energy barriers of 8.1 and 17.2 kJ mol^{-1} are observed, followed by the formation of metastable intermediate molecular complexes (MCPs), which are stabilized by 95.8 and 86.0 kJ mol^{-1}.
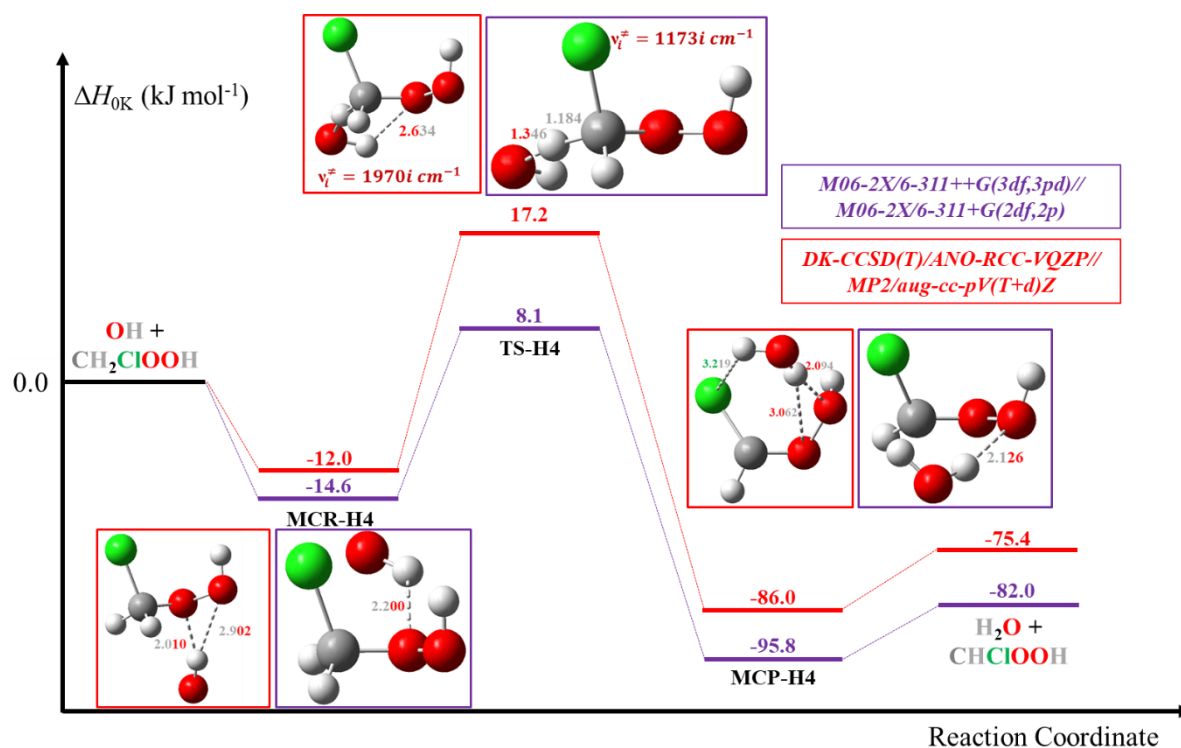
Figure II-15: *Energy profile at 0 K of the H4-abstraction pathway calculated at M06-2X/6-311++G(3df,3p) (in purple) and DK-CCSD(T)/ANO-RCC-VQZP (in red) levels of theory.*

Figure II-16 illustrates the energy profile at 0 K for the pathway where OH abstracts H5 from CH_2ClOOH. MCRs are formed and stabilized by 16.8 and 14.0 kJ mol^{-1} with respect to the reactants at M06-2X and DK-CCSD(T), respectively. The reactants then encounter a very low barrier (-0.8 kJ mol^{-1}) at M06-2X and a higher one (8.2 kJ mol^{-1}) at DK-CCSD(T). After crossing the barriers, the MCRs are converted into MCPs, which are stabilized and later decompose to produce the final products.
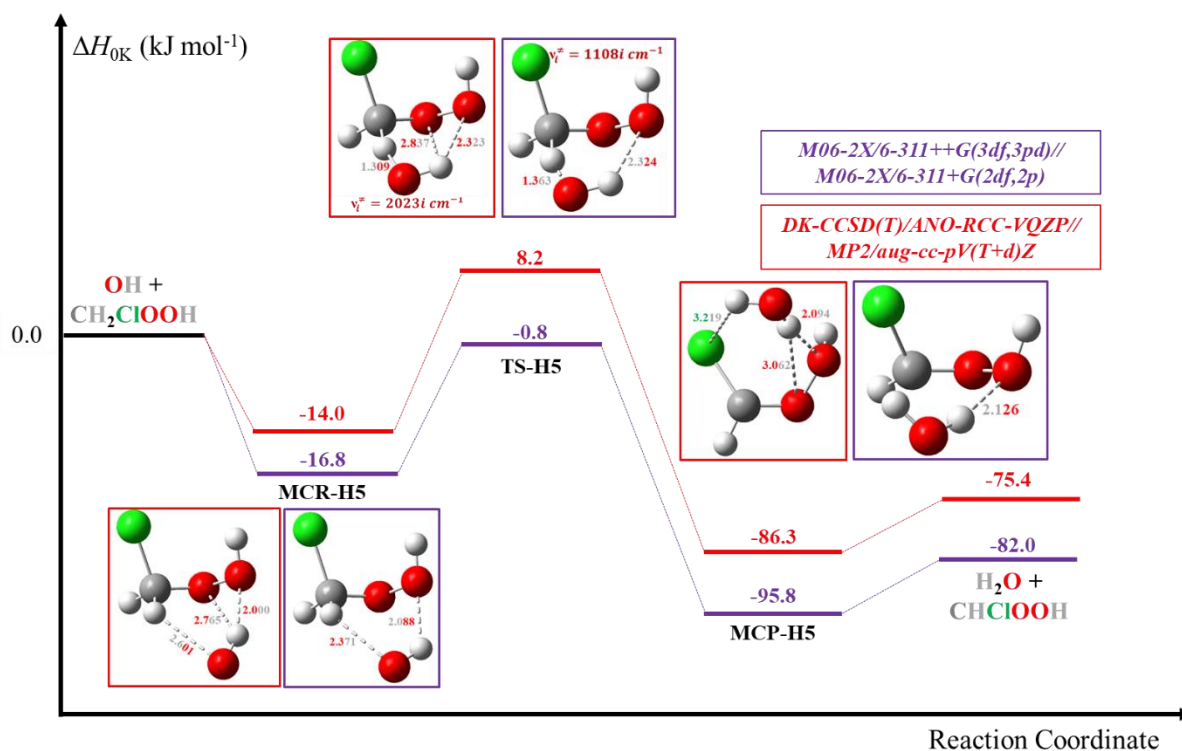
Figure II-16: *Energy profile at 0 K of the H5-abstraction pathway calculated at M06-2X/6-311++G(3df,3p) (in purple) and DK-CCSD(T)/ANO-RCC-VQZP (in red) levels of theory.*

Moreover, ***Figure II-17*** demonstrates the energy profile at 0 K of the H7-abstraction pathway. At both M06-2X and DK-CCSD(T) levels of theory, MCRs are formed and stabilized by 27.1 and 23.1 kJ mol^{-1}, respectively. The energy barrier at 0 K for M06-2X is very low (-8.6 kJ mol^{-1}) compared to that obtained at DK-CCSD(T) level (57.9 kJ mol^{-1}). The MCPs formed have similar structures and energies (124.7 and 117.2 kJ mol^{-1}).

To recap, detaching OH from CH$_2$ClOOH results in the addition of the SOC value of OH to the potential energy of MCR and TS. This holds true for MCR-H4, MCR-H5, and MCR-H7 at both levels of theory, as well as for TS-H4 and TS-H5 at the M06-2X level of theory.
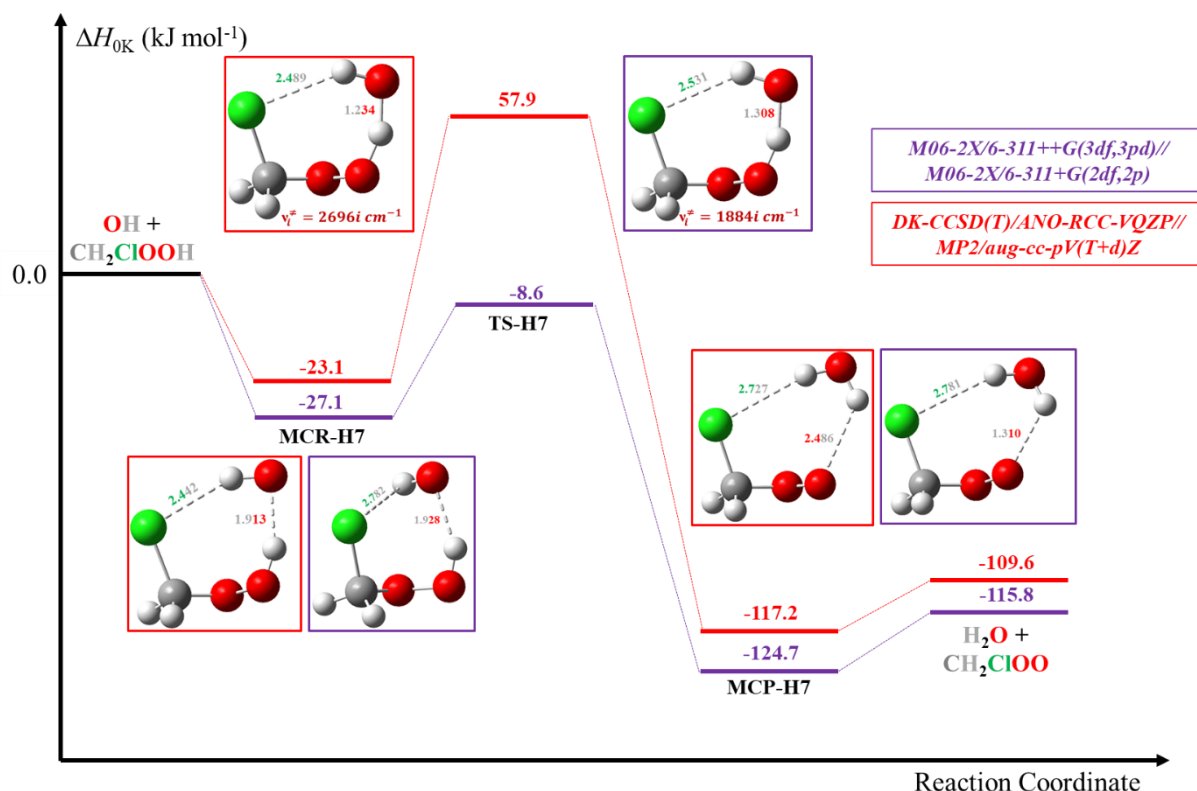
Figure II-17: *Energy profile at 0 K of the H7-abstraction pathway calculated at M06-2X/6-311++G(3df,3p) (in purple) and DK-CCSD(T)/ANO-RCC-VQZP (in red) levels of theory.*

The energy profiles of the abstraction of H4, H5, and H7 depicted in ***Figure II-15***, ***Figure II-16***, and ***Figure II-17*** respectively, demonstrate that although the intermediates optimized at the MP2/aug-cc-pV(T+d)Z level exhibit more intermolecular interactions (represented by dashed bonds in the intermediates' structures), they are more stable at the M06-2X/6-311+G(2df,2p) level.

In the case of these three pathways, the energy barrier is observed to be higher at the DK-CCSD(T) level of theory compared to the M06-2X level. However, the TS structures for these pathways at the different levels (as presented in ***Table II-6***) exhibit almost identical geometric parameters.

Furthermore, the energy profiles depicted in ***Figure II-15***, ***Figure II-16***, and ***Figure II-17*** demonstrate that the abstraction of H4, H5, and H7, respectively, lead to exothermic reactions. This outcome is consistent with Hammond's (1955) postulate, which proposes that a reactants-like TS structure (as indicated by the value of L parameter for the abstraction of the three hydrogens that are much less than 1 (***Table II-6***) and in ***section II.5.4.1***) corresponds to an exothermic reaction.

In ***Figure II-15*** and ***Figure II-16***, the energy profiles of H4 and H5 abstractions demonstrate that the MCPs and products of these two pathways align together at the two levels of theory. This observation can be attributed to the similarity in environment for the two hydrogens, as they both belong to the same methyl group.

II.5.6.2.   Cl-abstraction pathway

In **Figure II-18**, the energy profile of the Cl-abstraction pathway at 0 K is illustrated. The formation and stabilization of MCRs are evident at both M06-2X and DK-CCSD(T) levels of theory, with energy values of 27.1 and 23.1 kJ mol^{-1}, respectively. However, the energy barrier at 0 K is remarkably high at both levels, measuring 106.6 and 116.6 kJ mol^{-1} for M06-2X and DK-CCSD(T) respectively. The formed MCPs exhibit similar structures and energies, at 103.8 and 112.2 kJ mol^{-1}. Unlike previous energy profiles, the MCPs and products (HOCl and CH$_2$OOH) are less stable than the reactants, with even lower stability than the TS, conventionally the intermediate with the highest energy in a reaction profile. Therefore, the Cl-abstraction pathway is not of atmospheric importance and does not occur simultaneously. This hypothesis will later be substantiated through the study of each pathway's kinetic parameters.

Furthermore, as demonstrated by the energy profile, the Cl-abstraction pathway is endothermic at both levels of theory. This aligns with Hammond's (1955) postulate , which suggests that an endothermic reaction results from a product-like TS.
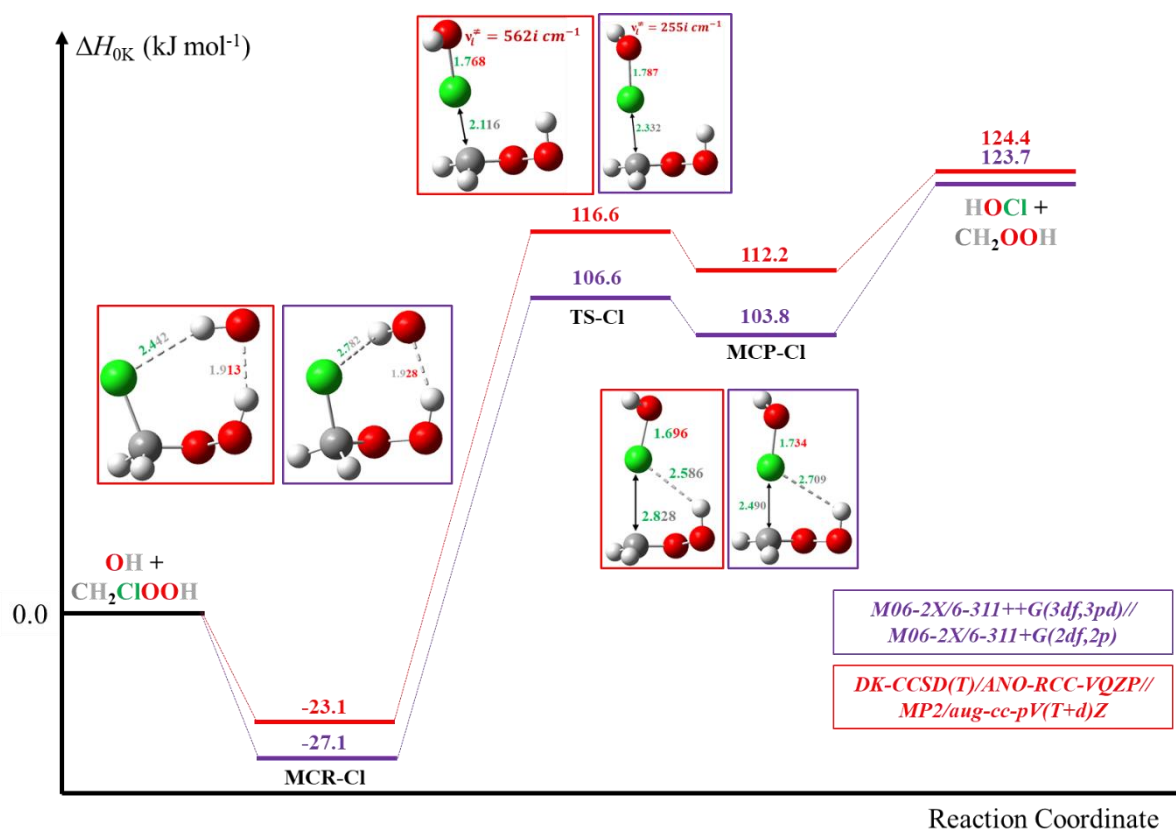
Figure II-18: *Energy profile at 0 K of the Cl-abstraction pathway calculated at M06-2X/6-311++G(3df,3p) (in purple) and DK-CCSD(T)/ANO-RCC-VQZP (in red) levels of theory.*

II.5.6.3. *OH-abstraction pathway*

Figure II-19 depicts the energy profile at 0 K for the pathway in which the OH radical abstracts the OH group from CH_2ClOOH. MCRs are formed and stabilized at M06-2X and DK-CCSD(T) levels, with respect to the reactants, by 27.1 and 23.1 kJ mol^{-1}, respectively. The reactants then encounter a significant energy barrier with very similar values, measuring 99.1 and 100.8 kJ mol^{-1} at M06-2X and DK-CCSD(T) respectively. Once the high barriers are overcome, MCPs are formed and stabilized by intermolecular interactions, which later decompose to produce the final products H_2O_2 and CH_2ClOOH.

Once more, in accordance with Hammond's (1955) postulate, this pathway is exothermic and results from a reactant-like TS.
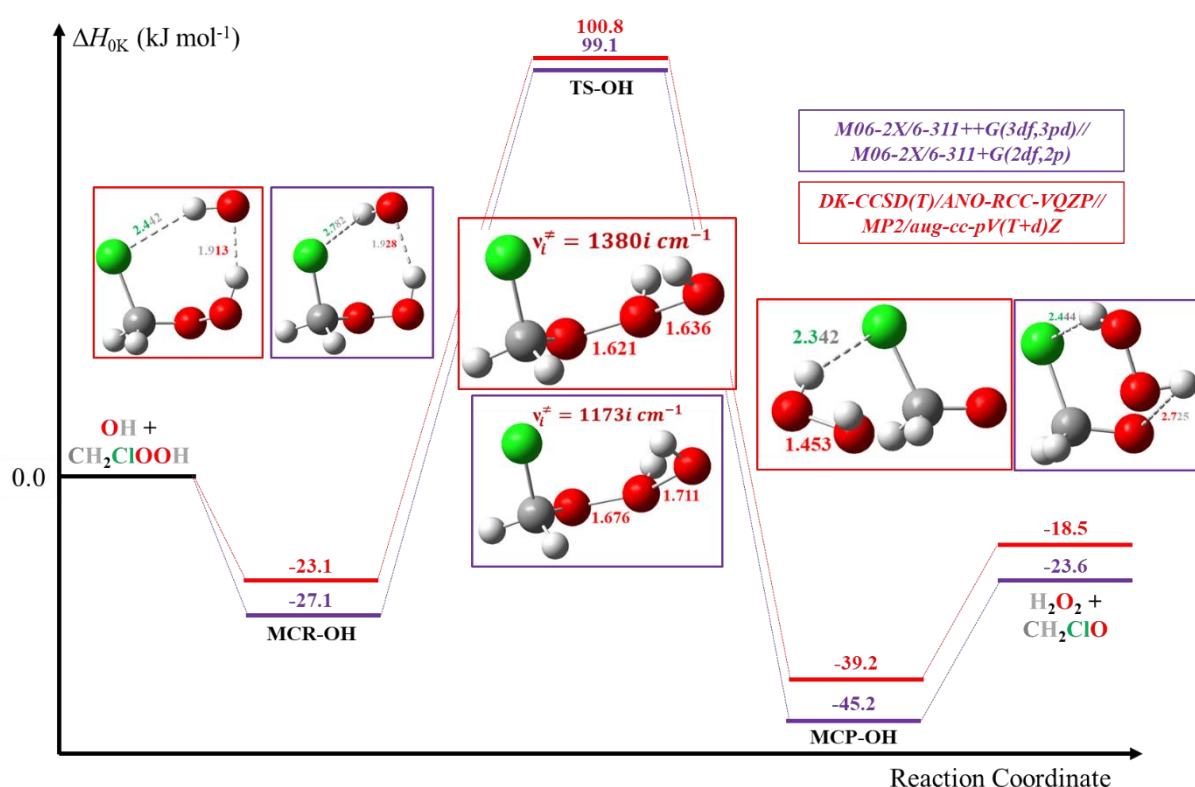
Figure II-19: *Energy profile at 0 K of the OH-abstraction pathway calculated at M06-2X/6-311++G(3df,3p) (in purple) and DK-CCSD(T)/ANO-RCC-VQZP (in red) levels of theory.*

In ***Table II-10***, ΔH_{0K} represents the energy of the MCR with respect to that of the reactants. E_0 is the vibrationally adiabatic barrier (E_0), which is equal to the energy of the TS with respect to that of the MCR. Moreover, $\Delta_r H_{0K}$ is the reaction enthalpy (ΔH_{0K}) representing the energy of the products with respect to that of the reactants. These energies are illustrated in ***Figure II-15*** through ***Figure II-19*** for the pathways involved in the reaction between OH and CH_2ClOOH.

Table II-10: *Vibrationally adiabatic barrier and reaction enthalpy calculated in kJ mol^{-1} at 0 K for each of the reaction pathways between OH and CH$_2$ClOOH calculated at M06-2X/6-311++G(3df,3p) and DK-CCSD(T)/ANO-RCC-VQZP levels of theory.*

	M06-2X/6-311++G(3df,3p)			*DK-CCSD(T)/ANO-RCC-VQZP*		
	ΔH_{0K}	E_0	$\Delta_r H_{0K}$	ΔH_{0K}	E_0	$\Delta_r H_{0K}$
H4-abstraction	-14.6	22.7	-82.0	−12.0	29.2	-75.4
H5-abstraction	-16.8	16.0	-82.0	−13.9	22.1	-75.4
H7-abstraction	-27.1	18.5	-115.8	−23.1	81.0	-109.6
Cl-abstraction	-27.1	106.6	123.6	−23.1	139.7	124.4
OH-abstraction	-27.1	126.2	-23.6	−23.1	123.9	-18.5

It is worth noting that, at both levels of theory, the MCR of the H7-, Cl-, OH-abstraction pathways possess identical geometrical characteristics, vibrational features, and energy levels.

II.5.7. Kinetic parameters

We performed calculations on the temperature-dependent rate constants for all the abstraction pathways using the indirect mechanism, incorporating two corrections (ZPE and SOC) at the two dual levels of theory: M06-2X/6-311+G(3df,3pd)//M06-2X/6-311+G(2df,2p) and DK-CCSD(T)/ANO-RCC-VQZP//MP2/aug-cc-pV(T+d)Z. For simplicity, they will be referred to by M06-2X/6-311+G(3df,3pd) and DK-CCSD(T)/ANO-RCC-VQZP, respectively.

Our rate constant values are calculated at the atmospheric temperature range 253 – 323 K with an interval of 5 K. Kinetic parameters are calculated for all the reaction pathways, firstly, without considering any tunnelling effects (**Table A.II-1**), secondly, adding Wigner tunnelling effects (**Table A.II-2**), and lastly, adding Eckart's tunnelling factor (**Table A.II-3**).

Table A.II-1, **Table A.II-2**, and **Table A.II-3** confirm that the Cl- and OH-abstraction pathways are insignificant throughout the entire temperature range studied, as supported by the energetic analysis presented in **Table II-10**. Both pathways have high vibrationally adiabatic barriers (exceeding 100 kJ mol^{-1}), requiring significant energy input to overcome. Additionally, the Cl-abstraction pathway results in the formation of less stable products (HOCl and CH$_2$OOH) compared to the reactants, making it an endothermic reaction. Consequently, these two pathways are deemed unfavourable at both levels of theory across the temperature range studied. Therefore, the effect of these two pathways on the overall rate constants of the reaction between OH radicals and CH$_2$ClOOH can be neglected.

Figure II-20, **Figure II-21**, and **Figure II-22** illustrate the relationship between the rate constant of the H4-, H5-, and H7-abstraction pathways and 1000/T, respectively, using both the M06-2X/6-311++G(3df,3p) and DK-CCSD(T)/ANO-RCC-VQZP levels of theory. The rate constants were computed without considering tunnelling, as well as with considering Wigner and Eckart tunnelling.
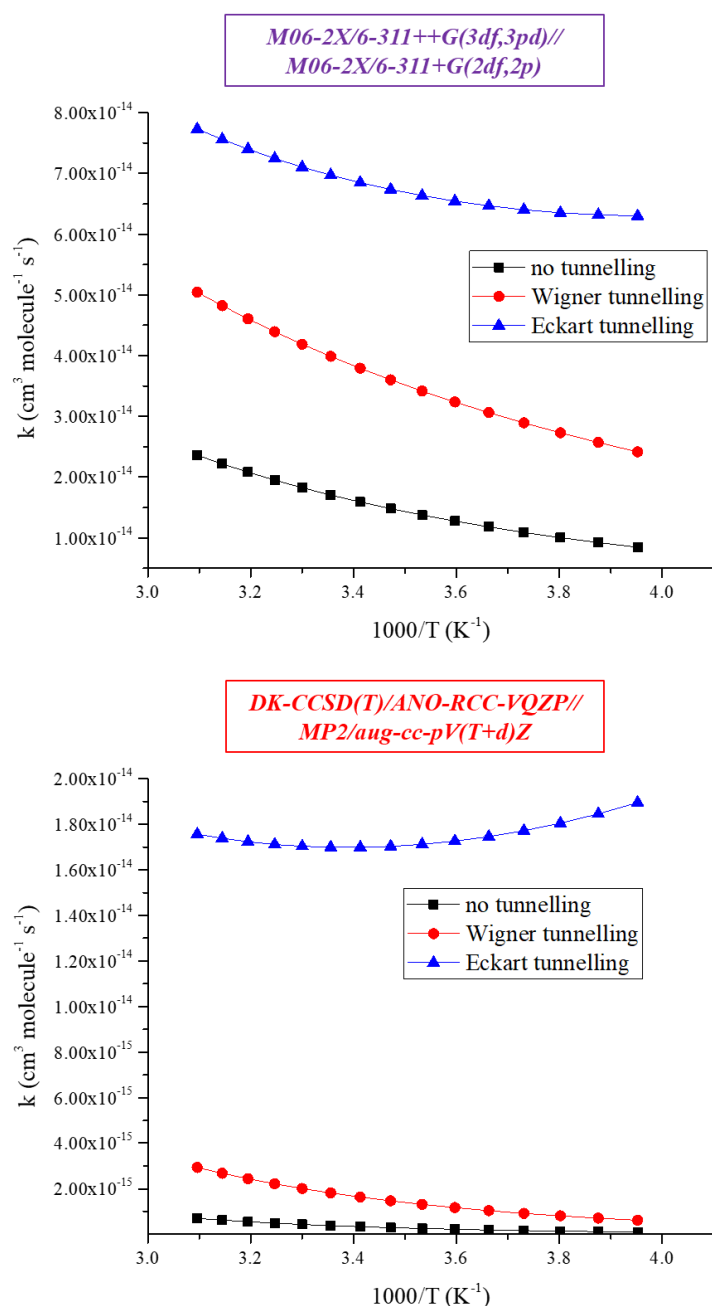
Figure II-20: *Evolution of the rate constant of H4-abstraction pathway as a function of 1000/T without and with considering the tunnelling effect.*

Compared to the DK-CCSD(T) level, the rate constants for these pathways are higher when calculated using the M06-2X level of theory. The rate constants are the lowest when no tunnelling is considered, and the highest values are obtained when Eckart tunnelling is considered, at both levels of theory. Additionally, the impact of tunnelling corrections is more significant at the DK-CCSD(T) level, while the M06-2X level exhibits very similar results between the three plots (with and without tunnelling). Therefore, for purposes of simplicity and clarity, rate constants for H-abstraction pathways considering Eckart tunnelling effects are only accounted in the following.
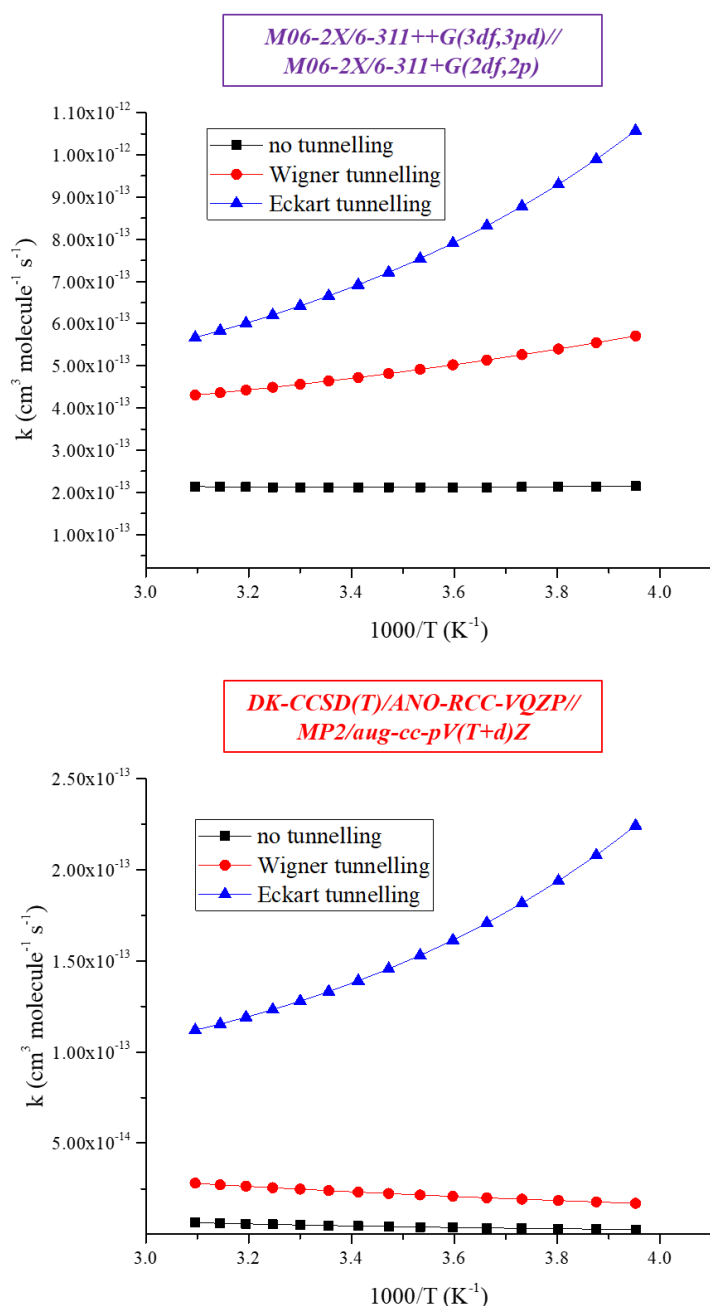
Figure II-21: *Evolution of the rate constant of H5-abstraction pathway as a function of 1000/T without and with considering the tunnelling effect.*

At the same time, for an abstraction reaction between OH radicals and CH_2ClOOH, we can define the branching ratio $f_X^{CH_2ClOOH}$ (in %) as the ratio of the rate constant for the X-abstraction pathway to the overall rate constant of the reaction. The branching ratios of all the pathways calculated using the indirect mechanism at the two levels of theory and considering Eckart tunnelling effects over the temperature range 253 - 323 K are gathered in **Table II-11**.

There are significant differences in the calculated branching ratios when comparing the two levels of theory, indicating that the most favourable pathways vary depending on the level of theory employed. At the DK-CCSD(T)/ANO-RCC-VQZP level of theory, H5-abstraction is

the dominant channel. Conversely, at the M06-2X/6-311++G(3df,3p) level of theory, H7-abstraction is the most favourable pathway.
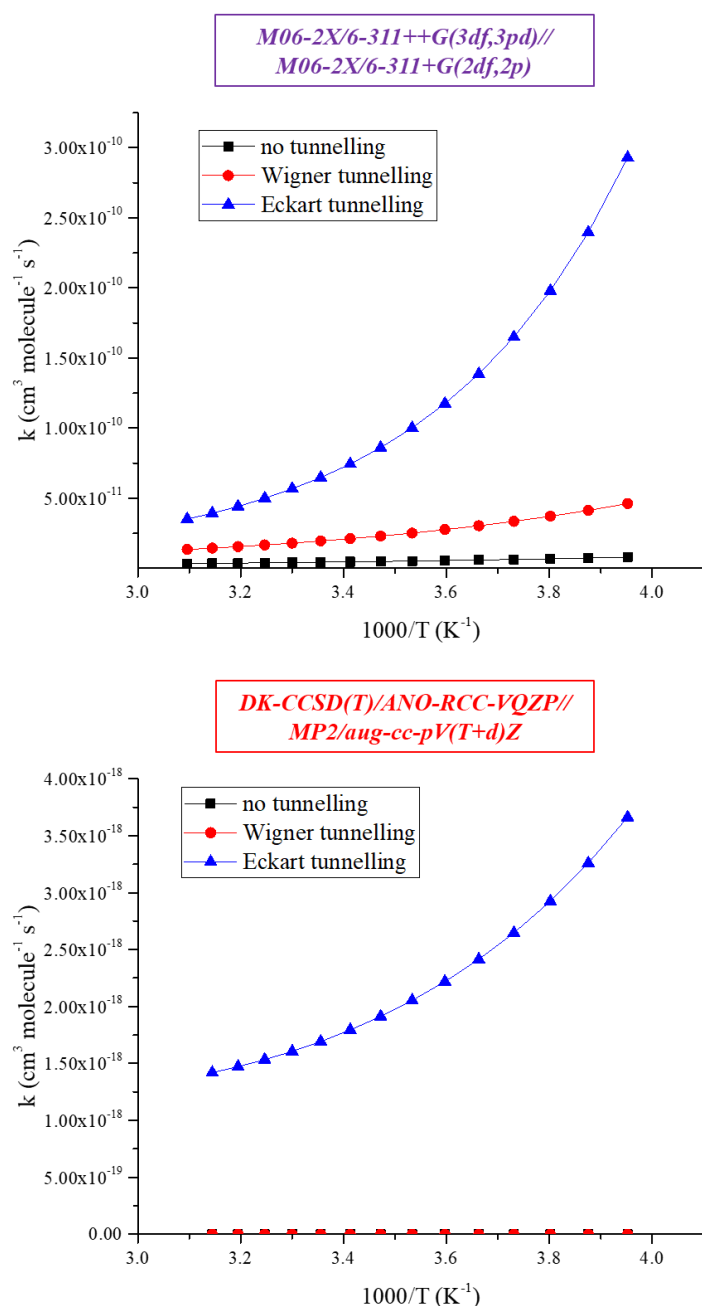
Figure II-22: *Evolution of the rate constant of H7-abstraction pathway as a function of 1000/T without and with considering the tunnelling effect.*

Table II-11 highlights that at the M06-2X/6-311++G(3df,3p) level of theory, there is a slight increase in $f_{H4}^{CH_2ClOOH}$ and $f_{H5}^{CH_2ClOOH}$ with increasing temperature, while $f_{H7}^{CH_2ClOOH}$ decreases slightly. Therefore, it is possible for H4 and H5 abstraction pathways to dominate outside of the tropospheric temperature range, such as in combustion processes. However, in the atmospheric temperature range studied (253 - 323 K), the H7-abstraction pathway remains the most favourable.

Chapter II. Molecular modelling

On the other hand, at the DK-CCSD(T)/ANO-RCC-VQZP level of theory, an increase in temperature results in an increase in $f_{H4}^{CH_2ClOOH}$ and decrease in $f_{H5}^{CH_2ClOOH}$. However, since both H4 and H5-abstraction pathways lead to the same products with identical energies, there might be significant impact of rate constants and branching ratios.

Table II-11: *Branching ratios $f_X^{CH_2ClOOH}$ in % calculated at the M06-2X/6-311++G(3df,3p) and DK-CCSD(T)/ANO-RCC-VQZP levels of theory for H-abstraction pathways using the indirect mechanism and Eckart tunnelling corrections.*

Temperature (K)							
$f_{H4}^{CH_2ClOOH}$							
253	**258**	**263**	**268**	**273**	**278**	**283**	**288**
0.02	0.03	0.03	0.04	0.05	0.06	0.07	0.08
7.79	*8.15*	*8.51*	*8.89*	*9.27*	*9.66*	*10.06*	*10.47*
293	**298**	**303**	**308**	**313**	**318**	**323**	
0.09	0.11	0.12	0.14	0.16	0.19	0.22	
10.89	*11.31*	*11.74*	*12.19*	*12.63*	*13.09*	*13.55*	
$f_{H5}^{CH_2ClOOH}$							
253	**258**	**263**	**268**	**273**	**278**	**283**	**288**
0.36	0.41	0.47	0.53	0.60	0.67	0.75	0.83
92.20	*91.85*	*91.48*	*91.11*	*90.73*	*90.34*	*89.94*	*89.53*
293	**298**	**303**	**308**	**313**	**318**	**323**	
0.92	1.02	1.12	1.23	1.34	1.46	1.58	
89.11	*88.69*	*88.25*	*87.81*	*87.36*	*86.91*	*86.44*	
$f_{H7}^{CH_2ClOOH}$							
253	**258**	**263**	**268**	**273**	**278**	**283**	**288**
99.62	99.56	99.50	99.43	99.36	99.28	99.19	99.09
0.00	*0.00*	*0.00*	*0.00*	*0.00*	*0.00*	*0.00*	*0.00*
293	**298**	**303**	**308**	**313**	**318**	**323**	
98.99	98.88	98.76	98.63	98.50	98.35	98.20	
0.00	*0.00*	*0.00*	*0.00*	*0.00*	*0.00*	*0.00*	
Values in Italics are computed at the DK-CCSD(T)/ANO-RCC-VQZP level of theory.							

By examining the curves presented in ***Figure II-20***, ***Figure II-21***, and ***Figure II-22***, with and without tunnelling effects, along with the summarized rate constant values in ***Table A.II-1***, ***Table A.II-2***, and ***Table A.II-3*** and branching ratios in ***Table II-11***, it is evident that the rate constant for the H7-abstraction pathway differs significantly between the M06-2X and DK-CCSD(T) levels of theory. Specifically, the H7-abstraction pathway is the most favourable at the M06-2X level, with branching ratios exceeding 90% within the selected temperature range, while it is negligible at the DK-CCSD(T) level, with branching ratios being zero.

The problem of multireference is the cause of the underestimation of the rate constant values for the H7-abstraction pathway during single-point energy calculations at the DK-CCSD(T)/ANO-RCC-VQZP level of theory for geometries optimized at the MP2/aug-cc-pV(T+d)Z level. The multireference problem arises when a system has more than one dominant configuration or electronic state that cannot be accurately represented by a single determinant (Shamasundar *et al.*, 2011). In such cases, a multireference wave function must be used, which

involves a linear combination of multiple determinants. However, calculating multireference wave functions is computationally intensive, and the resulting energies can be unreliable due to their strong dependence on the choice of reference configuration. This leads to errors in the calculation of rate constants, which depend primarily on the resulting energies.

The problem of multireference is addressed by T_1 diagnostic (T_1diag) values, which is obtained by diagonalization of the matrix of the second-order perturbation theory coefficients that describe the coupling between the reference and excited configurations. Specifically, T_1diag parameter represents the magnitude of the highest eigenvalue of this matrix. A value of T_1diag (0.2) is observed only during the calculations of the energetics of H7-abstraction pathway at the dual level DK-CCSD(T)/ANO-RCC-VQZP//MP2/aug-cc-pV(T+d)Z. This is higher than 0.045 which is an indication of the multireference problem (for open-shell system). The application of Complete Active Space second-order Perturbation Theory (CASPT2) can be used for accurate calculations (Gao *et al.*, 2018).

The kinetic parameters of the reaction of CH_2ClOOH with Cl atoms can be compared with the results of our study to figure out whether our work is reliable or not. Wallington *et al.* (1996) suggested that the reaction proceeds in two different pathways:

$$Cl + CH_2ClOOH \rightarrow CH_2ClOO + HCl \qquad (a)$$

$$Cl + CH_2ClOOH \rightarrow CHClOOH + HCl \qquad (b)$$
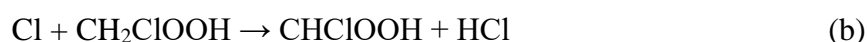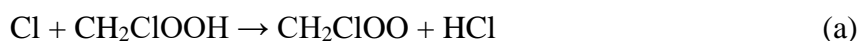
According to this study; the reaction proceeds 100% via pathway (a) and the rate constant is 5.90×10^{-13} cm^3 molecule^{-1} s^{-1}. It is also efficient to compare our results to those obtained when studying the reaction of OH radicals with CH_3OOH. Burkholder *et al.* (2020) suggested that the reaction can occur via two important channels as taken from Vaghjiani and Ravishankara (1989):

$$Cl + CH_3OOH \rightarrow CH_3OO + HCl \qquad \text{branching ratio} = 0.7$$

$$Cl + CH_3OOH \rightarrow CH_2OOH + HCl \qquad \text{branching ratio} = 0.3$$

Therefore, we can say that our reaction between OH and CH_2ClOOH proceeds via two major channels at 298 K similar to the previous studies (Vaghjiani and Ravishankara, 1989; Wallington *et al.*, 1996):

$$OH + CH_2ClOOH \rightarrow CH_2ClOO + H_2O \qquad (a)$$

$$OH + CH_2ClOOH \rightarrow CHClOOH + H_2O \qquad (b)$$
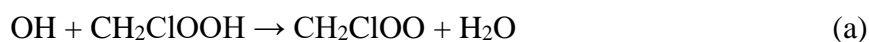
However, it is seen that the abstraction of H7 (hydrogen of the hydroxyl group of CH_2ClOOH) is more likely to occur. Then, the kinetic parameters computed at the M06-2X/6-311++G(3df,3pd)//M06-2X/6-311+G(2df,2p) dual level are more accurate than those calculated at DK-CCSD(T)/ANO-RCC-VQZP//MP2/aug-cc-pV(T+d)Z level of theory.

II.6. Conclusion and perspectives

This work allows the calculation of the thermokinetic parameters of the reaction of CH_2ClOOH with the tropospheric most abundant oxidant, OH radicals. This reaction proceeds through different channels including H-, Cl-, and OH-abstractions.

The geometries of all species and intermediates were optimized at M06-2X/6-311+G(2df,2p) and MP2/aug-cc-pV(T+d)Z levels of theory (MP2/aug-cc-pVTZ for species not containing Cl). Single point energies at the M06-2X/6-311++G(3df,3pd) and DK-CCSD(T)/ANO-RCC-VQZP are used to construct the energy profiles and to compute the kinetic parameters.

At the two levels of theory, it was found that Cl- and OH-abstraction pathways are insignificant. DK-CCSD(T)/ANO-RCC-VQZP revealed a multireference problem while calculating the energies of H7-abtraction pathway.

Additionally, the findings of this study can fill the gaps in the development of the mechanism used to investigate the reactivity of Cl in 0D and 3D atmospheric models, and enhance our understanding of Cl tropospheric chemistry.

To complete this work, it will be necessary to perform the CASPT2 calculations for H7-abstraction pathway in order to overcome the problem of multireference. It is also good to compute the rate constants using the CVT/SCT calculations, and to use polyrate to calculate the kinetic parameters.

Moreover, this study could be extended to multiple chlorinated species ($CHCl_2OOH$ and CCl_3OOH) and to different CH_2XOOH where X is a halogen (F, Br, or I). This enables the studying of the impact of the nature of the halogen on the reactivity of halogenated methyl hydroperoxide with OH radicals, and that of the degree of halogenation.

Chapter III.   Kinetic modelling

Tropospheric chlorine chemistry encompasses the investigation of reactions involving chlorine-containing species within the Earth's lower atmosphere, known as the troposphere. Previous studies (Badia *et al*., 2019; Eastham *et al*., 2014; Fan and Li, 2022; Hoffmann *et al*., 2019; Hossaini *et al*., 2016; Li *et al*., 2016; Ordóñez *et al*., 2012; Peng *et al*., 2021; Sander *et al*., 2011; Sander and Crutzen, 1996; Sherwen *et al*., 2016; Singh and Kasting, 1988; Sommariva and von Glasow, 2012; Soni *et al*., 2023) have explored this area, and are all listed in ***Table III-1***. For each of the mentioned studies, the total number of reactions of chlorinated species is listed which are further classified in details based on the nature of the species (organic or inorganic), and the type of the reaction (thermal or photolysis).

Table III-1: *Previous studies involving atmospheric models of gas-phase chlorine chemistry, with their total number of reactions of chlorinated species whether organic or inorganic species, thermal or photolysis reactions.*

Reference	Total number of reactions	Thermal		Photolysis		Model
		organic	inorganic	organic	inorganic	
(Singh and Kasting, 1988)	60	23	25	5	7	1D
(Sander and Crutzen, 1996)	17	5	7	0	5	0D (MOCCA)
(Sander *et al.*, 2011)	44	13	20	3	8	3D (CAABA /MECCA-3.0)
(Sommariva and von Glasow, 2012)	67	18	43	0	6	1D (MISTRA)
(Ordóñez *et al.*, 2012)	42	5	27	3	7	3D (CAM-Chem)
(Eastham *et al.*, 2014)	45	6	29	3	7	3D (GEOS-Chem)
(Sherwen *et al.*, 2016)	55	18	26	2	9	3D (GEOS-Chem)
(Hossaini *et al.*, 2016)	95	67	16	5	7	3D (TOMCAT)
(Li *et al.*, 2016)	24	14	6	1	3	3D (WRF-Chem)
(Badia *et al.*, 2019)	38	12	20	0	6	3D (WRF-Chem)
(Hoffmann *et al.*, 2019)	602	489	38	66	9	3D (SPACCIM)
(Peng *et al.*, 2021)	281	233	38	0	9	0D
(Fan and Li, 2022)	30	18	6	1	5	3D (CMAQ)
(Soni *et al.*, 2023)	35	21	9	0	5	0D (CAABA /MECCA v4.4.2)
Our work	**388**	**199**	**152**	**18**	**19**	**0D**

In general, atmospheric models simulate many processes including solar radiation, meteorology, emissions, transport, chemical processing, and removal processes of gases and aerosols (Jacobson, 2005). They aim to better understand the air composition and its physical and chemical properties. Concurrently, models are always improved in order to be used for forecasting and prediction of air quality and climate at the small and the large scales, respectively.

Chapter III. Kinetic modelling

Models representing the tropospheric Cl chemistry considered the multiphase halogen chemistry in both gaseous and aqueous phases. The other halogens (Br and I) were usually included (except in the models of Hossaini *et al*. (2016); Li *et al*. (2016); Singh and Kasting (1988); Soni *et al*. (2023)). Some of these studies focused on specific environments (marine atmosphere (Badia *et al*., 2019; Singh and Kasting, 1988), marine boundary layer (Sander and Crutzen, 1996), tropical Atlantic Ocean (Sommariva and von Glasow, 2012), southern China (Li *et al*., 2016), urban and maritime coastal area (Hoffmann *et al*., 2019), urban environments with different concentrations of NO$_x$: New Delhi (India) and Leicester (United Kingdom) (Soni *et al*., 2023)). Moreover, some models extended to the stratospheric chemistry (Badia *et al*., 2019; Eastham *et al*., 2014; Hossaini *et al*., 2016; Ordóñez *et al*., 2012; Sander *et al*., 2011; Singh and Kasting, 1988). Specifically, Peng *et al*. (2021) focused on winter time air quality in northern China, while Fan and Li (2022) studied the summer time chemistry in eastern Asia. Then, it can be seen that the mechanisms of the various research projects are simplified for targeted application (troposphere/ stratosphere, specific area (coastal, continental, ... etc), specific period of time).

However, in this study, the objective is to create a complete gas-phase mechanism for a global representation. It includes all reactions involving organic and inorganic chlorinated species in the troposphere. To achieve this, we have reviewed all available scientific data on the subject. The developed mechanism is then studied by the ASTEC (Accident Source Term Evaluation Code), a 0D box model developed by the French Nuclear Safety Institute (IRSN) (Chatelard *et al*., 2016).

Our team's selection of this model was the result of a long-standing partnership with the IRSN that began in 2009. Throughout the years, several PhD students, including Julien Trincal and Camille Fortin, have made significant contributions to this collaboration. Between 2012 and 2015, Julien Trincal's research focused on modelling the behaviour of iodine in the atmosphere. He used 0D simulations of the ATSEC model to investigate the discrepancy between measurements and simulations following the Fukushima accident (Trincal, 2015). Additionally, Camille Fortin's research from 2016 to 2019 was centred around atmospheric iodine reactivity. She worked on updating the mechanism of atmospheric iodine chemistry that was integrated into the ASTEC model (Fortin, 2019). She also performed the 3D simulations using Polair3D. The theses and ensuing studies of both students have led to the publication of numerous scientific papers on their topics (Canneaux *et al*., 2010; Fortin *et al*., 2019, 2018; Hammaecher *et al*., 2011; Khanniche *et al*., 2016; Sobanska *et al*., 2021; Taamalli *et al*., 2020; Xerri *et al*., 2012).

In this chapter, a detailed description of this model will be given in *section III.1*, then the input data and simulation setup will be summarized in *section III.2*. The model scenarios will be described in *section III.3*. All the results will be analysed in *section III.4*.

Chapter III. Kinetic modelling

III.1. ASTEC model design

The ASTEC code is a computer code that aims to simulate an entire severe accident sequence in a nuclear water-cooled reactor (Chatelard *et al.*, 2016). The code is designed to model the progression of an accident from the initiating event to the release of radioactive materials outside the containment.

Moreover, the ASTEC code is a comprehensive tool that includes modules for simulating various phenomena that occur during a severe accident, as shown in *Figure III-1*, such as core degradation, fission product release, transport through the reactor coolant system and containment, and interaction with the environment. The code is constantly being improved and updated to incorporate new knowledge and meet the evolving needs of the nuclear industry.
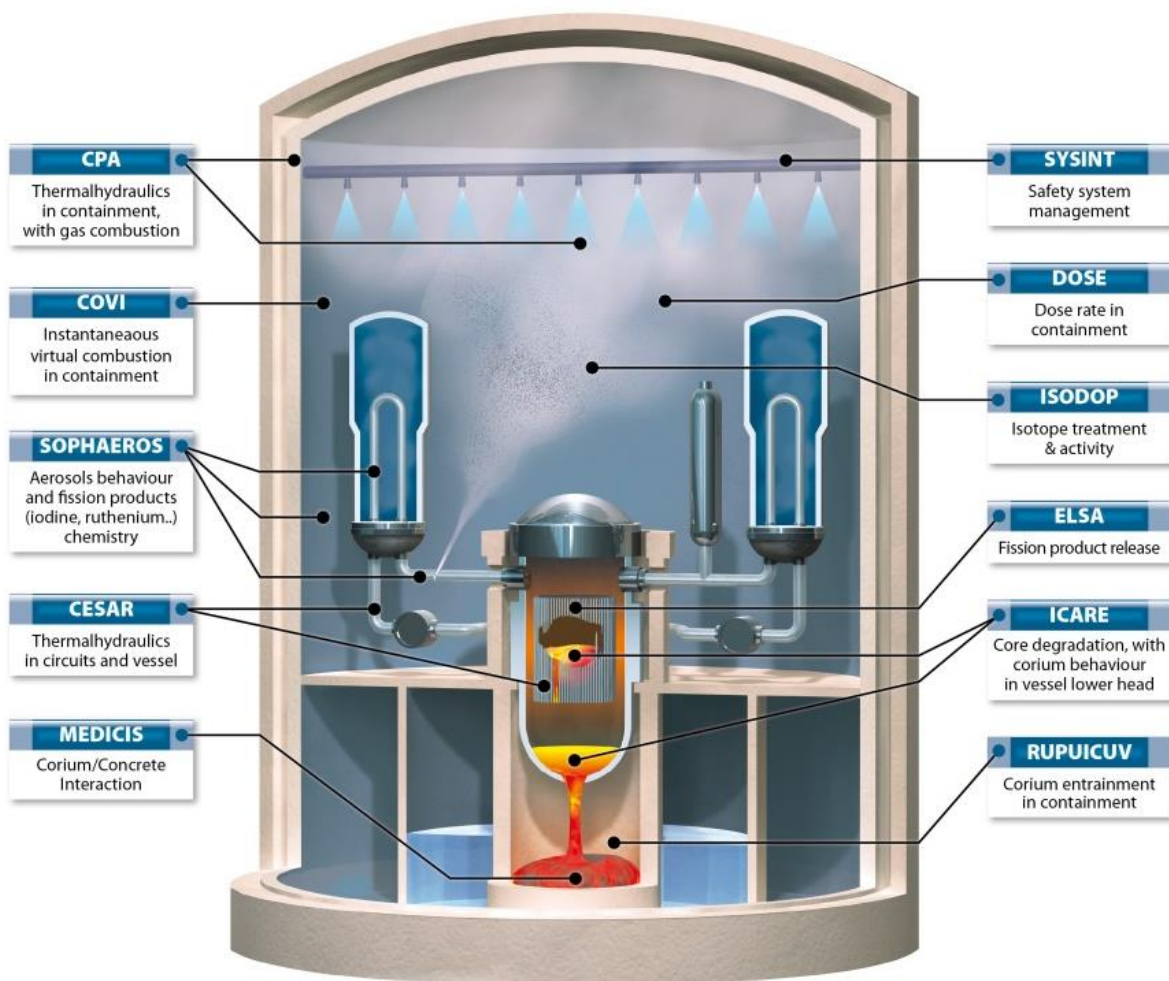
Figure III-1: Structure of the ASTEC software and presentation of the different modules from the IRSN site.

Chapter III. Kinetic modelling

While ASTEC includes models for three-dimensional phenomena, such as atmospheric dispersion and deposition, it is not strictly a 3D code. Rather, it is a multi-dimensional code that can handle a range of spatial dimensions, including zero-dimensional (0D), one-dimensional (1D), two-dimensional (2D), and three-dimensional (3D) models.

The SOPHAEROS module, originally designed to model the behaviour of fission products (such as iodine and ruthenium) in a reactor, was selected for its chemical solver capabilities. SOPHAEROS is a thermokinetic module that employs a 0D approach (Cousin *et al*., 2013). It simulates the principal physical and chemical processes taking place in the system and tracks the chemical evolution of various gaseous species and their concentrations at a given temperature (Bosland *et al*., 2010; Girault *et al*., 2012; Cantrel *et al*., 2014). Therefore, this module helps in the investigation of the gaseous reactivity in the atmosphere and is customized by adjusting different ambient parameters (such as pressure, temperature, volume, humidity, and initial concentrations) and incorporating specific velocity laws described later in *section III.2.1.1*.

Zero-dimensional (0D) models are mathematical models utilized to depict systems that lack spatial variation. In such models, the system is represented as a single point in space, and the variables are expressed as functions of time. 0D models are typically characterized by a set of differential equations that portray the system's dynamics over time. These equations encompass various physical and chemical processes, such as chemical reactions, mass and energy balances, and other relevant phenomena. One of the primary advantages of 0D models is their computational efficiency, which facilitates quick solutions. They are valuable for gaining insights into system behaviour, predicting component evolution, and identifying dominant reactions or species at specific conditions. *Figure III-2* shows the principle parameters involved in this type of simulation.

Originally, the SOPHAEROS module of the ASTEC software package uses numerical methods to solve a system of partial differential equations (PDEs) that govern the transport and transformation of radioactive materials during a nuclear power plant accident (Chatelard *et al*., 2014). The system of PDEs includes equations for conservation of mass, momentum, and energy, as well as equations that describe the transport and transformation of radioactive materials in the gas phase and on surfaces. The PDEs are typically solved using a finite volume method (FVM), which discretizes the equations into a set of algebraic equations that can be solved numerically. In order to solve the algebraic equations, SOPHAEROS uses a variety of numerical methods, including iterative methods like the Newton-Raphson method. The Newton-Raphson method is a commonly used iterative method for solving systems of nonlinear equations, which are frequently encountered in numerical simulations of complex physical systems like those in nuclear power plants.

A fixed volume defines the 0D (box) model. Constant temperature and pressure, VOCs, and NO_x emissions are the parameters used to describe the conditions of the box. These parameters are detailed in *section III.2*.

Chapter III. Kinetic modelling
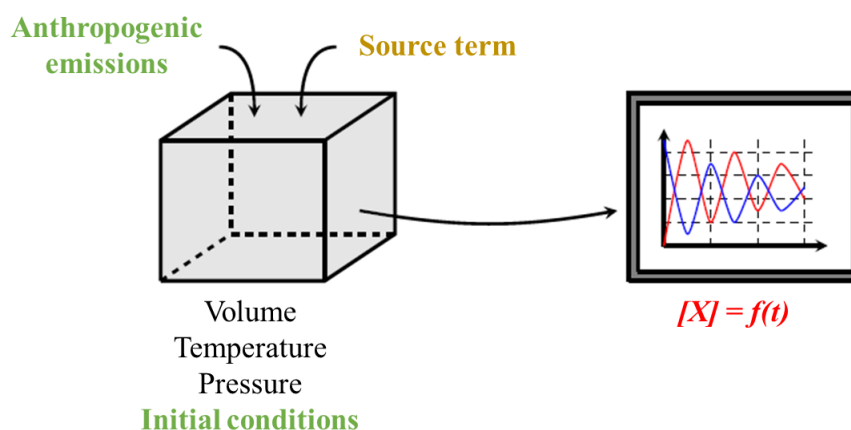
Figure III-2: Schematic representation of the operation of a 0D model.

III.2. Input data and simulation setup

III.2.1. Selection of the kinetic data

The reaction mechanism is initiated by gathering all gaseous phase reactions that involve chlorine-containing species within the tropospheric temperature range. These reactions are sourced from well-known international databases such as the MPI-Mainz UV/VIS Spectral Atlas (Keller-Rudek *et al*., 2013), the National Institute of Standards and Technology (NIST) kinetic database (Manion *et al*., 2023), and the Jet Propulsion Laboratory (JPL) evaluation (Burkholder *et al*., 2020).

Thermokinetic parameters for most of the collected reaction pathways are obtained from various literature studies, either through experimental or theoretical approaches, and show good agreement. In cases where there is disagreement, values from the most recent experimental studies are selected, and theoretical approaches are used if no experimental data is available.

It should be noted that the thermokinetic data for reactions involving chlorine are not analogous to those involving other halogens such as Br or I, or to reactions involving OH in this work. The gas-phase chlorine mechanism excludes reactions where thermokinetic parameters are merged with those of other halogen atoms due to the high uncertainties generated by such estimations. For instance, a previous study by Fortin *et al*. (2018), demonstrated the strong influence of the nature of the halogen atom on the rate constant of its reaction with hydrogen peroxide (H_2O_2). The value of the rate constant changed by about twelve orders of magnitude when the Br atom is replaced by an I atom.

Therefore, this work follows a similar strategy as that used by Fortin *et al*. (2019) in their study on the 0D modelling of the iodine tropospheric chemistry after a nuclear accident.

Our updated atmospheric gas-phase chlorine mechanism includes 388 reactions. These reactions are classified as 199 thermal organic reactions, 152 thermal inorganic reactions, 18 photolysis organic reactions, and 19 photolysis inorganic reactions. The detailed reactions implemented into this mechanism are listed in ***Appendix A.III***. These reactions involve 21 inorganic chlorinated species and 57 organic chlorinated species. These species are either

mono- or di-chlorinated. They represent stable molecules and free radicals. The reactions leading to the production of organic compounds with three and more chlorine atoms are not included in our mechanism since these compounds are less reactive in the troposphere.

Table III-1 reveals that the total number of reactions reported in the studies conducted by Hoffmann *et al.* (2019) and Peng *et al.* (2021) surpasses the count of reactions found during our bibliographic search. In their work, Hoffmann *et al.* (2019) incorporated the reactions of long-chain hydrocarbons into their mechanism, although they acknowledged that the significance of Cl is higher in the oxidation of short-chain alkanes, while its impact on long-chain hydrocarbons is considered negligible. Additionally, Peng *et al.* (2021) estimated that for 106 organic reactions, the involvement of Cl and OH in these reactions is equal.

III.2.1.1. Kinetics of the gaseous phase

a. Thermal reactions

In systems of atmospheric interest, the rate law or rate expression for a reaction is the equation expressing the dependence of the rate on the concentrations of the reactants, as well as the temperature and pressure values at which the reactions are occurring. For elementary bimolecular reactions only, the rate law may be written directly from the stoichiometric equation:

$$a\,A + b\,B \rightarrow c\,C + d\,D \qquad\qquad \textit{Eq. III-1}$$

$$v = k[A]^a[B]^b \qquad\qquad \textit{Eq. III-2}$$

At the same time, the overall rate of the reaction, v, is both equal to the rate of disappearance of the reactants or the rate of appearance of the products:

$$v = -\frac{1}{a}\frac{d[A]}{dt} = -\frac{1}{b}\frac{d[B]}{dt} = \frac{1}{c}\frac{d[C]}{dt} = \frac{1}{d}\frac{d[D]}{dt} \qquad\qquad \textit{Eq. III-3}$$

where k is the constant of proportionality in the expression. It relates the rate of the reaction to the concentrations of the reactants each expressed with the appropriate exponent. Simply, k is called the rate constant of the reaction. In gas phase reactions, concentrations are usually expressed in (molecules cm^{-3}) and time in seconds (s). Thus, the units of k, which depend on the global order of the reaction (a + b), are:

i. if the reaction is of order 1, the unit of k is (s^{-1}),

ii. if the reaction is of order 2, the unit of k is (cm^3 $molecule^{-1}$ s^{-1}),

iii. if the reaction is of order 3, the unit of k is (cm^6 $molecule^{-2}$ s^{-1}).

Empirical expressions are available in the literature to express the variation of the rate constant as a function of many parameters: temperature, pressure, and concentration of air molecules. The following list is not exhaustive but represents the cases encountered in this work for the air quality species and mechanisms of the organic and inorganic chlorinated species in the gas phase.

Chapter III. Kinetic modelling

The most frequent law is Arrhenius' law, which was proposed by Svante Arrhenius in 1889. It is an empirical law based on results observed during experiments. It can be expressed in two different formulations according to its dependence on temperature:

the empirical law:
$$k = A \exp(\frac{-E_a}{RT})$$
Eq. III-4

and the extended law:
$$k = A\, T^{\alpha} \exp(\frac{-E_a}{RT})$$
Eq. III-5

with A the pre-exponential factor (with same dimensions as k or k/T^{α}), E_a the activation energy of the reaction (in J mol^{-1}), R the ideal gas constant (R = 8.314 J mol^{-1} K^{-1}), and α the coefficient specific to each reaction.

For certain reactions, the rate is very dependent on pressure, as is the case for reactions that follow the Troe law developed by Carl Troe in 1963:

$$k = \frac{k_0[M]}{1+\frac{k_0[M]}{k_\infty}} F^{\left\{1+\left[log_{10}\left(\frac{k_0[M]}{k_\infty}\right)^2\right]\right\}^{-1}}$$
Eq. III-6

with
$$k_0 = k_0^{300} \times (\frac{T}{300})^{-n}$$
Eq. III-7

referring to the low-pressure limiting rate constant,

and
$$k_\infty = k_0^{\infty} \times (\frac{T}{300})^{-m}$$
Eq. III-8

referring to the high-pressure limiting rate constant.

In equation III-6, [M] represents the concentration of air molecules (in molecules cm^{-3}), k_0^{300} the low-pressure limiting rate constants at 300 K (in cm^6 molecule^{-2} s^{-1}), k_∞^{300} the high-pressure limiting rate constants at 300 K (in cm^3 molecule^{-1} s^{-1}), F the adjustment factor specific to the reaction under consideration, n and m the scaled coefficients also specific to the reaction under study. Moreover, the temperature dependence of the Troe law is captured in the temperature dependence of k_0 and k_∞.

It is worth mentioning that all the thermal reaction involved in the chlorine chemistry mechanism are probable to occur at the tropospheric temperature range (around 298 K). As a reminder, these are 199 thermal organic reactions and 152 thermal inorganic reactions.

b. Photolysis reactions

A photolysis reaction is a type of chemical reaction in which a molecule is broken down into smaller fragments by the absorption of light. These fragments can be radical species that can go on to participate in other chemical reactions. Photolysis reactions can be represented as unimolecular processes because they involve the decomposition of a single molecule into two or more fragments.

$$A + h\nu \rightarrow R_1 + R_2$$
Eq. III-10

where A is the species that photolyzes, R_1 and R_2 are the radicals produced, and hν is the energy produced by the light source in the wavelength range of the photolysis of A. As before, the

overall speed of a photolysis reaction is equal to the rate of disappearance of the reactants or the rate of appearance of the radicals:

$$v = -\frac{d[A]}{dt} = \frac{d[R_1]}{dt} = \frac{d[R_2]}{dt}$$

Eq. III-11

A photolysis reaction is an elementary act of order 1. Its rate depends on the intensity of the light, the absorption cross-section of the molecule, and the quantum yield, as well as the concentration of the molecule in the system.:

$$v = J[A]$$

Eq. III-12

where J is the photolysis constant expressed in s^{-1}. It is expressed as a function of the actinic flux, the effective cross section and the quantum efficiency, we then obtain the following expression:

$$J = \int_{\lambda_1}^{\lambda_2} F(\lambda)\sigma(\lambda)\,\phi(\lambda)\,d\lambda$$

Eq. III-13

where λ_1 and λ_2, are respectively the lower and upper limits of the wavelengths leading to photo dissociation in meters (m). $\phi(\lambda)$ is the quantum efficiency of the reaction, it represents the probability of dissociation to occur after a photon is being absorbed by the molecule. It is an experimentally determined parameter. $F(\lambda)$ is the actinic flux representing the amount of energy available per unit volume, it is expressed in (photons m^{-3} s^{-1}). It can be determined experimentally, either calculated from illumination values, or calculated from a radiative transfer code. $\sigma(\lambda)$ is the effective absorption cross section expressed in (m^2 molecule^{-1}), and is generally determined experimentally by Beer-Lambert's law:

$$\frac{dI_\lambda}{dl} = -\sigma_\lambda\,[A]\,I_\lambda$$

Eq. III-14

with I_λ the incident intensity of the radiation wavelength λ in (photons m^{-2} s^{-1}) and l the traversed length in (m).

It is worth mentioning that the tropospheric photolysis takes place at wavelength (λ) values ranging between 280 and 600 nm according to the TUV Radiation Model (NCAR, 2019). In *Appendix A.III*, the cross sections and quantum yields used are detailed for the organic and inorganic species, respectively. Again, a total of 18 photolysis organic reactions, and 19 photolysis inorganic reactions are collected from the databases.

III.2.2. Air quality conditions

Air quality conditions are important consideration in our box model simulations, which are conducted at a fixed volume of 10000 m^3 and atmospheric pressure of 1.013 bar. The temperature within the box varies depending on the season, with estimated average temperatures of 8 and 27 °C (281 and 300 K) during winter and summer, respectively (based on "Average weather August in Lille (Nord-Pas-de-Calais), France," 2013).

To accurately measure the reactivity of chlorinated species in the atmosphere, it is essential to create a realistic environment within the box that represents the molecules and radicals present in the troposphere. We used a variety of sources to determine the initial concentrations of different components, including permanent components such as H_2, O_2, and N_2, as reported by Jacob (1999) and later studies (Liang, 2013; Muralikrishna and Manickam, 2017). Concentrations of O_3 and NO were obtained from ("Qualité de l'air extérieur," 2013) at Avant-Port, while the overall average value of ground-measured NO_2 concentration was estimated from the study by Chi *et al.* (2021). Additionally, we obtained information on atmospheric daytime concentration of OH in the troposphere from a recent study by Zhao *et al.* (2022). ***Table III-2*** provides a summary of the initial concentrations of the main species used. Other species still exist

The volume mixing ratio is a way to express the concentration of a component in a mixture of gases. It is defined as the ratio of the volume of a particular gas to the total volume of the gas mixture. Here's the formula to calculate the volume mixing ratio:

$$volume\ mixing\ ratio = \frac{V_{gas}}{V_{total}}$$
Eq. III-15

where V_{gas} is the volume of the gas component and V_{total} is the total volume of the gas mixture.

The volume mixing ratio is typically expressed in parts per million (ppm) or parts per billion (ppb), representing the number of gas molecules per million or billion molecules of the entire gas mixture, respectively. It's important to note that the volume mixing ratio assumes ideal gas behaviour and assumes that the gas components do not interact significantly with each other.

Table III-2: *Initial conditions of the main species in the box model.*

Species	Concentration (species cm^{-3})	Volume mixing ratio	Reference
O_2	7.17×10^{18}	20.95 % (v)	(Jacob, 1999)
N_2	1.89×10^{19}	78.08 % (v)	(Jacob, 1999)
H_2	1.21×10^{13}	500.00 ppb	(Jacob, 1999)
O_3	5.57×10^{11}	22.93 ppb	("Qualité de l'air extérieur," 2013)
NO	3.56×10^{11}	14.67 ppb	("Qualité de l'air extérieur," 2013)
NO_2	3.47×10^{11}	14.29 ppb	(Chi *et al.*, 2021)
OH	9.72×10^{05}	0.04 ppt	(Zhao *et al.*, 2022)
N_2O_5	3.61×10^{07}	1.50 ppt	(Faxon *et al.*, 2015)

Furthermore, the emission fluxes of NO_x and VOCs were obtained from (Fortin *et al.*, 2019), which modelled the temporal variation of these species' emissions based on the values of Kuhn *et al.* (1998) (***Table III-3***). The NO_x speciation, with NO accounting for 98% and NO_2 accounting for 2%, was determined from measurements at a network station in the North of France (15 stations).

To model the VOCs, we aggregated the 67 species reported by Kuhn *et al.* (1998) into the RACM VOC chemical scheme, and their speciation is given in ***Table III-4***. Notably, the concentrations of NO_x and VOCs were not fixed, as they result from emissions and strongly influence the formation of ground-level ozone. As a result, our box model accurately represents an urban environment with moderately polluted conditions.

Table III-3: *Air pollutant emission flows.*

Species	Emission Flows (molecules cm^{-3} s^{-1})
NO_x	1.1×10^6
VOC	3.0×10^6

Table III-4: *Speciation of the RACM VOC mechanism.*

RACM Species	Speciation of the emission of VOC (%)
ALD	0.53
ORA2	1.54
ETE	6.71
ETH	3.53
HC3	24.93
HC5	23.34
HC8	7.60
HCHO	2.04
KET	6.49
OLI	2.87
OLT	3.11
TOL	7.90
XYL	9.41

To accurately simulate the fluctuation of NO_x and VOC emissions over time, we implemented an emission profile in ASTEC/SOPHAEROS. This profile was based on the hourly emission factors of the 10 SNAPs presented in ***Figure III-3***, which were obtained from EMEP (European Monitoring and Evaluation Program) emissions and published Menut *et al.* (2012). By averaging the emissions of the 10 SNAPs for each time step, we obtained an average profile, which is shown in ***Figure III-4***.

Chapter III. Kinetic modelling

The photolysis rate constants were computed using the Tropospheric Ultraviolet and Visible (TUV) Radiation Model of the National Centre for Atmospheric Research (NCAR, 2019). The actinic flux values were calculated at the beginning of January and August months, latitude 51°2′ 3.725″N and longitude 2°22′36.394″E, under clear sky conditions. These coordinates correspond to Dunkirk, a city in northern France with a significant industrial presence, including the third largest port in France and one of the largest industrial areas with high CO_2 emissions ("Dunkirk innovates for better air quality - SUEZ Group," 2013).
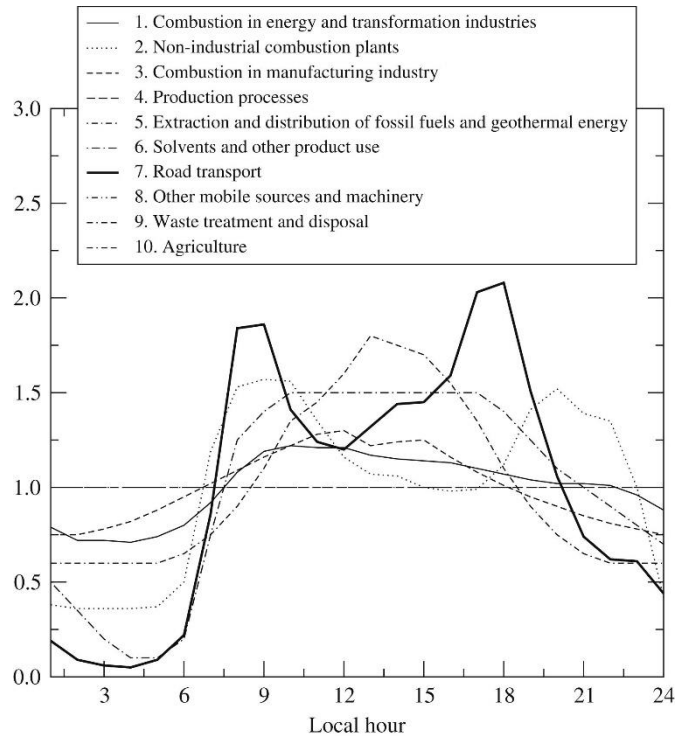
Figure III-3: Emissions hourly factors of the 10 SNAP anthropogenic activities sectors.
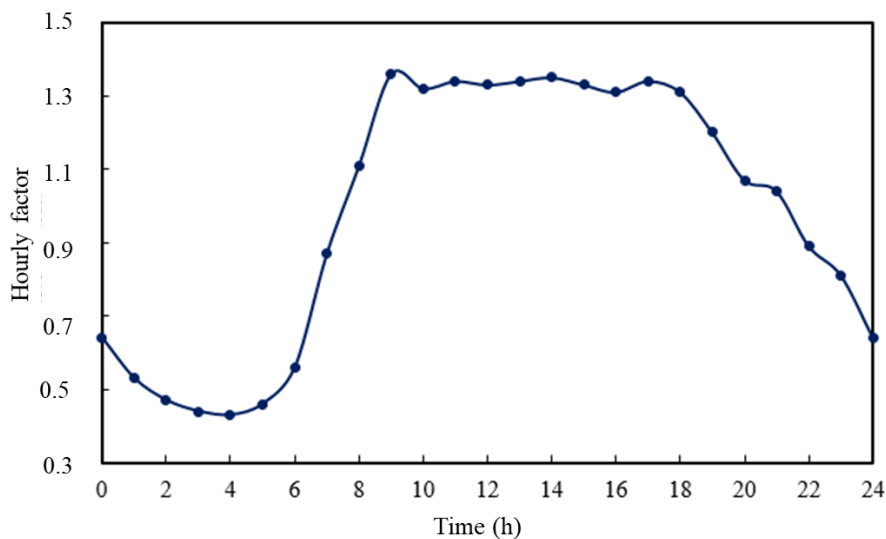
Figure III-4: Profile of hourly emission factors implemented in ASTEC.

94

III.2.3. Chlorine speciation and amount

Chlorine exists in various forms in the atmosphere, including particulate, inorganic gas, and chlorinated organic species. In the tropospheric gas phase, inorganic chlorine originates mainly from chloride anions (Cl^-) mobilized from sea-salt aerosols (SSA). Hydrogen chloride (HCl) is emitted directly to the atmosphere from various sources, such as coal combustion, water incineration, industrial processes, fugitive dust, road salt applications, and BB (Haskins *et al.*, 2020). Nitryl chloride ($ClNO_2$) is formed in the presence of aerosol chloride through the heterogeneous reaction with dinitrogen pentoxide (N_2O_5) (Lou *et al.*, 2022). $ClNO_2$ production can alter the cycling of regional NO_x and radical chemistry. The photolysis of $ClNO_2$ is a major source of Cl in the troposphere (Eger *et al.*, 2019).

Our mechanism models only the gas phase reactivity of chlorine-containing species, and we do not consider reactions that occur at the surface of aerosols or aqueous phases. The initial conditions of our box model include HCl and $ClNO_2$ concentrations, which serve as sources of atomic chlorine, in addition to the species present in ***Table III-2***. The tropospheric lifetime of HCl with respect to photolysis reaction and reaction with OH ([OH] = 1×10^6 radicals cm^{-3}) is 20 days (Kim *et al.*, 2008), and the nocturnal lifetime of $ClNO_2$ is estimated to be more than 30 hours (Eger *et al.*, 2019). However, $ClNO_2$ is rapidly photolyzed after sunrise, with an average photolysis lifetime of 30-60 minutes depending on the season and location (Kercher *et al.*, 2009).

To determine the initial chlorine concentration in our box, we needed to estimate the concentrations of these species on a global scale as given in ***Table III-5***. The total amount of chlorine in our box atmosphere is kept constant at around 372.5 parts per trillion (ppt), corresponding to the total initial concentration of atomic chlorine given in ***Table III-5***.

Table III-5: *Initial mixing ratios of the chlorine in the model.*

Species	Volume mixing ratio (ppt)	Concentration (species cm^{-3})	Reference
$ClNO_2$	50.0	1.21×10^9	(Kercher *et al.*, 2009)
HCl	322.5	7.84×10^9	(Wang, X. et al., 2019)

III.2.3.1. Classification of inorganic chlorinated species into families

To analyse the evolution of chlorine speciation over time, we categorized inorganic chlorinated species into three groups, based on their molecular composition and stability. **Stable chlorinated molecules**, including **Cl_2**, **HCl**, and **HOCl**, are shown in orange. **Chlorine nitroxides**, namely **ClNO** and **$ClNO_2$**, are represented in purple boxes. **Radical species**, such as **Cl** and **ClO**, are depicted in blue. These colours are used only in the reaction schemes for clarification.

Chapter III. Kinetic modelling

III.2.3.2. Classification of organic chlorinated species into Cl_RACM classes

We streamlined our modelling procedure by incorporating the RACM mechanism formulated by (Stockwell *et al.*, 1997) to integrate organic species. This approach categorizes organic species based on their reactivity towards OH radicals and functional groups, following the method described by Middleton *et al.* (1990) and Stockwell *et al.* (1990). We utilized the same categorization process for chlorinated organic species in our mechanism, producing 30 Cl_RACM classes composed of 57 specific organic chlorinated species (see ***Table III-6***). These classes include both stable molecules and radical species.

Table III-6: *Cl_RACM mechanism species list.*

Cl_RACM Class	Species
Cl_CH4	CH_3Cl
Cl2_CH4	CH_2Cl_2
Cl_MR	CH_2Cl
Cl2_MR	$CHCl_2$
Cl_ETE	$CH_2=CHCl$, $CHOH=CHCl$
Cl_ETER	$CH_2=CCl$, $CHCl=CH$
Cl_ETH	C_2H_5Cl
Cl2_ETH	CH_3CHCl_2, CH_2ClCH_2Cl
Cl_ETHR	CH_3CHCl, CH_2CH_2Cl, C_2H_4Cl (undefined isomer)
Cl2_ETHR	$CHCl_2CH_2$, CH_3CCl_2, $CH_2ClCHCl$
Cl_HC3	CH_2ClOH, CH_3OCl, $CH_2ClC≡CH$, CH_3OCH_2Cl, tert-C_4H_9Cl n-C_4H_9Cl, sec-C_4H_9Cl, n-C_3H_7Cl, iso-C_3H_7Cl
Cl_HC3R	CH_2ClO, $ClCHOH$, $ClCH_2CHCH_3$, $(CH_3)2CClCH_2$, CH_2OCl, CH_3CHClO, $CHClCH_2OH$, $CHClOHCH_2$, CH_2ClCH_2O
Cl_TOL	Chlorobenzene C_6H_5Cl, $C_6H_5CH_2Cl$
Cl_TOLR	2-chlorophenyl, 3-chlorophenyl, 4-chlorophenyl
Cl_HCHO	$HC(O)Cl$
Cl_HCHOR	$COCl$
Cl_ALD	CH_2ClCHO
Cl_DIEN	chlorocyclohexadiene
Cl_DIENR	$C_2H_2C_2H_2Cl$
Cl_ETHP	CH_3CHClO_2
Cl2_ETHP	$CH_2ClCHClO_2$
Cl_MO2	CH_2ClO_2
Cl2_MO2	$CHCl_2O_2$
Cl_OP1	CH_2ClOOH
Cl_OLT	$CH_2=CHCH_2Cl$
Cl_OLTR	$CH_2=C(CH_3)CHClCH_2$, $CH_2Cl-CH=CH$
Cl2_OLTR	$C_3H_3Cl_2$
Cl_ORA2R	$ClCH_2CHCOOH$
Cl_CSL	2-Chlorophenol C_6H_5OCl
Cl_PHO	2-Chlorophenoxy C_6H_4OCl

III.3. Model scenarios

Various scenarios are studied to evaluate the chlorine mechanism, including diurnal and seasonal cycles during both winter (January) and summer (August) in the northern hemisphere. These scenarios are applied separately to the organic and inorganic chlorinated species, as well as the whole mechanism (including both organic and inorganic species), in order to examine the relationship between them. The differences in thermal and photolytic conditions between the two seasons are considered, with average temperatures considered for each season and actinic flux values at the beginning of January and August controlling the photolytic effect. Mixing ratios of the species are calculated in parts per trillion (ppt) in the model.

III.4. Results and discussion

III.4.1. The chlorine mechanism

The temporal variation of the mixing ratios of the organic and inorganic chlorinated species are plotted for the first 48 hours after starting the model during both winter and summer seasons (*Figure III-5*, *Figure III-6*, *Figure III-9*, and *Figure III-10*). The temporal variation is given for two days (48 hours) to show the continuity of the behaviour of the mixing ratios of these species. The night-time is represented by the shaded grey part of the graphs, whereas the clear part represents the daytime. Each set of species with comparable mixing ratios are grouped together in one graph. The reactivities of these species during day and night times are summarized in reaction schemes showing the major production and loss pathways of these species for the two seasons (*Figure III-7*, *Figure III-8*, *Figure III-11*, and *Figure III-12*). While showing the reactivity of the species, a simple arrow represents the predominant loss and production pathways (> 50 %). A dash - point arrow symbolizes the important reactions (10 - 50 %). A dashed arrow shows that the reaction is of low effect (1 - 10 %), and a negligible pathway is represented by dash - double point arrow (0.1 - 1 %).

III.4.1.1. The inorganic chlorine mechanism

Figure III-5 and *Figure III-6* display the temporal variation of the mixing ratios of the main inorganic chlorinated species during summer and winter, respectively. *Figure III-7* and *Figure III-8* sum up the major production and loss pathways of the different inorganic chlorinated species and shows the importance of these reactions by using different arrow shapes.

The reactivity of HCl in the troposphere attracts our attention since HCl is one of the main atmospheric acidic gases that alter the air quality and the oxidative capacity of the atmosphere (Liakakou *et al.*, 2022). The mixing ratio of HCl increases slightly in both seasons during the daytime. This matches with the finding of Crisp *et al.* (2014) in their observations of the gas phase HCl in Los Angeles, which is a dry area with an environment similar to our conditions. HCl is mainly produced through the reaction pathways (*R5*) and (*R6*). Kumaran *et al.* (1994) indicated that reaction (*R5*) is known to be of atmospheric interest. Moreover, HCl is produced through the destruction pathway of nitrosyl chloride (ClNO) through its gaseous phase hydrolysis (*R6*). This is competitive with the photolysis reaction of ClNO (Karlsson and

LjungstrÖm, 1996), but still of lower importance as shown in **Figure III-7(a)** and **Figure III-8(a)**. Moreover, HCl is also a major chlorinated species, which is directly emitted into the troposphere as mentioned in **section III.2.3**.

$Cl + H_2 \rightarrow HCl + H$	**R5**
$ClNO + H_2O \rightarrow HCl + HONO$	**R6**

Then, we can say that HCl is indirectly produced through the photolysis of ClNO (**R7**), upon the reaction between atomic Cl produced and H_2 (**R8**).

$ClNO + h\nu \rightarrow Cl + NO$	**R7**
$Cl + H_2 \rightarrow HCl + H$	**R8**
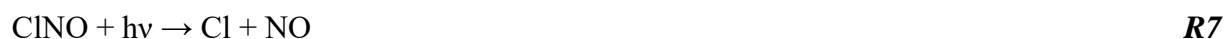
In the troposphere, the oxidation of HCl is a crucial source of Cl atoms. As demonstrated in **Figure III-7(b)** and **Figure III-8(b)**, HCl is oxidized by the nitrate radical (NO_3) during summer and winter nights. NO_3 is a significant nocturnal oxidant in the atmosphere (Brown and Stutz, 2012; Khan *et al*., 2015, 2008). The daytime HCl oxidation is governed by the atomic hydrogen (H) (**R9**) in summer (**Figure III-7(a)**) and OH (**R10**) in winter (**Figure III-8(a)**).

$HCl + H \rightarrow H_2 + Cl$	**R9**
$HCl + OH \rightarrow H_2O + Cl$	**R10**

In the troposphere, atomic H is produced by reaction (**R11**) (Novelli *et al*., 1999).

$H_2 + OH \rightarrow H_2O + H$	**R11**
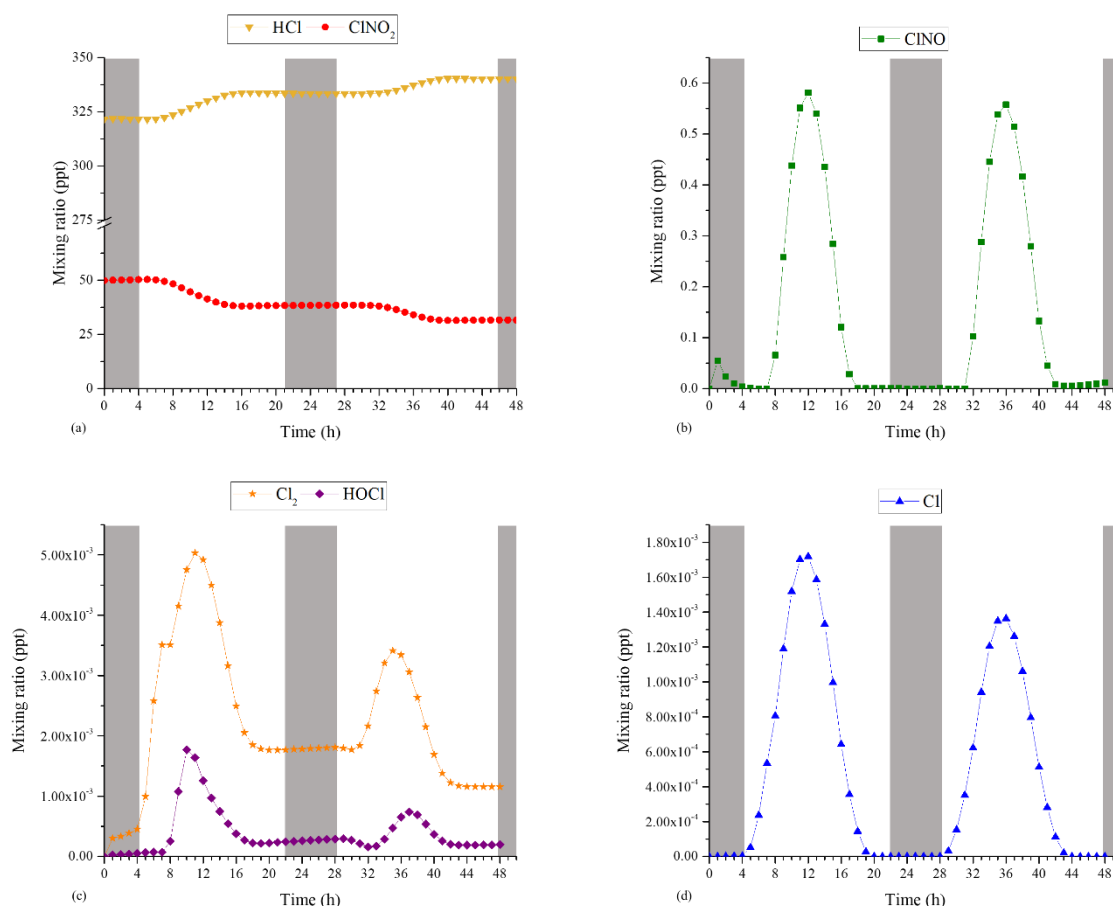
Figure III-5: *The temporal variation of the mixing ratios of the main inorganic chlorinated species during summer.*

This is explained by the fact that the concentration of OH in the atmosphere depends on the actinic flux because it is mainly produced by the reactions (***R12***) and (***R13***) (Monks, 2005). The tropospheric OH concentration is higher in summer than in winter as the photolytic effect is of less importance during winter. This makes the formation of H atoms by ***R11*** of higher significance during summer. Therefore, the reaction of HCl with H atoms is more important in summer. In addition, the concentrations of the species in ***Table III-2*** are the ones at the beginning of the calculation (time = 0 h), but they do not remain constant. Their variation depends on the photolytic effects.

$O_3 + h\nu \rightarrow O + O_2$ ***R12***
$O + H_2O \rightarrow 2\ OH$ ***R13***
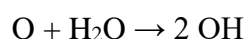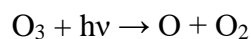
Furthermore, the photolysis of ClNO₂ is a significant contributor to the presence of chlorine (Cl) in the troposphere, as highlighted by Jeong *et al*. (2019) and Sarwar *et al*. (2014). In our model, ClNO₂ is generated through the addition of NO₂ to a chlorine atom. Although the heterogeneous formation reaction, which is not accounted for in our model, has a more substantial impact, Sarwar *et al*. (2014) demonstrated the importance of this gaseous production pathway.
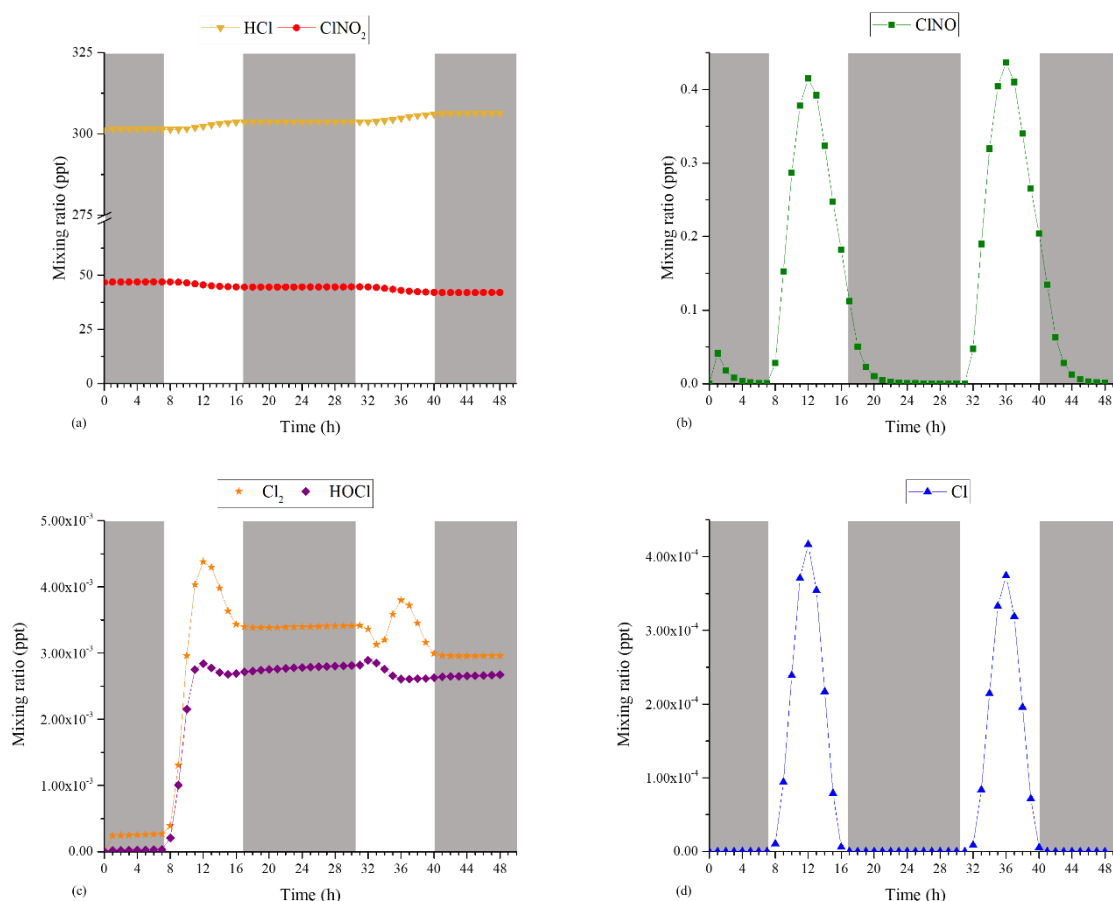
Figure III-6: *The temporal variation of the mixing ratios of the main inorganic chlorinated species during winter.*

Furthermore, the mixing ratios of ClNO, Cl_2, HCl, and Cl peak at 12 h in both seasons at which the actinic flux is the maximum according to the TUV Radiation Model (NCAR, 2019). The photolysis of $ClNO_2$, ClNO, Cl_2, and HOCl is an important part of the reaction scheme of the daytime reactivity of inorganic chlorinated species in both seasons as shown in ***Figure III-7(a)*** and ***Figure III-8(a)***. Crisp *et al*. (2014) mentioned that Cl atoms are produced in the polluted areas mainly from the photolysis of chlorine containing reservoirs (e.g., HCl, Cl_2, and HOCl). However, our model does not consider the photolysis of HCl since it is not likely to happen in the troposphere but in the stratosphere. The loss of HOCl and Cl_2 is negligible with respect to their formation during the night (***Figure III-7(b)*** and ***Figure III-8(b)***).

Chlorine monoxide (ClO) reactions play an important role in the cycling of atomic Cl. However, it has a very low mixing ratio (in the order of 10^{-8} ppt) that can be neglected with respect to the mixing ratios of the other species displayed in ***Figure III-5*** and ***Figure III-6***. ClO is a very reactive gas-phase chlorinated species that was significantly included in different previous tropospheric models (Badia *et al*., 2019; Eastham *et al*., 2014; Fan and Li, 2022; Hoffmann *et al*., 2019; Hossaini *et al*., 2016; Li *et al*., 2016; Ordóñez *et al*., 2012; Peng *et al*., 2021; Sander *et al*., 2011; Sherwen *et al*., 2016; Sommariva and von Glasow, 2012; Soni *et al*.,

2023; Wang, X. *et al*., 2019). In our mechanism, ClO is mainly produced through the reaction pathway (**R14**) and lost by (**R15**) as shown in *Figure III-7* and *Figure III-8*.
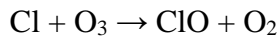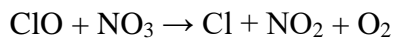
$$Cl + O_3 \rightarrow ClO + O_2 \hspace{4cm} \textbf{\textit{R14}}$$
$$ClO + NO_3 \rightarrow Cl + NO_2 + O_2 \hspace{3cm} \textbf{\textit{R15}}$$
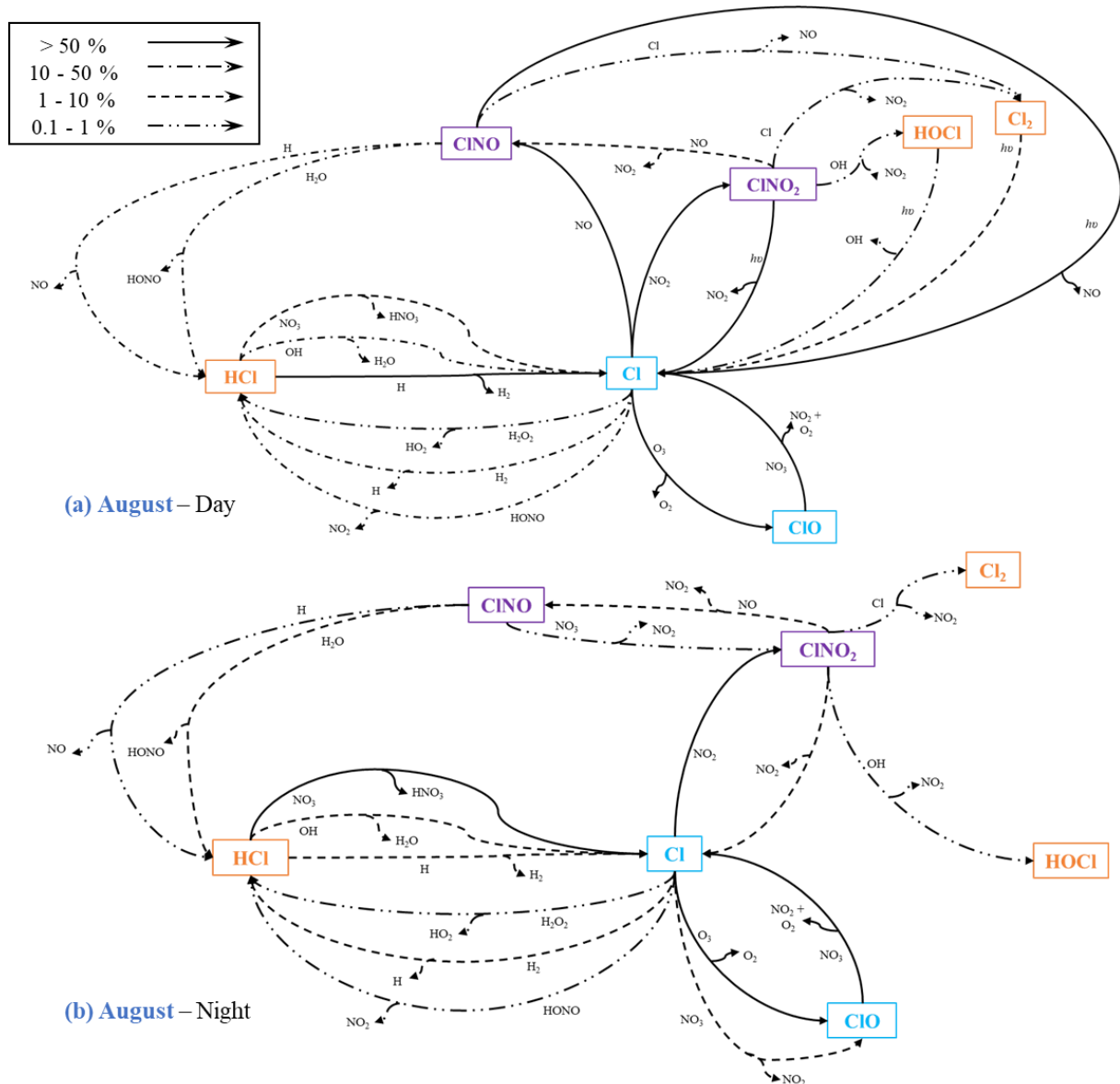
Figure III-7: *Reaction scheme of the inorganic chlorinated species during summer day (a) and night (b).*
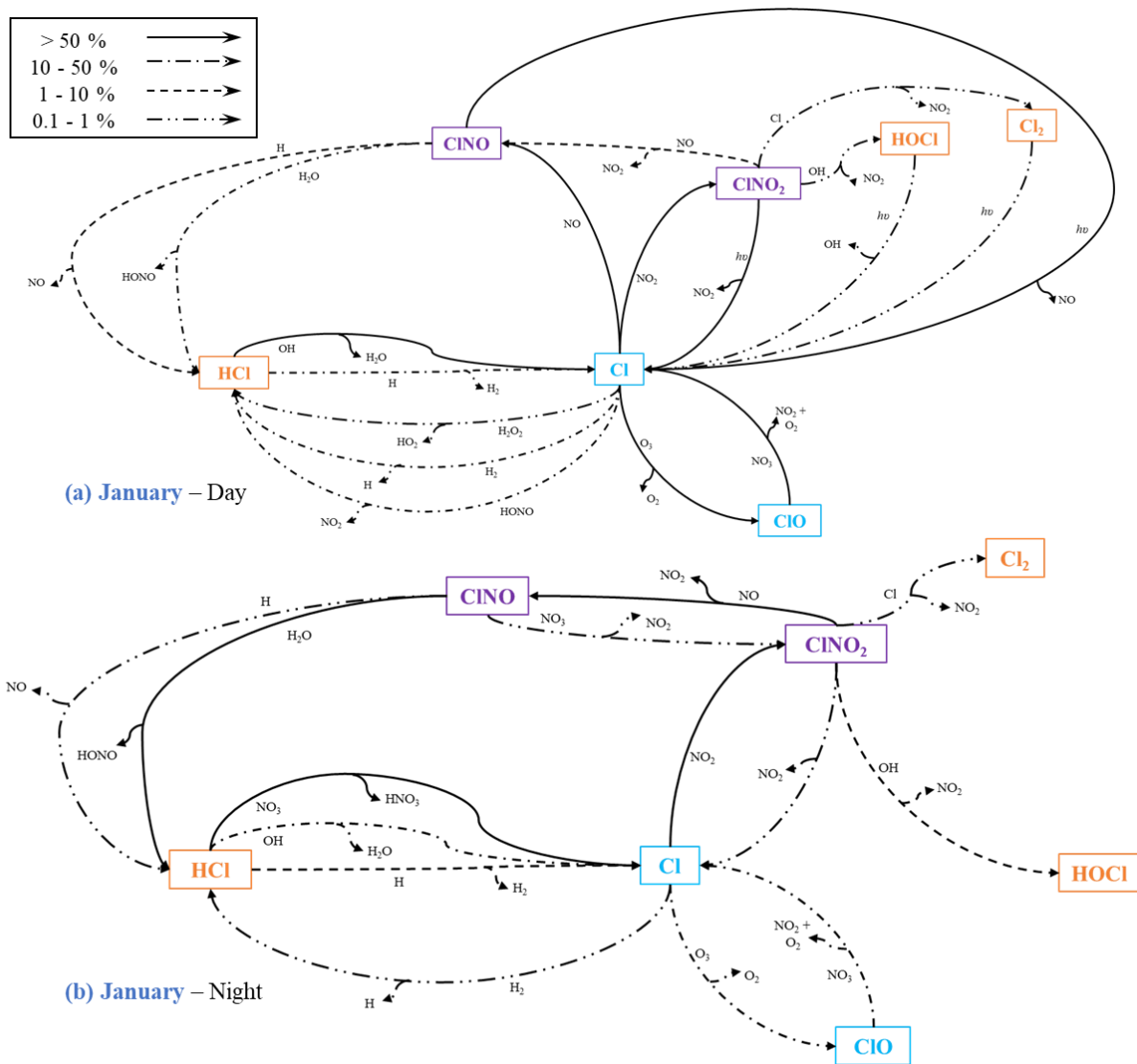
Figure III-8: *Reaction scheme of the inorganic chlorinated species during winter day (a) and night (b).*

All the reactions presented in final inorganic scheme (*Figure III-7* and *Figure III-8*) are summarized in *Table III-7*.

Table III-7: Photolysis and thermal reactions involved in the simplified reaction scheme of inorganic chlorinated species.

Photolysis Reactions		
$Cl_2 + h\nu \rightarrow 2Cl$		
$HOCl + h\nu \rightarrow Cl + OH$		
$ClNO + h\nu \rightarrow Cl + NO$		
$ClNO_2 + h\nu \rightarrow Cl + NO_2$		
Thermal Reactions		
Reaction	**Rate constant** (s^{-1}) **or** $(cm^3\ molecule^{-1}\ s^{-1})$ **or** $(cm^6\ molecule^{-2}\ s^{-1})$	**Literature**
$Cl + H_2 \rightarrow HCl + H$	$4.77 \times 10^{-16}\ T^{1.58}\ exp(-1610/T)$	(Kumaran et al., 1994)
$Cl + O_3 \rightarrow ClO + O_2$	$2.80 \times 10^{-11}\ exp(-250/T)$	(Atkinson et al., 2007)
$Cl + NO + M \rightarrow ClNO + M$	$1.26 \times 10^{-27}\ T^{-1.39}\ exp(-173/T)$	(Troe, 1979)
$Cl + NO_2 \rightarrow ClNO_2$	$k_0 = 1.30 \times 10^{-30}\ (T/298)^{-2}$, $k_\infty = 1.00 \times 10^{-10}\ (T/298)^{-1}$, $F_c = 0.6$	(Golden, 2007)
$Cl + NO_3 \rightarrow ClO + NO_2$	2.26×10^{-11}	(Becker *et al.*, 1991)
$Cl + H_2O_2 \rightarrow HCl + HO_2$	$1.10 \times 10^{-11}\ exp(-981/T)$	(Atkinson et al., 2007)
$Cl + HONO \rightarrow HCl + NO_2$	$5.86 \times 10^{-13}\ exp(1152/T)$	(Anglada and Solé, 2017)
$Cl + ClNO \rightarrow Cl_2 + NO$	$5.80 \times 10^{-11}\ exp(100/T)$	(Burkholder *et al.*, 2020)
$Cl + ClNO_2 \rightarrow Cl_2 + NO_2$	5.50×10^{-12}	(Nelson and Johnston, 1981)
$ClO + NO_3 \rightarrow Cl + O_2 + NO_2$	7.50×10^{-1}	(Boyd *et al.*, 1996)
$HCl + H \rightarrow Cl + H_2$	$2.01 \times 10^{-11}\ exp(-1790/T)$	(Kita and Stedman, 1982)
$HCl + OH \rightarrow Cl + H_2O$	$1.70 \times 10^{-12}\ exp(-230/T)$	(Atkinson et al., 2007)
$HCl + NO_3 \rightarrow Cl + HNO_3$	5.00×10^{-17}	(Mellouki *et al.*, 1989)
$ClNO + H \rightarrow HCl + NO$	1.96×10^{-11}	(Wategaonkar and Setser, 1989)
$ClNO + H_2O \rightarrow HCl + HONO$	7.41×10^{-22}	(Karlsson and LjungstrÖm, 1996)
$ClNO + NO_3 \rightarrow ClNO_2 + NO_2$	1.00×10^{-14}	(Cantrell *et al.*, 1987)
$ClNO_2 + NO \rightarrow ClNO + NO_2$	$2.34 \times 10^{-12}\ exp(-3470/T)$	(Wilkins *et al.*, 1974)
$ClNO_2 + OH \rightarrow HOCl + NO_2$	$2.40 \times 10^{-12}\ exp(-1250/T)$	(Atkinson et al., 2007)

Chapter III. Kinetic modelling

III.4.1.2. The organic chlorine mechanism

As mentioned before in ***section III.2.3.2***, our mechanism involves 57 specific organic chlorinated species classified into 30 Cl_RACM classes of stable and radical species as in ***Table III-6***. ***Figure III-9*** and ***Figure III-10*** show the temporal variation of the mixing ratios of these Cl_RACM classes involved in our mechanism in summer and winter, respectively. The model is not able to distinguish among the specific species when computing the mixing ratios evolution. ***Figure III-10*** and ***Figure III-11*** sum up the loss and production pathways of the specific organic chlorinated species in summer and winter, respectively. The results show that the cycling of the organic chlorinated species is much more complex than the inorganic chlorinated species. **Stable chlorinated species** are shown in red, and **radical species** are in green.

Atomic Cl and molecular chlorine (Cl_2) are the two inorganic species involved in the formation of organic chlorinated compounds as shown in ***Figure III-11*** and ***Figure III-12***. These compounds are produced through the addition of atomic chlorine on different VOCs (e.g.: C_2H_2 and $CH_3CH=CH_2$), or through the substitution reaction between Cl_2 and other VOCs (liked phenol C_6H_5OH) to give HCl and an organic chlorinated compound.
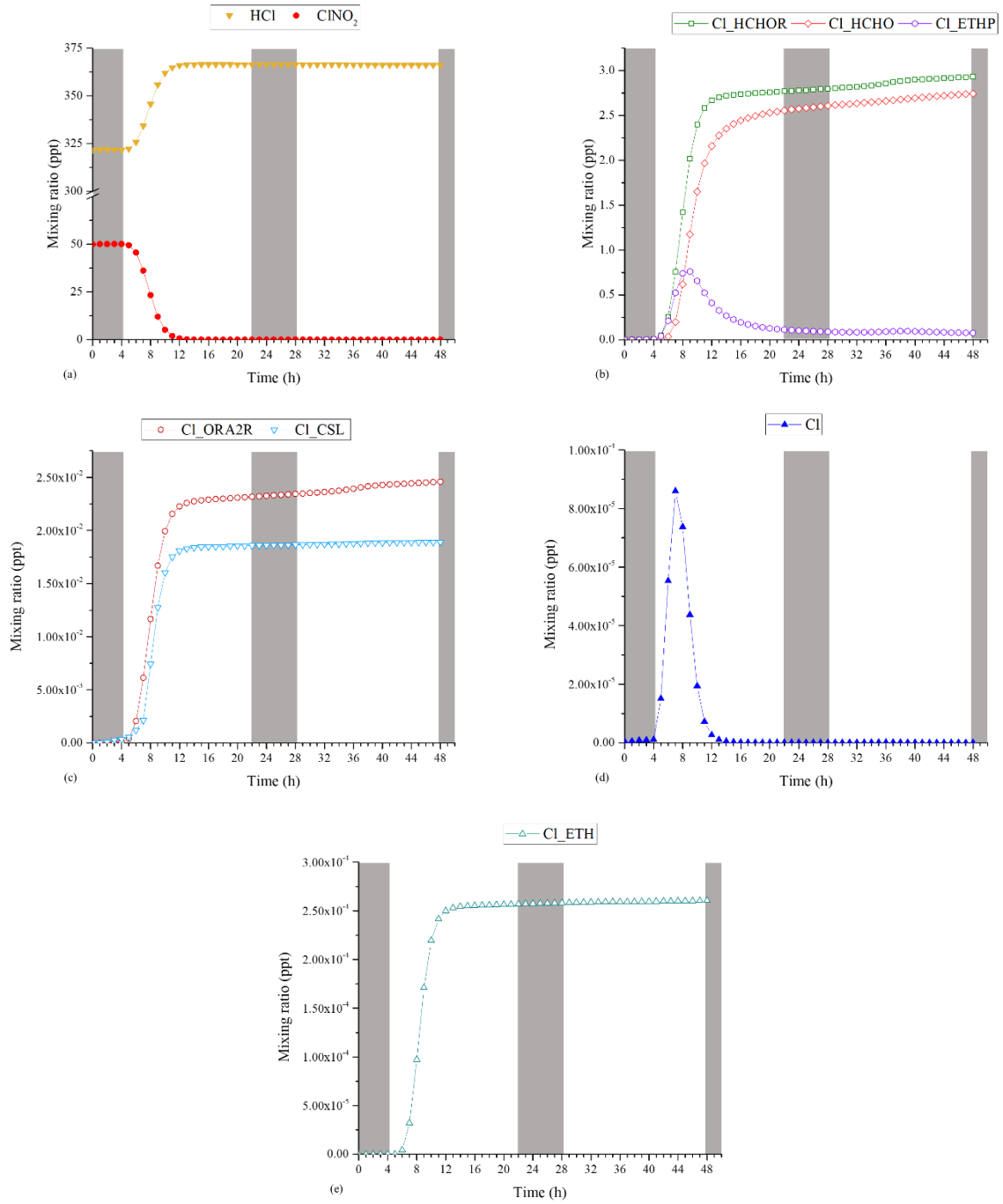
Figure III-9: *The temporal variation of the mixing ratios of the main Cl_RACM classes during summer.*
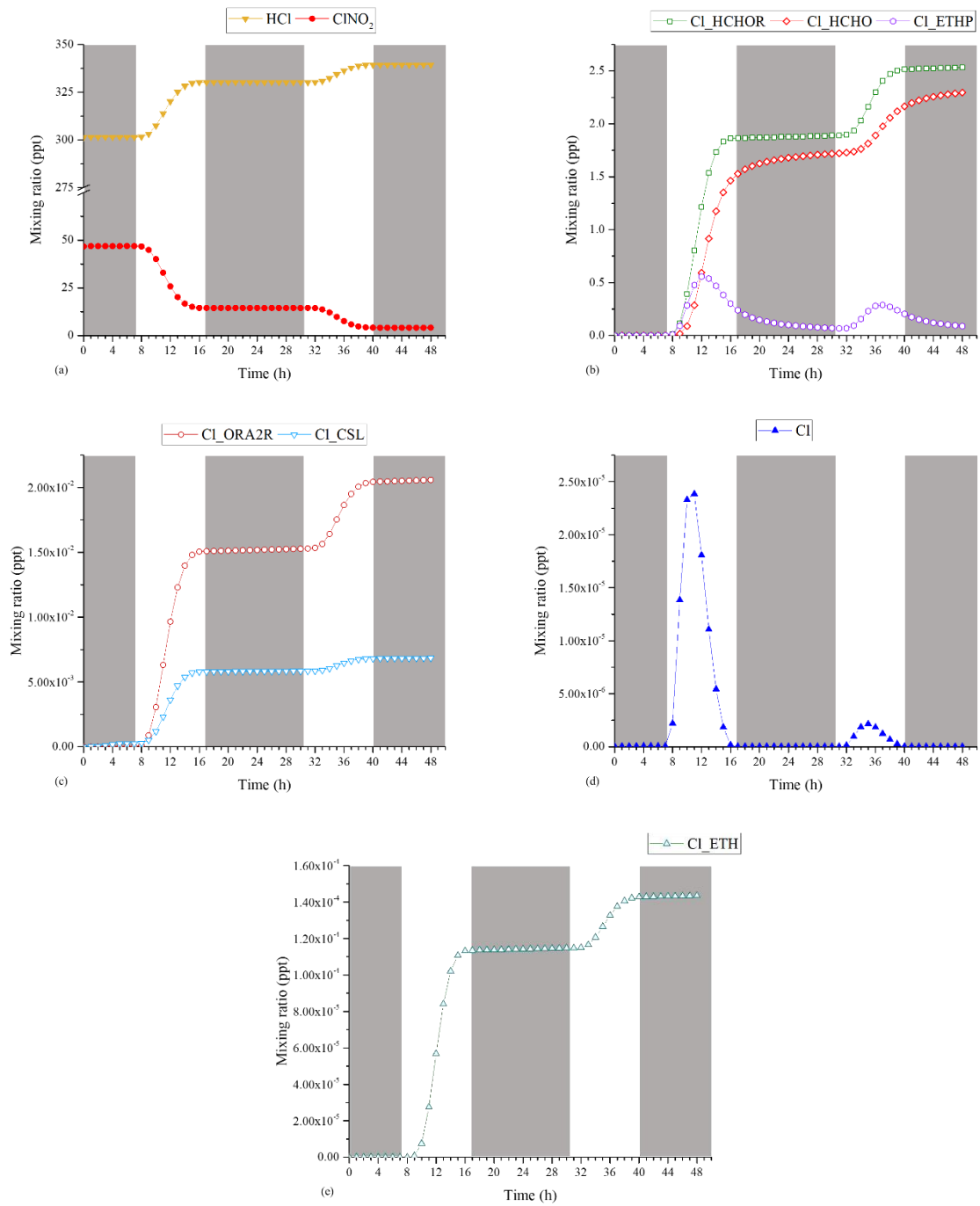
Figure III-10: *The temporal variation of the mixing ratios of the main Cl_RACM classes during winter.*
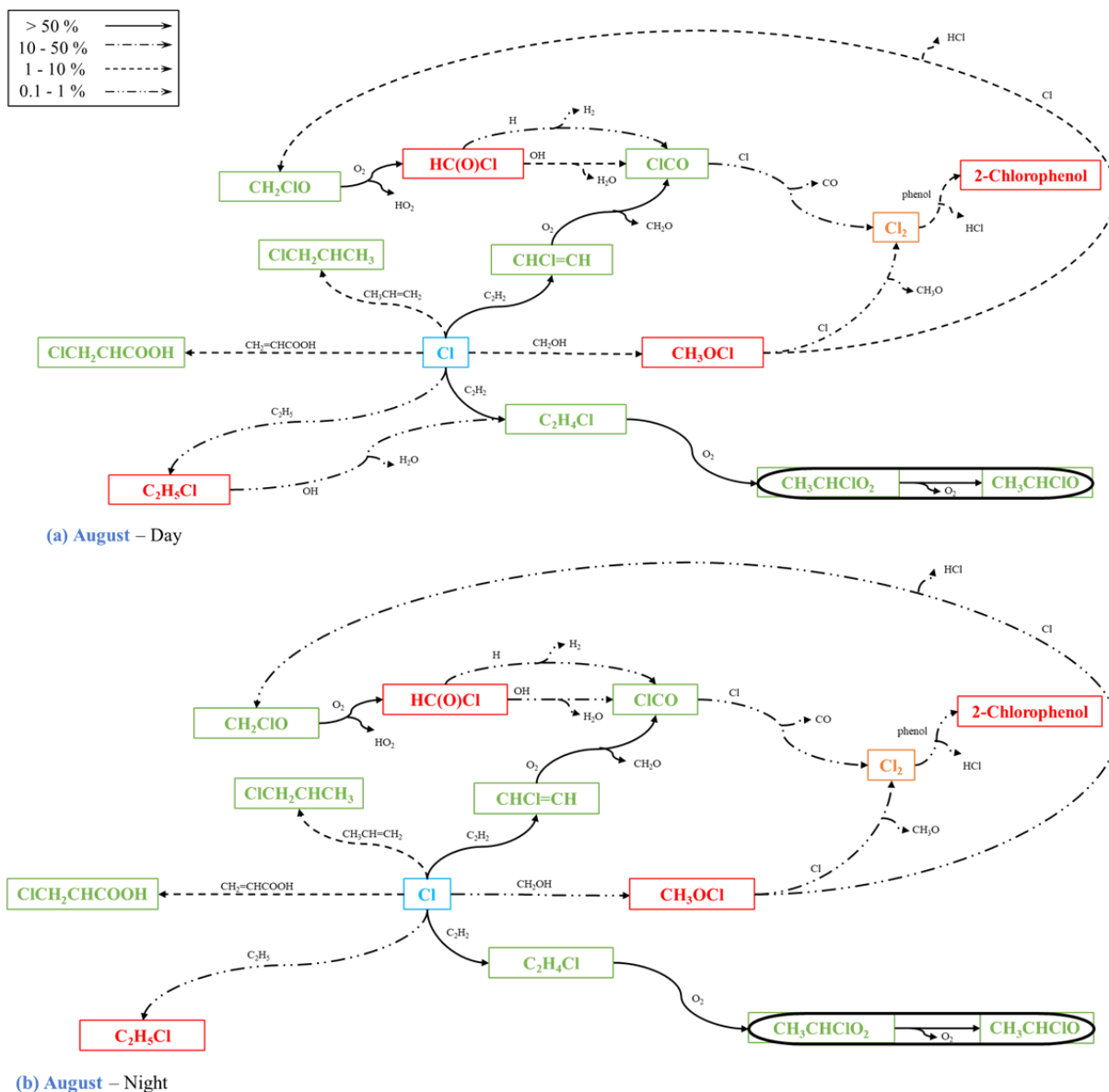
Figure III-11: *Reaction scheme of the main organic chlorinated species during summer day (a) and night (b).*

Similar to the inorganic species, the reactivity of the organic chlorinated species is negligible during the night through which their mixing ratios remain nearly constant. The mixing ratios attained during summer are higher than the mixing ratios reached during winter. However, and in contrary to the degradation of the inorganic species, photolysis has negligible effect on the loss of the organic chlorinated species. It is worth noting that these species are most likely to be photolyzed in the stratosphere and not in the troposphere.
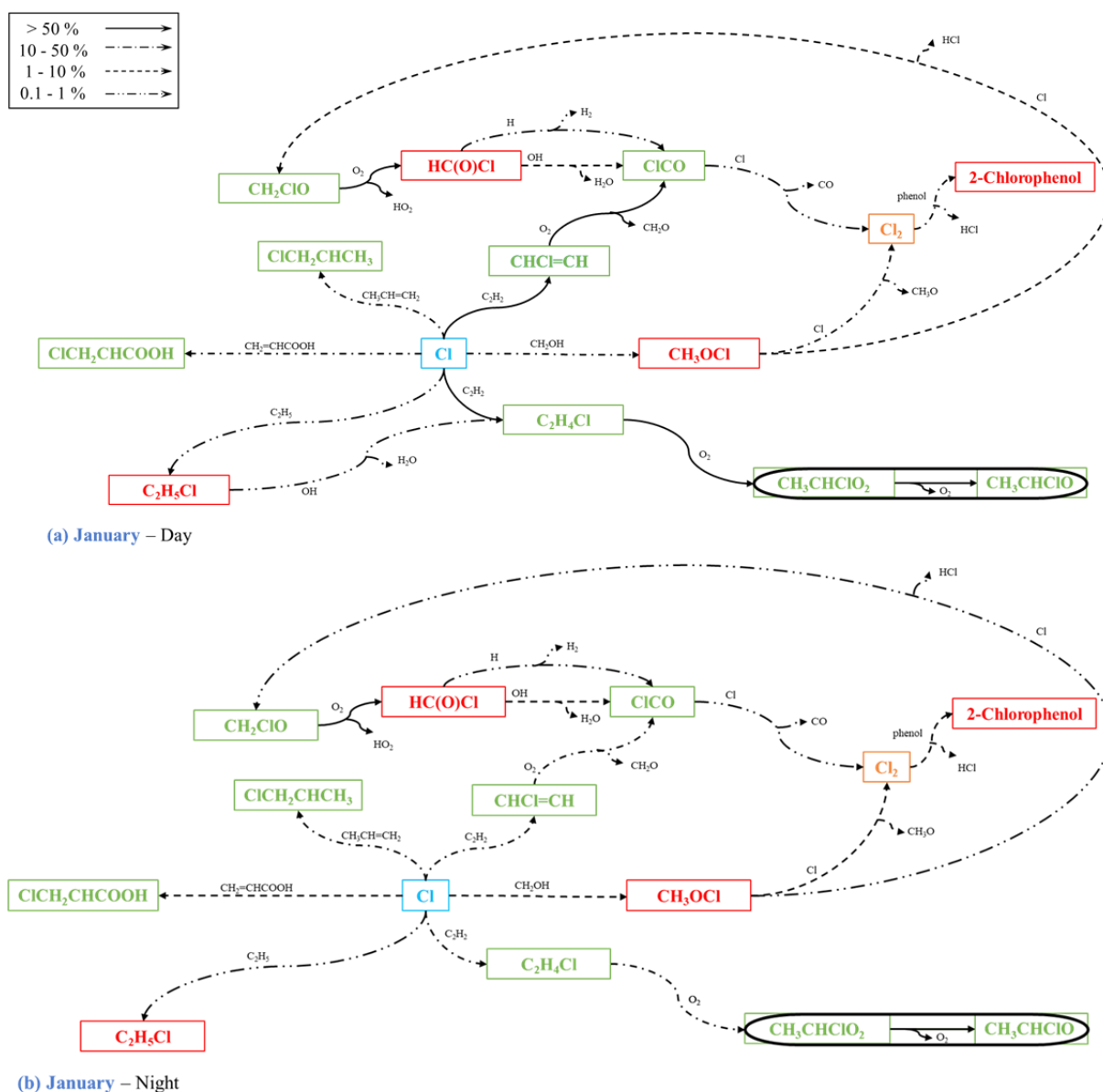
Figure III-12: *Reaction scheme of the organic chlorinated species during winter day (a) and night (b).*

The main Cl_RACM classes formed with the highest mixing ratios amongst the organic chlorinated species are Cl_HCHOR, Cl_HCHO, and Cl_ETHP. These classes correspond to the following species: ClCO, HC(O)Cl, and CH_3CHClO_2 respectively.

A recent publication by Vijayakumar and Wilmouth (2021) indicated that formyl chloride (HC(O)Cl) is a major degradation product of different chlorinated hydrocarbons and its oxidation yields the carbonyl chloride radical (ClCO) through the reaction with different oxidants (OH and Cl). The chlorinated alkoxy radical CH_3CHClO_2 is of significant interest in the atmospheric chemistry. This species is released into the atmosphere by biogenic and anthropogenic processes, and its degradation via a self-reaction, which is bordered by an oval shape (***Figure III-11*** and ***Figure III-12***), has been examined by different studies (Hou et al., 2000; Maricq et al., 1993). Moreover, the loss of ethyl chloride is negligible during the night.

Furthermore, 2-chlorophenol (Cl_CSL family) is a major chlorinated aromatic compound released and formed in the troposphere (Peng *et al*., 2018; Platz *et al*., 1998).

The mixing ratios of the other families are not very important. They can be considered as intermediates in the reactions of chlorinated organic species, especially Cl_HC3.

It is important to mention that the majority of organic species included in our final reaction schemes consist of radical species. Due to the model being run over a limited time scale, it is reasonable to expect that the model is only capable of simulating the behaviour of short-lived species whose lifetimes fall within a range of just a few days.

All the reactions presented in final organic scheme (***Figure III-11*** and ***Figure III-12***) are summarized in ***Table III-8***.

Table III-8: *Thermal reactions involved in the simplified reaction scheme of organic chlorinated species.*

Reaction	Rate constant (s^{-1}) or (cm^3 molecule^{-1} s^{-1}) or (cm^6 molecule^{-2} s^{-1})	Cl_RACM reaction	Literature
Cl + CH$_2$=CHCOOH → ClCH$_2$CHCOOH	2.70×10^{-11}	Cl + ORA2 → Cl_ORA2R	(Aranda et al., 2003)
Cl + M + C$_2$H$_4$ → M + CH$_2$CH$_2$Cl	7.00×10^{-69} T$^{-3.30}$	Cl + ETE → Cl_ETHR	(Atkinson et al., 2001)
Cl + C$_2$H$_5$ → C$_2$H$_5$Cl	4.55×10^{-10}	Cl + ETHR → Cl_ETH	(Timonen *et al.*, 1986)
Cl + CH$_3$CH=CH$_2$ → ClCH$_2$CHCH$_3$	2.71×10^{-10}	Cl + OLT → Cl_HC3R	(Kaiser and Wallington, 1996)
Cl + C$_2$H$_2$ → CHCl=CH	7.97×10^{-8} T$^{-1.04}$	Cl + HC3 → Cl_ETER	(Kaiser, 1992)
Cl + CH$_2$OH → CH$_3$OCl	1.03×10^{-11} T$^{0.29}$	Cl + HC3R → Cl_HC3	(Brudnik *et al.*, 2009)
C$_2$H$_5$Cl + OH → C$_2$H$_4$Cl + H$_2$O	1.50×10^{-12} T$^{0.50}$ exp(-674/T)	Cl_ETH + HO → Cl_ETHR + H2O	(Herndon *et al.*, 2001)
CH$_3$OCl + Cl → CH$_3$O + Cl$_2$	8.49×10^{-1}	Cl_HC3 + Cl → Cl2 + HC3R	(Kukui *et al.*, 1997)
CH$_3$OCl + Cl → HCl + CH$_2$OCl	2.00×10^{-1}	Cl_HC3 + Cl → HCl + Cl_HC3R	(Carl *et al.*, 1996)
HC(O)Cl + H → H$_2$ + ClCO	1.16×10^{-19} T$^{2.61}$ exp(-1018/T)	Cl_HCHO + H → H2 + Cl_HCHOR	(Li and Luo, 2003)
HC(O)Cl + OH → ClCO + H$_2$O	5.00×10^{-13}	Cl_HCHO + HO → Cl_HCHOR + H2O	(Atkinson et al., 2001)
Cl$_2$ + Phenyl → Chlorobenzene + Cl	1.00×10^{-12} exp(1000/T)	Cl2 + TOLR → Cl_TOL + Cl	(Tonokura *et al.*, 2002)
CH$_3$CHCl + O$_2$ → CH$_3$CHClO$_2$	1.04×10^{-11}	Cl_ETHR + O2 → Cl_ETHP	(Knyazev *et al.*, 1995)
CH$_3$CHClO$_2$ + CH$_3$CHClO$_2$ → 2 CH$_3$CHClO + O$_2$	4.90×10^{-12}	2Cl_ETHP → 2 Cl_HC3R + O2	(Maricq *et al.*, 1993)
CHCl=CH + O$_2$ → CH$_2$O + ClCO	5.00×10^{-12} exp(-166/T)	Cl_ETER + O2 → HCHO + Cl_HCHOR	(Russell et al., 1989)
CH$_2$ClO + O$_2$ → HC(O)Cl + HO$_2$	2.00×10^{-12} exp(-935/T)	Cl_HC3R + O2 → Cl_HCHO + HO2	(Wu and Carr, 2001)
ClCO + Cl → CO + Cl$_2$	2.16×10^{-9} exp(-1666/T)	Cl_HCHOR + Cl → CO + Cl2	(Baulch *et al.*, 1981)

Chapter III. Kinetic modelling

III.4.1.3. The full chlorine mechanism, organic/ inorganic

First of all, it is worth mentioning that the introduction of the reactions of the chlorinated organic species into the box model has its influence on the behaviour of the inorganic chlorinated species. When comparing the temporal variation of HCl and $ClNO_2$ before and after this introduction (***Figure III-5(a)*** to ***Figure III-9(a)*** during summer and ***Figure III-6(a)*** to ***Figure III-10(a)*** during winter). In the organic mechanism, HCl is mainly formed by the reaction of Cl with VOCs belonging to different classes of ***Table III-4*** via hydrogen abstraction by the atomic Cl, for example: HC5 ($1-C_6H_{14}$, $n-C_5H_{12}$, and cyclopentane) and HC3 ($1-C_4H_{10}$, $(CH_3)2O$, and cyclobutane).

$ClNO_2$ is still being photolyzed as in the case of inorganic mechanism. In the same way, the formation of $ClNO_2$ is predominantly via the reaction (***R16***). The efficiency of (***R16***) decreases in the organic mechanism since the mixing ratio of atomic Cl is lower (comparing ***Figure III-5(d)*** with ***Figure III-9(e)*** and ***Figure III-6(d)*** with ***Figure III-10(e)***). Therefore, the production of $ClNO_2$ is of lower importance in the organic mechanism.

$$Cl + NO_2 \rightarrow ClNO_2 \hspace{4cm} \textbf{\textit{R16}}$$

Simulations conducted to investigate the reactivity of atomic Cl during the daytime have revealed that its production predominantly occurs through the following pathways:

$$ClNO_2 + h\nu \rightarrow Cl + NO_2 \hspace{3cm} \textbf{\textit{R17}} (90.6\%)$$
$$ClO + NO_3 \rightarrow Cl + O_2 + NO_2 \hspace{2.5cm} \textbf{\textit{R18}} (3.7\%)$$
$$HCl + OH \rightarrow Cl + H_2O \hspace{3cm} \textbf{\textit{R19}} (2.0\%)$$
$$HCl + CH_2OH \rightarrow Cl + CH_3OH \hspace{2cm} \textbf{\textit{R20}} (1.1\%)$$

The remaining 2.6% primarily correspond to the reactions involving the abstraction of hydrogen from HCl by VOCs resulting in the formation of atomic Cl.

Similarly, simulations were conducted to study the routes of night-time reactivity of atomic Cl. The results are as follows:

$$HCl + CH_2OH \rightarrow Cl + CH_3OH \hspace{2.5cm} \textbf{\textit{R21}} (61.9\%)$$
$$HCl + NO_3 \rightarrow Cl + HNO_3 \hspace{3cm} \textbf{\textit{R22}} (19.3\%)$$
$$HCl + CH_3O \rightarrow Cl + CH_3OH \hspace{2.5cm} \textbf{\textit{R23}} (16.5\%)$$
$$HCl + OH \rightarrow Cl + H_2O \hspace{3.5cm} \textbf{\textit{R24}} (1.7\%)$$
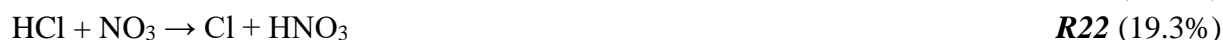
The differences between day and night production of atomic Cl mainly arise from the absence of photolytic effects during the night. It should be noted that these percentage values are specific to the summer season and may exhibit some variations during winter.

III.4.2. Influence of the added reactions on the general chlorine chemistry

Our model can be considered to include all tropospheric thermal and photolysis reactions of organic and inorganic chlorinated species that can take place in the gaseous phase only. It sums up all the literature about the degradation of these species and the chlorine cycling among them, which makes our mechanism capable of mimicking the free tropospheric chlorine cycling.

To show what our model brings new to chlorine tropospheric chemistry, it is crucial to compare it with one of the previous model studies listed in **Table III-1**. The most recent study of Fan and Li (2022) developed a model including different halogens (brominated and iodinated species) to determine the summer time tropospheric chemistry in eastern China. The model of Peng *et al*. (2021) was for a mixed halogenated mechanism and localized in North China. It considered the analogy between reactions with OH radicals and atomic Cl in the value of rate constants and branching ratios. Hoffmann *et al*. (2019) studied the impacts of mixed halogenated species in a specific environment (urban and maritime coastal area). Also, the mechanism of Badia *et al*. (2019) was simplified (only 38 reactions), localized (Tropical East Pacific), and for mixed halogenated species. Li *et al*. (2016) considered a simplified mechanism of the chlorinated species (only 24 reactions) over Southern China. Then, the mechanism developed in this work is compared with that of Hossaini *et al*. (2016), which focused primarily on chlorine chemistry on a global scale in the mentioned study.

The mechanism of Hossaini *et al*. (2016) is made under conditions close to the ones in our mechanism. In their model, 95 gas-phase reactions of chlorinated organic and inorganic species were included. These reactions are classified as the following: 67 thermal organic reactions, 16 thermal inorganic reactions, 5 photolysis organic reactions, and 7 photolysis inorganic reactions. There are 15 common reactions between our model and the model of Hossaini *et al*. (2016) with similar rate constants. Differences in kinetic data between the two models arise from referring to different literature studies to get the kinetic parameters.

The mechanism of Hossaini *et al*. (2016) involved the reactions of chlorinated organic species with more than two chlorine atoms ($CHCl_3$, $C_2Cl_4(OH)O_2$, $C_2Cl_5O_2$), which are, to our knowledge, non-reactive in the lower tropospheric levels (long-lived species), but reactive in the upper troposphere and stratosphere. In addition, it included phosgene (CCl_2O), which is very toxic. CCl_2O is released into the atmosphere at the upper tropospheric-stratospheric level (Harrison *et al*., 2019). It is mainly a product of the photolysis of carbon tetrachloride (CCl_4), which happens in the UV-C range (not in the troposphere). Hossaini *et al*. (2016) also added some reactions of mixed halogenated species including Cl ($CHBrCl_2$, $CHBr_2Cl$, CH_2ICl) to their mechanism.

The temporal variation of the mixing ratios of the main inorganic chlorinated species mentioned in the model of Hossaini *et al*. (2016) during summer time is represented in **Figure III-13**. The results during winter season are not presented since they are almost the same as in summer. The evolution of the mixing ratios of HCl and $ClNO_2$ in our mechanism and the mechanism of Hossaini *et al*. (2016) is similar (comparing **Figure III-9(a)** and **Figure III-13(a)**). HCl is being formed by the reaction (**R25**) mainly, which is the H abstraction from

methoxy radical (CH$_3$O) by atomic Cl. Therefore, in both mechanisms, ours and the one of Hossaini *et al.* (2016), the H abstraction from different VOCs (CH$_3$O, 1-C$_6$H$_{14}$, n-C$_5$H$_{12}$, cyclopentane, 1-C$_4$H$_{10}$, (CH$_3$)2O, and cyclobutane) constitutes the major way of producing of HCl in the troposphere (Crisp *et al.*, 2014; Dawe *et al.*, 2019).

Cl + CH$_3$O → HCl + HCHO **R25**

ClNO$_2$ is being photolyzed as the daytime starts in both mechanisms. Furthermore, Hossaini *et al.* (2016) focused more on the chlorine nitrate (ClONO$_2$) (***Figure III-13(b)***) and neglected the reactivity of ClNO in their mechanism. ClONO$_2$ is a stratospheric species and considered to be the reservoir of chlorine and nitrogen especially in the polar regions (von Clarmann and Johansson, 2018). Moreover, and due to the extension of the model of Hossaini *et al.* (2016) to include the stratospheric chemistry of chlorinated species, ClO becomes more and more important (Nedoluha *et al.*, 2016). It is still being produced by the reaction (***R14***), but the photolysis of ClONO$_2$, which occurs at wavelengths between 196 and 432 nm that is more important in the stratosphere and of very low efficiency in the troposphere (von Clarmann and Johansson, 2018), appears now to be the major source of ClO. This makes ClO more abundant than in our case (***Figure III-13(c)***).

Regarding the organic chlorinated species, Hossaini *et al.* (2016) focused primarily on the species with more than two chlorine atoms. The average mixing ratios of these species during 48 hours are given in ***Figure III-14***. As shown in the figure, these species are very scarce with very low mixing ratios (in the order of less than 10^{-17} ppt), i.e. their production is negligible under the ambient tropospheric conditions considered in our mechanism, but rather in the stratosphere. This validates our assumption of not involving species with more than two chlorine atoms in our model and neglecting their effects on the chlorine tropospheric chemistry.
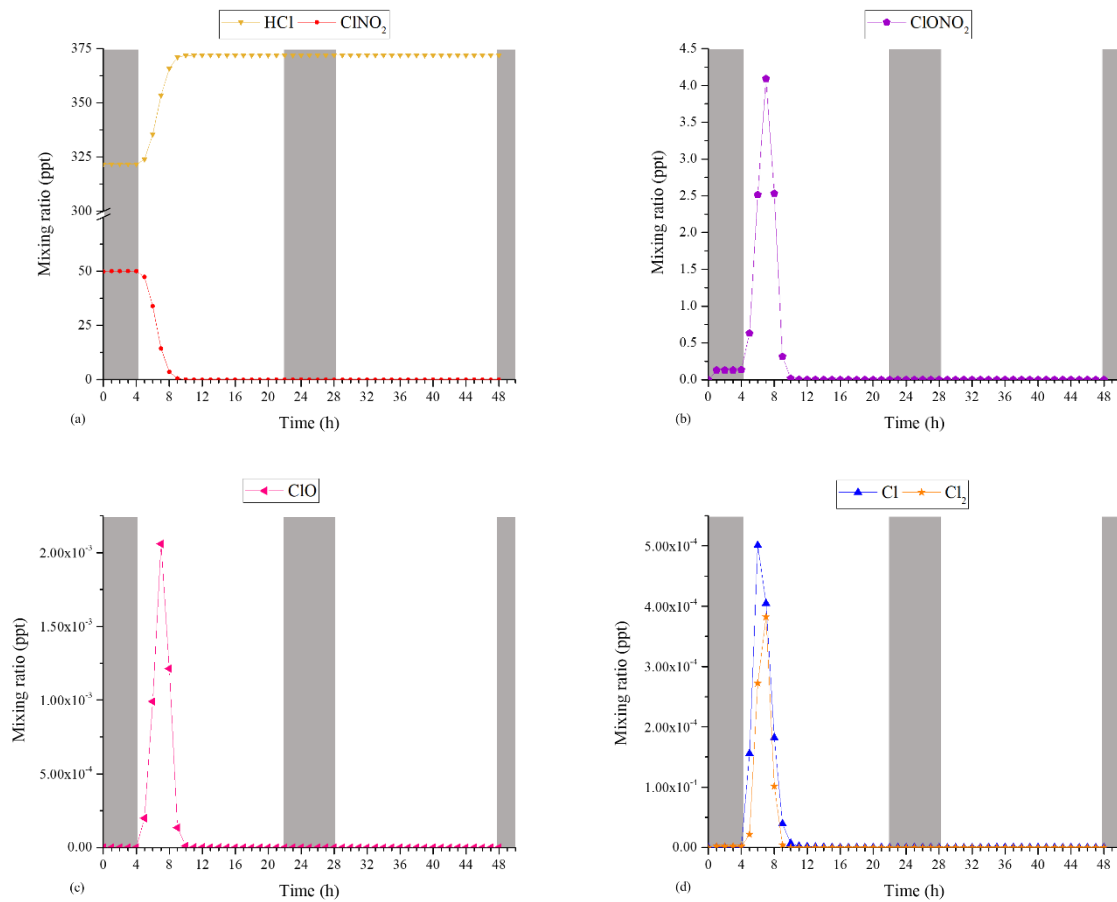
Figure III-13: *The temporal variation of the mixing ratios of the main inorganic chlorinated species mentioned in the model of Hossaini et al. (2016) during summer.*
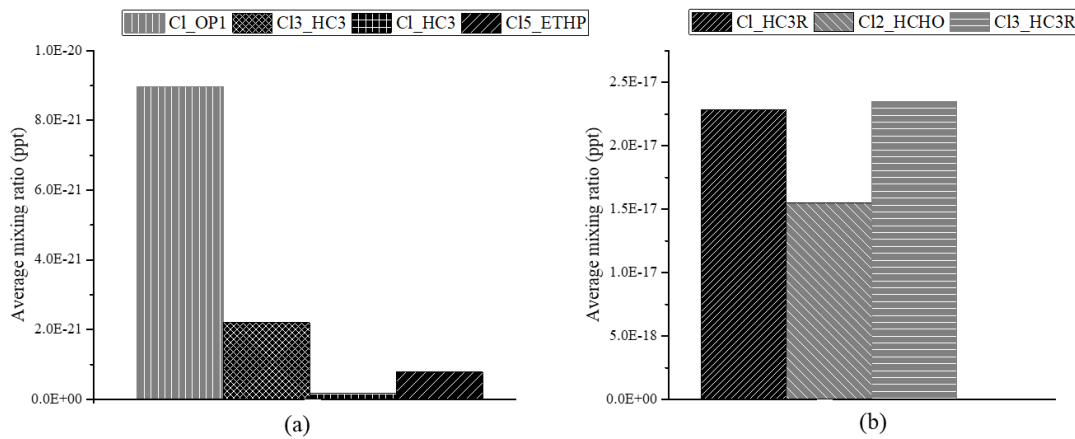
Figure III-14: *The average mixing ratios of the main Cl_RACM classes mentioned in the model of Hossaini et al. (2016) during summer given for 48 hours.*

114

Chapter III. Kinetic modelling

III.4.3. Limitations of the model

III.4.3.1. General limitations of 0D models

Zero-dimensional (0D) atmospheric models are simplified models that assume the atmosphere is uniform and well-mixed. While they can be useful for certain applications, such as modelling the global average temperature or the composition of the atmosphere, they have several important limitations:

- No spatial resolution: 0D models do not consider the spatial distribution of atmospheric parameters, such as temperature, pressure, and composition. As a result, they cannot capture regional or local variations in these parameters, which can be important for many applications.

- No temporal resolution: 0D models only provide an average value for atmospheric parameters over a given time period. They cannot capture the dynamics of atmospheric processes, such as the diurnal cycle of temperature or the seasonal cycle of atmospheric composition.

- Limited representation of physical processes: 0D models simplify the physics of the atmosphere and do not include many important processes, such as advection, convection, and turbulence. This can lead to inaccuracies in the results, especially for applications that require a high level of detail.

- Assumptions about atmospheric composition: 0D models often assume that the atmosphere is well-mixed and homogeneous, which may not be true in certain regions or for certain pollutants. This can lead to errors in the estimates of atmospheric composition, such as the concentration of greenhouse gases or pollutants.

Overall, 0D atmospheric models are useful for certain applications (air quality assessment, climate studies, chemical kinetics and mechanism development), but they have important limitations that must be considered when interpreting their results.

III.4.3.2. Specific limitations for the ASTEC 0D model

The availability and accuracy of input parameters such as temperature, pressure, and concentrations of atmospheric species are crucial for the accuracy of the SOPHAEROS module. However, measuring or estimating these parameters with high precision can be challenging, especially in regions with complex atmospheric dynamics or limited observations. Moreover, the mechanism used in the module may have uncertainties due to both thermokinetic and thermodynamic properties of the reactions involved, as highlighted by Chevalier-Jabet *et al*. (2014) in their investigation of iodine behaviour in the ASTEC model.

In addition, the model's shortcomings in studying chlorine atmospheric chemistry include its lack of heterogeneous (multiphase) reactions, which are crucial for this field. For example, as previously mentioned, the main production pathway for $ClNO_2$ is through the heterogeneous reactions with dinitrogen pentoxide (N_2O_5), as reported by Lou *et al*. (2022). This reaction is about three orders of magnitude more significant than the pathway in which NO_2 is added to atomic chlorine to form $ClNO_2$, as stated by Sarwar *et al*. (2014). Neglecting

the impact of mixed halogenated species, such as BrCl and ICl, further limits the model's mechanism and its ability to reflect the current understanding of tropospheric chemistry. Additionally, not considering the analogy between Cl reactivity and that of other halogens (Br and I) as well as that of OH radicals is not true for all reactions, since JPL and IUPAC have proven the kinetic parameters to be similar for some reactions with small uncertainties. All of these factors highlight the limitations of the model and emphasize the need for improvements to the ASTEC code to expand its capabilities in evaluating accidents and the evolution of radioactive species, as well as computing the reactivity of species relevant to atmospheric research.

III.5. Conclusion and perspectives

Based on the limitations identified in the earlier discussion, it is clear that there is a need for improvements to the ASTEC 0D model in studying chlorine atmospheric chemistry. These improvements include incorporating heterogeneous reactions and mixed halogenated species, as well as considering the analogy between Cl reactivity and that of other halogens and OH radicals.

However, it is encouraging to note that a new gas-phase chlorine mechanism, containing 388 reactions, has been implemented into the ASTEC 0D model to evaluate the behaviour of chlorinated species in the atmosphere. The resulting mechanism is up-to-date and is designed to mimic the chemistry of chlorinated species in the free troposphere at ambient temperature and pressure conditions. The simulations carried out in day and night times during both winter and summer times have shown promising results, indicating that the model can be simplified enough to be implemented into global and regional chemistry-transport models.

In conclusion, although there are limitations in the current ASTEC 0D model, the implementation of a new gas-phase chlorine mechanism represents a step forward in improving our understanding of chlorine atmospheric chemistry. Further research and improvements are still necessary to advance our knowledge in this field.

Moreover, and to complete this work, it will be important to include other halogens (Br for instance), mixed halogenated species (like BrCl, ICl), and chlorine heterogeneous chemistry. It will be also interesting to study the reactivity of chlorinated species over a longer time scale.

Chapter IV.   Global atmospheric modelling

IV.1. Introduction

This chapter describes MOCAGE, Model Of atmospheric Chemistry At larGE scale, used to carry out the simulations which are further analysed in the chapter. MOCAGE is a three-dimensional Chemistry-Transport Model (CTM) developed by the Centre National de Recherches Météorologiques (CNRM/Météo-France-CNRS). It is used to describe the chemical state of the atmosphere, from the surface up to an atmospheric pressure of 5 hPa, i.e. an altitude of about 35 km, covering the troposphere and part of the stratosphere.

In the original version of MOCAGE, the halogen chemistry is already implemented, namely chlorine and bromine. However, it only aims to represent stratospheric halogen chemistry. Regarding the chemistry of atmospheric chlorine, the effect of chlorine on VOCs and the impact of chlorinated VSLS on ozone, whether in the troposphere or in the stratosphere, are not taken into account despite the importance of the reactivity of chlorine towards VOCS and that of VSLS that are well described in *Chapter I*. In this chapter, we aim to further develop the chlorine chemistry in MOCAGE, and to highlight these two effects on the global scale. This work is done in a collaboration between PC2A laboratory in Lille, France and CNRM/Météo-France in Toulouse, France.

To do this work, several updates and new developments have been implemented in MOCAGE. The emissions of chlorinated species in MOCAGE are updated. Reactions of chlorine with certain VOCs are added. Chlorinated VSLS are implemented into the MOCAGE scheme, and reactions of VSLS are introduced. As a reminder, VSLS are species whose lifetimes are about 6 months. Therefore, MOCAGE enables the simulation of species that are important on a long-time scale.

In ASTEC, the mechanism of the cycling of the very reactive chlorinated species is at a very short time scale with mostly radical species, which are unstable in the atmosphere. Since MOCAGE simulations aim at studying much longer time scales, it is therefore not possible to use the ASTEC scheme directly in the developments of the chlorine chemistry in MOCAGE. Nevertheless, some of the ASTEC reactions are used in the new MOCAGE scheme.

A very short time duration was dedicated to the work presented in this chapter (about 4 months). Therefore, all the processes needed to fully represent tropospheric chlorine chemistry could not be implemented. Still, this work allows to analyse the effects of different updates of chlorine components on the tropospheric and stratospheric composition. Also, because of the lack of time, this is only a very preliminary analysis of the MOCAGE results that is presented in this chapter.

The organization of this chapter is as follows: in **section IV.2**, the MOCAGE model is presented, its geometry is described, together with its incorporated chemical and physical processes. The new developments made to evaluate the impact of chlorine atmospheric chemistry are also included. After that, the configurations of the different simulations are described in **section IV.3**. The results of these simulations are presented in **section IV.4**. Finally, a comprehensive discussion and brief conclusion are given in **section IV.5**.

IV.2. The chemistry transport model - MOCAGE

IV.2.1. General presentation

MOCAGE is an offline 3D CTM developed by CNRM (Centre National de Recherches Météorologiques) (Cussac *et al.*, 2020; Guth *et al.*, 2016). MOCAGE allows to model the chemical composition of the atmosphere (gases and aerosols) from global to regional scales. This is achieved by incorporating various physicochemical processes involved in the atmosphere, which can be broadly categorized into four groups: emission, transport, chemical transformation and deposition processes (**Figure IV-1**). MOCAGE allows the modelling of both primary and secondary aerosols, but since they are not studied in the present work which focuses on gaseous processes following the work of **Chapter III**, their representation in the model is not presented.
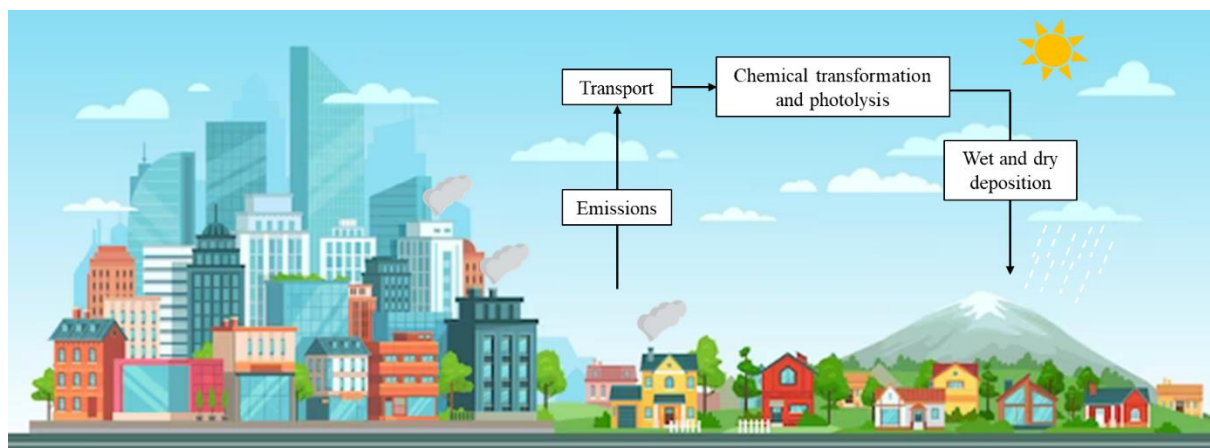
Figure IV-1: *Schematic presentation of the different processes presented in MOCAGE.*

As an offline model, MOCAGE uses meteorological fields (temperature, pressure, humidity, wind speed and direction, precipitation, and cloud) as inputs. These inputs are calculated by a separate meteorological model like Météo-France ARPEGE (Action de Recherche Petite Echelle Grande Echelle) or the European Centre for Medium-Range Weather Forecasts IFS (Integrated Forecasting System model) or climate models (e.g.: ARPEGE-Climat). The input and output data simulated by MOCAGE are summarized in **Figure IV-2**.

Chapter IV. Global atmospheric modelling
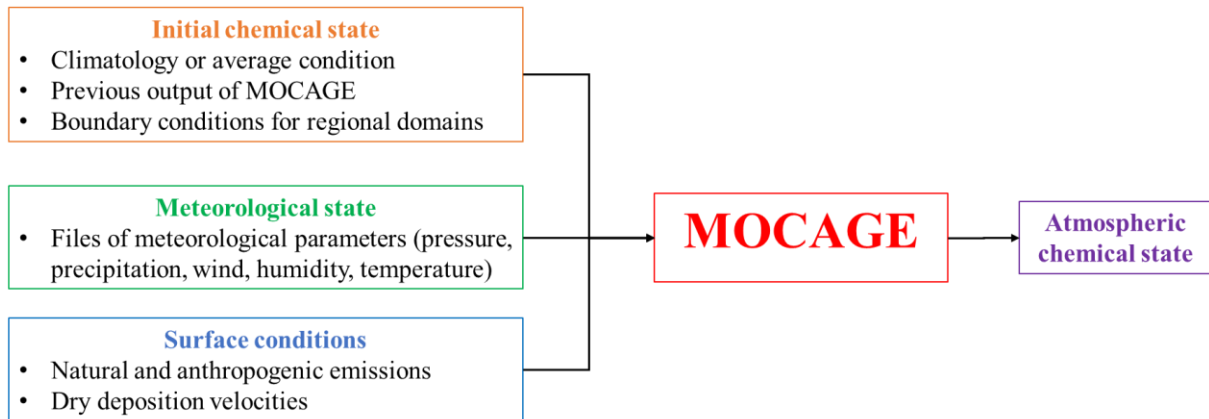
Figure IV-2: Schematic representation of the inputs and output of MOCAGE model.

The exploitation of the MOCAGE model is done for both operational purposes and scientific research. For example, in France, MOCAGE serves operational purposes by generating air quality forecasts within the PREV' AIR program (Rouil *et al.*, 2009). At the European level, CAMS (Copernicus Atmosphere Monitoring Service) coordinates the efforts of the operational prediction of the atmosphere composition, and in which MOCAGE participates with 10 other models (Marécal *et al.*, 2015). Moreover, it is utilized for research purposes for instance to examine the effects of climate changes on atmospheric composition, as in Lamarque *et al.* (2013), Lacressonnière *et al.* (2014), and Watson *et al.* (2015). The model can also be employed to investigate the gas composition of the upper troposphere and lower stratosphere, as shown in the studies of Barré *et al.* (2014) and Cussac *et al.* (2020).

IV.2.2. Geometry of the model

As mentioned, MOCAGE can be applied for both regional and global scales. In this research work, the model is used in its global horizontal resolution scale with a regular latitude and longitude grid ($1° \times 1°$). The model allows the implementation of nested domains for the regional modelling, but for the purposes of this thesis, this feature is not used.

In terms of vertical resolution, the atmosphere is subdivided into several levels in order to better understand the various physical and chemical processes from the surface to the lower stratosphere. In this study, a version with 47 vertical hybrid σ-pressure levels is used, ranging from the surface to 5 hPa (about 35 km). The distribution of these 47 levels is as follows: 7 levels in the boundary layer, 20 in the free troposphere, and 20 in the stratosphere. *Eq. IV-1* allows the calculation of the model's inter-level pressure. The inter-level pressures are then used to obtain the pressure P of the centre of mass of each vertical level of MOCAGE.

$$P_i = A_i + B_i P_s \qquad\qquad \textbf{\textit{Eq. IV-1}}$$

In *Eq. IV-1*, P_s is the pressure at the ground level. A_i and B_i are the coefficients used to calculate the inter-level pressure P_i. These coefficients and an example of vertical levels are shown in *Figure IV-3*.
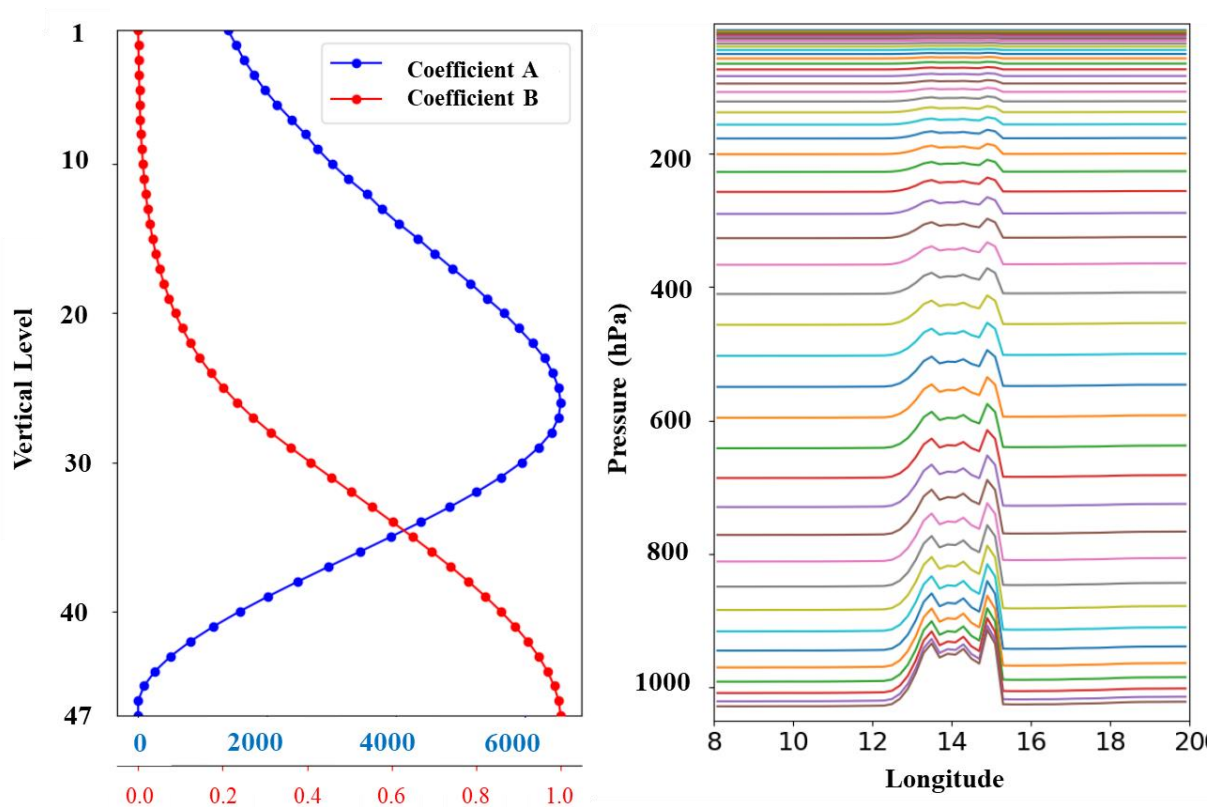
Figure IV-3: *Representation of the coefficient A_i (in blue) and B_i (in red) (figure on the left) presented in **Eq. IV-1**. The figure on the right shows the pressure (in hPa) corresponding to the vertical levels calculated using the same equation for a point located at 38 °N and for longitudes between 8 and 20 °E (Narivelo, 2019).*

IV.2.3. Chemical processes

IV.2.3.1. Chemical scheme

The chemistry of gaseous species in MOCAGE is treated with the RACMOBUS scheme, which is the result of the fusion of the tropospheric chemistry RACM (Regional Atmospheric Chemistry Mechanism (Stockwell *et al*., 1997)) and the scheme of the stratospheric chemistry REPROBUS (REactive Processes Ruling the Ozone Budget in the Stratosphere (Lefèvre *et al*., 1994)) whose specifications are detailed below.

RACM was created to model the composition of the troposphere from polluted chemical regimes in the atmospheric boundary layer to chemical regimes in the upper troposphere. In total, it includes the representation of 77 atmospheric species, 237 reactions including 23 photolysis reactions. For reasons of saving calculation time, some species are in fact groupings of several chemical compounds of the same family of species. This is particularly the case for certain families of organic compounds which represent a great diversity of species.

Used for the first time in the study of Lefèvre *et al.* (1994), the REPROBUS scheme has been designed to model the chemical composition of the stratosphere at a global scale. The objectives are the good presentation of the ozone layer, as well as its destruction at the poles in winter. The key mechanisms represented are the Chapman ozone production cycle, the different catalytic cycles of ozone destruction, and the heterogeneous reactions at the surface of polar clouds that cause ozone destruction. It includes a total of 41 species, 72 reactions in gaseous phase, 23 photolysis reactions, and 7 heterogeneous reactions.

The fusion of these two schemes results in a total of 112 species or families of species, as well as 434 chemical reactions. In order to complete the chemical cycle of nitrogen, 2 photolysis reactions have been added in the RACMOBUS scheme in order to consider the photolysis of the PAN, bringing the total of photolysis reactions considered in MOCAGE to 57. In addition, reactions are included to complete the sulphur cycle in the troposphere (Guth *et al.*, 2016).

The reaction constants are updated according to the recommendations of the JPL (Jet Propulsion Laboratory) and the IUPAC (International Union of Pure and Applied Chemistry). The calculation of the photolysis rates is done off-line by the TUV model (Tropospheric Ultraviolet and Visible radiation model (Madronich, 1987)) version 5.3.1. These photolysis rates are tabulated as a function of surface albedo, considered altitude, zenith angle, and ozone column above the considered point, and are then used in MOCAGE with an online correction for cloud cover according to Brasseur *et al.* (1998).

IV.2.3.2. Solver

The RACMOBUS scheme allows the calculation of the rates of chemical production Q_{prod} and chemical destruction Q_{loss} associated with every species in the model. The equation of chemical time variation of the mixing ratio C of a species is then:

$$\frac{\partial c}{\partial t} = Q_{prod} - Q_{loss}$$
Eq. IV-2

In a recent version of MOCAGE, the Rosenbrock solver generated by the Kinetic Pre-Processor (KPP) software is implemented (Sandu and Sander, 2006). The standard four-stages, third order Rosenbrock solver (Rodas3, Sandu *et al.* (1997)) is used.

IV.2.4. Physical processes

IV.2.4.1. Transport

In MOCAGE, the transport of species is of 3 types: the large-scale transport, the transport by convection, and the transport by turbulent diffusion. Each of these types is described below.

a. Large-scale transport:

The large-scale transport of air masses by the atmospheric circulation, and thus of the chemical species that compose them, corresponds to solving a problem of advection. Considering a transported species as a passive tracer ψ; i.e. a scalar which is conserved during the transport and which does not modify the flow; the transport equation is then written as:

$$\frac{\partial \psi}{\partial t} + \underline{u}\, \underline{\nabla}\, \psi = 0 \qquad\qquad \textbf{\textit{Eq. IV-3}}$$

where t is the time, and $\underline{u}$ represents the wind speed.

The calculation of the advection in MOCAGE is done with a semi-Lagrangian method, based on that of Williamson and Rasch (1989). This type of scheme calculates the transport through back-trajectories (Lagrangian approach) starting from different uniformly distributed grid points (Eulerian approach). The method of calculation to determine the evolution of a passive tracer ψ_i^t at different grid points x_i is as follows. At a timestep $t + \Delta t$, the value of $\psi_t^{t+\Delta t}$ is equal to the concentration of tracer ψ_0^t at the point x_0, located on the back trajectory starting from x_i and at time t. Since x_0 is a priori not a grid point, ψ_0^t is then computed by interpolation of the field ψ_i^t. This method is illustrated in **Figure IV-4**.
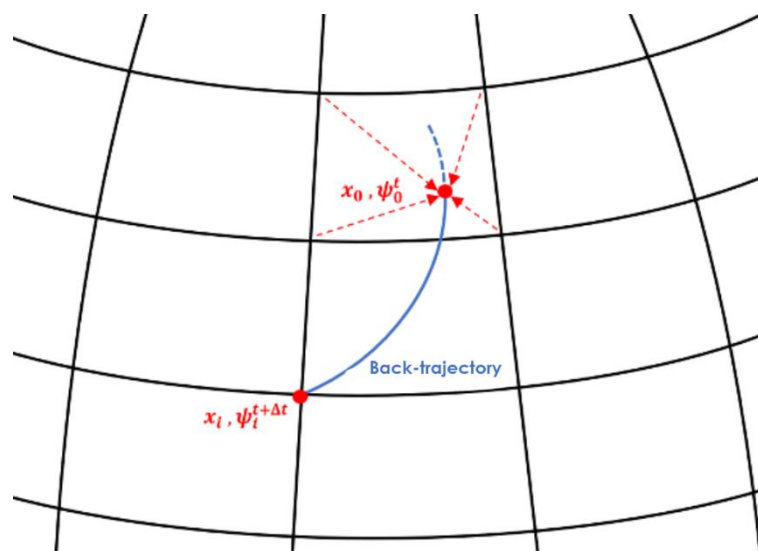
Figure IV-4: *Schematic diagram of the semi-Lagrangian method, allowing to evaluate $\psi_t^{t+\Delta t}$ through a back-trajectory calculation to find ψ_0^t (Cussac, 2020).*

b.   Transport by convection:

The phenomenon of convection is caused by instabilities in the atmosphere, the first manifestation of which are the cumulonimbus and/or thunderstorms. The general principle of this phenomenon is the heating of air masses by solar radiation, eventually increasing their buoyancy and causing a rapid vertical ascent associated with a descent of colder air. This is commonly called an *updraft* and a *downdraft*. To these two vertical movements inside convective clouds, we also associate the subsidence of the cloud environment, which compensates for the overall upward movement inside the cloud, schematized in ***Figure IV-5***. In addition, at the edges of the cloud, mixing takes place between the air in the cloud and the outside air, causing an input of outside air into the cloud (entrainment phenomenon) and an injection of the air of the cloud in the external environment (phenomenon of detrainment), also represented in ***Figure IV-5*** as well as the variation of their intensity with altitude.
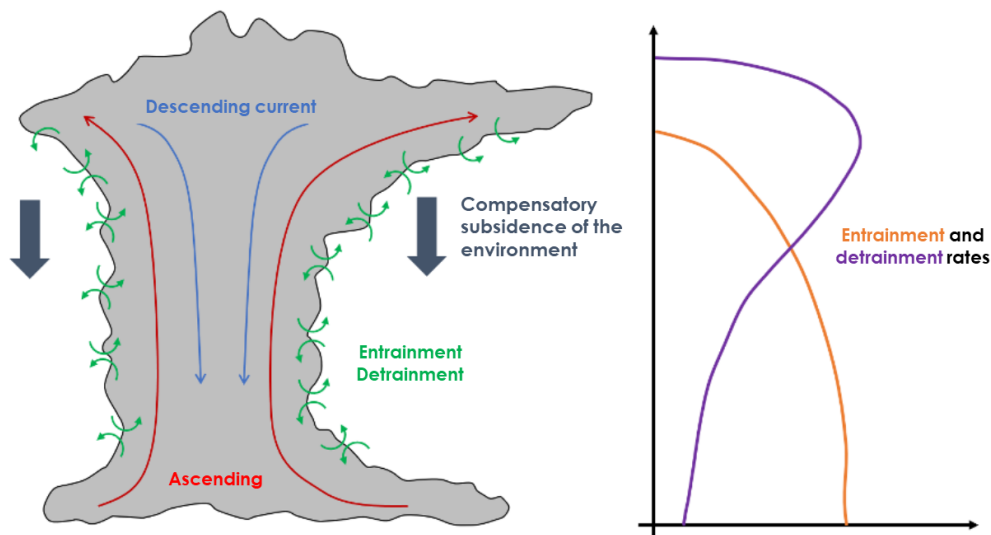
Figure IV-5: *Illustration of the convection phenomenon and the quantities represented in MOCAGE (left). Schematic vertical profile of the evolution of the entrainment and detrainment rates during a convective event (right) (Cussac, 2020).*

Convection is one of the most efficient means of vertical transport, allowing air masses at the surface to reach the upper troposphere in a few tens of minutes, thus participating in mixing in the troposphere. It is thus a key process to represent in a CTM, but its characteristic size, from about 1 km or to about 10 km, prevents an explicit representation for global modelling. A sub-grid parameterization is therefore used in MOCAGE, called KFB (for Kain-Frischt-Beschtold) according to the scheme of Bechtold *et al*. (2001), in which the computation of entrainment and detrainment rates is done according to the method of Kain and Fritsch (1990). Its implementation in MOCAGE and validation are detailed in the study of Josse *et al*. (2004).

c.   Transport by turbulent diffusion

Turbulent diffusion is also a fine-scale process responsible for vertical mixing, mainly in the lowest layers of the atmosphere. Because of its characteristic size and its complexity, it is also a process that requires parameterization. In MOCAGE, it is the Louis (1979) parameterization which is used. It is a first-order scheme based on a diagnosis of the stability of the atmosphere to estimate a diffusion coefficient K and thus the vertical transport for each species. The transport by turbulent diffusion increases with the instability of the atmosphere, in which the vertical wind gradient plays an important role.

IV.2.4.2. Deposition

Deposition is the main sink for the different chemical species present in the atmosphere. In the following, we distinguish the dry deposition from the wet deposition.

a.   Wet deposition

Wet deposition or scavenging corresponds to the process of elimination of soluble gases by precipitation. In practice, the elimination of species can take place either inside clouds, known as "rainout", or during the fall of raindrops or ice crystals, known as "washout". In the MOCAGE model, washout from stratiform and convective clouds is treated in different ways. For gases, scavenging by stratiform precipitation and under convective clouds follows the parameterization of Liu *et al*. (2001). The method of Mari *et al*. (2000), which is integrated into the convection scheme of Bechtold *et al*. (2001), is used for scavenging inside convective clouds.

b.   Dry deposition

Dry deposition, as opposed to wet deposition, occurs in the absence of precipitation, and corresponds to the capture of chemical species at the surface, whether by the vegetation, the soil, the different water bodies, the building, or ... etc. Its representation is often by a flux approach, with an analogy often made with the electric current. The relation of the deposition flux is the following:

$$F = -v_d C \hspace{4cm} \textbf{\textit{Eq. IV-4}}$$

For a given species, the dry deposition flux F can be compared to an electric current. The deposition velocity v_d can be compared to an electric conductance, i.e. the inverse of the electric resistance. Finally, the concentration of the deposited chemical species in the air C is comparable to the electrical potential. The resolution of the dry deposition flux comes back to the estimation of v_d, which, always in the idea of the analogy with the electric current, is done by calculating the inverse of the sum of the different resistance terms.

In the following, three resistances for the dry deposition are presented:

•   The aerodynamic resistance (R_a) which is the resistance to vertical transfer in the near-surface layer of air, and depends only on dynamic quantities. It is estimated according to Slinn and Slinn (1980).

- The resistance of the quasi-laminar layer (R_b), which corresponds to the capacity of a compound to cross the quasi-laminar layer of the surface. It also depends on the dynamics of the surface air layer, but also of the molecular diffusion related to the deposited species.

- The surface resistance (R_c) is the absorption resistance by soil, vegetation, or surface bodies. Its calculation is made according to Wesely (1989). We note that this resistance is the most complex to estimate, depending on the properties of the soil, the vegetation cover, but also on the meteorological conditions which influence for example the opening of the stomata of the plants.

The relationship among the deposition velocity and the three resistances of dry deposition is given by the following equation:

$$v_d = \frac{1}{R_a + R_b + R_c} \qquad\qquad \textbf{\textit{Eq. IV-5}}$$

In this equation (***Eq. IV-5***), R_a, R_b, and R_c are in s m^{-1}.

The dry deposition velocities do not depend on the concentration of the deposited species. They are pre-calculated using SUMO pre-processor (SUrface MOdel) before the simulation by using information on the surface (vegetation, soil, … etc.) and the same meteorological forcing as for MOCAGE simulation, allowing an economy of calculation time during the execution of MOCAGE.

IV.2.4.3. Emissions

Emissions are a necessary input for a CTM. In MOCAGE, most emissions come from emission inventories, but some are calculated on the basis of meteorological conditions. Emissions on the selected grid and domain are calculated using the SUMO pre-processor.

Regarding surface emissions, they are mostly taken from inventories. We only provide information of the inventories used here. The emissions of anthropogenic gaseous compounds are taken form MaCCity inventory (Lamarque *et al*., 2010). Soil emissions of NO$_x$ are provided by GEIA dataset (Yienger and Levy II, 1995), while those from lightening are parameterized from meteorological fields and are based on Price *et al*. (1997). Biogenic VOCs emissions are not taken from an inventory, but precalculated in SUMO using the MEGAN (Model of Emissions of Gases and Aerosols from Nature) model (Guenther *et al*., 2012). Regarding the oceanic DMS emissions, they are based on a monthly climatology (Kettle *et al*., 1999).

Quantities and heights of biomass burning emissions are taken from GFAS (Global Fire Assimilation System) products, which are based on Kaiser *et al*. (2012). In addition, the vertical injection profile of biomass fire has been parameterized and implemented into MOCAGE by Cussac *et al*. (2020). Concentrations of methane and Ozone Depleting Substances (ODS) such as CFCs are fixed at the surface.

IV.2.5. New developments

Halogen chemistry is already integrated into the MOCAGE original version, in which chlorinated and brominated species are implemented to represent the stratospheric chemistry due to their strong impact on ozone. Reactions in ***Table IV-1*** are the ones representing chlorine chemistry in MOCAGE. However, they do not fully represent the atmospheric chemistry.

Chlorinated VSLS, which are important players in the chlorine stratospheric chemistry are not involved into the model. Moreover, it does not take the reactivity of Cl with VOCs into account, which impacts the oxidation budget of the troposphere.

Therefore, in order to be able to represent the chlorine chemistry in the troposphere, the necessary modifications are made to the original chemical scheme of MOCAGE. These changes include the addition of gas-phase reactions of chlorinated organic and inorganic compounds, and setting the surface concentrations of the chlorinated VSLS that take part in the added reactions. In addition, the emissions of chlorinated species and the Henry's law constants for HCl have been updated.

Chapter IV. Global atmospheric modelling

Table IV-1: *Gaseous phase reactions of chlorinated species in the original version of MOCAGE.*

#	Reaction	Rate constant k [a] (cm^3 molecule^{-1} s^{-1})
1	$HOCl + h\nu \rightarrow Cl + OH$	-
2	$ClONO_2 + h\nu \rightarrow Cl + NO_3$	-
3	$ClONO_2 + h\nu \rightarrow ClO + NO_2$	-
4	$Cl_2O_2 + h\nu \rightarrow 2\ Cl + O_2$	-
5	$HCl + h\nu \rightarrow H + Cl$	-
6	$Cl_2 + h\nu \rightarrow 2\ Cl$	-
7	$ClNO_2 + h\nu \rightarrow Cl + NO_2$	-
8	$OClO + h\nu \rightarrow ClO + O(^3P)$	-
9	$BrCl + h\nu \rightarrow Br + Cl$	-
10	$Cl + HCHO \rightarrow HCl + HO_2 + CO$	8.10×10^{-11} exp(-30/T)
11	$MO2 + ClO \rightarrow CH_3O + Cl + O_2$	1.80×10^{-12} exp(-600/T)
12	$Cl + O_3 \rightarrow ClO + O_2$	2.30×10^{-11} exp(-200/T)
13	$ClO + O(^3P) \rightarrow Cl + O_2$	2.80×10^{-11} exp(85/T)
14	$ClO + NO \rightarrow NO_2 + Cl$	6.40×10^{-12} exp(290/T)
15	$Cl + CH_4 \rightarrow CH_3 + HCl$	7.10×10^{-12} exp(-1270/T)
16	$Cl + H_2 \rightarrow HCl + H$	3.05×10^{-11} exp(-2270/T)
17	$Cl + HO_2 \rightarrow HCl + O_2$	1.40×10^{-11} exp (270/T)
18	$Cl + HO_2 \rightarrow OH + ClO$	3.60×10^{-11} exp(-375/T)
19	$ClO + OH \rightarrow Cl + HO_2$	7.40×10^{-12} exp(270/T)
20	$ClO + OH \rightarrow HCl + O_2$	6.00×10^{-13} exp(230/T)
21	$HCl + OH \rightarrow H_2O + Cl$	1.80×10^{-12} exp(-250/T)
22	$ClO + NO_2 + M \rightarrow ClONO_2 + M$	K_{3rd} (T, cair, 1.80×10^{31}, 3.40, 1.50×10^{11}, 1.90, 0.60) [b]
23	$ClONO_2 + O(^3P) \rightarrow ClO + NO_3$	3.60×10^{-12} exp(-840/T)
24	$ClO + HO_2 \rightarrow O_2 + HOCl$	2.60×10^{-12} exp(290/T)
25	$HOCl + OH \rightarrow H_2O + ClO$	3.00×10^{-12} exp(-500/T)
26	$HOCl + O(^3P) \rightarrow ClO + OH$	1.70×10^{-13}
27	$Cl + NO_2 \rightarrow ClNO_2$	K_{3rd} (T, cair, 1.80×10^{31}, 2.00, 1.00×10^{11}, 1.00, 0.60) [b]
28	$HOCl + Cl \rightarrow OH + Cl_2$	3.40×10^{-12} exp(-130/T)
29	$ClO + ClO + M \rightarrow Cl_2O_2 + M$	$K_{ClO-ClO}$ (T, cair, 1.90×10^{32}, 3.60, 3.70×10^{12}, 1.60, 0.60) [b]

[a] All rate constants are taken from Burkholder *et al.* (2020).

[b] Rate constant of termolecular reaction in cm^6 molecule^{-2} s^{-1}

Table IV-1: Continued.

#	Reaction	Rate constant k [a] (cm^3 molecule^{-1} s^{-1})
30	$Cl_2O_2 + M \rightarrow M + 2\ ClO$	$A_{eq} = 2.16 \times 10^{27}\ B_{eq} = 8537k = (1/A_{eq})\exp(-B_{eq}/T) \times k_{ClO\text{-}ClO}$
31	$ClO + ClO \rightarrow Cl_2 + O_2$	$1.00 \times 10^{-12}\exp(-1590/T)$
32	$ClO + ClO \rightarrow OClO + Cl$	$3.50 \times 10^{-13}\exp(-1370/T)$
33	$BrO + ClO \rightarrow Br + OClO$	$9.50 \times 10^{-13}\exp(550/T)$
34	$BrO + ClO \rightarrow Br + Cl + O_2$	$2.30 \times 10^{-12}\exp(260/T)$
35	$BrO + ClO \rightarrow BrCl + O_2$	$4.10 \times 10^{-13}\exp(290/T)$

[a] All rate constants are taken from Burkholder *et al*. (2020).

[b] Rate constant of termolecular reaction in cm^6 molecule^{-2} s^{-1}

Chapter IV. Global atmospheric modelling

IV.2.5.1. Chemistry scheme

    a.   New species and reactions

Building on the initial model, a chlorine chemistry scheme has been developed and implemented into MOCAGE. The scheme includes the addition of 6 organic chlorinated species whose molar masses and Henry's law constants (a) and (b) are presented in ***Table IV-2***.

Table IV-2: *Molar masses and Henry's law constants of the organic chlorinated species added to MOCAGE original scheme.*

Species	Molar mass	Henry's constant (a) ($mol\ L^{-1}\ atm^{-1}$)	Henry's constant (b) (K^{-1})	Reference
CH_2Cl_2	84.9	3.6×10^{-3}	4100.0	(Staudinger and Roberts, 1996) [a]
$CHCl_3$	119.4	2.5×10^{-3}	4500.0	(Staudinger and Roberts, 1996) [a]
C_2Cl_4	165.8	9.9×10^{-4}	4600.0	(Hiatt, 2013) [a]
$CHCl_2O_2$	115.9	-	-	
$HCOCl$	64.5	7.4×10	0.0	(Krysztofiak *et al*., 2012) [b]
$COCl_2$	98.9	5.9×10^{-4}	3800.0	(de Bruyn *et al*., 1995) [a]

[a] Henry's constants compiled and suggested by Sander (2015).
[b] Assumed Henry's law constant of HCOCl analogous to that of HCOBr (Hossaini *et al*., 2016)

Out of these species, CH_2Cl_2, $CHCl_3$, and C_2Cl_4 are known as chlorinated VSLS. The sources of these species are detailed in ***section I.2.1***. Moreover, the reactivity and transport of the VSLS in the troposphere, together with the process of injection into the stratosphere are described in ***section I.2.5***.

In addition to the chlorinated VSLS, three other species are included to MOCAGE namely dichloromethylperoxy radical ($CHCl_2O_2$), formyl chloride (HCOCl) and carbonyl dichloride ($COCl_2$), known as phosgene. $CHCl_2O_2$, HCOCl, and $COCl_2$ are the products of the atmospheric degradation of the Cl-VSLS. Introducing these species into MOCAGE is expected to be mainly influencing the stratospheric chlorine and ozone budget.

HCOCl is included into MOCAGE model based on the fact that it is one of the most abundant chlorinated organic compounds in the troposphere (Hossaini *et al.*, 2016). HCOCl has a partial tropospheric mean lifetime of 32, 372, and 865 days against reaction with OH and NO_3, and due to photolysis respectively. Then, the only loss pathway we add into MOCAGE is its reaction with OH radical (Reaction 21 in ***Table IV-3***). In addition, using ASTEC model, HCOCl is found to be of important abundance and reactivity (see ***Chapter III section III.4.1.2***). therefore, this species is important at both short and long-time scales.

Moreover, and since our CTM extends to model upper tropospheric and stratospheric chemistry (unlike the 0D model ASTEC: ***Chapter III***), the inclusion of $COCl_2$ is important. $COCl_2$ is the most notorious (Harrison *et al*., 2019) as it was used as a chemical weapon in World War I. In their work, Harrison *et al*. (2019) show that this species is a product of the degradation of VSLS, and its observation in the upper troposphere and lower stratosphere can be used as a sign of product gases injection of VSLS into the stratosphere.

The reactions of Cl-VSLS are added to MOCAGE. Also, reactions of atomic Cl with VOCs producing HCl and other organic radicals are added. The reactivity of atomic Cl towards VOCs can be represented as a hydrogen abstraction reaction. Moreover, other diverse reactions of chlorinated organic and inorganic species are added. All these reactions are their corresponding rate constants are given in *Table IV-3*. These reactions mainly occur under tropospheric conditions.

The choice of these reactions to be included into MOCAGE is based on the fact that these reactions are frequently added to CTMs that aim to study and evaluate the chlorine tropospheric chemistry. For instance, reaction 18 in *Table IV-3* was previously added into 7 model of chlorine tropospheric chemistry, up to our knowledge (Badia *et al.*, 2019; Eastham *et al.*, 2014; Hossaini *et al.*, 2016; Ordóñez *et al.*, 2012; Sander *et al.*, 2011; Sherwen *et al.*, 2016; Sommariva and von Glasow, 2012) (see *Table III-1*). Moreover, it is worth mentioning that some of these reactions are present in the simplified mechanism resulting from ASTEC simulations (R17 and R20 in *Table IV-3*).

Table IV-3: *Reactions and kinetic data for reactions added to MOCAGE chemistry scheme.*

	Reaction	Rate constant k (cm^3 molecule^{-1} s^{-1})	Reference
	Reactions of VSLS and their products		
1	$CH_2Cl_2 + OH \rightarrow CHCl_2O_2 + H_2O$	1.92×10^{-12} exp(-880/T)	(a)
2	$CHCl_3 + OH \rightarrow COCl_2 + Cl + H_2O$	2.20×10^{-12} exp(-920/T)	(a)
3	$CH_2Cl_2 + Cl \rightarrow CHCl_2O_2 + HCl$	7.40×10^{-12} exp(-910/T)	(a)
4	$CHCl_3 + Cl \rightarrow COCl_2 + Cl + HCl$	3.30×10^{-12} exp(-990/T)	(a)
5	$C_2Cl_4 + OH \rightarrow 0.47 \; COCl_2 + 3.06 \; Cl$	4.70×10^{-12} exp(-990/T)	(a)
6	$CHCl_2O_2 + NO \rightarrow 2 \; Cl + NO_2 + CO + HO_2$	4.05×10^{-12} exp(360/T)	(b)
7	$CHCl_2O_2 + HO_2 \rightarrow COCl_2 + H_2O$	3.92×10^{-13} exp(700/T)	(b)
8	$CHCl_2O_2 + HO_2 \rightarrow HO_2 + CO + Cl + HOCl$	1.68×10^{-13} exp(700/T)	(b)
9	$CHCl_2O_2 + MO2 \rightarrow 2 \; Cl + 2 \; HO_2 + CO + HCHO$	1.20×10^{-12}	(b)
10	$CHCl_2O_2 + MO2 \rightarrow COCl_2 + HCHO + HO_2$	8.00×10^{-13}	(b)
11	$COCl_2 + O(^1D) \rightarrow CO + ClO + Cl$	1.76×10^{-10} exp(30/T)	(a)
	Reactions of Cl with VOCs		
12	$Cl + ALD + O_2 \rightarrow HCl + ETHP$	8.00×10^{-11}	(c)
13	$Cl + HC3 \rightarrow HCl + 0.92 \; ALD + 0.92 \; HO_2 + 0.08 \; ETHP$	8.60×10^{-11} exp(45/T)	(c)
14	$Cl + MO2 \rightarrow 0.5 \; HCHO + 0.5 \; CO + 0.5 \; H_2O + 0.5 \; HO_2 + 0.5 \; HCl + 0.5 \; ClO$	1.60×10^{-10}	(a)
15	$Cl + ETH \rightarrow MO2 + HCl$	7.20×10^{-11} exp(-70/T)	(a)
16	$Cl + ETE \rightarrow HCOCl + 2 \; XO2 + HO_2 + HCHO$	1.07×10^{-10}	(c)
	Other reactions		
17	$ClNO_2 + OH \rightarrow HOCl + NO_2$	2.40×10^{-12} exp(-1250/T)	(a)
18	$Cl + ClONO_2 \rightarrow Cl_2 + NO_3$	6.20×10^{-12} exp(145/T)	(c)
19	$ClONO_2 + OH \rightarrow 0.5 \; ClO + 0.5 \; HNO_3 + 0.5 \; HOCl + 0.5 \; NO_3$	1.20×10^{-12} exp(-330/T)	(c)
20	$Cl + H_2O_2 \rightarrow HCl + HO_2$	1.10×10^{-11} exp(-980/T)	(a)
21	$HCOCl + OH \rightarrow Cl + CO$	5.00×10^{-13}	(c)

(a) JPL 2020 (Burkholder *et al.*, 2020)

(b) MCM3.1 (Jenkin *et al.*, 1997)

(c) IUPAC (Atkinson et al., 2007)

b.   Henry's law of HCl

In the original MOCAGE version, the values of Henry's law constants of HCl are taken from Leriche *et al.* (2003) (see ***Table IV-4***). However, the original value of Henry's law constant (a) is considered to be very low but, since HCl is a strong acid whose pK_a = -5.9 in the gaseous phase (Trummal *et al.*, 2016), it dissociates very rapidly in water according to the following reaction:

$$HCl + H_2O \rightarrow H_3O^+ + Cl^- \hspace{4cm} \textbf{\textit{R1}}$$

Therefore, the Henry's law constant of HCl is updated according to the values given in ***Table IV-4***. The updated value is called the effective Henry's law constant, which depends on the pH of the solution and pK_a of HCl. The pH is assumed to be 4.5 for a typical cloud droplet following Sherwen *et al.* (2016).

Table IV-4: *Henry's law constants of HCl in the original and updated MOCAGE versions.*

	Henry's constant (a) $(mol\ L^{-1}\ atm^{-1})$	Henry's constant (b) (K^{-1})	Reference
Henry's law constant	1.5×10^0	9000.0	(Leriche *et al.*, 2003)
Effective Henry's law constant	7.1×10^{15}	5900.0	(Sherwen *et al.*, 2016)

This update is made to calculate the exact wet deposition of HCl, and hence is expected to increase the removal of this species from the atmosphere compared to the original model version.

IV.2.5.2.   Emissions

In the original MOCAGE version, chlorine is emitted in the form of HCl. These emissions are taken from the Global Emissions InitiAtive dataset, GEIA-Reactive-Chlorines (Cunnold *et al.*, 1994). Based on this dataset, HCl oceanic and anthropogenic emissions in the year 1990 are considered. The distribution of the average emissions in December 2014 is illustrated in ***Figure IV-6***. According to GEIA dataset, emissions of HCl arise mainly from the Northern Hemisphere (NH). Anthropogenic sources come from the industrial countries, namely China, India, European countries, and United States of America. In addition, oceans in the NH are more releasing HCl than oceans in Southern Hemisphere (SH).

In our work, we update the emissions of HCl and add those of $ClNO_2$. This is similar to the initial conditions in the box model, where these two species are the sources of Cl (***section III.2.3***). In the updated emissions from recent publications, HCl originates from acid displacement, and $ClNO_2$ is the product of the heterogeneous reaction between chloride ions and N_2O_5. These two sources are considered to be oceanic and replace the heterogeneous reactions responsible for these emissions (refer to ***section I.2.1***). HCl is also released to the atmosphere from anthropogenic sources. The estimated fluxes of these emissions (original and updated) are given in ***Table IV-5***. Because there is no recent inventory that provides the geographical distribution of the emissions of chlorinated species, we assume that these fluxes are homogeneously distributed over land for anthropogenic emissions, and over ocean for

oceanic emissions. This is a crude assumption that prevents the analysis of the regional effects. Still, this approach allows to analyse the global impact of the up-to-date chlorine emissions.
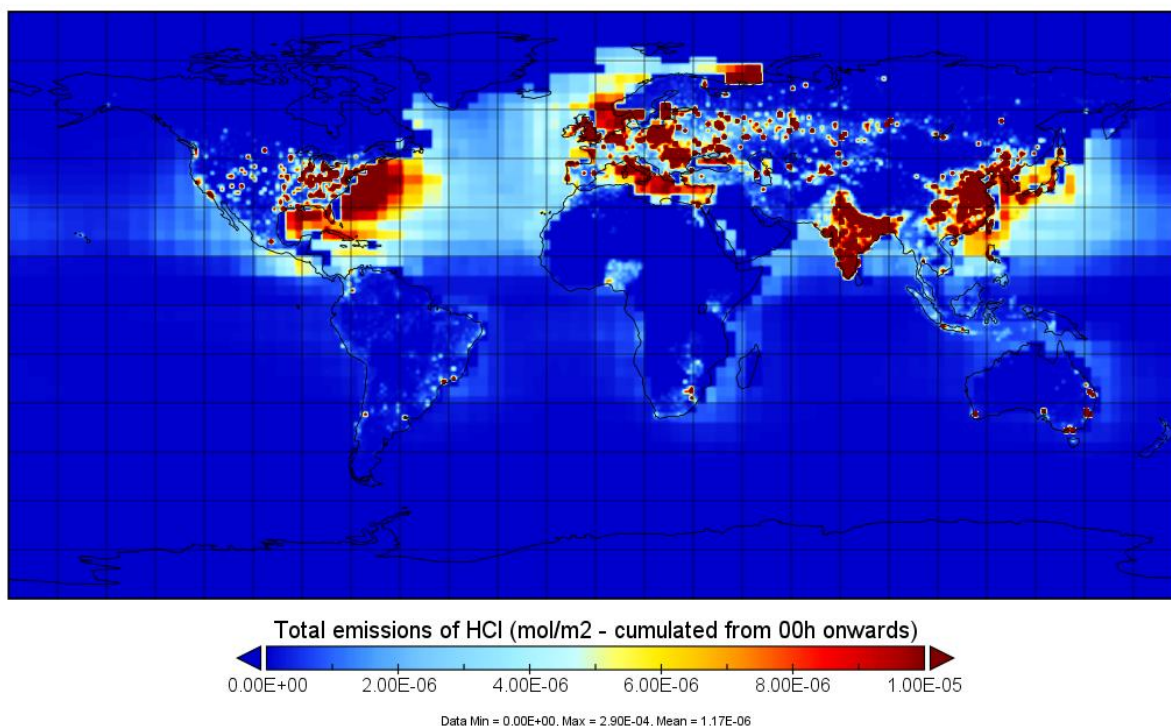
Figure IV-6: Total emissions of HCl in December 2014 based on GEIA dataset.

Table IV-5: Original and updated emissions of chlorinated species in MOCAGE.

Species	Emission flux (Gg Cl year⁻¹)	Source	Year	Reference
		Original		
HCl	6950	Oceanic	1990	(Cunnold *et al.*, 1994)
	6640	Anthropogenic	1990	(Cunnold *et al.*, 1994)
		Updated emissions		
HCl	52000	Oceanic	2016	(Wang, X. *et al.*, 2019)
	1906	Anthropogenic	2014	(Zhang *et al.*, 2022)
ClNO₂	1810	Oceanic	2016	(Wang, X. *et al.*, 2019)

According to *Table IV-5*, the updated anthropogenic emissions are less in the year 2014 than in 1990. Zhang *et al.* (2022) mentions that anthropogenic emissions of HCl have been declining due to the air pollution control strategies. These anthropogenic sources include: energy, industry, and residential sources. *Figure IV-7* shows that HCl anthropogenic emissions reached their peak in the period 1970-1990. After that, they have been declining constantly. Note that the original anthropogenic emissions (resp. oceanic) emissions of HCl from GEIA that were for the year 1990 are much higher (resp. much lower) than those estimated recently by Zhang *et al.* (2022) (resp. (Wang X. *et al.*, 2019)).
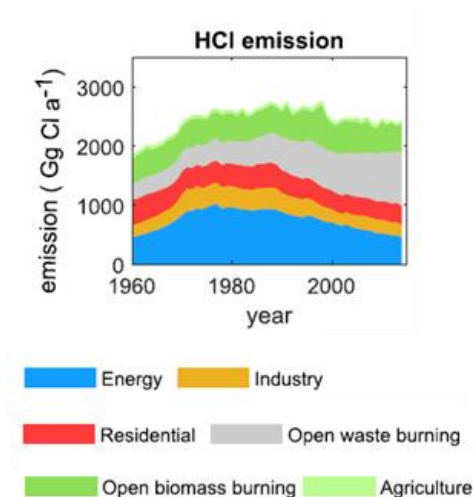
Figure IV-7: *Evolution of the emissions of HCl (in Gg Cl year^{-1}) from different sectors according to Zhang et al. (2022).*

Regarding the distribution of chlorinated VSLS, we choose the same approach as in the previous study of Hossaini *et al*. (2016). The concentrations of the VSLS are set at the surface, instead of including the emission fluxes of these species. The chemical boundary conditions of these species are based on surface observations in 2014. The volume mixing ratios of the VSLS included in the model are given in **Table IV-6**. For instance, CH_2Cl_2 originates mainly from anthropogenic sources, with minor natural sources. For $CHCl_3$, it is mainly released from natural sources and minor anthropogenic sources. C_2Cl_4 is emitted by anthropogenic sources only.

Table IV-6: *Latitude dependent volume mixing ratios (ppt) of VSLS in 2014 (Hossaini et al., 2016).*

	Latitude Band				
Species	**> 60 °N**	**30-60 °N**	**0-30 °N**	**0-30 °S**	**< 30°S**
CH_2Cl_2	60.0	63.3	56.1	20.0	17.0
$CHCl_3$	13.0	8.6	6.7	5.4	5.7
C_2Cl_4	2.3	3.4	1.7	0.6	0.5

IV.3. Configuration of the simulations

In this research work, the model is used in its global configuration with a regular latitude and longitude grid (1° × 1°). The vertical resolution is a version with 47 levels as described previously is *section IV.2.2*.

The model is run for two years 2013 and 2014 with 3-hourly outputs. We test the effects of all the new developments with respect to the original version of MOCAGE, as described in *section IV.2.5* by running different MOCAGE experiments over these 2 years. A two-year period allows the system to achieve chemical equilibrium of the new components added in MOCAGE, in particular the Cl-VSLS. The simulation named "**Original**" represents the basic version of MOCAGE without any changes, while the simulations named "FULL" includes all the new developments.

In addition to the "FULL" and "Original", several intermediate simulations are done to investigate in an incremental way the effect of each of the new developments applied to MOCAGE. Firstly, the Henry's law constant of HCl is changed to check the effect of correcting the Henry's constant by the effective Henry's constant on the wet deposition and therefore on the amount of HCl reaching the free troposphere and the stratosphere.

This simulation is named "**Original_HC**". Based on this simulation, in the next step, the updated HCl and ClNO$_2$ emissions described in *section IV.2.5.1.b* are applied to the model: "**Original_emis_HC**" simulation. In the step after, the reactions of chlorinated species listed in *Table IV-3* are added: "**Cl_emis_HC**" simulation. Finally, the boundary conditions for VSLS given in *section IV.2.5.1.b* are added to get the "**FULL**" simulation. These MOCAGE experiments with the changes made are summarized in *Figure IV-8*. These changes are also presented in *Table IV-7*.
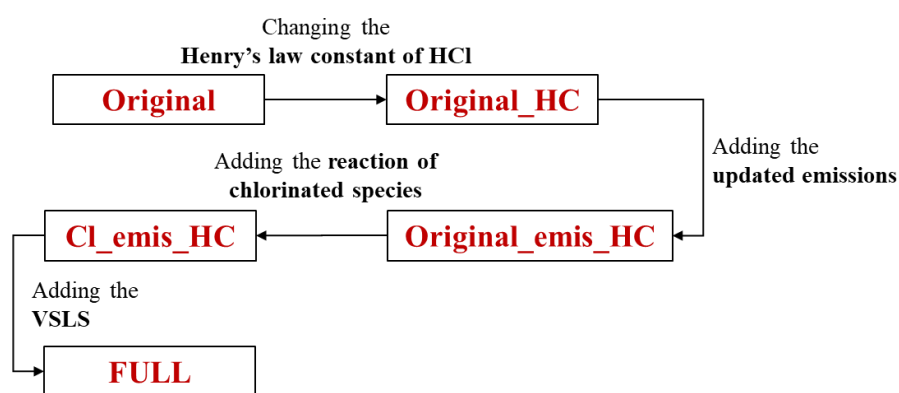
Figure IV-8: *Illustration of the different tests done to simulate the chlorine atmospheric chemistry.*

Table IV-7: *Input parameters of the different simulations made to investigate chlorine atmospheric chemistry.*

Simulation	Reactions	Henry's law constant of HCl	Emissions	VSLS
Original	Original	Original	Original	No VSLS
Original_HC	Original	Updated	Original	No VSLS
Original_emis_HC	Original	Updated	Updated	No VSLS
Cl_emis_HC	Original + added reactions of Cl	Updated	Updated	No VSLS
FULL	Original + added reactions of Cl	Updated	Updated	VSLS included

IV.4. Analysis of the results

In this section, the fields are given as monthly averages in December 2014 (last month of the simulated time period). All the plots represent the zonal average distribution of the species concentrations or difference in concentrations with respect to the model vertical levels, level 47 being the surface level. Southern Hemisphere (SH) extends over the latitude band (-90 0 °N or 90°S 0°N), and Northern Hemisphere covers the region extending over the latitudes (0 90 °N).

IV.4.1. Plots of major species

In this section, we present some of the fields of the all simulations that are being or expected to be significantly changed due to the developments applied to the original MOCAGE scheme. For all the simulations presented in ***Table IV-7***, the distributions of HCl, ClNO$_2$, ClO, and O$_3$ are given in the figures below. The distribution of HCl is important due to the changes in the Henry's law constants of this species. Moreover, HCl and ClNO$_2$ are chosen to be presented since their emissions are changed significantly from the original MOCAGE emissions. ClO is thought to be the most important chlorinated species active on ozone depletion. The impact of all developments on ozone is one of the main objectives of this study. These figures are only briefly and qualitatively compared here with an analysis of the differences between the simulations that is provided in the next sections.

In the "Original" simulation, no changes are applied to the original MOCAGE scheme and emissions. This is used as a reference simulation to which developments are applied. The zonal average distribution of species as a function of the model vertical levels in the "Original" simulation are plotted in ***Figure IV-9***. Note that, a logarithmic scale is used.
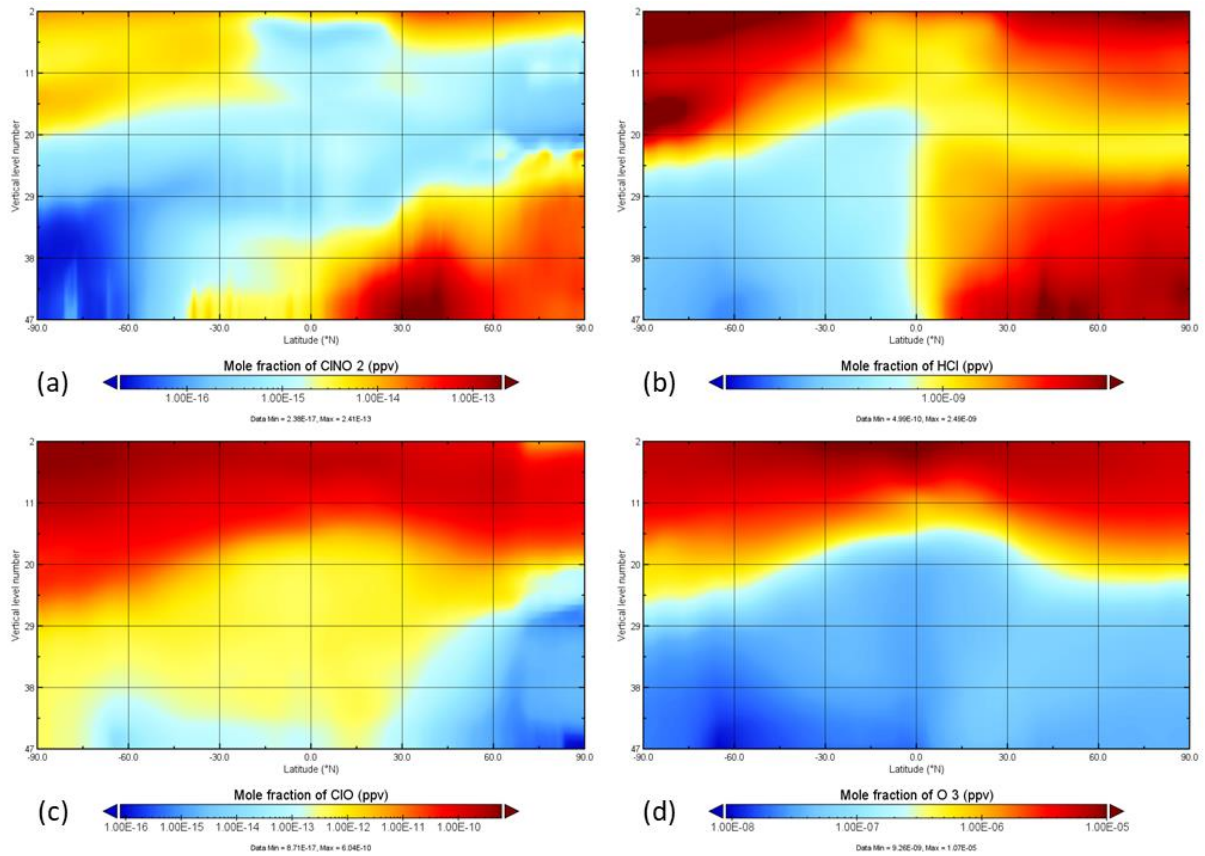
Figure IV-9: *Zonal average distribution of ClNO₂ (a), HCl (b), ClO (c), and O₃ (d) in ppv as a function of the model vertical levels in the "Original" simulation. The level 47 is the surface level. For all the species, a logarithmic scale is used.*

For the simulation "Original_HC", in which the Henry's law constant of HCl in the original MOCAGE version is changed, the plots are given in ***Figure IV-10***. The differences with the "Original" simulation are only slightly visible on the HCl field (for instance around the tropopause in the Antarctic region).
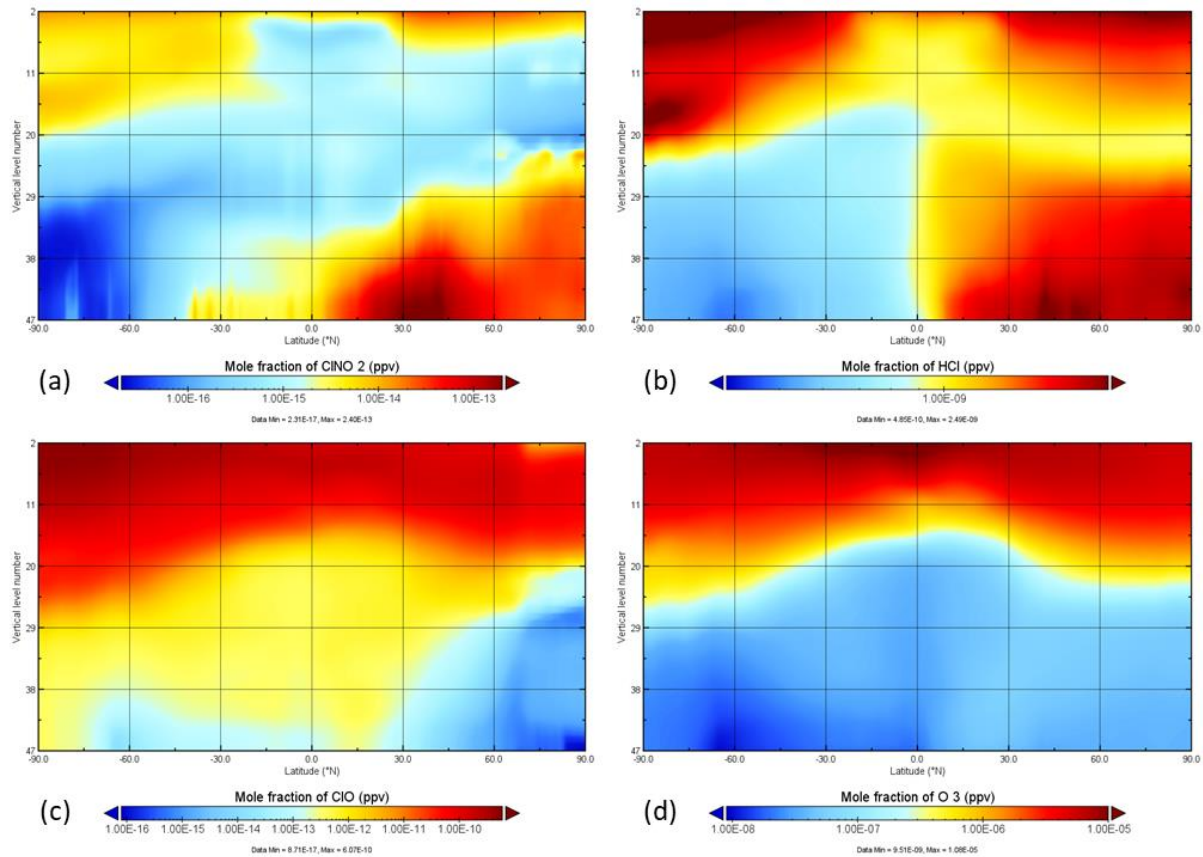
Figure IV-10: *Zonal average distribution of ClNO$_2$ (a), HCl (b), ClO (c), and O$_3$ (d) in ppv as a function of the model vertical levels in the "Original_HC" simulation. The level 47 is the surface level. For all the species, a logarithmic scale is used.*

Then, after updating the emissions of the original MOCAGE version, we get the simulation "Original_emis_HC". The plots of this simulation are given in ***Figure IV-11***. Note that the scales for ClNO₂ ***(a)*** and HCl ***(b)*** are changed compared to ***Figure IV-9*** and ***Figure IV-10*** because of the large increase in the emissions of ClNO₂ and HCl in "Original_emis_HC" compared to "Original" and "Original_HC" simulations. This induces a general increase in ClO concentration and significant changes on ozone.
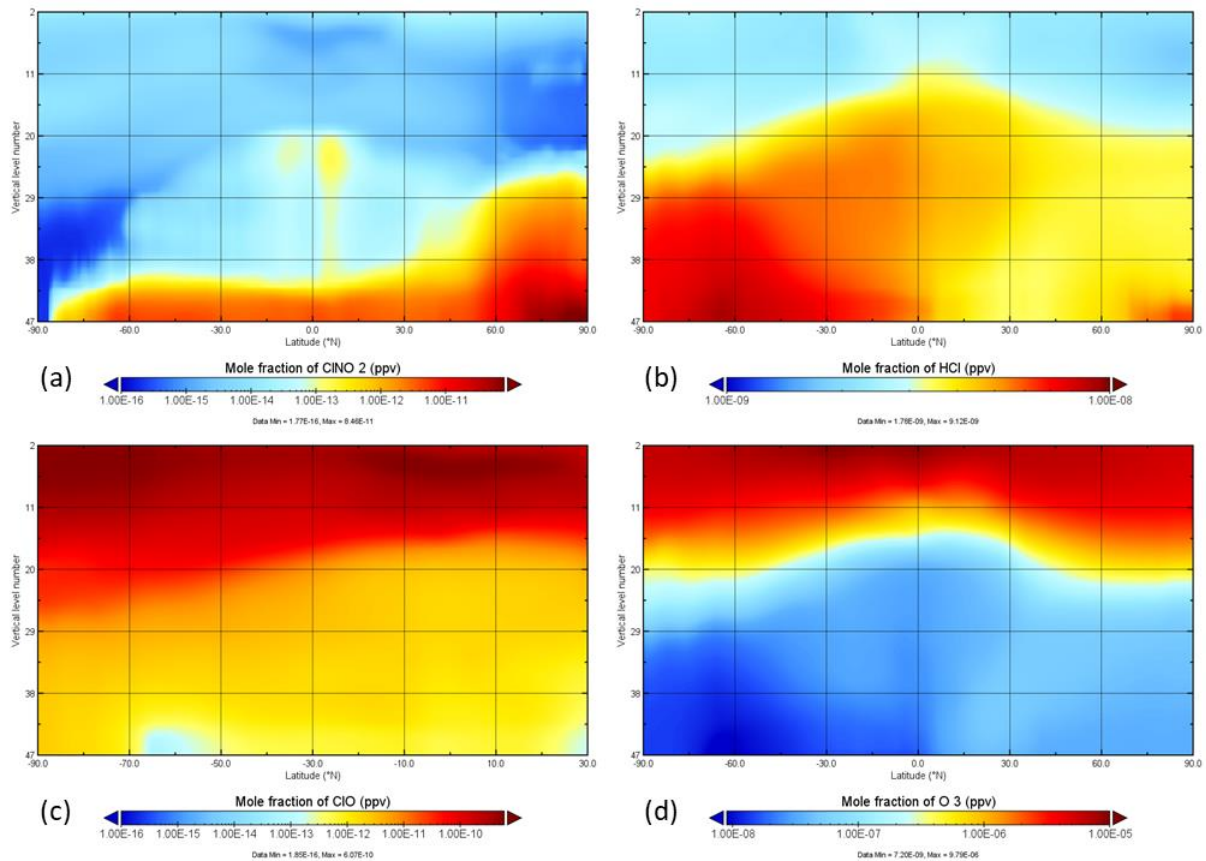
Figure IV-11: *Zonal average distribution of ClNO₂ (a), HCl (b), ClO (c), and O₃ (d) in ppv as a function of the model vertical levels in the "Original_emis_HC" simulation. The level 47 is the surface level. For all the species, a logarithmic scale is used.*

After that, adding the reactions listed in **Table IV-3**, we get the simulation "Cl_emis_HC". The zonal average distribution of $ClNO_2$, HCl, ClO, and O_3 in this simulation are given in **Figure IV-12**. The "Cl_emis_HC" simulation gives large changes in both, the troposphere and the stratosphere for all the species. The scale used for HCl is changed **(b)** from **Figure IV-11(b)**.
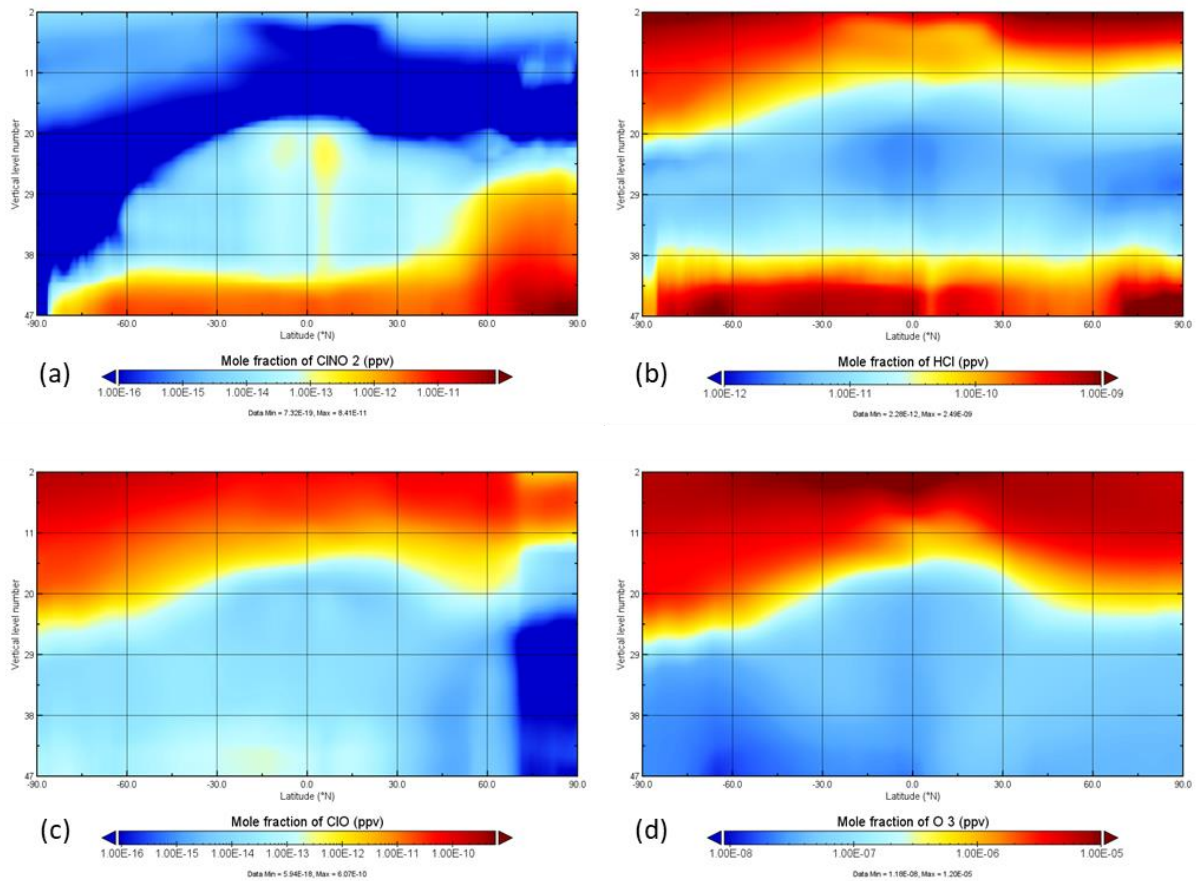
Figure IV-12: *Zonal average distribution of $ClNO_2$ (a), HCl (b), ClO (c), and O_3 (d) in ppv as a function of the model vertical levels in the "Cl_emis_HC" simulation. The level 47 is the surface level. For all species, a logarithmic scale is used.*

Now, setting the surface concentrations of Cl-VSLS, and after adding all other developments, we get the "FULL" simulation. The plots for this simulation are given in *Figure IV-13*. These plots do not show noticeable changes compared to the "Cl_emis_HC" simulation.
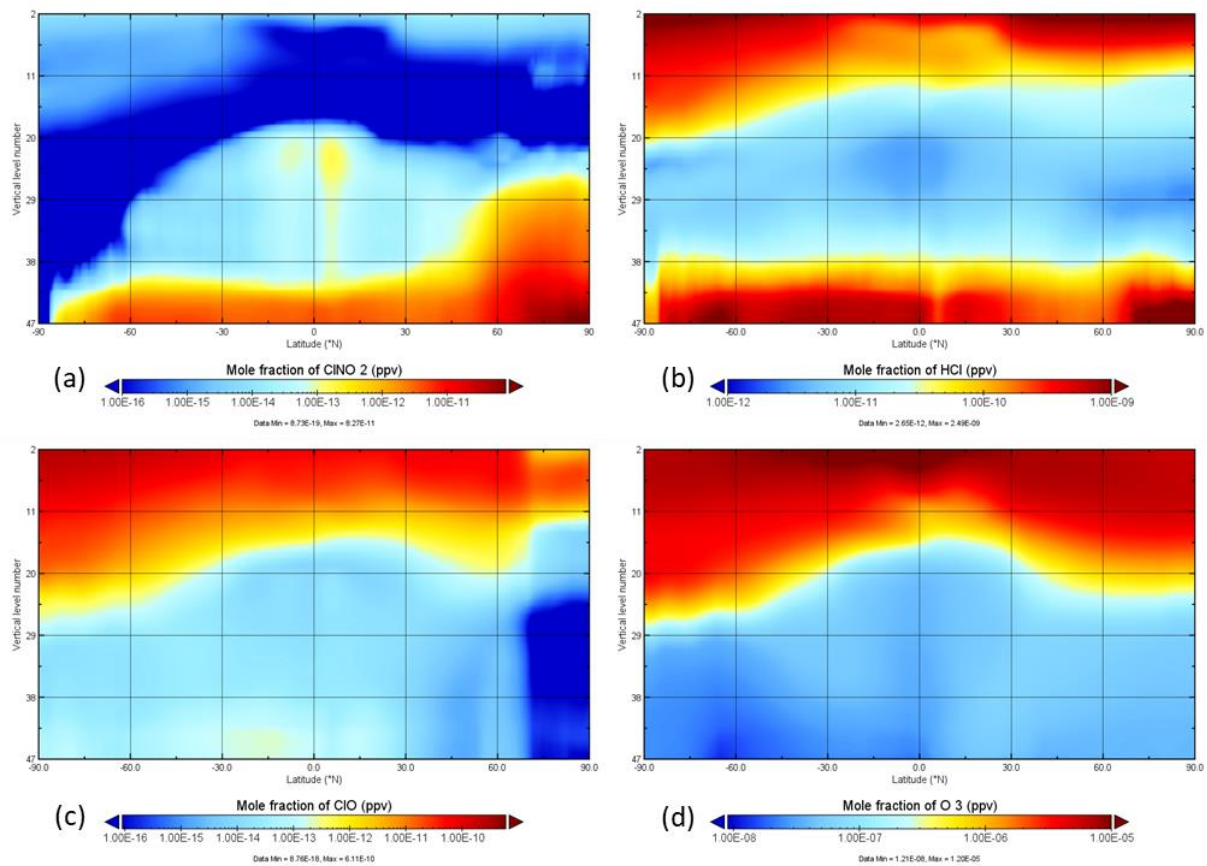
Figure IV-13: Zonal average distribution of ClNO$_2$ (a), HCl (b), ClO (c), and O$_3$ (d) in ppv as a function of the model vertical levels in the "FULL" simulation. The level 47 is the surface level. For all species, a logarithmic scale is used.

IV.4.2. Henry's law constant effect

The effect of wet deposition can be shown by comparing the "Original_HC" and "Original" simulations. Changing the Henry's law constant of HCl, as indicated in *Table IV-4*, is affecting the wet deposition of HCl primarily. HCl is being more scavenged in the "Original_HC" simulation, as less HCl is found in the atmosphere in general (*Figure IV-14*). This effect is slightly more significant in the stratosphere than in the troposphere, as less HCl is being injected into the stratosphere from the troposphere where more HCl is scavenged around the tropopause.

Consequently, of less chlorine in the troposphere and stratosphere, less ozone destruction occurs in both layers, and higher ozone levels are generally seen. This relative effect is higher around the tropopause (*Figure IV-15(a)*), particularly in the polar SH reaching 11.6% because there is a stronger decrease of HCl (*Figure IV-14*) in this region.
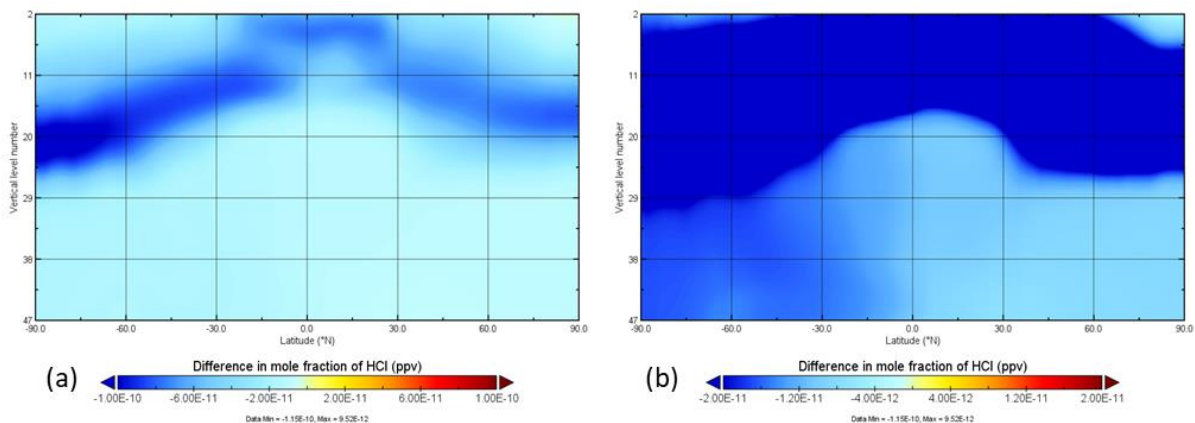
Figure IV-14: *Difference in the zonal average distribution of HCl with a scale adapted to the stratosphere (a) and to the troposphere (b) in ppv as a function of the model vertical levels between "Original_HC" and "Original" simulations. The level 47 is the surface level.*
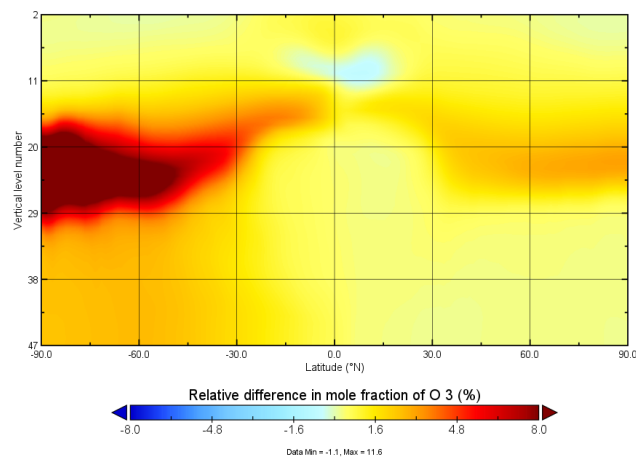
Figure IV-15: *Relative difference in the zonal average distribution of O_3 in % as a function of the model vertical levels between "Original_HC" and "Original" simulations. The level 47 in the surface level.*

IV.4.3. Effect of updated emissions

In this section, the difference between the two simulations "Original_emis_HC" and "Original_HC" is investigated to analyse the effect of the updated emissions on the composition of the atmosphere.

The difference in the distribution of $ClNO_2$ in the troposphere is plotted in ***Figure IV-16(a)*** and can be compared to the "Original_HC" $ClNO_2$ field (***Figure IV-10(a)***). When using the updated emissions, much higher $ClNO_2$ levels, by more than one order of magnitude, are observed in the whole atmosphere, which is related to the fact that there are no $ClNO_2$ emissions in "Original_HC" while $ClNO_2$ oceanic emissions are taken into account in the "Original_emis_HC" simulation. In ***Figure IV-16(a)***, we can see that $ClNO_2$ is more abundant in the NH in the polar regions, where in December, there is full darkness at the Arctic region. The photolysis is not active during this period. Therefore, $ClNO_2$, that is mainly lost by photolysis, is accumulating in the NH Arctic region from the emissions. For the other regions,

ClNO₂ is mainly in the boundary layer, thanks to the emissions, while it undergoes strong loss by photolysis above this layer. Note that the variations of ClNO₂ in the boundary layer from 90°S to 50°N are related to the assumption of homogeneous emissions from the oceans combined to the fact that the ocean surface varies with latitude.

When the emissions are updated, the levels of HCl show an increase in the entire atmosphere (***Figure IV-16(b,c)***). This increase is more pronounced in the SH compared to the NH. In the original emissions, HCl is primarily emitted from anthropogenic sources in the NH (***Figure IV-6***). However, in the updated emissions, anthropogenic emissions are reduced, and HCl is predominantly released from the oceans in much higher quantities than in the original emissions. Since the SH has larger oceanic surfaces compared to the NH and because it is assumed that the emissions are homogeneously distributed over the oceans, more HCl is emitted in the SH. As a consequence, more HCl is transported into the stratosphere in the "Original_emis_HC" in the SH than in the NH because of higher levels in the troposphere.
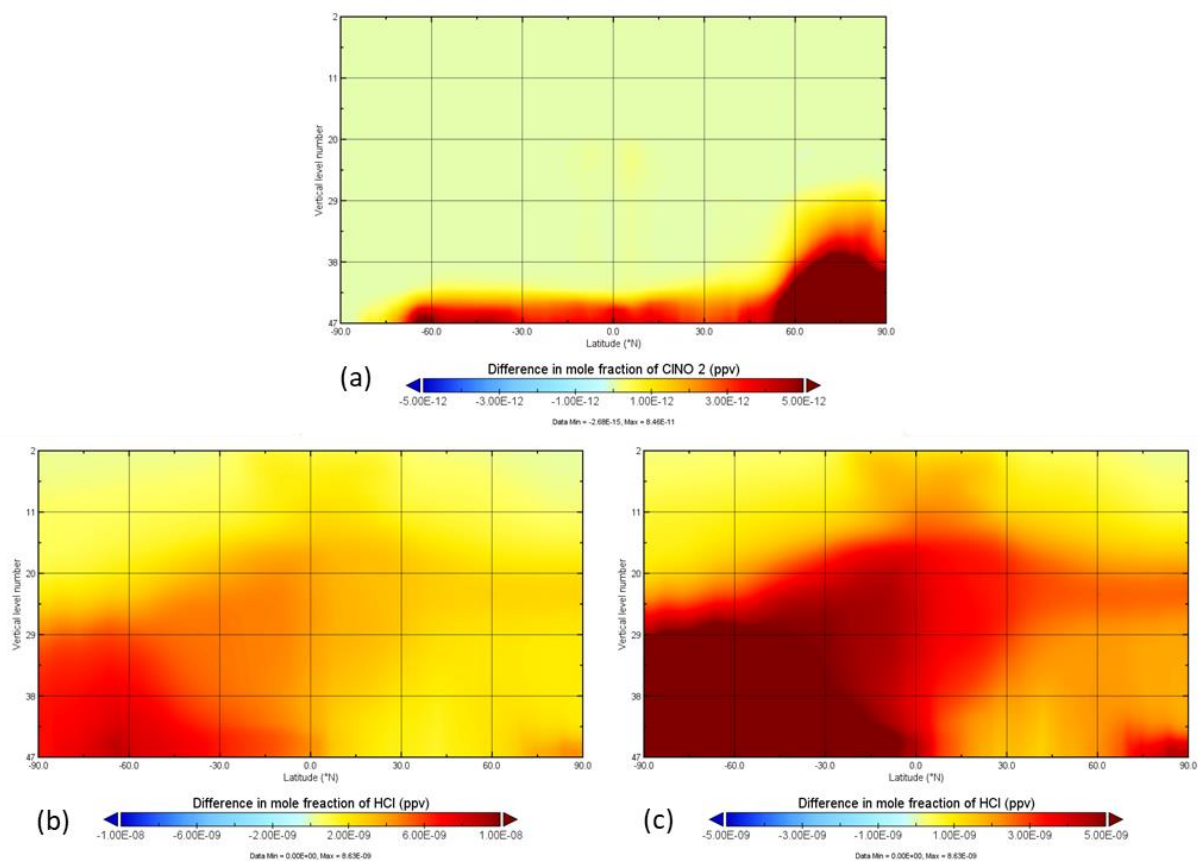
Figure IV-16: *Difference in the zonal average distribution of ClNO₂ (a) and of HCl with a scale adapted to the troposphere (b) and to the stratosphere (c) in ppv as a function of the model vertical levels between "Original_emis_HC" and "Original_HC" simulations. The level 47 is the surface level.*

Because of the significant changes of HCl in the troposphere and in the stratosphere, the updated emissions are affecting both stratospheric and tropospheric ozone levels. The effect is very strong in the troposphere and lower stratosphere of the NH and reaches values > 100% (***Figure IV-17***).
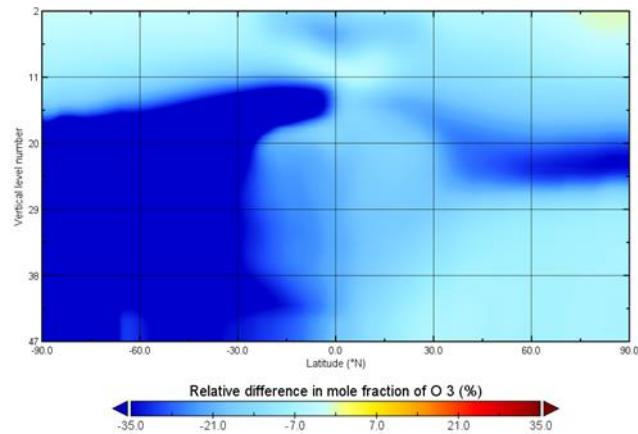
***Figure IV-17:** Relative difference in the zonal average distribution of O₃ in % as a function of the model vertical levels between "Original_emis_HC" and "Original_HC" simulations. The level 47 in the surface level.*

To interpret the results, it is useful to observe the impact of the updated emissions on the distribution of ClO, which is the most abundant active chlorine compound that act on the tropospheric ozone destruction (***Figure IV-18***). Comparing the impact of the updated emissions on O_3 and ClO levels, we can see that the distribution of these two species is being inversely affected in the troposphere, i.e. higher ClO levels lead to lower ozone. In the SH lower stratosphere and around the tropopause, there is a decrease in ozone linked to an increase in inorganic chlorine.
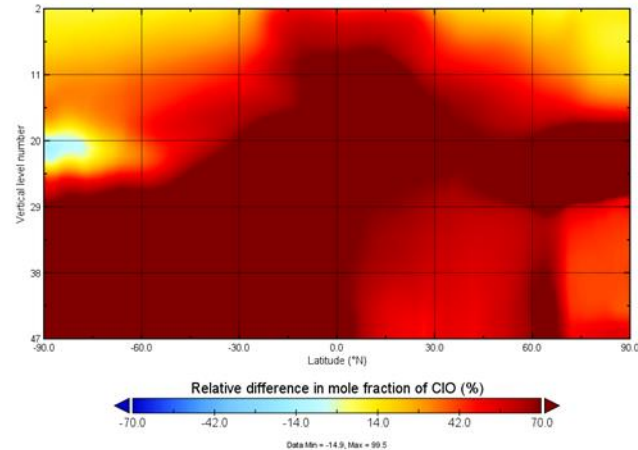
***Figure IV-18:** Relative difference in the zonal average distribution of ClO in % as a function of the model vertical levels between "Original_emis_HC" and "Original_HC" simulations. The level 47 in the surface level.*

IV.4.4. Effect of added reactions

In this section, the effect of the reactions listed in ***Table IV-3*** (reactions 12 – 21) on MOCAGE is analysed. In the simulation "Cl_emis_HC", these reactions are added to the simulation "Original_emis_HC".

As these reactions are added to MOCAGE scheme, less inorganic compounds are being formed in the troposphere, HCl in particular (***Figure IV-19(a)***), although most of the reactions are showing to be producing HCl.
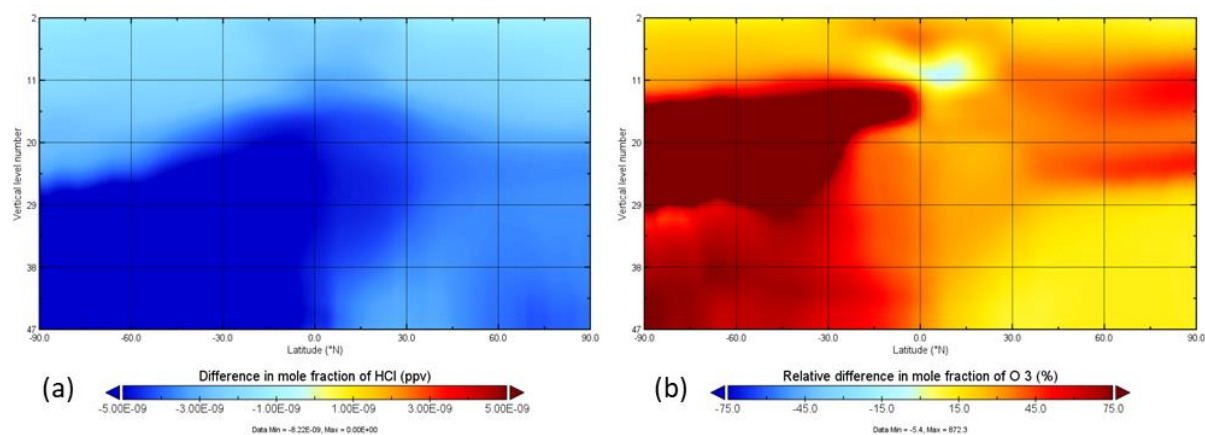
Figure IV-19: *Difference in the zonal average distribution of HCl (a), and relative difference in the zonal average difference of O₃ (b) in the entire atmosphere in % as a function of the model vertical levels between "Cl_emis_HC" and "Original_emis_HC" simulations. The level 47 in the surface level.*

Originally, a concurrent cycle between HCl and atomic Cl exists in the troposphere. However, in the presence of VOCs, this cycle is disturbed. Atomic Cl reacts with VOCs to form either HCl by hydrogen abstraction or other halogenated species by chlorine addition. This cycle is schematized in ***Figure IV-20***.
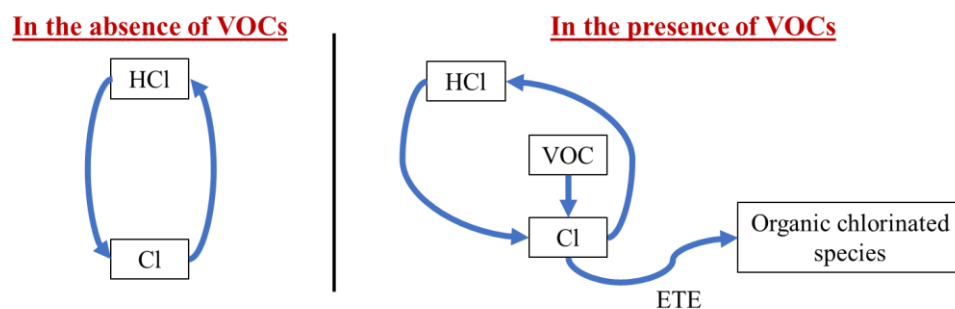
Figure IV-20: *Schematic representation of the concurrent cycle between HCl and atomic Cl in the absence and presence of VOCs.*

Whether the reaction between atomic Cl and VOCs proceeds to form HCl or organic chlorinated species depends on the rate constant of the reaction and the abundance of the VOC involved in the corresponding reaction. As seen in **Table IV-3**, the rate constant of reaction 16 ($k = 1.07 \times 10^{-10}$ cm^3 molecules^{-1} s^{-1}) is the highest among the reactions of atomic Cl with VOCs. HCOCl is an important product of the oxidation of ethene (ETE) in our scheme. Moreover, it is being lost through reaction 21, whose rate constant is three order of magnitude lower than that of the production route ($k = 5.00 \times 10^{-13}$ cm^3 molecules^{-1} s^{-1}). Therefore, HCOCl is accumulating in the atmosphere. According to Hossaini *et al.* (2016), HCOCl is one of the most abundant chlorine containing organic compounds in the atmosphere. The distribution of this species from "Cl_emis_HC" simulation (**Figure IV-21**) shows that there is a large concentration of HCOCl produced by ethene oxidation with higher values in NH, where there are more anthropogenic emissions.
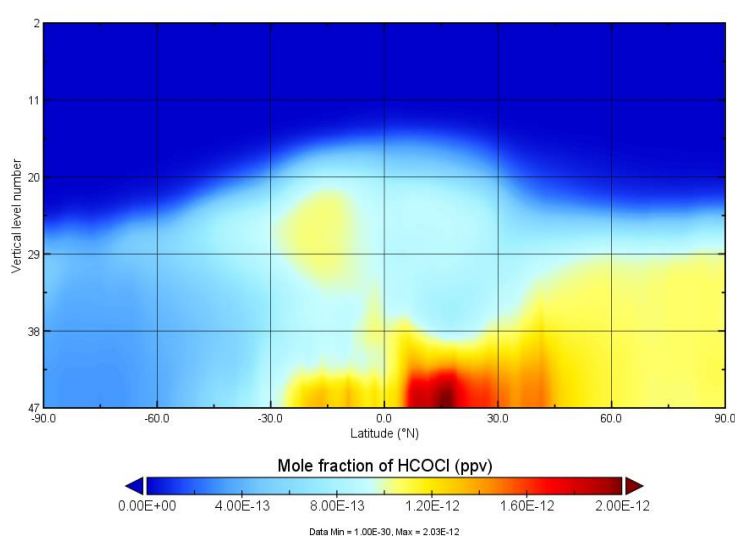
Figure IV-21: Zonal average distribution of HCOCl in ppv as a function of the model vertical levels in the "Cl_emis_HC" simulation. The level 47 is the surface level.

These reactions have an influence on stratospheric HCl, mainly near the SH tropopause while the impact on ozone is an increase in this region, but also extending above (in the lower stratosphere). More investigation is needed to understand this result.

IV.4.5. Impact of the addition of VSLS

In this section, the impact of adding the VSLS on the MOCAGE scheme is analysed. This is done by setting the concentrations of VSLS at the surface as indicated in **Table IV-6** and adding the reactions (1 - 11) (**Table IV-3**) to the scheme. Now, this simulation involves all the changes done on the original scheme and it is named "FULL". To analyse the impact of VSLS on the scheme, the results of this simulation are compared to those of the simulation "Cl_emis_HC".

Upon adding the effect of VSLS, higher HCl and ClO levels are observed in both layers, the troposphere and the stratosphere (***Figure IV-22(a,b)***). Reactions (1 - 11) in ***Table IV-3*** show that HCl is being formed via the oxidation of VSLS (CH_2Cl_2 and $CHCl_3$) by atomic Cl (reactions 3 and 4). ClO is produced via reaction 11 involving the oxidation of $COCl_2$. However, it is surprising that O_3 levels are higher in the "FULL" simulation than in the "Cl_emis_simulation".
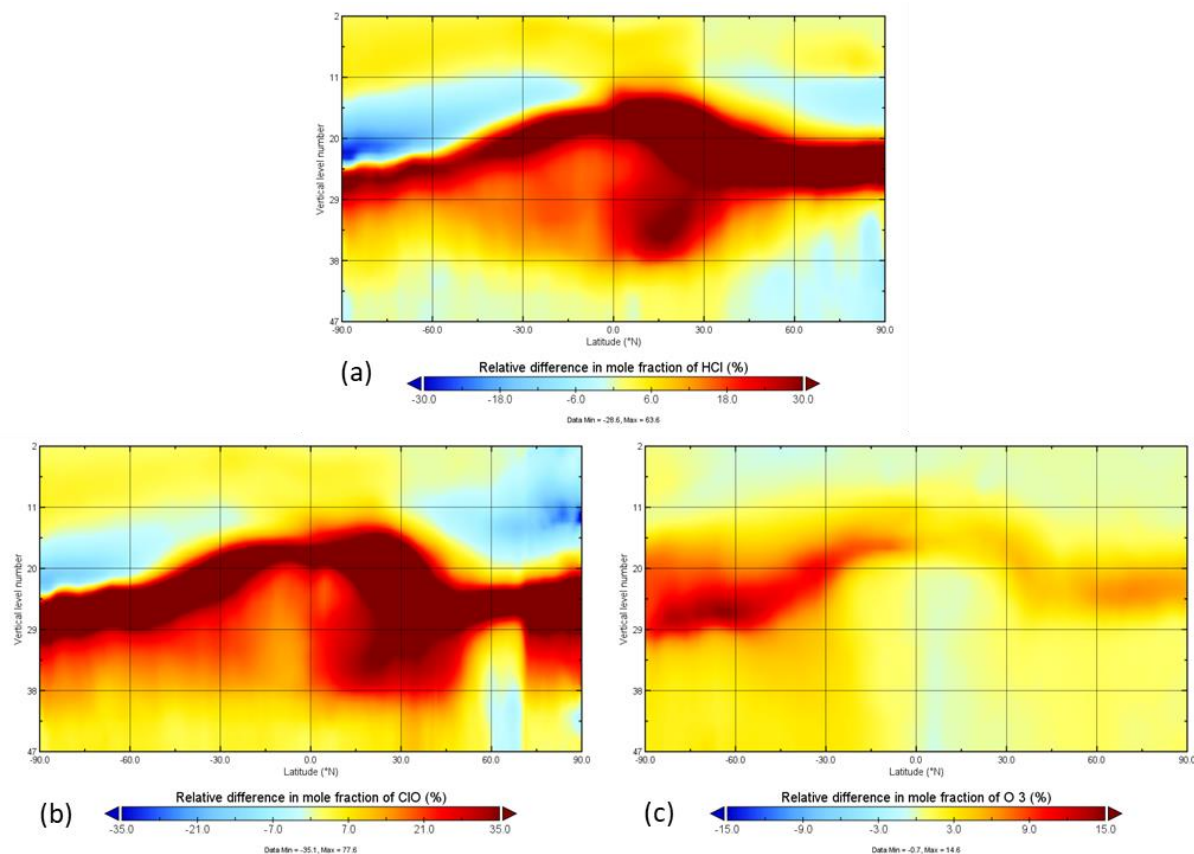
Figure IV-22: *Relative difference in the zonal average distribution of HCl (a) ClO (b), and O_3 (c) in the entire atmosphere in % as a function of the model vertical levels between "FULL" and "Cl_emis_HC" simulations. The level 47 in the surface level.*

$COCl_2$ and $CHCl_2O_2$ are produced in this simulation. Both species are formed by the oxidation of VSLS. They are abundant in the atmosphere, mainly the troposphere (***Figure IV-23***). $COCl_2$ is produced in the troposphere mainly in the tropics from the oxidation of $CHCl_3$ and from $CHCl_2O_2$ degradation. This is why $COCl_2$ is much more abundant than $CHCl_2O_2$. $COCl_2$ is then transported to the stratosphere mainly by tropical deep convection and slow radiative ascent (***Figure IV-23(a)***). Moreover, we can see that $COCl_2$ and $CHCl_2O_2$ are more abundant in the NH than in the SH. This can be related to the fact that VSLS have higher surface concentrations in the NH as shown in ***Table IV-6***.
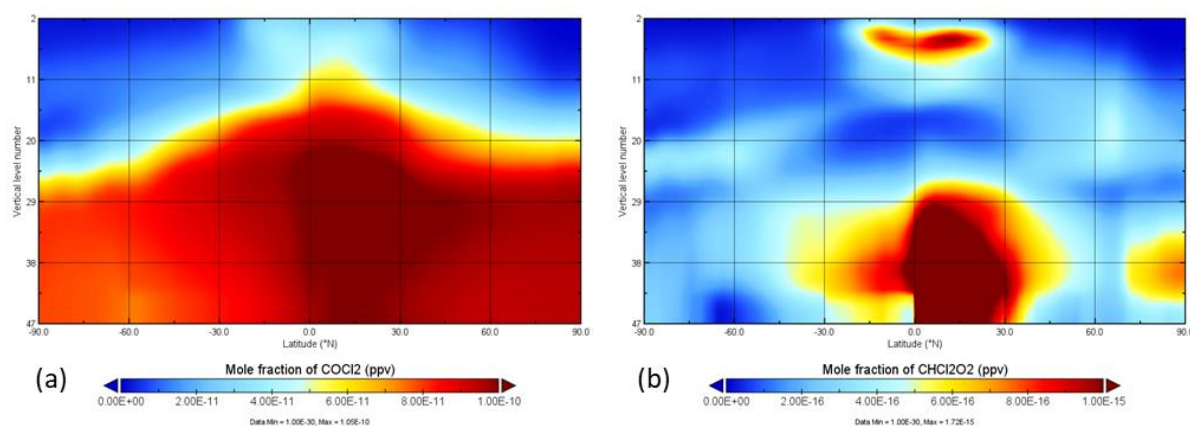
Figure IV-23: *Zonal average distribution of COCl₂ (a) and CHCl₂O₂ (b) in ppv as a function of the model vertical levels in the "FULL" simulation. The level 47 is the surface level.*

The impact of including the VSLS is generally an increase in ozone levels, mainly in the lower stratosphere and around the tropopause. In the lower stratosphere, the increase of ozone can be linked to the decrease of HCl and ClO. Around the tropopause, this is counterintuitive that the increase of chlorine induces an increase of ozone. More investigation is needed to understand this result.

IV.5. Conclusion and perspectives

As this work is done in a very short time, a first goal is achieved, which is to test how different factors for the representation of tropospheric chlorine affect the partitioning of chlorine species and their impact on ozone. The main findings of the simulations can be summarized as:

- Changing the Henry's law constants of HCl, by setting the effective constant, lessens the amount of HCl present in the atmosphere by the more efficient scavenging by precipitation. This leads to a general increase of ozone in the troposphere and stratosphere.
- Updating the emissions of HCl by decreasing the land anthropogenic emissions and increasing the oceanic emissions, besides adding the oceanic ClNO₂ emissions, results in more chlorine in the troposphere and the stratosphere, and consequently higher ozone destruction.
- Adding the chlorine reactions and in particular with VOCs adds up the production of a new important organic chlorinated species to MOCAGE scheme, namely HCOCl. HCOCl is one of the most abundant chlorinated products in the troposphere from VOCs.
- Setting the surface concentration of Cl-VSLS favours the formation of HCl and ClO, mainly in the troposphere and in the tropopause region. The main organic chlorinated products of the oxidation of these species are COCl₂ and CHCl₂O₂.

This work is only very preliminary. It has to be completed by a more in-depth analysis of the results based on other diagnostic/visualization tools than the zonal-vertical cross sections used here. In particular, more diagnostics are needed for a better understanding of the response of stratospheric ozone to the different changes tested in the thesis. For this, we need to

investigate the combined role of chemistry and transport processes. Moreover, the analysis is done so far for the month of December. It would be useful to extend it to other seasons to have a full picture of temporal evolution during the year and analyse the impacts of the upgrades.

This work can also be considered as very preliminary because it does not include some of the processes required to fully represent tropospheric chlorine chemistry or it uses crude assumptions. Without these improvements, it is not possible to study and quantify the full effect of chlorine on tropospheric chemistry and its indirect effect on stratospheric chemistry. More thermal and photolytic reactions will be added to the scheme that represent the real atmospheric chemistry of chlorine. Reactions resulting from the simplified mechanism of ASTEC can be a part of the reactions to be added. The emissions need to be added in a more realistic way that consider the spatial and temporal variations of both anthropogenic and oceanic emissions, rather than being evenly distributed. Additional Cl-VSLS could be added to the scheme. Heterogeneous reactions of chlorinated species in the troposphere and stratosphere have to be also implemented. The model could be run for a longer time than 2 years, to allow the scheme to fully attain an equilibrium state due to the chemical reactivity of the species and their transport, in particular VSLS. To achieve the goal of a full and accurate modelling of tropospheric chlorine chemistry in MOCAGE is therefore a long-term effort. This is linked to the developments listed above but also because errors in chlorine amounts and partitioning in the troposphere that have non-negligible impacts on stratospheric ozone.

General conclusions and perspectives

In 1974, Crutzen, Molina, and Rowland recognized the role of chlorine in stratospheric ozone depletion, and their work led to the awarding of the 1995 Nobel Prize in Chemistry. Since then, a huge effort was put to understand the chlorine stratospheric chemistry. Recently, scientists are being interested to analyse and quantify the impact of chlorine on the troposphere. Inspired by these studies, and based on the continuing development of this research domain, our aim is to take part in the investigation of tropospheric chlorine chemistry by numerical tools.

This thesis work presents the modelling of the chemistry of chlorine in the atmosphere, mainly in the troposphere, by three different aspects: quantum chemistry tools, a kinetic model, and a global model.

The **quantum chemistry tools** are used to compute the thermokinetic properties of species and their reactions. In the frame of this thesis, these tools are applied on the reaction between CH_2ClOOH and OH, the most abundant tropospheric oxidant. CH_2ClOOH is an important intermediate in low-temperature combustion processes. Upon reviewing the literature, we find that this is the first time to compute the thermokinetic data of this reaction. The thermokinetic and energetic properties of this reaction are computed at two dual levels of theory: M06-2X/6-311+G(3df,3pd)//M06-2X/6-311+G(2df,2p) and DK-CCSD(T)/ANO-RCC-VQZP//MP2/aug-cc-pV(T+d)Z. The latter level of theory shows a multireference problem, and therefore, the DFT level of theory, M06-2X/6-311+G(3df,3pd)//M06-2X/6-311+G(2df,2p), is more accurate in computing the thermokinetic data. The overall rate constant of this reaction is 6.55×10^{-11} cm^3 molecule^{-1} s^{-1} at the levels of theory at 298 K using a two-step mechanism and asymmetrical one-dimensional Eckart tunnelling.

The findings of this investigation can be used to complete the mechanisms implemented into 0D and global models that simulate the chlorine atmospheric chemistry. They can be also applied to figure out the effect of this reactivity on the atmospheric chlorine budget and on the air quality.

In the **0D model**, the reactivity and speciation of chlorinated species are simulated. The kinetic model, ASTEC, used in this work, simulates the chlorine reactivity in the gaseous phase over a very short time scale (in the range of few hours or days). A total of 388 reactions of organic and inorganic chlorinated species are implemented into this model which is set under suitable conditions. The simplified mechanism resulting from this model summarizes the cycling of the very reactive chlorinated organic and inorganic species in the troposphere. This model makes it clear that photolysis reactions are the main route of destruction of inorganic chlorinated species, whereas, oxidation governs the reactivity of organic chlorinated species.

The simplified mechanism determined by the kinetic model, can be as an input in global models to check its importance on a global scale, and for a longer time range.

General conclusions and perspectives

The chemistry-transport model MOCAGE is used as a **global model**. It allows to model the chemical composition of the atmosphere. Unlike ASTEC, MOCAGE considers the different physicochemical processes that take place in the atmosphere and the meteorological conditions. These factors have impacts on the atmospheric composition. In the context of this thesis, new developments are added to MOCAGE to make it possible to model the chlorine chemistry in both, the troposphere and the stratosphere. The results show that changing the Henry's law constant of one species can alter the atmospheric composition and the abundance of different species by changing the efficiency of the scavenging process. Emissions of chlorinated species can be not only affecting the troposphere, but also transported into the stratosphere. Addition of the reactions involving chlorinated species is essential to model the chemical reactivity of these species and adding up the effect of other species that are not present in the original MOCAGE version.

This work opens up a number of avenues to be investigated:

- On the quantum chemistry aspect, thermokinetic parameters of the reaction between CH_2XOOH (X = F, Br, or I) and OH will be determined to figure out the effect of halogen type on the reactivity. Moreover, the effect of multiple halogenation species $CH_{(n-x)}X_xOOH$ can be a subject of interest. Reactivity with other atmospheric oxidants (e.g.: O_3 or Cl) can be also computed.
- The 0D model will be improved to overcome its limitations to model the chlorine chemistry over a longer time scale. Other halogenated and mixed halogenated species will be added to determine whether they affect each other and how. In addition, the input reaction should always be updated to include newly determined kinetic parameters, just like the ones obtained during this thesis while studying the reactivity of CH_2ClOOH with OH radicals.
- The chlorine chemistry in the global model will be improved by adding more gaseous reactions of chlorinated species and the heterogeneous reactions. The impact of iodinated and brominated species can be analysed over a global scale. The chemistry of iodine can be simulated following an accident like the Fukushima nuclear disaster. The chemistry of bromine can be modelled following a volcanic explosion.

The results of this thesis work are valorised by:

- **2** oral communications in international conferences,
- **3** oral communications in workshops and national conferences,
- **9** posters in national and international conferences and events.

Moreover, I would like to thank my supervisors, who gave me the opportunity of being a part of other projects. I had the chance to perform thermokinetic computations of the reactivity of OH radical with pesticides (metazachlor and quinmerac). In addition, I gained some skills related to adsorption models, thanks to Dr. Lotfi SELLAOUI, who was a post-doctoral student in our team. These projects are valorised by the publication of 4 scientific articles, presented in 2 oral communications, and 10 posters.

Bibliography

Abbatt, J.P.D., Demerjian, K.L., Anderson, J.G., 1990. A new approach to free-radical kinetics: radially and axially resolved high-pressure discharge flow with results for hydroxyl + (ethane, propane, n-butane, n-pentane) = products at 297 K. Journal of Physical Chemistry 94, 4566–4575. https://doi.org/10.1021/j100374a039

Agrawal, S.K., Chakraborty, A., Chakraborty, S., 2023. Atmospherically relevant halogen- and hydrogen- bond complex [CCl_4 ($H_2Y)_n$] with Y = O and S, n≤4: A computational study on Rayleigh scattering properties. Computational and Theoretical Chemistry 1229, 114293. https://doi.org/10.1016/j.comptc.2023.114293

Anderson, J.G., Brune, W.H., Proffitt, M.H., 1989. Ozone destruction by chlorine radicals within the Antarctic vortex: The spatial and temporal evolution of ClO-O_3 anticorrelation based on in situ ER-2 data. Journal of Geophysical Research: Atmospheres 94, 11465–11479. https://doi.org/10.1029/JD094iD09p11465

Anderson, W.D., Gerry, M.C.L., Davis, R.W., 1986. The microwave spectrum of isotopically substituted hypochlorous acid: Determination of the molecular structure. Journal of Molecular Spectroscopy 115, 117–130. https://doi.org/10.1016/0022-2852(86)90280-8

Anglada, J.M., Olivella, S., Solé, A., 2006. Mechanistic Study of the CH_3O_2• + HO_2• → CH_3O_2H + O_2 Reaction in the Gas Phase. Computational Evidence for the Formation of a Hydrogen-Bonded Diradical Complex. Journal of Physical Chemistry A 110, 6073–6082. https://doi.org/10.1021/jp060798u

Anglada, J.M., Solé, A., 2017. The Atmospheric Oxidation of HONO by OH, Cl, and ClO Radicals. Journal of Physical Chemistry A 121, 9698–9707. https://doi.org/10.1021/acs.jpca.7b10715

Aquilante, F., Autschbach, J., Baiardi, A., Battaglia, S., Borin, V.A., Chibotaru, L.F., Conti, I., De Vico, L., Delcey, M., Fdez. Galván, I., Ferré, N., Freitag, L., Garavelli, M., Gong, X., Knecht, S., Larsson, E.D., Lindh, R., Lundberg, M., Malmqvist, P.Å., Nenov, A., Norell, J., Odelius, M., Olivucci, M., Pedersen, T.B., Pedraza-González, L., Phung, Q.M., Pierloot, K., Reiher, M., Schapiro, I., Segarra-Martí, J., Segatta, F., Seijo, L., Sen, S., Sergentu, D.-C., Stein, C.J., Ungur, L., Vacher, M., Valentini, A., Veryazov, V., 2020. Modern quantum chemistry with [Open]Molcas. Journal of Physical Chemistry 152, 214117. https://doi.org/10.1063/5.0004835

Aranda, A., Martínez, E., Díaz de Mera, Y., Rodríguez, A., Rodríguez, D., Cuartero, J., 2003. Low-pressure study of the reactions of Cl atoms with acrylic acid and allyl alcohol. Atmospheric Environment 37, 4361–4369. https://doi.org/10.1016/S1352-2310(03)00573-9

Argento, D.C., Stone, J.O., Keith Fifield, L., Tims, S.G., 2010. Chlorine-36 in seawater. Nuclear Instruments and Methods in Physics Research Section B: Beam Interactions with Materials and Atoms, Proceedings of the Eleventh International Conference on Accelerator Mass Spectrometry 268, 1226–1228. https://doi.org/10.1016/j.nimb.2009.10.139

Atkinson, R., Baulch, D.L., Cox, R.A., Crowley, J.N., Hampson, R.F., 2001. Summary of Evaluated Kinetic and Photochemical Data for Atmospheric Chemistry 1–56.

Atkinson, R., Baulch, D.L., Cox, R.A., Crowley, J.N., Hampson, R.F., Hynes, R.G., Jenkin, M.E., Rossi, M.J., Troe, J., 2007a. Evaluated kinetic and photochemical data for atmospheric chemistry: Volume III – gas phase reactions of inorganic halogens. Atmospheric Chemistry and Physics 7, 981–1191. https://doi.org/10.5194/acp-7-981-2007

Atlas, E., Pollock, W., Greenberg, J., Heidt, L., Thompson, A.M., 1993. Alkyl nitrates, nonmethane hydrocarbons, and halocarbon gases over the equatorial Pacific Ocean

Bibliography

during SAGA 3. Journal of Geophysical Research: Atmospheres 98, 16933–16947. https://doi.org/10.1029/93JD01005

Average weather August in Lille (Nord-Pas-de-Calais), France [WWW Document], 2013. . World Weather & Climate Information. URL https://weather-and-climate.com:80/lille-August-averages (accessed 1.10.23).

Badia, A., Reeves, C.E., Baker, A.R., Saiz-Lopez, A., Volkamer, R., Koenig, T.K., Apel, E.C., Hornbrook, R.S., Carpenter, L.J., Andrews, S.J., Sherwen, T., von Glasow, R., 2019. Importance of reactive halogens in the tropical marine atmosphere: a regional modelling study using WRF-Chem. Atmospheric Chemistry and Physics 19, 3161–3189. https://doi.org/10.5194/acp-19-3161-2019

Bari, A., Ferraro, V., Wilson, L.R., Luttinger, D., Husain, L., 2003. Measurements of gaseous HONO, HNO_3, SO_2, HCl, NH_3, particulate sulfate and PM2.5 in New York, NY. Atmospheric Environment 37, 2825–2835. https://doi.org/10.1016/S1352-2310(03)00199-7

Barletta, B., Meinardi, S., Simpson, I.J., Atlas, E.L., Beyersdorf, A.J., Baker, A.K., Blake, N.J., Yang, M., Midyett, J.R., Novak, B.J., McKeachie, R.J., Fuelberg, H.E., Sachse, G.W., Avery, M.A., Campos, T., Weinheimer, A.J., Rowland, F.S., Blake, D.R., 2009. Characterization of volatile organic compounds (VOCs) in Asian and north American pollution plumes during INTEX-B: identification of specific Chinese air mass tracers. Atmospheric Chemistry and Physics 9, 5371–5388. https://doi.org/10.5194/acp-9-5371-2009

Barré, J., Peuch, V.H., Lahoz, W.A., Attié, J.L., Josse, B., Piacentini, A., Eremenko, M., Dufour, G., Nedelec, P., von Clarmann, T., El Amraoui, L., 2014. Combined data assimilation of ozone tropospheric columns and stratospheric profiles in a high-resolution CTM. Quarterly Journal of the Royal Meteorological Society 140, 966–981. https://doi.org/10.1002/qj.2176

Baulch, D.L., Campbell, I.M., Saunders, S.M., 1985. Rate constants for the reactions of hydroxyl radicals with propane and ethane. Journal of the Chemical Society, Faraday Transactions 1: Physical Chemistry in Condensed Phases 1 81, 259–263. https://doi.org/10.1039/F19858100259

Baulch, D.L., Duxbury, J., Grant, S., Montague, D., 1981. Evaluated Kinetic Data for High Temperature Reactions. Volume 4. Homogeneous Gas Phase Reactions of Halogen- and Cyanide-Containing Species. Journal of Physical and Chemical Reference Data 10.

Bechtold, P., Bazile, E., Guichard, F., Mascart, P., Richard, E., 2001. A mass-flux convection scheme for regional and global models. Quarterly Journal of the Royal Meteorological Society 127, 869–886. https://doi.org/10.1002/qj.49712757309

Becker, E., Wille, U., Rahman, M.M., Schindler, R.N., 1991. An Investigation of the Reactions of NO_3 Radicals with Cl and ClO. Berichte der Bunsengesellschaft für physikalische Chemie 95, 1173–1179. https://doi.org/10.1002/bbpc.19910951003

Bednarz, E.M., Hossaini, R., Chipperfield, M.P., Abraham, N.L., Braesicke, P., 2022. Atmospheric impacts of chlorinated very short-lived substances over the recent past – Part 1: Stratospheric chlorine budget and the role of transport. Atmospheric Chemistry and Physics 22, 10657–10676. https://doi.org/10.5194/acp-22-10657-2022

Begum, S., Subramanian, R., 2014. Bonding and spectroscopic properties of complexes of SO_2 – O_2 and SO_2 – N_2 and its atmospheric consequences. Physical Chemistry Chemical Physics 16, 17658–17669. https://doi.org/10.1039/C4CP01084A

Bonard, A., Daële, V., Delfau, J.-L., Vovelle, C., 2002. Kinetics of OH Radical Reactions with Methane in the Temperature Range 295−660 K and with Dimethyl Ether and Methyl-tert-butyl Ether in the Temperature Range 295−618 K. Journal of Physical Chemistry A 106, 4384–4389. https://doi.org/10.1021/jp012425t

Bibliography

Born, M., Oppenheimer, R., 1927. Zur Quantentheorie der Molekeln. Annalen der Physik 389, 457–484. https://doi.org/10.1002/andp.19273892002

Bosland, L., Cantrel, L., Girault, N., Clement, B., 2010. Modeling of Iodine Radiochemistry in the ASTEC Severe Accident Code: Description and Application to FPT-2 PHEBUS Test. Nuclear Technology 171, 88–107. https://doi.org/10.13182/NT10-A10774

Boudries, H., Bottenheim, J.W., 2000. Cl and Br atom concentrations during a surface boundary layer ozone depletion event in the Canadian High Arctic. Geophysical Research Letters 27, 517–520. https://doi.org/10.1029/1999GL011025

Bourmada, N., Lafage, C., Devolder, P., 1987. Absolute rate constants of the reactions of OH with cyclohexane and ethane at 296 ± 2 K by the discharge flow method. Chemical Physics Letters 136, 209–214. https://doi.org/10.1016/0009-2614(87)80443-8

Boyd, A.A., Marston, G., Wayne, R.P., 1996. Kinetic Studies of the Reaction between NO_3 and OClO at T = 300 K and P = 2−8 Torr. Journal of Physical Chemistry 100, 130–137. https://doi.org/10.1021/jp9509931

Brasseur, G.P., Hauglustaine, D.A., Walters, S., Rasch, P.J., Müller, J.-F., Granier, C., Tie, X.X., 1998. MOZART, a global chemical transport model for ozone and related chemical tracers: 1. Model description. Journal of Geophysical Research: Atmospheres 103, 28265–28289. https://doi.org/10.1029/98JD02397

Brown, S.S., Stutz, J., 2012. Nighttime radical observations and chemistry. Chemical Society Reviews 41, 6405–6447. https://doi.org/10.1039/C2CS35181A

Brudnik, K., Gola, A.A., Jodkowski, J.T., 2009. Theoretical kinetic study of the formation reactions of methanol and methyl hypohalites in the gas phase. Journal of Molecular Modeling 15, 1061–1066. https://doi.org/10.1007/s00894-009-0461-x

Bryukov, M.G., Knyazev, V.D., Lomnicki, S.M., McFerrin, C.A., Dellinger, B., 2004. Temperature-Dependent Kinetics of the Gas-Phase Reactions of OH with Cl_2, CH_4, and C_3H_8. Journal of Physical Chemistry A 108, 10464–10472. https://doi.org/10.1021/jp047340h

Bryukov, M.G., Slagle, I.R., Knyazev, V.D., 2003. Kinetics of Reactions of Cl Atoms with Ethane, Chloroethane, and 1,1-Dichloroethane. Journal of Physical Chemistry A 107, 6565–6573. https://doi.org/10.1021/jp0275138

Bryukov, M.G., Slagle, I.R., Knyazev, V.D., 2002. Kinetics of Reactions of Cl Atoms with Methane and Chlorinated Methanes. Journal of Physical Chemistry A 106, 10532–10542. https://doi.org/10.1021/jp0257909

Burkholder, J.B., Abbatt, J.P.D., Cappa, C., Dibble, T.S., Kolb, C.E., Wilmouth, D.M., Sander, S.P., Barker, J.R., Crounse, J.D., Huie, R.E., Kurylo, M.J., Percival, C.J., Wine, P.H., 2020. Chemical Kinetics and Photochemical Data for Use in Atmospheric Studies, Evaluation No. 19-5, JPL Publication 19-5. Jet Propulsion Laboratory, Pasadena.

Canneaux, S., Xerri, B., Louis, F., Cantrel, L., 2010. Theoretical Study of the Gas-Phase Reactions of Iodine Atoms ($^2P_{3/2}$) with H_2, H_2O, HI, and OH. Journal of Physical Chemistry A 114, 9270–9288. https://doi.org/10.1021/jp104163t

Cantrel, L., Cousin, F., Bosland, L., Chevalier-Jabet, K., Marchetto, C., 2014. ASTEC V2 severe accident integral code: Fission product modelling and validation. Nuclear Engineering and Design 272, 195–206. https://doi.org/10.1016/j.nucengdes.2014.01.011

Cantrell, C.A., Davidson, J.A., Shetter, R.E., Anderson, B.A., Calvert, J.G., 1987. Reactions of nitrate radical and nitrogen oxide (N_2O_5) with molecular species of possible atmospheric interest. Journal of Physical Chemistry 91, 6017–6021. https://doi.org/10.1021/j100307a040

Bibliography

Carl, S.A., Roehl, M., Müller, R., Moortgat, G.K., Crowley, J.N., 1996. Rate Constant and Mechanism of the Reaction between Cl and CH_3OCl at 295 K. Journal of Physical Chemistry 100, 17191–17201. https://doi.org/10.1021/jp9611075

Cavalli, F., Glasius, M., Hjorth, J., Rindone, B., Jensen, N.R., 1998. Atmospheric lifetimes, infrared spectra and degradation products of a series of hydrofluoroethers. Atmospheric Environment 32, 3767–3773. https://doi.org/10.1016/S1352-2310(98)00106-X

Chase, M.W., 1998. NIST-JANAF Thermochemical Tables, 4th Edition. Journal of Physical Chemistry Monograph No. 9.

Chatelard, P., Belon, S., Bosland, L., Carénini, L., Coindreau, O., Cousin, F., Marchetto, C., Nowack, H., Piar, L., Chailan, L., 2016. Main modelling features of the ASTEC V2.1 major version. Annals of Nuclear Energy, ERMSAR-2015 conference of SARNET in the frame of the NUGENIA Technical Area 2 93, 83–93. https://doi.org/10.1016/j.anucene.2015.12.026

Chatelard, P., Reinke, N., Arndt, S., Belon, S., Cantrel, L., Carenini, L., Chevalier-Jabet, K., Cousin, F., Eckel, J., Jacq, F., Marchetto, C., Mun, C., Piar, L., 2014. ASTEC V2 severe accident integral code main features, current V2.0 modelling status, perspectives. Nuclear Engineering and Design 272, 119–135. https://doi.org/10.1016/j.nucengdes.2013.06.040

Chen, Y., Tschuikow-Roux, E., 1992. Ab initio study of the structures, rotation/inversion barriers, fundamental frequencies, and thermodynamic functions of beta-chloroethyl, alpha-chloroethyl, and alpha, alpha-dichloroethyl radicals. Journal of Physical Chemistry 96, 7266–7272. https://doi.org/10.1021/j100197a026

Chevalier-Jabet, K., Cousin, F., Cantrel, L., Séropian, C., 2014. Source term assessment with ASTEC and associated uncertainty analysis using SUNSET tool. Nuclear Engineering and Design 272, 207–218. https://doi.org/10.1016/j.nucengdes.2013.06.042

Chi, Y., Fan, M., Zhao, C., Sun, L., Yang, Y., Yang, X., Tao, J., 2021. Ground-level NO_2 concentration estimation based on OMI tropospheric NO_2 and its spatiotemporal characteristics in typical regions of China. Atmospheric Research 264, 105821. https://doi.org/10.1016/j.atmosres.2021.105821

Clarke, J.S., Kroll, J.H., Donahue, N.M., Anderson, J.G., 1998. Testing Frontier Orbital Control: Kinetics of OH with Ethane, Propane, and Cyclopropane from 180 to 360K. Journal of Physical Chemistry A 102, 9847–9857. https://doi.org/10.1021/jp982922i

Claxton, T., Hossaini, R., Wilson, C., Montzka, S.A., Chipperfield, M.P., Wild, O., Bednarz, E.M., Carpenter, L.J., Andrews, S.J., Hackenberg, S.C., Mühle, J., Oram, D., Park, S., Park, M.-K., Atlas, E., Navarro, M., Schauffler, S., Sherry, D., Vollmer, M., Schuck, T., Engel, A., Krummel, P.B., Maione, M., Arduini, J., Saito, T., Yokouchi, Y., O'Doherty, S., Young, D., Lunder, C., 2020. A Synthesis Inversion to Constrain Global Emissions of Two Very Short Lived Chlorocarbons: Dichloromethane, and Perchloroethylene. Journal of Geophysical Research: Atmospheres 125, e2019JD031818. https://doi.org/10.1029/2019JD031818

Cleary, P.A., Romero, M.T.B., Blitz, M.A., Heard, D.E., Pilling, M.J., Seakins, P.W., Wang, L., 2006. Determination of the temperature and pressure dependence of the reaction OH + C_2H_4 from 200–400 K using experimental and master equation analyses. Physical Chemistry Chemical Physics 8, 5633–5642. https://doi.org/10.1039/B612127F

Cohen, N., Benson, S.W., 1987. Transition-state-theory calculations for reactions of hydroxyl radicals with haloalkanes. Journal of Physical Chemistry 91, 162–170. https://doi.org/10.1021/j100285a036

Cousin, F., Kissane, M.P., Girault, N., 2013. Modelling of fission-product transport in the reactor coolant system. Annals of Nuclear Energy, Special Issue: Phebus FP Final Seminar 61, 135–142. https://doi.org/10.1016/j.anucene.2013.02.035

Bibliography

Cox, J.D., Wagman, D.D., Medvedev, V.A., 1990. CODATA — Key Values for Thermodynamics, Aus Der Reihe: CODATA, Series on Thermodynamic Properties. Hemisphere Publishing Corporation: New York, Washington, Philadelphia, London. Berichte der Bunsengesellschaft für physikalische Chemie 94, 93. https://doi.org/10.1002/bbpc.19900940121

Cox, M.L., Sturrock, G.A., Fraser, P.J., Siems, S.T., Krummel, P.B., O'Doherty, S., 2003. Regional Sources of Methyl Chloride, Chloroform and Dichloromethane Identified from AGAGE Observations at Cape Grim, Tasmania, 1998–2000. Journal of Atmospheric Chemistry 45, 79–99. https://doi.org/10.1023/A:1024022320985

Crisp, T.A., Lerner, B.M., Williams, E.J., Quinn, P.K., Bates, T.S., Bertram, T.H., 2014. Observations of gas phase hydrochloric acid in the polluted marine boundary layer. Journal of Geophysical Research: Atmospheres 119, 6897–6915. https://doi.org/10.1002/2013JD020992

Cristofanelli, P., Arduini, J., Calzolari, F., Giostra, U., Bonasoni, P., Maione, M., 2020. First Evidences of Methyl Chloride (CH_3Cl) Transport from the Northern Italy Boundary Layer during Summer 2017. Atmosphere 11, 238. https://doi.org/10.3390/atmos11030238

Crowley, J.N., Campuzano-Jost, P., Moortgat, G.K., 1996. Temperature Dependent Rate Constants for the Gas-Phase Reaction between OH and CH_3OCl. Journal of Physical Chemistry 100, 3601–3606. https://doi.org/10.1021/jp953018i

Crutzen, P.J., 1970. The influence of nitrogen oxides on the atmospheric ozone content. Quarterly Journal of the Royal Meteorological Society 96, 320–325. https://doi.org/10.1002/qj.49709640815

Cunnold, D.M., Fraser, P.J., Weiss, R.F., Prinn, R.G., Simmonds, P.G., Miller, B.R., Alyea, F.N., Crawford, A.J., 1994. Global trends and annual releases of CCl_3F and CCl_2F_2 estimated from ALE/GAGE and other measurements from July 1978 to June 1991. Journal of Geophysical Research: Atmospheres 99, 1107–1126. https://doi.org/10.1029/93JD02715

Cussac, M., 2020. La composition chimique de la haute troposphère : étude de l'impact des feux de biomasse et des processus de transports verticaux avec le modèle MOCAGE et les mesures IAGOS (These de doctorat). Toulouse, INPT.

Cussac, M., Marécal, V., Thouret, V., Josse, B., Sauvage, B., 2020. The impact of biomass burning on upper tropospheric carbon monoxide: a study using MOCAGE global model and IAGOS airborne data. Atmospheric Chemistry and Physics 20, 9393–9417. https://doi.org/10.5194/acp-20-9393-2020

Dao, D.Q., Taamalli, S., Louis, F., Kdouh, D., Srour, Z., Ngo, T.C., Truong, D.H., Fèvre-Nollet, V., Ribaucour, M., El Bakali, A., Černušák, I., 2023. Hydroxyl radical-initiated decomposition of metazachlor herbicide in the gaseous and aqueous phases: Mechanism, kinetics, and toxicity evaluation. Chemosphere 312, 137234. https://doi.org/10.1016/j.chemosphere.2022.137234

Dawe, K.E.R., Furlani, T.C., Kowal, S.F., Kahan, T.F., VandenBoer, T.C., Young, C.J., 2019. Formation and emission of hydrogen chloride in indoor air. Indoor Air 29, 70–78. https://doi.org/10.1111/ina.12509

de Bruyn, W.J., Shorter, J.A., Davidovits, Paul., Worsnop, D.R., Zahniser, M.S., Kolb, C.E., 1995. Uptake of Haloacetyl and Carbonyl Halides by Water Surfaces. Environmental Science & Technology 29, 1179–1185. https://doi.org/10.1021/es00005a007

de Zafra, R.L., Jaramillo, M., Parrish, A., Solomon, P., Connor, B., Barrett, J., 1987. High concentrations of chlorine monoxide at low altitudes in the Antarctic spring stratosphere: diurnal variation. Nature 328, 408–411. https://doi.org/10.1038/328408a0

Bibliography

DeMore, W.B., Bayes, K.D., 1999. Rate Constants for the Reactions of Hydroxyl Radical with Several Alkanes, Cycloalkanes, and Dimethyl Ether. Journal of Physical Chemistry A 103, 2649–2654. https://doi.org/10.1021/jp983273d

Dillon, T.J., Hölscher, D., Sivakumaran, V., Horowitz, A., Crowley, J.N., 2005. Kinetics of the reactions of HO with methanol (210 - 351 K) and with ethanol (216 - 368 K). Physical Chemistry Chemical Physics 7, 349–355. https://doi.org/10.1039/B413961E

DóBé, S., Turányi, T., Iogansen, A.A., Bérces, T., 1992. Rate constants of the reactions of OH radicals with cyclopropane and cyclobutane. International Journal of Chemical Kinetics 24, 191–198. https://doi.org/10.1002/kin.550240207

Donahue, N.M., Anderson, J.G., Demerjian, K.L., 1998. New Rate Constants for Ten OH Alkane Reactions from 300 to 400 K: An Assessment of Accuracy. Journal of Physical Chemistry A 102, 3121–3126. https://doi.org/10.1021/jp980532q

Douglas, M., Kroll, N.M., 1974. Quantum electrodynamical corrections to the fine structure of helium. Annals of Physics 82, 89–155. https://doi.org/10.1016/0003-4916(74)90333-9

Droege, A.T., Tully, F.P., 1986. Hydrogen-atom abstraction from alkanes by hydroxyl. 3. Propane. Journal of Physical Chemistry 90, 1949–1954. https://doi.org/10.1021/j100400a042

Dunkirk innovates for better air quality - SUEZ Group [WWW Document], 2013. URL https://www.suez.com/en/news/dunkirk-innovates-for-better-air-quality (accessed 11.27.22).

Dunning, T.H., 1989. Gaussian basis sets for use in correlated molecular calculations. I. The atoms boron through neon and hydrogen. Journal of Chemical Physics 90, 1007–1023. https://doi.org/10.1063/1.456153

Dunning, T.H., Peterson, K.A., Wilson, A.K., 2001. Gaussian basis sets for use in correlated molecular calculations. X. The atoms aluminum through argon revisited. Journal of Chemical Physics 114, 9244–9253. https://doi.org/10.1063/1.1367373

Eastham, S.D., Weisenstein, D.K., Barrett, S.R.H., 2014. Development and evaluation of the unified tropospheric–stratospheric chemistry extension (UCX) for the global chemistry-transport model GEOS-Chem. Atmospheric Environment 89, 52–63. https://doi.org/10.1016/j.atmosenv.2014.02.001

Eckart, C., 1930. The Penetration of a Potential Barrier by Electrons. Physical Review 35, 1303–1309. https://doi.org/10.1103/PhysRev.35.1303

Eger, P.G., Friedrich, N., Schuladen, J., Shenolikar, J., Fischer, H., Tadic, I., Harder, H., Martinez, M., Rohloff, R., Tauer, S., Drewnick, F., Fachinger, F., Brooks, J., Darbyshire, E., Sciare, J., Pikridas, M., Lelieveld, J., Crowley, J.N., 2019. Shipborne measurements of $ClNO_2$ in the Mediterranean Sea and around the Arabian Peninsula during summer. Atmospheric Chemistry and Physics 19, 12121–12140. https://doi.org/10.5194/acp-19-12121-2019

Engel, A., Rigby, M., 2018. Update on Ozone-Depleting Substances (ODSs) and Other Gases of Interest to the Montreal Protocol, in: Scientific Assessment of Ozone Depletion: 2018. World Meteorological Organization, Geneva, Switzerland, p. 1.1-1.87.

Eyring, H., 1935. The Activated Complex in Chemical Reactions. Journal of Chemical Physics 3, 107–115. https://doi.org/10.1063/1.1749604

Fahad, 2021. Earth Reminder. Earth Reminder. URL https://www.earthreminder.com/describe-the-composition-of-the-earths-atmosphere/ (accessed 6.21.23).

Fan, S., Li, Y., 2022. The impacts of marine-emitted halogens on OH radicals in East Asia during summer. Atmospheric Chemistry and Physics 22, 7331–7351. https://doi.org/10.5194/acp-22-7331-2022

Fan, X., Cai, J., Yan, C., Zhao, J., Guo, Y., Li, C., Dällenbach, K.R., Zheng, F., Lin, Z., Chu, B., Wang, Y., Dada, L., Zha, Q., Du, W., Kontkanen, J., Kurtén, T., Iyer, S., Kujansuu,

Bibliography

    J.T., Petäjä, T., Worsnop, D.R., Kerminen, V.-M., Liu, Y., Bianchi, F., Tham, Y.J., Yao, L., Kulmala, M., 2021. Atmospheric gaseous hydrochloric and hydrobromic acid in urban Beijing, China: detection, source identification and potential atmospheric impacts. Atmospheric Chemistry and Physics 21, 11437–11452. https://doi.org/10.5194/acp-21-11437-2021

Farman, J.C., Gardiner, B.G., Shanklin, J.D., 1985. Large losses of total ozone in Antarctica reveal seasonal ClO_x/NO_x interaction. Nature 315, 207–210. https://doi.org/10.1038/315207a0

Faxon, C.B., Allen, D.T., Faxon, C.B., Allen, D.T., 2013. Chlorine chemistry in urban atmospheres: a review. Environmental Chemistry 10, 221–233. https://doi.org/10.1071/EN13026

Faxon, C.B., Bean, J.K., Ruiz, L.H., 2015. Inland Concentrations of Cl_2 and $ClNO_2$ in Southeast Texas Suggest Chlorine Chemistry Significantly Contributes to Atmospheric Reactivity. Atmosphere 6, 1487–1506. https://doi.org/10.3390/atmos6101487

Finlayson-Pitts, B.J., Hernandez, S.K., Berko, H.N., 1993. A new dark source of the gaseous hydroxyl radical for relative rate measurements. Journal of Physical Chemistry 97, 1172–1177. https://doi.org/10.1021/j100108a012

Finley, B.D., Saltzman, E.S., 2008. Observations of Cl_2, Br_2, and I_2 in coastal marine air. Journal of Geophysical Research: Atmospheres 113. https://doi.org/10.1029/2008JD010269

Finley, B.D., Saltzman, E.S., 2006. Measurement of Cl_2 in coastal urban air. Geophysical Research Letters 33. https://doi.org/10.1029/2006GL025799

Fortin, C., 2019. Etudes par simulations numériques et moléculaires de la réactivité atmosphérique de l'iode (Thèse de doctorat). University of Lille.

Fortin, C., Fèvre-Nollet, V., Cousin, F., Lebègue, P., Louis, F., 2019. Box modelling of gas-phase atmospheric iodine chemical reactivity in case of a nuclear accident. Atmospheric Environment 214, 116838. https://doi.org/10.1016/j.atmosenv.2019.116838

Fortin, C., Khanniche, S., Khiri, D., Fèvre-Nollet, V., Lebègue, P., Cousin, F., Černušák, I., Louis, F., 2018. Reactivity of Hydrogen Peroxide with Br and I Atoms. Journal of Physical Chemistry A 122, 1053–1063. https://doi.org/10.1021/acs.jpca.7b10318

Frisch, M.J., Trucks, G.W., Schlegel, H.B., Scuseria, G.E., Robb, M.A., Cheeseman, J.R., Scalmani, G., Barone, V., Petersson, G.A., Nakatsuji, H., Li, X., Caricato, M., Marenich, A.V., Bloino, J., Janesko, B.G., Gomperts, R., Mennucci, B., Hratchian, H.P., Ortiz, J.V., Izmaylov, A.F., Sonnenberg, J.L., Williams-Young, D., Ding, F., Lipparini, F., Egidi, F., Goings, J., Peng, B., Petrone, A., Henderson, T., Ranasinghe, D., Zakrzewski, V.G., Gao, J., Rega, N., Zhang, G., Liang, W., Hada, M., Ehara, M., Toyota, K., Fukuda, R., Hasegawa, J., Ishida, M., Nakajima, T., Honda, Y., Kitao, O., Nakai, H., Vreven, T., Throssell, K., Montgomery, J.A., Peralta, Jr., J.E., Ogliaro, F., Bearpark, M.J., Heyd, J.J., Brothers, E.N., Kudin, K.N., Staroverov, V.N., Keith, T.A., Kobayashi, R., Normand, J., Raghavachari, K., Rendell, A.P., Burant, J.C., Iyengar, F., Tomasi, J., Cossi, M., Millam, J.M., Klene, M., Adamo, C., Cammi, R., Ochterski, J.W., Morokuma, K., Farkas, O., Foresman, J.B., Fox, D.J., 2016. Gaussian. Wallingford CT.

Fukui, K., 1970. Formulation of the reaction coordinate. Journal of Physical Chemistry 74, 4161–4163. https://doi.org/10.1021/j100717a029

Gao, L.G., Zheng, J., Fernández-Ramos, A., Truhlar, D.G., Xu, X., 2018. Kinetics of the Methanol Reaction with OH at Interstellar, Atmospheric, and Combustion Temperatures. Journal of the American Chemical Society 140, 2906–2918. https://doi.org/10.1021/jacs.7b12773

Gautrois, M., Brauers, T., Koppmann, R., Rohrer, F., Stein, O., Rudolph, J., 2003. Seasonal variability and trends of volatile organic compounds in the lower polar troposphere.

Bibliography

Journal of Geophysical Research: Atmospheres 108. https://doi.org/10.1029/2002JD002765

Gerlach, T.M., 2004. Volcanic sources of tropospheric ozone-depleting trace gases. Geochemistry, Geophysics, Geosystems 5. https://doi.org/10.1029/2004GC000747

Ghoshal, S., Hazra, M.K., 2014. New Mechanism for Autocatalytic Decomposition of H_2CO_3 in the Vapor Phase. Journal of Physical Chemistry A 118, 2385–2392. https://doi.org/10.1021/jp412239e

Girault, N., Bosland, L., Dickinson, S., Funke, F., Güntay, S., Herranz, L.E., Powers, D., 2012. LWR severe accident simulation: Iodine behaviour in FPT2 experiment and advances on containment iodine chemistry. Nuclear Engineering and Design 243, 371–392. https://doi.org/10.1016/j.nucengdes.2011.11.011

Golden, D.M., 2007. The Reaction $Cl + NO_2 \rightarrow ClONO$ and $ClNO_2$. Journal of Physical Chemistry A 111, 6772–6780. https://doi.org/10.1021/jp069000x

Graedel, T.E., Keene, W.C., 1995. Tropospheric budget of reactive chlorine. Global Biogeochemical Cycles 9, 47–77. https://doi.org/10.1029/94GB03103

Guenther, A.B., Jiang, X., Heald, C.L., Sakulyanontvittaya, T., Duhl, T., Emmons, L.K., Wang, X., 2012. The Model of Emissions of Gases and Aerosols from Nature version 2.1 (MEGAN2.1): an extended and updated framework for modeling biogenic emissions. Geoscientific Model Development 5, 1471–1492. https://doi.org/10.5194/gmd-5-1471-2012

Gurvich, L.V., Veits, I.V., Alcock, C.B., 1989. Thermodynamics properties of individual substances., 4th ed. New York.

Guth, J., Josse, B., Marécal, V., Joly, M., Hamer, P., 2016. First implementation of secondary inorganic aerosols in the MOCAGE version R2.15.0 chemistry transport model. Geoscientific Model Development 9, 137–160. https://doi.org/10.5194/gmd-9-137-2016

Hägele, J., Lorenz, K., Rhäsa, D., Zellner, R., 1983. Rate Constants and CH_3O Product Yield of the Reaction $OH + CH_3OH \rightarrow$ Products. Berichte der Bunsengesellschaft für physikalische Chemie 87, 1023–1026. https://doi.org/10.1002/bbpc.19830871112

Hall, R., Nepotchatykh, O., Nepotchatykh, E., Ariya, P.A., 2020. Anthropogenic Photolabile Chlorine in the Cold-Climate City of Montreal. Atmosphere 11, 812. https://doi.org/10.3390/atmos11080812

Hammaecher, C., Canneaux, S., Louis, F., Cantrel, L., 2011. A Theoretical Study of the H-Abstraction Reactions from HOI by Moist Air Radiolytic Products (H, OH, and O (^{3}P)) and Iodine Atoms ($^2P_{3/2}$). Journal of Physical Chemistry A 115, 6664–6674. https://doi.org/10.1021/jp202760u

Hammond, G.S., 1955. A Correlation of Reaction Rates. Journal of the American Chemical Society 77, 334–338. https://doi.org/10.1021/ja01607a027

Harrison, J.J., Chipperfield, M.P., Hossaini, R., Boone, C.D., Dhomse, S., Feng, W., Bernath, P.F., 2019. Phosgene in the Upper Troposphere and Lower Stratosphere: A Marker for Product Gas Injection Due to Chlorine-Containing Very Short-Lived Substances. Geophysical Research Letters 46, 1032–1039. https://doi.org/10.1029/2018GL079784

Haskins, J.D., Jaeglé, L., Thornton, J.A., 2020. Significant Decrease in Wet Deposition of Anthropogenic Chloride Across the Eastern United States, 1998 - 2018. Geophysical Research Letters 47, e2020GL090195. https://doi.org/10.1029/2020GL090195

Haskins, J.D., Lee, B.H., Lopez-Hilifiker, F.D., Peng, Q., Jaeglé, L., Reeves, J.M., Schroder, J.C., Campuzano-Jost, P., Fibiger, D., McDuffie, E.E., Jiménez, J.L., Brown, S.S., Thornton, J.A., 2019. Observational Constraints on the Formation of Cl_2 From the Reactive Uptake of $ClNO_2$ on Aerosols in the Polluted Marine Boundary Layer. Journal

of Geophysical Research: Atmospheres 124, 8851–8869. https://doi.org/10.1029/2019JD030627

Heathfield, A.E., Anastasi, C., Pagsberg, P., McCulloch, A., 1998. Atmospheric lifetimes of selected fluorinated ether compounds. Atmospheric Environment 32, 711–717. https://doi.org/10.1016/S1352-2310(97)00330-0

Herndon, S.C., Gierczak, T., Talukdar, R.K., Ravishankara, A.R., 2001. Kinetics of the reactions of OH with several alkyl halides. Physical Chemistry Chemical Physics 3, 4529–4535. https://doi.org/10.1039/B105188C

Hess, B.A., 1986. Relativistic electronic-structure calculations employing a two-component no-pair formalism with external-field projection operators. Physical Review A 33, 3742–3748. https://doi.org/10.1103/PhysRevA.33.3742

Hess, B.A., Buenker, R.J., Marian, C.M., Peyerimhoff, S.D., 1982. Investigation of electron correlation on the theoretical prediction of zero-field splittings of $^2\Pi$ molecular states. Chemical Physics Letters 89, 459–462. https://doi.org/10.1016/0009-2614(82)83046-7

Hess, W.P., Tully, F.P., 1989. Hydrogen-atom abstraction from methanol by hydroxyl radical. Journal of Physical Chemistry 93, 1944–1947. https://doi.org/10.1021/j100342a049

Hiatt, M.H., 2013. Determination of Henry's Law Constants Using Internal Standards with Benchmark Values. Journal of Chemical & Engineering Data 58, 902–908. https://doi.org/10.1021/je3010535

Hoffmann, E.H., Tilgner, A., Vogelsberg, U., Wolke, R., Herrmann, H., 2019. Near-Explicit Multiphase Modeling of Halogen Chemistry in a Mixed Urban and Maritime Coastal Area. ACS Earth and Space Chemistry 3, 2452–2471. https://doi.org/10.1021/acsearthspacechem.9b00184

Hossaini, R., Atlas, E., Dhomse, S.S., Chipperfield, M.P., Bernath, P.F., Fernando, A.M., Mühle, J., Leeson, A.A., Montzka, S.A., Feng, W., Harrison, J.J., Krummel, P., Vollmer, M.K., Reimann, S., O'Doherty, S., Young, D., Maione, M., Arduini, J., Lunder, C.R., 2019. Recent Trends in Stratospheric Chlorine from Very Short-Lived Substances. Journal of Geophysical Research: Atmospheres 124, 2318–2335. https://doi.org/10.1029/2018JD029400

Hossaini, R., Chipperfield, M.P., Saiz-Lopez, A., Fernandez, R., Monks, S., Feng, W., Brauer, P., von Glasow, R., 2016. A global model of tropospheric chlorine chemistry: Organic versus inorganic sources and impact on methane oxidation. Journal of Geophysical Research: Atmospheres 121, 14,271-14,297. https://doi.org/10.1002/2016JD025756

Hou, H., Wang, B., Gu, Y., 2000. Decomposition and Isomerization of the CH_3CHClO Radical: ab Initio and RRKM Study. Journal of Physical Chemistry A 104, 1570–1575. https://doi.org/10.1021/jp9930999

Howard, C.J., Evenson, K.M., 1976. Rate constants for the reactions of OH with ethane and some halogen substituted ethanes at 296 K. The Journal of Chemical Physics 64, 4303–4306. https://doi.org/10.1063/1.432115

Hoy, A.R., Bunker, P.R., 1979. A precise solution of the rotation bending Schrödinger equation for a triatomic molecule with application to the water molecule. Journal of Molecular Spectroscopy 74, 1–8. https://doi.org/10.1016/0022-2852(79)90019-5

Huber, K.P., Herzberg, G., 1979. Molecular Spectra and Molecular Structure. IV. Constants of Diatomic Molecules. Van Nostrand Co.: New York. https://doi.org/10.1007/978-1-4757-0961-2

Irikura, K.K., 1998. Appendix B: Essential Statistical Thermodynamics, in: Computational Thermochemistry, ACS Symposium Series. American Chemical Society, pp. 402–418. https://doi.org/10.1021/bk-1998-0677.ch022

IUPAC, 1991. Isotopic compositions of the elements 1989. Pure and Applied Chemistry 63, 991–1002. https://doi.org/10.1351/pac199163070991

Bibliography

Jacob, D.J., 1999. Introduction to Atmospheric Chemistry, Introduction to Atmospheric Chemistry. Princeton University Press. https://doi.org/10.1515/9781400841547

Jacobson, M.Z., 2005. Fundamentals of Atmospheric Modeling, 2nd ed. Cambridge University Press, Cambridge. https://doi.org/10.1017/CBO9781139165389

Jacox, M.E., 1994. Vibrational and Electronic Energy Levels of Polyatomic Transient Molecules. Journal of Physical Chemistry Ref. Data, Monograph 3.

Jayaraj, R., Megha, P., Sreedev, P., 2016. Organochlorine pesticides, their toxic effects on living organisms and their fate in the environment. Interdisciplinary Toxicology 9, 90–100. https://doi.org/10.1515/intox-2016-0012

Jenkin, M.E., Saunders, S.M., Pilling, M.J., 1997. The tropospheric degradation of volatile organic compounds: a protocol for mechanism development. Atmospheric Environment 31, 81–104. https://doi.org/10.1016/S1352-2310(96)00105-7

Jeong, D., Seco, R., Gu, D., Lee, Youngro, Nault, B.A., Knote, C.J., Mcgee, T., Sullivan, J.T., Jimenez, J.L., Campuzano-Jost, P., Blake, D.R., Sanchez, D., Guenther, A.B., Tanner, D., Huey, L.G., Long, R., Anderson, B.E., Hall, S.R., Ullmann, K., Shin, H., Herndon, S.C., Lee, Youngjae, Kim, D., Ahn, J., Kim, S., 2019. Integration of airborne and ground observations of nitryl chloride in the Seoul metropolitan area and the implications on regional oxidation capacity during KORUS-AQ 2016. Atmospheric Chemistry and Physics 19, 12779–12795. https://doi.org/10.5194/acp-19-12779-2019

Jiménez, E., Gilles, M.K., Ravishankara, A.R., 2003. Kinetics of the reactions of the hydroxyl radical with CH_3OH and C_2H_5OH between 235 and 360 K. Journal of Photochemistry and Photobiology A: Chemistry, Atmospheric Photochemistry 157, 237–245. https://doi.org/10.1016/S1010-6030(03)00073-X

Jobson, B.T.., Niki, H., Yokouchi, Y., Bottenheim, J., Hopper, F., Leaitch, R., 1994. Measurements of C_2-C_6 hydrocarbons during the Polar Sunrise1992 Experiment: Evidence for Cl atom and Br atom chemistry. Journal of Geophysical Research: Atmospheres 99, 25355–25368. https://doi.org/10.1029/94JD01243

Jodkowski, J.T., Rayez, M.-T., Rayez, J.-C., Bérces, T., Dóbé, S., 1998. Theoretical Study of the Kinetics of the Hydrogen Abstraction from Methanol. 2. Reaction of Methanol with Chlorine and Bromine Atoms. Journal of Physical Chemistry A 102, 9230–9243. https://doi.org/10.1021/jp980846d

Johnson III, R.D., Richter, U., Manichaikul, A., Schneider, B., Acevedo, C., Cockrell, B., Minne, E., Reed, J., Parsons, M., Fahey, M., 2022. NIST Computational Chemistry Comparison and Benchmark Database, NIST Standard Reference Database Number 101. ed.

Johnston, H.S., 1966. Gas phase reaction rate theory, in: Gas Phase Reaction Rate Theory, Modern Concepts in Chemistry. Ronald Press Co., New York, NY.

Josse, B., Simon, P., Peuch, V.-H., 2004. Radon global simulations with the multiscale chemistry and transport model MOCAGE. Tellus B 56, 339–356. https://doi.org/10.1111/j.1600-0889.2004.00112.x

Jourdain, B., Legrand, M., 2002. Year-round records of bulk and size-segregated aerosol composition and HCl and HNO_3 levels in the Dumont d'Urville (coastal Antarctica) atmosphere: Implications for sea-salt aerosol fractionation in the winter and summer. Journal of Geophysical Research: Atmospheres 107, ACH 20-1-ACH 20-13. https://doi.org/10.1029/2002JD002471

Joy, F., Rajakumar, B., 2023. Photo-oxidation reaction of tert -butyl chloride with OH radicals and Cl atoms in the troposphere and its implications. Physical Chemistry Chemical Physics 25, 7901–7916. https://doi.org/10.1039/D2CP03503K

Bibliography

Kain, J.S., Fritsch, J.M., 1990. A One-Dimensional Entraining/Detraining Plume Model and Its Application in Convective Parameterization. Journal of the Atmospheric Sciences 47, 2784–2802. https://doi.org/10.1175/1520-0469(1990)047<2784:AODEPM>2.0.CO;2

Kaiser, E.W., 1992. Pressure dependence of the reaction $Cl + C_2H_2$ over the temperature range 230 to 370 K. International Journal of Chemical Kinetics 24, 179–189. https://doi.org/10.1002/kin.550240206

Kaiser, E.W., Wallington, T.J., 1996. Pressure Dependence of the Reaction $Cl + C_3H_6$. Journal of Physical Chemistry 100, 9788–9793. https://doi.org/10.1021/jp960406r

Kaiser, J.W., Heil, A., Andreae, M.O., Benedetti, A., Chubarova, N., Jones, L., Morcrette, J.-J., Razinger, M., Schultz, M.G., Suttie, M., van der Werf, G.R., 2012. Biomass burning emissions estimated with a global fire assimilation system based on observed fire radiative power. Biogeosciences 9, 527–554. https://doi.org/10.5194/bg-9-527-2012

Kanchanakungwankul, S., Bao, J.L., Zheng, J., Alecu, I.M., Lynch, B.J., Zhao, Y., Truhlar, D.G., 2018. Database of Frequency Scale Factors for Electronic Model Chemistries, Version 4 [WWW Document]. URL https://comp.chem.umn.edu/freqscale/190107_Database_of_Freq_Scale_Factors_v4.p d (accessed 5.27.23).

Karlsson, R.S., LjungstrÖm, E.B., 1996. Laboratory Study of ClNO: Hydrolysis. Environmental Science & Technology 30, 2008–2013. https://doi.org/10.1021/es950801f

Keene, W.C., Pszenny, A.A.P., Jacob, D.J., Duce, R.A., Galloway, J.N., Schultz-Tokos, J.J., Sievering, H., Boatman, J.F., 1990. The geochemical cycling of reactive chlorine through the marine troposphere. Global Biogeochemical Cycles 4, 407–430. https://doi.org/10.1029/GB004i004p00407

Keene, W.C., Savoie, D.L., 1998. The pH of deliquesced sea-salt aerosol in polluted marine air. Geophysical Research Letters 25, 2181–2184. https://doi.org/10.1029/98GL01591

Keene, William.C., Khalil, M.A.K., Erickson III, David.J., McCulloch, A., Graedel, T.E., Lobert, J.M., Aucott, M.L., Gong, S.L., Harper, D.B., Kleiman, G., Midgley, P., Moore, R.M., Seuzaret, C., Sturges, W.T., Benkovitz, C.M., Koropalov, V., Barrie, L.A., Li, Y.F., 1999. Composite global emissions of reactive chlorine from anthropogenic and natural sources: Reactive Chlorine Emissions Inventory. Journal of Geophysical Research: Atmospheres 104, 8429–8440. https://doi.org/10.1029/1998JD100084

Keller-Rudek, H., Moortgat, G.K., Sander, R., Sörensen, R., 2013. The MPI-Mainz UV/VIS Spectral Atlas of Gaseous Molecules of Atmospheric Interest. Earth System Science Data 5, 365–373. https://doi.org/10.5194/essd-5-365-2013

Kendall, R.A., Dunning, T.H., Harrison, R.J., 1992. Electron affinities of the first-row atoms revisited. Systematic basis sets and wave functions. Journal of Chemical Physics 96, 6796–6806. https://doi.org/10.1063/1.462569

Kercher, J.P., Riedel, T.P., Thornton, J.A., 2009. Chlorine activation by N_2O_5: simultaneous, in situ detection of $ClNO_2$ and N_2O_5 by chemical ionization mass spectrometry. Atmospheric Measurement Techniques 2, 193–204. https://doi.org/10.5194/amt-2-193-2009

Kettle, A., Andreae, M., Amouroux, D., Andreae, T., Bates, T., Berresheim, H., Bingemer, H., Boniforti, R., Curran, M., Ditullio, G., Helas, G., Jones, G., Keller, M., Kiene, R., Leck, C., Levasseur, M., Malin, G., Maspero, M., Matrai, P., Mctaggart, A., Mihalopoulos, N., Nguyen, B., Novo, A., Putaud, J., Rapsomanikis, S., Roberts, G., Schebeske, G., Sharma, S., Simó, R., Staubes, R., Turner, S., Uher, G., 1999. A global database of sea surface dimethylsulfide (DMS) measurements and a procedure to predict sea surface DMS as a function of latitude, longitude, and month. Global Biogeochemical Cycles 13, 399. https://doi.org/10.1029/1999GB900004

Bibliography

Khalil, M. a. K., Moore, R.M., Harper, D.B., Lobert, J.M., Erickson, D.J., Koropalov, V., Sturges, W.T., Keene, W.C., 1999. Natural emissions of chlorine-containing gases: Reactive Chlorine Emissions Inventory. Journal of Geophysical Research 104, 8333–8346. https://doi.org/10.1029/1998JD100079

Khalil, M.A.K., Rasmussen, R.A., 1981. Atmospheric methylchloride (CH_3Cl). Chemosphere 10, 1019–1023. https://doi.org/10.1016/0045-6535(81)90204-6

Khan, M.A.H., Ashfold, M.J., Nickless, G., Martin, D., Watson, L.A., Hamer, P.D., Wayne, R.P., Canosa-Mas, C.E., Shallcross, D.E., 2008. Night-time NO_3 and OH radical concentrations in the United Kingdom inferred from hydrocarbon measurements. Atmospheric Science Letters 9, 140–146. https://doi.org/10.1002/asl.175

Khan, M.A.H., Cooke, M.C., Utembe, S.R., Archibald, A.T., Derwent, R.G., Xiao, P., Percival, C.J., Jenkin, M.E., Morris, W.C., Shallcross, D.E., 2015. Global modeling of the nitrate radical (NO_3) for present and pre-industrial scenarios. Atmospheric Research 164–165, 347–357. https://doi.org/10.1016/j.atmosres.2015.06.006

Khanniche, S., Louis, F., Cantrel, L., Černušák, I., 2016. Computational study of the I_2O_5 + H_2O = 2 $HOIO_2$ gas-phase reaction. Chemical Physics Letters 662, 114–119. https://doi.org/10.1016/j.cplett.2016.09.023

Khiri, D., Černušák, I., Louis, F., 2018. Theoretical Study of the Reactions of H Atoms with CH_3I and CH_2I_2. Journal of Physical Chemistry A 122, 6546–6557. https://doi.org/10.1021/acs.jpca.8b04748

Kim, S., Huey, L.G., Stickel, R.E., Pierce, R.B., Chen, G., Avery, M.A., Dibb, J.E., Diskin, G.S., Sachse, G.W., McNaughton, C.S., Clarke, A.D., Anderson, B.E., Blake, D.R., 2008. Airborne measurements of HCl from the marine boundary layer to the lower stratosphere over the North Pacific Ocean during INTEX-B. Atmospheric Chemistry and Physics Discussions 8, 3563–3595. https://doi.org/10.5194/acpd-8-3563-2008

Kita, D., Stedman, D.H., 1982. Kinetic studies of reactions of hydrogen atoms with HCl, Cl_2 and NOCl, and chlorine atoms with H_2 and NOCl. Journal of Chemical Society, Faraday Trans. 2 78, 1249. https://doi.org/10.1039/f29827801249

Knyazev, V.D., Bencsura, A., Dubinsky, I.A., Gutman, D., Melius, C.F., Senkan, S.M., 1995. Kinetics and Thermochemistry of the Reaction of 1-Chloroethyl Radical with Molecular Oxygen. Journal of Physical Chemistry 99, 230–238. https://doi.org/10.1021/j100001a036

Knyazev, V.D., Kalinovski, I.J., Slagle, I.R., 1999. Kinetics of the $CH_2CH_2Cl \rightleftarrows C_2H_4 + Cl$ Reaction. Journal of Physical Chemistry A 103, 3216–3221. https://doi.org/10.1021/jp984207e

Kozlov, S.N., Orkin, V.L., Huie, R.E., Kurylo, M.J., 2003. OH Reactivity and UV Spectra of Propane, n-Propyl Bromide, and Isopropyl Bromide. Journal of Physical Chemistry A 107, 1333–1338. https://doi.org/10.1021/jp021806j

Krysztofiak, G., Catoire, V., Poulet, G., Marécal, V., Pirre, M., Louis, F., Canneaux, S., Josse, B., 2012. Detailed modeling of the atmospheric degradation mechanism of very-short lived brominated species. Atmospheric Environment 59, 514–532. https://doi.org/10.1016/j.atmosenv.2012.05.026

Kuhn, M., Builtjes, P.J.H., Poppe, D., Simpson, D., Stockwell, W.R., Andersson-Sko¨ld, Y., Baart, A., Das, M., Fiedler, F., Hov, Ø., Kirchner, F., Makar, P.A., Milford, J.B., Roemer, M.G.M., Ruhnke, R., Strand, A., Vogel, B., Vogel, H., 1998. Intercomparison of the gas-phase chemistry in several chemistry and transport models. Atmospheric Environment 32, 693–709. https://doi.org/10.1016/S1352-2310(97)00329-4

Kukui, A.S., Roggenbuck, J., Schindler, R.N., 1997. Mechanism and rate constants for the reactions of Cl atoms with HOCl, CH_3OCl and tert-C_4H_9OCl. Ber. Bunsenges. Physik. Chem. 101, 281–286. https://doi.org/10.1002/bbpc.19971010217

Bibliography

Kumaran, S.S., Lim, K.P., Michael, J.V., 1994a. Thermal rate constants for the Cl+H$_2$ and Cl+D$_2$ reactions between 296 and 3000 K. Journal of Chemical Physics 101, 9487–9498. https://doi.org/10.1063/1.468486

Kurth, S., Marques, M.A.L., Gross, E.K.U., 2005. Density-Functional Theory, in: Bassani, F., Liedl, G.L., Wyder, P. (Eds.), Encyclopedia of Condensed Matter Physics. Elsevier, Oxford, pp. 395–402. https://doi.org/10.1016/B0-12-369401-9/00445-9

Kwon, H.-Y., Morrow, Z., Kelley, C.T., Jakubikova, E., 2021. Interpolation Methods for Molecular Potential Energy Surface Construction. Journal of Physical Chemistry A 125, 9725–9735. https://doi.org/10.1021/acs.jpca.1c06812

Kyasa, S., Puffer, B.W., Dussault, P.H., 2013. Synthesis of Alkyl Hydroperoxides via Alkylation of gem-Dihydroperoxides. The Journal of Organic Chemistry 78, 3452–3456. https://doi.org/10.1021/jo4001564

Lacressonnière, G., Peuch, V.-H., Vautard, R., Arteta, J., Déqué, M., Joly, M., Josse, B., Marécal, V., Saint-Martin, D., 2014. European air quality in the 2030s and 2050s: Impacts of global and regional emission trends and of climate change. Atmospheric Environment 92, 348–358. https://doi.org/10.1016/j.atmosenv.2014.04.033

Lamarque, J.-F., Bond, T.C., Eyring, V., Granier, C., Heil, A., Klimont, Z., Lee, D., Liousse, C., Mieville, A., Owen, B., Schultz, M.G., Shindell, D., Smith, S.J., Stehfest, E., Van Aardenne, J., Cooper, O.R., Kainuma, M., Mahowald, N., McConnell, J.R., Naik, V., Riahi, K., van Vuuren, D.P., 2010. Historical (1850 - 2000) gridded anthropogenic and biomass burning emissions of reactive gases and aerosols: methodology and application. Atmospheric Chemistry and Physics 10, 7017–7039. https://doi.org/10.5194/acp-10-7017-2010

Lamarque, J.-F., Shindell, D.T., Josse, B., Young, P.J., Cionni, I., Eyring, V., Bergmann, D., Cameron-Smith, P., Collins, W.J., Doherty, R., Dalsoren, S., Faluvegi, G., Folberth, G., Ghan, S.J., Horowitz, L.W., Lee, Y.H., MacKenzie, I.A., Nagashima, T., Naik, V., Plummer, D., Righi, M., Rumbold, S.T., Schulz, M., Skeie, R.B., Stevenson, D.S., Strode, S., Sudo, K., Szopa, S., Voulgarakis, A., Zeng, G., 2013. The Atmospheric Chemistry and Climate Model Intercomparison Project (ACCMIP): overview and description of models, simulations and climate diagnostics. Geoscientific Model Development 6, 179–206. https://doi.org/10.5194/gmd-6-179-2013

Laube, J.C., Tegtmeier, S., 2022. Update on Ozone-Depleting Substances (ODSs) and Other Gases of Interest to the Montreal Protocol, in: Scientific Assessment of Ozone Depletion: 2022. World Meteorological Organization (WMO), Geneva, Switzerland, pp. 51–113.

Lawler, M.J., Finley, B.D., Keene, W.C., Pszenny, A. a. P., Read, K.A., von Glasow, R., Saltzman, E.S., 2009. Pollution-enhanced reactive chlorine chemistry in the eastern tropical Atlantic boundary layer. Geophysical Research Letters 36. https://doi.org/10.1029/2008GL036666

Lawler, M.J., Sander, R., Carpenter, L.J., Lee, J.D., von Glasow, R., Sommariva, R., Saltzman, E.S., 2011. HOCl and Cl$_2$ observations in marine air. Atmospheric Chemistry and Physics 11, 7617–7628. https://doi.org/10.5194/acp-11-7617-2011

Le Breton, M., Hallquist, Å.M., Pathak, R.K., Simpson, D., Wang, Y., Johansson, J., Zheng, J., Yang, Y., Shang, D., Wang, H., Liu, Q., Chan, C., Wang, T., Bannan, T.J., Priestley, M., Percival, C.J., Shallcross, D.E., Lu, K., Guo, S., Hu, M., Hallquist, M., 2018. Chlorine oxidation of VOCs at a semi-rural site in Beijing: significant chlorine liberation from ClNO$_2$ and subsequent gas- and particle-phase Cl–VOC production. Atmospheric Chemistry and Physics 18, 13013–13030. https://doi.org/10.5194/acp-18-13013-2018

Bibliography

Lee, J.H., Tang, I.N., 1982. Absolute rate constants for the hydroxyl radical reactions with ethane, furan, and thiophene at room temperature. The Journal of Chemical Physics 77, 4459–4463. https://doi.org/10.1063/1.444367

Leedham Elvidge, E.C., Oram, D.E., Laube, J.C., Baker, A.K., Montzka, S.A., Humphrey, S., O'Sullivan, D.A., Brenninkmeijer, C. a. M., 2015. Increasing concentrations of dichloromethane, CH_2Cl_2, inferred from CARIBIC air samples collected 1998–2012. Atmospheric Chemistry and Physics 15, 1939–1958. https://doi.org/10.5194/acp-15-1939-2015

Lefèvre, F., Brasseur, G.P., Folkins, I., Smith, A.K., Simon, P., 1994. Chemistry of the 1991 - 1992 stratospheric winter: Three-dimensional model simulations. Journal of Geophysical Research: Atmospheres 99, 8183–8195. https://doi.org/10.1029/93JD03476

Leriche, M., Deguillaume, L., Chaumerliac, N., 2003. Modeling study of strong acids formation and partitioning in a polluted cloud during wintertime. Journal of Geophysical Research: Atmospheres 108. https://doi.org/10.1029/2002JD002950

Leu, M.T., 1979. Rate constant for the reaction $HO_2 + NO \rightarrow OH + NO_2$. The Journal of Chemical Physics 70, 1662–1666. https://doi.org/10.1063/1.437680

Li, L., Yin, S., Huang, L., Yi, X., Wang, Y., Zhang, K., Ooi, C.G., Allen, D.T., 2020. An emission inventory for Cl_2 and HOCl in Shanghai, 2017. Atmospheric Environment 223, 117220. https://doi.org/10.1016/j.atmosenv.2019.117220

Li, Q., Osborne, M.C., Smith, I.W.M., 2000. Rate constants for the reactions of Cl atoms with HCOOH and with HOCO radicals. International Journal of Chemical Kinetics 32, 85–91. https://doi.org/10.1002/(SICI)1097-4601(2000)32:2<85::AID-KIN3>3.0.CO;2-I

Li, Q., Zhang, L., Wang, T., Tham, Y.J., Ahmadov, R., Xue, L., Zhang, Q., Zheng, J., 2016. Impacts of heterogeneous uptake of dinitrogen pentoxide and chlorine activation on ozone and reactive nitrogen partitioning: improvement and application of the WRF-Chem model in southern China. Atmospheric Chemistry and Physics 16, 14875–14890. https://doi.org/10.5194/acp-16-14875-2016

Li, Q.S., Luo, Q., 2003. Direct ab Initio Dynamics Study of the Reaction of the Hydrogen Atom with Formyl Chloride. Journal of Physical Chemistry A 107, 10435–10440. https://doi.org/10.1021/jp0360568

Liakakou, E., Fourtziou, L., Paraskevopoulou, D., Speyer, O., Lianou, M., Grivas, G., Myriokefalitakis, S., Mihalopoulos, N., 2022. High-Resolution Measurements of SO_2, HNO_3 and HCl at the Urban Environment of Athens, Greece: Levels, Variability and Gas to Particle Partitioning. Atmosphere 13, 218. https://doi.org/10.3390/atmos13020218

Liang, J., 2013. Chemical composition of the atmosphere of the Earth, in: Liang, J. (Ed.), Chemical Modeling for Air Resources. Academic Press, Boston, pp. 3–20. https://doi.org/10.1016/B978-0-12-408135-2.00001-X

Liao, J., Huey, L.G., Liu, Z., Tanner, D.J., Cantrell, C.A., Orlando, J.J., Flocke, F.M., Shepson, P.B., Weinheimer, A.J., Hall, S.R., Ullmann, K., Beine, H.J., Wang, Y., Ingall, E.D., Stephens, C.R., Hornbrook, R.S., Apel, E.C., Riemer, D., Fried, A., Mauldin, R.L., Smith, J.N., Staebler, R.M., Neuman, J.A., Nowak, J.B., 2014. High levels of molecular chlorine in the Arctic atmosphere. Nature Geosci 7, 91–94. https://doi.org/10.1038/ngeo2046

Lindgren, P.F., 1992. Diffusion scrubber-ion chromatography for the measurement of trace levels of atmospheric HCl. Atmospheric Environment. Part A. General Topics 26, 43–49. https://doi.org/10.1016/0960-1686(92)90259-N

Liu, H., Jacob, D.J., Bey, I., Yantosca, R.M., 2001. Constraints from ^{210}Pb and [7]Be on wet deposition and transport in a global three-dimensional chemical tracer model driven by

Bibliography

assimilated meteorological fields. Journal of Geophysical Research: Atmospheres 106, 12109–12128. https://doi.org/10.1029/2000JD900839

Liu, X., Qu, H., Huey, L.G., Wang, Y., Sjostedt, S., Zeng, L., Lu, K., Wu, Y., Hu, M., Shao, M., Zhu, T., Zhang, Y., 2017. High Levels of Daytime Molecular Chlorine and Nitryl Chloride at a Rural Site on the North China Plain. Environmental Science & Technology 51, 9588–9595. https://doi.org/10.1021/acs.est.7b03039

Lobert, J.M., Keene, W.C., Logan, J.A., Yevich, R., 1999. Global chlorine emissions from biomass burning: Reactive Chlorine Emissions Inventory. Journal of Geophysical Research: Atmospheres 104, 8373–8389. https://doi.org/10.1029/1998JD100077

Lou, S., Tan, Z., Gan, G., Chen, J., Wang, Haichao, Gao, Y., Huang, D., Huang, Congyan, Li, X., Song, R., Wang, Hongli, Wang, M., Wang, Q., Wu, Y., Huang, Cheng, 2022. Observation based study on atmospheric oxidation capacity in Shanghai during late-autumn: Contribution from nitryl chloride. Atmospheric Environment 271, 118902. https://doi.org/10.1016/j.atmosenv.2021.118902

Louis, F., 2015. A Theoretical Study of the Kinetics of the Hydrogen Atom Abstraction Reactions from Cyclopropane by H, O (^{3}P), and Cl (^{2}P$_{3/2}$) Atoms and OH Radicals. International Journal of Chemical Kinetics 47, 232–245. https://doi.org/10.1002/kin.20905

Louis, J.-F., 1979. A parametric model of vertical eddy fluxes in the atmosphere. Boundary-Layer Meteorology 17, 187–202. https://doi.org/10.1007/BF00117978

Luo, J., Jia, X., Gao, Y., Song, G., Yu, Y., Wang, R., Pan, X., 2011. Theoretical study on the kinetics of OH radical reactions with CH_3OOH and CH_3CH_2OOH. Journal of Computational Chemistry 32, 987–997. https://doi.org/10.1002/jcc.21684

Madronich, S., 1987. Photodissociation in the atmosphere: 1. Actinic flux and the effects of ground reflections and clouds. Journal of Geophysical Research: Atmospheres 92, 9740–9752. https://doi.org/10.1029/JD092iD08p09740

Manion, J.A., Huie, R.E., Levin, R.D., Burgess Jr., D.R., Orkin, V.L., Tsang, W., McGivern, W.S., Hudgens, J.W., Knyazev, V.D., Atkinson, D.B., Chai, E., Tereza, A.M., Lin, C.-Y., Allison, T.C., Mallard, W.G., Westley, F., Herron, J.T., Hampson, R.F., Frizzell, D.H., 2023. NIST Chemical Kinetics Database, NIST Standard Reference Database 17, Version 7.1 (Web Version), Release 1.6.8, Data version 2023, National Institute of Standards and Technology, Gaithersburg, Maryland, 20899-8320. [WWW Document]. URL https://kinetics.nist.gov/

Marché, P., Barbe, A., Secroun, C., Corr, J., Jouve, P., 1980. Ground based spectroscopic measurements of HCl. Geophysical Research Letters 7, 869–872. https://doi.org/10.1029/GL007i011p00869

Marécal, V., Peuch, V.-H., Andersson, C., Andersson, S., Arteta, J., Beekmann, M., Benedictow, A., Bergström, R., Bessagnet, B., Cansado, A., Chéroux, F., Colette, A., Coman, A., Curier, R.L., Denier van der Gon, H. a. C., Drouin, A., Elbern, H., Emili, E., Engelen, R.J., Eskes, H.J., Foret, G., Friese, E., Gauss, M., Giannaros, C., Guth, J., Joly, M., Jaumouillé, E., Josse, B., Kadygrov, N., Kaiser, J.W., Krajsek, K., Kuenen, J., Kumar, U., Liora, N., Lopez, E., Malherbe, L., Martinez, I., Melas, D., Meleux, F., Menut, L., Moinat, P., Morales, T., Parmentier, J., Piacentini, A., Plu, M., Poupkou, A., Queguiner, S., Robertson, L., Rouïl, L., Schaap, M., Segers, A., Sofiev, M., Tarasson, L., Thomas, M., Timmermans, R., Valdebenito, Á., van Velthoven, P., van Versendaal, R., Vira, J., Ung, A., 2015. A regional air quality forecasting system over Europe: the MACC-II daily ensemble production. Geoscientific Model Development 8, 2777–2813. https://doi.org/10.5194/gmd-8-2777-2015

Bibliography

Mari, C., Jacob, D.J., Bechtold, P., 2000. Transport and scavenging of soluble gases in a deep convective cloud. Journal of Geophysical Research: Atmospheres 105, 22255–22267. https://doi.org/10.1029/2000JD900211

Maricq, M.M., Shi, J., Szente, J.J., Rimai, L., Kaiser, E.W., 1993. Evidence for the three-center elimination of hydrogen chloride from 1-chloroethoxy. Journal of Physical Chemistry 97, 9686–9694.

Matsumoto, M., Okita, T., 1998. Long term measurements of atmospheric gaseous and aerosol species using an annular denuder system in Nara, Japan. Atmospheric Environment 32, 1419–1425. https://doi.org/10.1016/S1352-2310(97)00270-7

McCaulley, J.A., Anderson, S.M., Jeffries, J.B., Kaufman, F., 1985. Kinetics of the reaction of CH_3O with NO_2. Chemical Physics Letters 115, 180–186. https://doi.org/10.1016/0009-2614(85)80675-8

McCulloch, A., 2003. Chloroform in the environment: occurrence, sources, sinks and effects. Chemosphere 50, 1291–1308. https://doi.org/10.1016/S0045-6535(02)00697-5

McCulloch, A., Aucott, M.L., Benkovitz, C.M., Graedel, T.E., Kleiman, G., Midgley, P.M., Li, Y.-F., 1999. Global emissions of hydrogen chloride and chloromethane from coal combustion, incineration and industrial activities: Reactive Chlorine Emissions Inventory. Journal of Geophysical Research: Atmospheres 104, 8391–8403. https://doi.org/10.1029/1999JD900025

Meier, U., Grotheer, H.H., Just, Th., 1984. Temperature dependence and branching ratio of the CH_3OH + OH reaction. Chemical Physics Letters 106, 97–101. https://doi.org/10.1016/0009-2614(84)87019-0

Mellouki, A., Poulet, G., Le Bras, G., Singer, R., Burrows, J.P., Moortgat, G.K., 1989. Discharge flow kinetic study of the reactions of nitrate radical with bromine, bromine monoxide, hydrogen bromide, and hydrogen chloride. Journal of Physical Chemistry 93, 8017–8021. https://doi.org/10.1021/j100361a012

Mellouki, A., Téton, S., Laverdet, G., Quilgars, A., Bras, G.L., 1994. Kinetic studies of OH reactions with H_2O_2, C_3H_8 and CH_4 using the pulsed laser photolysis - laser induced fluorescence method. Journal de Chimie Physique 91, 473–487. https://doi.org/10.1051/jcp/1994910473

Menut, L., Goussebaile, A., Bessagnet, B., Khvorostiyanov, D., Ung, A., 2012. Impact of realistic hourly emissions profiles on air pollutants concentrations modelled with CHIMERE. Atmospheric Environment 49, 233–244. https://doi.org/10.1016/j.atmosenv.2011.11.057

Middleton, P., Stockwell, W.R., Carter, W.P.L., 1990. Aggregation and analysis of volatile organic compound emissions for regional modeling. Atmospheric Environment. Part A. General Topics 24, 1107–1133. https://doi.org/10.1016/0960-1686(90)90077-Z

Mielke, L.H., Furgeson, A., Odame-Ankrah, C.A., Osthoff, H.D., 2016. Ubiquity of $ClNO_2$ in the urban boundary layer of Calgary, Alberta, Canada. Canadian Journal of Chemistry 94, 414–423. https://doi.org/10.1139/cjc-2015-0426

Mielke, L.H., Furgeson, A., Osthoff, H.D., 2011. Observation of $ClNO_2$ in a Mid-Continental Urban Environment. Environmental Science & Technology 45, 8889–8896. https://doi.org/10.1021/es201955u

Mielke, L.H., Stutz, J., Tsai, C., Hurlock, S.C., Roberts, J.M., Veres, P.R., Froyd, K.D., Hayes, P.L., Cubison, M.J., Jimenez, J.L., Washenfelder, R.A., Young, C.J., Gilman, J.B., de Gouw, J.A., Flynn, J.H., Grossberg, N., Lefer, B.L., Liu, J., Weber, R.J., Osthoff, H.D., 2013. Heterogeneous formation of nitryl chloride and its role as a nocturnal NO_x reservoir species during CalNex-LA 2010. Journal of Geophysical Research: Atmospheres 118, 10,638-10,652. https://doi.org/10.1002/jgrd.50783

Bibliography

Miller, W.H., Smith, F.T., 1978. Semiclassical perturbation theory of electron-molecule collisions. Physical Review A 17, 939–953. https://doi.org/10.1103/PhysRevA.17.939

Miyoshi, A., 2022. GPOP software, rev. 2022.01.20m1, available from the author. See http://akrmys.com/gpop/.

Molina, M.J., Rowland, F.S., 1974. Stratospheric sink for chlorofluoromethanes: chlorine atom-catalysed destruction of ozone. Nature 249, 810–812.

Møller, Chr., Plesset, M.S., 1934. Note on an Approximation Treatment for Many-Electron Systems. Physical Review 46, 618–622. https://doi.org/10.1103/PhysRev.46.618

Monks, P.S., 2005. Gas-phase radical chemistry in the troposphere. Chemical Society Reviews 34, 376–395. https://doi.org/10.1039/B307982C

Morin, J., Romanias, M.N., Bedjanian, Y., 2015. Experimental Study of the Reactions of OH Radicals with Propane, n-Pentane, and n-Heptane over a Wide Temperature Range. International Journal of Chemical Kinetics 47, 629–637. https://doi.org/10.1002/kin.20936

Muralikrishna, I.V., Manickam, V., 2017. Chapter Fourteen - Air Pollution Control Technologies, in: Environmental Management. Butterworth-Heinemann, pp. 337–397. https://doi.org/10.1016/B978-0-12-811989-1.00014-2

Narivelo, H. luc angelo, 2019. ETUDE DE L'IMPACT DES ESPECES HALOGENES EMISES PAR LES VOLCANS SUR LA CHIMIE TROPOSPHERIQUE (These en préparation). Toulouse 3.

NCAR, 2019. Tropospheric Ultraviolet and Visible (TUV) Radiation Model | Atmospheric Chemistry Observations & Modeling (ACOM) [WWW Document]. URL https://www2.acom.ucar.edu/modeling/tropospheric-ultraviolet-and-visible-tuv-radiation-model (accessed 5.18.22).

Nedoluha, G.E., Connor, B.J., Mooney, T., Barrett, J.W., Parrish, A., Gomez, R.M., Boyd, I., Allen, D.R., Kotkamp, M., Kremser, S., Deshler, T., Newman, P., Santee, M.L., 2016. 20 years of ClO measurements in the Antarctic lower stratosphere. Atmospheric Chemistry and Physics 16, 10725–10734. https://doi.org/10.5194/acp-16-10725-2016

Nelson, H.H., Johnston, H.S., 1981. Kinetics of the reaction of chlorine atoms with nitrosyl chloride and nitryl chloride and the photochemistry of nitryl chloride. Journal of Physical Chemistry 85, 3891–3896. https://doi.org/10.1021/j150625a036

Neogrády, P., Urban, M., 1995. Spin-Adapted restricted Hartree–Fock reference coupled-cluster theory for open-shell systems: Noniterative triples for noncanonical orbitals. International Journal of Quantum Chemistry 55, 187–203. https://doi.org/10.1002/qua.560550214

Neogrády, P., Urban, M., Hubač, I., 1994. Spin adapted restricted Hartree–Fock reference coupled cluster theory for open shell systems. Journal of Chemical Physics 100, 3706–3716. https://doi.org/10.1063/1.466359

Ngo, T.C., Taamalli, S., Srour, Z., Fèvre-Nollet, V., El Bakali, A., Louis, F., Černušák, I., Dao, D.Q., 2023. Theoretical insights into the oxidation of quinmerac herbicide initiated by HO• radical in aqueous media: Mechanism, kinetics, and ecotoxicity. Journal of Environmental Chemical Engineering 11, 109941. https://doi.org/10.1016/j.jece.2023.109941

Niedzielski, J., Tschuikow-Roux, E., Yano, T., 1984. Hydrogen/deuterium abstraction by chlorine atoms from gaseous ethyl chlorides. Secondary kinetic isotope effects in the system CH_3CH_2Cl, CH_3CHDCl, CH_3CD_2Cl. International Journal of Chemical Kinetics 16, 621–631. https://doi.org/10.1002/kin.550160602

NOAA Chemical Sciences, 1994. NOAA CSL: Scientific Assessment of Ozone Depletion: 1994 [WWW Document]. URL

Bibliography

https://csl.noaa.gov/assessments/ozone/1994/commonquestions3.html (accessed 5.18.23).

Nobel Prize in Chemistry [WWW Document], 1995. URL https://www.nobelprize.org/prizes/chemistry/1995/summary/ (accessed 5.14.23).

Novelli, P.C., Lang, P.M., Masarie, K.A., Hurst, D.F., Myers, R., Elkins, J.W., 1999. Molecular hydrogen in the troposphere: Global distribution and budget. Journal of Geophysical Research: Atmospheres 104, 30427–30444. https://doi.org/10.1029/1999JD900788

Ordóñez, C., Lamarque, J.-F., Tilmes, S., Kinnison, D.E., Atlas, E.L., Blake, D.R., Sousa Santos, G., Brasseur, G., Saiz-Lopez, A., 2012. Bromine and iodine chemistry in a global chemistry-climate model: description and evaluation of very short-lived oceanic sources. Atmospheric Chemistry and Physics 12, 1423–1447. https://doi.org/10.5194/acp-12-1423-2012

Osthoff, H.D., Roberts, J.M., Ravishankara, A.R., Williams, E.J., Lerner, B.M., Sommariva, R., Bates, T.S., Coffman, D., Quinn, P.K., Dibb, J.E., Stark, H., Burkholder, J.B., Talukdar, R.K., Meagher, J., Fehsenfeld, F.C., Brown, S.S., 2008. High levels of nitryl chloride in the polluted subtropical marine boundary layer. Nature Geoscience 1, 324–328. https://doi.org/10.1038/ngeo177

Overend, R., Paraskevopoulos, G., 1978. Rates of hydroxyl radical reactions. 4. Reactions with methanol, ethanol, 1-propanol, and 2-propanol at 296 K. Journal of Physical Chemistry 82, 1329–1333. https://doi.org/10.1021/j100501a001

Overend, R.P., Paraskevopoulos, G., Cvetanović, R.J., 1975. Rates of OH Radical Reactions. I. Reactions with H_2, CH_4, C_2H_6, and C_3H_8 at 295 K. Canadian Journal of Chemistry 53, 3374–3382. https://doi.org/10.1139/v75-482

Papajak, E., Truhlar, D.G., 2010. Efficient Diffuse Basis Sets for Density Functional Theory. Journal of Chemical Theory and Computation 6, 597–601. https://doi.org/10.1021/ct900566x

Peng, A., Gao, J., Chen, Z., Wang, Y., Li, H., Ma, L.Q., Gu, C., 2018. Interactions of Gaseous 2-Chlorophenol with Fe^{3+}-Saturated Montmorillonite and Their Toxicity to Human Lung Cells. Environmental Science & Technology 52, 5208–5217. https://doi.org/10.1021/acs.est.7b06664

Peng, X., Wang, T., Wang, W., Ravishankara, A.R., George, C., Xia, M., Cai, M., Li, Q., Salvador, C.M., Lau, C., Lyu, X., Poon, C.N., Mellouki, A., Mu, Y., Hallquist, M., Saiz-Lopez, A., Guo, H., Herrmann, H., Yu, C., Dai, J., Wang, Y., Wang, X., Yu, A., Leung, K., Lee, S., Chen, J., 2022. Photodissociation of particulate nitrate as a source of daytime tropospheric Cl_2. Nature Communications 13, 939. https://doi.org/10.1038/s41467-022-28383-9

Peng, X., Wang, W., Xia, M., Chen, H., Ravishankara, A.R., Li, Q., Saiz-Lopez, A., Liu, P., Zhang, F., Zhang, C., Xue, L., Wang, X., George, C., Wang, J., Mu, Y., Chen, J., Wang, T., 2021. An unexpected large continental source of reactive bromine and chlorine with significant impact on wintertime air quality. National Science Review 8, nwaa304. https://doi.org/10.1093/nsr/nwaa304

Phillips, G.J., Tang, M.J., Thieser, J., Brickwedde, B., Schuster, G., Bohn, B., Lelieveld, J., Crowley, J.N., 2012. Significant concentrations of nitryl chloride observed in rural continental Europe associated with the influence of sea salt chloride and anthropogenic emissions. Geophysical Research Letters 39. https://doi.org/10.1029/2012GL051912

Platz, J., Nielsen, O.J., Wallington, T.J., Ball, J.C., Hurley, M.D., Straccia, A.M., Schneider, W.F., Sehested, J., 1998. Atmospheric Chemistry of the Phenoxy Radical, $C_6H_5O(\bullet)$: UV Spectrum and Kinetics of Its Reaction with NO, NO_2, and O_2. Journal of Physical Chemistry A 102, 7964–7974. https://doi.org/10.1021/jp982221l

Bibliography

Pöhler, D., Vogel, L., Frieß, U., Platt, U., 2010. Observation of halogen species in the Amundsen Gulf, Arctic, by active long-path differential optical absorption spectroscopy. Proceedings of the National Academy of Sciences 107, 6582–6587. https://doi.org/10.1073/pnas.0912231107

Price, C., Penner, J., Prather, M., 1997. NO$_x$ from lightning: 1. Global distribution based on lightning physics. Journal of Geophysical Research: Atmospheres 102, 5929–5941. https://doi.org/10.1029/96JD03504

Priestley, M., le Breton, M., Bannan, T.J., Worrall, S.D., Bacak, A., Smedley, A.R.D., Reyes-Villegas, E., Mehra, A., Allan, J., Webb, A.R., Shallcross, D.E., Coe, H., Percival, C.J., 2018. Observations of organic and inorganic chlorinated compounds and their contribution to chlorine radical concentrations in an urban environment in northern Europe during the wintertime. Atmospheric Chemistry and Physics 18, 13481–13493. https://doi.org/10.5194/acp-18-13481-2018

Pszenny, A. a. P., Keene, W.C., Jacob, D.J., Fan, S., Maben, J.R., Zetwo, M.P., Springer-Young, M., Galloway, J.N., 1993. Evidence of inorganic chlorine gases other than hydrogen chloride in marine surface air. Geophysical Research Letters 20, 699–702. https://doi.org/10.1029/93GL00047

Qualité de l'air extérieur : état des lieux [WWW Document], 2013. URL https://environnement.brussels/outils-et-donnees/etat-des-lieux-de-lenvironnement/qualite-de-lair-exterieur-etat-des-lieux (accessed 11.25.22).

Rahn, K.A., Borys, R.D., Butler, E.L., Duce, R.A., 1979. Gaseous and Particulate Halogens in the New York City Atmosphere*. Annals of the New York Academy of Sciences 322, 143–151. https://doi.org/10.1111/j.1749-6632.1979.tb14123.x

Ravishankara, A.R., Davis, D.D., 1978. Kinetic rate constants for the reaction of hydroxyl with methanol, ethanol, and tetrahydrofuran at 298 K. Journal of Physical Chemistry 82, 2852–2853. https://doi.org/10.1021/j100515a022

Rawas, H.K.A., Mawla, R.A., Pham, T.Y.N., Truong, D.H., Nguyen, T.L.A., Taamalli, S., Ribaucour, M., Bakali, A.E., Černušák, I., Dao, D.Q., Louis, F., 2023. New insight into environmental oxidation of phosmet insecticide initiated by HO˙ radicals in gas and water – a theoretical study. Environmental Science: Processes & Impacts. https://doi.org/10.1039/D3EM00325F

Redeker, K.R., Meinardi, S., Blake, D., Sass, R., 2003. Gaseous emissions from flooded rice paddy agriculture. Journal of Geophysical Research: Atmospheres 108, 4386–4398. https://doi.org/10.1029/2002JD002814

Redington, R.L., Olson, W.B., Cross, P.C., 1962. Studies of Hydrogen Peroxide: The Infrared Spectrum and the Internal Rotation Problem. Journal of Chemical Physics 36, 1311–1326. https://doi.org/10.1063/1.1732733

Riedel, T.P., Bertram, T.H., Crisp, T.A., Williams, E.J., Lerner, B.M., Vlasenko, A., Li, S.-M., Gilman, J., de Gouw, J., Bon, D.M., Wagner, N.L., Brown, S.S., Thornton, J.A., 2012. Nitryl Chloride and Molecular Chlorine in the Coastal Marine Boundary Layer. Environmental Science & Technology 46, 10463–10470. https://doi.org/10.1021/es204632r

Riedel, T.P., Wolfe, G.M., Danas, K.T., Gilman, J.B., Kuster, W.C., Bon, D.M., Vlasenko, A., Li, S.-M., Williams, E.J., Lerner, B.M., Veres, P.R., Roberts, J.M., Holloway, J.S., Lefer, B., Brown, S.S., Thornton, J.A., 2014. An MCM modeling study of nitryl chloride (ClNO$_2$) impacts on oxidation, ozone production and nitrogen oxide partitioning in polluted continental outflow. Atmospheric Chemistry and Physics 14, 3789–3800. https://doi.org/10.5194/acp-14-3789-2014

Bibliography

Roberts, J.M., Osthoff, H.D., Brown, S.S., Ravishankara, A.R., 2008. N_2O_5 Oxidizes Chloride to Cl_2 in Acidic Atmospheric Aerosol. Science 321, 1059–1059. https://doi.org/10.1126/science.1158777

Rouil, L., Honoré, C., Vautard, R., Beekmann, M., Bessagnet, B., Malherbe, L., Meleux, F., Dufour, A., Elichegaray, C., Flaud, J.-M., Menut, L., Martin, D., Peuch, A., Peuch, V.-H., Poisson, N., 2009. Prev'air: An Operational Forecasting and Mapping System for Air Quality in Europe. Bulletin of the American Meteorological Society 90, 73–84. https://doi.org/10.1175/2008BAMS2390.1

Rowland, F.S., 1990. Stratospheric Ozone Depletion by Chlorofluorocarbons. Ambio 19, 281–292.

Russell, J.J., Seetula, J.A., Gutman, D., Senkan, S.M., 1989. Kinetics of reactions of chlorinated vinyl radicals (CH_2CCl and C_2Cl_3) with molecular oxygen. Journal of Physical Chemistry 93, 1934–1938. https://doi.org/10.1021/j100342a047

Saiz-Lopez, A., von Glasow, R., 2012. Reactive halogen chemistry in the troposphere. Chemical Society Reviews 41, 6448–6472. https://doi.org/10.1039/C2CS35208G

Sander, R., 2015. Compilation of Henry's law constants (version 4.0) for water as solvent. Atmospheric Chemistry and Physics 15, 4399–4981. https://doi.org/10.5194/acp-15-4399-2015

Sander, R., Baumgaertner, A., Gromov, S., Harder, H., Jöckel, P., Kerkweg, A., Kubistin, D., Regelin, E., Riede, H., Sandu, A., Taraborrelli, D., Tost, H., Xie, Z.-Q., 2011. The atmospheric chemistry box model CAABA/MECCA-3.0. Geoscientific Model Development 4, 373–380. https://doi.org/10.5194/gmd-4-373-2011

Sander, R., Crutzen, P.J., 1996. Model study indicating halogen activation and ozone destruction in polluted air masses transported to the sea. Journal of Geophysical Research: Atmospheres 101, 9121–9138. https://doi.org/10.1029/95JD03793

Sandu, A., Sander, R., 2006. Technical note: Simulating chemical systems in Fortran90 and Matlab with the Kinetic PreProcessor KPP-2.1. Atmospheric Chemistry and Physics 6, 187–195. https://doi.org/10.5194/acp-6-187-2006

Sandu, A., Verwer, J.G., Blom, J.G., Spee, E.J., Carmichael, G.R., Potra, F.A., 1997. Benchmarking stiff ode solvers for atmospheric chemistry problems II: Rosenbrock solvers. Atmospheric Environment 31, 3459–3472. https://doi.org/10.1016/S1352-2310(97)83212-8

Sanhueza, E., Garaboto, A., 2002. Gaseous HCl at a remote tropical continental site. Tellus B: Chemical and Physical Meteorology 54, 412–415. https://doi.org/10.3402/tellusb.v54i4.16675

Sarwar, G., Simon, H., Xing, J., Mathur, R., 2014. Importance of tropospheric $ClNO_2$ chemistry across the Northern Hemisphere. Geophysical Research Letters 41, 4050–4058. https://doi.org/10.1002/2014GL059962

Scheeren, H.A., Lelieveld, J., de Gouw, J.A., van der Veen, C., Fischer, H., 2002. Methyl chloride and other chlorocarbons in polluted air during INDOEX. Journal of Geophysical Research: Atmospheres 107, INX2 14-1-INX2 14-18. https://doi.org/10.1029/2001JD001121

Schiffman, A., Nelson, D.D.Jr., Robinson, M.S., Nesbitt, D.J., 1991. High-resolution infrared flash kinetic spectroscopy of hydroxyl radicals. Journal of Physical Chemistry 95, 2629–2636. https://doi.org/10.1021/j100160a004

Schlegel, H.B., 2003. Exploring potential energy surfaces for chemical reactions: An overview of some practical methods. Journal of Computational Chemistry 24, 1514–1527. https://doi.org/10.1002/jcc.10231

Schmidt, J.A., Jacob, D.J., Horowitz, H.M., Hu, L., Sherwen, T., Evans, M.J., Liang, Q., Suleiman, R.M., Oram, D.E., Le Breton, M., Percival, C.J., Wang, S., Dix, B.,

Bibliography

Volkamer, R., 2016. Modeling the observed tropospheric BrO background: Importance of multiphase chemistry and implications for ozone, OH, and mercury. Journal of Geophysical Research: Atmospheres 121, 11,819-11,835. https://doi.org/10.1002/2015JD024229

Schmidt, V., Zhu, G.Y., Becker, K.H., Fink, E.H., 1985. Study of OH Reactions at High Pressures by Excimer Laser Photolysis - Dye Laser Fluorescence. Berichte der Bunsengesellschaft für physikalische Chemie 89, 321–322. https://doi.org/10.1002/bbpc.19850890337

Schrödinger, E., 1926. An Undulatory Theory of the Mechanics of Atoms and Molecules. Physical Review 28, 1049–1070. https://doi.org/10.1103/PhysRev.28.1049

Scott, A.P., Radom, L., 1996. Harmonic Vibrational Frequencies: An Evaluation of Hartree−Fock, Møller−Plesset, Quadratic Configuration Interaction, Density Functional Theory, and Semiempirical Scale Factors. Journal of Physical Chemistry 100, 16502–16513. https://doi.org/10.1021/jp960976r

Shamasundar, K.R., Knizia, G., Werner, H.-J., 2011. A new internally contracted multi-reference configuration interaction method. Journal of Chemical Physics 135, 054101. https://doi.org/10.1063/1.3609809

Sherwen, T., Schmidt, J.A., Evans, M.J., Carpenter, L.J., Großmann, K., Eastham, S.D., Jacob, D.J., Dix, B., Koenig, T.K., Sinreich, R., Ortega, I., Volkamer, R., Saiz-Lopez, A., Prados-Roman, C., Mahajan, A.S., Ordóñez, C., 2016. Global impacts of tropospheric halogens (Cl, Br, I) on oxidants and composition in GEOS-Chem. Atmospheric Chemistry and Physics 16, 12239–12271. https://doi.org/10.5194/acp-16-12239-2016

Shimanouchi, T., 1972. Tables of Molecular Vibrational Frequencies Consolidated. Volume I.

Simmonds, P.G., Derwent, R.G., Manning, A.J., Fraser, P.J., Krummel, P.B., O'Doherty, S., Prinn, R.G., Cunnold, D.M., Miller, B.R., Wang, H.J., Ryall, D.B., Porter, L.W., Weiss, R.F., Salameh, P.K., 2004. AGAGE Observations of Methyl Bromide and Methyl Chloride at Mace Head, Ireland, and Cape Grim, Tasmania, 1998–2001. Journal of Atmospheric Chemistry 47, 243–269. https://doi.org/10.1023/B:JOCH.0000021136.52340.9c

Simmonds, P.G., Manning, A.J., Cunnold, D.M., McCulloch, A., O'Doherty, S., Derwent, R.G., Krummel, P.B., Fraser, P.J., Dunse, B., Porter, L.W., Wang, R.H.J., Greally, B.R., Miller, B.R., Salameh, P., Weiss, R.F., Prinn, R.G., 2006. Global trends, seasonal cycles, and European emissions of dichloromethane, trichloroethene, and tetrachloroethene from the AGAGE observations at Mace Head, Ireland, and Cape Grim, Tasmania. Journal of Geophysical Research: Atmospheres 111. https://doi.org/10.1029/2006JD007082

Simpson, I.J., Akagi, S.K., Barletta, B., Blake, N.J., Choi, Y., Diskin, G.S., Fried, A., Fuelberg, H.E., Meinardi, S., Rowland, F.S., Vay, S.A., Weinheimer, A.J., Wennberg, P.O., Wiebring, P., Wisthaler, A., Yang, M., Yokelson, R.J., Blake, D.R., 2011. Boreal forest fire emissions in fresh Canadian smoke plumes: C_1-C_{10} volatile organic compounds (VOCs), CO_2, CO, NO_2, NO, HCN and CH_3CN. Atmospheric Chemistry and Physics 11, 6445–6463. https://doi.org/10.5194/acp-11-6445-2011

Simpson, W.R., Brown, S.S., Saiz-Lopez, A., Thornton, J.A., von Glasow, R., 2015. Tropospheric Halogen Chemistry: Sources, Cycling, and Impacts. Chemical Reviews 115, 4035–4062. https://doi.org/10.1021/cr5006638

Singh, H.B., Kasting, J.F., 1988. Chlorine-hydrocarbon photochemistry in the marine troposphere and lower stratosphere. Journal of Atmospheric Chemistry 7, 261–285. https://doi.org/10.1007/BF00130933

Bibliography

Singleton, D.L., Cvetanovic, R.J., 1976. Temperature dependence of the reaction of oxygen atoms with olefins. Journal of the American Chemical Society 98, 6812–6819. https://doi.org/10.1021/ja00438a006

Slinn, S.A., Slinn, W.G.N., 1980. Predictions for particle deposition on natural waters. Atmospheric Environment (1967) 14, 1013–1016. https://doi.org/10.1016/0004-6981(80)90032-3

Smith, C.A., Molina, L.T., Lamb, J.J., Molina, M.J., 1984. Kinetics of the reaction of OH with pernitric and nitric acids. International Journal of Chemical Kinetics 16, 41–55. https://doi.org/10.1002/kin.550160107

Smith, G.P., Fairchild, P.W., Crosley, D.R., 1984. The pressure and temperature dependence of the $OH+C_2H_2$ reaction above 800 K. The Journal of Chemical Physics 81, 2667–2677. https://doi.org/10.1063/1.447976

Sobanska, S., Houjeij, H., Coussan, S., Aupetit, C., Taamalli, S., Louis, F., Cantrel, L., Gregoire, A.C., Mascetti, J., 2021. Infrared matrix-isolation and theoretical studies of interactions between CH_3I and water. Journal of Molecular Structure 1236, 130342. https://doi.org/10.1016/j.molstruc.2021.130342

Solomon, S., 1990. Progress towards a quantitative understanding of Antarctic ozone depletion. Nature 347, 347–354. https://doi.org/10.1038/347347a0

Solomon, S., Mount, G.H., Sanders, R.W., Schmeltekopf, A.L., 1987. Visible spectroscopy at McMurdo Station, Antarctica: 2. Observations of OClO. Journal of Geophysical Research: Atmospheres 92, 8329–8338. https://doi.org/10.1029/JD092iD07p08329

Sommariva, R., von Glasow, R., 2012. Multiphase Halogen Chemistry in the Tropical Atlantic Ocean. Environmental Science & Technology 46, 10429–10437. https://doi.org/10.1021/es300209f

Soni, M., Sander, R., Sahu, L.K., Taraborrelli, D., Liu, P., Patel, A., Girach, I.A., Pozzer, A., Gunthe, S.S., Ojha, N., 2023. Comprehensive multiphase chlorine chemistry in the box model CAABA/MECCA: Implications to atmospheric oxidative capacity. EGUsphere 1–24. https://doi.org/10.5194/egusphere-2023-652

Spicer, C.W., 1986. Patterns of atmospheric nitrates, sulfate, and hydrogen chloride in the central Ohio River Valley over a one-year period. Environment International 12, 513–518. https://doi.org/10.1016/0160-4120(86)90145-5

Stachnik, R.A., Molina, L.T., Molina, M.J., 1986. Pressure and temperature dependences of the reaction of hydroxyl radical with nitric acid. Journal of Physical Chemistry 90, 2777–2780. https://doi.org/10.1021/j100403a044

Staudinger, J., Roberts, P.V., 1996. A critical review of Henry's law constants for environmental applications. Critical Reviews in Environmental Science and Technology 26, 205–297. https://doi.org/10.1080/10643389609388492

Sommariva, R., von Glasow, R., 2012. Multiphase Halogen Chemistry in the Tropical Atlantic Ocean. Environmental Science & Technology 46, 10429–10437. https://doi.org/10.1021/es300209f

Stockwell, W.R., Middleton, P., Chang, J.S., Tang, X., 1990. The second-generation regional acid deposition model chemical mechanism for regional air quality modeling. Journal of Geophysical Research: Atmospheres 95, 16343–16367. https://doi.org/10.1029/JD095iD10p16343

Stutz, J., Ackermann, R., Fast, J.D., Barrie, L., 2002. Atmospheric reactive chlorine and bromine at the Great Salt Lake, Utah. Geophysical Research Letters 29, 18-1-18–4. https://doi.org/10.1029/2002GL014812

Sun, H., Bozzelli, J.W., 2001. Structures, Intramolecular Rotation Barriers, and Thermochemical Properties: Ethanol, α-Monoethanols, Dichloroethanols, and

Bibliography

Corresponding Radicals Derived from H Atom Loss. Journal of Physical Chemistry A 105, 9543–9552. https://doi.org/10.1021/jp011949q

Sun, H., Chen, C.-J., Bozzelli, J.W., 2000. Structures, Intramolecular Rotation Barriers, and Thermodynamic Properties (Enthalpies, Entropies and Heat Capacities) of Chlorinated Methyl Hydroperoxides (CH_2ClOOH, $CHCl_2OOH$, and CCl_3OOH). Journal of Physical Chemistry A 104, 8270–8282. https://doi.org/10.1021/jp0013917

Taamalli, S., Khiri, D., Suliman, S., Khanniche, S., Černušák, I., Cantrel, L., Ribaucour, M., Louis, F., 2020. Unraveling the Tropospheric Microhydration Processes of Iodous Acid HOIO. ACS Earth and Space Chemistry 4, 92–100. https://doi.org/10.1021/acsearthspacechem.9b00257

Talukdar, R.K., Mellouki, A., Gierczak, T., Barone, S., Chiang, S.-Y., Ravishankara, A.R., 1994. Kinetics of the reactions of OH with alkanes. International Journal of Chemical Kinetics 26, 973–990. https://doi.org/10.1002/kin.550261003

Textor, C., Graf, H.-F., Timmreck, C., Robock, A., 2004. Emissions from volcanoes, in: Granier, C., Artaxo, P., Reeves, C.E. (Eds.), Emissions of Atmospheric Trace Compounds, Advances in Global Change Research. Springer Netherlands, Dordrecht, pp. 269–303. https://doi.org/10.1007/978-1-4020-2167-1_7

Tham, Y.J., Wang, Z., Li, Q., Yun, H., Wang, W., Wang, X., Xue, L., Lu, K., Ma, N., Bohn, B., Li, X., Kecorius, S., Größ, J., Shao, M., Wiedensohler, A., Zhang, Y., Wang, T., 2016. Significant concentrations of nitryl chloride sustained in the morning: investigations of the causes and impacts on ozone production in a polluted region of northern China. Atmospheric Chemistry and Physics 16, 14959–14977. https://doi.org/10.5194/acp-16-14959-2016

Thornton, J.A., Kercher, J.P., Riedel, T.P., Wagner, N.L., Cozic, J., Holloway, J.S., Dubé, W.P., Wolfe, G.M., Quinn, P.K., Middlebrook, A.M., Alexander, B., Brown, S.S., 2010. A large atomic chlorine source inferred from mid-continental reactive nitrogen chemistry. Nature 464, 271–274. https://doi.org/10.1038/nature08905

Timonen, R.S., Kalliorinne, K., Koskikallio, J., 1986. Kinetics of Reactions of Methyl and Ethyl Radicals with Chlorine in the Gas Phase Studied by Photochlorination of Methane. Acta Chemica Scandinavica 40a, 459–466. https://doi.org/10.3891/acta.chem.scand.40a-0459

Tonokura, K., Norikane, Y., Koshi, M., Nakano, Y., Nakamichi, S., Goto, M., Hashimoto, S., Kawasaki, M., Sulbaek Andersen, M.P., Hurley, M.D., Wallington, T.J., 2002. Cavity Ring-down Study of the Visible Absorption Spectrum of the Phenyl Radical and Kinetics of Its Reactions with Cl, Br, Cl_2, and O_2. Journal of Physical Chemistry A 106, 5908–5917. https://doi.org/10.1021/jp025585t

Trincal, J., 2015. Modélisation du comportement de l'iode dans l'atmosphère (Thèse de doctorat). University of Lille.

Troe, J., 1979. Predictive possibilities of unimolecular rate theory. Journal of Physical Chemistry 83, 114–126. https://doi.org/10.1021/j100464a019

Trummal, A., Lipping, L., Kaljurand, I., Koppel, I.A., Leito, I., 2016. Acidity of Strong Acids in Water and Dimethyl Sulfoxide. Journal of Physical Chemistry A 120, 3663–3669. https://doi.org/10.1021/acs.jpca.6b02253

Tully, F.P., Droege, A.T., Koszykowski, M.L., Melius, C.F., 1986. Hydrogen-atom abstraction from alkanes by hydroxyl. 2. Ethane. Journal of Physical Chemistry 90, 691–698. https://doi.org/10.1021/j100276a042

Tully, F.P., Ravishankara, A.R., Carr, K., 1983. Kinetic study of the reactions of the hydroxyl radical with ethane and propane. International Journal of Chemical Kinetics 15, 1111–1118. https://doi.org/10.1002/kin.550151014

Bibliography

Tyndall, G.S., Cox, R.A., Granier, C., Lesclaux, R., Moortgat, G.K., Pilling, M.J., Ravishankara, A.R., Wallington, T.J., 2001. Atmospheric chemistry of small organic peroxy radicals. Journal of Geophysical Research: Atmospheres 106, 12157–12182. https://doi.org/10.1029/2000JD900746

Vaghjiani, G.L., Ravishankara, A.R., 1989. Kinetics and mechanism of hydroxyl radical reaction with methyl hydroperoxide. Journal of Physical Chemistry 93, 1948–1959. https://doi.org/10.1021/j100342a050

Vidal, C.M., Métrich, N., Komorowski, J.-C., Pratomo, I., Michel, A., Kartadinata, N., Robert, V., Lavigne, F., 2016. The 1257 Samalas eruption (Lombok, Indonesia): the single greatest stratospheric gas release of the Common Era. Scientific Reports 6, 34868. https://doi.org/10.1038/srep34868

Vijayakumar, S., Wilmouth, D.M., 2021. Atmospheric fate of formyl chloride and mechanisms of the gas-phase reactions with OH radicals and Cl atoms. Chemical Physics Letters 777, 138709. https://doi.org/10.1016/j.cplett.2021.138709

von Clarmann, T., 2013. Chlorine in the stratosphere. Atmósfera 26, 415–458. https://doi.org/10.1016/S0187-6236(13)71086-5

von Clarmann, T., Johansson, S., 2018. Chlorine nitrate in the atmosphere. Atmospheric Chemistry and Physics 18, 15363–15386. https://doi.org/10.5194/acp-18-15363-2018

von Glasow, R., Bobrowski, N., Kern, C., 2009. The effects of volcanic eruptions on atmospheric chemistry. Chemical Geology, Halogens in Volcanic Systems and Their Environmental Impacts 263, 131–142. https://doi.org/10.1016/j.chemgeo.2008.08.020

Wallington, T.J., Bilde, M., Møgelberg, T.E., Sehested, J., Nielsen, O.J., 1996. Atmospheric Chemistry of 1,2-Dichloroethane: UV Spectra of $CH_2ClCHCl$ and $CH_2ClCHClO_2$ Radicals, Kinetics of the Reactions of $CH_2ClCHCl$ Radicals with O_2 and $CH_2ClCHClO_2$ Radicals with NO and NO_2, and Fate of the Alkoxy Radical $CH_2ClCHClO$. Journal of Physical Chemistry 100, 5751–5760. https://doi.org/10.1021/jp952149g

Wallington, T.J., Dagaut, P., Kurylo, M.J., 1992. UV absorption cross sections and reaction kinetics and mechanisms for peroxy radicals in the gas phase. Chemical Review 92, 667–710. https://doi.org/10.1021/cr00012a008

Wallington, T.J., Kurylo, M.J., 1987. The gas phase reactions of hydroxyl radicals with a series of aliphatic alcohols over the temperature range 240 - 440 K. International Journal of Chemical Kinetics 19, 1015–1023. https://doi.org/10.1002/kin.550191106

Wallington, T.J., Neuman, D.M., Kurylo, M.J., 1987. Kinetics of the gas phase reaction of hydroxyl radicals with ethane, benzene, and a series of halogenated benzenes over the temperature range 234 - 438 K. International Journal of Chemical Kinetics 19, 725–739. https://doi.org/10.1002/kin.550190806

Wang, T., Tham, Y.J., Xue, L., Li, Q., Zha, Q., Wang, Z., Poon, S.C.N., Dubé, W.P., Blake, D.R., Louie, P.K.K., Luk, C.W.Y., Tsui, W., Brown, S.S., 2016. Observations of nitryl chloride and modeling its source and effect on ozone in the planetary boundary layer of southern China. Journal of Geophysical Research: Atmospheres 121, 2476–2489. https://doi.org/10.1002/2015JD024556

Wang, X., Jacob, D.J., Eastham, S.D., Sulprizio, M.P., Zhu, L., Chen, Q., Alexander, B., Sherwen, T., Evans, M.J., Lee, B.H., Haskins, J.D., Lopez-Hilfiker, F.D., Thornton, J.A., Huey, G.L., Liao, H., 2019. The role of chlorine in global tropospheric chemistry. Atmospheric Chemistry and Physics 19, 3981–4003. https://doi.org/10.5194/acp-19-3981-2019

Wang, Z., Herbinet, O., Hansen, N., Battin-Leclerc, F., 2019. Exploring hydroperoxides in combustion: History, recent advances and perspectives. Progress in Energy and Combustion Science 73, 132–181. https://doi.org/10.1016/j.pecs.2019.02.003

Bibliography

Wategaonkar, S.J., Setser, D.W., 1989. Infrared chemiluminescence studies of H atom reactions with Cl_2O, $ClNO$, F_2O, CF_3OF, ClO_2, NO_2, and ClO. Journal of Chemical Physics 90, 251–264. https://doi.org/10.1063/1.456527

Watson, L., Lacressonnière, G., Gauss, M., Engardt, M., Andersson, C., Josse, B., Marécal, V., Nyiri, A., Sobolowski, S., Siour, G., Vautard, R., 2015. The impact of meteorological forcings on gas phase air pollutants over Europe. Atmospheric Environment 119, 240–257. https://doi.org/10.1016/j.atmosenv.2015.07.037

Wesely, M.L., 1989. Parameterization of surface resistances to gaseous dry deposition in regional-scale numerical models. Atmospheric Environment (1967) 23, 1293–1304. https://doi.org/10.1016/0004-6981(89)90153-4

Wigner, E., 1932. On the Quantum Correction For Thermodynamic Equilibrium. Physical Review 40, 749–759. https://doi.org/10.1103/PhysRev.40.749

Wilkins, R.A., Dodge, M.C., Hisatsune, I.C., 1974. Kinetics of nitric oxide catalyzed decomposition of nitryl chloride and its related nitrogen isotope exchange reactions. Journal of Physical Chemistry 78, 2073–2076. https://doi.org/10.1021/j100614a001

Williamson, D.L., Rasch, P.J., 1989. Two-Dimensional Semi-Lagrangian Transport with Shape-Preserving Interpolation. Monthly Weather Review 117, 102–129. https://doi.org/10.1175/1520-0493(1989)117<0102:TDSLTW>2.0.CO;2

Wu, F., Carr, R.W., 2001. Kinetics of CH_2ClO Radical Reactions with O_2 and NO, and the Unimolecular Elimination of HCl. Journal of Physical Chemistry A 105, 1423–1432. https://doi.org/10.1021/jp001953m

Xerri, B., Canneaux, S., Louis, F., Trincal, J., Cousin, F., Badawi, M., Cantrel, L., 2012. Ab initio calculations and iodine kinetic modeling in the reactor coolant system of a pressurized water reactor in case of severe nuclear accident. Computational and Theoretical Chemistry, Chemical reactivity, from accurate theories to simple models, in honor of Professor Jean-Claude Rayez 990, 194–208. https://doi.org/10.1016/j.comptc.2012.02.024

Xia, M., Peng, X., Wang, W., Yu, C., Wang, Z., Tham, Y.J., Chen, J., Chen, H., Mu, Y., Zhang, C., Liu, P., Xue, L., Wang, X., Gao, J., Li, H., Wang, T., 2021. Winter $ClNO_2$ formation in the region of fresh anthropogenic emissions: seasonal variability and insights into daytime peaks in northern China. Atmospheric Chemistry and Physics 21, 15985–16000. https://doi.org/10.5194/acp-21-15985-2021

Yang, X., Wang, Q., Ma, N., Hu, W., Gao, Y., Huang, Z., Zheng, J., Yuan, B., Yang, N., Tao, J., Hong, J., Cheng, Y., Su, H., 2022. The impact of chlorine chemistry combined with heterogeneous N_2O_5 reactions on air quality in China. Atmospheric Chemistry and Physics 22, 3743–3762. https://doi.org/10.5194/acp-22-3743-2022

Yi, X., Yin, S., Huang, L., Li, H., Wang, Y., Wang, Q., Chan, A., Traoré, D., Ooi, M.C.G., Chen, Y., Allen, D.T., Li, L., 2021. Anthropogenic emissions of atomic chlorine precursors in the Yangtze River Delta region, China. Science of Total Environment 771, 144644. https://doi.org/10.1016/j.scitotenv.2020.144644

Yienger, J.J., Levy II, H., 1995. Empirical model of global soil-biogenic NO_x emissions. Journal of Geophysical Research: Atmospheres 100, 11447–11464. https://doi.org/10.1029/95JD00370

Yokouchi, Y., Noijiri, Y., Barrie, L.A., Toom-Sauntry, D., Machida, T., Inuzuka, Y., Akimoto, H., Li, H.J., Fujinuma, Y., Aoki, S., 2000. A strong source of methyl chloride to the atmosphere from tropical coastal land. Nature 403, 295–298. https://doi.org/10.1038/35002049

Young, A.H., Keene, W.C., Pszenny, A.A.P., Sander, R., Thornton, J.A., Riedel, T.P., Maben, J.R., 2013. Phase partitioning of soluble trace gases with size-resolved aerosols in near-surface continental air over northern Colorado, USA, during winter. Journal of

Bibliography

Geophysical Research: Atmospheres 118, 9414–9427. https://doi.org/10.1002/jgrd.50655

Zabarnick, S., Fleming, J.W., Lin, M.C., 1988. Kinetics of hydroxyl radical reactions with formaldehyde and 1,3,5-trioxane between 290 and 600 K. International Journal of Chemical Kinetics 20, 117–129. https://doi.org/10.1002/kin.550200205

Zhang, B., Shen, H., Yun, X., Zhong, Q., Henderson, B.H., Wang, X., Shi, L., Gunthe, S.S., Huey, L.G., Tao, S., Russell, A.G., Liu, P., 2022. Global Emissions of Hydrogen Chloride and Particulate Chloride from Continental Sources. Environ. Sci. Technol. 56, 3894–3904. https://doi.org/10.1021/acs.est.1c05634

Zhao, X., Teng, Z., Wang, J., Ma, X., Sun, Y., Gao, R., Xu, F., Zhang, Q., Wang, W., 2022. Barrierless HNO_3 formation from the hydrolysis reaction of NO_2 with Cl atom in the atmosphere. Atmospheric Environment 270, 118871. https://doi.org/10.1016/j.atmosenv.2021.118871

Zhao, Y., Truhlar, D.G., 2008. The M06 suite of density functionals for main group thermochemistry, thermochemical kinetics, noncovalent interactions, excited states, and transition elements: two new functionals and systematic testing of four M06-class functionals and 12 other functionals. Theoretical Chemistry Accounts 120, 215–241. https://doi.org/10.1007/s00214-007-0310-x

Appendices

Appendix A.I: Acronyms

Abbreviation	Full term
UV	UltraViolet
O_3	Ozone
ppt	Part per trillion
VOC	Volatile Organic Compound
CFC	Chlorofluorocarbons
VSLS	Very Short-Lived Species
BB	Biomass burning
SG	Source Gas
PG	Product Gas
SOA	Secondary Organic Aerosols
SSA	Sea-Salt Aerosols
PES	Potential Energy Surface
ZPE	Zero-Point Energy
IRC	Intrinsic Reaction Coordinate
MP2	second order Møller-Plesset perturbation theory
TST	Transition State Theory
CVT	Canonical Variational Theory
ASTEC	Accident Source Term Evaluation Code
IRSN	Institut de Radioprotection et de Sûreté Nucléaire (French Nuclear Safety Institute)
0D	zero-dimensional
PDE	Partial Differential Equations
UV/VIS	Ultra-Violet/VISible
NIST	National Institute of Standards and Technology
JPL	Jet Propulsion Laboratory
RACM	Regional Atmospheric Chemistry Mechanism
MOCAGE	MOdèle de Chimie Atmosphérique de Grande Echelle
VSLS	Very Short-Lived Species
REPROBUS	REactive Processes Ruling the Ozone BUdget in the Stratosphere
CTM	Chemistry-Transport Model

Appendices

Appendix A.II: Kinetic parameters of the reaction OH + CH₂ClOOH

Appendix A.II: Kinetic parameters of the reaction OH + CH$_2$ClOOH

Table A.II-1: *Rate constants in cm^3 molecule^{-1} s^{-1} calculated at different temperatures at the M06-2X/6-311++G(3df,3p) and DK-CCSD(T)/ANO-RCC-VQZP levels of theory for H-, Cl-, and OH-abstraction pathways and the overall reaction OH and CH$_2$ClOOH using the indirect mechanism **without considering any tunnelling corrections**.*

	M06-2X/6-311++G(3df,3p)							
	253	258	263	268	273	278	283	288
H4-abstraction	8.46×10^{-15}	9.23×10^{-15}	1.00×10^{-14}	1.09×10^{-14}	1.18×10^{-14}	1.28×10^{-14}	1.38×10^{-14}	1.48×10^{-14}
H5-abstraction	2.15×10^{-13}	2.14×10^{-13}	2.13×10^{-13}	2.13×10^{-13}	2.12×10^{-13}	2.12×10^{-13}	2.12×10^{-13}	2.12×10^{-13}
H7-abstraction	7.99×10^{-12}	7.38×10^{-12}	6.85×10^{-12}	6.37×10^{-12}	5.94×10^{-12}	5.56×10^{-12}	5.22×10^{-12}	4.91×10^{-12}
Cl-abstraction	4.41×10^{-35}	1.20×10^{-34}	3.14×10^{-34}	7.94×10^{-34}	1.94×10^{-33}	4.60×10^{-33}	1.06×10^{-32}	2.37×10^{-32}
OH-abstraction	1.89×10^{-33}	4.76×10^{-33}	1.16×10^{-32}	2.73×10^{-32}	6.23×10^{-32}	1.38×10^{-31}	2.98×10^{-31}	6.27×10^{-31}
overall	8.22×10^{-12}	7.61×10^{-12}	7.07×10^{-12}	6.59×10^{-12}	6.17×10^{-12}	5.79×10^{-12}	5.45×10^{-12}	5.14×10^{-12}
	293	298	303	308	313	318	323	
H4-abstraction	1.59×10^{-14}	1.71×10^{-14}	1.83×10^{-14}	1.95×10^{-14}	2.08×10^{-14}	2.22×10^{-14}	2.36×10^{-14}	
H5-abstraction	2.12×10^{-13}	2.12×10^{-13}	2.12×10^{-13}	2.12×10^{-13}	2.13×10^{-13}	2.13×10^{-13}	2.14×10^{-13}	
H7-abstraction	4.63×10^{-12}	4.38×10^{-12}	4.15×10^{-12}	3.95×10^{-12}	3.75×10^{-12}	3.58×10^{-12}	3.42×10^{-12}	
Cl-abstraction	5.16×10^{-32}	1.10×10^{-31}	2.27×10^{-31}	4.60×10^{-31}	9.12×10^{-31}	1.77×10^{-30}	3.36×10^{-30}	
OH-abstraction	1.29×10^{-30}	2.58×10^{-30}	5.05×10^{-30}	9.68×10^{-30}	1.28×10^{-29}	3.35×10^{-29}	6.06×10^{-29}	
overall	4.86×10^{-12}	4.61×10^{-12}	4.38×10^{-12}	4.18×10^{-12}	3.99×10^{-12}	3.82×10^{-12}	3.66×10^{-12}	
	DK-CCSD(T)/ANO-RCC-VQZP							
	253	258	263	268	273	278	283	288
H4-abstraction	9.91×10^{-17}	1.17×10^{-16}	1.38×10^{-16}	1.62×10^{-16}	1.89×10^{-16}	2.19×10^{-16}	2.53×10^{-16}	2.91×10^{-16}
H5-abstraction	2.61×10^{-15}	2.28×10^{-15}	3.04×10^{-15}	3.26×10^{-15}	3.50×10^{-15}	3.74×10^{-15}	4.00×10^{-15}	4.26×10^{-15}
H7-abstraction	1.11×10^{-25}	1.89×10^{-25}	3.15×10^{-25}	5.14×10^{-25}	8.27×10^{-25}	1.31×10^{-24}	2.03×10^{-24}	3.11×10^{-24}
Cl-abstraction	7.40×10^{-37}	2.20×10^{-36}	6.28×10^{-38}	1.73×10^{-35}	4.57×10^{-35}	1.17×10^{-34}	2.90×10^{-34}	6.97×10^{-34}
OH-abstraction	4.97×10^{-34}	1.27×10^{-33}	3.12×10^{-33}	7.42×10^{-33}	1.71×10^{-32}	3.84×10^{-32}	8.36×10^{-32}	1.77×10^{-31}
overall	2.71×10^{-15}	2.94×10^{-15}	3.18×10^{-15}	3.43×10^{-15}	6.69×10^{-15}	3.96×10^{-15}	4.25×10^{-15}	4.55×10^{-15}
	293	298	303	308	313	318	323	
H4-abstraction	3.34×10^{-16}	3.81×10^{-16}	4.32×10^{-16}	4.89×10^{-16}	5.52×10^{-16}	6.21×10^{-16}	6.96×10^{-15}	
H5-abstraction	4.54×10^{-15}	4.82×10^{-15}	5.11×10^{-15}	5.42×10^{-15}	5.73×10^{-15}	6.06×10^{-15}	6.39×10^{-15}	
H7-abstraction	4.70×10^{-24}	7.00×10^{-24}	1.03×10^{-23}	1.50×10^{-23}	2.15×10^{-23}	3.06×10^{-23}	4.30×10^{-23}	
Cl-abstraction	1.63×10^{-33}	3.69×10^{-33}	8.15×10^{-33}	1.75×10^{-32}	3.69×10^{-32}	7.59×10^{-32}	1.53×10^{-31}	
OH-abstraction	3.67×10^{-31}	7.41×10^{-31}	1.46×10^{-30}	2.82×10^{-30}	5.35×10^{-20}	9.92×10^{-30}	1.81×10^{-29}	
overall	4.87×10^{-15}	5.20×10^{-15}	5.55×10^{-15}	5.91×10^{-15}	6.28×10^{-15}	6.68×10^{-15}	7.09×10^{-15}	

Appendices

Table A.II-2: Rate constants in cm³ molecule⁻¹ s⁻¹ calculated at different temperatures at the M06-2X/6-311++G(3df,3p) and DK-CCSD(T)/ANO-RCC-VQZP levels of theory for H-, Cl-, and OH-abstraction pathways and the overall reaction OH and CH₂ClOOH using the indirect mechanism considering Wigner tunnelling corrections.

	M06-2X/6-311++G(3df,3p)							
	253	**258**	**263**	**268**	**273**	**278**	**283**	**288**
H4-abstraction	2.42×10^{-14}	2.57×10^{-14}	2.73×10^{-14}	2.89×10^{-14}	3.06×10^{-14}	3.24×10^{-14}	3.42×10^{-14}	3.60×10^{-14}
H5-abstraction	5.71×10^{-13}	5.55×10^{-13}	5.40×10^{-13}	5.26×10^{-13}	5.14×10^{-13}	5.02×10^{-13}	4.91×10^{-13}	4.82×10^{-13}
H7-abstraction	4.62×10^{-11}	4.13×10^{-11}	3.71×10^{-11}	3.35×10^{-11}	3.04×10^{-11}	2.76×10^{-11}	2.52×10^{-11}	2.30×10^{-11}
Cl-abstraction	4.79×10^{-35}	1.30×10^{-34}	3.39×10^{-34}	8.56×10^{-34}	2.09×10^{-33}	4.94×10^{-33}	1.13×10^{-32}	2.53×10^{-32}
OH-abstraction	5.29×10^{-33}	1.30×10^{-32}	3.09×10^{-32}	7.10×10^{-32}	1.59×10^{-31}	3.44×10^{-31}	7.27×10^{-31}	1.50×10^{-30}
overall	4.68×10^{-11}	4.19×10^{-11}	3.77×10^{-11}	3.41×10^{-11}	3.09×10^{-11}	2.81×10^{-11}	2.57×10^{-11}	2.36×10^{-11}
	293	**298**	**303**	**308**	**313**	**318**	**323**	
H4-abstraction	3.79×10^{-14}	3.99×10^{-14}	4.19×10^{-14}	4.39×10^{-14}	4.61×10^{-14}	4.82×10^{-14}	5.05×10^{-14}	
H5-abstraction	4.72×10^{-13}	4.64×10^{-13}	4.56×10^{-13}	4.49×10^{-13}	4.42×10^{-13}	4.36×10^{-13}	4.31×10^{-13}	
H7-abstraction	2.12×10^{-11}	1.95×10^{-11}	1.80×10^{-11}	1.67×10^{-11}	1.55×10^{-11}	1.44×10^{-11}	1.35×10^{-11}	
Cl-abstraction	5.50×10^{-32}	1.17×10^{-31}	2.41×10^{-31}	4.87×10^{-31}	9.64×10^{-31}	1.87×10^{-30}	3.54×10^{-30}	
OH-abstraction	3.01×10^{-30}	5.91×10^{-30}	1.14×10^{-29}	2.14×10^{-29}	3.95×10^{-29}	7.16×10^{-29}	1.27×10^{-28}	
overall	2.17×10^{-11}	2.00×10^{-11}	1.85×10^{-11}	1.72×10^{-11}	1.60×10^{-11}	1.49×10^{-11}	1.39×10^{-11}	
	DK-CCSD(T)/ANO-RCC-VQZP							
	253	**258**	**263**	**268**	**273**	**278**	**283**	**288**
H4-abstraction	6.17×10^{-16}	7.08×10^{-16}	8.08×10^{-16}	9.18×10^{-16}	1.04×10^{-15}	1.17×10^{-15}	1.31×10^{-15}	1.47×10^{-15}
H5-abstraction	1.70×10^{-14}	1.78×10^{-14}	1.85×10^{-14}	1.93×10^{-14}	2.01×10^{-14}	2.08×10^{-14}	2.16×10^{-14}	2.24×10^{-14}
H7-abstraction	1.20×10^{-24}	1.97×10^{-24}	3.17×10^{-24}	5.00×10^{-24}	7.78×10^{-24}	1.18×10^{-23}	1.79×10^{-23}	2.66×10^{-23}
Cl-abstraction	1.05×10^{-36}	3.10×10^{-36}	8.75×10^{-36}	2.38×10^{-35}	6.24×10^{-35}	1.58×10^{-34}	3.88×10^{-34}	9.25×10^{-34}
OH-abstraction	1.77×10^{-33}	4.39×10^{-33}	1.05×10^{-33}	2.44×10^{-32}	5.49×10^{-32}	1.20×10^{-31}	2.55×10^{-31}	5.28×10^{-31}
overall	1.76×10^{-14}	1.85×10^{-14}	1.93×10^{-14}	2.02×10^{-14}	2.11×10^{-14}	2.20×10^{-14}	2.29×10^{-14}	2.39×10^{-14}
	293	**298**	**303**	**308**	**313**	**318**	**323**	
H4-abstraction	1.63×10^{-15}	1.81×10^{-15}	2.01×10^{-15}	2.22×10^{-15}	2.44×10^{-15}	2.68×10^{-15}	2.93×10^{-15}	
H5-abstraction	2.32×10^{-14}	2.40×10^{-14}	2.48×10^{-14}	2.56×10^{-14}	2.64×10^{-14}	2.72×10^{-14}	2.80×10^{-14}	
H7-abstraction	3.90×10^{-23}	5.64×10^{-23}	8.07×10^{-23}	1.14×10^{-22}	1.59×10^{-22}	2.20×10^{-22}	3.01×10^{-22}	
Cl-abstraction	2.14×10^{-33}	4.82×10^{-33}	1.06×10^{-32}	2.26×10^{-32}	4.72×10^{-32}	9.63×10^{-32}	1.92×10^{-31}	
OH-abstraction	1.07×10^{-30}	2.11×10^{-30}	4.08×10^{-30}	7.72×10^{-30}	1.43×10^{-29}	2.60×10^{-29}	4.65×10^{-29}	
overall	2.48×10^{-14}	2.58×10^{-14}	2.68×10^{-14}	2.78×10^{-14}	2.88×10^{-14}	2.99×10^{-14}	3.09×10^{-14}	

Appendices

Table A.II-3: *Rate constants in cm^3 molecule^{-1} s^{-1} calculated at different temperatures at the M06-2X/6-311++G(3df,3p) and DK-CCSD(T)/ANO-RCC-VQZP levels of theory for H-, Cl-, and OH-abstraction pathways and the overall reaction OH and CH$_2$ClOOH using the indirect mechanism considering Eckart tunnelling corrections*.

	M06-2X/6-311++G(3df,3p)							
	253	**258**	**263**	**268**	**273**	**278**	**283**	**288**
H4-abstraction	6.30×10^{-14}	6.23×10^{-14}	6.35×10^{-14}	6.40×10^{-14}	6.47×10^{-14}	6.54×10^{-14}	6.63×10^{-14}	6.74×10^{-14}
H5-abstraction	1.06×10^{-12}	9.89×10^{-13}	9.30×10^{-13}	8.78×10^{-13}	8.32×10^{-13}	7.91×10^{-13}	7.54×10^{-13}	7.21×10^{-13}
H7-abstraction	2.93×10^{-10}	2.40×10^{-10}	1.98×10^{-10}	1.65×10^{-10}	1.39×10^{-10}	1.17×10^{-10}	1.00×10^{-10}	8.61×10^{-11}
Cl-abstraction	4.51×10^{-35}	1.22×10^{-34}	3.20×10^{-34}	8.08×10^{-34}	1.97×10^{-33}	4.67×10^{-33}	1.07×10^{-32}	2.40×10^{-32}
OH-abstraction	3.91×10^{-32}	8.01×10^{-32}	1.62×10^{-31}	3.25×10^{-31}	6.40×10^{-31}	1.24×10^{-30}	2.38×10^{-30}	4.49×10^{-30}
overall	2.94×10^{-10}	2.41×10^{-10}	1.99×10^{-10}	1.66×10^{-10}	1.40×10^{-10}	1.18×10^{-10}	1.01×10^{-10}	8.69×10^{-11}
	293	**298**	**303**	**308**	**313**	**318**	**323**	
H4-abstraction	6.85×10^{-14}	6.77×10^{-14}	7.10×10^{-14}	7.25×10^{-14}	7.40×10^{-14}	7.56×10^{-14}	7.73×10^{-14}	
H5-abstraction	6.92×10^{-13}	6.66×10^{-13}	6.42×10^{-13}	6.20×10^{-13}	6.01×10^{-13}	5.83×10^{-13}	5.67×10^{-13}	
H7-abstraction	7.44×10^{-11}	6.48×10^{-11}	5.67×10^{-11}	4.99×10^{-11}	4.42×10^{-11}	3.93×10^{-11}	3.51×10^{-11}	
Cl-abstraction	5.22×10^{-32}	1.11×10^{-31}	2.29×10^{-31}	4.64×10^{-31}	9.19×10^{-31}	1.78×10^{-30}	3.39×10^{-30}	
OH-abstraction	8.35×10^{-30}	1.53×10^{-29}	2.75×10^{-29}	4.89×10^{-29}	8.56×10^{-29}	1.48×10^{-28}	2.52×10^{-28}	
overall	7.52×10^{-11}	6.55×10^{-11}	5.74×10^{-11}	5.06×10^{-11}	4.49×10^{-11}	4.00×10^{-11}	3.58×10^{-11}	
	DK-CCSD(T)/ANO-RCC-VQZP							
	253	**258**	**263**	**268**	**273**	**278**	**283**	**288**
H4-abstraction	1.90×10^{-14}	1.85×10^{-14}	1.80×10^{-14}	1.77×10^{-14}	1.75×10^{-14}	1.73×10^{-14}	1.71×10^{-14}	1.70×10^{-14}
H5-abstraction	2.24×10^{-13}	2.08×10^{-13}	1.94×10^{-13}	1.82×10^{-13}	1.71×10^{-13}	1.61×10^{-13}	1.53×10^{-13}	1.46×10^{-13}
H7-abstraction	4.15×10^{-18}	3.66×10^{-18}	3.26×10^{-18}	2.92×10^{-18}	2.65×10^{-18}	2.41×10^{-18}	2.22×10^{-18}	2.05×10^{-18}
Cl-abstraction	1.01×10^{-36}	2.98×10^{-36}	8.40×10^{-36}	2.28×10^{-35}	5.99×10^{-35}	1.52×10^{-34}	3.73×10^{-34}	8.88×10^{-34}
OH-abstraction	1.36×10^{-31}	2.29×10^{-31}	3.85×10^{-31}	6.53×10^{-31}	1.11×10^{-30}	1.88×10^{-30}	3.19×10^{-30}	5.40×10^{-30}
overall	2.43×10^{-13}	2.26×10^{-13}	2.12×10^{-13}	1.99×10^{-13}	1.88×10^{-13}	1.79×10^{-13}	1.70×10^{-13}	1.63×10^{-13}
	293	**298**	**303**	**308**	**313**	**318**	**323**	
H4-abstraction	1.70×10^{-14}	1.70×10^{-14}	1.70×10^{-14}	1.71×10^{-14}	1.72×10^{-14}	1.74×10^{-14}	1.76×10^{-14}	
H5-abstraction	1.39×10^{-13}	1.33×10^{-13}	1.28×10^{-13}	1.23×10^{-13}	1.19×10^{-13}	1.15×10^{-13}	1.12×10^{-13}	
H7-abstraction	1.91×10^{-18}	1.79×10^{-18}	1.69×10^{-18}	1.61×10^{-18}	1.53×10^{-18}	1.47×10^{-18}	1.42×10^{-18}	
Cl-abstraction	2.06×10^{-33}	4.63×10^{-33}	1.01×10^{-32}	2.17×10^{-32}	4.54×10^{-32}	9.27×10^{-32}	1.85×10^{-31}	
OH-abstraction	9.12×10^{-30}	1.53×10^{-29}	2.55×10^{-29}	4.24×10^{-29}	6.97×10^{-29}	1.14×10^{-29}	1.84×10^{-28}	
overall	1.56×10^{-13}	1.50×10^{-13}	1.45×10^{-13}	1.40×10^{-13}	1.36×10^{-13}	1.33×10^{-13}	1.30×10^{-13}	

Appendices

Table A.II-4: Values of Wigner tunnelling corrections at the M06-2X/6-311++G(3df,3p) and DK-CCSD(T)/ANO-RCC-VQZP levels of theory for H-, Cl-, and OH-abstraction pathways and the overall reaction OH and CH₂ClOOH.

	M06-2X/6-311++G(3df,3p)							
	253	**258**	**263**	**268**	**273**	**278**	**283**	**288**
H4-abstraction	2.86	2.78	2.72	2.65	2.59	2.54	2.48	2.43
H5-abstraction	2.65	2.59	2.53	2.47	2.42	2.37	2.32	2.28
H7-abstraction	5.78	5.60	5.42	5.26	5.11	4.96	4.82	4.69
Cl-abstraction	1.09	1.08	1.08	1.08	1.08	1.07	1.07	1.07
OH-abstraction	2.80	2.73	2.66	2.60	2.54	2.49	2.44	2.39
	293	**298**	**303**	**308**	**313**	**318**	**323**	
H4-abstraction	2.38	2.34	2.29	2.25	2.21	2.17	2.14	
H5-abstraction	2.23	2.19	2.15	2.12	2.08	2.05	2.01	
H7-abstraction	4.56	4.45	4.33	4.23	4.12	4.03	3.93	
Cl-abstraction	1.07	1.06	1.06	1.06	1.06	1.06	1.05	
OH-abstraction	2.34	2.29	2.25	2.21	2.17	2.14	2.10	
	DK-CCSD(T)/ANO-RCC-VQZP							
	253	**258**	**263**	**268**	**273**	**278**	**283**	**288**
H4-abstraction	6.23	6.03	5.84	5.66	5.49	5.33	5.18	5.03
H5-abstraction	6.51	6.30	6.10	5.91	5.74	5.57	5.41	5.25
H7-abstraction	10.79	10.42	10.06	9.73	9.41	9.11	8.83	8.56
Cl-abstraction	1.43	1.41	1.39	1.38	1.37	1.35	1.34	1.33
OH-abstraction	3.57	3.47	3.37	3.29	3.20	3.13	3.05	2.98
	293	**298**	**303**	**308**	**313**	**318**	**323**	
H4-abstraction	4.90	4.77	4.64	4.53	4.42	4.31	4.21	
H5-abstraction	8.30	8.06	7.83	7.61	7.40	7.20	7.01	
H7-abstraction	1.32	1.31	1.30	1.29	1.28	1.27	1.26	
Cl-abstraction	2.91	2.85	2.79	2.73	2.68	2.62	2.57	
OH-abstraction	5.11	4.97	4.84	4.72	4.60	4.49	4.38	

Table A.II-5: *Values of **Eckart tunnelling corrections** at the M06-2X/6-311++G(3df,3p) and DK-CCSD(T)/ANO-RCC-VQZP levels of theory for H-, Cl-, and OH-abstraction pathways and the overall reaction OH and CH₂ClOOH.*

	M06-2X/6-311++G(3df,3p)							
	253	**258**	**263**	**268**	**273**	**278**	**283**	**288**
H4-abstraction	7.44	6.84	6.32	5.87	5.47	5.13	4.82	4.55
H5-abstraction	4.91	4.62	4.36	4.13	3.92	3.73	3.56	3.41
H7-abstraction	36.66	32.46	28.92	25.90	23.33	21.11	19.19	17.52
Cl-abstraction	1.02	1.02	1.02	1.02	1.02	1.02	1.01	1.01
OH-abstraction	20.66	16.81	14.00	11.89	10.27	9.00	7.99	7.17
	293	**298**	**303**	**308**	**313**	**318**	**323**	
H4-abstraction	4.30	4.09	3.89	3.71	3.55	3.41	3.28	
H5-abstraction	3.27	3.14	3.03	2.92	2.83	2.74	2.65	
H7-abstraction	16.06	14.78	13.66	12.66	11.77	10.98	10.27	
Cl-abstraction	1.01	1.01	1.01	1.01	1.01	1.01	1.01	
OH-abstraction	6.49	5.93	5.46	5.05	4.71	4.41	4.15	
	DK-CCSD(T)/ANO-RCC-VQZP							
	253	**258**	**263**	**268**	**273**	**278**	**283**	**288**
H4-abstraction	191.28	157.15	130.41	109.24	92.31	78.66	67.56	58.45
H5-abstraction	85.82	73.75	63.85	55.66	48.83	43.11	38.27	34.16
H7-abstraction	3.74×10^7	1.94×10^7	1.04×10^7	5.68×10^6	3.20×10^6	1.85×10^6	1.09×10^6	6.60×10^5
Cl-abstraction	1.37	1.35	1.34	1.32	1.31	1.30	1.29	1.28
OH-abstraction	274.28	180.39	123.60	87.90	64.66	49.02	38.19	30.48
	293	**298**	**303**	**308**	**313**	**318**	**323**	
H4-abstraction	50.92	44.65	39.40	34.97	31.21	27.99	25.23	
H5-abstraction	30.65	27.63	25.03	22.76	20.79	19.06	17.54	
H7-abstraction	4.07×10^5	2.56×10^5	1.64×10^5	1.07×10^5	7.13×10^4	4.81×10^4	3.30×10^4	
Cl-abstraction	1.26	1.26	1.25	1.24	1.23	1.22	1.21	
OH-abstraction	24.86	20.67	17.47	15.00	13.04	11.48	10.21	

Appendices

Appendix A.III: Thermal and photolysis reactions of chlorinated species

Appendix A.III-1: Organic chlorine gas-phase mechanism

Table A.III-1: Cl_RACM mechanism species list.

Cl_RACM Class	Species
Cl_CH4	CH_3Cl
Cl2_CH4	CH_2Cl_2
Cl_MR	CH_2Cl
Cl2_MR	$CHCl_2$
Cl_ETE	$CH_2=CHCl$, $CHOH=CHCl$
Cl_ETER	$CH_2=CCl$, $CHCl=CH$
Cl_ETH	C_2H_5Cl
Cl2_ETH	CH_3CHCl_2, CH_2ClCH_2Cl
Cl_ETHR	CH_3CHCl, CH_2CH_2Cl, C_2H_4Cl (undefined isomer)
Cl2_ETHR	$CHCl_2CH_2$, CH_3CCl_2, $CH_2ClCHCl$
Cl_HC3	CH_2ClOH, CH_3OCl, $CH_2ClC≡CH$, CH_3OCH_2Cl, tert-C_4H_9Cl, n-C_4H_9Cl, sec C_4H_9Cl, n-C_3H_7Cl, iso-C_3H_7Cl
Cl_HC3R	CH_2ClO, $ClCHOH$, $ClCH_2CHCH_3$, $(CH_3)2CClCH_2$, CH_2OCl, CH_3CHClO, $CHClCH_2OH$, $CHClOHCH_2$, CH_2ClCH_2O
Cl_TOL	Chlorobenzene (C_6H_5Cl), $C_6H_5CH_2Cl$
Cl_TOLR	2-chlorophenyl, 3-chlorophenyl, 4-chlorophenyl
Cl_HCHO	$HC(O)Cl$
Cl_HCHOR	$ClCO$
Cl_ALD	CH_2ClCHO
Cl_DIEN	chlorocyclohexadiene
Cl_DIENR	$C_2H_2C_2H_2Cl$
Cl_ETHP	CH_3CHClO_2
Cl2_ETHP	$CH_2ClCHClO_2$
Cl_MO2	CH_2ClO_2
Cl2_MO2	$CHCl_2O_2$
Cl_OP1	CH_2ClOOH
Cl_OLT	$CH_2=CHCH_2Cl$
Cl_OLTR	$CH_2=C(CH_3)CHClCH_2$, $CH_2Cl-CH=CH$
Cl2_OLTR	$C_3H_3Cl_2$
Cl_ORA2R	$ClCH_2CHCOOH$
Cl_CSL	2-Chlorophenol (C_6H_5OCl)
Cl_PHO	2-Chlorophenoxy (C_6H_4OCl)

Appendix

Table A.III-2: *Organic chlorine gas-phase mechanism.*

#	Reaction	Rate constant (s^{-1}) or $(cm^3\ molecule^{-1}\ s^{-1})$ or $(cm^6\ molecule^{-2}\ s^{-1})$	Cl_RACM reaction	Literature
1	$HCl + CH_2=CCl \rightarrow Cl + CH_2=CHCl$	2.19×10^{-13}	$HCl + Cl\_ETER \rightarrow Cl + Cl\_ETE$	(Russell *et al.*, 1989b)
2	$HCl + CH_2Cl \rightarrow CH_2Cl_2 + H$	$1.71 \times 10^{-22}\ T^{2.85}\ exp(-14300/T)$	$HCl + Cl\_MR \rightarrow Cl2\_CH4 + H$	(Bryukov *et al.*, 2001)
3	$HCl + CH_2Cl \rightarrow Cl + CH_3Cl$	$3.12 \times 10^{-17}\ T^{1.57}\ exp(-2100/T)$	$HCl + Cl\_MR \rightarrow Cl\_CH4 + Cl$	(Brudnik *et al.*, 2013a)
4	$HCl + CH_2OH \rightarrow Cl + CH_3OH$	$5.80 \times 10^{-13}\ exp(-2754/T)$	$HCl + HC3R \rightarrow Cl + HC3$	(Jodkowski *et al.*, 1998)
5	$HCl + Phenyl \rightarrow Cl + Benzene$	$1.14 \times 10^{-12}\ exp(625/T)$	$HCl + TOLR \rightarrow Cl + TOL$	(Alecu *et al.*, 2007)
6	$HCl + CH_3O \rightarrow Cl + CH_3OH$	$1.74 \times 10^{-20}\ T^{2.50}\ exp(-2230/T)$	$HCl + HC3R \rightarrow Cl + HC3$	(Jodkowski *et al.*, 1998)
7	$HCl + CH_3 \rightarrow CH_3Cl + H$	$6.40 \times 10^{-23}\ T^{2.56}\ exp(-13230/T)$	$HCl + MR \rightarrow Cl\_CH4 + H$	(Bryukov *et al.*, 2001)
8	$HCl + C_2H_3 \rightarrow Cl + C_2H_4$	$8.70 \times 10^{-13}\ exp(-100/T)$	$HCl + ETER \rightarrow Cl + ETE$	(Dobis and Benson, 1991)
9	$HCl + CH_3 \rightarrow Cl + CH_4$	$5.60 \times 10^{-13}\ exp(-752/T)$	$HCl + MR \rightarrow Cl + CH4$	(Chen *et al.*, 1991)
10	$CH_3Cl + Cl \rightarrow HCl + CH_2Cl$	$1.70 \times 10^{-11}\ exp(-1040/T)$	$Cl\_CH4 + Cl \rightarrow HCl + Cl\_MR$	(Sarzyński *et al.*, 2009)
11	$CH_3Cl + Cl \rightarrow Cl_2 + CH_3$	$1.91 \times 10^{-15}\ T^{1.63}\ exp(-12749/T)$	$Cl\_CH4 + Cl \rightarrow Cl2 + MR$	(Brudnik *et al.*, 2013b)
12	$CH_3Cl + O(^3P) \rightarrow CH_2Cl + OH$	$2.82 \times 10^{-11}\ exp(-3690/T)$	$Cl\_CH4 + O3P \rightarrow Cl\_MR + HO$	(Herron and Huie, 1973)
13	$CH_3Cl + O(^1D) \rightarrow CH_2Cl + OH$	3.40×10^{-10}	$Cl\_CH4 + O1D \rightarrow Cl\_MR + HO$	(Matsumi *et al.*, 1993)
14	$CH_3Cl + H \rightarrow HCl + CH_3$	$1.83 \times 10^{-11}\ exp(-2320/T)$	$Cl\_CH4 + H \rightarrow HCl + MR$	(Aders *et al.*, 1975)
15	$CH_3Cl + H \rightarrow CH_2Cl + H_2$	$4.65 \times 10^{-19}\ T^{2.59}\ exp(-3848/T)$	$Cl\_CH4 + H \rightarrow Cl\_MR + H2$	(Bryukov *et al.*, 2001)
16	$CH_3Cl + OH \rightarrow CH_2Cl + H_2O$	$3.80 \times 10^{-12}\ exp(-1340/T)$	$Cl\_CH4 + HO \rightarrow Cl\_MR + H2O$	(Atkinson *et al.*, 2001)
17	$CH_3Cl + CH_3 \rightarrow CH_4 + CH_2Cl$	$2.09 \times 10^{-12}\ exp(-5840/T)$	$Cl\_CH4 + MR \rightarrow Cl\_MR + CH4$	(Macken and Sidebottom, 1979)
18	$CH_2Cl_2 + Cl \rightarrow CH_2Cl + Cl_2$	$2.12 \times 10^{-14}\ T^{1.23}\ exp(-10957/T)$	$Cl2\_CH4 + Cl \rightarrow Cl\_MR + Cl2$	(Brudnik *et al.*, 2013b)
19	$CH_2Cl_2 + Cl \rightarrow CHCl_2 + HCl$	$1.48 \times 10^{-16}\ T^{1.58}\ exp(-360/T)$	$Cl2\_CH4 + Cl \rightarrow Cl2\_MR + HCl$	(Bryukov *et al.*, 2002)
20	$CH_2Cl_2 + O(^3P) \rightarrow CHCl_2 + OH$	$9.86 \times 10^{-12}\ exp(-2875/T)$	$Cl2\_CH4 + O3P \rightarrow Cl2\_MR + HO$	(Barassin *et al.*, 1975)
21	$CH_2Cl_2 + H \rightarrow CH_2Cl + HCl$	$1.79 \times 10^{-11}\ exp(-3067/T)$	$Cl2\_CH4 + H \rightarrow Cl\_MR + HCl$	(Combourieu *et al.*, 1973)
22	$CH_2Cl_2 + H \rightarrow H_2 + CHCl_2$	$1.52 \times 10^{-19}\ T^{2.66}\ exp(-3067/T)$	$Cl2\_CH4 + H \rightarrow Cl2\_MR + H2$	(Bryukov *et al.*, 2001)
23	$CH_2Cl_2 + OH \rightarrow CHCl_2 + H_2O$	$4.04 \times 10^{-15}\ T^{1.09}\ exp(-771/T)$	$Cl2\_CH4 + HO \rightarrow Cl2\_MR + H2O$	(Taylor *et al.*, 1993)
24	$CH_2Cl_2 + CH_3 \rightarrow CHCl_2 + CH_4$	$1.05 \times 10^{-12}\ exp(-4534/T)$	$Cl2\_CH4 + MR \rightarrow Cl2\_MR + CH4$	(Macken and Sidebottom, 1979)
25	$Cl + HC(O)H \rightarrow HCl + HC(O)$	6.98×10^{-11}	$Cl + HCHO \rightarrow HCl + HCHOR$	(Seakins *et al.*, 2004)
26	$Cl + CH_3CHCl \rightarrow HCl + CH_2=CHCl$	1.18×10^{-11}	$Cl + Cl\_ETHR \rightarrow HCl + Cl\_ETE$	(Dobis and Benson, 2000)
27	$Cl + CH_2ClOH \rightarrow HCl + CH_2ClO$	$4.83 \times 10^{-19}\ T^{2.23}\ exp(-4931/T)$	$Cl + Cl\_HC3 \rightarrow HCl + Cl\_HC3R$	(Ji *et al.*, 2006)
28	$Cl + CH_2ClOH \rightarrow HCl + ClCHOH$	$1.99 \times 10^{-16}\ T^{1.81}\ exp(-722/T)$	$Cl + Cl\_HC3 \rightarrow HCl + Cl\_HC3R$	(Ji *et al.*, 2006)
29	$Cl + Cyclohexadienyl \rightarrow Chlorocyclohexadiene$	1.00×10^{-10}	$Cl + DIENR \rightarrow Cl\_DIEN$	(Berho *et al.*, 1999)
30	$Cl + CH_3C(O) \rightarrow HCl + H_2C=C(O)$	1.79×10^{-10}	$Cl + ALDR \rightarrow HCl + ALD$	(Maricq *et al.*, 1999)
31	$Cl + C_2H_5O_2 \rightarrow HCl + CH_3CHOO$	7.69×10^{-11}	$Cl + ETHP \rightarrow HCl + ETHP$	(Burkholder *et al.*, 2020)
32	$Cl + C_2H_5O_2 \rightarrow ClO + CH_3CH_2O$	7.41×10^{-11}	$Cl + ETHP \rightarrow ClO + HC3R$	(Burkholder *et al.*, 2020)
33	$Cl + CH_2OH \rightarrow CH_3OCl$	$1.03 \times 10^{-11}\ T^{0.29}$	$Cl + HC3R \rightarrow Cl\_HC3$	(Brudnik *et al.*, 2009)
34	$Cl + CH_2OH \rightarrow HCl + HC(O)H$	6.64×10^{-10}	$Cl + HC3R \rightarrow HCl + HCHO$	(Pagsberg *et al.*, 1988)

Appendix

#	Reaction	Rate	Reaction (model)	Reference
35	$Cl + HC(O)Cl \rightarrow HCl + C(O)Cl$	$1.20 \times 10^{-11} \exp(-815/T)$	$Cl + Cl\_HCHO \rightarrow HCl + Cl\_HCHOR$	(Atkinson $et\ al.$, 2001)
36	$Cl + Phenyl \rightarrow Chlorobenzene$	1.20×10^{-10}	$Cl + TOLR \rightarrow Cl\_TOL$	(Tonokura $et\ al.$, 2002)
37	$Cl + CH_3 \rightarrow CH_3Cl$	$9.21 \times 10^{-12} T^{0.30} \exp(54/T)$	$Cl + MR \rightarrow Cl\_CH4$	(Parker $et\ al.$, 2007)
38	$Cl + Benzyl \rightarrow C_6H_5CH_2Cl$	6.91×10^{-10}	$Cl + TOLR \rightarrow Cl\_TOL$	(Markert and Pagsberg, 1993)
39	$Cl + CH_3O \rightarrow HCl + HC(O)H$	1.91×10^{-11}	$Cl + HC3R \rightarrow HCl + HCHO$	(Daële $et\ al.$, 1996)
40	$Cl + CH_3O_2 \rightarrow HCl + CH_2OO$	2.01×10^{-10}	$Cl + MO2 \rightarrow HCl + MO2$	(Daële and Poulet, 1996)
41	$Cl + CH_3O_2 \rightarrow CH_3O + ClO$	2.01×10^{-11}	$Cl + MO2 \rightarrow ClO + HC3R$	(Daële and Poulet, 1996)
42	$Cl + C_2H_5 \rightarrow C_2H_5Cl$	4.55×10^{-10}	$Cl + ETHR \rightarrow Cl\_ETH$	(Timonen $et\ al.$, 1986)
43	$Cl + C_2H_5 \rightarrow HCl + C_2H_4$	$7.57 \times 10^{-10} \exp(-290/T)$	$Cl + ETHR \rightarrow HCl + ETE$	(Maricq $et\ al.$, 1993b)
44	$Cl + (CH_3O)2 \rightarrow CH_2OOCH_3 + HCl$	$3.72 \times 10^{-11} \exp(413/T)$	$Cl + OP2 \rightarrow HCl + OP2R$	(Senkan and Quam, 1992)
45	$Cl + CH_2ClC\equiv CH \rightarrow C_3H_3Cl_2$	1.20×10^{-10}	$Cl + Cl\_HC3 \rightarrow Cl2\_OLTR$	(Atkinson and Hudgens, 1999)
46	$Cl + M + C_2H_4 \rightarrow M + CH_2CH_2Cl$	$7.00 \times 10^{-69} T^{-3.30}$	$Cl + ETE \rightarrow Cl\_ETHR$	(Atkinson $et\ al.$, 2001)
47	$Cl + M + C_2H_2 \rightarrow M + CH_2=CCl$	$4.55 \times 10^{-70} T^{-3.00}$	$Cl + HC3 \rightarrow Cl\_ETER$	(Atkinson $et\ al.$, 2001)
48	$Cl + CH_2O \rightarrow HCO + HCl$	$8.20 \times 10^{-11} \exp(-34/T)$	$Cl + HCHO \rightarrow HCl + HCHOR$	(Atkinson $et\ al.$, 2001)
49	$Cl + HCOOH \rightarrow HOCO + HCl$	1.83×10^{-13}	$Cl + ORA1 \rightarrow HCl + ORA1R$	(Li $et\ al.$, 2000)
50	$Cl + CH_3OH \rightarrow CH_3O + HCl$	$9.65 \times 10^{-19} T^{2.50} \exp(-3668/T)$	$Cl + HC3 \rightarrow HCl + HC3R$	(Jodkowski $et\ al.$, 1998)
51	$Cl + CH_3OH \rightarrow CH_2OH + HCl$	$6.60 \times 10^{-11} \exp(23/T)$	$Cl + HC3 \rightarrow HCl + HC3R$	(Jodkowski $et\ al.$, 1998)
52	$Cl + n\text{-}C_3H_7OH \rightarrow CH_3CHCH_2OH + HCl$	4.35×10^{-11}	$Cl + HC3 \rightarrow HCl + HC3R$	(Yamanaka $et\ al.$, 2008)
53	$Cl + n\text{-}C_3H_7OH \rightarrow CH_2CH_2CH_2OH + HCl$	2.61×10^{-11}	$Cl + HC3 \rightarrow HCl + HC3R$	(Yamanaka $et\ al.$, 2008)
54	$Cl + n\text{-}C_3H_7OH \rightarrow C_2H_5CHOH + HCl$	1.04×10^{-10}	$Cl + HC3 \rightarrow HCl + HC3R$	(Yamanaka $et\ al.$, 2008)
55	$Cl + Benzene \rightarrow Phenyl + HCl$	$6.10 \times 10^{-11} \exp(-3801/T)$	$Cl + TOL \rightarrow TOLR + HCl$	(Alecu $et\ al.$, 2007)
56	$Cl + CH_4 \rightarrow CH_3 + HCl$	$1.30 \times 10^{-19} T^{2.69} \exp(-497/T)$	$Cl + CH4 \rightarrow HCl + MR$	(Bryukov $et\ al.$, 2002)
57	$Cl + C_2H_6 \rightarrow C_2H_5 + HCl$	$4.91 \times 10^{-12} T^{0.47} \exp(-82/T)$	$Cl + ETH \rightarrow HCl + ETHR$	(Bryukov $et\ al.$, 2003)
58	$Cl + C_2H_4 \rightarrow C_2H_3 + HCl$	$1.15 \times 10^{-10} \exp(-1612/T)$	$Cl + ETE \rightarrow HCl + ETER$	(Dobis and Benson, 1991)
59	$Cl + C_2H_4 \rightarrow CH_2CH_2Cl$	$2.96 \times 10^{-14} T^{1.31} \exp(518/T)$	$Cl + ETE \rightarrow Cl\_ETHR$	(Knyazev $et\ al.$, 1999)
60	$Cl + C_2H_2 \rightarrow CHCl=CH$	$7.97 \times 10^{-8} T^{-1.04}$	$Cl + HC3 \rightarrow Cl\_ETER$	(Kaiser, 1992)
61	$Cl + C_3H_8 \rightarrow 1\text{-}C_3H_7 + HCl$	1.40×10^{-10}	$Cl + HC3 \rightarrow HCl + HC3R$	(Atkinson $et\ al.$, 2001)
62.	$Cl + C_3H_8 \rightarrow iso\text{-}C_3H_7 + HCl$	$8.14 \times 10^{-11} \exp(-86/T)$	$Cl + HC3 \rightarrow HCl + HC3R$	(Tschuikow-Roux $et\ al.$, 1985)
63	$Cl + CH_3CCH \rightarrow CH_2C\equiv CH + HCl$	$1.41 \times 10^{-17} T^{2.00} \exp(-500/T)$	$Cl + HC3 \rightarrow HCl + HC3R$	(Farrell and Taatjes, 1998)
64	$Cl + C_2H_5Cl \rightarrow C_2H_4Cl + HCl$	$2.55 \times 10^{-19} T^{2.60} \exp(793/T)$	$Cl + Cl\_ETH \rightarrow HCl + Cl\_ETHR$	(He $et\ al.$, 2006)
65	$Cl + CH_2=CHCl \rightarrow CHCl_2CH_2$	$5.25 \times 10^{-12} \exp(-503/T)$	$Cl + Cl\_ETE \rightarrow Cl2\_ETHR$	(Ayscough $et\ al.$, 1961)
66	$Cl + CH_3CHO \rightarrow CH_3CO + HCl$	7.20×10^{-11}	$Cl + ALD \rightarrow HCl + ALDR$	(Atkinson $et\ al.$, 2001)
67	$Cl + Cyclopropane \rightarrow Cyclopropyl + HCl$	1.21×10^{-13}	$Cl + HC3 \rightarrow HCl + HC3R$	(Baghal-Vayjooee and Benson, 1979)
68	$Cl + Oxirane \rightarrow HCl + Oxiranyl$	2.82×10^{-11}	$Cl + HC3 \rightarrow HCl + HC3R$	(Bartels $et\ al.$, 1989)
69	$Cl + iso\text{-}C_4H_{10} \rightarrow tert\text{-}C_4H_9 + HCl$	$2.89 \times 10^{-11} \exp(-138/T)$	$Cl + HC3 \rightarrow HCl + HC3R$	(Cadman $et\ al.$, 1976)
70	$Cl + iso\text{-}C_4H_{10} \rightarrow iso\text{-}C_4H_9 + HCl$	$8.52 \times 10^{-11} \exp(-292/T)$	$Cl + HC3 \rightarrow HCl + HC3R$	(Cadman $et\ al.$, 1976)
71	$Cl + CH_3CHCl_2 \rightarrow HCl + CH_3CCl_2$	$1.92 \times 10^{-11} \exp(-732/T)$	$Cl + Cl2\_ETH \rightarrow HCl + Cl2\_ETHR$	(Bryukov $et\ al.$, 2003)
72	$Cl + CH_3CHCl_2 \rightarrow HCl + CHCl_2CH_2$	$2.98 \times 10^{-11} \exp(-1686/T)$	$Cl + Cl2\_ETH \rightarrow HCl + Cl2\_ETHR$	(Bryukov $et\ al.$, 2003)
73	$Cl + CH_2=C(CH_3)CH=CH_2 \rightarrow CH_2=C(CH_3)CHClCH_2$	3.40×10^{-10}	$Cl + DIEN \rightarrow Cl\_OLTR$	(Suh and Zhang, 2000)

Appendix

#	Reaction	Rate	Reaction	Reference
74	$Cl + CH_2=C(CH_3)CH=CH_2 \rightarrow H_2C=CHC(CH_3)=CH + HCl$	6.60×10^{-11}	$Cl + DIEN \rightarrow HCl + DIENR$	(Suh and Zhang, 2000)
75	$Cl + sec\text{-}C_4H_9OH \rightarrow CH_3CHCH(OH)CH_3 + HCl$	9.88×10^{-11}	$Cl + HC3 \rightarrow HCl + HC3R$	(Garzón et al., 2009)
76	$Cl + sec\text{-}C_4H_9OH \rightarrow CH_3CH_2C(OH)CH_3 + HCl$	1.57×10^{-9}	$Cl + HC3 \rightarrow HCl + HC3R$	(Garzón et al., 2009)
77	$Cl + C_2H_5COCH_3 \rightarrow CH_2C(O)C_2H_5 + HCl$	$2.30 \times 10^{-11} \exp(-906/T)$	$Cl + KET \rightarrow HCl + KETR$	(Kaiser et al., 2009)
78	$Cl + C_2H_5COCH_3 \rightarrow HCl + CH_2CH_2C(O)CH_3$	$1.90 \times 10^{-11} \exp(-237/T)$	$Cl + KET \rightarrow HCl + KETR$	(Kaiser et al., 2009)
79	$Cl + CH_2=CHCOOH \rightarrow ClCH_2CHCOOH$	2.70×10^{-11}	$Cl + ORA2 \rightarrow Cl\_ORA2R$	(Aranda et al., 2003b)
80	$Cl + CH_3C(O)OCH_3 \rightarrow CH_3C(O)OCH_2 + HCl$	2.44×10^{-12}	$Cl + HC3 \rightarrow HCl + HC3R$	(Deka and Mishra, 2014)
81	$Cl + CH_3C(O)OCH_3 \rightarrow HCl + CH_2C(O)OCH_3$	1.68×10^{-13}	$Cl + HC3 \rightarrow HCl + HC3R$	(Deka and Mishra, 2014)
82	$Cl + 2\text{-Chlorophenol} \rightarrow 2\text{-chlorophenoxy} + HCl$	$1.84 \times 10^{-16} T^{1.47} \exp(582/T)$	$Cl + Cl\_CSL \rightarrow HCl + Cl\_PHO$	(Altarawneh et al., 2008)
83	$Cl + 1\text{-}C_4H_{10} \rightarrow sec\text{-}C_4H_9 + HCl$	$3.32 \times 10^{-11} \exp(-150/T)$	$Cl + HC3 \rightarrow HCl + HC3R$	(Galiba et al., 1964)
84	$Cl + 1\text{-}C_4H_{10} \rightarrow 1\text{-}C_4H_9 + HCl$	2.20×10^{-10}	$Cl + HC3 \rightarrow HCl + HC3R$	(Atkinson et al., 2001)
85	$Cl + CH_2=CHCHO \rightarrow HCl + CH_2=CHCO$	$5.40 \times 10^{-10} \exp(-748/T)$	$Cl + ALD \rightarrow HCl + ALDR$	(Aranda et al., 2003a)
86	$Cl + CH_2ClCH_2Cl \rightarrow HCl + CH_2ClCHCl$	$1.99 \times 10^{-11} \exp(-777/T)$	$Cl + Cl2\_ETH \rightarrow HCl + Cl2\_ETHR$	(Sarzyński et al., 2014)
87	$Cl + CH_2=CHCH_2OH \rightarrow C_3H_6O + HCl$	2.90×10^{-11}	$Cl + OLT \rightarrow HCl + KET$	(Aranda et al., 2003b)
88	$Cl + HC(O)OCH_3 \rightarrow HC(O)OCH_2 + HCl$	2.80×10^{-13}	$Cl + HC3 \rightarrow HCl + HC3R$	(Good et al., 2000)
89	$Cl + HC(O)OCH_3 \rightarrow HCl + CH_3C(O)O$	2.50×10^{-12}	$Cl + HC3 \rightarrow HCl + ORA2R$	(Good et al., 2000)
90	$Cl + Toluene \rightarrow Benzyl + HCl$	5.65×10^{-11}	$Cl + TOL \rightarrow HCl + TOLR$	(Markert and Pagsberg, 1993)
91	$Cl + n\text{-}C_5H_{12} \rightarrow CH_3CH_2CH_2CHCH_3 + HCl$	2.46×10^{-10}	$Cl + HC5 \rightarrow HCl + HC5R$	(Qian et al., 2002)
92	$Cl + 1\text{-}C_6H_{14} \rightarrow 2\text{-hexyl radical} + HCl$	3.44×10^{-10}	$Cl + HC5 \rightarrow HCl + HC5R$	(Qian et al., 2002)
93	$Cl + CH_3CH=CH_2 \rightarrow CH_2CH=CH_2 + HCl$	$4.90 \times 10^{-11} \exp(-90/T)$	$Cl + OLT \rightarrow HCl + OLTR$	(Pilgrim and Taatjes, 1997)
94	$Cl + CH_3CH=CH_2 \rightarrow ClCH_2CHCH_3$	2.71×10^{-10}	$Cl + OLT \rightarrow Cl\_HC3R$	(Kaiser and Wallington, 1996)
95	$Cl + (CH_3)2O \rightarrow HCl + CH_3OCH_2$	1.91×10^{-10}	$Cl + HC3 \rightarrow HCl + HC3R$	(Jenkin et al., 1993)
96	$Cl + Cyclobutane \rightarrow Cyclobutyl + HCl$	$4.25 \times 10^{-10} \exp(-415/T)$	$Cl + HC3 \rightarrow HCl + HC3R$	(Knox and Nelson, 1959)
97	$Cl + Cyclopentane \rightarrow Cyclopentyl + HCl$	2.31×10^{-10}	$Cl + HC5 \rightarrow HCl + HC5R$	(Rowley et al., 1992)
98	$Cl + neo\text{-}C_5H_{12} \rightarrow Neopentyl + HCl$	1.01×10^{-10}	$Cl + HC5 \rightarrow HCl + HC5R$	(Qian et al., 2002)
99	$Cl + tert\text{-}C_4H_9Cl \rightarrow HCl + (CH_3)2CClCH_2$	1.30×10^{-11}	$Cl + Cl\_HC3 \rightarrow HCl + Cl\_HC3R$	(Donaghy et al., 1993)
100	$Cl + (CH_3)3C(CH_2)3CH_3 \rightarrow HCl + n\text{-}C_4H_9C(CH_3)2CH_2$	$8.32 \times 10^{-12} \exp(-302/T)$	$Cl + HC3 \rightarrow HCl + HC3R$	(Desai et al., 1970)
101	$Cl + HCOO(CH_2)3CH_3 \rightarrow HCl + HC(O)OCH_2CHCH_2CH_3$	$1.05 \times 10^{-11} \exp(-150/T)$	$Cl + HC5 \rightarrow HCl + HC5R$	(Singh and Tedder, 1966)
102	$ClO + CH_3 \rightarrow CH_3OCl$	$5.69 \times 10^{-11} T^{0.35}$	$ClO + MR \rightarrow Cl\_HC3$	(Brudnik et al., 2009)
103	$ClO + CH_3O \rightarrow CH_2O + HOCl$	2.31×10^{-11}	$ClO + HC3R \rightarrow HOCl + ALD$	(Daële et al., 1996)
104	$ClO + CH_3O_2 \rightarrow CH_3O + ClOO$	$5.00 \times 10^{-12} \exp(-51/T)$	$ClO + ORA1R \rightarrow OClO + HC3R$	(Kukui, A. S. et al., 1994)
105	$ClO + CH_3O_2 \rightarrow CH_3OCl + O_2$	$1.50 \times 10^{-14} \exp(920/T)$	$ClO + ORA1R \rightarrow Cl\_HC3R + O2$	(Kukui, A. S. et al., 1994)
106	$ClO + CH_4 \rightarrow CH_3 + HOCl$	$3.00 \times 10^{-21} T^{2.89} \exp(-6365/T)$	$ClO + CH4 \rightarrow HOCl + MR$	(Louis et al., 2001)
107	$ClO + CH_2O \rightarrow HCO + HOCl$	$2.99 \times 10^{-13} T^{0.60} \exp(-3015/T)$	$ClO + ALD \rightarrow HOCl + ALDR$	(Tian et al., 2006)
108	$C_2H_5Cl + H \rightarrow C_2H_5 + HCl$	$6.57 \times 10^{-16} T^{1.46} \exp(-4080/T)$	$Cl\_ETH + H \rightarrow HCl + ETHR$	(Sheng et al., 2004)
109	$C_2H_5Cl + H \rightarrow H_2 + CH_3CHCl$	$1.09 \times 10^{-18} T^{2.38} \exp(-2723/T)$	$Cl\_ETH + H \rightarrow Cl\_ETHR + H2$	(Sheng et al., 2004)
110	$C_2H_5Cl + H \rightarrow H_2 + CH_2CH_2Cl$	$2.16 \times 10^{-20} T^{2.90} \exp(-3471/T)$	$Cl\_ETH + H \rightarrow Cl\_ETHR + H2$	(Sheng et al., 2004)
111	$C_2H_5Cl + OH \rightarrow C_2H_4Cl + H_2O$	$1.50 \times 10^{-12} T^{0.50} \exp(-674/T)$	$Cl\_ETH + HO \rightarrow Cl\_ETHR + H2O$	(Herndon et al., 2001)
112	$C_2H_5Cl \rightarrow CH_3 + CH_2Cl$	$1.71 \times 10^{16} \exp(-44741/T)$	$Cl\_ETH \rightarrow MR + Cl\_MR$	(Karra and Senkan, 1988)

Appendix

113	$C_2H_5Cl \rightarrow C_2H_5 + Cl$	$5.00 \times 10^{15} \exp(-41735/T)$	$Cl\_ETH \rightarrow ETHR + Cl$	(Karra and Senkan, 1988)
114	$C_2H_5Cl \rightarrow C_2H_4 + HCl$	$4.49 \times 10^{10} T^{1.05} \exp(-29106/T)$	$Cl\_ETH \rightarrow ETE + HCl$	(Ahubelem et al., 2014)
115	$C_2H_5Cl + Cl \rightarrow HCl + CH_3CHCl$	$1.36 \times 10^{-11} \exp(-202/T)$	$Cl\_ETH + Cl \rightarrow Cl\_ETHR + HCl$	(Sarzyński et al., 2012)
116	$C_2H_5Cl + Cl \rightarrow HCl + CH_2CH_2Cl$	$1.14 \times 10^{-11} \exp(-592/T)$	$Cl\_ETH + Cl \rightarrow Cl\_ETHR + HCl$	(Sarzyński et al., 2012)
117	$2CH_3CHCl \rightarrow C_2H_5Cl + CH_2=CHCl$	1.83×10^{-12}	$2Cl\_ETHR \rightarrow Cl\_ETH + Cl\_ETE$	(Dobis and Benson, 2000)
118	$CH_3CHCl \rightarrow CH_2=CHCl + H$	$1.94 \times 10^{9} T^{1.22} \exp(-19484/T)$	$Cl\_ETHR \rightarrow Cl\_ETE + H$	(Knyazev et al., 1994)
119	$CH_2CH_2Cl \rightarrow CH_2=CHCl + H$	$1.40 \times 10^{13} \exp(-21168/T)$	$Cl\_ETHR \rightarrow Cl\_ETE + H$	(Barat and Bozzelli, 1992)
120	$CH_2CH_2Cl \rightarrow C_2H_4 + Cl$	$2.25 \times 10^{9} T^{-5.43} \exp(-9370/T)$	$Cl\_ETHR \rightarrow Cl + ETE$	(Knyazev et al., 1999)
121	$CH_3CHCl + Cl_2 \rightarrow CH_3CHCl_2 + Cl$	1.70×10^{-13}	$Cl\_ETHR + Cl2 \rightarrow Cl2\_ETH + Cl$	(Dobis and Benson, 2000)
122	$CH_3CHCl + O_2 \rightarrow CH_3CHClO_2$	1.04×10^{-11}	$Cl\_ETHR + O2 \rightarrow Cl\_ETHP$	(Knyazev et al., 1995)
123	$CH_2Cl + C_2H_2 \rightarrow CH_2Cl\text{-}CH=CH$	$8.35 \times 10^{22} T^{-11.54} \exp(-9661/T)$	$Cl\_MR + HC3R \rightarrow Cl\_OLTR$	(Knyazev, 2018)
124	$CH_2Cl + H_2 \rightarrow CH_3Cl + H$	$1.73 \times 10^{-21} T^{2.78} \exp(-5826/T)$	$Cl\_MR + H2 \rightarrow Cl\_CH4 + H$	(Bryukov et al., 2001)
125	$CH_2Cl + CH_2Cl \rightarrow CH_2ClCH_2Cl$	$3.56 \times 10^{-9} T^{-0.85}$	$Cl\_MR + Cl\_MR \rightarrow Cl2\_ETH$	(Roussel et al., 1991)
126	$CH_2Cl + HCl \rightarrow CH_3Cl + Cl$	$3.12 \times 10^{-17} T^{1.57} \exp(-2100/T)$	$Cl\_MR + HCl \rightarrow Cl\_CH4 + Cl$	(Brudnik et al., 2013a)
127	$CH_2Cl + HCl \rightarrow CH_2Cl_2 + H$	$1.71 \times 10^{-22} T^{2.85} \exp(-14312/T)$	$Cl\_MR + HCl \rightarrow Cl2\_CH4 + H$	(Bryukov et al., 2001)
128	$CH_2Cl + O_2 \rightarrow CH_2ClO_2$	$2.71 \times 10^{-9} T^{-1.20}$	$Cl\_MR + O2 \rightarrow Cl\_MO2$	(Burkholder et al., 2020)
129	$CH_2Cl + Cl_2 \rightarrow CH_2Cl_2 + Cl$	$2.11 \times 10^{-17} T^{1.43} \exp(390/T)$	$Cl\_MR + Cl2 \rightarrow Cl2\_CH4 + Cl$	(Brudnik et al., 2013b)
130	Chlorobenzene $+ OH \rightarrow$ 2-chlorophenyl $+ H_2O$	$3.64 \times 10^{-31} T^{6.01} \exp(320/T)$	$Cl\_TOL + HO \rightarrow Cl\_TOLR + H2O$	(Bryukov et al., 2009)
131	Chlorobenzene $+ OH \rightarrow$ 3-chlorophenyl $+ H_2O$	$5.17 \times 10^{-27} T^{4.74} \exp(140/T)$	$Cl\_TOL + HO \rightarrow Cl\_TOLR + H2O$	(Bryukov et al., 2009)
132	Chlorobenzene $+ OH \rightarrow$ 4-chlorophenyl $+ H_2O$	$1.10 \times 10^{-27} T^{4.83} \exp(177/T)$	$Cl\_TOL + HO \rightarrow Cl\_TOLR + H2O$	(Bryukov et al., 2009)
133	Chlorobenzene $+ OH \rightarrow$ Phenol $+ Cl$	$3.09 \times 10^{-19} T^{2.10} \exp(-1867/T)$	$Cl\_TOL + HO \rightarrow CSL + Cl$	(Bryukov et al., 2009)
134	$Cl_2 + CH_3CHCl \rightarrow CH_3CHCl_2 + Cl$	4.37×10^{-12}	$Cl2 + Cl\_ETHR \rightarrow Cl2\_ETH + Cl$	(Knyazev et al., 1995)
135	$Cl_2 + CH_3OCH_2 \rightarrow CH_3OCH_2Cl + Cl$	$1.79 \times 10^{-11} \exp(360/T)$	$Cl2 + HC3R \rightarrow Cl\_HC3 + Cl$	(Maricq et al., 1997)
136	$Cl_2 + C_2H_3 \rightarrow CH_2=CHCl + Cl$	$4.64 \times 10^{-12} \exp(-375/T)$	$Cl2 + ETER \rightarrow Cl\_ETE + Cl$	(Eskola and Timonen, 2003)
137	$Cl_2 + HCO \rightarrow HC(O)Cl + Cl$	$6.31 \times 10^{-12} \exp(-36/T)$	$Cl2 + HCHOR \rightarrow Cl\_HCHO + Cl$	(Timonen et al., 1988)
138	$Cl_2 + 1\text{-}C_4H_9 \rightarrow n\text{-}C_4H_9Cl + Cl$	$1.74 \times 10^{-5} T^{-2.38}$	$Cl2 + HC3R \rightarrow Cl\_HC3 + Cl$	(Eskola et al., 2007)
139	$Cl_2 + Phenyl \rightarrow$ Chlorobenzene $+ Cl$	$1.00 \times 10^{-12} \exp(1000/T)$	$Cl2 + TOLR \rightarrow Cl\_TOL + Cl$	(Tonokura et al., 2002)
140	$Cl_2 + sec\text{-}C_4H_9 \rightarrow sec\text{-}C_4H_9Cl + Cl$	6.79×10^{-12}	$Cl2 + HC3R \rightarrow Cl\_HC3 + Cl$	(Nesbitt and Leone, 1982)
141	$Cl_2 + CH_3 \rightarrow CH_3Cl + Cl$	$9.72 \times 10^{-20} T^{2.52} \exp(664/T)$	$Cl2 + MR \rightarrow Cl\_CH4 + Cl$	(Eskola et al., 2008)
142	$Cl_2 + 1\text{-}C_3H_7 \rightarrow n\text{-}C_3H_7Cl + Cl$	$1.46 \times 10^{-7} T^{-1.57}$	$Cl2 + HC3R \rightarrow Cl\_HC3 + Cl$	(Eskola et al., 2007)
143	$Cl_2 + C_2H_5 \rightarrow C_2H_5Cl + Cl$	$2.80 \times 10^{-7} T^{-1.73}$	$Cl2 + ETHR \rightarrow Cl\_ETH + Cl$	(Eskola et al., 2007)
144	$Cl_2 + iso\text{-}C_3H_7 \rightarrow iso\text{-}C_3H_7Cl + Cl$	$2.51 \times 10^{-11} \exp(241/T)$	$Cl2 + HC3R \rightarrow Cl\_HC3 + Cl$	(Timonen, 1988)
145	$Cl_2 + CH_2CH=CH_2 \rightarrow CH_2=CHCH_2Cl + Cl$	$1.55 \times 10^{-11} \exp(-2160/T)$	$Cl2 + OLTR \rightarrow Cl\_OLT + Cl$	(Timonen, 1988)
146	$Cl_2 + tert\text{-}C_4H_9 \rightarrow tert\text{-}C_4H_9Cl + Cl$	3.99×10^{-11}	$Cl2 + HC3R \rightarrow Cl\_HC3 + Cl$	(Timonen, 1988)
147	$CH_3OCl + Cl \rightarrow HCl + CH_2OCl$	2.00×10^{-1}	$Cl\_HC3 + Cl \rightarrow HCl + Cl\_HC3R$	(Carl et al., 1996)
148	$CH_3OCl + Cl \rightarrow CH_3O + Cl_2$	8.49×10^{-1}	$Cl\_HC3 + Cl \rightarrow Cl2 + HC3R$	(Kukui et al., 1997)
149	$CH_3OCl + OH \rightarrow H_2O + CH_2OCl$	$3.45 \times 10^{-20} T^{2.78} \exp(126/T)$	$Cl\_HC3 + HO \rightarrow H2O + Cl\_HC3R$	(He et al., 2005)
150	$CH_3OCl + OH \rightarrow CH_3O + HOCl$	$1.87 \times 10^{-21} T^{2.67} \exp(535/T)$	$Cl\_HC3 + HO \rightarrow HC3R + HOCl$	(He et al., 2005)
151	$CH_3OCl \rightarrow CH_3 + ClO$	$2.60 \times 10^{14} T^{0.77} \exp(-38950/T)$	$Cl\_HC3 \rightarrow MR + ClO$	(Brudnik et al., 2009)

Appendix

152	$CH_3OCl \rightarrow CH_3O + Cl$	$6.59 \times 10^{15} T^{-0.17} \exp(-25230/T)$	$Cl\_HC3 \rightarrow HC3R + Cl$	(Brudnik et al., 2009)
153	$ClCH_2OH \rightarrow CH_2O + HCl$	1.60×10^{-3}	$Cl\_HC3 \rightarrow HCHO + HCl$	(Tyndall et al., 1993)
154	$CH_2=CHCl + O \rightarrow CH_3 + ClCO$	1.40×10^{-13}	$Cl\_ETE + O \rightarrow MR + Cl\_HCHOR$	(Slagle et al., 1975)
155	$CH_2=CHCl + H \rightarrow CH_3CHCl$	$4.50 \times 10^{-12} T^{0.86} \exp(-75/T)$	$Cl\_ETE + H \rightarrow Cl\_ETHR$	(Knyazev et al., 1994)
156	$CH_2=CHCl + H \rightarrow CH_2CH_2Cl$	$2.49 \times 10^{-11} \exp(-2920/T)$	$Cl\_ETE + H \rightarrow Cl\_ETHR$	(Barat and Bozzelli, 1992)
157	$CH_2=CHCl + OH \rightarrow H_2O + CHCl=CH$	$5.81 \times 10^{-17} T^{2.00} \exp(-3170/T)$	$Cl\_ETE + HO \rightarrow H2O + Cl\_ETER$	(Yamada et al., 2001)
158	$CH_2=CHCl + OH \rightarrow H_2O + CH_2=CCl$	$3.02 \times 10^{-17} T^{2.00} \exp(-2214/T)$	$Cl\_ETE + HO \rightarrow H2O + Cl\_ETER$	(Yamada et al., 2001)
159	$CH_2=CHCl + OH \rightarrow CHClCH_2OH$	$1.25 \times 10^{-18} T^{2.10} \exp(805/T)$	$Cl\_ETE + HO \rightarrow Cl\_HC3R$	(Yamada et al., 2001)
160	$CH_2=CHCl + OH \rightarrow CHClOHCH_2$	$9.58 \times 10^{-20} T^{2.35} \exp(-1208/T)$	$Cl\_ETE + HO \rightarrow Cl\_HC3R$	(Yamada et al., 2001)
161	$CHCl=CH + O_2 \rightarrow CH_2O + ClCO$	$5.00 \times 10^{-12} \exp(-166/T)$	$Cl\_ETER + O2 \rightarrow HCHO + Cl\_HCHOR$	(Russell et al., 1989a)
162	$CHCl=CH + C_2H_2 \rightarrow C_2H_2C_2H_2Cl$	1.66×10^{-18}	$Cl\_ETER + HC3 \rightarrow Cl\_DIENR$	(Resende et al., 1998)
163	$HC(O)Cl + H \rightarrow HCO + HCl$	$1.16 \times 10^{-17} T^{1.90} \exp(-3017/T)$	$Cl\_HCHO + H \rightarrow HCHOR + HCl$	(Li and Luo, 2003)
164	$HC(O)Cl + H \rightarrow H_2 + ClCO$	$1.16 \times 10^{-19} T^{2.61} \exp(-1018/T)$	$Cl\_HCHO + H \rightarrow H2 + Cl\_HCHOR$	(Li and Luo, 2003)
165	$HC(O)Cl + OH \rightarrow ClCO + H_2O$	5.00×10^{-13}	$Cl\_HCHO + HO \rightarrow Cl\_HCHOR + H2O$	(Atkinson et al., 2001)
166	$ClCO + Cl \rightarrow CO + Cl_2$	$2.16 \times 10^{-9} \exp(-1666/T)$	$Cl\_HCHOR + Cl \rightarrow CO + Cl2$	(Baulch et al., 1981)
167	$CHCl_2 + O \rightarrow CO + HCl + Cl$	7.10×10^{-1}	$Cl2\_MR + O \rightarrow CO + HCl + Cl$	(Hold et al., 2009)
168	$CHCl_2 + H \rightarrow CHCl + HCl$	5.96	$Cl2\_MR + H \rightarrow Cl\_MR + HCl$	(Clark and Tedder, 1966)
169	$CHCl_2 + C_2H_5 \rightarrow C_2H_4 + CH_2Cl_2$	7.00×10^{-2}	$Cl2\_MR + ETHR \rightarrow ETE + Cl2\_CH4$	(Yu and Wijnen, 1970)
170	$CHCl_2 + H_2 \rightarrow CH_2Cl_2 + H$	$3.22 \times 10^{-22} T^{3.03} \exp(-16838/T)$	$Cl2\_MR + H2 \rightarrow Cl2\_CH4 + H$	(Bryukov et al., 2001)
171	$CHCl_2 + Toluene \rightarrow CH_2Cl_2 + Benzyl$	$1.66 \times 10^{-13} \exp(-4030/T)$	$Cl2\_MR + TOL \rightarrow Cl2\_CH4 + TOLR$	(Benson and Weissman, 1982)
172	$CH_2ClCH_2Cl + O \rightarrow OH + CH_2ClCHCl$	$8.15 \times 10^{-12} \exp(-2530/T)$	$Cl2\_ETH + O \rightarrow HO + Cl2\_ETHR$	(Barassin et al., 1977)
173	$CH_2ClCH_2Cl + OH \rightarrow H_2O + CH_2ClCHCl$	$8.92 \times 10^{-12} \exp(-1090/T)$	$Cl2\_ETH + HO \rightarrow H2O + Cl2\_ETHR$	(Xing et al., 1992)
174	$CH_3CHCl_2 + OH \rightarrow H_2O + CHCl_2CH_2$	1.22×10^{-15}	$Cl2\_ETH + HO \rightarrow H2O + Cl2\_ETHR$	(Chandra and Uchimaru, 1999)
175	$CH_3CHCl_2 + O(^3P) \rightarrow OH + CHCl_2CH_2$	$1.09 \times 10^{-18} T^{2.30} \exp(-5644/T)$	$Cl2\_ETH + O3P \rightarrow HO + Cl2\_ETHR$	(Zhang et al., 2003)
176	$CH_3CHCl_2 + O(^3P) \rightarrow OH + CH_3CCl_2$	$2.60 \times 10^{-21} T^{2.95} \exp(-1423/T)$	$Cl2\_ETH + O3P \rightarrow HO + Cl2\_ETHR$	(Zhang et al., 2003)
177	$CH_2ClCHCl + O_2 \rightarrow CH_2ClCHClO_2$	2.41×10^{-12}	$Cl2\_ETHR + O2 \rightarrow Cl2\_ETHP$	(Wallington et al., 1996a)
178	$CH_2ClO_2 + CH_2ClO_2 \rightarrow O_2 + 2 CH_2ClO$	$2.00 \times 10^{-13} \exp(870/T)$	$2 Cl\_MO2 \rightarrow O2 + 2Cl\_HC3R$	(Atkinson et al., 2001)
179	$CH_2ClO_2 + NO \rightarrow NO_2 + CH_2ClO$	$7.01 \times 10^{-12} \exp(300/T)$	$Cl\_MO2 + NO \rightarrow Cl\_HC3R + NO2$	(Burkholder et al., 2020)
180	$CH_2ClO_2 + HO_2 \rightarrow O_2 + CH_2ClOOH$	$3.20 \times 10^{-13} \exp(820/T)$	$Cl\_MO2 + HO2 \rightarrow O2 + Cl\_OP1$	(Atkinson et al., 2001)
181	$CH_2ClO_2 + HO_2 \rightarrow HC(O)Cl + H_2O + O_2$	7.29×10^{-1}	$Cl\_MO2 + HO2 \rightarrow Cl\_HCHO + H2O + O2$	(Wallington et al., 1996b)
182	$CH_3CHClO_2 + CH_3CHClO_2 \rightarrow 2 CH_3CHClO + O_2$	4.90×10^{-12}	$2Cl\_ETHP \rightarrow 2 Cl\_HC3R + O2$	(Maricq et al., 1993a)
183	$CH_2OH + Cl_2 \rightarrow ClCH_2OH + Cl$	2.90×10^{-11}	$Cl2 + HC3R \rightarrow Cl\_HC3 + Cl$	(Tyndall et al., 1999)
184	$CHClOHCH_2 \rightarrow CH_2=CHCl + OH$	$3.67 \times 10^{10} T^{0.91} \exp(-15399/T)$	$Cl\_HC3 \rightarrow Cl\_ETE + HO$	(Yamada et al., 2001)
185	$C_2H_2 + Cl_2 \rightarrow Cl + CHCl=CH$	1.66×10^{-38}	$Cl2 + HC3 \rightarrow Cl\_ETER + Cl$	(Resende et al., 1998)
186	$C_2H_2 + Cl \rightarrow CH_2=CCl$	$4.55 \times 10^{-70} T^{-3.00}$	$Cl + HC3 \rightarrow Cl\_ETER$	(Atkinson et al., 2001)
187	$CH_2ClCH_2O \rightarrow CH_2ClCHO + H$	$1.94 \times 10^{9} T^{1.88} \exp(-10080/T)$	$Cl\_HC3R \rightarrow Cl\_ALD + H$	(Zhu et al., 1999)

Appendix

188	$CH_3CHClO \rightarrow CH_3 + HC(O)Cl$	$1.70 \times 10^8 \exp(-5142/T)$	$Cl\_HC3R \rightarrow Cl\_HCHO + MR$	(Hou *et al.*, 2000)
189	$CHClCH_2OH \rightarrow CHOH=CHCl + H$	$3.10 \times 10^7 \ T^{1.69} \exp(-19003/T)$	$Cl\_HC3R \rightarrow Cl\_ETE + H$	(Zhu *et al.*, 1999)
190	$CHClOHCH_2 \rightarrow CH_2ClCHO + H$	$2.32 \times 10^9 \ T^{1.06} \exp(-18282/T)$	$Cl\_HC3R \rightarrow Cl\_ALD + H$	(Zhu *et al.*, 1999)
191	$CH_2ClO + O_2 \rightarrow HC(O)Cl + HO_2$	$2.00 \times 10^{-12} \exp(-935/T)$	$Cl\_HC3R + O2 \rightarrow Cl\_HCHO + HO2$	(Wu and Carr, 2001)
192	$CHCl_2CO \rightarrow CO + CHCl_2$	$1.10 \times 10^{14} \exp(-4426/T)$	$Cl2\_ALDR \rightarrow Cl2\_MR + CO$	(Méreau *et al.*, 2001)
193	$C_2H_2 + Cl \rightarrow CH_2CH_2Cl$	1.11×10^{-29}	$Cl + HC3 \rightarrow Cl\_ETHR$	(Zhu *et al.*, 1993)
194	$CH_2ClCHClO_2 \rightarrow O_2 + CH_2ClCHCl$	$1.10 \times 10^{13} \exp(-12148/T)$	$Cl2\_ETHP \rightarrow Cl2\_ETHR + O2$	(Bertrand *et al.*, 1972)
195	$CHCl_2 + O_2 \rightarrow CHCl_2O_2$	$8.18 \times 10^{-9} \ T^{-1.40}$	$Cl2\_MR + O2 \rightarrow Cl2\_MO2$	(Burkholder *et al.*, 2020)
196	Phenol + $Cl_2 \rightarrow$ 2-Chlorophenol + HCl	2.80×10	$Cl2 + CSL \rightarrow Cl\_CSL + HCl$	(Platz *et al.*, 1998)
197	2-Chlorophenol + O $\rightarrow$ 2-chlorophenoxy + OH	$2.13 \times 10^{-11} \exp(-1459/T)$	$Cl\_CSL + O \rightarrow Cl\_PHO + HO$	(Evans and Dellinger, 2005)
198	2-Chlorophenol + OH $\rightarrow$ 2-chlorophenoxy + H_2O	$3.44 \times 10^{-21} \ T^{2.68} \exp(-1070/T)$	$Cl\_CSL + HO \rightarrow Cl\_PHO + H2O$	(Altarawneh *et al.*, 2008)
199	2-Chlorophenol $\rightarrow$ Cl + Phenyl, 2-hydroxy-	$1.05 \times 10^{13} \ T^{0.45} \exp(-43058/T)$	$Cl\_CSL \rightarrow Cl + PHO$	(Altarawneh *et al.*, 2008)

Appendix

Appendix A.III-2: Inorganic chlorine gas-phase mechanism

Table A.III-3: *Classification of the inorganic chlorinated species.*

Inorganic chlorinated class	Species
Cl_x	Cl, Cl_2, Cl_3
Cl_xO_y	ClO, ClO_2, $OClO$, ClO_3, ClO_4, Cl_2O, Cl_2O_2, Cl_2O_4
$ClNO_x$	$ClNO$, $ClNO_2$, $ClONO_2$, $NOClO_4$
$HClO_x$	HCl, $HOCl$, $HOClO$, $HOClO_2$, $HOClO_3$

Table A.III-4: *Inorganic chlorine gas-phase mechanism.*

#	Reaction	Rate constant (s^{-1}) or $(cm^3$ molecule^{-1} s$^{-1})$ or $(cm^6$ molecule^{-2} s$^{-1})$	Literature
1	$HCl + H \rightarrow Cl + H_2$	2.01×10^{-11} exp(-1790/T)	(Kita and Stedman, 1982)
2	$HCl + OH \rightarrow Cl + H_2O$	1.70×10^{-12} exp(-230/T)	(Atkinson *et al.*, 2007)
3	$HCl + Cl \rightarrow Cl_2 + H$	1.66×10^{-7} exp(-23935/T)	(Baulch *et al.*, 1981)
4	$HCl + NO \rightarrow Cl + HNO$	2.62×10^{-11} exp(-25270/T)	(Higashihara *et al.*, 1978)
5	$HCl + NO_2 \rightarrow Cl + HONO$	6.61×10^{-13} exp(-11805/T)	(Rosser and Wise, 1960)
6	$HCl + NO_3 \rightarrow Cl + HNO_3$	5.00×10^{-17}	(Mellouki *et al.*, 1989)
7	$HCl + N_2O_5 \rightarrow ClNO_2 + HNO_3$	8.40×10^{-21}	(Leu *et al.*, 1989)
8	$HCl + O(^3P) \rightarrow Cl + OH$	1.00×10^{-18} $T^{2.11}$ exp(-2025/T)	(Xie *et al.*, 2003)
9	$HCl + O(^1D) \rightarrow Cl + OH$	1.00×10^{-10}	(Chichinin, 2000)
10	$HCl + O(^1D) \rightarrow ClO + H$	3.60×10^{-11}	(Chichinin, 2000)
11	$HCl + O_3 \rightarrow HOCl + O_2$	4.70×10^{-24}	(Leu *et al.*, 1989)
12	$HCl + HONO \rightarrow ClNO + H_2O$	1.15×10^{-22} $T^{3.12}$ exp(-5870/T)	(Lu *et al.*, 2000)
13	$HCl + HNO_4 \rightarrow HOCl + HNO_3$	9.00×10^{-22}	(Leu *et al.*, 1989)
14	$HCl + ClONO_2 \rightarrow Cl_2 + HNO_3$	2.01×10^{-20}	(Atkinson *et al.*, 1989)
15	$HOCl + H \rightarrow HCl + OH$	5.27×10^{-15} $T^{1.2}$ exp(-188/T)	(Wang *et al.*, 2003)
16	$HOCl + H \rightarrow ClO + H_2$	7.31×10^{-28} $T^{4.89}$ exp(-214/T)	(Wang *et al.*, 2003)
17	$HOCl + HNO \rightarrow Cl + NO + H_2O$	5.77×10^{-22} $T^{3.06}$ exp(-3055/T)	(Xu and Lin, 2010a)
18	$HOCl + HONO \rightarrow ClNO_2 + H_2O$	1.35×10^{-22} $T^{2.86}$ exp(-1405/T)	(Xu and Lin, 2010a)
19	$HOCl + HNO_3 \rightarrow ClONO_2 + H_2O$	4.24×10^{-23} $T^{3.08}$ exp(-25271/T)	(Xu and Lin, 2010a)
20	$HOCl + OH \rightarrow ClO + H_2O$	3.01×10^{-12} exp(-500/T)	(Burkholder *et al.*, 2020)
21	$HOCl + Cl \rightarrow HCl + ClO$	5.91×10^{-25} $T^{4.07}$ exp(170/T)	(Wang *et al.*, 2003)
22	$HOCl + Cl \rightarrow Cl_2 + OH$	2.45×10^{-16} $T^{1.39}$ exp(177/T)	(Bryukov *et al.*, 2004)

Appendix

23	$HOCl + ClO \rightarrow Cl_2O + OH$	$2.29 \times 10^{-17}\, T^{1.77}\, \exp(-9386/T)$	(Xu and Lin, 2010b)
24	$HOCl + ClO_2 \rightarrow HOClO + ClO$	$1.08 \times 10^{-21}\, T^{2.48}\, \exp(-11666/T)$	(Xu and Lin, 2010b)
25	$HOCl + ClO_3 \rightarrow HOClO_2 + ClO$	$3.87 \times 10^{-30}\, T^{5.45}\, \exp(-3867/T)$	(Xu and Lin, 2010b)
26	$HOCl + ClO_3 \rightarrow Cl_2O_3 + OH$	$2.79 \times 10^{-17}\, T^{2.04}\, \exp(-8231/T)$	(Xu and Lin, 2010b)
27	$HOCl + HOCl \rightarrow Cl_2O + H_2O$	$1.13 \times 10^{-22}\, T^{3.03}\, \exp(-11686/T)$	(Xu and Lin, 2010a)
28	$HOCl + ClO_4 \rightarrow OH + HOClO_3$	$1.35 \times 10^{-18}\, T^{1.73}\, \exp(-1017/T)$	(Xu and Lin, 2010b)
29	$HOCl + O(^3P) \rightarrow ClO + OH$	$1.05 \times 10^{-16}\, T^{1.46}\, \exp(-469/T)$	(Wang $et\ al.$, 2005)
30	$Cl + H_2 \rightarrow HCl + H$	$4.77 \times 10^{-16}\, T^{1.58}\, \exp(-1610/T)$	(Kumaran $et\ al.$, 1994)
31	$Cl + H_2O \rightarrow HCl + OH$	$1.94 \times 10^{-16}\, T^{1.67}\, \exp(-7679/T)$	(Bryukov $et\ al.$, 2006)
32	$Cl + H_2O_2 \rightarrow HCl + HO_2$	$1.10 \times 10^{-11}\, \exp(-981/T)$	(Atkinson $et\ al.$, 2007)
33	$Cl + OH \rightarrow HCl + O(^3P)$	$9.80 \times 10^{-12}\, \exp(-2860/T)$	(Baulch $et\ al.$, 1981)
34	$Cl + OH \rightarrow ClO + H$	$2.51 \times 10^{-10}\, \exp(-32232/T)$	(Garrett and Truhlar, 1979)
35	$Cl + HO_2 \rightarrow HCl + O_2$	$1.40 \times 10^{-11}\, \exp(270/T)$	(Hickson and Keyser, 2005)
36	$Cl + HO_2 \rightarrow ClO + OH$	$3.60 \times 10^{-11}\, \exp(-375/T)$	(Hickson and Keyser, 2005)
37	$Cl + HONO \rightarrow HCl + NO_2$	$5.86 \times 10^{-13}\, \exp(1152/T)$	(Anglada and Solé, 2017)
38	$Cl + Cl + M \rightarrow Cl_2 + M$	$6.15 \times 10^{-34}\, \exp(906/T)$	(Baulch $et\ al.$, 1981)
39	$Cl + Cl_2 \rightarrow Cl_3$	1.51×10^{-16}	(Hutton and Wright, 1965)
40	$Cl + Cl_3 \rightarrow 2\,Cl_2$	2.82×10^{-10}	(Hutton and Wright, 1965)
41	$Cl + ClNO \rightarrow Cl_2 + NO$	$5.80 \times 10^{-11}\, \exp(100/T)$	(Burkholder $et\ al.$, 2020)
42	$Cl + ClNO_2 \rightarrow Cl_2 + NO_2$	5.50×10^{-12}	(Nelson and Johnston, 1981)
43	$Cl + ClONO_2 \rightarrow Cl_2 + NO_3$	$6.20 \times 10^{-12}\, \exp(146/T)$	(Atkinson $et\ al.$, 2007)
44	$Cl + ClO \rightarrow Cl_2O$	$4.55 \times 10^{-11}\, T^{0.07}\, \exp(-94/T)$	(Xu and Lin, 2010c)
45	$Cl + ClO \rightarrow Cl_2 + O(^3P)$	$2.18 \times 10^{-14}\, T^{1}\, \exp(-4762/T)$	(Xu and Lin, 2010c)
46	$Cl + ClO_2 \rightarrow 2\,ClO$	$3.20 \times 10^{-11}\, \exp(170/T)$	(Atkinson $et\ al.$, 2007)
47	$Cl + OClO \rightarrow 2\,ClO$	1.20×10^{-11}	(Burkholder $et\ al.$, 2020)
48	$Cl + OClO \rightarrow Cl_2 + O_2$	2.31×10^{-10}	(Burkholder $et\ al.$, 2020)
49	$Cl + ClO_4 \rightarrow ClO_3 + ClO$	$7.96 \times 10^{-11}\, T^{0.16}\, \exp(-49/T)$	(Xu and Lin, 2003)
50	$Cl + Cl_2O \rightarrow Cl_2 + ClO$	$6.20 \times 10^{-11}\, \exp(130/T)$	(Atkinson $et\ al.$, 2007)
51	$Cl + Cl_2O_2 \rightarrow Cl_2O + ClO$	$2.19 \times 10^{-14}\, T^{0.7}\, \exp(-1110/T)$	(Zhu and Lin, 2003a)
52	$Cl + Cl_2O_2 \rightarrow Cl_2 + OClO$	$7.60 \times 10^{-11}\, \exp(65/T)$	(Atkinson $et\ al.$, 2007)
53	$Cl + HOClO_3 \rightarrow HOCl + ClO_3$	$1.33 \times 10^{-12}\, T^{0.67}\, \exp(-9657/T)$	(Zhu and Lin, 2010)
54	$Cl + HOClO_3 \rightarrow HCl + ClO_4$	$1.75 \times 10^{-16}\, T^{1.63}\, \exp(-11156/T)$	(Zhu and Lin, 2010)
55	$Cl + NO + M \rightarrow ClNO + M$	$1.26 \times 10^{-27}\, T^{-1.39}\, \exp(-173/T)$	(Troe, 1979)
56	$Cl + NO_2 \rightarrow ClNO_2$	$k_0 = 1.30 \times 10^{-30}\, (T/298)^{-2},\ k_\infty = 1.00 \times 10^{-10}\, (T/298)^{-1},\ F_c = 0.6$	(Golden, 2007)
57	$Cl + NO_3 \rightarrow ClO + NO_2$	2.26×10^{-11}	(Becker $et\ al.$, 1991)
58	$Cl + N_2O \rightarrow ClO + N_2$	$1.28 \times 10^{-10}\, \exp(-16360/T)$	(Lesar $et\ al.$, 1996)
59	$Cl + HNO_3 \rightarrow HCl + NO_3$	2.00×10^{-16}	(Atkinson $et\ al.$, 2001)
60	$Cl + O_2 \rightarrow ClO + O(^3P)$	$1.46 \times 10^{-9}\, \exp(-27677/T)$	(Baulch $et\ al.$, 1981)
61	$Cl + O_3 \rightarrow ClO + O_2$	$2.80 \times 10^{-11}\, \exp(-250/T)$	(Atkinson et al., 2007)
62	$Cl_2 + H \rightarrow HCl + Cl$	8.66×10^{-12}	(Dobis and Benson, 2002)
63	$Cl_2 + OH \rightarrow HOCl + Cl$	$3.59 \times 10^{-16}\, T^{1.35}\, \exp(-745/T)$	(Bryukov $et\ al.$, 2004)

Appendix

64	$Cl_2 + O(^3P) \rightarrow ClO + Cl$	6.90×10^{-14}	(Larin $et\ al.$, 2009)
65	$Cl_2 + O(^1D) \rightarrow ClO + Cl$	$1.29 \times 10^{-10}\ T^{-0.19}\ exp(-45/T)$	(Xu and Lin, 2010c)
66	$Cl_2 + O(^1D) \rightarrow Cl_2 + O(^3P)$	2.19×10^{-10}	(Fletcher and Husain, 1976)
67	$Cl_2 + O_3 \rightarrow OClO + ClO$	2.99×10^{-28}	(Bodenstein $et\ al.$, 1929)
68	$Cl_2 \rightarrow 2\ Cl$	$1.41 \times 10^{-8}\ exp(-28160/T)$	(Huybrechts $et\ al.$, 1996)
69	$Cl_2 + OClO \rightarrow Cl_2O + ClO$	3.40×10^{-12}	(Baer et al., 1991)
70	$Cl_2 + NO \rightarrow ClNO + Cl$	$2.94 \times 10^{-15}\ exp(-6700/T)$	(Ashmore and Spencer, 1959)
71	$Cl_2 + 2NO \rightarrow 2\ ClNO$	$1.14 \times 10^{-37}\ exp(-2280/T)$	(Hisatsune and Zafonte, 1969)
72	$ClNO + ClNO \rightarrow Cl_2 + 2\ NO$	$5.25 \times 10^{-12}\ exp(-11800/T)$	(Deklau and Palmer, 1961)
73	$ClNO + O(^3P) \rightarrow ClO + NO$	$8.30 \times 10^{-12}\ exp(-1520/T)$	(Abbatt $et\ al.$, 1989)
74	$ClNO + ClO \rightarrow ClNO_2 + Cl$	3.32×10^{-17}	(Knauth, 1978)
75	$ClNO + ClONO_2 \rightarrow Cl_2 + 2NO_2$	1.96×10^{-20}	(Knauth, 1978)
76	$ClNO + H \rightarrow HCl + NO$	1.96×10^{-11}	(Wategaonkar and Setser, 1989)
77	$ClNO + NO_3 \rightarrow ClNO_2 + NO_2$	1.00×10^{-14}	(Cantrell $et\ al.$, 1987)
78	$ClNO + NO_2 \rightarrow ClNO_2 + NO$	$2.96 \times 10^{-16}\ exp(-3350/T)$	(Sharma and Sood, 1974)
79	$ClNO + N_2O_5 \rightarrow ClNO_2 + N_2O_4$	9.00×10^{-18}	(Cantrell $et\ al.$, 1987)
80	$ClNO + H_2O \rightarrow HCl + HONO$	7.41×10^{-22}	(Karlsson and LjungstrÖm, 1996)
81	$ClNO + OH \rightarrow HOCl + NO$	$9.00 \times 10^{-12}\ exp(-1130/T)$	(Abbatt $et\ al.$, 1989)
82	$ClNO + OH \rightarrow Cl + HONO$	$4.71 \times 10^{-18}\ T^{1.74}\ exp(247/T)$	(Abbatt $et\ al.$, 1989)
83	$ClNO_2 \rightarrow Cl + NO_2$	$7.26 \times 10^{19}\ T^{-1.89}\ exp(-16838/T)$	(Zhu and Lin, 2011)
84	$ClNO_2 + NO \rightarrow ClNO + NO_2$	$2.34 \times 10^{-12}\ exp(-3470/T)$	(Wilkins $et\ al.$, 1974)
85	$ClNO_2 + OH \rightarrow HOCl + NO_2$	$2.40 \times 10^{-12}\ exp(-1250/T)$	(Atkinson $et\ al.$, 2007)
86	$ClO + H_2 \rightarrow HOCl + H$	1.10×10^{-20}	(Su $et\ al.$, 1979)
87	$ClO + H_2 \rightarrow HCl + OH$	4.98×10^{-16}	(Clyne $et\ al.$, 1968)
88	$ClO + OH \rightarrow HCl + O_2$	$6.30 \times 10^{-13}\ exp(230/T)$	(Burkholder $et\ al.$, 2020)
89	$ClO + OH \rightarrow Cl + HO_2$	$7.40 \times 10^{-12}\ exp(270/T)$	(Burkholder $et\ al.$, 2020)
90	$ClO + HO_2 \rightarrow HOCl + O_2$	$2.60 \times 10^{-12}\ exp(290/T)$	(Burkholder $et\ al.$, 2020)
91	$ClO + HO_2 \rightarrow HCl + O_3$	2.10×10^{-14}	(Atkinson $et\ al.$, 1989)
92	$ClO + HO_2 \rightarrow ClO_2 + OH$	$2.22 \times 10^{-21}\ T^{2.32}\ exp(-2565/T)$	(Zhu and Lin, 2011)
93	$ClO + HO_2 \rightarrow OClO + OH$	$7.60 \times 10^{-19}\ T^{1.80}\ exp(-1065/T)$	(Zhu and Lin, 2011)
94	$ClO + HO_2 \rightarrow HOClO_2$	$9.03 \times 10^{-17}\ T^{1.22}\ exp(898/T)$	(Xu $et\ al.$, 2003a)
95	$ClO + H_2O_2 \rightarrow HOCl + HO_2$	5.06×10^{-13}	(Su $et\ al.$, 1979)
96	$ClO + ClO \rightarrow Cl_2 + O_2$	$2.90 \times 10^{-14}\ exp(-283/T)$	(Ferracci and Rowley, 2012)
97	$ClO + ClO \rightarrow 2\ Cl + O_2$	4.20×10^{-1}	(Horowitz $et\ al.$, 1993)
98	$ClO + ClO \rightarrow Cl + OClO$	$3.50 \times 10^{-13}\ exp(-1370/T)$	(Atkinson $et\ al.$, 2007)
99	$ClO + ClO \rightarrow Cl + ClO_2$	$3.00 \times 10^{-11}\ exp(-2450/T)$	(Atkinson $et\ al.$, 2007)
100	$ClO + ClO + M \rightarrow Cl_2O_2 + M$	$k_0 = 1.90 \times 10^{-32}\ (T/298)^{-3.6},\ k_\infty = 3.70 \times 10^{-12}\ (T/298)^{-1.6},\ F_c = 0.6$	(Burkholder $et\ al.$, 2020)
101	$ClO + ClO_2 \rightarrow Cl_2O_3$	3.00×10^{-10}	(Zhu and Lin, 2011)
102	$ClO + ClO_2 \rightarrow OClO + ClO$	$1.18 \times 10^{-29}\ T^{2.80}\ exp(-78/T)$	(Zhu and Lin, 2003b)
103	$ClO + ClO_2 \rightarrow Cl_2O + O_2$	$1.11 \times 10^{-27}\ T^{2.40}\ exp(-1670/T)$	(Zhu and Lin, 2003b)
104	$ClO + ClO_3 \rightarrow 2\ ClO_2$	$1.42 \times 10^{-18}\ T^{2.11}\ exp(-2870/T)$	(Xu and Lin, 2003)

Appendix

105	ClO + ClO$_3$ → OClO + ClO$_2$	1.85×10^{-18} T$^{2.28}$ exp(-2419/T)	(Xu and Lin, 2003)
106	ClO + ClO$_3$ → Cl$_2$O$_4$	8.61×10^{15} T$^{-9.75}$ exp(-1727/T)	(Xu and Lin, 2003)
107	ClO + Cl$_2$O → OClO + Cl$_2$	4.32×10^{-16}	(Basco $et\ al.$, 1971a)
108	ClO + Cl$_2$O → Cl$_2$ + Cl + O$_2$	1.80×10^{-15}	(Basco $et\ al.$, 1971a)
109	ClO + NO → Cl + NO$_2$	6.20×10^{-12} exp(295/T)	(Atkinson $et\ al.$, 2007)
110	ClO + NO$_2$ + M → ClONO$_2$ + M	$k_0 = 1.80 \times 10^{-31}$ (T/298)$^{-3.4}$, $k_\infty = 1.50 \times 10^{-11}$ (T/298)$^{-1.9}$, $F_c = 0.6$	(Burkholder $et\ al.$, 2020)
111	ClO + NO$_3$ → ClO$_2$ + NO$_2$	1.46×10^{-13}	(Kukui, A. $et\ al.$, 1994)
112	ClO + NO$_3$ → OClO + NO$_2$	4.70×10^{-13}	(Burkholder $et\ al.$, 2020)
113	ClO + NO$_3$ → Cl + O$_2$ + NO$_2$	7.50×10^{-1}	(Boyd $et\ al.$, 1996)
114	ClO + HONO → HOCl + NO$_2$	8.56×10^{-16} exp(-891/T)	(Anglada and Solé, 2017)
115	ClO + O(^{3}P) → Cl + O$_2$	2.50×10^{-11} exp(109/T)	(Atkinson $et\ al.$, 2007)
116	ClO + O(^{3}P) → ClO$_2$	4.33×10^{-11} T$^{-0.03}$ exp(43/T)	(Zhu and Lin, 2003c)
117	ClO + O$_3$ → ClO$_2$ + O$_2$	1.00×10^{-18}	(Wongdontri-Stuper $et\ al.$, 1979)
118	ClO + O$_3$ → OClO + O$_2$	1.00×10^{-18}	(Wongdontri-Stuper $et\ al.$, 1979)
119	ClO + O$_3$ → Cl + 2 O$_2$	5.25×10^{-15}	(Clyne $et\ al.$, 1968)
120	ClO$_2$ + H → ClO + OH	7.80×10^{-11}	(Wategaonkar and Setser, 1989)
121	ClO$_2$ + OH → HOClO$_2$	1.36×10^{4} T$^{-6.61}$ exp(-537/T)	(Xu $et\ al.$, 2003b)
122	ClO$_2$ + OH → HOCl + O$_2$	5.47×10^{-20} T$^{2.07}$ exp(2065/T)	(Xu $et\ al.$, 2003b)
123	ClO$_2$ + OH → ClO + HO$_2$	1.22×10^{-22} T$^{2.75}$ exp(1682/T)	(Xu $et\ al.$, 2003b)
124	ClO$_2$ + NO → ClO + NO$_2$	1.04×10^{-13} exp(348/T)	(Li $et\ al.$, 2002)
125	ClO$_2$ + NO$_3$ → NOClO$_4$	2.01×10^{-14}	(Friedl $et\ al.$, 1992)
126	ClO$_2$ + NO$_3$ → ClO + NO$_2$ + O$_2$	2.01×10^{-15}	(Friedl $et\ al.$, 1992)
127	ClO$_2$ + O(^{3}P) → ClO$_3$	1.18×10^{-10} T$^{-0.04}$ exp(51/T)	(Zhu and Lin, 2002)
128	ClO$_2$ + O(^{3}P) → ClO + O$_2$	1.00×10^{-16} T$^{1.44}$ exp(-469/T)	(Zhu and Lin, 2002)
129	ClO$_2$ + O$_3$ → ClO$_3$ + O$_2$	2.10×10^{-12} exp(-4700/T)	(Atkinson $et\ al.$, 2007)
130	ClO$_2$ → Cl + O$_2$	1.11×10^{16} T$^{-0.28}$ exp(-29587/T)	(Zhu and Lin, 2003c)
131	OClO + NO → ClO + NO$_2$	1.48×10^{-24} T$^{3.99}$ exp(1711T)	(Raghunath and Lin, 2012)
132	OClO + NO → ClNO + O$_2$	2.65×10^{-16} T$^{1.91}$ exp(342/T)	(Raghunath and Lin, 2012)
133	OClO + NO$_2$ → ClO + NO$_3$	7.07×10^{-23}	(Martin and Kohnlein, 1958)
134	OClO + O(^{3}P) → ClO + O$_2$	4.98×10^{-11}	(Basco $et\ al.$, 1971b)
135	OClO + H → ClO + OH	5.65×10^{-11}	(Baulch $et\ al.$, 1981)
136	ClO$_2$ → Cl + O$_2$	6.17×10^{15} T$^{-0.46}$ exp(-2570/T)	(Zhu and Lin, 2003c)
137	ClO$_3$ + O$_3$ → OClO + 2 O$_2$	1.53×10^{-18}	(Bodenstein $et\ al.$, 1929)
138	Cl$_2$O + O(^{3}P) → 2 ClO	2.71×10^{-11} exp(-510/T)	(Stevens and Anderson, 1992)
139	Cl$_2$O + H → HCl + ClO	4.10×10^{-11}	(Wategaonkar and Setser, 1989)
140	Cl$_2$O + NO$_2$ → ClO + ClNO$_2$	7.22×10^{-14} exp(-5840/T)	(Martin $et\ al.$, 1960)
141	Cl$_2$O → ClO + Cl	1.88×10^{17} T$^{-0.75}$ exp(-16477/T)	(Xu and Lin, 2010a)
142	Cl$_2$O + H$_2$O → 2HOCl	1.21×10^{-21} T$^{2.82}$ exp(-13237/T)	(Xu and Lin, 2010b)
143	Cl$_2$O + OH → ClO + HOCl	6.47×10^{-16} T$^{1.39}$ exp(415/T)	(Xu and Lin, 2010c)
144	Cl$_2$O$_2$ + O$_3$ → OClO + ClO + O$_2$	1.00×10^{-19}	(DeMore and Tschuikow-Roux, 1990)
145	Cl$_2$O$_2$ + M → ClO + ClO + M	3.70×10^{-7} exp(-7694/T)	(Atkinson $et\ al.$, 2007)

Appendix

146	$Cl_2O_2 + OH \rightarrow OClO + HOCl$	$6.00 \times 10^{-13} \exp(670/T)$	(Hansen *et al.*, 2008)
147	$Cl_2O_3 \rightarrow ClO + ClO_2$	1.80×10^5	(Atkinson *et al.*, 2007)
148	$ClONO_2 \rightarrow ClO + NO_2$	$2.76 \times 10^{-6} \exp(-11406/T)$	(Anderson and Fahey, 1990)
149	$ClONO_2 + H_2O \rightarrow HOCl + HNO_3$	5.00×10^{-21}	(Atkinson *et al.*, 1989)
150	$HOClO_3 + H \rightarrow HOClO_2 + OH$	$6.08 \times 10^{-17} T^{1.96} \exp(-7733/T)$	(Zhu and Lin, 2010)
151	$HOClO_3 + H \rightarrow ClO_4 + H_2$	$1.07 \times 10^{-17} T^{1.97} \exp(-7485/T)$	(Zhu and Lin, 2010)
152	$HOClO_3 + OH \rightarrow ClO_4 + H_2O$	$1.24 \times 10^{-8} T^{-2.99} \exp(1665/T)$	(Zhu and Lin, 2010)

Appendix

Appendix A.III-3: Photolysis reactions of organic chlorinated species

The photolysis constants **J** presented in this appendix were calculated under clear skies in early January for a latitude of 51 °N (at ground level: $\lambda > 280$ nm and for solar zenith angle of 35°).

$CCl_4 + h\nu \rightarrow Cl + CCl_3$		$J = 0.00 \times 10^{-0}$ s^{-1}	$\varphi1 = 1$		**D01**
$CCl_4 + h\nu \rightarrow 2\ Cl + CCl_2$		$J = 0.00 \times 10^{-0}$ s^{-1}	$\varphi2 = 0$		**D02**

λ (nm)	σ (cm² molecule^{-1})	λ (nm)	σ (cm² molecule^{-1})	λ (nm)	σ (cm² molecule^{-1})
174	9.56×10^{-18}	196	6.95×10^{-19}	218	2.38×10^{-19}
176	1.01×10^{-17}	198	6.80×10^{-19}	220	1.89×10^{-19}
178	9.83×10^{-18}	200	6.78×10^{-19}	222	1.47×10^{-19}
180	8.06×10^{-18}	202	6.48×10^{-19}	224	1.13×10^{-19}
182	6.47×10^{-18}	204	6.19×10^{-19}	226	8.53×10^{-20}
184	4.79×10^{-18}	206	5.79×10^{-19}	228	6.63×10^{-20}
186	3.39×10^{-18}	208	5.30×10^{-19}	230	4.71×10^{-20}
188	2.27×10^{-18}	210	4.74×10^{-19}	232	3.48×10^{-20}
190	1.46×10^{-18}	212	4.13×10^{-19}	234	2.57×10^{-20}
192	9.96×10^{-19}	214	3.52×10^{-19}		
194	7.67×10^{-19}	216	2.93×10^{-19}		

For ($174 < \lambda < 192$): The values of the cross sections are from Hubrich and Stuhl (1980), and those of the quantum yields are taken from Simon *et al*. (1988).

For ($194 < \lambda < 198$): The values of the cross sections are from Simon *et al*. (1988).

For ($200 < \lambda < 234$): The values of the cross sections are from Rontu Carlon *et al*. (2010).

CH$_3$OCl + hν → CH$_3$O + Cl J = 1.98 × 10^{-5} s^{-1} φ1 = 0.95 **D03**
CH$_3$OCl + hν → CH$_2$O + HCl J = 1.04 × 10^{-6} s^{-1} φ2 = 0.05 **D04**

λ (nm)	σ (cm² molecule^{-1})	λ (nm)	σ (cm² molecule^{-1})	λ (nm)	σ (cm² molecule^{-1})
230	1.49 × 10^{-19}	286	1.33 × 10^{-20}	342	8.75 × 10^{-21}
232	1.54 × 10^{-19}	288	1.32 × 10^{-20}	344	8.22 × 10^{-21}
234	1.57 × 10^{-19}	290	1.32 × 10^{-20}	346	7.60 × 10^{-21}
236	1.59 × 10^{-19}	292	1.34 × 10^{-20}	348	7.09 × 10^{-21}
238	1.58 × 10^{-19}	294	1.35 × 10^{-20}	350	6.62 × 10^{-21}
240	1.55 × 10^{-19}	296	1.37 × 10^{-20}	352	6.11 × 10^{-21}
242	1.49 × 10^{-19}	298	1.40 × 10^{-20}	354	5.74 × 10^{-21}
244	1.42 × 10^{-19}	300	1.43 × 10^{-20}	356	5.29 × 10^{-21}
246	1.32 × 10^{-19}	302	1.45 × 10^{-20}	358	4.82 × 10^{-21}
248	1.22 × 10^{-19}	304	1.47 × 10^{-20}	360	4.45 × 10^{-21}
250	1.11 × 10^{-19}	306	1.48 × 10^{-20}	362	4.11 × 10^{-21}
252	9.96 × 10^{-20}	308	1.49 × 10^{-20}	364	3.89 × 10^{-21}
254	8.86 × 10^{-20}	310	1.49 × 10^{-20}	366	3.56 × 10^{-21}
256	7.77 × 10^{-20}	312	1.48 × 10^{-20}	368	3.31 × 10^{-21}
258	6.80 × 10^{-20}	314	1.47 × 10^{-20}	370	2.98 × 10^{-21}
260	5.87 × 10^{-20}	316	1.46 × 10^{-20}	372	2.73 × 10^{-21}
262	5.05 × 10^{-20}	318	1.43 × 10^{-20}	374	2.46 × 10^{-21}
264	4.31 × 10^{-20}	320	1.41 × 10^{-20}	376	2.25 × 10^{-21}
266	3.69 × 10^{-20}	322	1.37 × 10^{-20}	378	2.09 × 10^{-21}
268	3.16 × 10^{-20}	324	1.33 × 10^{-20}	380	2.02 × 10^{-21}
270	2.71 × 10^{-20}	326	1.30 × 10^{-20}	382	1.86 × 10^{-21}
272	2.35 × 10^{-20}	328	1.24 × 10^{-20}	384	1.70 × 10^{-21}
274	2.06 × 10^{-20}	330	1.20 × 10^{-20}	386	1.60 × 10^{-21}
276	1.83 × 10^{-20}	332	1.14 × 10^{-20}	388	1.50 × 10^{-21}
278	1.64 × 10^{-20}	334	1.09 × 10^{-20}	390	1.30 × 10^{-21}
280	1.53 × 10^{-20}	336	1.04 × 10^{-20}	392	1.40 × 10^{-21}
282	1.42 × 10^{-20}	338	9.80 × 10^{-21}	394	1.30 × 10^{-21}
284	1.37 × 10^{-20}	340	9.18 × 10^{-21}		

The values of the cross sections are from Crowley *et al.* (1994) and Jungkamp *et al.* (1995), and those of the quantum yields are taken from Schindler *et al.* (1997).

CHCl$_3$ + hν → CHCl$_2$ + Cl $J = 0.00 \times 10^{-0}$ s^{-1} $\varphi_1 = 1$ **D05**
CHCl$_3$ + hν → CCl$_3$ + H $J = 0.00 \times 10^{-0}$ s^{-1} $\varphi_2 = 0$ **D06**

λ (nm)	σ (cm^2 molecule^{-1})	λ (nm)	σ (cm^2 molecule^{-1})	λ (nm)	σ (cm^2 molecule^{-1})
180	3.72×10^{-18}	206	2.07×10^{-19}	232	1.58×10^{-21}
182	3.17×10^{-18}	208	1.51×10^{-19}	234	1.07×10^{-21}
184	2.48×10^{-18}	210	1.07×10^{-19}	236	7.30×10^{-22}
186	1.86×10^{-18}	212	7.48×10^{-20}	238	5.03×10^{-22}
188	1.44×10^{-18}	214	5.24×10^{-20}	240	3.47×10^{-22}
190	1.13×10^{-18}	216	3.60×10^{-20}	242	3.23×10^{-22}
192	8.99×10^{-19}	218	2.48×10^{-20}	244	1.51×10^{-22}
194	7.61×10^{-19}	220	1.69×10^{-20}	246	1.02×10^{-22}
196	6.42×10^{-19}	222	1.13×10^{-20}	248	6.94×10^{-23}
198	5.30×10^{-19}	224	7.50×10^{-21}	250	4.70×10^{-23}
200	4.26×10^{-19}	226	5.03×10^{-21}	252	3.19×10^{-23}
202	3.44×10^{-19}	228	3.42×10^{-21}	254	2.16×10^{-23}
204	2.72×10^{-19}	230	2.34×10^{-21}	256	1.47×10^{-23}

For (180 < λ < 240): The values of the cross sections are from Hubrich and Stuhl (1980), and those of the quantum yields are taken from Simon *et al.* (1988).

For (242 < λ < 256): The recommended absorption cross sections are obtained by extrapolation, log σ (λ) = −1.2277 −0.0844 λ. The values of the quantum yields are taken from Richard A. Brownsword *et al.* (1997).

CH$_2$Cl$_2$ + hν → CH$_2$Cl + Cl $J = 0.00 \times 10^{-0}$ s^{-1} $\varphi_1 = 1$ **D07**
CH$_2$Cl$_2$ + hν → CHCl$_2$ + H $J = 0.00 \times 10^{-0}$ s^{-1} $\varphi_2 = 0$ **D08**

λ (nm)	σ (cm^2 molecule^{-1})	λ (nm)	σ (cm^2 molecule^{-1})	λ (nm)	σ (cm^2 molecule^{-1})
176	1.86×10^{-18}	204	4.41×10^{-20}	222	1.35×10^{-21}
178	1.82×10^{-18}	206	3.07×10^{-20}	224	9.18×10^{-22}
180	1.73×10^{-18}	208	2.13×10^{-20}	226	6.23×10^{-22}
182	1.56×10^{-18}	210	1.45×10^{-20}	228	4.22×10^{-22}
184	1.35×10^{-18}	212	9.78×10^{-21}	230	2.86×10^{-22}
186	1.10×10^{-18}	214	6.51×10^{-21}	232	1.94×10^{-22}
188	8.42×10^{-19}	216	4.35×10^{-21}	234	1.32×10^{-22}
190	6.10×10^{-19}	248	8.66×10^{-24}	236	8.92×10^{-23}
192	4.39×10^{-19}	250	5.87×10^{-24}	238	6.05×10^{-23}
194	3.05×10^{-19}	252	3.98×10^{-24}	240	4.10×10^{-23}
196	2.06×10^{-19}	254	2.70×10^{-24}	242	2.78×10^{-23}
198	1.41×10^{-19}	256	1.83×10^{-24}	244	1.88×10^{-23}
200	9.48×10^{-20}	218	2.91×10^{-21}	246	1.28×10^{-23}
202	6.40×10^{-20}	220	1.90×10^{-21}		

For (176 < λ < 220): The values of the cross sections are from Hubrich and Stuhl (1980), and those of the quantum yields are taken from Simon *et al.* (1988).

For (222 < λ (nm) < 256): The recommended absorption cross sections are obtained by extrapolation, log σ (λ) = −2.1337 −0.08439 λ. The values of the quantum yield are taken from R. A. Brownsword *et al.* (1997).

Appendix

| CH₃Cl + hν → CH₃ + Cl | J = 0.00 × 10⁻⁰ s⁻¹ | φ1 = 1 | D09 |

$CH_3Cl + h\nu \rightarrow CH_3 + Cl$ $\quad$ J = 0.00 × 10^{-0} s^{-1} $\quad$ φ1 = 1 $\quad$ **D09**

$CH_3Cl + h\nu \rightarrow CH_2Cl + H$ $\quad$ J = 0.00 × 10^{-0} s^{-1} $\quad$ φ2 = 0 $\quad$ **D10**

λ (nm)	σ (cm² molecule⁻¹)	λ (nm)	σ (cm² molecule⁻¹)	λ (nm)	σ (cm² molecule⁻¹)
174	1.10×10^{-18}	196	3.96×10^{-20}	218	3.45×10^{-22}
176	9.39×10^{-19}	198	2.68×10^{-20}	220	2.20×10^{-22}
178	7.82×10^{-19}	200	1.77×10^{-20}	222	1.35×10^{-22}
180	6.36×10^{-19}	202	1.13×10^{-20}	224	8.59×10^{-23}
182	4.65×10^{-19}	204	7.31×10^{-21}	226	5.49×10^{-23}
184	3.50×10^{-19}	206	4.82×10^{-21}	228	3.50×10^{-23}
186	2.58×10^{-19}	208	3.13×10^{-21}	230	2.24×10^{-23}
188	1.84×10^{-19}	210	2.00×10^{-21}	232	1.43×10^{-23}
190	1.28×10^{-19}	212	1.27×10^{-21}	234	9.10×10^{-24}
192	8.84×10^{-20}	214	8.60×10^{-22}	236	5.80×10^{-24}
194	5.83×10^{-20}	216	5.34×10^{-22}		

The values of the cross sections are from Hubrich and Stuhl (1980), and those of the quantum yields are taken from Simon *et al.* (1988).

For (174 < λ < 184): The values of the cross sections are from Hubrich *et al.* (1977), Robbins, 1976, and Simon *et al.*, (1988).

For (186 < λ < 216): The values of the cross sections are from Hubrich *et al.* (1977), Robbins (1976), Simon *et al.* (1988), and Vanlaethem-Meurée *et al.* (1978).

For (218 < λ < 220): The values of the cross sections are from Hubrich *et al.* (1977) and Robbins (1976).

For (222 < λ < 236): The recommended absorption cross sections fit to data by extrapolation, $\log \sigma (\lambda) = -0.24164 - 0.09743 \lambda$ given by Hubrich *et al.* (1977).

The values of quantum yields are taken from R. A. Brownsword *et al.* (1997).

Appendix

$CCl_2O + h\nu \rightarrow CO + Cl_2$	$J = 0.00 \times 10^{-0}$ s^{-1}	$\varphi1 = 0$	D11
$CCl_2O + h\nu \rightarrow ClCO + Cl$	$J = 0.00 \times 10^{-0}$ s^{-1}	$\varphi2 = 0$	D12
$CCl_2O + h\nu \rightarrow CO + 2\ Cl$	$J = 1.54 \times 10^{-11}$ s^{-1}	$\varphi3 = 1$	D13
$CCl_2O + h\nu \rightarrow CCl_2 + O$	$J = 0.00 \times 10^{-0}$ s^{-1}	$\varphi4 = 0$	D14

λ (nm)	σ (cm² molecule^{-1})	λ (nm)	σ (cm² molecule^{-1})	λ (nm)	σ (cm² molecule^{-1})
168.10	3.01×10^{-18}	201.01	2.57×10^{-19}	245.41	1.04×10^{-19}
170.95	4.33×10^{-18}	203.05	2.07×10^{-19}	248.45	9.07×10^{-20}
173.15	4.93×10^{-18}	205.14	1.72×10^{-19}	251.59	7.75×10^{-20}
174.65	5.09×10^{-18}	207.26	1.47×10^{-19}	254.79	6.32×10^{-20}
176.20	4.75×10^{-18}	209.43	1.30×10^{-19}	258.08	5.02×10^{-20}
177.80	4.27×10^{-18}	211.65	1.19×10^{-19}	261.45	3.77×10^{-20}
179.40	3.69×10^{-18}	213.89	1.14×10^{-19}	264.92	2.68×10^{-20}
181.00	3.13×10^{-18}	216.20	1.13×10^{-19}	268.50	1.85×10^{-20}
182.65	2.61×10^{-18}	218.59	1.15×10^{-19}	272.12	1.17×10^{-20}
184.35	2.10×10^{-18}	221.00	1.22×10^{-19}	275.88	6.89×10^{-21}
186.05	1.78×10^{-18}	223.47	1.26×10^{-19}	279.74	3.70×10^{-21}
187.80	1.37×10^{-18}	226.00	1.30×10^{-19}	283.70	1.82×10^{-21}
189.60	1.12×10^{-18}	228.58	1.32×10^{-19}	287.78	7.71×10^{-22}
191.40	8.89×10^{-19}	231.23	1.34×10^{-19}	291.99	2.98×10^{-22}
193.25	6.88×10^{-19}	233.93	1.35×10^{-19}	296.32	1.04×10^{-22}
195.15	5.21×10^{-19}	236.69	1.30×10^{-19}	300.77	3.23×10^{-23}
197.05	4.06×10^{-19}	239.53	1.24×10^{-19}	305.36	9.60×10^{-24}
199.00	3.17×10^{-19}	242.43	1.15×10^{-19}		

Data of absorption cross sections are taken from:

For (168.10 < λ (nm) < 173.15): (Gillotay *et al*., 1993),

For (174.65 < λ (nm) < 182.65): (Gillotay *et al*., 1993) and (Jäger *et al*., 1996),

For (184.5 < λ (nm) < 199): (Chou *et al*., 1977), (Gillotay *et al*., 1993), and (Jäger *et al*., 1996),

For (201.01 < λ (nm) < 218.59): (Chou *et al*., 1977), (Gillotay *et al*., 1993), (Jäger *et al*., 1996), and (Meller *et al*., 1991)

For (221 < λ (nm) < 226): (Chou *et al*., 1977), (Gillotay *et al*., 1993), and (Meller *et al*., 1991),

For (228.58 < λ (nm) < 305.36): (Gillotay *et al*., 1993) and (Meller *et al*., 1991).

Photolysis quantum yields of Okabe (1983), Wijnen (1961), Heicklen (1965), and (Calvert and Pitts, 1966).

Appendix

CCl$_3$CHO + h$\nu \rightarrow$ CCl$_3$ + HCO	**J = 0.00 × 10^{-0} s^{-1}**	**φ1 = 0**	**D15**
CCl$_3$CHO + h$\nu \rightarrow$ CCl$_3$CO + H	**J = 0.00 × 10^{-0} s^{-1}**	**φ2 = 0**	**D16**
CCl$_3$CHO + h$\nu \rightarrow$ CCl$_2$CHO + Cl	**J = 1.05 × 10^{-5} s^{-1}**	**φ3 = 1**	**D17**
CCl$_3$CHO + h$\nu \rightarrow$ CCl$_3$H + CO	**J = 0.00 × 10^{-0} s^{-1}**	**φ4 = 0**	**D18**

λ (nm)	σ (cm^2 molecule^{-1})	λ (nm)	σ (cm^2 molecule^{-1})	λ (nm)	σ (cm^2 molecule^{-1})
200	1.87×10^{-18}	250	2.18×10^{-20}	300	9.25×10^{-20}
202	1.53×10^{-18}	252	2.54×10^{-20}	302	8.77×10^{-20}
204	1.22×10^{-18}	254	2.92×10^{-20}	304	8.17×10^{-20}
206	9.57×10^{-19}	256	3.36×10^{-20}	306	7.50×10^{-20}
208	7.38×10^{-19}	258	3.84×10^{-20}	308	6.86×10^{-20}
210	5.63×10^{-19}	260	4.35×10^{-20}	310	6.18×10^{-20}
212	4.26×10^{-19}	262	4.90×10^{-20}	312	5.58×10^{-20}
214	3.18×10^{-19}	264	5.48×10^{-20}	314	4.98×10^{-20}
216	2.38×10^{-19}	266	6.07×10^{-20}	316	4.33×10^{-20}
218	1.71×10^{-19}	268	6.68×10^{-20}	318	3.68×10^{-20}
220	1.31×10^{-19}	270	7.28×10^{-20}	320	3.09×10^{-20}
222	9.75×10^{-20}	272	7.88×10^{-20}	322	2.51×10^{-20}
224	7.24×10^{-20}	274	8.46×10^{-20}	324	2.09×10^{-20}
226	5.39×10^{-20}	276	8.99×10^{-20}	326	1.76×10^{-20}
228	4.06×10^{-20}	278	9.49×10^{-20}	328	1.43×10^{-20}
230	3.07×10^{-20}	280	9.94×10^{-20}	330	1.12×10^{-20}
232	2.39×10^{-20}	282	1.03×10^{-19}	332	8.49×10^{-21}
234	1.90×10^{-20}	284	1.06×10^{-19}	334	5.90×10^{-21}
236	1.62×10^{-20}	286	1.08×10^{-19}	336	3.73×10^{-21}
238	1.43×10^{-20}	288	1.09×10^{-19}	338	2.61×10^{-21}
240	1.39×10^{-20}	290	1.09×10^{-19}	340	1.88×10^{-21}
242	1.41×10^{-20}	292	1.08×10^{-19}	342	1.36×10^{-21}
244	1.53×10^{-20}	294	1.06×10^{-19}	344	1.00×10^{-21}
246	1.66×10^{-20}	296	1.03×10^{-19}		
248	1.91×10^{-20}	298	9.92×10^{-20}		

Absorption cross sections and photolysis quantum yields are recommended by Talukdar *et al.* (2001).

Appendix A.III-4: Photolysis reactions of organic chlorinated species

The photolysis constants **J** presented in this appendix were calculated under clear skies in early January for a latitude of 51 °N (at ground level: $\lambda > 280$ nm and for solar zenith angle of 35°).

$Cl_2 + h\nu \rightarrow Cl + Cl$		J = 6.64×10^{-4} s⁻¹		$\varphi = 1$	B01
λ (nm)	σ (cm² molecule⁻¹)	λ (nm)	σ (cm² molecule⁻¹)	λ (nm)	σ (cm² molecule⁻¹)
260	1.98×10^{-21}	360	1.32×10^{-19}	460	2.58×10^{-21}
270	8.24×10^{-21}	370	8.41×10^{-20}	470	1.62×10^{-21}
280	2.85×10^{-20}	380	5.00×10^{-20}	480	9.57×10^{-22}
290	6.22×10^{-20}	390	2.94×10^{-20}	490	5.34×10^{-22}
300	1.19×10^{-19}	400	1.84×10^{-20}	500	2.83×10^{-22}
310	1.85×10^{-19}	410	1.28×10^{-20}	510	1.42×10^{-22}
320	2.37×10^{-19}	420	9.56×10^{-21}	520	6.81×10^{-23}
330	2.56×10^{-19}	430	7.32×10^{-21}	530	3.13×10^{-23}
340	2.35×10^{-19}	440	5.46×10^{-21}	540	1.37×10^{-23}
350	1.88×10^{-19}	450	3.87×10^{-21}	550	5.80×10^{-24}

All values are recommended by Burkholder *et al*. (2020).

$ClO + h\nu \rightarrow Cl + O(^1D)$		J = 1.15×10^{-5} s⁻¹		$\varphi = 1$	B02
λ (nm)	σ (cm² molecule⁻¹)	λ (nm)	σ (cm² molecule⁻¹)	λ (nm)	σ (cm² molecule⁻¹)
245	2.60×10^{-18}	269	5.29×10^{-18}	293	1.61×10^{-18}
246	2.79×10^{-18}	270	5.75×10^{-18}	294	1.02×10^{-18}
247	2.97×10^{-18}	271	4.89×10^{-18}	295	9.45×10^{-19}
248	3.15×10^{-18}	272	5.32×10^{-18}	296	2.06×10^{-18}
249	3.33×10^{-18}	273	5.15×10^{-18}	297	8.31×10^{-19}
250	3.52×10^{-18}	274	4.70×10^{-18}	298	6.51×10^{-19}
251	3.71×10^{-18}	275	5.07×10^{-18}	299	7.48×10^{-19}
252	3.88×10^{-18}	276	4.56×10^{-18}	300	1.33×10^{-18}
253	4.07×10^{-18}	277	4.18×10^{-18}	301	5.66×10^{-19}
254	4.25×10^{-18}	278	5.01×10^{-18}	302	4.52×10^{-19}
255	4.42×10^{-18}	279	2.83×10^{-18}	303	4.49×10^{-19}
256	4.57×10^{-18}	280	5.38×10^{-18}	304	8.78×10^{-19}
257	4.73×10^{-18}	281	3.29×10^{-18}	305	4.55×10^{-19}
258	4.86×10^{-18}	282	3.11×10^{-18}	306	3.32×10^{-19}
259	5.00×10^{-18}	283	4.45×10^{-18}	307	3.31×10^{-19}
260	5.11×10^{-18}	284	2.45×10^{-18}	308	4.77×10^{-19}
261	5.20×10^{-18}	285	2.92×10^{-18}	309	4.19×10^{-19}
262	5.29×10^{-18}	286	3.62×10^{-18}	310	2.87×10^{-19}
263	5.36×10^{-18}	287	2.00×10^{-18}	311	2.73×10^{-19}
264	5.40×10^{-18}	288	1.97×10^{-18}	312	3.31×10^{-19}
265	5.41×10^{-18}	289	3.37×10^{-18}	313	3.25×10^{-19}
266	5.49×10^{-18}	290	1.65×10^{-18}	314	2.89×10^{-19}
267	5.46×10^{-18}	291	1.11×10^{-18}	315	2.78×10^{-19}
268	5.29×10^{-18}	292	2.70×10^{-18}	316	2.68×10^{-19}

All values are recommended by Sander and Friedl (1989).

Appendix

ClOO + hν → Cl + O₂ **J = 0.00 × 10⁻⁰ s⁻¹** **φ = 1** **B03**

λ (nm)	σ (cm² molecule⁻¹)	λ (nm)	σ (cm² molecule⁻¹)	λ (nm)	σ (cm² molecule⁻¹)
220	6.11×10^{-18}	242	2.91×10^{-17}	264	1.12×10^{-17}
222	6.70×10^{-18}	244	2.96×10^{-17}	266	9.05×10^{-18}
224	7.47×10^{-18}	246	2.98×10^{-17}	268	7.25×10^{-18}
226	9.51×10^{-18}	248	2.95×10^{-17}	270	5.96×10^{-18}
228	1.10×10^{-17}	250	2.80×10^{-17}	272	4.35×10^{-18}
230	1.40×10^{-17}	252	2.63×10^{-17}	274	3.44×10^{-18}
232	1.65×10^{-17}	254	2.37×10^{-17}	276	2.82×10^{-18}
234	1.96×10^{-17}	256	2.12×10^{-17}	278	2.10×10^{-18}
236	2.24×10^{-17}	258	1.89×10^{-17}	280	2.00×10^{-18}
238	2.52×10^{-17}	260	1.61×10^{-17}		
240	2.73×10^{-17}	262	1.37×10^{-17}		

All values are recommended by Burkholder *et al*. (2020).

OClO + hν → ClO + O(³P) **J = 2.52 × 10⁻² s⁻¹** **φ = 1** **B04**

λ (nm)	σ (cm² molecule⁻¹)	λ (nm)	σ (cm² molecule⁻¹)	λ (nm)	σ (cm² molecule⁻¹)
247	3.56×10^{-19}	294	9.41×10^{-19}	341	2.50×10^{-18}
248	3.44×10^{-19}	295	1.47×10^{-18}	342	4.14×10^{-18}
249	3.37×10^{-20}	296	1.72×10^{-18}	343	9.25×10^{-18}
250	3.46×10^{-19}	297	1.22×10^{-18}	344	1.09×10^{-19}
251	3.43×10^{-19}	298	9.20×10^{-19}	345	3.88×10^{-18}
252	3.46×10^{-19}	299	1.06×10^{-18}	346	1.76×10^{-18}
253	3.41×10^{-19}	300	2.26×10^{-18}	347	1.61×10^{-18}
254	3.49×10^{-19}	301	2.22×10^{-18}	348	2.58×10^{-18}
255	3.43×10^{-19}	302	1.43×10^{-18}	349	3.20×10^{-18}
256	3.48×10^{-19}	303	9.43×10^{-19}	350	5.81×10^{-18}
257	3.48×10^{-19}	304	9.61×10^{-19}	351	1.10×10^{-17}
258	3.51×10^{-19}	305	2.76×10^{-18}	352	9.93×10^{-18}
259	3.50×10^{-19}	306	3.28×10^{-18}	353	3.30×10^{-18}
260	3.58×10^{-19}	307	1.90×10^{-18}	354	1.64×10^{-18}
261	3.65×10^{-19}	308	1.16×10^{-18}	355	1.90×10^{-18}
262	3.75×10^{-19}	309	8.54×10^{-19}	356	2.76×10^{-18}
263	3.82×10^{-19}	310	1.68×10^{-18}	357	3.43×10^{-18}
264	3.80×10^{-19}	311	5.11×10^{-18}	358	5.97×10^{-18}
265	3.88×10^{-19}	312	3.38×10^{-18}	359	8.30×10^{-18}
266	3.99×10^{-19}	313	1.74×10^{-18}	360	1.21×10^{-17}
267	4.04×10^{-19}	314	1.07×10^{-18}	361	4.77×10^{-18}
268	4.23×10^{-19}	315	9.42×10^{-19}	362	1.73×10^{-18}
269	4.46×10^{-19}	316	2.39×10^{-18}	363	1.79×10^{-18}
270	4.43×10^{-19}	317	6.86×10^{-18}	364	2.07×10^{-18}
271	4.57×10^{-19}	318	3.60×10^{-18}	365	3.61×10^{-18}
272	4.99×10^{-19}	319	1.76×10^{-18}	366	4.03×10^{-18}
273	4.91×10^{-19}	320	1.14×10^{-18}	367	6.25×10^{-18}
274	4.81×10^{-19}	321	1.25×10^{-18}	368	9.19×10^{-18}
275	5.48×10^{-19}	322	2.79×10^{-18}	369	9.03×10^{-18}
276	5.83×10^{-19}	323	8.73×10^{-18}	370	2.68×10^{-18}
277	5.25×10^{-19}	324	4.43×10^{-18}	371	1.07×10^{-18}
278	5.43×10^{-19}	325	1.92×10^{-18}	372	1.80×10^{-18}
279	6.74×10^{-19}	326	1.21×10^{-18}	373	1.70×10^{-18}
280	6.72×10^{-19}	327	1.47×10^{-18}	374	3.64×10^{-18}
281	5.83×10^{-19}	328	2.21×10^{-18}	375	3.76×10^{-18}
282	6.54×10^{-19}	329	8.38×10^{-18}	376	5.54×10^{-18}

283	8.24×10^{-19}	330	7.82×10^{-18}	377	7.18×10^{-18}
284	7.76×10^{-19}	331	2.85×10^{-18}	378	8.81×10^{-18}
285	6.72×10^{-19}	332	1.55×10^{-18}	379	2.78×10^{-18}
286	7.77×10^{-19}	333	1.47×10^{-18}	380	9.24×10^{-19}
287	1.00×10^{-18}	334	2.08×10^{-18}	381	1.35×10^{-18}
288	9.37×10^{-19}	335	3.55×10^{-18}	382	1.48×10^{-18}
289	7.94×10^{-19}	336	1.09×10^{-17}	383	2.66×10^{-18}
290	9.05×10^{-19}	337	7.82×10^{-18}	384	2.98×10^{-18}
291	1.27×10^{-18}	338	2.66×10^{-18}	385	4.40×10^{-18}
292	1.16×10^{-18}	339	1.55×10^{-18}	386	3.45×10^{-18}
293	9.09×10^{-19}	340	1.67×10^{-18}	387	7.62×10^{-18}
388	5.91×10^{-18}	417	1.00×10^{-18}	446	4.68×10^{-19}
389	1.73×10^{-18}	418	1.07×10^{-18}	447	5.52×10^{-19}
390	7.14×10^{-19}	419	7.51×10^{-19}	448	1.84×10^{-19}
391	1.23×10^{-18}	420	8.14×10^{-19}	449	7.17×10^{-20}
392	1.09×10^{-18}	421	3.23×10^{-18}	450	6.96×10^{-20}
393	2.03×10^{-18}	422	1.51×10^{-18}	451	4.50×10^{-20}
394	2.70×10^{-18}	423	5.00×10^{-19}	452	1.66×10^{-20}
395	2.85×10^{-18}	424	2.38×10^{-19}	453	3.57×10^{-20}
396	2.75×10^{-18}	425	2.33×10^{-19}	454	9.07×10^{-21}
397	3.70×10^{-18}	426	1.45×10^{-19}	455	1.33×10^{-20}
398	6.53×10^{-18}	427	4.38×10^{-19}	456	9.70×10^{-20}
399	2.25×10^{-18}	428	9.95×10^{-19}	457	4.76×10^{-20}
400	7.01×10^{-19}	429	4.69×10^{-19}	458	4.25×10^{-20}
401	4.56×10^{-19}	430	4.43×10^{-19}	459	3.98×10^{-20}
402	9.69×10^{-19}	431	2.33×10^{-19}	460	1.84×10^{-20}
403	5.63×10^{-19}	432	4.70×10^{-19}	461	1.71×10^{-19}
404	1.96×10^{-18}	433	1.73×10^{-18}	462	1.79×10^{-19}
405	1.94×10^{-18}	434	6.96×10^{-19}	463	1.18×10^{-19}
406	1.85×10^{-18}	435	2.46×10^{-19}	464	1.00×10^{-19}
407	1.60×10^{-18}	436	1.12×10^{-19}	465	4.01×10^{-20}
408	1.58×10^{-18}	437	7.68×10^{-20}	466	1.40×10^{-20}
409	4.93×10^{-18}	438	9.09×10^{-20}	467	2.53×10^{-20}
410	2.10×10^{-18}	439	5.13×10^{-20}	468	1.01×10^{-19}
411	7.16×10^{-19}	440	1.25×10^{-19}	469	1.50×10^{-19}
412	3.40×10^{-19}	441	4.78×10^{-19}	470	7.69×10^{-20}
413	4.68×10^{-19}	442	2.32×10^{-19}	471	6.14×10^{-20}
414	4.46×10^{-19}	443	1.47×10^{-19}	472	3.18×10^{-20}
415	3.00×10^{-19}	444	7.59×10^{-20}		
416	1.64×10^{-18}	445	3.96×10^{-20}		

The values of the cross sections are from Wahner *et al.* (1987), and those of the quantum yields are recommended by Burkholder *et al.* (2020).

Appendix

$Cl_2O + h\nu \rightarrow Cl + ClO$ $J = 2.70 \times 10^{-4}\ s^{-1}$ $\varphi 1 = 1$ **B05**

$Cl_2O + h\nu \rightarrow Cl_2 + O(^1D)$ $J = 6.76 \times 10^{-5}\ s^{-1}$ $\varphi 2 = 0.25$ **B06**

λ (nm)	σ (cm² molecule^{-1})	λ (nm)	σ (cm² molecule^{-1})	λ (nm)	σ (cm² molecule^{-1})
200	6.94×10^{-19}	246	1.56×10^{-18}	292	9.43×10^{-19}
201	6.38×10^{-19}	247	1.64×10^{-18}	293	9.13×10^{-19}
202	5.83×10^{-19}	248	1.71×10^{-18}	294	8.83×10^{-19}
203	5.27×10^{-19}	249	1.78×10^{-18}	295	8.53×10^{-19}
204	4.76×10^{-19}	250	1.83×10^{-18}	296	8.22×10^{-19}
205	4.31×10^{-19}	251	1.87×10^{-18}	297	7.91×10^{-19}
206	3.88×10^{-19}	252	1.91×10^{-18}	298	7.59×10^{-19}
207	3.47×10^{-19}	253	1.94×10^{-18}	299	7.26×10^{-19}
208	3.09×10^{-19}	254	1.95×10^{-18}	300	6.93×10^{-19}
209	2.74×10^{-19}	255	1.96×10^{-18}	301	6.61×10^{-19}
210	2.44×10^{-19}	256	1.95×10^{-18}	302	6.28×10^{-19}
211	2.15×10^{-19}	257	1.93×10^{-18}	303	5.97×10^{-19}
212	1.90×10^{-19}	258	1.91×10^{-18}	304	5.66×10^{-19}
213	1.68×10^{-19}	259	1.89×10^{-18}	305	5.35×10^{-19}
214	1.49×10^{-19}	260	1.86×10^{-18}	306	5.05×10^{-19}
215	1.34×10^{-19}	261	1.82×10^{-18}	307	4.76×10^{-19}
216	1.20×10^{-19}	262	1.78×10^{-18}	308	4.47×10^{-19}
217	1.10×10^{-19}	263	1.74×10^{-18}	309	4.20×10^{-19}
218	1.02×10^{-19}	264	1.69×10^{-18}	310	3.94×10^{-19}
219	9.77×10^{-20}	265	1.65×10^{-18}	311	3.69×10^{-19}
220	9.66×10^{-20}	266	1.60×10^{-18}	312	3.45×10^{-19}
221	9.85×10^{-20}	267	1.56×10^{-18}	313	3.22×10^{-19}
222	1.03×10^{-19}	268	1.52×10^{-18}	314	3.00×10^{-19}
223	1.11×10^{-19}	269	1.48×10^{-18}	315	2.79×10^{-19}
224	1.22×10^{-19}	270	1.45×10^{-18}	316	2.59×10^{-19}
225	1.38×10^{-19}	271	1.42×10^{-18}	317	2.41×10^{-19}
226	1.58×10^{-19}	272	1.38×10^{-18}	318	2.23×10^{-19}
227	1.83×10^{-19}	273	1.36×10^{-18}	319	2.07×10^{-19}
228	2.12×10^{-19}	274	1.33×10^{-18}	320	1.92×10^{-19}
229	2.46×10^{-19}	275	1.30×10^{-18}	321	1.77×10^{-19}
230	2.85×10^{-19}	276	1.28×10^{-18}	322	1.64×10^{-19}
231	3.31×10^{-19}	277	1.27×10^{-18}	323	1.51×10^{-19}
232	3.84×10^{-19}	278	1.25×10^{-18}	324	1.39×10^{-19}
233	4.43×10^{-19}	279	1.23×10^{-18}	325	1.28×10^{-19}
234	5.07×10^{-19}	280	1.21×10^{-18}	326	1.18×10^{-19}
235	5.75×10^{-19}	281	1.19×10^{-18}	327	1.09×10^{-19}
236	6.50×10^{-19}	282	1.17×10^{-18}	328	1.00×10^{-19}
237	7.31×10^{-19}	283	1.15×10^{-18}	329	9.25×10^{-20}
238	8.19×10^{-19}	284	1.13×10^{-18}	330	8.52×10^{-20}
239	9.11×10^{-19}	285	1.11×10^{-18}	331	7.84×10^{-20}
240	1.00×10^{-18}	286	1.09×10^{-18}	332	7.21×10^{-20}
241	1.10×10^{-18}	287	1.07×10^{-18}	333	6.63×10^{-20}
242	1.19×10^{-18}	288	1.05×10^{-18}	334	6.09×10^{-20}
243	1.29×10^{-18}	289	1.03×10^{-18}	335	5.61×10^{-20}
244	1.38×10^{-18}	290	9.99×10^{-19}	336	5.16×10^{-20}
245	1.47×10^{-18}	291	9.72×10^{-19}	337	4.76×10^{-20}
338	4.39×10^{-20}	387	5.41×10^{-21}	436	1.22×10^{-20}
339	4.04×10^{-20}	388	5.56×10^{-21}	437	1.20×10^{-20}
340	3.73×10^{-20}	389	5.75×10^{-21}	438	1.18×10^{-20}
341	3.43×10^{-20}	390	5.97×10^{-21}	439	1.16×10^{-20}
342	3.16×10^{-20}	391	6.20×10^{-21}	440	1.14×10^{-20}

Appendix

343	2.91×10^{-20}	392	6.42×10^{-21}	441	1.12×10^{-20}
344	2.69×10^{-20}	393	6.64×10^{-21}	442	1.10×10^{-20}
345	2.48×10^{-20}	394	6.89×10^{-21}	443	1.07×10^{-20}
346	2.30×10^{-20}	395	7.18×10^{-21}	444	1.04×10^{-20}
347	2.13×10^{-20}	396	7.47×10^{-21}	445	1.02×10^{-20}
348	1.98×10^{-20}	397	7.75×10^{-21}	446	9.96×10^{-21}
349	1.84×10^{-20}	398	8.00×10^{-21}	447	9.69×10^{-21}
350	1.71×10^{-20}	399	8.25×10^{-21}	448	9.44×10^{-21}
351	1.59×10^{-20}	400	8.53×10^{-21}	449	9.17×10^{-21}
352	1.48×10^{-20}	401	8.83×10^{-21}	450	8.91×10^{-21}
353	1.38×10^{-20}	402	9.16×10^{-21}	451	8.65×10^{-21}
354	1.28×10^{-20}	403	9.46×10^{-21}	452	8.39×10^{-21}
355	1.19×10^{-20}	404	9.72×10^{-21}	453	8.12×10^{-21}
356	1.11×10^{-20}	405	9.98×10^{-21}	454	7.87×10^{-21}
357	1.04×10^{-20}	406	1.02×10^{-20}	455	7.65×10^{-21}
358	9.74×10^{-21}	407	1.05×10^{-20}	456	7.42×10^{-21}
359	9.20×10^{-21}	408	1.08×10^{-20}	457	7.19×10^{-21}
360	8.71×10^{-21}	409	1.11×10^{-20}	458	6.92×10^{-21}
361	8.28×10^{-21}	410	1.14×10^{-20}	459	6.65×10^{-21}
362	7.85×10^{-21}	411	1.16×10^{-20}	460	6.42×10^{-21}
363	7.43×10^{-21}	412	1.18×10^{-20}	461	6.23×10^{-21}
364	7.02×10^{-21}	413	1.20×10^{-20}	462	6.04×10^{-21}
365	6.64×10^{-21}	414	1.22×10^{-20}	463	5.81×10^{-21}
366	6.30×10^{-21}	415	1.24×10^{-20}	464	5.54×10^{-21}
367	6.02×10^{-21}	416	1.26×10^{-20}	465	5.32×10^{-21}
368	5.79×10^{-21}	417	1.27×10^{-20}	466	5.13×10^{-21}
369	5.60×10^{-21}	418	1.29×10^{-20}	467	4.97×10^{-21}
370	5.43×10^{-21}	419	1.30×10^{-20}	468	4.82×10^{-21}
371	5.26×10^{-21}	420	1.31×10^{-20}	469	4.66×10^{-21}
372	5.09×10^{-21}	421	1.32×10^{-20}	470	4.52×10^{-21}
373	4.95×10^{-21}	422	1.32×10^{-20}	471	4.40×10^{-21}
374	4.85×10^{-21}	423	1.32×10^{-20}	472	4.29×10^{-21}
375	4.76×10^{-21}	424	1.32×10^{-20}	473	4.13×10^{-21}
376	4.70×10^{-21}	425	1.32×10^{-20}	474	3.96×10^{-21}
377	4.66×10^{-21}	426	1.33×10^{-20}	475	3.79×10^{-21}
378	4.64×10^{-21}	427	1.33×10^{-20}	476	3.66×10^{-21}
379	4.67×10^{-21}	428	1.32×10^{-20}	477	$3.56 \; 10^{-21}$
380	4.72×10^{-21}	429	1.31×10^{-20}	478	3.47×10^{-21}
381	4.78×10^{-21}	430	1.30×10^{-20}	479	3.39×10^{-21}
382	4.86×10^{-21}	431	1.30×10^{-20}	480	3.29×10^{-21}
383	4.96×10^{-21}	432	1.29×10^{-20}	481	3.19×10^{-21}
384	5.06×10^{-21}	433	1.27×10^{-20}	482	3.11×10^{-21}
385	5.17×10^{-21}	434	1.26×10^{-20}	483	3.04×10^{-21}
386	5.29×10^{-21}	435	1.24×10^{-20}	484	2.98×10^{-21}
485	2.87×10^{21}	491	2.59×10^{-21}	497	2.52×10^{-21}
486	2.76×10^{-21}	492	2.51×10^{-21}	498	2.48×10^{-21}
487	2.69×10^{-21}	493	2.44×10^{-21}	499	2.40×10^{-21}
488	2.63×10^{-21}	494	2.42×10^{-21}	500	2.38×10^{-21}
489	2.61×10^{-21}	495	2.43×10^{-21}		
490	2.62×10^{-21}	496	2.49×10^{-21}		

The values of the cross sections are from Papanastasiou *et al.* (2011). Those of the quantum yields are taken from Nelson and Johnston (1981) and Sander and Friedl (1989) for B06 ($\varphi1$) and B07 ($\varphi2$) respectively.

Appendix

| Cl$_2$O$_2$ + hν → Cl + ClO$_2$ | | J = 4.00 × 10^{-4} s^{-1} | φ1 = 0.9 | B07 |
| Cl$_2$O$_2$ + hν → ClO + ClO | | J = 4.45 × 10^{-5} s^{-1} | φ2 = 0.1 | B08 |

λ (nm)	σ (cm² molecule^{-1})	λ (nm)	σ (cm² molecule^{-1})	λ (nm)	σ (cm² molecule^{-1})
200	4.23 × 10^{-18}	246	7.53 × 10^{-18}	292	9.82 × 10^{-19}
201	4.09 × 10^{-18}	247	7.44 × 10^{-18}	293	9.35 × 10^{-19}
202	3.95 × 10^{-18}	248	7.32 × 10^{-18}	294	8.89 × 10^{-19}
203	3.78 × 10^{-18}	249	7.16 × 10^{-18}	295	8.46 × 10^{-19}
204	3.62 × 10^{-18}	250	6.94 × 10^{-18}	296	8.05 × 10^{-19}
205	3.47 × 10^{-18}	251	6.75 × 10^{-18}	297	7.66 × 10^{-19}
206	3.31 × 10^{-18}	252	6.51 × 10^{-18}	298	7.29 × 10^{-19}
207	3.17 × 10^{-18}	253	6.26 × 10^{-18}	299	6.95 × 10^{-19}
208	3.03 × 10^{-18}	254	6.01 × 10^{-18}	300	6.61 × 10^{-19}
209	2.90 × 10^{-18}	255	5.75 × 10^{-18}	301	6.30 × 10^{-19}
210	2.77 × 10^{-18}	256	5.49 × 10^{-18}	302	5.99 × 10^{-19}
211	2.66 × 10^{-18}	257	5.21 × 10^{-18}	303	5.71 × 10^{-19}
212	2.55 × 10^{-18}	258	4.95 × 10^{-18}	304	5.44 × 10^{-19}
213	2.46 × 10^{-18}	259	4.69 × 10^{-18}	305	5.20 × 10^{-19}
214	2.38 × 10^{-18}	260	4.45 × 10^{-18}	306	4.97 × 10^{-19}
215	2.32 × 10^{-18}	261	4.22 × 10^{-18}	307	4.75 × 10^{-19}
216	2.28 × 10^{-18}	262	4.00 × 10^{-18}	308	4.54 × 10^{-19}
217	2.26 × 10^{-18}	263	3.80 × 10^{-18}	309	4.34 × 10^{-19}
218	2.25 × 10^{-18}	264	3.60 × 10^{-18}	310	4.16 × 10^{-19}
219	2.27 × 10^{-18}	265	3.42 × 10^{-18}	311	3.99 × 10^{-19}
220	2.32 × 10^{-18}	266	3.25 × 10^{-18}	312	3.82 × 10^{-19}
221	2.40 × 10^{-18}	267	3.09 × 10^{-18}	313	3.67 × 10^{-19}
222	2.49 × 10^{-18}	268	2.94 × 10^{-18}	314	3.53 × 10^{-19}
223	2.62 × 10^{-18}	269	2.81 × 10^{-18}	315	3.40 × 10^{-19}
224	2.77 × 10^{-18}	270	2.68 × 10^{-18}	316	3.28 × 10^{-19}
225	2.95 × 10^{-18}	271	2.57 × 10^{-18}	317	3.16 × 10^{-19}
226	3.16 × 10^{-18}	272	2.46 × 10^{-18}	318	3.04 × 10^{-19}
227	3.40 × 10^{-18}	273	2.35 × 10^{-18}	319	2.93 × 10^{-19}
228	3.66 × 10^{-18}	274	2.25 × 10^{-18}	320	2.82 × 10^{-19}
229	3.94 × 10^{-18}	275	2.15 × 10^{-18}	321	2.72 × 10^{-19}
230	4.24 × 10^{-18}	276	2.06 × 10^{-18}	322	2.63 × 10^{-19}
231	4.55 × 10^{-18}	277	1.97 × 10^{-18}	323	2.55 × 10^{-19}
232	4.88 × 10^{-18}	278	1.89 × 10^{-18}	324	2.47 × 10^{-19}
233	5.22 × 10^{-18}	279	1.81 × 10^{-18}	325	2.39 × 10^{-19}
234	5.55 × 10^{-18}	280	1.73 × 10^{-18}	326	2.32 × 10^{-19}
235	5.87 × 10^{-18}	281	1.65 × 10^{-18}	327	2.25 × 10^{-19}
236	6.18 × 10^{-18}	282	1.58 × 10^{-18}	328	2.19 × 10^{-19}
237	6.47 × 10^{-18}	283	1.51 × 10^{-18}	329	2.13 × 10^{-19}
238	6.74 × 10^{-18}	284	1.44 × 10^{-18}	330	2.07 × 10^{-19}
239	6.98 × 10^{-18}	285	1.38 × 10^{-18}	331	2.01 × 10^{-19}
240	7.19 × 10^{-18}	286	1.31 × 10^{-18}	332	1.95 × 10^{-19}
241	7.35 × 10^{-18}	287	1.25 × 10^{-18}	333	1.89 × 10^{-19}
242	7.47 × 10^{-18}	288	1.19 × 10^{-18}	334	1.84 × 10^{-19}
243	7.55 × 10^{-18}	289	1.14 × 10^{-18}	335	1.78 × 10^{-19}
244	7.58 × 10^{-18}	290	1.08 × 10^{-18}	336	1.73 × 10^{-19}
245	7.57 × 10^{-18}	291	1.03 × 10^{-18}	337	1.68 × 10^{-19}
338	1.63 × 10^{-19}	387	2.14 × 10^{-20}	436	4.54 × 10^{-21}
339	1.59 × 10^{-19}	388	2.04 × 10^{-20}	437	4.41 × 10^{-21}
340	1.54 × 10^{-19}	389	1.95 × 10^{-20}	438	4.29 × 10^{-21}

341	1.49×10^{-19}	390	1.87×10^{-20}	439	4.17×10^{-21}
342	1.45×10^{-19}	391	1.78×10^{-20}	440	4.06×10^{-21}
343	1.41×10^{-19}	392	1.71×10^{-20}	441	3.94×10^{-21}
344	1.36×10^{-19}	393	1.65×10^{-20}	442	3.83×10^{-21}
345	1.32×10^{-19}	394	1.58×10^{-20}	443	3.73×10^{-21}
346	1.27×10^{-19}	395	1.52×10^{-20}	444	3.63×10^{-21}
347	1.23×10^{-19}	396	1.47×10^{-20}	445	3.62×10^{-21}
348	1.19×10^{-19}	397	1.41×10^{-20}	446	3.43×10^{-21}
349	1.14×10^{-19}	398	1.36×10^{-20}	447	3.33×10^{-21}
350	1.11×10^{-19}	399	1.31×10^{-20}	448	3.24×10^{-21}
351	1.07×10^{-19}	400	1.26×10^{-20}	449	3.15×10^{-21}
352	1.03×10^{-19}	401	1.22×10^{-20}	450	3.06×10^{-21}
353	9.91×10^{-20}	402	1.18×10^{-20}	451	2.98×10^{-21}
354	9.55×10^{-20}	403	1.14×10^{-20}	452	2.89×10^{-21}
355	9.20×10^{-20}	404	1.11×10^{-20}	453	2.81×10^{-21}
356	8.82×10^{-20}	405	1.08×10^{-20}	454	2.74×10^{-21}
357	8.47×10^{-20}	406	1.05×10^{-20}	455	2.66×10^{-21}
358	8.10×10^{-20}	407	1.02×10^{-20}	456	2.59×10^{-21}
359	7.76×10^{-20}	408	9.88×10^{-21}	457	2.52×10^{-21}
360	7.43×10^{-20}	409	9.61×10^{-21}	458	2.45×10^{-21}
361	7.12×10^{-20}	410	9.33×10^{-21}	459	2.38×10^{-21}
362	6.81×10^{-20}	411	9.07×10^{-21}	460	2.31×10^{-21}
363	6.51×10^{-20}	412	8.78×10^{-21}	461	2.25×10^{-21}
364	6.24×10^{-20}	413	8.57×10^{-21}	462	2.19×10^{-21}
365	5.98×10^{-20}	414	8.31×10^{-21}	463	2.13×10^{-21}
366	5.72×10^{-20}	415	8.01×10^{-21}	464	2.07×10^{-21}
367	5.47×10^{-20}	416	7.78×10^{-21}	465	2.01×10^{-21}
368	5.23×10^{-20}	417	7.61×10^{-21}	466	1.95×10^{-21}
369	4.99×10^{-20}	418	7.38×10^{-21}	467	1.90×10^{-21}
370	4.77×10^{-20}	419	7.25×10^{-21}	468	1.85×10^{-21}
371	4.55×10^{-20}	420	7.12×10^{-21}	469	1.80×10^{-21}
372	4.35×10^{-20}	421	6.92×10^{-21}	470	1.75×10^{-21}
373	4.15×10^{-20}	422	6.73×10^{-21}	471	1.70×10^{-21}
374	3.95×10^{-20}	423	6.54×10^{-21}	472	1.65×10^{-21}
375	3.77×10^{-20}	424	6.36×10^{-21}	473	1.61×10^{-21}
376	3.60×10^{-20}	425	6.18×10^{-21}	474	1.56×10^{-21}
377	3.43×10^{-20}	426	6.01×10^{-21}	475	1.52×10^{-21}
378	3.27×10^{-20}	427	5.85×10^{-21}	476	1.47×10^{-21}
379	3.12×10^{-20}	428	5.68×10^{-21}	477	1.43×10^{-21}
380	2.97×10^{-20}	429	5.53×10^{-21}	478	1.39×10^{-21}
381	2.83×10^{-20}	430	5.37×10^{-21}	479	1.36×10^{-21}
382	2.70×10^{-20}	431	5.22×10^{-21}	480	1.32×10^{-21}
383	2.57×10^{-20}	432	5.08×10^{-21}	481	1.28×10^{-21}
384	2.45×10^{-20}	433	4.94×10^{-21}	482	1.25×10^{-21}
385	2.34×10^{-20}	434	4.80×10^{-21}	483	1.21×10^{-21}
386	2.24×10^{-20}	435	4.67×10^{-21}	484	1.18×10^{-21}
485	1.15×10^{-21}	507	6.17×10^{-22}	529	3.33×10^{-22}
486	1.11×10^{-21}	508	6.00×10^{-22}	530	3.23×10^{-22}
487	1.08×10^{-21}	509	5.84×10^{-22}	531	3.14×10^{-22}
488	1.05×10^{-21}	510	5.67×10^{-22}	532	3.06×10^{-22}
489	1.02×10^{-21}	511	5.52×10^{-22}	533	2.97×10^{-22}
490	9.95×10^{-22}	512	5.36×10^{-22}	534	2.89×10^{-22}
491	9.68×10^{-22}	513	5.21×10^{-22}	535	2.81×10^{-22}
492	9.41×10^{-22}	514	5.07×10^{-22}	536	2.73×10^{-22}

493	9.15×10^{-22}	515	4.93×10^{-22}	537	2.66×10^{-22}
494	8.89×10^{-22}	516	4.79×10^{-22}	538	2.58×10^{-22}
495	8.65×10^{-22}	517	4.66×10^{-22}	539	2.51×10^{-22}
496	8.41×10^{-22}	518	4.53×10^{-22}	540	2.44×10^{-22}
497	8.18×10^{-22}	519	4.41×10^{-22}	541	2.37×10^{-22}
498	7.95×10^{-22}	520	4.28×10^{-22}	542	2.31×10^{-22}
499	7.73×10^{-22}	521	4.16×10^{-22}	543	2.24×10^{-22}
500	7.51×10^{-22}	522	4.05×10^{-22}	544	2.18×10^{-22}
501	7.31×10^{-22}	523	3.94×10^{-22}	545	2.12×10^{-22}
502	7.10×10^{-22}	524	3.83×10^{-22}	546	2.06×10^{-22}
503	6.91×10^{-22}	525	3.72×10^{-22}	547	2.01×10^{-22}
504	6.72×10^{-22}	526	3.62×10^{-22}	548	1.95×10^{-22}
505	6.53×10^{-22}	527	3.52×10^{-22}	549	1.90×10^{-22}
506	6.35×10^{-22}	528	3.42×10^{-22}	550	1.84×10^{-22}

The values of the cross sections are from Papanastasiou *et al.* (2009), and those of the quantum yields are taken from Moore *et al.* (1999)

Appendix

Cl$_2$O$_3$ + hν → ClO + OClO   **J = 7.33 × 10^{-5} s^{-1}**   **φ = 1**   **B09**

λ (nm)	σ (cm² molecule^{-1})	λ (nm)	σ (cm² molecule^{-1})	λ (nm)	σ (cm² molecule^{-1})
201	4.40 × 10^{-18}	241	7.40 × 10^{-18}	281	1.05 × 10^{-17}
202	4.50 × 10^{-18}	242	7.60 × 10^{-18}	282	1.00 × 10^{-17}
203	4.90 × 10^{-18}	243	7.70 × 10^{-18}	283	9.60 × 10^{-18}
204	4.90 × 10^{-18}	244	8.00 × 10^{-18}	284	9.10 × 10^{-18}
205	4.90 × 10^{-18}	245	8.10 × 10^{-18}	285	8.70 × 10^{-18}
206	5.30 × 10^{-18}	246	8.40 × 10^{-18}	286	8.20 × 10^{-18}
207	5.40 × 10^{-18}	247	8.60 × 10^{-18}	287	7.70 × 10^{-18}
208	5.70 × 10^{-18}	248	8.90 × 10^{-18}	288	7.30 × 10^{-18}
209	5.70 × 10^{-18}	249	9.30 × 10^{-18}	289	6.90 × 10^{-18}
210	5.90 × 10^{-18}	250	9.60 × 10^{-18}	290	6.50 × 10^{-18}
211	6.30 × 10^{-18}	251	1.00 × 10^{-17}	291	6.10 × 10^{-18}
212	6.30 × 10^{-18}	252	1.04 × 10^{-17}	292	5.70 × 10^{-18}
213	6.70 × 10^{-18}	253	1.07 × 10^{-17}	293	5.30 × 10^{-18}
214	7.00 × 10^{-18}	254	1.11 × 10^{-17}	294	5.00 × 10^{-18}
215	7.20 × 10^{-18}	255	1.15 × 10^{-17}	295	4.60 × 10^{-18}
216	7.40 × 10^{-18}	256	1.19 × 10^{-17}	296	4.30 × 10^{-18}
217	7.40 × 10^{-18}	257	1.23 × 10^{-17}	297	4.00 × 10^{-18}
218	7.50 × 10^{-18}	258	1.27 × 10^{-17}	298	3.70 × 10^{-18}
219	7.50 × 10^{-18}	259	1.30 × 10^{-17}	299	3.50 × 10^{-18}
220	7.70 × 10^{-18}	260	1.33 × 10^{-17}	300	3.20 × 10^{-18}
221	7.70 × 10^{-18}	261	1.36 × 10^{-17}	301	2.90 × 10^{-18}
222	7.70 × 10^{-18}	262	1.39 × 10^{-17}	302	2.70 × 10^{-18}
223	7.60 × 10^{-18}	263	1.41 × 10^{-17}	303	2.50 × 10^{-18}
224	7.80 × 10^{-18}	264	1.43 × 10^{-17}	304	2.40 × 10^{-18}
225	7.70 × 10^{-18}	265	1.43 × 10^{-17}	305	2.10 × 10^{-18}
226	7.60 × 10^{-18}	266	1.44 × 10^{-17}	306	1.90 × 10^{-18}
227	7.60 × 10^{-18}	267	1.44 × 10^{-17}	307	1.80 × 10^{-18}
228	7.50 × 10^{-18}	268	1.44 × 10^{-17}	308	1.70 × 10^{-18}
229	7.50 × 10^{-18}	269	1.43 × 10^{-17}	309	1.60 × 10^{-18}
230	7.40 × 10^{-18}	270	1.41 × 10^{-17}	310	1.40 × 10^{-18}
231	7.40 × 10^{-18}	271	1.40 × 10^{-17}	311	1.10 × 10^{-18}
232	7.40 × 10^{-18}	272	1.38 × 10^{-17}	312	1.10 × 10^{-18}
233	7.20 × 10^{-18}	273	1.36 × 10^{-17}	313	1.10 × 10^{-18}
234	7.20 × 10^{-18}	274	1.33 × 10^{-17}	314	1.00 × 10^{-18}
235	7.20 × 10^{-18}	275	1.30 × 10^{-17}	315	9.00 × 10^{-19}
236	7.20 × 10^{-18}	276	1.25 × 10^{-17}	316	1.00 × 10^{-18}
237	7.20 × 10^{-18}	277	1.21 × 10^{-17}	317	6.00 × 10^{-19}
238	7.20 × 10^{-18}	278	1.18 × 10^{-17}	318	6.00 × 10^{-19}
239	7.30 × 10^{-18}	279	1.14 × 10^{-17}	319	6.00 × 10^{-19}
240	7.40 × 10^{-18}	280	1.10 × 10^{-17}	320	6.00 × 10^{-19}

The value of the cross sections are taken from Burkholder *et al*. (1993), and those of the quantum yields are taken from Harwood *et al*. (1995).

Appendix

Cl₂O₄ + hν → ClO + ClO₃ $Cl_2O_4 + h\nu \rightarrow ClO + ClO_3$ **J = 1.87 × 10⁻⁵ s⁻¹** $J = 1.87 \times 10^{-5}\ s^{-1}$ **φ = 1** $\varphi = 1$ **B10**

λ (nm)	σ (cm² molecule⁻¹)	λ (nm)	σ (cm² molecule⁻¹)	λ (nm)	σ (cm² molecule⁻¹)
200	9.68×10^{-19}	247	6.23×10^{-19}	294	1.50×10^{-20}
201	9.28×10^{-19}	248	5.95×10^{-19}	295	1.34×10^{-20}
202	8.79×10^{-19}	249	5.66×10^{-19}	296	1.21×10^{-20}
203	8.29×10^{-19}	250	5.38×10^{-19}	297	1.10×10^{-20}
204	7.78×10^{-19}	251	5.11×10^{-19}	298	1.01×10^{-20}
205	7.52×10^{-19}	252	4.86×10^{-19}	299	9.40×10^{-21}
206	7.32×10^{-19}	253	4.58×10^{-19}	300	8.80×10^{-21}
207	6.93×10^{-19}	254	4.33×10^{-19}	301	8.50×10^{-21}
208	6.75×10^{-19}	255	4.09×10^{-19}	302	8.30×10^{-21}
209	6.50×10^{-19}	256	3.85×10^{-19}	303	8.30×10^{-21}
210	6.46×10^{-19}	257	3.64×10^{-19}	304	8.30×10^{-21}
211	6.22×10^{-19}	258	3.43×10^{-19}	305	8.50×10^{-21}
212	6.18×10^{-19}	259	3.23×10^{-19}	306	8.80×10^{-21}
213	6.20×10^{-19}	260	3.03×10^{-19}	307	9.20×10^{-21}
214	6.17×10^{-19}	261	3.84×10^{-19}	308	9.70×10^{-21}
215	6.29×10^{-19}	262	2.66×10^{-19}	309	1.02×10^{-20}
216	6.35×10^{-19}	263	2.51×10^{-19}	310	1.08×10^{-20}
217	6.51×10^{-19}	264	2.36×10^{-19}	311	1.14×10^{-20}
218	6.66×10^{-19}	265	2.21×10^{-19}	312	1.21×10^{-20}
219	6.85×10^{-19}	266	2.06×10^{-19}	313	1.28×10^{-20}
220	7.08×10^{-19}	267	1.93×10^{-19}	314	1.35×10^{-20}
221	7.31×10^{-19}	268	1.80×10^{-19}	315	1.42×10^{-20}
222	7.50×10^{-19}	269	1.69×10^{-19}	316	1.49×10^{-20}
223	7.75×10^{-19}	270	1.58×10^{-19}	317	1.55×10^{-20}
224	7.79×10^{-19}	271	1.47×10^{-19}	318	1.62×10^{-20}
225	8.18×10^{-19}	272	1.36×10^{-19}	319	1.68×10^{-20}
226	8.39×10^{-19}	273	1.28×10^{-19}	320	1.74×10^{-20}
227	8.55×10^{-19}	274	1.18×10^{-19}	321	1.79×10^{-20}
228	8.72×10^{-19}	275	1.08×10^{-19}	322	1.83×10^{-20}
229	8.83×10^{-19}	276	9.95×10^{-20}	323	1.88×10^{-20}
230	8.92×10^{-19}	277	9.14×10^{-20}	324	1.91×10^{-20}
231	8.99×10^{-19}	278	8.38×10^{-20}	325	1.94×10^{-20}
232	9.01×10^{-19}	279	7.66×10^{-20}	326	1.96×10^{-20}
233	9.01×10^{-19}	280	6.98×10^{-20}	327	1.97×10^{-20}
234	8.97×10^{-19}	281	6.35×10^{-20}	328	1.98×10^{-20}
235	8.89×10^{-19}	282	5.76×10^{-20}	329	1.97×10^{-20}
236	8.79×10^{-19}	283	5.21×10^{-20}	330	1.96×10^{-20}
237	8.66×10^{-19}	284	4.70×10^{-20}	331	1.95×10^{-20}
238	7.49×10^{-19}	285	4.22×10^{-20}	332	1.92×10^{-20}
239	8.31×10^{-19}	286	3.79×10^{-20}	333	1.89×10^{-20}
240	8.10×10^{-19}	287	3.39×10^{-20}	334	1.85×10^{-20}
241	7.87×10^{-19}	288	3.03×10^{-20}	335	1.80×10^{-20}
242	7.61×10^{-19}	289	2.70×10^{-20}	336	1.75×10^{-20}
243	7.36×10^{-19}	290	2.40×10^{-20}	337	1.70×10^{-20}
244	7.10×10^{-19}	291	2.13×10^{-20}	338	1.63×10^{-20}
245	6.81×10^{-19}	292	1.89×10^{-20}	339	1.57×10^{-20}
246	6.52×10^{-19}	293	1.68×10^{-20}	340	1.50×10^{-20}
341	1.43×10^{-20}	345	1.17×10^{-20}	349	9.90×10^{-21}
342	1.36×10^{-20}	346	1.11×10^{-20}	350	9.80×10^{-21}
343	1.30×10^{-20}	347	1.06×10^{-20}		
344	1.23×10^{-20}	348	1.02×10^{-20}		

Appendix

The values of the cross sections are from Green *et al*. (2004), and those of quantum yields are taken from Harwood *et al*. (1995).

HCl + hν → H + Cl			**J = 0.00 × 10^{-0} s^{-1}**	**φ = 0.95**	**B11**
λ (nm)	σ (cm² molecule^{-1})	λ (nm)	σ (cm² molecule^{-1})	λ (nm)	σ (cm² molecule^{-1})
143	2.47×10^{-18}	173	1.30×10^{-18}	203	1.31×10^{-20}
144	2.62×10^{-18}	174	1.16×10^{-18}	204	1.08×10^{-20}
145	2.79×10^{-18}	175	1.06×10^{-18}	205	9.03×10^{-21}
146	2.93×10^{-18}	176	9.58×10^{-19}	206	7.26×10^{-21}
147	3.10×10^{-18}	177	8.41×10^{-19}	207	5.84×10^{-21}
148	3.19×10^{-18}	178	7.51×10^{-19}	208	4.79×10^{-21}
149	3.28×10^{-18}	179	6.67×10^{-19}	209	3.83×10^{-21}
150	3.34×10^{-18}	180	5.89×10^{-19}	210	3.10×10^{-21}
151	3.38×10^{-18}	181	5.17×10^{-19}	211	2.54×10^{-21}
152	3.39×10^{-18}	182	4.56×10^{-19}	212	2.00×10^{-21}
153	3.48×10^{-18}	183	3.91×10^{-19}	213	1.60×10^{-21}
154	3.42×10^{-18}	184	3.45×10^{-19}	214	1.28×10^{-21}
155	3.43×10^{-18}	185	2.94×10^{-19}	215	1.01×10^{-21}
156	3.41×10^{-18}	186	2.55×10^{-19}	216	7.87×10^{-22}
157	3.26×10^{-18}	187	2.20×10^{-19}	217	6.38×10^{-22}
158	3.25×10^{-18}	188	1.89×10^{-19}	218	4.99×10^{-22}
159	3.17×10^{-18}	189	1.61×10^{-19}	219	3.96×10^{-22}
160	3.06×10^{-18}	190	1.38×10^{-19}	220	2.97×10^{-22}
161	2.89×10^{-18}	191	1.15×10^{-19}	221	2.35×10^{-22}
162	2.83×10^{-18}	192	9.78×10^{-20}	222	1.90×10^{-22}
163	2.68×10^{-18}	193	8.37×10^{-20}	223	1.53×10^{-22}
164	2.55×10^{-18}	194	7.10×10^{-20}	224	1.22×10^{-22}
165	2.40×10^{-18}	195	5.96×10^{-20}	225	9.95×10^{-23}
166	2.20×10^{-18}	196	4.99×10^{-20}	226	7.81×10^{-23}
167	2.10×10^{-18}	197	4.16×10^{-20}	227	6.29×10^{-23}
168	1.95×10^{-18}	198	3.49×10^{-20}	228	4.92×10^{-23}
169	1.79×10^{-18}	199	2.91×10^{-20}	229	3.97×10^{-23}
170	1.63×10^{-18}	200	2.39×10^{-20}	230	3.35×10^{-23}
171	1.55×10^{-18}	201	1.99×10^{-20}		
172	1.42×10^{-18}	202	1.62×10^{-20}		

The values of the cross sections are from Cheng *et al*. (2002)

Appendix

HOCl + hν → Cl + HO **J = 6.48 × 10⁻⁵ s⁻¹** **φ = 1** **B12**

λ (nm)	σ (cm² molecule⁻¹)	λ (nm)	σ (cm² molecule⁻¹)	λ (nm)	σ (cm² molecule⁻¹)
200	7.18×10^{-20}	274	5.26×10^{-20}	348	1.55×10^{-20}
202	6.39×10^{-20}	276	4.94×10^{-20}	350	1.43×10^{-20}
204	5.81×10^{-20}	278	4.74×10^{-20}	352	1.33×10^{-20}
206	5.46×10^{-20}	280	4.64×10^{-20}	354	1.24×10^{-20}
208	5.37×10^{-20}	282	4.62×10^{-20}	356	1.17×10^{-20}
210	5.54×10^{-20}	284	4.68×10^{-20}	358	1.11×10^{-20}
212	5.98×10^{-20}	286	4.79×10^{-20}	360	1.06×10^{-20}
214	6.68×10^{-20}	288	4.95×10^{-20}	362	1.02×10^{-20}
216	7.63×10^{-20}	290	5.13×10^{-20}	364	9.85×10^{-21}
218	8.81×10^{-20}	292	5.33×10^{-20}	366	9.51×10^{-21}
220	1.02×10^{-19}	294	5.52×10^{-20}	368	9.19×10^{-21}
222	1.16×10^{-19}	296	5.71×10^{-20}	370	8.88×10^{-21}
224	1.32×10^{-19}	298	5.86×10^{-20}	372	8.55×10^{-21}
226	1.47×10^{-19}	300	5.99×10^{-20}	374	8.22×10^{-21}
228	1.62×10^{-19}	302	6.08×10^{-20}	376	7.86×10^{-21}
230	1.75×10^{-19}	304	6.12×10^{-20}	378	7.48×10^{-21}
232	1.87×10^{-19}	306	6.12×10^{-20}	380	7.08×10^{-21}
234	1.96×10^{-19}	308	6.07×10^{-20}	382	6.67×10^{-21}
236	2.02×10^{-19}	310	5.97×10^{-20}	384	6.24×10^{-21}
238	2.05×10^{-19}	312	5.84×10^{-20}	386	5.80×10^{-21}
240	2.06×10^{-19}	314	5.66×10^{-20}	388	5.35×10^{-21}
242	2.03×10^{-19}	316	5.45×10^{-20}	390	4.91×10^{-21}
244	1.98×10^{-19}	318	5.21×10^{-20}	392	4.47×10^{-21}
246	1.90×10^{-19}	320	4.95×10^{-20}	394	4.05×10^{-21}
248	1.81×10^{-19}	322	4.67×10^{-20}	396	3.64×10^{-21}
250	1.70×10^{-19}	324	4.38×10^{-20}	398	3.25×10^{-21}
252	1.58×10^{-19}	326	4.09×10^{-20}	400	2.88×10^{-21}
254	1.46×10^{-19}	328	3.79×10^{-20}	402	2.54×10^{-21}
256	1.33×10^{-19}	330	3.50×10^{-20}	404	2.22×10^{-21}
258	1.21×10^{-19}	332	3.21×10^{-20}	406	1.94×10^{-21}
260	1.09×10^{-19}	334	2.94×10^{-20}	408	1.68×10^{-21}
262	9.73×10^{-20}	336	2.68×10^{-20}	410	1.44×10^{-21}
264	8.68×10^{-20}	338	2.44×10^{-20}	412	1.24×10^{-21}
266	7.75×10^{-20}	340	2.22×10^{-20}	414	1.05×10^{-21}
268	6.94×10^{-20}	342	2.02×10^{-20}	416	8.90×10^{-22}
270	6.25×10^{-20}	344	1.84×10^{-20}	418	7.50×10^{-22}
272	5.69×10^{-20}	346	1.69×10^{-20}	420	6.30×10^{-22}

The values of the cross sections are from Barnes *et al*. (1998), and those of quantum yields are recommended by Burkholder *et al*. (2020).

Appendix

| HOClO₂ + hν → OClO + HO | | J = 2.07 × 10⁻⁹ s⁻¹ | φ = 1 | | B13 |

HOClO$_2$ + hν → OClO + HO   **J = 2.07 × 10^{-9} s^{-1}**   **φ = 1**   **B13**

λ (nm)	σ (cm² molecule⁻¹)	λ (nm)	σ (cm² molecule⁻¹)	λ (nm)	σ (cm² molecule⁻¹)
169.13	5.06×10^{-18}	193.88	5.27×10^{-18}	233.40	6.04×10^{-18}
170.95	4.90×10^{-18}	195.23	5.54×10^{-18}	234.92	5.74×10^{-18}
171.99	5.24×10^{-18}	196.14	5.29×10^{-18}	236.57	6.07×10^{-18}
172.28	5.73×10^{-18}	196.91	4.99×10^{-18}	237.77	6.49×10^{-18}
173.02	6.35×10^{-18}	197.38	4.26×10^{-18}	238.81	6.86×10^{-18}
173.60	7.04×10^{-18}	198.15	3.78×10^{-18}	239.56	7.14×10^{-18}
174.19	7.57×10^{-18}	198.62	3.30×10^{-18}	240.31	7.32×10^{-18}
175.38	8.05×10^{-18}	199.84	2.92×10^{-18}	241.52	7.12×10^{-18}
176.45	7.61×10^{-18}	201.03	3.27×10^{-18}	243.04	6.73×10^{-18}
176.47	7.04×10^{-18}	201.93	3.59×10^{-18}	244.41	6.36×10^{-18}
177.24	6.51×10^{-18}	203.28	3.88×10^{-18}	246.54	5.94×10^{-18}
178.30	6.19×10^{-18}	205.25	3.49×10^{-18}	247.76	5.44×10^{-18}
179.66	6.39×10^{-18}	207.23	3.12×10^{-18}	248.68	4.90×10^{-18}
180.25	6.58×10^{-18}	208.14	2.79×10^{-18}	250.21	4.27×10^{-18}
181.32	6.30×10^{-18}	210.57	2.35×10^{-18}	251.74	3.79×10^{-18}
181.78	5.98×10^{-18}	212.68	2.41×10^{-18}	253.25	3.52×10^{-18}
182.83	6.28×10^{-18}	215.25	2.51×10^{-18}	255.67	3.38×10^{-18}
183.12	6.70×10^{-18}	216.59	2.88×10^{-18}	257.34	3.04×10^{-18}
183.86	7.19×10^{-18}	217.03	3.30×10^{-18}	258.11	2.64×10^{-18}
184.14	7.74×10^{-18}	217.63	3.62×10^{-18}	259.93	2.18×10^{-18}
185.19	8.23×10^{-18}	218.98	3.81×10^{-18}	262.06	1.70×10^{-18}
185.78	8.58×10^{-18}	220.50	3.62×10^{-18}	264.34	1.34×10^{-18}
187.01	7.65×10^{-18}	221.71	3.25×10^{-18}	266.91	1.17×10^{-18}
187.34	7.01×10^{-18}	223.84	2.88×10^{-18}	270.23	1.06×10^{-18}
187.51	6.29×10^{-18}	225.64	3.11×10^{-18}	273.11	7.98×10^{-19}
187.98	5.52×10^{-18}	226.23	3.50×10^{-18}	275.53	5.43×10^{-19}
188.61	4.86×10^{-18}	227.28	3.99×10^{-18}	278.26	2.88×10^{-19}
189.08	4.18×10^{-18}	228.46	4.64×10^{-18}	282.64	1.39×10^{-19}
190.15	3.75×10^{-18}	229.20	5.35×10^{-18}	286.84	7.85×10^{-19}
191.20	3.97×10^{-18}	230.24	5.84×10^{-18}	292.60	8.66×10^{-20}
192.39	4.46×10^{-18}	230.68	6.09×10^{-18}	296.83	5.73×10^{-20}
193.44	4.90×10^{-18}	232.04	6.26×10^{-18}	299.85	9.46×10^{-20}

The values of the cross sections are from Tham *et al.* (2020).

Appendix

HOClO₃ + hν → ClO₃ + HO $J = 0.00 \times 10^{-0} \text{ s}^{-1}$ $\varphi = 1$ **B14**

λ (nm)	σ (cm² molecule⁻¹)	λ (nm)	σ (cm² molecule⁻¹)	λ (nm)	σ (cm² molecule⁻¹)
169.77	2.51×10^{-18}	192.73	2.55×10^{-18}	216.10	1.27×10^{-18}
170.52	2.70×10^{-18}	193.48	2.72×10^{-18}	216.72	1.15×10^{-18}
170.96	2.87×10^{-18}	194.84	2.89×10^{-18}	217.50	9.43×10^{-19}
171..86	3.01×10^{-18}	195.61	2.76×10^{-18}	218.12	7.28×10^{-19}
172.18	2.89×10^{-18}	196.38	2.57×10^{-18}	218.74	5.40×10^{-19}
172.80	2.71×10^{-18}	196.86	2.35×10^{-18}	219.82	3.78×10^{-19}
173.27	2.47×10^{-18}	197.33	2.09×10^{-18}	221.80	3.02×10^{-19}
173.75	2.22×10^{-18}	197.96	1.82×10^{-18}	223.17	3.51×10^{-19}
174.08	1.92×10^{-18}	198.43	1.64×10^{-18}	224.53	3.92×10^{-19}
175.46	1.67×10^{-18}	199.51	1.48×10^{-18}	226.52	3.31×10^{-19}
176.51	1.86×10^{-18}	200.41	1.66×10^{-18}	228.04	2.29×10^{-19}
176.95	2.12×10^{-18}	201.00	1.86×10^{-18}	230.48	1.72×10^{-19}
177.08	2.36×10^{-18}	201.59	2.05×10^{-18}	232.15	2.25×10^{-19}
177.52	2.60×10^{-18}	202.34	2.27×10^{-18}	233.67	3.04×10^{-19}
177.81	2.94×10^{-18}	203.24	2.42×10^{-18}	235.33	3.56×10^{-19}
178.40	3.01×10^{-18}	203.86	2.28×10^{-18}	237.01	2.77×10^{-19}
179.15	3.17×10^{-18}	204.64	2.05×10^{-18}	238.70	1.60×10^{-19}
180.83	3.12×10^{-18}	205.26	1.85×10^{-18}	341.29	5.39×10^{-20}
182.04	3.15×10^{-18}	205.88	1.62×10^{-18}	245.85	3.81×10^{-20}
183.12	3.04×10^{-18}	206.66	1.47×10^{-18}	251.48	2.97×10^{-20}
184.65	2.90×10^{-18}	207.12	1.33×10^{-18}	258.17	1.73×10^{-20}
186.04	2.91×10^{-18}	208.50	1.25×10^{-18}	263.50	1.64×10^{-20}
186.94	2.81×10^{-18}	209.86	1.34×10^{-18}	266.38	4.60×10^{-20}
188.01	2.64×10^{-18}	210.76	1.47×10^{-18}	268.82	6.45×10^{-20}
189.09	2.44×10^{-18}	212.43	1.56×10^{-18}	272.62	2.99×10^{-20}
190.78	2.24×10^{-18}	213.65	1.49×10^{-18}	277.19	1.04×10^{-20}
191.99	2.36×10^{-18}	215.18	1.40×10^{-18}		

The values of the cross sections are from Tham *et al*. (2020).

Appendix

ClNO + hν → Cl + NO **J = 1.27 × 10⁻³ s⁻¹** **φ = 1** **B15**

λ (nm)	σ (cm² molecule⁻¹)	λ (nm)	σ (cm² molecule⁻¹)	λ (nm)	σ (cm² molecule⁻¹)
190	4.32×10^{-17}	237	1.14×10^{-18}	284	9.99×10^{-20}
191	4.80×10^{-17}	238	1.01×10^{-18}	285	9.91×10^{-20}
192	5.34×10^{-17}	239	9.00×10^{-19}	286	9.84×10^{-20}
193	5.80×10^{-17}	240	8.26×10^{-19}	287	9.73×10^{-20}
194	6.15×10^{-17}	241	7.42×10^{-19}	288	9.71×10^{-20}
195	6.36×10^{-17}	242	6.72×10^{-19}	289	9.67×10^{-20}
196	6.48×10^{-17}	243	6.13×10^{-19}	290	9.64×10^{-20}
197	6.45×10^{-17}	244	5.51×10^{-19}	291	9.60×10^{-20}
198	6.31×10^{-17}	245	5.00×10^{-19}	292	9.63×10^{-20}
199	3.12×10^{-17}	246	4.52×10^{-19}	293	9.61×10^{-20}
200	5.86×10^{-17}	247	4.16×10^{-19}	294	9.69×10^{-20}
201	5.58×10^{-17}	248	3.77×10^{-19}	295	9.67×10^{-20}
202	5.25×10^{-17}	249	3.48×10^{-19}	296	9.71×10^{-20}
203	4.90×10^{-17}	250	3.17×10^{-19}	297	9.83×10^{-20}
204	4.54×10^{-17}	251	2.94×10^{-19}	298	9.69×10^{-20}
205	4.20×10^{-17}	252	2.74×10^{-19}	299	9.92×10^{-20}
206	3.84×10^{-17}	253	2.66×10^{-19}	300	1.00×10^{-19}
207	3.51×10^{-17}	254	2.37×10^{-19}	301	1.01×10^{-19}
208	3.21×10^{-17}	255	2.24×10^{-19}	302	1.03×10^{-19}
209	2.92×10^{-17}	256	2.13×10^{-19}	303	1.03×10^{-19}
210	2.63×10^{-17}	257	2.00×10^{-19}	304	1.05×10^{-19}
211	2.37×10^{-17}	258	1.90×10^{-19}	305	1.07×10^{-19}
212	2.18×10^{-17}	259	1.82×10^{-19}	306	1.08×10^{-19}
213	1.96×10^{-17}	260	1.75×10^{-19}	307	1.10×10^{-19}
214	1.76×10^{-17}	261	1.70×10^{-19}	308	1.11×10^{-19}
215	1.67×10^{-17}	262	1.65×10^{-19}	309	1.13×10^{-19}
216	1.40×10^{-17}	263	1.59×10^{-19}	310	1.15×10^{-19}
217	1.26×10^{-17}	264	1.53×10^{-19}	311	1.17×10^{-19}
218	1.11×10^{-17}	265	1.49×10^{-19}	312	1.19×10^{-19}
219	1.00×10^{-17}	266	1.44×10^{-19}	313	1.20×10^{-19}
220	8.96×10^{-18}	267	1.40×10^{-19}	314	1.22×10^{-19}
221	7.91×10^{-18}	268	1.36×10^{-19}	315	1.24×10^{-19}
222	7.07×10^{-18}	269	1.33×10^{-19}	316	1.25×10^{-19}
223	6.27×10^{-18}	270	1.29×10^{-19}	317	1.28×10^{-19}
224	5.52×10^{-18}	271	1.26×10^{-19}	318	1.30×10^{-19}
225	4.89×10^{-18}	272	1.23×10^{-19}	319	1.32×10^{-19}
226	4.36×10^{-18}	273	1.20×10^{-19}	320	1.34×10^{-19}
227	3.85×10^{-18}	274	1.18×10^{-19}	321	1.35×10^{-19}
228	3.39×10^{-18}	275	1.16×10^{-19}	322	1.36×10^{-19}
229	3.04×10^{-18}	276	1.13×10^{-19}	323	1.39×10^{-19}
230	2.66×10^{-18}	277	1.11×10^{-19}	324	1.40×10^{-19}
231	2.37×10^{-18}	278	1.07×10^{-19}	325	1.42×10^{-19}
232	2.12×10^{-18}	279	1.07×10^{-19}	326	1.43×10^{-19}
233	1.86×10^{-18}	280	1.06×10^{-19}	327	1.46×10^{-19}
234	1.64×10^{-18}	281	1.04×10^{-19}	328	1.46×10^{-19}
235	1.45×10^{-18}	282	1.02×10^{-19}	329	1.46×10^{-19}
236	1.20×10^{-18}	283	1.01×10^{-19}	330	1.47×10^{-19}
331	1.48×10^{-19}	348	1.49×10^{-19}	425	2.45×10^{-20}
332	1.49×10^{-19}	349	1.48×10^{-19}	430	2.21×10^{-20}
333	1.49×10^{-19}	350	1.45×10^{-19}	435	2.20×10^{-20}
334	1.51×10^{-19}	355	1.36×10^{-19}	440	2.20×10^{-20}
335	1.52×10^{-19}	360	1.29×10^{-19}	445	2.07×10^{-20}

Appendix

336	1.53×10^{-19}	365	1.20×10^{-19}	450	1.87×10^{-20}
337	1.54×10^{-19}	370	1.10×10^{-19}	455	1.79×10^{-20}
338	1.53×10^{-19}	375	9.95×10^{-20}	460	1.95×10^{-20}
339	1.53×10^{-19}	380	8.86×10^{-20}	465	2.25×10^{-20}
340	1.52×10^{-19}	385	7.82×10^{-20}	470	2.50×10^{-20}
341	1.53×10^{-19}	390	6.86×10^{-20}	475	2.61×10^{-20}
342	1.53×10^{-19}	395	5.97×10^{-20}	480	2.53×10^{-20}
343	1.53×10^{-19}	400	5.13×10^{-20}	485	2.33×10^{-20}
344	1.51×10^{-19}	405	4.40×10^{-20}	490	2.07×10^{-20}
345	1.49×10^{-19}	410	3.83×10^{-20}	495	1.78×10^{-20}
346	1.51×10^{-19}	415	3.38×10^{-20}	500	1.50×10^{-20}
347	1.49×10^{-19}	420	2.89×10^{-20}		

For a step of 1 nm ($190 < \lambda < 350$): The values of the cross sections are from Tyndall *et al.* (1987).

For a step of 5 nm ($355 < \lambda < 650$): The values of the cross sections are from Roehl *et al.* (1992).

The values of the quantum yields are taken from Calvert and Pitts (1966)

Appendix

| ClNO₂ + hv → Cl + NO₂ | | J = 7.52 × 10⁻⁵ s⁻¹ | φ = 0.93 | | B16 |

$ClNO_2 + h\nu \rightarrow Cl + NO_2$ $\quad J = 7.52 \times 10^{-5}\ s^{-1} \quad \varphi = 0.93 \quad$ **B16**

λ (nm)	σ (cm² molecule⁻¹)	λ (nm)	σ (cm² molecule⁻¹)	λ (nm)	σ (cm² molecule⁻¹)
200	4.02×10^{-18}	247	1.03×10^{-18}	295	1.58×10^{-19}
201	3.64×10^{-18}	248	9.98×10^{-19}	296	1.56×10^{-19}
202	3.36×10^{-18}	249	9.56×10^{-19}	297	4.54×10^{-19}
203	3.19×10^{-18}	250	9.29×10^{-19}	298	1.52×10^{-19}
204	3.10×10^{-18}	251	8.87×10^{-19}	299	1.50×10^{-19}
205	3.06×10^{-18}	252	8.53×10^{-19}	300	1.48×10^{-19}
206	3.06×10^{-18}	253	8.24×10^{-19}	301	1.45×10^{-19}
207	3.09×10^{-18}	254	7.86×10^{-19}	302	1.43×10^{-19}
208	3.14×10^{-18}	255	7.59×10^{-19}	303	1.40×10^{-19}
209	3.20×10^{-18}	257	6.88×10^{-19}	304	1.37×10^{-19}
210	3.26×10^{-18}	258	6.61×10^{-19}	305	1.35×10^{-19}
211	3.33×10^{-18}	259	6.28×10^{-19}	306	1.32×10^{-19}
212	3.38×10^{-18}	260	5.96×10^{-19}	307	1.29×10^{-19}
213	3.43×10^{-18}	261	5.70×10^{-19}	308	1.26×10^{-19}
214	3.46×10^{-18}	262	5.39×10^{-19}	309	1.23×10^{-19}
215	3.48×10^{-18}	263	5.10×10^{-19}	310	1.20×10^{-19}
216	3.48×10^{-18}	264	4.86×10^{-19}	311	1.17×10^{-19}
217	3.47×10^{-18}	265	4.59×10^{-19}	312	1.14×10^{-19}
218	3.44×10^{-18}	266	4.32×10^{-19}	313	1.11×10^{-19}
219	3.39×10^{-18}	267	4.10×10^{-19}	314	1.07×10^{-19}
220	3.32×10^{-18}	268	3.88×10^{-19}	315	1.04×10^{-19}
221	3.24×10^{-18}	269	3.66×10^{-19}	316	1.01×10^{-19}
222	3.15×10^{-18}	270	3.48×10^{-19}	317	9.76×10^{-20}
223	3.05×10^{-18}	271	3.30×10^{-19}	318	9.44×10^{-20}
224	2.94×10^{-18}	272	3.12×10^{-19}	319	9.12×10^{-20}
225	2.82×10^{-18}	273	2.96×10^{-19}	320	8.81×10^{-20}
226	2.69×10^{-18}	274	2.82×10^{-19}	321	8.49×10^{-20}
227	2.57×10^{-18}	275	2.68×10^{-19}	322	8.18×10^{-20}
228	2.45×10^{-18}	276	2.56×10^{-19}	323	7.85×10^{-20}
229	2.32×10^{-18}	277	2.45×10^{-19}	324	7.54×10^{-20}
230	2.20×10^{-18}	278	2.35×10^{-19}	325	7.24×10^{-20}
231	2.09×10^{-18}	279	2.26×10^{-19}	326	6.94×10^{-20}
232	1.98×10^{-18}	280	2.18×10^{-19}	327	6.62×10^{-20}
233	1.88×10^{-18}	281	2.10×10^{-19}	328	6.37×10^{-20}
234	1.78×10^{-18}	282	2.03×10^{-19}	329	6.09×10^{-20}
235	1.70×10^{-18}	283	1.97×10^{-19}	330	5.82×10^{-20}
236	1.61×10^{-18}	284	1.92×10^{-19}	331	5.56×10^{-20}
237	1.54×10^{-18}	285	1.88×10^{-19}	332	5.30×10^{-20}
238	1.47×10^{-18}	286	1.83×10^{-19}	333	5.06×10^{-20}
239	1.40×10^{-18}	287	1.79×10^{-19}	334	4.82×10^{-20}
240	1.35×10^{-18}	288	1.76×10^{-19}	335	4.59×10^{-20}
241	1.29×10^{-18}	289	1.73×10^{-19}	336	4.37×10^{-20}
242	1.24×10^{-18}	290	1.70×10^{-19}	337	4.16×10^{-20}
243	1.19×10^{-18}	291	1.68×10^{-19}	338	3.95×10^{-20}
244	1.15×10^{-18}	292	1.65×10^{-19}	339	3.75×10^{-20}
245	1.11×10^{-18}	293	1.63×10^{-19}	340	3.56×10^{-20}
246	1.07×10^{-18}	294	1.60×10^{-19}	341	3.38×10^{-20}
342	3.21×10^{-20}	387	2.38×10^{-21}	432	2.03×10^{-22}
343	3.04×10^{-20}	388	2.24×10^{-21}	433	1.85×10^{-22}
344	2.88×10^{-20}	389	2.13×10^{-21}	434	1.75×10^{-22}
345	2.73×10^{-20}	390	2.01×10^{-21}	435	1.69×10^{-22}
346	2.58×10^{-20}	391	1.89×10^{-21}	436	1.54×10^{-22}

Appendix

347	2.44×10^{-20}	392	1.77×10^{-21}	437	1.50×10^{-22}
348	2.31×10^{-20}	393	1.67×10^{-21}	438	1.40×10^{-22}
349	2.19×10^{-20}	394	1.58×10^{-21}	439	1.28×10^{-22}
350	2.07×10^{-20}	395	1.49×10^{-21}	440	1.22×10^{-22}
351	1.96×10^{-20}	396	1.41×10^{-21}	441	1.13×10^{-22}
352	1.85×10^{-20}	397	1.33×10^{-21}	442	1.13×10^{-22}
353	1.75×10^{-20}	398	1.25×10^{-21}	443	1.07×10^{-22}
354	1.65×10^{-20}	399	1.18×10^{-21}	444	9.84×10^{-23}
355	1.56×10^{-20}	400	1.12×10^{-21}	445	9.05×10^{-23}
356	1.47×10^{-20}	401	1.06×10^{-21}	446	8.99×10^{-23}
357	1.39×10^{-20}	402	1.00×10^{-21}	447	8.39×10^{-23}
358	1.31×10^{-20}	403	9.48×10^{-22}	448	7.58×10^{-23}
359	1.24×10^{-20}	404	8.91×10^{-22}	449	7.73×10^{-23}
360	1.17×10^{-20}	405	8.39×10^{-22}	450	7.90×10^{-23}
361	1.10×10^{-20}	406	7.96×10^{-22}	451	7.24×10^{-23}
362	1.04×10^{-20}	407	7.61×10^{-22}	452	6.95×10^{-23}
363	9.79×10^{-21}	408	7.15×10^{-22}	453	6.94×10^{-23}
364	9.23×10^{-21}	409	6.75×10^{-22}	454	6.14×10^{-23}
365	8.70×10^{-21}	410	6.42×10^{-22}	455	6.35×10^{-23}
366	8.19×10^{-21}	411	6.08×10^{-22}	456	6.14×10^{-23}
367	7.73×10^{-21}	412	5.69×10^{-22}	457	4.72×10^{-23}
368	7.28×10^{-21}	413	5.36×10^{-22}	458	5.34×10^{-23}
369	6.87×10^{-21}	414	5.12×10^{-22}	459	5.97×10^{-23}
370	6.48×10^{-21}	415	4.86×10^{-22}	460	5.47×10^{-23}
371	6.11×10^{-21}	416	4.60×10^{-22}	461	4.71×10^{-23}
372	5.76×10^{-21}	417	4.34×10^{-22}	462	3.51×10^{-23}
373	5.43×10^{-21}	418	4.11×10^{-22}	463	3.57×10^{-23}
374	5.12×10^{-21}	419	3.87×10^{-22}	464	4.18×10^{-23}
375	4.82×10^{-21}	420	3.60×10^{-22}	465	3.69×10^{-23}
376	4.54×10^{-21}	421	3.36×10^{-22}	466	3.84×10^{-23}
377	4.27×10^{-21}	422	3.19×10^{-22}	467	3.69×10^{-23}
378	4.03×10^{-21}	423	2.97×10^{-22}	468	3.76×10^{-23}
379	3.80×10^{-21}	424	2.88×10^{-22}	469	4.39×10^{-23}
380	3.58×10^{-21}	425	2.82×10^{-22}	470	3.21×10^{-23}
381	3.38×10^{-21}	426	2.75×10^{-22}	471	2.28×10^{-23}
382	3.18×10^{-21}	427	2.46×10^{-22}	472	2.21×10^{-23}
383	3.01×10^{-21}	428	2.38×10^{-22}	473	2.68×10^{-23}
384	2.84×10^{-21}	429	2.27×10^{-22}	474	3.39×10^{-23}
385	2.68×10^{-21}	430	2.12×10^{-22}	475	2.05×10^{-23}
386	2.53×10^{-21}	431	2.04×10^{-22}		

The values of the cross sections are from Ghosh *et al.* (2012), and those of the quantum yields are taken from Nelson and Johnston (1981).

Appendix

| ClONO₂ + hν → Cl + NO₃ | | J = 1.04 × 10⁻⁵ s⁻¹ | φ1 = 0.6 | B17 |

ClONO₂ + hν → Cl + NO₃   J = 1.04×10^{-5} s⁻¹   φ1 = 0.6   **B17**
ClONO₂ + hν → ClO + NO₂   J = 1.26×10^{-6} s⁻¹   φ1 = 0.4   **B18**
ClONO₂ + hν → ClNO₂ + O (³P)   J = 0.00×10^{-0} s⁻¹   φ3 = 0   **B19**
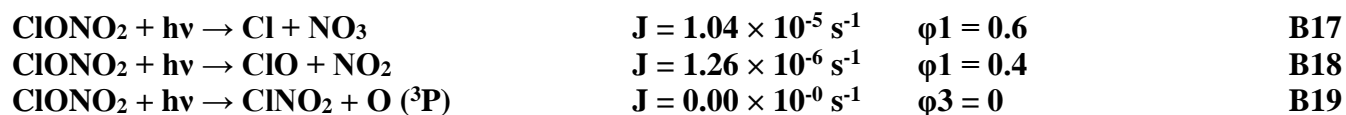
λ (nm)	σ (cm² molecule⁻¹)	λ (nm)	σ (cm² molecule⁻¹)	λ (nm)	σ (cm² molecule⁻¹)
196	3.10×10^{-18}	276	1.49×10^{-19}	356	2.05×10^{-21}
198	2.94×10^{-18}	278	1.33×10^{-19}	358	2.03×10^{-21}
200	2.82×10^{-18}	280	1.19×10^{-19}	360	2.00×10^{-21}
202	2.77×10^{-18}	282	1.05×10^{-19}	362	1.90×10^{-21}
204	2.80×10^{-18}	284	9.35×10^{-20}	364	1.84×10^{-21}
206	2.88×10^{-18}	286	8.26×10^{-20}	366	1.75×10^{-21}
208	3.00×10^{-18}	288	7.24×10^{-20}	368	1.66×10^{-21}
210	3.14×10^{-18}	290	6.41×10^{-20}	370	1.59×10^{-21}
212	3.29×10^{-18}	292	5.50×10^{-20}	372	1.51×10^{-21}
214	3.39×10^{-18}	294	4.67×10^{-20}	374	1.44×10^{-21}
216	3.45×10^{-18}	296	4.09×10^{-20}	376	1.38×10^{-21}
218	3.41×10^{-18}	298	3.57×10^{-20}	378	1.29×10^{-21}
220	3.32×10^{-18}	300	3.13×10^{-20}	380	1.21×10^{-21}
222	3.14×10^{-18}	302	2.74×10^{-20}	382	1.15×10^{-21}
224	2.91×10^{-18}	304	2.39×10^{-20}	384	1.08×10^{-21}
226	2.64×10^{-18}	306	2.09×10^{-20}	386	1.03×10^{-21}
228	2.35×10^{-18}	308	1.83×10^{-20}	388	9.70×10^{-22}
230	2.08×10^{-18}	310	1.60×10^{-20}	390	9.09×10^{-22}
232	1.82×10^{-18}	312	1.40×10^{-20}	392	8.49×10^{-22}
234	1.58×10^{-18}	314	1.22×10^{-20}	394	7.80×10^{-22}
236	1.38×10^{-18}	316	1.07×10^{-20}	396	7.40×10^{-22}
238	1.20×10^{-18}	318	9.47×10^{-21}	398	7.10×10^{-22}
240	1.05×10^{-18}	320	8.31×10^{-21}	400	6.38×10^{-22}
242	9.19×10^{-19}	322	7.31×10^{-21}	402	5.99×10^{-22}
244	8.12×10^{-19}	324	6.47×10^{-21}	404	5.68×10^{-22}
246	7.16×10^{-19}	326	5.78×10^{-21}	406	5.13×10^{-22}
248	6.24×10^{-19}	328	5.18×10^{-21}	408	4.81×10^{-22}
250	5.60×10^{-19}	330	4.66×10^{-21}	410	4.44×10^{-22}
252	5.02×10^{-19}	332	4.20×10^{-21}	412	4.13×10^{-22}
254	4.53×10^{-19}	334	3.82×10^{-21}	414	3.73×10^{-22}
256	4.10×10^{-19}	336	3.51×10^{-21}	416	3.56×10^{-22}
258	3.72×10^{-19}	338	3.26×10^{-21}	418	3.17×10^{-22}
260	3.38×10^{-19}	340	3.02×10^{-21}	420	3.16×10^{-22}
262	3.06×10^{-19}	342	2.82×10^{-21}	422	2.75×10^{-22}
264	2.78×10^{-19}	344	2.64×10^{-21}	424	2.42×10^{-22}
266	2.52×10^{-19}	346	2.52×10^{-21}	426	2.22×10^{-22}
268	2.27×10^{-19}	348	2.43×10^{-21}	428	2.07×10^{-22}
270	2.05×10^{-19}	350	2.29×10^{-21}	430	1.89×10^{-22}
272	1.85×10^{-19}	352	2.18×10^{-21}	432	1.88×10^{-22}
274	1.66×10^{-19}	354	2.12×10^{-21}		

The values of the cross sections are from Burkholder *et al.* (1994), and those of the quantum yields (φ1 and φ2) are from Burkholder *et al.* (2020), and for (φ3) by Keller-Rudek *et al.* (2013).

φ3 = 0.73 for λ ≤ 220 nm, φ3 = 0.13 for 222 nm ≤ λ ≤ 246 nm, and φ3 = 0 for λ ≥ 248 nm

Appendix

Cl₂O₆ + hν → OClO + ClO₄ $\quad$ **J = 7.05 × 10⁻³ s⁻¹** $\quad$ **φ = 1** $\quad$ **BXXX**

λ (nm)	σ (cm² molecule⁻¹)	λ (nm)	σ (cm² molecule⁻¹)	λ (nm)	σ (cm² molecule⁻¹)
200	1.10×10^{-17}	248	1.09×10^{-17}	295	1.20×10^{-17}
201	1.13×10^{-17}	249	1.10×10^{-17}	296	1.17×10^{-17}
202	1.14×10^{-17}	250	1.11×10^{-17}	297	1.14×10^{-17}
203	1.16×10^{-17}	251	1.13×10^{-17}	298	1.12×10^{-17}
204	1.16×10^{-17}	252	1.14×10^{-17}	299	1.09×10^{-17}
205	1.18×10^{-17}	253	1.16×10^{-17}	300	1.06×10^{-17}
206	1.21×10^{-17}	254	1.18×10^{-17}	301	1.03×10^{-17}
207	1.21×10^{-17}	255	1.20×10^{-17}	302	9.97×10^{-18}
208	1.23×10^{-17}	256	1.22×10^{-17}	303	9.68×10^{-18}
209	1.24×10^{-17}	257	1.24×10^{-17}	304	9.39×10^{-18}
210	1.25×10^{-17}	258	1.26×10^{-17}	305	9.10×10^{-18}
211	1.25×10^{-17}	259	1.28×10^{-17}	306	8.80×10^{-18}
212	1.26×10^{-17}	260	1.30×10^{-17}	307	8.51×10^{-18}
213	1.27×10^{-17}	261	1.32×10^{-17}	308	8.22×10^{-18}
214	1.27×10^{-17}	262	1.34×10^{-17}	309	7.94×10^{-18}
215	1.26×10^{-17}	263	1.36×10^{-17}	310	7.67×10^{-18}
216	1.26×10^{-17}	264	1.38×10^{-17}	311	7.40×10^{-18}
217	1.25×10^{-17}	265	1.39×10^{-17}	312	7.14×10^{-18}
218	1.25×10^{-17}	266	1.41×10^{-17}	313	6.89×10^{-18}
219	1.24×10^{-17}	267	1.43×10^{-17}	314	6.64×10^{-18}
220	1.23×10^{-17}	268	1.44×10^{-17}	315	6.39×10^{-18}
221	1.22×10^{-17}	269	1.45×10^{-17}	316	6.15×10^{-18}
222	1.21×10^{-17}	270	1.47×10^{-17}	317	5.92×10^{-18}
223	1.19×10^{-17}	271	1.48×10^{-17}	318	5.69×10^{-18}
224	1.18×10^{-17}	272	1.49×10^{-17}	319	5.47×10^{-18}
225	1.17×10^{-17}	273	1.49×10^{-17}	320	5.26×10^{-18}
226	1.16×10^{-17}	274	1.50×10^{-17}	321	5.06×10^{-18}
227	1.14×10^{-17}	275	1.50×10^{-17}	322	4.85×10^{-18}
228	1.13×10^{-17}	276	1.50×10^{-17}	323	4.65×10^{-18}
229	1.12×10^{-17}	277	1.50×10^{-17}	324	4.47×10^{-18}
230	1.11×10^{-17}	278	1.50×10^{-17}	325	4.29×10^{-18}
231	1.10×10^{-17}	279	1.49×10^{-17}	326	4.12×10^{-18}
232	1.09×10^{-17}	280	1.49×10^{-17}	327	3.96×10^{-18}
233	1.08×10^{-17}	281	1.48×10^{-17}	328	3.80×10^{-18}
234	1.07×10^{-17}	282	1.47×10^{-17}	329	3.65×10^{-18}
235	1.06×10^{-17}	283	1.46×10^{-17}	330	3.50×10^{-18}
236	1.05×10^{-17}	284	1.44×10^{-17}	331	3.37×10^{-18}
237	1.05×10^{-17}	285	1.43×10^{-17}	332	3.22×10^{-18}
238	1.04×10^{-17}	286	1.41×10^{-17}	333	3.09×10^{-18}
239	1.04×10^{-17}	287	1.39×10^{-17}	334	2.96×10^{-18}
240	1.04×10^{-17}	288	1.37×10^{-17}	335	2.84×10^{-18}
241	1.04×10^{-17}	289	1.35×10^{-17}	336	2.71×10^{-18}
242	1.04×10^{-17}	290	1.33×10^{-17}	337	2.61×10^{-18}
244	1.05×10^{-17}	291	1.31×10^{-17}	338	2.51×10^{-18}
245	1.06×10^{-17}	292	1.28×10^{-17}	339	2.54×10^{-18}
246	1.07×10^{-17}	293	1.26×10^{-17}	340	2.31×10^{-18}
247	1.07×10^{-17}	294	1.23×10^{-17}	341	2.22×10^{-18}
342	2.12×10^{-18}	379	5.00×10^{-19}	416	1.60×10^{-19}
343	2.03×10^{-18}	380	4.90×10^{-19}	417	1.60×10^{-19}
344	1.95×10^{-18}	381	4.70×10^{-19}	418	1.60×10^{-19}
345	1.88×10^{-18}	382	7.60×10^{-19}	419	1.50×10^{-19}
346	1.80×10^{-18}	383	4.40×10^{-19}	420	1.50×10^{-19}

347	1.74×10^{-18}	384	4.30×10^{-19}	421	1.40×10^{-19}
348	1.67×10^{-18}	385	4.10×10^{-19}	422	1.40×10^{-19}
349	1.60×10^{-18}	386	4.00×10^{-19}	423	1.40×10^{-19}
350	1.53×10^{-18}	387	3.80×10^{-19}	424	1.30×10^{-19}
351	1.46×10^{-18}	388	3.70×10^{-19}	425	1.40×10^{-19}
352	1.41×10^{-18}	389	3.60×10^{-19}	426	1.40×10^{-19}
353	1.36×10^{-18}	390	3.60×10^{-19}	427	1.40×10^{-19}
354	1.30×10^{-18}	391	3.40×10^{-19}	428	1.30×10^{-19}
355	1.26×10^{-18}	392	3.30×10^{-19}	429	1.30×10^{-19}
356	1.21×10^{-18}	393	3.10×10^{-19}	430	1.30×10^{-19}
357	1.17×10^{-18}	394	3.10×10^{-19}	431	1.20×10^{-19}
358	1.11×10^{-18}	395	2.90×10^{-19}	432	1.20×10^{-19}
359	1.07×10^{-18}	396	2.90×10^{-19}	433	1.30×10^{-19}
360	1.03×10^{-18}	397	2.80×10^{-19}	434	1.20×10^{-19}
361	9.90×10^{-19}	398	2.60×10^{-19}	435	1.20×10^{-19}
362	9.60×10^{-19}	399	2.60×10^{-19}	436	1.20×10^{-19}
363	9.20×10^{-19}	400	2.60×10^{-19}	437	1.20×10^{-19}
364	8.90×10^{-19}	401	2.50×10^{-19}	438	1.20×10^{-19}
365	8.50×10^{-19}	402	2.40×10^{-19}	439	1.10×10^{-19}
366	8.10×10^{-19}	403	2.40×10^{-19}	440	1.20×10^{-19}
367	7.80×10^{-19}	404	2.20×10^{-19}	441	1.10×10^{-19}
368	7.50×10^{-19}	405	2.10×10^{-19}	442	1.00×10^{-19}
369	7.30×10^{-19}	406	2.10×10^{-19}	443	1.00×10^{-19}
370	7.10×10^{-19}	407	2.00×10^{-19}	444	1.10×10^{-19}
371	6.90×10^{-19}	408	2.00×10^{-19}	445	1.00×10^{-19}
372	6.60×10^{-19}	409	1.90×10^{-19}	446	1.00×10^{-19}
373	6.40×10^{-19}	410	1.90×10^{-19}	447	1.00×10^{-19}
374	6.10×10^{-19}	411	1.90×10^{-19}	448	1.00×10^{-19}
375	5.80×10^{-19}	412	1.80×10^{-19}	449	1.10×10^{-19}
376	2.70×10^{-19}	413	1.80×10^{-19}	450	1.10×10^{-19}
377	5.40×10^{-19}	414	1.80×10^{-19}		
378	5.20×10^{-19}	415	1.80×10^{-19}		

The values of the cross sections are from Green *et al.* (2004), and those of the quantum yields are taken from Harwood *et al.* (1995)

Appendix

Cl₂O₇ + hν → ClO₃ + ClO₄ — $Cl_2O_7 + h\nu \rightarrow ClO_3 + ClO_4$ — **J = 1.29 × 10⁻⁸ s⁻¹** **φ = 1** **BXXX**

λ (nm)	σ (cm² molecule⁻¹)	λ (nm)	σ (cm² molecule⁻¹)	λ (nm)	σ (cm² molecule⁻¹)
180	1.19×10^{-17}	225	7.97×10^{-19}	270	3.77×10^{-20}
185	9.09×10^{-18}	230	6.10×10^{-19}	275	2.57×10^{-20}
190	6.75×10^{-18}	235	4.56×10^{-19}	280	1.70×10^{-20}
195	4.75×10^{-18}	240	3.46×10^{-19}	285	1.20×10^{-20}
200	3.22×10^{-18}	245	2.47×10^{-19}	290	7.05×10^{-21}
205	2.32×10^{-18}	250	1.75×10^{-19}	295	5.21×10^{-21}
210	1.69×10^{-18}	255	1.20×10^{-20}	300	3.68×10^{-21}
215	1.32×10^{-18}	260	7.74×10^{-20}	305	2.03×10^{-21}
220	1.02×10^{-18}	265	5.37×10^{-20}	310	1.04×10^{-21}

The values of the cross sections are from Lin (1976), and those of the quantum yields are taken from Harwood *et al.* (1995).

ClONO + hν → Cl + NO₂ — $ClONO + h\nu \rightarrow Cl + NO_2$ — **J = 6.47 × 10⁻⁸ s⁻¹** **φ = 1** **BXXX**

λ (nm)	σ (cm² molecule⁻¹)	λ (nm)	σ (cm² molecule⁻¹)	λ (nm)	σ (cm² molecule⁻¹)
235	2.15×10^{-18}	300	1.29×10^{-18}	350	2.69×10^{-19}
240	1.76×10^{-18}	305	1.14×10^{-18}	355	2.29×10^{-19}
245	1.37×10^{-18}	310	1.05×10^{-18}	360	1.61×10^{-19}
250	1.06×10^{-18}	315	9.81×10^{-19}	365	1.13×10^{-19}
255	6.50×10^{-19}	320	8.03×10^{-19}	370	9.00×10^{-20}
260	6.46×10^{-19}	325	7.54×10^{-19}	375	6.90×10^{-20}
265	6.93×10^{-19}	330	5.87×10^{-19}	380	4.10×10^{-20}
270	9.03×10^{-19}	320	8.03×10^{-19}	385	3.30×10^{-20}
275	1.10×10^{-18}	325	7.54×10^{-19}	390	2.20×10^{-20}
280	1.32×10^{-18}	330	5.87×10^{-19}	395	1.50×10^{-20}
285	1.44×10^{-18}	335	5.77×10^{-19}	400	6.00×10^{-21}
290	1.44×10^{-18}	340	4.37×10^{-19}		
295	1.42×10^{-18}	345	3.57×10^{-19}		

The values of the cross sections are recommended by Burkholder *et al.* (2020).

Appendix

Bibliography of Appendix AIII

Abbatt, J.P.D., Toohey, D.W., Fenter, F.F., Stevens, P.S., Brune, W.H., Anderson, J.G., 1989. Kinetics and mechanism of X + ClNO → XCl + NO (X = Cl, F, Br, OH, O, N) from 220 to 450 K. Correlation of reactivity and activation energy with electron affinity of X. Journal of Physical Chemistry 93, 1022–1029.

Aders, W.K., Pangritz, D., Wagner, H.G., 1975. Investigations on the reaction of hydrogen atoms with methylfluoride, methyl chloride and methyl bromide. Berichte Bunsenges. Für Phys. Chem., Untersuchungen zur Reaktion von Wasserstoffatomen mit Methylfluorid, Methylchlorid und Methylbromid 79, 90–94.

Ahubelem, N., Altarawneh, M., Dlugogorski, B.Z., 2014. Dehydrohalogenation of ethyl halides. Tetrahedron Letters 55, 4860–4868. https://doi.org/10.1016/j.tetlet.2014.07.009

Alecu, I.M., Gao, Y., Hsieh, P.-C., Sand, J.P., Ors, A., McLeod, A., Marshall, P., 2007. Studies of the Kinetics and Thermochemistry of the Forward and Reverse Reaction $Cl + C_6H_6 = HCl + C_6H_5$. The Journal of Physical Chemistry A 111, 3970–3976. https://doi.org/10.1021/jp067212o

Altarawneh, M., Dlugogorski, B.Z., Kennedy, E.M., Mackie, J.C., 2008. Quantum Chemical and Kinetic Study of Formation of 2-Chlorophenoxy Radical from 2-Chlorophenol: Unimolecular Decomposition and Bimolecular Reactions with H, OH, Cl, and O_2. The Journal of Physical Chemistry A 112, 3680–3692. https://doi.org/10.1021/jp712168n

Anderson, L.C., Fahey, D.W., 1990. Studies with nitryl hypochlorite: thermal dissociation rate and catalytic conversion to nitric oxide using an NO/O_3 chemiluminescence detector. The Journal of Physical Chemistry 94, 644–652. https://doi.org/10.1021/j100365a027

Anglada, J.M., Solé, A., 2017. The Atmospheric Oxidation of HONO by OH, Cl, and ClO Radicals. The Journal of Physical Chemistry A 121, 9698–9707. https://doi.org/10.1021/acs.jpca.7b10715

Aranda, A., Díaz de Mera, Y., Rodríguez, A., Rodríguez, D., Martínez, E., 2003a. A Kinetic and Mechanistic Study of the Reaction of Cl Atoms with Acrolein: Temperature Dependence for Abstraction Channel. The Journal of Physical Chemistry A 107, 5717–5721. https://doi.org/10.1021/jp027767t

Aranda, A., Martínez, E., Díaz de Mera, Y., Rodríguez, A., Rodríguez, D., Cuartero, J., 2003b. Low-pressure study of the reactions of Cl atoms with acrylic acid and allyl alcohol. Atmospheric Environment 37, 4361–4369. https://doi.org/10.1016/S1352-2310(03)00573-9

Ashmore, P.G., Spencer, M.S., 1959. Concurrent molecular and chlorine atom mechanisms in the reversible dissociation of nitrosyl chloride. Transactions of the Faraday Society 55, 1868–1883. https://doi.org/10.1039/TF9595501868

Atkinson, D.B., Hudgens, J.W., 1999. Chlorination Chemistry I: Rate Coefficients, Reaction Mechanisms, and Spectra of the Chlorine and Bromine Adducts of Propargyl Halides. The Journal of Physical Chemistry A 103, 7978. https://doi.org/10.1021/jp991076o

Atkinson, R., Baulch, D.L., Cox, R.A., Crowley, J.N., Hampson, R.F., 2001. Summary of Evaluated Kinetic and Photochemical Data for Atmospheric Chemistry 1–56.

Atkinson, R., Baulch, D.L., Cox, R.A., Crowley, J.N., Hampson, R.F., Hynes, R.G., Jenkin, M.E., Rossi, M.J., Troe, J., 2007. Evaluated kinetic and photochemical data for atmospheric chemistry: Volume III – gas phase reactions of inorganic halogens. Atmospheric Chemistry and Physics 7, 981–1191. https://doi.org/10.5194/acp-7-981-2007

Atkinson, R., Baulch, D.L., Cox, R.A., Hampson, R.F., Kerr (Chairman), J.A., Troe, J., 1989. Evaluated Kinetic and Photochemical Data for Atmospheric Chemistry: Supplement III.

Appendix

IUPAC Subcommittee on Gas Kinetic Data Evaluation for Atmospheric Chemistry. Journal of Physical and Chemical Reference Data 18, 881–1097. https://doi.org/10.1063/1.555832

Ayscough, P.B., Cocker, A.J., Dainton, F.S., Hirst, S., Weston, M., 1961. Excited chloroethyl radicals $C_2H_2Cl_{5-x}$. Proceedings of the Chemical Society 244.

Baer, S., Hippler, H., Rahn, R., Siefke, M., Seitzinger, N., Troe, J., 1991. Thermodynamic and kinetic properties of the reaction $Cl + O_2 + M \rightleftarrows ClOO + M$ in the range 160–300 K and 1–1000 bar. The Journal of Chemical Physics 95, 6463–6470. https://doi.org/10.1063/1.461543

Baghal-Vayjooee, M.H., Benson, S.W., 1979. Kinetics and Thermochemistry of the Reaction $Cl + Cyclopropane \leftrightarrows HCl + Cyclopropyl$. Heat of Formation of the Cyclopropyl Radical. Journal of the American Chemical Society 101, 2838–2840. https://doi.org/10.1021/ja00505a005

Barassin, J., Lebreton, J., Combourieu, J., 1975. Étude cinétique des réactions entre l'oxygène atomique et les dérivés chlorés du méthane. Calcul théorique des constantes de vitesse. Journal de Chimie Physique 72, 1080–1086. https://doi.org/10.1051/jcp/1975721080

Barassin, J., Richoux, M., Combourieu, J., 1977. Etude cinetique des reactions entre l'oxygene atomique et les derives chlores de l'ethane. Bulletin de la Société Chimique de France 69–73.

Barat, R.B., Bozzelli, J.W., 1992. Kinetic and Product Distribution Analysis of the Reaction of Atomic Hydrogen with Vinyl Chloride. The Journal of Physical Chemistry 96, 2494–2501. https://doi.org/10.1021/j100185a021

Barnes, R.J., Sinha, A., Michelsen, H.A., 1998. Assessing the Contribution of the Lowest Triplet State to the Near-UV Absorption Spectrum of HOCl. The Journal of Physical Chemistry A 102, 8855–8859. https://doi.org/10.1021/jp9835869

Bartels, M., Hoyermann, K., Lange, U., 1989. An Experimental Study of the Reactions $CH_3CHO + Cl$, $C_2H_4O + Cl$, and $C_2H_4O + F$ in the Gas-Phase. Berichte der Bunsengesellschaft für physikalische Chemie 93, 423–427. https://doi.org/10.1002/bbpc.19890930403

Basco, N., Dogra, S.K., Norrish, R.G.W., 1971a. Reactions of halogen oxides studied by flash photolysis II. The flash photolysis of chlorine monoxide and of the ClO free radical. Proceedings of the Royal Society of London. A. Mathematical and Physical Sciences 323, 401–415. https://doi.org/10.1098/rspa.1971.0112

Basco, N., Dogra, S.K., Norrish, R.G.W., 1971b. Reactions of halogen oxides studied by flash photolysis. I. The flash photolysis of chlorine dioxide. Proceedings of the Royal Society of London. A. Mathematical and Physical Sciences 323, 29–68. https://doi.org/10.1098/rspa.1971.0087

Baulch, D.L., Duxbury, J., Grant, S., Montague, D., 1981. Evaluated Kinetic Data for High Temperature Reactions. Volume 4. Homogeneous Gas Phase Reactions of Halogen- and Cyanide-Containing Species. Journal of Physical and Chemical Reference Data 10.

Becker, E., Wille, U., Rahman, M.M., Schindler, R.N., 1991. An Investigation of the Reactions of NO_3 Radicals with Cl and ClO. Berichte der Bunsengesellschaft für physikalische Chemie 95, 1173–1179. https://doi.org/10.1002/bbpc.19910951003

Benson, S.W., Weissman, M., 1982. Mechanism of the pyrolysis of C_2HCl_5, molecular and radical steps. International Journal of Chemical Kinetics 14, 1287–1304. https://doi.org/10.1002/kin.550141202

Berho, F., Rayez, M.-T., Lesclaux, R., 1999. UV Absorption Spectrum and Self-Reaction Kinetics of the Cyclohexadienyl Radical, and Stability of a Series of Cyclohexadienyl-Type Radicals. The Journal of Physical Chemistry A 103, 5501–5509. https://doi.org/10.1021/jp9904318

Appendix

Bertrand, L., Bizongwako, J., Huybrechts, G., Olbregts, J., 1972. Oxygen-inhibited photochlorination of 1,2-dichloroethane. Bulletin des Sociétés Chimiques Belges 81, 73–80. https://doi.org/10.1002/bscb.19720810106

Bodenstein, M., Padelt, E., Schumacher, H.-J., 1929. Die thermische Reaktion zwischen Chlor und Ozon. Zeitschrift für Physikalische Chemie 5BB, 209–232. https://doi.org/10.1515/zpch-1929-0514

Boyd, A.A., Marston, G., Wayne, R.P., 1996. Kinetic Studies of the Reaction between NO_3 and OClO at T = 300 K and P = 2−8 Torr. The Journal of Physical Chemistry 100, 130–137. https://doi.org/10.1021/jp9509931

Brownsword, Richard A., Hillenkamp, M., Laurent, T., Vatsa, R.K., Volpp, H.-R., Wolfrum, J., 1997. Dynamics of H Atom Formation in the Photodissociation of Chloromethanes at 193.3 nm. The Journal of Physical Chemistry A 101, 5222–5227. https://doi.org/10.1021/jp963811r

Brownsword, R. A., Hillenkamp, M., Laurent, T., Vatsa, R.K., Volpp, H.-R., Wolfrum, J., 1997. Photodissociation dynamics of the chloromethanes at the Lyman-α wavelength (121.6 nm). The Journal of Chemical Physics 106, 1359–1366. https://doi.org/10.1063/1.473304

Brudnik, K., Gola, A.A., Jodkowski, J.T., 2009. Theoretical kinetic study of the formation reactions of methanol and methyl hypohalites in the gas phase. Journal of Molecular Modeling 15, 1061–1066. https://doi.org/10.1007/s00894-009-0461-x

Brudnik, K., Twarda, M., Sarzyński, D., Jodkowski, J.T., 2013a. Theoretical study of the kinetics of reactions of the monohalogenated methanes with atomic chlorine. Journal of Molecular Modeling 19, 1489–1505. https://doi.org/10.1007/s00894-012-1709-4

Brudnik, K., Twarda, M., Sarzyński, D., Jodkowski, J.T., 2013b. Theoretical study of the kinetics of chlorine atom abstraction from chloromethanes by atomic chlorine. Journal of Molecular Modeling 19, 4181–4193. https://doi.org/10.1007/s00894-013-1779-y

Bryukov, M.G., Dellinger, B., Knyazev, V.D., 2006. Kinetics of the Gas-Phase Reaction of OH with HCl. The Journal of Physical Chemistry A 110, 936–943. https://doi.org/10.1021/jp053615x

Bryukov, M.G., Knyazev, V.D., Gehling, W.M., Dellinger, B., 2009. Kinetics of the Gas-Phase Reaction of OH with Chlorobenzene. The Journal of Physical Chemistry A 113, 10452–10459. https://doi.org/10.1021/jp9049186

Bryukov, M.G., Knyazev, V.D., Lomnicki, S.M., McFerrin, C.A., Dellinger, B., 2004. Temperature-Dependent Kinetics of the Gas-Phase Reactions of OH with Cl_2, CH_4, and C_3H_8. The Journal of Physical Chemistry A 108, 10464–10472. https://doi.org/10.1021/jp047340h

Bryukov, M.G., Slagle, I.R., Knyazev, V.D., 2003. Kinetics of Reactions of Cl Atoms with Ethane, Chloroethane, and 1,1-Dichloroethane. The Journal of Physical Chemistry A 107, 6565–6573. https://doi.org/10.1021/jp0275138

Bryukov, M.G., Slagle, I.R., Knyazev, V.D., 2002. Kinetics of Reactions of Cl Atoms with Methane and Chlorinated Methanes. The Journal of Physical Chemistry A 106, 10532–10542. https://doi.org/10.1021/jp0257909

Bryukov, M.G., Slagle, I.R., Knyazev, V.D., 2001. Kinetics of Reactions of H Atoms with Methane and Chlorinated Methanes. The Journal of Physical Chemistry A 105, 3107–3122. https://doi.org/10.1021/jp0023359

Burkholder, J.B., Abbatt, J.P.D., Cappa, C., Dibble, T.S., Kolb, C.E., Wilmouth, D.M., Sander, S.P., Barker, J.R., Crounse, J.D., Huie, R.E., Kurylo, M.J., Percival, C.J., Wine, P.H., 2020. Chemical Kinetics and Photochemical Data for Use in Atmospheric Studies, Evaluation No. 19-5, JPL Publication 19-5. Jet Propulsion Laboratory, Pasadena.

Appendix

Burkholder, J.B., Mauldin, R.L., Yokelson, R.J., Solomon, S., Ravishankara, A.R., 1993. Kinetic, thermochemical, and spectroscopic study of chlorine oxide (Cl_2O_3). The Journal of Physical Chemistry 97, 7597–7605. https://doi.org/10.1021/j100131a032

Burkholder, J.B., Talukdar, R.K., Ravishankara, A.R., 1994. Temperature dependence of the $ClONO_2$ UV absorption spectrum. Geophysical Research Letters 21, 585–588. https://doi.org/10.1029/93GL03303

Cadman, P., Kirk, A.W., Trotman-Dickenson, A.F., 1976. Reactions of chlorine atoms with ethane, propane, isobutane, fluoroethane, 1,1-difluoroethane, 1,1,1-trifluoroethane and cyclopropane. Journal of the Chemical Society, Faraday Transactions 1: Physical Chemistry in Condensed Phases 72, 1027–1032. https://doi.org/10.1039/F19767201027

Calvert, J.G., Pitts, J.N., 1966. Photochemistry. John Wiley & Sons Inc, New York.

Cantrell, C.A., Davidson, J.A., Shetter, R.E., Anderson, B.A., Calvert, J.G., 1987. Reactions of nitrate radical and nitrogen oxide (N_2O_5) with molecular species of possible atmospheric interest. The Journal of Physical Chemistry 91, 6017–6021. https://doi.org/10.1021/j100307a040

Carl, S.A., Roehl, M., Müller, R., Moortgat, G.K., Crowley, J.N., 1996. Rate Constant and Mechanism of the Reaction between Cl and CH_3OCl at 295 K. The Journal of Physical Chemistry 100, 17191–17201. https://doi.org/10.1021/jp9611075

Chandra, A.K., Uchimaru, T., 1999. An ab Initio Investigation of the Reactions of 1,1- and 1,2-Dichloroethane with Hydroxyl Radical. The Journal of Physical Chemistry A 103, 10874–10883. https://doi.org/10.1021/jp991660x

Chen, Y., Rauk, A., Tschuikow-Roux, E., 1991. On the question of negative activation energies: absolute rate constants by RRKM and G1 theory for methyl + hydrogen halide → methane + halogen (Cl, Br) reactions. The Journal of Physical Chemistry 95, 9900–9908. https://doi.org/10.1021/j100177a053

Cheng, B.-M., Chung, C.-Y., Bahou, M., Lee, Y.-P., Lee, L.C., 2002. Quantitative spectral analysis of HCl and DCl in 120-220 nm: Effects of singlet-triplet mixing. The Journal of Physical Chemistry 117, 4293–4298. https://doi.org/10.1063/1.1496476

Chichinin, A.I., 2000. Isotope effects in the deactivation of $O(^1D)$ atoms by XCl and XF (X = H, D). Chemical Physics Letters 316, 425–432. https://doi.org/10.1016/S0009-2614(99)01325-1

Chou, C.C., Crescentini, G., Vera-Ruiz, H., Smith, W.S., Rowland, F.S., 1977. Stratospheric photochemistry of CF_2O, $CClFO$, and CCl_2O. 173rd American Chemical Society Meeting, New Orleans, LA.

Clark, D.T., Tedder, J.M., 1966. Reaction of hydrogen atoms with halogeno-methanes. Part 2.-Bromotrichloromethane and fluorotrichloromethane. Transactions of the Faraday Society 62, 399–404. https://doi.org/10.1039/TF9666200399

Clyne, M.A.A., Coxon, J.A., Linnett, J.W., 1968. Kinetic studies of oxy-halogen radical systems. Proceedings of the Royal Society of London. Series A. Mathematical and Physical Sciences 303, 207–231. https://doi.org/10.1098/rspa.1968.0048

Combourieu, J., Le Bras, G., Paty, C., 1973. Reaction of H atoms with CH_2Cl_2 application to the inhibition of flames. Symposium (International) on Combustion, Fourteenth Symposium (International) on Combustion 14, 485–492. https://doi.org/10.1016/S0082-0784(73)80047-5

Crowley, J.N., Helleis, F., Müller, R., Moortgat, G.K., Crutzen, P.J., Orlando, J.J., 1994. CH_3OCl: UV/visible absorption cross sections, J values and atmospheric significance. Journal of Geophysical Research: Atmospheres 99, 20683–20688. https://doi.org/10.1029/94JD01829

Appendix

Daële, V., Laverdet, G., Poulet, G., 1996. Kinetics of the reactions of CH_3O with Cl and ClO. International Journal of Chemical Kinetics 28, 589–598. https://doi.org/10.1002/(SICI)1097-4601(1996)28:8<589::AID-KIN4>3.0.CO;2-R

Daële, V., Poulet, G., 1996. Kinetics and products of the reactions of CH_3O_2 with Cl and ClO. Journal de Chimie Physique 93, 1081–1099. https://doi.org/10.1051/jcp/1996931081

Deka, R.C., Mishra, B.K., 2014. A theoretical investigation on the kinetics, mechanism and thermochemistry of gas-phase reactions of methyl acetate with chlorine atoms at 298K. Chemical Physics Letters 595–596, 43–47. https://doi.org/10.1016/j.cplett.2014.01.049

Deklau, B., Palmer, H.B., 1961. The rate of decomposition of nitrosyl chloride in shock waves. Symp. Int. Combust., Eighth Symposium (International) on Combustion 8, 139–150. https://doi.org/10.1016/S0082-0784(06)80496-0

DeMore, W.B., Tschuikow-Roux, E., 1990. Ultraviolet spectrum and chemical reactivity of the chlorine monoxide dimer. The Journal of Physical Chemistry 94, 5856–5860. https://doi.org/10.1021/j100378a046

Desai, V.R., Nechvatal, A., Tedder, J.M., 1970. Free-radical substitution in aliphatic compounds. Part XIX. Chlorination of 2,2-dimethylhexane. Journal of the Chemical Society B: Physical Organic 386–388. https://doi.org/10.1039/J29700000386

Dobis, O., Benson, S.W., 2002. Some Complexities in the Reaction of Hydrogen Atoms Generated in H_2 Discharge with Molecular Chlorine. The Journal of Physical Chemistry A 106, 4403–4410. https://doi.org/10.1021/jp014385z

Dobis, O., Benson, S.W., 2000. Kinetics of Cl Atom Reactions with C_2H_5Cl and C_2H_4Cl Radical and the Disproportionation of $2C_2H_4Cl$ at 298 K and at Millitorr Pressures. The Journal of Physical Chemistry A 104, 5503–5510. https://doi.org/10.1021/jp993163m

Dobis, O., Benson, S.W., 1991. Temperature coefficients of the rates of chlorine atom reactions with C_2H_6, C_2H_5, and C_2H_4. The rates of disproportionation and recombination of ethyl radicals. Journal of the American Chemical Society 113, 6377–6386. https://doi.org/10.1021/ja00017a004

Donaghy, T., Shanahan, I., Hande, M., Fitzpatrick, S., 1993. Rate constants and atmospheric lifetimes for the reactions of OH radicals and Cl atoms with haloalkanes. International Journal of Chemical Kinetics 25, 273–284. https://doi.org/10.1002/kin.550250407

Eskola, A.J., Lozovsky, V.A., Timonen, R.S., 2007. Kinetics of the reactions of C_2H_5, n-C_3H_7, and n-C_4H_9 radicals with Cl_2 at the temperature range 190–360 K. International Journal of Chemical Kinetics 39, 614–619. https://doi.org/10.1002/kin.20272

Eskola, A.J., Timonen, R.S., 2003. Kinetics of the reactions of vinyl radicals with molecular oxygen and chlorine at temperatures 200–362 K. Physical Chemistry Chemical Physics 5, 2557–2561. https://doi.org/10.1039/B302894A

Eskola, A.J., Timonen, R.S., Marshall, P., Chesnokov, E.N., Krasnoperov, L.N., 2008. Rate constants and hydrogen isotope substitution effects in the CH_3 + HCl and CH_3 + Cl_2 reactions. The Journal of Physical Chemistry. A 112, 7391–7401. https://doi.org/10.1021/jp801999w

Evans, C.S., Dellinger, B., 2005. Mechanisms of Dioxin Formation from the High-Temperature Oxidation of 2-Chlorophenol. Environmental Science & Technology 39, 122–127. https://doi.org/10.1021/es049355z

Farrell, J.T., Taatjes, C.A., 1998. Infrared Frequency-Modulation Probing of Cl + C_3H_4 (Allene, Propyne) Reactions: Kinetics of HCl Production from 292 to 850 K. The Journal of Physical Chemistry A 102, 4846–4856. https://doi.org/10.1021/jp981265r

Ferracci, V., Rowley, D.M., 2012. The temperature dependence of the bimolecular channels of the ClO + ClO reaction over the range T = 298–323 K. International Journal of Chemical Kinetics 44, 386–397. https://doi.org/10.1002/kin.20573

Appendix

Fletcher, I.S., Husain, D., 1976. The Reaction of $O(2^1D_2)$ with Molecular Chlorine Studied by Atomic Absorption Spectroscopy in the Vacuum Ultra-Violet. Berichte der Bunsengesellschaft für physikalische Chemie 80, 982–985. https://doi.org/10.1002/bbpc.19760801011

Friedl, R.R., Sander, S.P., Yung, Y.L., 1992. Chloryl nitrate: a novel product of the OClO + NO_3 + M recombination. The Journal of Physical Chemistry 96, 7490–7493. https://doi.org/10.1021/j100198a002

Galiba, I., Tedder, J.M., Watson, R.A., 1964. Free-radical substitution in aliphatic compounds. Part V. The halogenation of 1,1,1-trifluoropentane. Journal of the Chemical Society (Resumed) 1321–1324. https://doi.org/10.1039/JR9640001321

Garrett, B.C., Truhlar, D.G., 1979. Generalized transition state theory. Canonical variational calculations using the bond energy-bond order method for bimolecular reactions of combustion products. Journal of the American Chemical Society 101, 5207–5217. https://doi.org/10.1021/ja00512a016

Garzón, A., Moral, M., Notario, A., Albaladejo, J., Fernández-Gómez, M., 2009. Theoretical calculation of atmospheric reactions. The case of $CH_3–CH_xOH(CH_3)_{1-x}–CH_y(CH_3)_{3-y}$, (x=1,0; y=2,1)+Cl. Chemical Physics 1–3, 132–140. https://doi.org/10.1016/j.chemphys.2009.03.017

Ghosh, B., Papanastasiou, D.K., Talukdar, R.K., Roberts, J.M., Burkholder, J.B., 2012. Nitryl Chloride ($ClNO_2$): UV/Vis Absorption Spectrum between 210 and 296 K and $O(^3P)$ Quantum Yield at 193 and 248 nm. The Journal of Physical Chemistry A 116, 5796–5805. https://doi.org/10.1021/jp207389y

Gillotay, D., Simon, P.C., Dierickx, 1993. Ultraviolet absorption cross-sections of some carbonyl compounds and their temperature dependence. Aeronomica Acta A 368, 1–15.

Golden, D.M., 2007. The Reaction Cl + $NO_2 \rightarrow$ ClONO and $ClNO_2$. The Journal of Physical Chemistry A 111, 6772–6780. https://doi.org/10.1021/jp069000x

Good, D.A., Hansen, J., Kamboures, M., Santiono, R., Francisco, J.S., 2000. An Experimental and Computational Study of the Kinetics and Mechanism of the Reaction of Methyl Formate with Cl Atoms. The Journal of Physical Chemistry A 104, 1505–1511. https://doi.org/10.1021/jp992478z

Green, T.J., Islam, M., Canosa-Mas, C.E., Marston, G., Wayne, R.P., 2004. Higher oxides of chlorine: absorption cross-sections of Cl_2O_6 and Cl_2O_4, the decomposition of Cl_2O_6, and the reactions of OClO with O and O_3. Journal of Photochemistry and Photobiology A - Chemistry 162, 353–370.

Hansen, J.C., Friedl, R.R., Sander, S.P., 2008. Kinetics of the OH + ClOOCl and OH + Cl_2O Reactions: Experiment and Theory. The Journal of Physical Chemistry A 112, 9229–9237. https://doi.org/10.1021/jp8007706

Harwood, M.H., Rowley, D.M., Freshwater, R.A., Cox, R.A., Jones, R.L., 1995. A spectroscopic study of Cl_2O_3. Journal of the Chemical Society, Faraday Transactions 91, 3027–3032. https://doi.org/10.1039/FT9959103027

He, H., Liu, J., Li, Z., Sun, C., 2006. Theoretical study for the reaction of C_2H_5Cl/C_2D_5Cl with Cl atom. Journal of Molecular Structure: THEOCHEM 763, 59–66. https://doi.org/10.1016/j.theochem.2005.12.038

He, H., Liu, J., Li, Z., Sun, C., 2005. Direct ab initio dynamics calculation of the reaction rates of CH_3OCl with OH. The Journal of Physical Chemistry A 109, 3235–3240. https://doi.org/10.1021/jp045065t

Heicklen, J., 1965. The photolysis of phosgene-ethylene mixtures. Journal of the American Chemical Society 87, 445–453. https://doi.org/10.1021/ja01081a010

Appendix

Herndon, S.C., Gierczak, T., Talukdar, R.K., Ravishankara, A.R., 2001. Kinetics of the reactions of OH with several alkyl halides. Physical Chemistry Chemical Physics 3, 4529–4535. https://doi.org/10.1039/B105188C

Herron, J.T., Huie, R.E., 1973. Rate Constants for the Reactions of Atomic Oxygen (O ^{3}P) with Organic Compounds in the Gas Phase. Journal of Physical and Chemical Reference Data 2, 467–518. https://doi.org/10.1063/1.3253125

Hickson, K.M., Keyser, L.F., 2005. A kinetic and product study of the Cl + HO$_2$ reaction. The Journal of Physical Chemistry A 109, 6887–6900. https://doi.org/10.1021/jp051176w

Higashihara, T., Saito, K., Murakami, I., 1978. The Reaction of Hydrogen Chloride with Nitrogen Oxide in Shock Waves. Bulletin of the Chemical Society of Japan 51, 3426–3429. https://doi.org/10.1246/bcsj.51.3426

Hisatsune, I.C., Zafonte, L., 1969. Kinetic study of some third-order reactions of nitric oxide. The Journal of Physical Chemistry 73, 2980–2989. https://doi.org/10.1021/j100843a034

Hold, M., Hoyermann, K., Morozov, I., Zeuch, T., 2009. CH$_2$Cl and CHCl$_2$ Radical Chemistry: The Formation by the Reactions CH$_3$Cl + F and CH$_2$Cl$_2$ + F and The Destruction by the Reactions CH$_2$Cl + O and CHCl$_2$ + O. Zeitschrift für Physikalische Chemie 223, 409–426. https://doi.org/10.1524/zpch.2009.6044

Horowitz, A., Bauer, D., Crowley, J.N., Moortgat, G.K., 1993. Determination of product branching ratio of the ClO self-reaction at 298 K. Geophysical Research Letters 20, 1423–1426. https://doi.org/10.1029/93GL01383

Hou, H., Wang, B., Gu, Y., 2000. Decomposition and Isomerization of the CH$_3$CHClO Radical: ab Initio and RRKM Study. The Journal of Physical Chemistry A 104, 1570–1575. https://doi.org/10.1021/jp9930999

Hubrich, C., Stuhl, F., 1980. The ultraviolet absorption of some halogenated methanes and ethanes of atmospheric interest. Journal of Photochemistry 12, 93–107. https://doi.org/10.1016/0047-2670(80)85031-3

Hubrich, C., Zetzsch, C., Stuhl, F., 1977. Absorptionsspektren von halogenierten Methanen im Bereich von 275 bis 160 nm bei Temperaturen von 298 und 208 K. Berichte der Bunsengesellschaft für physikalische Chemie 81, 437–442. https://doi.org/10.1002/bbpc.19770810417

Hutton, E., Wright, M., 1965. Photoemissive and recombination reactions of atomic chlorine. Transactions of the Faraday Society 61, 78–89. https://doi.org/10.1039/TF9656100078

Huybrechts, G., Narmon, M., Mele, B.V., 1996. The pyrolysis of CCl$_4$ and C$_2$Cl$_6$ in the gas phase. Mechanistic modeling by thermodynamic and kinetic parameter estimation. International Journal of Chemical Kinetics 28, 27–36. https://doi.org/10.1002/(SICI)1097-4601(1996)28:1<27::AID-KIN4>3.0.CO;2-O

Jäger, M., Heydtmann, H., Zetzsch, C., 1996. Vacuum ultraviolet spectrum and quantum yield of the 193 nm photolysis of phosgene. Chemical Physics Letters 263, 817–821. https://doi.org/10.1016/S0009-2614(96)01278-X

Jenkin, M.E., Hayman, G.D., Wallington, T.J., Hurley, M.D., Ball, J.C., Nielsen, O.J., Ellermann, T., 1993. Kinetic and mechanistic study of the self-reaction of methoxymethylperoxy radicals at room temperature. The Journal of Physical Chemistry 97, 11712–11723. https://doi.org/10.1021/j100147a027

Ji, Y.-M., Wu, J., Liu, J., Li, Z., Sun, C., 2006. Theoretical study and rate constants calculation for the ClCH$_2$OH + Cl reaction. Chemical Physics Letters 417, 345–350. https://doi.org/10.1016/j.cplett.2005.10.009

Jodkowski, J.T., Rayez, M.-T., Rayez, J.-C., Bérces, T., Dóbé, S., 1998. Theoretical Study of the Kinetics of the Hydrogen Abstraction from Methanol. 2. Reaction of Methanol with

Appendix

Chlorine and Bromine Atoms. The Journal of Physical Chemistry A 102, 9230–9243. https://doi.org/10.1021/jp980846d

Jungkamp, T.P.W., Kirchner, U., Schmidt, M., Schindler, R.N., 1995. UV absorption cross-section data for the hypochlorites ROCl (R=H, CH_3, C_2H_5, i-C_3H_7, tert-C_4H_9). Journal of Photochemistry and Photobiology A: Chemistry 91, 1–6. https://doi.org/10.1016/1010-6030(95)04074-P

Kaiser, E.W., 1992. Pressure dependence of the reaction $Cl + C_2H_2$ over the temperature range 230 to 370 K. International Journal of Chemical Kinetics 24, 179–189. https://doi.org/10.1002/kin.550240206

Kaiser, E.W., Wallington, T.J., 1996. Pressure Dependence of the Reaction $Cl + C_3H_6$. The Journal of Physical Chemistry 100, 9788–9793. https://doi.org/10.1021/jp960406r

Kaiser, E.W., Wallington, T.J., Hurley, M.D., 2009. Products and Mechanism of the Reaction of Cl with Butanone in N_2/O_2 Diluent at 297−526 K. The Journal of Physical Chemistry A 113, 2424–2437. https://doi.org/10.1021/jp809169h

Karlsson, R.S., LjungstrÖm, E.B., 1996. Laboratory Study of ClNO: Hydrolysis. Environmental Science & Technology 30, 2008–2013. https://doi.org/10.1021/es950801f

Karra, S.B., Senkan, S.M., 1988. Analysis of the chemically activated CH_2Cl/CH_2Cl and CH_3/CH_2Cl recombination reactions at elevated temperatures using the bimolecular Quantam Rice-Ramsperger-Kassel (QRRK) method. Industrial & Engineering Chemistry Research 27, 447–451. https://doi.org/10.1021/ie00075a014

Keller-Rudek, H., Moortgat, G.K., Sander, R., Sörensen, R., 2013. The MPI-Mainz UV/VIS Spectral Atlas of Gaseous Molecules of Atmospheric Interest. Earth System Science Data 5, 365–373. https://doi.org/10.5194/essd-5-365-2013

Kita, D., Stedman, D.H., 1982. Kinetic studies of reactions of hydrogen atoms with HCl, Cl_2 and NOCl, and chlorine atoms with H_2 and NOCl. Journal of the Chemical Society, Faraday Transactions 2 78, 1249. https://doi.org/10.1039/f29827801249

Knauth, H.-D., 1978. Über die Reaktionen von NO und von ClNO mit $ClONO_2$ in der Gasphase (Teil 2). Berichte der Bunsengesellschaft für physikalische Chemie 82, 428–435. https://doi.org/10.1002/bbpc.197800077

Knox, J.H., Nelson, R.L., 1959. Competitive chlorination reactions in the gas phase: hydrogen and C_1—C_5 saturated hydrocarbons. Transactions of the Faraday Society 55, 937–946. https://doi.org/10.1039/TF9595500937

Knyazev, V.D., 2018. Kinetics and mechanism of the reactions of chloromethyl radical with acetylene and decomposition of 1-chloroallyl and 2-chloromethyl vinyl radicals. Chemical Physics Letters 691, 431–436. https://doi.org/10.1016/j.cplett.2017.11.057

Knyazev, V.D., Bencsura, A., Dubinsky, I.A., Gutman, D., Melius, C.F., Senkan, S.M., 1995. Kinetics and Thermochemistry of the Reaction of 1-Chloroethyl Radical with Molecular Oxygen. The Journal of Physical Chemistry 99, 230–238. https://doi.org/10.1021/j100001a036

Knyazev, V.D., Bencsura, Á., Dubinsky, I.A., Gutman, D., Senkan, S.M., 1994. The unimolecular decomposition of 1-chloroethyl radical. Symposium (International) on Combustion, Twenty-Fifth Symposium (International) on Combustion 25, 817–824. https://doi.org/10.1016/S0082-0784(06)80715-0

Knyazev, V.D., Kalinovski, I.J., Slagle, I.R., 1999. Kinetics of the $CH_2CH_2Cl \rightleftarrows C_2H_4 + Cl$ Reaction. The Journal of Physical Chemistry A 103, 3216–3221. https://doi.org/10.1021/jp984207e

Kukui, A., Jungkamp, T.P.W., Schindler, R.N., 1994. Determination of the product branching ratio in the reaction of NO_3 with OCl at 300 K. Berichte der Bunsengesellschaft für physikalische Chemie 98, 1619–1621. https://doi.org/10.1002/bbpc.19940981219

Appendix

Kukui, A.S., Jungkamp, T.P.W., Schindler, R.N., 1994. Determination of the rate constant and of product branching ratios in the reaction of CH_3O_2 with OCl between 233 and 300 K. Berichte der Bunsengesellschaft für physikalische Chemie 98, 1298–1302. https://doi.org/10.1002/bbpc.19940981013

Kukui, A.S., Roggenbuck, J., Schindler, R.N., 1997. Mechanism and rate constants for the reactions of Cl atoms with HOCl, CH_3OCl and tert-C_4H_9OCl. Berichte der Bunsengesellschaft für physikalische Chemie 101, 281–286. https://doi.org/10.1002/bbpc.19971010217

Kumaran, S.S., Lim, K.P., Michael, J.V., 1994. Thermal rate constants for the Cl + H_2 and Cl + D_2 reactions between 296 and 3000 K. The Journal of Chemical Physics 101, 9487–9498. https://doi.org/10.1063/1.468486

Larin, I.K., Spasskii, A.I., Trofimova, E.M., Turkin, L.E., 2009. Measurement of the reaction rate constants of oxygen atoms with chlorine and iodomethane using a resonance fluorescence technique. Kinetics and Catalysis 50, 474–480. https://doi.org/10.1134/S0023158409040028

Lesar, A., Hodošček, M., Senegačnik, M., 1996. Experimental and theoretical studies of the decomposition of N_2O catalyzed by chlorine. The Journal of Chemical Physics 105, 917–926. https://doi.org/10.1063/1.471935

Leu, M.T., Hatakeyama, S., Hsu, K.J., 1989. Rate constants for reactions between atmospheric reservoir species. 1. Hydrogen chloride. The Journal of Physical Chemistry 93, 5778–5784. https://doi.org/10.1021/j100352a026

Li, Q., Osborne, M.C., Smith, I.W.M., 2000. Rate constants for the reactions of Cl atoms with HCOOH and with HOCO radicals. International Journal of Chemical Kinetics 32, 85–91. https://doi.org/10.1002/(SICI)1097-4601(2000)32:2<85::AID-KIN3>3.0.CO;2-I

Li, Q.S., Luo, Q., 2003. Direct ab Initio Dynamics Study of the Reaction of the Hydrogen Atom with Formyl Chloride. The Journal of Physical Chemistry A 107, 10435–10440. https://doi.org/10.1021/jp0360568

Li, Z., Wuebbles, R.D., Pylawka, N.J., 2002. Rate constant measurement for the reaction of OClO with NO at 220–367 K. Chemical Physics Letters 354, 491–497. https://doi.org/10.1016/S0009-2614(02)00181-1

Lin, C.-L., 1976. Extinction coefficients of chlorine monoxide and chlorine heptoxide. Journal of Chemical & Engineering Data 21, 411–413. https://doi.org/10.1021/je60071a030

Louis, F., Allison, T.C., Gonzalez, C.A., Sawerysyn, J.-P., 2001. Computational Study of the Reactions of Methane with XO Radicals (X = F, Cl, or Br): Implications in Combustion Chemistry. The Journal of Physical Chemistry A 105, 4284–4289. https://doi.org/10.1021/jp0028498

Lu, X., Park, J., Lin, M.C., 2000. Gas Phase Reactions of HONO with NO_2, O_3, and HCl: Ab Initio and TST Study. The Journal of Physical Chemistry A 104, 8730–8738. https://doi.org/10.1021/jp001610o

Macken, K.V., Sidebottom, H.W., 1979. The reactions of methyl radicals with chloromethanes. International Journal of Chemical Kinetics 11, 511–527. https://doi.org/10.1002/kin.550110505

Maricq, M.M., Ball, J.C., Straccia, A.M., Szente, J.J., 1999. A diode laser study of the Cl + CH_3CO reaction. International Journal of Chemical Kinetics 29, 421–429.

Maricq, M.M., Shi, J., Szente, J.J., Rimai, L., Kaiser, E.W., 1993a. Evidence for the three-center elimination of hydrogen chloride from 1-chloroethoxy. Journal of Physical Chemistry 97, 9686–9694.

Maricq, M.M., Szente, J.J., Hybl, J.D., 1997. Kinetic Studies of the Oxidation of Dimethyl Ether and Its Chain Reaction with Cl_2. The Journal of Physical Chemistry A 101, 5155–5167. https://doi.org/10.1021/jp9709666

Appendix

Maricq, M.M., Szente, J.J., Kaiser, E.W., 1993b. A diode laser study of the chlorine atom + ethyl reaction. The Journal of Physical Chemistry 97, 7970–7977. https://doi.org/10.1021/j100132a028

Markert, F., Pagsberg, P., 1993. UV spectra and kinetics of radicals produced in the gas phase reactions of Cl, F and OH with toluene. Chemical Physics Letters 209, 445–454. https://doi.org/10.1016/0009-2614(93)80115-6

Martin, H., Kohnlein, E., 1958. Die Reaktion des Chlordioxyds mit Nitrosylchlorid in der Gasphase. Zeitschrift für Physikalische Chemie 17, 375–398. https://doi.org/10.1524/zpch.1958.17.5_6.375

Martin, H., Meise, W., Engelmann, E., 1960. Über die Kinetik der Reaktion des Dichlormonoxyds mit Stickstoffdioxyd in der Gasphase und im flüssigen Kondensat. Zeitschrift für Physikalische Chemie 24, 285–299. https://doi.org/10.1524/zpch.1960.24.5_6.285

Matsumi, Y., Tonokura, K., Inagaki, Y., Kawasaki, M., 1993. Isotopic branching ratios and translational energy release of hydrogen and deuterium atoms in reaction of oxygen (^{3}D) atoms with alkanes and alkyl chlorides. The Journal of Physical Chemistry 97, 6816–6821. https://doi.org/10.1021/j100128a012

Meller, R., Boglu, D., Moortgat, G.K., 1991. "UV spectra of several halogenated carbonyl compounds and FTIR studies of the degradation of CF_3COCl, HCFC-123 and HFC-143a"; Kinetics and Mechanisms for the Reactions of Halogenated Organic Compounds in the Troposphere. Presented at the STEPHALOCSIDE/ AFEAS WORKSHOP, Dublin, Ireland.

Mellouki, A., Poulet, G., Le Bras, G., Singer, R., Burrows, J.P., Moortgat, G.K., 1989. Discharge flow kinetic study of the reactions of nitrate radical with bromine, bromine monoxide, hydrogen bromide, and hydrogen chloride. The Journal of Physical Chemistry 93, 8017–8021. https://doi.org/10.1021/j100361a012

Méreau, R., Rayez, M.-T., Rayez, J.-C., Caralp, F., Lesclaux, R., 2001. Theoretical study on the atmospheric fate of carbonyl radicals: kinetics of decomposition reactions. Physical Chemistry Chemical Physics 3, 4712–4717. https://doi.org/10.1039/B105824J

Moore, T.A., Okumura, M., Seale, J.W., Minton, T.K., 1999. UV Photolysis of ClOOCl. The Journal of Physical Chemistry A 103, 1691–1695. https://doi.org/10.1021/jp984410+

Nelson, H.H., Johnston, H.S., 1981. Kinetics of the reaction of chlorine atoms with nitrosyl chloride and nitryl chloride and the photochemistry of nitryl chloride. The Journal of Physical Chemistry 85, 3891–3896. https://doi.org/10.1021/j150625a036

Nesbitt, D.J., Leone, S.R., 1982. Laser-initiated chlorine/hydrocarbon chain reactions: time-resolved infrared emission spectra of product vibrational excitation. The Journal of Physical Chemistry 86, 4962–4973. https://doi.org/10.1021/j100222a027

Okabe, H., 1983. Photochemistry of acetylene at 1849 Å. The Journal of Chemical Physics 78, 1312–1317. https://doi.org/10.1063/1.444868

Pagsberg, P., Munk, J., Sillesen, A., Anastasi, C., 1988. UV spectrum and kinetics of hydroxymethyl radicals. Chemical Physics Letters 146, 375–381. https://doi.org/10.1016/0009-2614(88)87462-1

Papanastasiou, D.K., Feierabend, K.J., Burkholder, J.B., 2011. Cl_2O photochemistry: Ultraviolet/vis absorption spectrum temperature dependence and O(^{3}P) quantum yield at 193 and 248 nm. The Journal of Chemical Physics 134, 204310. https://doi.org/10.1063/1.3592662

Papanastasiou, D.K., Papadimitriou, V.C., Fahey, D.W., Burkholder, J.B., 2009. UV absorption spectrum of the ClO dimer (Cl_2O_2) between 200 and 420 nm. The Journal of Physical Chemistry A 113, 13711–13726. https://doi.org/10.1021/jp9065345

Appendix

Parker, J.K., Payne, W.A., Cody, R.J., Nesbitt, F.L., Stief, L.J., Klippenstein, S.J., Harding, L.B., 2007. Direct measurement and theoretical calculation of the rate coefficient for $Cl+CH_3$ in the range from T=202-298 K. The Journal of Physical Chemistry A 111, 1015–1023. https://doi.org/10.1021/jp066231v

Pilgrim, J.S., Taatjes, C.A., 1997. Infrared Absorption Probing of the $Cl + C_3H_6$ Reaction: Rate Coefficients for HCl Production between 290 and 800 K. The Journal of Physical Chemistry A 101, 5776–5782. https://doi.org/10.1021/jp971405h

Platz, J., Nielsen, O.J., Wallington, T.J., Ball, J.C., Hurley, M.D., Straccia, A.M., Schneider, W.F., Sehested, J., 1998. Atmospheric Chemistry of the Phenoxy Radical, $C_6H_5O(\bullet)$: UV Spectrum and Kinetics of Its Reaction with NO, NO_2, and O_2. The Journal of Physical Chemistry A 102, 7964–7974. https://doi.org/10.1021/jp982221l

Qian, H.-B., Turton, D., Seakins, P.W., Pilling, M.J., 2002. A laser flash photolysis/IR diode laser absorption study of the reaction of chlorine atoms with selected alkanes. International Journal of Chemical Kinetics 34, 86–94. https://doi.org/10.1002/kin.10025

Raghunath, P., Lin, M.C., 2012. Ab initio chemical kinetics for the ClOO + NO reaction: Effects of temperature and pressure on product branching formation. The Journal of Chemical Physics 137, 014315. https://doi.org/10.1063/1.4731883

Resende, S.M., Jr, J.R.P., Almeida, W.B.D., 1998. Free radical mechanism of the Cl_2 addition to acetylene. Journal of the Chemical Society, Faraday Transactions 94, 2895–2900. https://doi.org/10.1039/A803923B

Robbins, D.E., 1976. Photodissociation of methyl chloride and methyl bromide in the atmosphere. Geophysical Research Letters 3, 213–216. https://doi.org/10.1029/GL003i004p00213

Roehl, C.M., Orlando, J.J., Calvert, J.G., 1992. The temperature dependence of the UV—visible absorption cross-sections of NOCl. Journal of Photochemistry and Photobiology A: Chemistry 69, 1–5. https://doi.org/10.1016/1010-6030(92)85253-Q

Rontu Carlon, N., Papanastasiou, D.K., Fleming, E.L., Jackman, C.H., Newman, P.A., Burkholder, J.B., 2010. UV absorption cross sections of nitrous oxide (N_2O) and carbon tetrachloride (CCl_4) between 210 and 350 K and the atmospheric implications. Atmospheric Chemistry and Physics 10, 6137–6149. https://doi.org/10.5194/acp-10-6137-2010

Rosser, W.A., Wise, H., 1960. Kinetics of the gas phase oxidation of hydrogen chloride and of hydrogen bromide by nitrogen dioxide. The Journal of Physical Chemistry 64, 602–604. https://doi.org/10.1021/j100834a022

Roussel, P.B., Lightfoot, P.D., Caralp, F., Catoire, V., Lesclaux, R., Forst, W., 1991. Ultraviolet absorption spectra of the CH_2Cl and $CHCl_2$ radicals and the kinetics of their self-recombination reactions from 273 to 686 K. Journal of the Chemical Society, Faraday Transactions 87, 2367–2377. https://doi.org/10.1039/FT9918702367

Rowley, D.M., Lesclaux, R., Lightfoot, P.D., Noziere, B., Wallington, T.J., Hurley, M.D., 1992. Kinetic and mechanistic studies of the reactions of cyclopentylperoxy and cyclohexylperoxy radicals with hydroperoxy radical. The Journal of Physical Chemistry 96, 4889–4894. https://doi.org/10.1021/j100191a031

Russell, J.J., Seetula, J.A., Gutman, D., Senkan, S.M., 1989a. Kinetics of reactions of chlorinated vinyl radicals (CH_2CCl and C_2Cl_3) with molecular oxygen. The Journal of Physical Chemistry 93, 1934–1938. https://doi.org/10.1021/j100342a047

Russell, J.J., Senkan, S.M., Seetula, J.A., Gutman, D., 1989b. Kinetics and thermochemistry of ethenyl and chloroethenyl radicals: study of the ethenyl + hydrogen chloride = ethene + chlorine atom and chloroethenyl + hydrogen chloride = chloroethene + chlorine atom

reactions. The Journal of Physical Chemistry 93, 5184–5188. https://doi.org/10.1021/j100350a032

Sander, S.P., Friedl, R.R., 1989. Kinetics and product studies of the reaction chlorine monoxide + bromine monoxide using flash photolysis-ultraviolet absorption. The Journal of Physical Chemistry 93, 4764–4771. https://doi.org/10.1021/j100349a017

Sarzyński, D.S., Fojcik, Ł., Gola, A.A., Berkowski, R., Jodkowski, J.T., Latajka, Z., 2014. Experimental and theoretical studies of the reactions of chlorine atoms with 1,2-dichloroethane and 1,2-dichloroethane-d_4 in the gas phase. The kinetics of hydrogen atom abstraction from the –CH_2Cl group in chloroethane and 1,2-dichloroethane. Chemical Physics Letters 597, 86–93. https://doi.org/10.1016/j.cplett.2014.02.026

Sarzyński, D.S., Gola, A.A., Brudnik, K., Berkowski, R., Jodkowski, J.T., 2012. Temperature dependence of the kinetic isotopic effect of the reaction of Cl atoms with C_2H_5Cl between 298 and 550K. Chemical Physics Letters 554, 20–26. https://doi.org/10.1016/j.cplett.2012.09.072

Sarzyński, D.S., Gola, A.A., Dryś, A., Jodkowski, J.T., 2009. Kinetic study of the reaction of chlorine atoms with chloromethane in the gas phase. Chemical Physics Letters 476, 138–142. https://doi.org/10.1016/j.cplett.2009.04.086

Schindler, R.N., Liesner, M., Schmidt, S., Kirchner, U., Benter, Th., 1997. Identification of nascent products formed in the laser photolysis of CH_3OCl and $HOCl$ at 308 nm and around 235 nm. Total Cl-atom quantum yields and the state and velocity distributions of $Cl(^2P_j)$. Journal of Photochemistry and Photobiology A: Chemistry 107, 9–19. https://doi.org/10.1016/S1010-6030(96)04583-2

Seakins, P.W., Orlando, J.J., Tyndall, G.S., 2004. Rate coefficients and production of vibrationally excited HCl from the reactions of chlorine atoms with methanol, ethanol, acetaldehyde and formaldehyde. Physical Chemistry Chemical Physics 6, 2224–2229. https://doi.org/10.1039/B402167C

Senkan, S.M., Quam, D., 1992. Correlation of reaction rate coefficients for the abstraction of hydrogen atoms from organic compounds by chlorine radical attack. The Journal of Physical Chemistry 96, 10837–10842. https://doi.org/10.1021/j100205a044

Sharma, H.D., Sood, S.P., 1974. Isotopic exchange reactions between nitrogen oxides and oxyhalides. The Journal of Physical Chemistry 78, 402–405. https://doi.org/10.1021/j100597a016

Sheng, L., Li, Z.-S., Liu, J.-Y., Xiao, J.-F., Sun, C.-C., 2004. Ab initio direct dynamics studies on the reaction of H atom with CH_3CH_2Cl. Journal of Computational Chemistry 25, 72–82. https://doi.org/10.1002/jcc.10305

Simon, P.C., Gillotay, D., Vanlaethem-Meuree, N., Wisemberg, J., 1988. Ultraviolet absorption cross-sections of chloro and chlorofluoro-methanes at stratospheric temperatures. Journal of Atmospheric Chemistry 7, 107–135. https://doi.org/10.1007/BF00048042

Singh, H., Tedder, J.M., 1966. Free-radical substitution in aliphatic compounds. Part XIV. The halogenation of esters of butan-1-ol. Journal of the Chemical Society B: Physical Organic 608–611. https://doi.org/10.1039/J29660000608

Slagle, I.R., Gutman, D., Gilbert, J.R., 1975. Direct identification of products and measurement of branching ratios for the reactions of oxygen atoms with vinylfluoride, vinylchloride, and vinylbromide. Symposium (International) on Combustion, Fifteenth Symposium (International) on Combustion 15, 785–793. https://doi.org/10.1016/S0082-0784(75)80347-X

Stevens, P.S., Anderson, J.G., 1992. Kinetic and mechanistic study of X + ClOCl → products (X = Br, Cl, F, O, OH, N) over the temperature range 240-373 K. Journal of Physical Chemistry 96, 1708–1718.

Appendix

Su, F., Calvert, J.G., Lindley, C.R., Uselman, W.M., Shaw, J.H., 1979. Fourier transform infrared kinetic study of hypochlorous acid and its absolute integrated infrared band intensities. Journal of Physical Chemistry 83, 912–920. https://doi.org/10.1021/j100471a006

Suh, I., Zhang, R., 2000. Kinetic Studies of Isoprene Reactions Initiated by Chlorine Atom. The Journal of Physical Chemistry A 104, 6590–6596. https://doi.org/10.1021/jp000605h

Talukdar, R.K., Mellouki, A., Burkholder, J.B., Gilles, M.K., Le Bras, G., Ravishankara, A.R., 2001. Quantification of the Tropospheric Removal of Chloral (CCl_3CHO): Rate Coefficient for the Reaction with OH, UV Absorption Cross Sections, and Quantum Yields. The Journal of Physical Chemistry A 105, 5188–5196. https://doi.org/10.1021/jp004632j

Taylor, P.H., Jiang, Z., Dellinger, B., 1993. Determination of the gas-phase reactivity of hydroxyl with chlorinated methanes at high temperature: Effects of laser/thermal photochemistry. International Journal of Chemical Kinetics 25, 9–23. https://doi.org/10.1002/kin.550250103

Tham, Y.J., Sarnela, N., Cuevas, C.A., Siddharth, I., Beck, L., Saiz-Lopez, A., Sipilä, M., 2020. Observation of $HClO_3$ and $HClO_4$ in the Arctic atmosphere. Copernicus Meetings https://doi.org/10.5194/egusphere-egu2020-16908

Tian, Y., Wei, W.-M., Tian, Z.-M., Yang, H.-Y., He, T.-J., Liu, F.-C., Chen, D.-M., 2006. Ab Initio/Density Functional Theory and Multichannel RRKM Study for the $ClO + CH_2O$ Reaction. The Journal of Physical Chemistry A 110, 11145–11150. https://doi.org/10.1021/jp061314x

Timonen, R.S., 1988. Kinetics of the reactions of some polyatomic free radicals with Cl_2 and Br_2, and reactions of formyl radicals with O_2, NO_2, Cl_2, Br_2, and H atoms. Annales Academiae Scientiarum Fennicae. Series A. II, Chemica 218, 5–45.

Timonen, R.S., Kalliorinne, K., Koskikallio, J., 1986. Kinetics of Reactions of Methyl and Ethyl Radicals with Chlorine in the Gas Phase Studied by Photochlorination of Methane. Acta Chemica Scandinavica 40a, 459–466. https://doi.org/10.3891/acta.chem.scand.40a-0459

Timonen, R.S., Ratajczak, E., Gutman, D., 1988. Kinetics of the reactions of the formyl radical with oxygen, nitrogen dioxide, chlorine, and bromine. The Journal of Physical Chemistry 92, 651–655. https://doi.org/10.1021/j100314a017

Tonokura, K., Norikane, Y., Koshi, M., Nakano, Y., Nakamichi, S., Goto, M., Hashimoto, S., Kawasaki, M., Sulbaek Andersen, M.P., Hurley, M.D., Wallington, T.J., 2002. Cavity Ring-down Study of the Visible Absorption Spectrum of the Phenyl Radical and Kinetics of Its Reactions with Cl, Br, Cl_2, and O_2. The Journal of Physical Chemistry A 106, 5908–5917. https://doi.org/10.1021/jp025585t

Troe, J., 1979. Predictive possibilities of unimolecular rate theory. The Journal of Physical Chemistry 83, 114–126. https://doi.org/10.1021/j100464a019

Tschuikow-Roux, E., Yano, T., Niedzielski, J., 1985. Reactions of ground state chlorine atoms with fluorinated methanes and ethanes. The Journal of Chemical Physics 82, 65–74. https://doi.org/10.1063/1.448737

Tyndall, G.S., Orlando, J.J., Kegley-Owen, C.S., Wallington, T.J., Hurley, M.D., 1999. Rate coefficients for the reactions of chlorine atoms with methanol and acetaldehyde. International Journal of Chemical Kinetics 31, 776–784. https://doi.org/10.1002/(SICI)1097-4601(1999)31:11<776::AID-JCK3>3.0.CO;2-Q

Tyndall, G.S., Stedman, K.M., Schneider, W., Burrows, J.P., Moortgat, G.K., 1987. The absorption spectrum of ClNO between 190 and 350 nm. Journal of Photochemistry 36, 133–139. https://doi.org/10.1016/0047-2670(87)87070-3

Appendix

Tyndall, G.S., Wallington, T.J., Hurley, M.D., Schneider, W.F., 1993. Rate coefficient for the reaction of hydroxymethyl radicals with chlorine and infrared spectra of chloromethanol and dichloromethanol. The Journal of Physical Chemistry 97, 1576–1582. https://doi.org/10.1021/j100110a019

Vanlaethem-Meurée, N., Wisemberg, J., Simon, P.C., 1978. Absorption des chlorométhanes dans l'ultraviolet : mesures des sections efficaces d'absorption en fonction de la température. Bulletins de l'Académie Royale de Belgique 64, 31–41. https://doi.org/10.3406/barb.1978.58340

Wahner, Andreas., Tyndall, G.S., Ravishankara, A.R., 1987. Absorption cross sections for symmetric chlorine dioxide as a function of temperature in the wavelength range 240-480nm. The Journal of Physical Chemistry 91, 2734–2738. https://doi.org/10.1021/j100295a018

Wallington, T.J., Bilde, M., Møgelberg, T.E., Sehested, J., Nielsen, O.J., 1996a. Atmospheric Chemistry of 1,2-Dichloroethane: UV Spectra of $CH_2ClCHCl$ and $CH_2ClCHClO_2$ Radicals, Kinetics of the Reactions of $CH_2ClCHCl$ Radicals with O_2 and $CH_2ClCHClO_2$ Radicals with NO and NO_2, and Fate of the Alkoxy Radical $CH_2ClCHClO$. The Journal of Physical Chemistry 100, 5751–5760. https://doi.org/10.1021/jp952149g

Wallington, T.J., Hurley, M.D., Schneider, W.F., 1996b. Atmospheric chemistry of CH_3Cl: mechanistic study of the reaction of CH_2ClO_2 radicals with HO_2. Chemical Physics Letters 251, 164–173. https://doi.org/10.1016/0009-2614(96)00080-2

Wang, L., Liu, J., Li, Z., Huang, X., Sun, C., 2003. Theoretical Study and Rate Constant Calculation of the Cl + HOCl and H + HOCl Reactions. The Journal of Physical Chemistry A 107, 4921–4928. https://doi.org/10.1021/jp0277558

Wang, L., Liu, J., Li, Z., Sun, C., 2005. Ab initio and DFT theoretical studies and rate constants calculation on the reactions O (^{3}P) atoms with HOX (X = Cl, Br). Chemical Physics Letters 411, 225–232. https://doi.org/10.1016/j.cplett.2005.05.071

Wategaonkar, S.J., Setser, D.W., 1989. Infrared chemiluminescence studies of H atom reactions with Cl_2O, ClNO, F_2O, CF_3OF, ClO_2, NO_2, and ClO. The Journal of Chemical Physics 90, 251–264. https://doi.org/10.1063/1.456527

Wijnen, M.H., 1961. Photolysis of phosgene in the presence of ethylene. Journal of the American Chemical Society 83, 3014–3017. https://doi.org/10.1021/ja01475a009

Wilkins, R.A., Dodge, M.C., Hisatsune, I.C., 1974. Kinetics of nitric oxide catalyzed decomposition of nitryl chloride and its related nitrogen isotope exchange reactions. The Journal of Physical Chemistry 78, 2073–2076. https://doi.org/10.1021/j100614a001

Wongdontri-Stuper, W., Jayanty, R.K.M., Simonaitis, R., Heicklen, J., 1979. The Cl_2 photosensitized decomposition of O_3: the reactions of ClO and OClO with O_3. Journal of Photochemistry 10, 163–186. https://doi.org/10.1016/0047-2670(79)80004-0

Wu, F., Carr, R.W., 2001. Kinetics of CH_2ClO Radical Reactions with O_2 and NO, and the Unimolecular Elimination of HCl. The Journal of Physical Chemistry A 105, 1423–1432. https://doi.org/10.1021/jp001953m

Xie, T., Bowman, J.M., Peterson, K.A., Ramachandran, B., 2003. Quantum calculations of the rate constant for the O(^{3}P) + HCl reaction on new *ab initio* ^{3}A″ and ^{3}A′ surfaces. The Journal of Chemical Physics 119, 9601–9608. https://doi.org/10.1063/1.1612918

Xing, S.-B., Shi, S.-H., Qiu, L.-X., 1992. Kinetics studies of reactions of OH radicals with four haloethanes part I. Experiment and BEBO calculation. International Journal of Chemical Kinetics 24, 1–10. https://doi.org/10.1002/kin.550240102

Xu, Z.F., Lin, M.C., 2010a. Ab initio chemical kinetic study on Cl + ClO and related reverse processes. The Journal of Physical Chemistry A 114, 11477–11482. https://doi.org/10.1021/jp102947w

Appendix

Xu, Z.F., Lin, M.C., 2010b. Computational Studies on Metathetical and Redox Processes of HOCl in Gas Phase. III. Its Self-Reaction and Interactions with HNO_x ($x = 1-3$). The Journal of Physical Chemistry A 114, 5320–5326. https://doi.org/10.1021/jp100977k

Xu, Z.F., Lin, M.C., 2010c. Computational Studies on Metathetical and Redox Processes of HOCl in the Gas Phase: (II) Reactions with ClO_x ($x = 1-4$). The Journal of Physical Chemistry A 114, 833–838. https://doi.org/10.1021/jp908882b

Xu, Z.F., Lin, M.C., 2003. Ab initio studies of ClO_x reactions. IX. Combination and disproportionation reactions of ClO and s-ClO_3 radicals. The Journal of Chemical Physics 119, 8897–8904. https://doi.org/10.1063/1.1613632

Xu, Z.F., Zhu, R.S., Lin, M.C., 2003a. Ab Initio Studies of ClO_x Reactions: VI. Theoretical Prediction of Total Rate Constant and Product Branching Probabilities for the HO_2 + ClO Reaction. The Journal of Physical Chemistry A 107, 3841–3850. https://doi.org/10.1021/jp0221237

Xu, Z.F., Zhu, R.S., Lin, M.C., 2003b. Ab Initio Studies of ClOx Reactions. 3. Kinetics and Mechanism for the OH + OClO Reaction. The Journal of Physical Chemistry A 107, 1040–1049. https://doi.org/10.1021/jp021183+

Yamada, T., Siraj, M., Taylor, P.H., Peng, J., Hu, X., Marshall, P., 2001. Rate Coefficients and Mechanistic Analysis for Reaction of OH with Vinyl Chloride between 293 and 730 K. The Journal of Physical Chemistry A 105, 9436–9444. https://doi.org/10.1021/jp011545y

Yamanaka, T., Kawasaki, M., Hurley, M.D., Wallington, T.J., Xiao, L., Schneider, W.F., 2008. Experimental and Computational Investigation of Gas-Phase Reaction of Chlorine with n-Propanol: Observation of Chloropropanol Conformational Isomerization at Room Temperature. The Journal of Physical Chemistry A 112, 2773–2781. https://doi.org/10.1021/jp711882c

Yu, W.H.S., Wijnen, M.H.J., 1970. Photolysis of Chloroform in the Presence of Ethane at 25°C. The Journal of Physical Chemistry 52, 2736–2739. https://doi.org/10.1063/1.1673367

Zhang, Q., Wang, S., Gu, Y., 2003. A theoretical investigation on the mechanism and kinetics for the reaction of atomic O (^{3}P) with CH_3CHCl_2. The Journal of Chemical Physics 119, 11172–11179. https://doi.org/10.1063/1.1622928

Zhu, L., Bozzelli, J.W., Ho, W.-P., 1999. Reaction of OH Radical with C_2H_3Cl: Rate Constant and Reaction Pathway Analysis. The Journal of Physical Chemistry A 103, 7800–7810. https://doi.org/10.1021/jp9904015

Zhu, L., Chen, W., Hase, W.L., Kaiser, E.W., 1993. Comparison of Models for Treating Angular Momentum in RRKM Calculations with Vibrator Transition States. Pressure and Temperature Dependence of Cl + C_2H_2 Association. The Journal of Physical Chemistry 97, 311–322. https://doi.org/10.1021/j100104a010

Zhu, R.S., Lin, M.C., 2011. Ab initio chemical kinetics for ClO reactions with HO_x, ClO_x and NO_x (x=1, 2): A review. Computational and Theoretical Chemistry, Theoretical chemistry of atmospheric processes 965, 328–339. https://doi.org/10.1016/j.comptc.2010.12.002

Zhu, R.S., Lin, M.C., 2010. An ab initio chemical kinetic study on the reactions of H, OH, and Cl with $HOClO_3$. International Journal of Chemical Kinetics 42, 253–261. https://doi.org/10.1002/kin.20459

Zhu, R.S., Lin, M.C., 2003a. Ab Initio Studies of ClO_x Radical Reactions: V. Evidence for a New Path in the Cl + ClOOCl Reaction. The Journal of Physical Chemistry A 107, 3836–3840. https://doi.org/10.1021/jp0218894

Zhu, R.S., Lin, M.C., 2003b. Ab initio studies of ClO_x reactions. VII. Isomers of Cl_2O_3 and their roles in the ClO + OClO reaction. Journal of Chemical Physics 118, 8645–8655.

Appendix

Zhu, R.S., Lin, M.C., 2003c. Ab initio studies of ClO_x reactions. VIII. Isomerization and decomposition of ClO_2 radicals and related bimolecular processes. Journal of Chemical Physics 119, 2075–2082. https://doi.org/10.1063/1.1585027

Zhu, R.S., Lin, M.C., 2002. Ab Initio Studies of ClO_x Reactions. 2. Unimolecular Decomposition of s-ClO_3 and the Bimolecular O + OClO Reaction. The Journal of Physical Chemistry A 106, 8386–8390. https://doi.org/10.1021/jp020015e